



Phytochemical, Biological, and Molecular Docking
Studies on
Fraxinus excelsior, Stachys arabica,
Pelargonium sidoides, and Pelargonium reniforme

by

Rana Mohammad Qasaymeh

Strathclyde Institute of Pharmacy
and Biomedical Sciences (SIPBS), Glasgow, UK

A thesis submitted to the University of Strathclyde in fulfilment of
the requirements for the degree of Doctor of Philosophy

August 2021

Declaration

'This thesis is the result of the author's original research. It has been composed by the author and has not been previously submitted for examination which has led to the award of a degree.'

'The copyright of this thesis belongs to the author under the terms of the United Kingdom Copyright Acts as qualified by University of Strathclyde Regulation 3.50. Due acknowledgement must always be made of the use of any material contained in, or derived from, this thesis.'

Signed:

Date:

Dedication

By the name of Allah

This thesis is proudly dedicated to my beloved parents.

To the soul of my father, and my beloved mother.

Dad, your passing away before starting my writing this thesis gave me the will-power/strength to succeed, because I always knew that you believed in me and wanted the best for me.

I miss you and I wish you could have been with me to share this moment together (with me)...

Mom, I cannot find the appropriate words that would describe properly my deepest gratitude for your endless love, sacrifice and honest prayers

Dad & Mom...

Without you none of my success would be possible.

I love you and I hope you are proud....

Alhamdulillah for all blessing and guidance

Acknowledgements

I would like to express my greatest gratitude to **Allah (SWT)** for blessing me and giving me the strength, knowledge, ability that has led me to finalise this thesis.

The journey is easier when you have accompaniment/ companions, as our life is based on interdependence and mutual support. During the time of my PhD, I have been supported by wonderful people. This work would not have been possible without them.

I would like to express my deepest gratitude and appreciation to my supervisor **Dr Veronique Seidel** for her support, excellent guidance, and wise criticism throughout the time of this research. Her meticulous attention to details, and providing constructive feedback helped me a lot in writing this thesis. My sincere appreciation to my co-supervisor **Dr Dino Rotondo**, who introduced me to the biology world which was a new adventure for me. His kindness, guidance and fruitful suggestions were invaluable contributions to my PhD experience. I am indebted to both of them for optimising my research skills to a higher level, improving my way of thinking, and on a more personal level, for their patience, help, and for their warm feeling during tough times in my sickness, my father passing away, and my mother illness due to COVID -19.

My sincere thanks to my academic assessor, **Prof. Yvonne Perrie**, for her motivation during my mini-vivas and regular reviewing of my research progress. I am grateful to **Dr Mohammad Al-Garaibah** (plant taxonomist, JUST) for his collaboration with the plant material of *Stachys arabica*.

I am grateful to **Dr Christopher Lawson, Dr Ruangelie Edrada-Ebel, Miss Grace Tedman and Mr. Craig Irving**. I will never forget their kindness, and their positive contributions during my journey. I will never forget **Dr Christopher Lawson** for his assistance in isolating 390RQ5, for useful time-sharing experiences and information,

and for his brother-like caring. I also would like to thank the members of staff in SIPBS who facilitated my resuming the lab work during the COVID-19 pandemic.

I would like to acknowledge **Jordan University of Science and Technology (JUST)** for awarding me this scholarship, and the opportunity to pursue my PhD studies in the United Kingdom, without which this study would not have been possible.

Warmest thanks to **all my friends**, for assistance, offering advice, sharing times and moments. Their lovely spirits were a milestone in the completion of this journey.

Finally, my heartfelt gratitude goes to all my beloved family (**Mom, Razan, Mahmoud, Marwan and Husam**) for their love, unlimited support, and encouragement. I am indebted to **Husam**, who helped me settle in Glasgow in my first year of study.

To all of you who made it possible for me to accomplish this adventure... May almighty Allah bless you all.

Publications and presentations

Publications

Rana M Qasaymeh, Dino Rotondo, Carel B Oosthuizen, Namrita Lall, Veronique Seidel. Predictive Binding Affinity of Plant-Derived Natural Products Towards the Protein Kinase G Enzyme of *Mycobacterium tuberculosis* (MtPknG). *Plants*, 2019, 8(11), 477; <https://doi.org/10.3390/plants8110477> (This article belongs to the Special Issue [Plant-Derived Chemicals: A Source of Inspiration for New Drugs](#)).

Poster communications

Rana M. Qasaymeh, Dino Rotondo and Veronique Seidel. Molecular docking of metabolites from *Pelargonium* spp. on the PknG enzyme from *Mycobacterium tuberculosis* 2018, Young Scientists' Meeting-Phytochemical Society of Europe - Trends in Natural Products Research, Liverpool, UK- July 2-5, 2018. Awarded Prize for Best Poster presentation.

Rana M. Qasaymeh, Dino Rotondo and Veronique Seidel. Predictive binding affinity of plant-derived natural products towards the protein kinase G enzyme of *Mycobacterium tuberculosis* (MtPknG). 2nd International Conference on Herbal and Traditional Medicine, Dubai, United Arab Emirates - June 20-21,2019.

Rana M. Qasaymeh, Dino Rotondo and Veronique Seidel. Predictive binding affinity of plant-derived natural products towards the protein kinase G enzyme of *Mycobacterium tuberculosis* (MtPknG). SIPBS Symposium, University of Strathclyde, Glasgow, Scotland, January 30th , 2020

Table of Contents

Declaration	II
Dedication	III
Acknowledgements	IV
Publications and presentations	VI
Table of Contents	VII
List of Abbreviations	XV
List of Figures	XVIII
List of Tables	XXIV
List of Protocols	XXVII
Abstract	XXVIII
Chapter One: INTRODUCTION	1
1.1 Tuberculosis: Disease, treatment, and challenges	1
1.2 Medicinal plants and natural products as a source of new drugs	5
1.2.1 General overview	5
1.2.2 Traditional antitubercular plant remedies and natural products.....	5
1.2.3 Selection of plants for phytochemical and biological evaluation.....	9
1.2.3.1 Ethno-guided or classical knowledge-based approach.....	9
1.2.3.2 Chemotaxonomical approach.....	9
1.2.3.3 Random approach	10
1.2.3.4 Computational approach	10
1.3 Medicinal plants selected for this study	12
1.3.1 <i>Fraxinus excelsior</i> L.	12
1.3.1.1 Botanical description	12
1.3.1.2 Traditional uses	12
1.3.1.3 Previous phytochemical work	13
1.3.1.4 Previous biological work	24
1.3.2 <i>Stachys arabica</i> Hornem	26
1.3.2.1 Botanical description	26
1.3.2.2 Traditional uses	27

1.3.2.3 Previous phytochemical work	27
1.3.2.4 Previous biological work	27
1.3.3 <i>Pelargonium sidoides</i> DC and <i>Pelargonium reniforme</i> Curt.	28
1.3.3.1 Botanical description	28
1.3.3.2 Traditional uses: Historical and modern uses	28
1.3.3.3 Previous phytochemical work	29
1.3.3.4 Previous biological work	30
1.4 The immune system	32
1.4.1 Innate and adaptive immunity	32
1.4.2 The innate immune response against Mtb	33
1.5 Inflammation	34
1.5.1 Pattern recognition receptors (PRRs)	35
1.5.2 Toll-like receptors (TLRs)	35
1.5.3 The TLR signalling pathways	38
1.6 Cytokines	40
1.6.1 Tumour Necrosis Factor-alpha (TNF- α)	41
1.6.2 Interleukin 12 (IL-12)	42
1.7 Host-Directed Therapies (HDT) and Pathogen-Directed Therapy (PDT) to tackle TB infection	43
1.7.1 Adjunct host-directed therapies (HDTs)	43
1.7.2 Adjunct pathogen-directed therapies (PDTs): Protein kinase G from <i>M. tuberculosis</i> (<i>MtPknG</i>) as a target for new antitubercular agents.	45
1.8 Aims and objectives	48
Chapter Two: MATERIALS AND METHODS	49
2.1 General	49
2.1.1 Solvents, chemicals and consumables used in phytochemical work.	49

2.1.2 Solvents, chemicals and consumables used in biology work	50
2.1.3 Cell lines and modulator	51
2.1.4 Enzyme-linked immunosorbent assay (ELISA) materials	51
2.1.5 Equipment and Instruments	52
2.1.6 Software packages and databases used in the molecular docking study	53
2.1.6.1 SciFinder	53
2.1.6.2 BIOVIA Discovery Studio Visualizer	53
2.1.6.3 ChemOffice	53
2.1.6.4 MGL Tools	53
2.1.6.5 Protein Data Bank	54
2.2 Plant material	54
2.3 Extraction	55
2.4 Chromatographic techniques	55
2.4.1 Vacuum liquid chromatography (VLC)	55
2.4.2 Thin layer chromatography (TLC)	56
2.4.3 Column chromatography (CC)	57
2.4.3.1 Size exclusion chromatography (SEC)	57
2.4.3.2 Silica gel column chromatography (SiCC)	57
2.4.4 Flash chromatography (FC)	58
2.5 Extraction and isolation protocols	59
2.6 Structure elucidation	64
2.6.1 NMR spectroscopy	64
2.6.2 Mass spectrometry (MS)	64
2.7 Cell viability assessment using colorimetric MTT assay	65
2.7.1 Cell culture	65
2.7.1.1 Preparation of culture medium	65
2.7.1.2 Preparation of K562 cells for experimental use	65

2.7.1.3 Preparation of THP-1 cells for experimental use	66
2.7.1.4 Storage and recovery of THP-1 cells	66
2.7.2 Plant extracts and phytochemicals - sample preparation	66
2.7.3 Preparation of MTT assay solutions	67
2.7.4 Protocol used	67
2.7.4.1 K562 MTT assay protocol	67
2.7.4.2 THP-1 MTT assay protocol	68
2.8 Measurement of cytokine production using ELISA	69
2.8.1 Preparation of THP-1 cells	69
2.8.2 THP-1 cell incubation protocol	69
2.8.3 Preparation of plant extracts and isolated phytochemicals for experimental use	70
2.8.4 Preparation of ELISA buffers and solutions	70
2.8.5 Preparation of ELISA antibody solutions	71
2.8.5.1 Preparation of TNF- α ELISA coating and detection antibody solutions.....	71
2.8.5.2 Preparation of IL-12 ELISA coating and detection antibody solutions	71
2.8.6 Preparation of ELISA standards solutions.....	72
2.8.6.1 Preparation of TNF- α standards	72
2.8.6.2 Preparation of IL-12 standards	72
2.8.7 ELISA protocol	73
2.9 Data analysis and statistical analysis	75
2.10 Molecular docking protocol	78
2.10.1 Ligand selection and preparation before docking	78
2.10.2 Target protein preparation before docking	78
2.10.3 Docking preparation	79
2.10.4 Docking experiment and visualisation of results.....	79
2.10.5 Protein-Ligand interactions and identification of binding site residues	80

Chapter Three: RESULTS AND DISCUSSION	82
Part A Phytochemical study	82
3.1 Characterisation of isolated phytochemicals	82
3.1.1 Terpenoids and phytosterols.....	83
3.1.1.1 Characterisation of 370RQ7/370RQ2 as a mixture of oleanolic acid (a) and ursolic acid (b).....	83
3.1.1.2 Characterisation of 370RQ25 as ursolic acid	102
3.1.1.3 Characterisation of 390RQ5 as a mixture of stigmasterol (a), β -sitosterol (b) and campesterol (c).....	107
3.1.1.4 Characterisation of 390RQ3/ 370RQ24 as a mixture of steryl fatty acid esters (a) and phytyl fatty acid esters (b)	116
3.1.2 Pheophytins	124
3.1.2.1 General NMR assignments	125
3.1.2.2 Characterisation of 390RQ10 as pheophytin a	126
3.1.2.3 Characterisation of 390RQ27 as a mixture of ^{13}C (S)-hydroxy pheophytin a and ^{13}C (R)-hydroxy pheophytin a	133
3.1.2.4 Characterisation of 390RQ28 as pheophytin b.....	140
3.1.3 Miscellaneous compounds.....	146
3.1.3.1 Characterization of 370RQ1 as a mixture of squalene (a) and nonacosane (b).....	146
3.1.3.2 Characterisation of 370RQ20 as pinocembrin.....	152
3.1.3.3 Characterisation of 370RQ19 as a mixture of phenylethanoid esters.....	159
3.1.3.4 Characterization of 390RQ1 and 370RQ22 as a mixture of acyclic alkanes	166
3.1.3.5 Others	170
Part B Biological studies	173
3.2 Evaluation of the effect of various crude extracts from <i>Fraxinus excelsior</i> leaves, <i>Stachys arabica</i> aerial parts, and selected isolated phytochemicals on cell viability using an MTT assay	173

3.2.1 Effect of varying K562 and THP-1 cell concentrations on cell viability.....	173
3.2.2 Effect of the various crude extracts of <i>Fraxinus excelsior</i> leaves (370) on cell viability.....	176
3.2.3 Effect of the various crude extracts of <i>Stachys arabica</i> aerial parts (390) on cell viability	179
3.2.4 Effect of selected phytochemicals isolated from EtOAc extract of <i>Fraxinus excelsior</i> leaves (370E) on THP-1 cell viability	182
3.2.5 Effect of phytochemicals isolated from EtOAc extracts of <i>Stachys arabica</i> aerial parts (390E) on THP-1 cell viability	187

3.3 Determination of the effect of various crude extracts from *F. excelsior* leaves, *S. arabica* aerial parts, and selected isolated phytochemicals on pro-inflammatory cytokines (TNF- α and IL-12) production from THP-1 cells....191

3.3.1 The effect of LPS on TNF- α and IL-12 production from THP-1 cells....	191
3.3.2 The effect of various crude extracts of <i>F. excelsior</i> leaves (370) on LPS-stimulated TNF- α production from THP-1 cells	194
3.3.3 The effect of various crude extract of <i>S. arabica</i> aerial parts (390) on LPS-stimulated TNF- α production from THP-1 cells	196
3.3.4 The effect of selected phytochemicals isolated from <i>F. excelsior</i> leaves (370E) on LPS-stimulated TNF- α production from THP-1 cells	199
3.3.5 The effect of selected phytochemicals isolated of <i>S. arabica</i> aerial parts (390E) on LPS-stimulated TNF- α production from THP-1 cells	203
3.3.6 The effect of various crude extract of <i>F. excelsior</i> leaves (370) on LPS-stimulated IL-12 production from THP-1 cells	206
3.3.7 The effect of various crude extracts of <i>S. arabica</i> aerial parts (390) on LPS-stimulated IL-12 production from THP-1 cells	208
3.3.8 The effect of selected phytochemicals isolated from <i>F. excelsior</i> leaves (370E) on LPS-stimulated IL-12 production from THP-1 cells	211
3.3.9 The effect of selected phytochemicals isolated from <i>S. arabica</i> aerial parts (390E) on LPS-stimulated IL-12 production from THP-1 cells	215

3.4 Modulation of cell viability by various crude extracts and purified phytochemicals.....	218
3.4.1 Modulation of cell viability by crude extracts of <i>F. excelsior</i> leaves (370) and their purified phytochemicals	218
3.4.2 Modulation of cell viability by crude extracts of <i>S. arabica</i> aerial parts (390) and their purified phytochemicals	220
3.5 Suppression of pro-inflammatory cytokines (TNF- α and IL-12) production from LPS- stimulated THP-1 cells	222
3.5.1. Suppression of pro-inflammatory cytokines (TNF- α and IL-12) production from LPS- stimulated THP-1 cells by crude extracts of <i>F. excelsior</i> leaves (370) and their purified phytochemicals.....	222
3.5.2 Suppression of pro-inflammatory cytokines (TNF- α and IL-12) production from LPS- stimulated THP-1 cells by crude extracts of <i>S. arabica</i> aerial parts (390) and their purified phytochemicals.....	228
3.5.3 Putative mode(s) of action of the plant extracts/phytochemicals	232
Part C Molecular docking studies	234
3.6 Molecular docking of ligands towards the protein kinase G enzyme of <i>Mycobacterium tuberculosis</i> (<i>MtPknG</i>).....	234
3.6.1 Phytochemicals from <i>Pelargonium reniforme</i> and <i>Pelargonium sidoides</i>	233
3.6.2 Selected phytochemicals isolated from <i>Fraxinus excelsior</i> and <i>Stachys arabica</i>	235
3.7 Evaluation of the docking studies	253
Chapter Four: CONCLUSION AND FUTURE WORK	257
4.1 Conclusion	257
4.2 Recommendations for future work	262

Appendices	263
Appendix I: Chemical structures of phytochemicals isolated from <i>Pelargonium reniforme</i> and <i>Pelargonium sidoides</i>	263
Appendix II: Mass Spectrometry Results	276
Appendix III: Others	301
References	306

List of Abbreviations

370E	Ethyl acetate extract of <i>Fraxinus excelsior</i> leaves
370H	Hexane extract of <i>Fraxinus excelsior</i> leaves
370M	Methanol extract of <i>Fraxinus excelsior</i> leaves
390E	Ethyl acetate extract of <i>Stachys arabica</i> aerial parts
390H	Hexane extract of <i>Stachys arabica</i> aerial parts
390M	Methanol extract of <i>Stachys arabica</i> aerial parts
1D-NMR	One dimensional- Nuclear Magnetic Resonance
2D-NMR	Two dimensional- Nuclear Magnetic Resonance
AECs	Airway epithelial cells
AIDS	Acquired Immune Deficiency Syndrome
ANOVA	Analysis of variance
ASAP-MS	Atmospheric Solids Analysis Probe Mass Spectrometry
BSA	Bovine serum albumin
CC	Open Column Chromatography
CD14	Cluster of Differentiation 14
CDCl ₃	Deuterated Chloroform
CRs	Complement receptors
DCs	Dendritic cells
DCM	Dichloromethane
DEPTQ	Distortionless Enhancement by Polarization Transfer including the detection of Quaternary nuclei
DMSO	Dimethyl Sulfoxide
DS-TB	Drug susceptible- tuberculosis
DSS	Dextrin Sodium Sulphate
ECACC	European Type Cell Culture
ELISA	Enzyme linked immunosorbent assay
ETM	European traditional medicine
EtOAc	Ethyl acetate
FBS	Foetal Bovine Serum
FC	Flash Chromatography
HIV	Human Immunodeficiency Virus
HSP65	Heat shock protein 65

HSQC	Heteronuclear Single Quantum Correlation
HMBC	Heteronuclear Multiple Bond Correlation
HR- nanoESI-MS	High Resolution nano Electron Spray Ionization Mass Spectrometry
HR-GC-EI-MS	High Resolution Gas Chromatography Electron Impact Mass Spectrometry
Hydroxy pheo a	13^2 (R,S)-hydroxy pheophytin a
IC ₅₀	the concentration required for 50% inhibition of the cell viability with respect to untreated cells
IL-12	Interleukin 12
iNOS	Inducible nitric oxide synthase
INH	Isoniazid
IRAK	IL-1 Receptor-Associated Kinase
LBS	LPS-binding protein
LAM	Lipoarabinomannan
LM	Lipomannan
LPS	Lipopolysaccharide
MAPK	Mitogen-Activated Protein Kinases
MD2	Myeloid differentiation protein 2
MDR-TB	Multidrug-resistant Tuberculosis
MeOH	Methanol
MIC	Minimum Inhibitory Concentration
Mtb	<i>Mycobacterium tuberculosis</i>
MtPknG	<i>Mycobacterium tuberculosis</i> protein kinase G enzyme
MTT	3-[4,5-Dimethylthiazol-2-yl]-2,5 diphenyl tetrazolium bromide / Thiazolyl blue tetrazolium
MS	Mass Spectrometry
MyD88	Myeloid differentiation factor 88
Nano-ESI	Nano-electrospray ionization
NF-κB	Nuclear factor-kappa beta
NK	Natural killer
NMR	Nuclear Magnetic Resonance
NMSF	National Mass Spectrometry Facility
NPs	Natural Products

NO	Nitric oxide
NLRs	NOD-Like receptors
OA	Oleanolic acid
PAMP	Pathogen-associated molecular pattern
PBS	Phosphate buffered saline
PGE2	Prostaglandin E2
PRRs	Pattern recognition receptors
PFAEs	Phytol fatty acid esters
RIF	Rifampicin
RMSD	Root mean square deviation
RPMI	Roswell Park Memorial Institute
ROS	Reactive oxygen species
s.d.	Standard deviation
SDS	Sodium Dodecyl Sulphate
SEC	Size exclusion chromatography
SFAEs	Steryl fatty acid esters
SiCC	Silica Column Chromatography
TB	Tuberculosis
THP-1	Human Leukaemia Monocytic Cell Line
TLC	Thin layer chromatography
TLRs	Toll-like receptors
TLR4	Toll like receptor 4
TNF- α	Tumour necrosis factor-alpha
TOF	Time-of-flight analyser
UA	Ursolic acid
UV	Ultraviolet Light
VLC	Vacuum Liquid Chromatography
XDR-TB	Extensively Drug-resistant Tuberculosis

List of Figures

Chapter One

Figure 1.1	Estimated TB incidence in 2019	2
Figure 1.2	Leaves of <i>Fraxinus excelsior</i> L	12
Figure 1.3	Structures of flavonoids reported in <i>F. excelsior</i>	21
Figure 1.4	Structures of terpenoids and sterol isolated from <i>F. excelsior</i>	22
Figure 1.5	Structures of phenolic acid and their derivatives isolated from <i>F. excelsior</i>	23
Figure 1.6	Structures of other phytochemicals isolated from <i>F. excelsior</i>	24
Figure 1.7	Aerial parts of <i>Stachys arabica</i> Hornem	26
Figure 1.8	Simplified diagram of MyD88-dependent pathway following TLR4 activation by LPS	39

Chapter Two

Figure 2.1	Simplified diagram of ELISA procedure steps followed in this study	74
Figure 2.2	Typical TNF- α standard curve for ELISA assay	76
Figure 2.3	Typical IL-12 standard curve for ELISA assay	77
Figure 2.4	Protocol used for the molecular docking study	81

Chapter Three

Figure 3.1	Summary of the isolated phytochemicals identified in <i>Fraxinus excelsior</i> leaves (370), and <i>Stachys arabica</i> aerial parts (390).	82
Figure 3.2	Structures of 370RQ7/370RQ2 or oleanolic acid (a) and ursolic acid (b) with selected HMBC correlations.	83
Figure 3.3	^1H NMR spectrum (CDCl_3^* , 600 MHz) of 370RQ7	92
Figure 3.4	^{13}C -DEPTQ NMR spectrum (CDCl_3^* , 150 MHz) of 370RQ7	93
Figure 3.5	HSQC spectrum (CDCl_3^* , 500 MHz) of 370RQ7	94
Figure 3.6	Selected expansion of HMBC spectrum (CDCl_3^* , 600 MHz) of 370RQ7	95

Figure 3.7	^1H NMR spectrum (CDCl_3^* , 500 MHz) of 370RQ2	98
Figure 3.8	^{13}C -DEPTQ NMR spectrum (CDCl_3^* , 125 MHz) of 370RQ2	99
Figure 3.9	HSQC spectrum (CDCl_3^* , 500 MHz) of 370RQ2	100
Figure 3.10	HMBC spectrum (CDCl_3^* , 500 MHz) of 370RQ2	101
Figure 3.11	^1H NMR spectrum (CDCl_3^* , 500 MHz) of 370RQ25	105
Figure 3.12	^{13}C -DEPTQ NMR spectrum (CDCl_3^* , 125 MHz) of 370RQ25	106
Figure 3.13	Structures of 390RQ5 or stigmasterol (a), β -sitosterol (b) and campesterol (c)	107
Figure 3.14	^1H NMR spectrum (CDCl_3^* , 500 MHz) of 390RQ5	113
Figure 3.15	^{13}C -DEPTQ NMR spectrum (CDCl_3^* , 125 MHz) of 390RQ5	114
Figure 3.16	HMBC spectrum (CDCl_3^* , 500 MHz) of 390RQ5	115
Figure 3.17	Structures of 390RQ3/370RQ24 or mixture of steryl fatty acid esters (SFAEs) (a) and a mixture of phytyl fatty acid esters (PFAEs) (b)	116
Figure 3.18	^1H NMR spectra (CDCl_3^* , 500 MHz) of 390RQ3 and 370RQ24	121
Figure 3.19	^{13}C DEPTQ NMR spectra (CDCl_3^* , 125 MHz) of 390RQ3 and 370RQ24	122
Figure 3.20	HMBC spectrum (CDCl_3^* , 500 MHz) of 390RQ3	123
Figure 3.21	Structures of 390RQ10, 390RQ27, and 390RQ28	124
Figure 3.22	Structure of 390RQ10 or pheophytin a	126
Figure 3.23	^1H NMR spectrum (CDCl_3^* , 500 MHz) of 390RQ10	131
Figure 3.24	^{13}C -DEPTQ NMR spectrum (CDCl_3^* , 125 MHz) of 390RQ10	132
Figure 3.25	Structure of 390RQ27 or $13^2(R,S)$ -hydroxy pheophytin a	133
Figure 3.26	^1H NMR spectrum (CDCl_3^* , 400 MHz) of 390RQ27	138
Figure 3.27	^{13}C -DEPTQ NMR spectrum (CDCl_3^* , 100 MHz) of 390RQ27	139
Figure 3.28	Structure of 390RQ28 or pheophytin b	140
Figure 3.29	^1H NMR spectrum (CDCl_3^* , 500 MHz) of 390RQ28	144
Figure 3.30	^{13}C -DEPTQ NMR spectrum (CDCl_3^* , 125 MHz) of 390RQ28	145
Figure 3.31	Structures of 370RQ1 or squalene (a) and nonacosane (b)	146

Figure 3.32	^1H NMR spectrum (CDCl_3^* , 500 MHz) of 370RQ1	150
Figure 3.33	^{13}C -DEPTQ NMR spectrum (CDCl_3^* , 125 MHz) of 370RQ1	151
Figure 3.34	Structure of 370RQ20 or pinocembrin with the key HMBC correlations.	152
Figure 3.35	^1H NMR spectrum (CDCl_3^* , 500 MHz) of 370RQ20	156
Figure 3.36	^{13}C -DEPTQ NMR spectrum (CDCl_3^* , 125 MHz) of 370RQ20	157
Figure 3.37	HMBC spectrum (CDCl_3^* , 500 MHz) of 370RQ20	158
Figure 3.38	Structure of 370RQ19 or phenylethanoid esters	159
Figure 3.39	^1H NMR spectrum (CDCl_3^* , 500 MHz) of 370RQ19	164
Figure 3.40	^{13}C -DEPTQ NMR spectrum (CDCl_3^* , 125 MHz) of 370RQ19	165
Figure 3.41	Structures of 390RQ1 / 370RQ22 or a mixture of acyclic alkanes	166
Figure 3.42	^1H NMR spectrum (CDCl_3^* , 500 MHz) spectra of 390RQ1/370RQ22	168
Figure 3.43	^{13}C NMR spectrum (CDCl_3^* , 125 MHz) spectra of 390RQ1/370RQ22	169
Figure 3.44	Structure of 370RQ4 or dioctyl phthalate (BEHP)	170
Figure 3.45	K562 cell viability with increasing cell numbers	174
Figure 3.46	THP-1 cell viability with increasing cell numbers	175
Figure 3.47	Effect of the various crude extracts of <i>Fraxinus excelsior</i> leaves (370) on the viability of K562 cells	177
Figure 3.48	Effects of the various crude extracts of <i>Fraxinus excelsior</i> leaves (370) on the viability of THP-1 cells	178
Figure 3.49	Effect of the various crude extracts of <i>Stachys arabica</i> aerial parts (390) on the viability of K562 cells	180
Figure 3.50	Effect of the various crude extracts of <i>Stachys arabica</i> aerial parts (390) on the viability of THP-1 cells	181
Figure 3.51	Effect of the various concentrations of pinocembrin on the viability of THP-1 cells	183
Figure 3.52	Effect of the various concentrations of UA on the viability of THP-1 cells	184

Figure 3.53	Effect of the various concentrations of OA on the viability of THP-1 cells	185
Figure 3.54	Effect of the various concentration of the mixture of phenylethanoid esters on the viability of THP-1 cells	186
Figure 3.55	Effect of the various concentration of pheophytin a on the viability of THP-1 cells	188
Figure 3.56	Effect of the various concentration of 13 ² (<i>R,S</i>)-hydroxy pheophytin a on the viability of THP-1 cells	189
Figure 3.57	Effect of the various concentration of pheophytin b on the viability of THP-1 cells	190
Figure 3.58	The effect of various concentrations of LPS on TNF- α production from THP-1 cells	192
Figure 3.59	The effect of various concentrations of LPS on IL-12 production from THP-1 cells	193
Figure 3.60	The effect of various crude extract of <i>F. excelsior</i> leaves (370) on LPS-stimulated TNF- α production from THP-1 cells	195
Figure 3.61	The effect of <i>n</i> -hexane and EtOAc crude extract of <i>S. arabica</i> aerial parts (390H & 390E) on LPS-stimulated TNF- α production from THP-1 cells	197
Figure 3.62	The effect of MeOH crude extract of <i>S. arabica</i> aerial parts (390M) on LPS-stimulated TNF- α production from THP-1 cells	198
Figure 3.63	The effect of different concentrations of UA & Pinocembrin on LPS-stimulated TNF- α production from THP-1 cells	200
Figure 3.64	The effect of different concentrations of OA on LPS-stimulated TNF- α production from THP-1 cells	201
Figure 3.65	The effect of different concentrations of the mixture of phenylethanoid esters on LPS-stimulated TNF- α production from THP-1 cells	202
Figure 3.66	The effect of different concentrations of pheophytin a on LPS-stimulated TNF- α production from THP-1 cells	204

Figure 3.67	The effect of different concentrations of 13 ² (<i>R,S</i>)-hydroxy pheophytin a & pheophytin b on LPS-stimulated TNF- α production from THP-1 cells	205
Figure 3.68	The effect of various crude extracts of <i>F. excelsior</i> leaves (370) on LPS-stimulated IL-12 production from THP-1 cells	207
Figure 3.69	The effect of <i>n</i> -hexane and EtOAc crude extracts of <i>S. arabica</i> aerial parts (390H & 390E) on LPS-stimulated IL-12 production from THP-1 cells	209
Figure 3.70	The effect of MeOH crude extract of <i>S. arabica</i> aerial parts (390M) on LPS-stimulated IL-12 production from THP-1 cells	210
Figure 3.71	The effect of different concentrations of UA & Pinocembrin on LPS-stimulated IL-12 production from THP-1	212
Figure 3.72	The effect of different concentrations of OA on LPS-stimulated IL-12 production from THP-1 cells	213
Figure 3.73	The effect of different concentrations of the mixture of phenylethanoid esters on LPS-stimulated IL-12 production from THP-1 cells	214
Figure 3.74	The effect of different concentrations of pheophytin a on LPS-stimulated IL-12 production from THP-1 cells	216
Figure 3.75	The effect of different concentrations of 13 ² (<i>R,S</i>)-hydroxy pheophytin a & pheophytin b on LPS-stimulated IL-12 production from THP-1 cells	217
Figure 3.76	Proposed mechanisms representing the effect of <i>F. excelsior</i> , <i>S. arabica</i> , and selected phytochemicals on LPS-stimulated THP-1 cells.	233
Figure 3.77	Predicted binding free energy (docking score) and detailed molecular interactions of the control inhibitor AX20017 within the active site of <i>MtPknG</i> .	247
Figure 3.78	Predicted binding free energy (docking score) and detailed molecular interactions of isoorientin 2''- <i>O</i> -gallate (79) within the active site of <i>MtPknG</i> .	248

Figure 3.79	Predicted binding free energy (docking score) and detailed molecular interactions of isovitexin 2"-O-gallate (77) within the active site of <i>MtPknG</i> .	249
Figure 3.80	Predicted binding free energy (docking score) and detailed molecular interactions of kaempferol 3-O-β-D- rutinoside (nicotiflorin) (61) within the active site of <i>MtPknG</i> .	250
Figure 3.81	Predicted binding free energy (docking score) and detailed molecular interactions of orientin (74) within the active site of <i>MtPknG</i> .	251
Figure 3.82	Predicted binding free energy (docking score) and detailed molecular interactions of kaempferol 7-O-β-D-glucoside (populnin) (60) within the active site of <i>MtPknG</i> .	252
Figure 3.83	Graphical summary of the present study	260

List of Tables

Chapter One

Table 1.1	Current anti-TB drug regimen recommended by the WHO	4
Table 1.2	List of selected medicinal plants used as remedies for TB and TB-related symptoms	7
Table 1.3	Example of phytochemicals with anti-TB activity	8
Table 1.4	Coumarins previously isolated from <i>F. excelsior</i>	14
Table 1.5	Secoiridoids previously isolated from <i>F. excelsior</i>	15
Table 1.6	Phenylethanoids previously isolated from <i>F. excelsior</i>	19
Table 1.7	Number and types of phytochemicals previously isolated from <i>P. sidoides</i> / <i>P. reniforme</i> roots and aerial parts	30
Table 1.8	Examples of Human Toll-Like Receptors (TLRs) and their ligands	37

Chapter Two

Table 2.1	Plant material used for the phytochemical investigation	55
Table 2.2	Gradient elution used in FC	58

Chapter Three

Table 3.1	^1H (600 MHz) and ^{13}C (150 MHz) NMR chemical shift values* for 370RQ7a (recorded in CDCl_3) in comparison with literature data.	88
Table 3.2	^1H (600 MHz) and ^{13}C (150 MHz) NMR chemical shift values* for 370RQ7b (recorded in CDCl_3) in comparison with literature data.	90
Table 3.3	^1H (500 MHz) and ^{13}C (125 MHz) NMR chemical shift values* for 370RQ2 (recorded in CDCl_3)	96
Table 3.4	^1H (500 MHz) and ^{13}C (125 MHz) NMR chemical shift values* for 370RQ25 (recorded in CDCl_3) in comparison with literature data	103
Table 3.5	Molecular ions adduct peaks observed in the mass spectrum of 390RQ5	108

Table 3.6	^1H (500MHz) and ^{13}C (125 MHz) NMR chemical shift values* for 390RQ5 (recorded in CDCl_3) in comparison with literature data	111
Table 3.7	^1H (500MHz) and ^{13}C (125 MHz) NMR chemical shift values* for 390RQ3/ 370RQ 24 recorded in CDCl_3	119
Table 3.8	Molecular ions adduct peaks observed in the mass spectra of 390RQ3 & 370RQ24	118
Table 3.9	^1H (500 MHz) and ^{13}C (125 MHz) NMR chemical shift values* for 390RQ10 recorded in CDCl_3 in comparison to literature data	129
Table 3.10	^1H (400 MHz) and ^{13}C (100 MHz) NMR chemical shift values* for 390RQ27 recorded in CDCl_3 in comparison with literature data	136
Table 3.11	^1H (500 MHz) and ^{13}C (125 MHz) NMR chemical shift values* for 390RQ28 recorded in CDCl_3 in comparison to literature	142
Table 3.12	^1H (500 MHz) and ^{13}C (125 MHz) NMR chemical shift values* for 370RQ1 (a) (recorded in CDCl_3) in comparison with literature data.	149
Table 3.13	^1H (500 MHz) and ^{13}C NMR (125 MHz) chemical shift values* for 370RQ20 (recorded in CDCl_3) in comparison with literature data	155
Table 3.14	Molecular ion peaks of ammonium adduct observed in the mass spectrum of 370RQ19	160
Table 3.15	Methyl fatty acid esters molecular ion peaks observed in the mass spectrum of 370RQ19	161
Table 3.16	^1H (500 MHz) and ^{13}C (125 MHz) NMR chemical shift values* for 370RQ19 (recorded in CDCl_3) in comparison with literature data.	163
Table 3.17	Molecular ions in the GC-EI-MS spectra of 370RQ22 and 390RQ1	167
Table 3.18	Table 3.18 ^1H (600 MHz) NMR chemical shift values* and proton assignments of 370RQ3 (recorded in CDCl_3)	172

Table 3.19	Predicted binding free energies (docking scores (ΔG in kcal/mol) and ligand efficiencies* (LEs) of <i>P. reniforme</i> and <i>P. sidoides</i> root constituents and re-docked control inhibitor AX20017** towards <i>MtPknG</i> .	236
Table 3.20	Predicted binding free energies (docking scores (ΔG in kcal/mol) and ligand efficiencies* (LEs) of <i>P. reniforme</i> and <i>P. sidoides</i> aerial parts constituents and re-docked control inhibitor AX20017** towards <i>MtPknG</i>	240
Table 3.21	Predicted binding free energies ΔG in kcal/mol and ligand efficiencies* (LE) of selected phytochemicals isolated from <i>F. excelsior</i> and <i>S. arabica</i> and of the re-docked control inhibitor AX20017** towards <i>MtPknG</i> .	243
Table 3.22	List of best ligands obtained in this study, ranked according to their predicted free binding energy (docking score) and SILE towards <i>MtPknG</i>	244
Table 3.23	Detailed molecular interactions between the top ranked ligands of <i>Pelargonium</i> spp. and <i>MtPknG</i>	245
Table 3.24	Summary of biology results (IC_{50} values & observed effect on cytokines production using LPS stimulated THP-1 cells)	261

List of Protocols

Protocol 1	Large-scale extraction of a- <i>Fraxinus excelsior</i> leaves (370), b- <i>Stachys arabica</i> aerial leaves (390)	59
Protocol 2	Fractionation and isolation of phytochemicals from the <i>n</i> -hexane extract of <i>Fraxinus excelsior</i> leaves (370H)	60
Protocol 3	Fractionation and isolation of phytochemicals from the ethyl acetate extract of <i>Fraxinus excelsior</i> leaves (370E)	61
Protocol 4	Fractionation and isolation of phytochemicals from the <i>n</i> -hexane extract of <i>Stachys arabica</i> aerial parts (390H)	62
Protocol 5	Fractionation and isolation of phytochemicals from the ethyl acetate extract of <i>Stachys arabica</i> aerial parts (390E)	63

Abstract

Plants have a long history of use in traditional medicine and several plant species are natural cures for tuberculosis (TB) or TB-related symptoms. Such natural sources can be a worthy starting point in the search for new drugs since they are rich in diverse phytochemicals which may possess antimicrobial and/or immunomodulatory activity. TB is still a growing public health concern worldwide, especially with the emerging challenge of drug resistance to current anti-TB drugs. There is an urgent need for effective and safe therapeutic interventions to tackle TB globally. One approach to achieve this goal is to combine host directed therapies (HDT) with current anti-TB therapies. Pro-inflammatory cytokines (TNF- α and IL-12) are essential for an effective immune response against bacterial infections and play a crucial role in controlling TB. Another promising approach is to identify compounds that could target key virulence enzymes of Mtb such as protein kinase G (*MtPKnG*).

This study describes the phytochemical investigation of two medicinal plants (*Fraxinus excelsior* and *Stachys arabica*) selected based on their traditional and/or chemo-taxonomical use in the treatment for TB or TB-related symptoms. The work also focused on the evaluation of these plant extracts and selected isolated phytochemicals for their potential immunomodulatory effect in LPS-stimulated THP-1 cells.

A total of 28 phytochemicals were isolated and characterised from both plants. The phytochemical investigation of the *n*-hexane and ethyl acetate extracts of *F. excelsior* leaves revealed the presence of 20 phytochemicals. The isolated phytochemicals included two pentacyclic triterpenoids (oleanolic acid and ursolic acid), squalene, one flavonoid (pinocembrin), five phenylethanoid esters (4-hydroxyphenethyl dotriacontanoate, 4-hydroxyphenethyl triacontanoate, 4-hydroxyphenethyl octacosanoate, 4-hydroxyphenethyl hexacosanoate, and 4-hydroxyphenethyl tetracosanoate), steryl fatty acid esters (β -sitosterol oleate), phytyl fatty acid esters (phytyl palmitate, phytyl oleate, and phytyl linolenate), and a mixture of acyclic alkanes (heptacosane, octacosane, nonacosane, triacontane, hentriacontane, dotriacontane and tritriacontane). Although ursolic acid, phytyl linolenate, nonacosane, and hentriacontane have already been reported in *F. excelsior* leaves, all other phytochemicals are reported here for the first time.

A total of 17 phytochemicals were isolated from the *n*-hexane and ethyl acetate extracts of *S. arabica* leaves. This included pheophytins (pheophytin a, 13² (*R,S*)-hydroxy pheophytin a, and pheophytin b), a mixture of phytosterols (stigmasterol, β -sitosterol and campesterol), a mixture of steryl fatty acid esters (β -sitosterol oleate & campesterol oleate), a mixture of phytyl fatty acid esters (phytyl palmitate, phytyl oleate), and a mixture of acyclic alkanes (heptacosane, octacosane, nonacosane, triacontane, hentriacontane and tritriacontane). Although all are known compounds, they are reported from *S. arabica* for the first time.

When screened for potential Immunomodulatory effect in LPS-stimulated THP-1 cells, all the plant extracts and selected purified phytochemicals (oleanolic acid, ursolic acid, pinocembrin, and pheophytins) were able to reduce the production of the pro-inflammatory cytokines (TNF- α and IL-12). The mixture of phenylethanoid esters did not appear to influence the production of either of the cytokines studied. Our results indicate that the two plant extracts and their selected phytochemicals (oleanolic acid, ursolic acid, pinocembrin, and pheophytins) exhibited anti-inflammatory effect that could validate to a certain extent their potential use for complications associated with inflammation including TB as adjunct host therapy.

Molecular docking using AutoDock Vina was conducted to predict the interactions between *MtPknG* and eighty-four phytochemicals from *Pelargonium sidoides* and *Pelargonium reniforme* as well as six selected phytochemicals identified through the phytochemical work. The flavonoids present in the aerial parts of *Pelargonium* plants displayed the best predicted binding energy towards *MtPknG*. The highest binding affinity towards *MtPknG* was recorded for isoorientin 2''-*O*-gallate (**79**), isovitexin 2''-*O*-gallate (**77**), nicotiflorin (**61**), orientin (**74**) and populnin (**60**) (-13.2, -12.6, -12.2, -11.8, and -11.6 kcal/mol, respectively) accompanied with SILE values (4.27, 4.11, 3.98, 4.17 and 4.10, respectively) that were superior to the control inhibitor AX20017 (-7.9 kcal/mol and SILE value of 3.32, respectively).

Medicinal plants and their phytochemicals, owing to their abundance and diversity, could provide valuable alternatives for design of new generation of anti-TB drugs by serving as adjunct host-directed therapy and/or pathogen-directed therapy.

CHAPTER ONE

INTRODUCTION

1. Introduction

1.1 Tuberculosis: Disease, treatment, and challenges

Tuberculosis (TB), also known as phthisis or consumption, is a disease that has plagued mankind for many millennia. Early evidence of this disease has been detected in Egyptian mummies (Daniel, 2006). In the Middle Ages, scrofula was described as a new clinical form of TB and it was known in England and France as the "King's evil" (Barberis *et al.*, 2017). During the 17th and 18th centuries, TB was called the "White Plague" and it contributed to 20 % of all human death (Bloom and Murray, 1992). In the early 1980s, TB cases were relatively low, but this changed with the arrival of the HIV epidemic in the early 1990s (Phillips, 2013). This resurgence in TB cases worldwide led the World Health Organization to declare TB a global emergency in 1993.

TB is a contagious airborne disease caused by a slow-growing bacterium called *Mycobacterium tuberculosis* (Mtb) which was first discovered by Robert Koch, a German physician, in 1882. TB is transmitted through the inhalation of droplets coming from a person with active TB disease (via coughing or sneezing) (Raja, 2004; Dheda *et al.*, 2016; World Health Organization, 2018a; National Health Service, 2018). This usually occurs after prolonged contact with a TB-infected person. In a healthy person, the immune system is usually strong enough to clear Mtb and there are no symptoms. However, sometimes the immune system cannot eliminate this pathogen completely and Mtb can remain in a dormant state (latent TB). People with latent TB are not infectious to others. However, latent TB might develop into an active TB disease if the immune system becomes weakened by human immunodeficiency virus (HIV), diabetes, use of immunosuppressive drugs, or other risk factors include poverty, malnutrition, alcohol abuse, poor ventilation and overcrowding (Narasimhan *et al.*, 2013; Dheda *et al.*, 2016; World Health Organization, 2018a). Even though the lungs are the initial infection site (pulmonary TB), the disease can spread throughout the body (extra-pulmonary TB). The typical symptoms of active TB disease include a persistent cough that lasts more than three weeks and usually brings up phlegm (which may be bloody), weight loss, night sweats, fever, tiredness and loss of appetite (National Health Service, 2018; World Health Organization, 2018b).

In 2019, the World Health Organization (WHO) stated that TB is the leading infectious disease killer and one of the top ten causes of death worldwide and the leading cause of death (ranking above HIV/AIDS since 2007) from a single infectious agent. In 2019, there were an estimated 10.0 million new TB cases worldwide, with people living with HIV accounting for 10% of this total and most of the estimated number of cases occurring in South-East Asia (44%) and Africa (25%). Notably in India, Indonesia, China, the Philippines, Pakistan, Nigeria, and South Africa (Figure 1.1). In 2019, 1.4 million people died of TB (World Health Organization, 2020a).

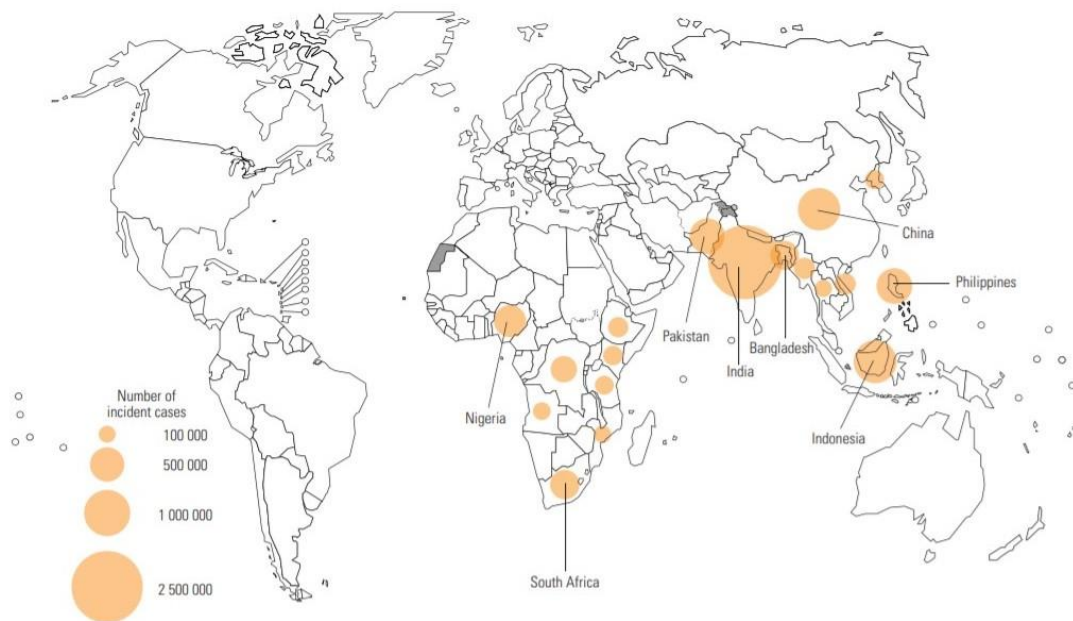


Figure 1.1 Estimated TB incidence in 2019 (World Health Organization, 2020a).

TB has become a global threat to public health due to the rapid spread of bacterial strains resistant to current drugs. The treatment of TB is a long process that involves complex drug regimens. The standard therapy for Drug susceptible- tuberculosis (DS-TB) usually involves taking a four-drug regimen for six-months (first-line treatment). The initial phase starts with isoniazid, rifampicin, pyrazinamide, and ethambutol for the first two months followed by a continuation phase of isoniazid and rifampicin for the last four months. The purpose of this combined treatment is to avoid the emergence of drug-resistant strains. However, this treatment uses drugs with adverse effects and interactions, and often leads to poor patient compliance which in turn

results in the emergence of resistant strains of bacteria (Tiberi *et al.*, 2018; Chan and Iseman, 2002; Wong *et al.*, 2013; Dheda *et al.*, 2016).

Multidrug-resistant TB (MDR-TB) is resistant to at least isoniazid and rifampicin, the two most important first-line anti-TB drugs. The current WHO guidelines recommend that patients with MDR-TB should receive drugs that are categorized into groups A, B and C as listed in Table 1.1. If the minimum of effective TB medicines cannot be composed as above, an agent from group D may be added. Extensively drug resistant (XDR-TB) is resistant to isoniazid and rifampicin as well as any fluoroquinolones and any of the second-line anti-TB injectable drugs (amikacin, kanamycin or capreomycin) (World Health Organization, 2020b). A treatment regimen for 6–9 months, composed of bedaquiline, pretomanid and linezolid (BPaL) is recommended for the treatment of adults with pulmonary XDR-TB or for nonresponsive MDR-TB (Shirley, 2020; World Health Organization, 2020b). The treatment of MDR-TB and XDR-TB can take up to 18-24 months and requires more toxic and expensive drugs (Maitre *et al.*, 2017; Singh and Mizrahi, 2017).

The current COVID-19 pandemic has a negative impact on health services worldwide, which led to an increase in the global number of TB deaths by around 0.2–0.4 million in 2020. There is no doubt that the COVID-19 pandemic has highlighted the importance of infection prevention and control in health care settings worldwide (World Health Organization, 2020a) .

The major side effects of current anti-TB drugs are gastrointestinal disturbance, hepatotoxicity, peripheral neuropathy, nephrotoxicity, psychiatric disorder, and arthralgia which accounted for patient's withdrawal and the increase of MDR TB cases (Ramappa and Aithal, 2013; Yang *et al.*, 2017; Molla *et al.*, 2021; Lange *et al.*, 2014) . New anti-TB drugs are also needed to shorten the treatment duration of drug-sensitive-TB and achieve better patient compliance , thereby overall preventing the development of further drug resistance (Liu *et al.*, 2012b; Janssen *et al.*, 2012).

Table 1.1 Current anti-TB drug regimen recommended by the WHO

Drug classes	Anti-TB Drugs (year of introduction)	Mechanisms of action
First-line TB medicines DS-TB	Rifampicin (1972)	Inhibition of RNA synthesis
	Isoniazid (1952)	Inhibition of cell wall mycolic acid synthesis
	Ethambutol (1966)	Inhibition of cell wall arabinogalactan synthesis
	Pyrazinamide (1955)	Disrupt membrane energy
Second-line MDR-TB		
Group A: Include all three medicines	Levofloxacin (1992) Moxifloxacin (1995)	Inhibition of DNA gyrase and topoisomerase IV
	Bedaquiline (2012)	Inhibition of ATP synthase.
	Linezolid (2003)	Inhibition of protein synthesis
	Group B: Add one or both	Clofazimine (1986)
Cycloserine (1964)/ terizidone (1978)		Inhibition of peptidoglycan synthesis
Group C: Add to complete the regimen, and when medicines from Group A & B can not be used	Ethambutol	
	Delamanid (2013)	Inhibition of mycolic acid synthesis
	Pyrazinamide	
	Imipenem-cilastatin (1985)/Meropenem(1995)	
	Amikacin (1972) Streptomycin (1944)	Inhibition of protein synthesis
	Ethionamide/ prothionamide (1965)	Inhibition of cell wall mycolic acid synthesis
	p-aminosalicylic acid (1948)	Inhibition of folic acid synthesis
Group D: Other medicines (not part of the core MDR-TB regimen)	High dose of Isoniazid	
	Amoxicillin-clavulanic acid	Inhibition of cell wall synthesis
	Gatifloxacin (1999)	Inhibition of DNA gyrase
	Pretomanid (2020)	Inhibition of cell wall mycolic acid synthesis

Adapted from (World Health Organization, 2020b; Bahuguna and Rawat, 2020; Olaru *et al.*, 2015; Prasad *et al.*, 2019; Dookie *et al.*, 2018; Palomino and Martin, 2014)

1.2 Medicinal plants and natural products as a source of new drugs

1.2.1 General overview

Plants continue to be used in medicinal practice in many countries. This is the case for example in traditional Ayurvedic (Indian), Chinese, Arabic, and African medicine. Medicinal plants are used to treat a range of symptoms. They are also a source of new chemical entities with therapeutic potential (Shakya, 2016; Mandal *et al.*, 2015). In most cases, knowledge on the use of medicinal plants is transmitted orally from one generation to another with little written evidence (Gupta *et al.*, 2017; Ojha *et al.*, 2020).

Plants synthesise phytochemicals as a result of their adaptation to the environment, to assist and improve their survival (e.g., as a defence mechanism against herbivores). They are neither essential for the reproduction nor the development of plants, and often have some biological activity that can be exploited to design new drug leads (Dewick, 2009). The most famous example of drugs from natural products (NPs) is the alkaloid morphine isolated from *Papaver somniferum* (opium poppy) (Dias *et al.*, 2012). Another example includes reserpine, an antihypertensive agent isolated from the root of *Rauwolfia serpentina* (Indian snakeroot). Artemisinin is a sesquiterpene lactone from *Artemisia annua* (sweet wormwood) with antimalarial activity. Other examples of plant-derived drugs include the anticancer agents vinblastine and vincristine from *Catharanthus roseus*, camptothecin and its derivatives from *Camptotheca acuminata*, and paclitaxel from the Pacific yew tree (*Taxus brevifolia*) (Mandal *et al.*, 2015; Shakya, 2016; Balunas and Kinghorn, 2005; Sun *et al.*, 2019).

Natural products play an important role in the discovery of new drug leads, and provide some inspiration for the design and synthesis of new structural mimics (Newman and Cragg, 2016).

1.2.2 Traditional antitubercular plant remedies and natural products

Plant-based medicines have been used traditionally in different parts of the world to treat TB and TB-related symptoms. Infusions, macerations, and other forms of

traditional remedies prepared from different plant parts (flowers, leaves, roots) are still used by native people/local healers in many countries. Several plant species have been evaluated phytochemically and biologically, and have displayed interesting antimycobacterial activity. (Sharifi-Rad *et al.*, 2017; Newton *et al.*, 2000; Newton *et al.*, 2002; Gautam *et al.*, 2007; Chinsembu, 2016). Some examples of medicinal plants used for this purpose are presented in Table 1.2.

Due to their structural diversity and complexity, plant NPs are considered an attractive and relatively untapped source of inspiration for new antitubercular agents. Different classes of phytochemicals (e.g., alkaloids, flavonoids, terpenes, phenolics, steroids, fatty acids) have anti-TB activity (Okunade *et al.*, 2004; García *et al.*, 2012; Veluthoor *et al.*, 2012; Dong *et al.*, 2017). Ursolic acid and cucurbitacin E 2-O- β -glucopyranoside, isolated from *Citrullus colocynthis* fruits (a traditional Indian TB remedy) inhibited the growth of Mtb H37Rv (MIC values of 50 and 25 μ g/mL, respectively) (Mehta *et al.*, 2013). Plumericin and isoplumericin, two iridoids from the Indian medicinal plant *Plumeria bicolor*, were also active against Mtb H37Rv (MIC values of 2.1 and 2.4 μ g/mL, respectively). Both compounds had excellent activity against four MDR strains of Mtb (MIC values of 1.5 and 3.8 μ g/mL) and showed better MIC values when compared to the standard drugs rifampicin and isoniazid (Kumar *et al.*, 2013).

The flavonoid, 3,4-methylenedioxy-10-methoxy-7-oxo[2]benzopyrano[4,3b] benzopyran, isolated from the roots of *Derris indica*, exhibited activity against Mtb H37Ra (MIC value of 6.25 mg/mL). Seven other flavonoids from this plant also had anti-Mtb H37Ra activity (MICs of 12.5 - 50 mg/mL) (Koysoomboon *et al.*, 2006). In a study on the inhibitory activity of 100 plant-derived NPs on the Mtb proteasome, twelve (including 10 flavonoids) showed >65% inhibition, suggesting that flavonoids represent a basis for the rational design of novel anti-TB drugs (Zheng *et al.*, 2014). Other examples of plant phytochemicals with anti-TB activity are listed in Table 1.3.

Considering all of the above, medicinal plants and their isolated phytochemicals provide an interesting approach with regard to TB treatment owing to their ability to inhibit the growth of Mtb (including drug-resistant strains), modulate the host's immune system, exhibit synergistic activity with anti-TB drugs, alleviate TB symptoms, and/or minimise the side effects caused by anti-TB drugs (Gupta *et al.*, 2017; Mangwani *et al.*, 2020; Sieniawska *et al.*, 2020).

Table 1.2 List of selected medicinal plants used as remedies for TB and TB-related symptoms

Botanical name	Part Used	Common name	Reference(s)
<i>Artemisia absinthium</i>	Herb/powder	Wormwood	(Duke, 2008; Grange and Davey, 1990; Gautam <i>et al.</i> , 2007; Sharifi-Rad <i>et al.</i> , 2017; Kayani <i>et al.</i> , 2014)
<i>Achillea millefolium</i>	Herb/powder	Yarrow	(Duke, 2008; Gautam <i>et al.</i> , 2007; Kayani <i>et al.</i> , 2014)
<i>Azadiracta indica</i>	leaf	Neem	(Newton <i>et al.</i> , 2000; Gautam <i>et al.</i> , 2007; Sharifi-Rad <i>et al.</i> , 2017)
<i>Centella asiatica</i>	Herb/Powder	Gotu Kola	(Duke, 2008; Sharifi-Rad <i>et al.</i> , 2017; Gautam <i>et al.</i> , 2007; Newton <i>et al.</i> , 2002; Newton <i>et al.</i> , 2000)
<i>Fraxinus excelsior</i>	Leaves	Ash	(Gautam <i>et al.</i> , 2007; Lucas <i>et al.</i> , 1951; Orwa, 2009)
<i>Humulus lupulus</i>	flowers	Hops	(Duke, 2008; Gautam <i>et al.</i> , 2007; Newton <i>et al.</i> , 2000; Grange and Davey, 1990)
<i>Plantago lanceolata</i>	Leave, whole	Plantain	(Duke, 2008; Gautam <i>et al.</i> , 2007)
<i>Tinospora cordifolia</i>	leaves	Guduchi	(Duke, 2008; Gautam <i>et al.</i> , 2007; Sharifi-Rad <i>et al.</i> , 2017)
<i>Urtica dioica</i>	Root powder	Nettle	(Duke, 2008; Mccutcheon <i>et al.</i> , 1997)
<i>Withania somnifera</i>	Root Powder	Ashwagandha	(Duke, 2008; Gautam <i>et al.</i> , 2007; Sharifi-Rad <i>et al.</i> , 2017; Newton <i>et al.</i> , 2002)
<i>Stachys sieboldii</i>	Tubers	Chinese artichoke	(Feng <i>et al.</i> , 2015)

Table 1.3 Example of phytochemicals with anti-TB activity

Plant	Part used	NPs class	Reference
<i>Zanthoxylum capense</i>	Root	Alkaloids	(Luo <i>et al.</i> , 2013)
<i>Goniothalamus laoticus</i>	Flowers	Alkaloids	(Lekphrom <i>et al.</i> , 2009)
<i>Galenia africana</i>	leaves	Flavonoids	(Mativandlela <i>et al.</i> , 2009)
<i>Pelargonium reniforme/ sidoides</i>	Root	Flavonoids	(Kim <i>et al.</i> , 2009)
<i>Aristolochia taliscana</i>	Root	Neolignane	(León-Díaz <i>et al.</i> , 2010)
<i>Citrullus colocynthis</i>	Fruit	Ursolic acid, cucurbitacin derivatives	(Mehta <i>et al.</i> , 2013)
<i>Terminalia avicennioides</i>	Root bark	Triterpenoids	(Mann <i>et al.</i> , 2012)
<i>Borrchia frutescens</i>	Whole plant	Triterpenoids	(Cantrell <i>et al.</i> , 1996)
<i>Ferula hermonis</i>	Root	Sesquiterpenoids	(Liu <i>et al.</i> , 2012b; Zeid <i>et al.</i> , 2012)
<i>Juniperus communis</i>	Root and aerial parts	Sesquiterpenoids, diterpenoids	(Gordien <i>et al.</i> , 2009)
<i>Salvia miltiorrhiza</i>	Root	Norditerpenoids	(Luo, 1982 in- Liu <i>et al.</i> , 2012b)
<i>Euclea natalensis</i>	Root	Naphthoquinones	(Van Der Kooy <i>et al.</i> , 2006)
<i>Diospyros anisandra</i>	Stem bark	Naphthoquinones	(Uc-Cachón <i>et al.</i> , 2014)

1.2.3 Selection of plants for phytochemical and biological evaluation

Many plant species have been largely unexplored phytochemically. Although many species are used as medicinal plants, several have yet to be investigated for any type of pharmacological activity. The discovery of new drugs from plants rely on ethno-guided, chemotaxonomical, random, and computational approaches (Atanasov *et al.*, 2015).

1.2.3.1 Ethno-guided or classical knowledge-based approach

This is an interdisciplinary approach based on botany, chemistry, and pharmacology where the plant species under study are selected according to the available indigenous knowledge that has been recorded in specific traditional health systems. The basis of this approach is to evaluate traditionally-used plant remedies and their bioactivity. The plants being investigated are collected and identified by plant taxonomists, and interviews with local traditional healers are conducted by a team of experts (Heinrich and Gibbons, 2001; Heinrich, 2010; Fabricant and Farnsworth, 2001; Gyllenhaal *et al.*, 2012).

It is worth mentioning that most of the plants which have reported in *vitro* antitubercular activity are traditional remedies for cough, fever, chest complaints, and respiratory disorders. This indicates that the investigation of traditionally used plant remedies can be a valuable approach in the search for new anti-TB drug leads (Gupta *et al.*, 2017).

1.2.3.2 Chemotaxonomical approach

This approach, also called chemosystematic or phylogenetic, uses chemotaxonomic knowledge and molecular phylogenetic information to select a plant based on the biological activity and/or phytochemical knowledge of related species within its genus or family (Atanasov *et al.*, 2015). For example, chemosystematic studies confirmed the presence of the alkaloid galantamine, and acetylcholinesterase inhibitory activity in several species of the genus *Galanthus*, following the isolation of galantamine from *Galanthus nivalis* (Amaryllidaceae) (Larsen *et al.*, 2010). Another example is the isolation of paclitaxel-related compounds in needles of the European yew (*Taxus baccata*), following the initial isolation of paclitaxel from the bark of the Pacific yew tree (*Taxus brevifolia*) (Miele *et al.*, 2012).

1.2.3.3 Random approach

The random approach has been recognised as an approach which does not rely on any specific criteria, but rather on the random selection of plant species for investigation, based on their availability (Atanasov *et al.*, 2015; Spjut, 1985).

1.2.3.4 Computational approach

Computational methods have become an important component of modern drug discovery research. One of the most important techniques in Computer-Aided-Drug-Discovery (CADD) approaches is virtual screening (VS) which can be used to predict the way molecules will interact with a specific target. Two generally accepted approaches can be taken in virtual screening. One is the ligand-based virtual screening (LBVS), the other is the structure-based virtual screening (SBVS). The difference between the two approaches is that the structural information on the target, which is usually obtained from X-ray crystallography or NMR data, is a basic requirement for SBVS. In ligand-based (LBVS), there is no structural information about the target. Both QSAR (Quantitative Structure-Activity Relationships) and pharmacophore pattern are examples of LBVS (Tringali, 2012). Many current drug discovery studies use these approaches to accelerate lead identification and optimisation (Kumar and Jha, 2017; Sliwoski *et al.*, 2014).

Structure-based virtual screening (SBVS), or molecular docking, can be used to virtually screen potential drug candidates before starting any laboratory experiments. Molecular docking is an efficient screening method that can predict the preferred orientation of a ligand (drug candidate) inside a macromolecule (protein) binding site. However, neither the ligand nor the protein are rigid structures (Tringali, 2012). Ideally, the geometrical structure of a target protein as well as of the potential ligands are needed to perform this type of docking. 3D structural data of large biological molecules such as proteins can be obtained from the Protein Data Bank (<http://www.rcsb.org>) (Khamis *et al.*, 2015; Tringali, 2012)

Computer software available to perform SBVS include AutoDock, Flex-X, GOLD, Glide, AutoDock Vina (also known as Vina). They are used to determine the position of a ligand within the binding pocket of a target protein and to calculate binding affinities (docking scores) (Waszkowycz *et al.*, 2011). Vina is one of the most widely used docking packages in molecular docking (Chen, 2015). The Vina software consists of two major elements: a search algorithm, and a scoring function. The

search algorithm (or optimisation algorithm) is responsible for finding the best conformations (position and orientation) of a given ligand relative to a given protein. The scoring function shows how strongly a ligand will interact with a given protein. All Vina scores are given as the predicted binding free energies (negative values in kcal/mol) (Trott and Olson, 2010).

A computational approach can be employed to identify plants containing the most promising phytochemicals (ligands) for further biological investigation (Atanasov *et al.*, 2015). An investigation of the anti-cancer activity of NPs from Korean *Panax ginseng* using pharmacophore-based virtual screening and molecular docking studies on EGFR (epidermal growth factor receptor) tyrosine kinase domain identified fourteen NPs that could be used to design new EGFR tyrosine kinase inhibitors (Sathishkumar *et al.*, 2013).

Ligand efficiency indices (LEIs) are generally accepted as valuable parameters to analyse molecular docking results in drug discovery research (Cavalluzzi *et al.*, 2017). The concept of a ligand efficiency index was firstly described as the free energy of binding (ΔG) per number of heavy or non-hydrogen atom (NHA) bound to a target ($LE = \Delta G/NHA$) and served as a useful guide to optimize fragment and lead selection (Hopkins *et al.*, 2004). Other LEIs were later introduced. The analysis of a large number of protein-ligand complexes showed that ligand efficiency (LE) depends on ligand size, with smaller ligands showing greater efficiencies on average than larger ligands (Reynolds *et al.*, 2008; Hopkins *et al.*, 2014). This led to an assumption that LE cannot be applied for all molecular size ranges without some type of normalization for size. An alternative is to adopt a size-independent metric such as a described by Nissink (2009) (size-independent ligand efficiency SILE = $(\Delta G) / NHA^{(0.3)}$). The latter is a simple metric to evaluate how efficiently a ligand binds relative to other ligands across a wide range of sizes. This correction is useful in experimental drug optimisation, and in applications like protein-ligand docking, where calculated free energy of binding and scores tend to show a strong dependency on compound size (Nissink, 2009; Hopkins *et al.*, 2014; Cavalluzzi *et al.*, 2017). The use of SILE has been reported in previous studies (Ferenczy and Keserű, 2010; Ferenczy and Keserű, 2013; Leeson *et al.*, 2021).

Taking everything into account, combining traditionally used plant remedies with virtual screening is strongly suggested and could lead to new drug candidates.

1.3 Medicinal plants selected for this study

1.3.1 *Fraxinus excelsior* L. (Oleaceae)

1.3.1.1 Botanical description

Fraxinus excelsior, known as European or common ash, is a medium-sized deciduous broadleaved tree native to the temperate zones of Europe and south-western Asia. European ash grows up to 40 m high. The leaves appear relatively late in spring from May to October. They are compound, with 7-13 leaflets, odd pinnate, serrated, and stalkless. The individual leaflets measure 5-12 cm long. The flowers are purple and bloom before the leaves from April to May. The seeds ripen individually in oval-shaped samaras, flattened, 2.5-5 cm long, that by the end of summer from September to January hang in bunches from the branches (Plantfile Online Database, 2018; Royal Botanic Gardens, 2019; Humphries, 1981).

After *Quercus* species, *Fraxinus excelsior* is the second most abundant tree species in small woodland patches in the UK (Maskell *et al.*, 2013).



Figure 1.2 Leaves of *Fraxinus excelsior* L. (Ughetto, 2014)

1.3.1.2 Traditional uses

In European traditional medicine (ETM), common ash (*F. excelsior*) leaves are used to treat a wide range of illnesses including arthritis, gout, rheumatism, fever, hypercholesterolemia, obesity. They are also employed as a diuretic and anti-

catarrhal remedy (Neves *et al.*, 2009; Menković *et al.*, 2011; Cavero and Calvo, 2015; Vitalini *et al.*, 2015; Pranskuniene *et al.*, 2018; Kostova and lossifova, 2007). Common ash is also reported to be used to treat malaria and tuberculosis (Orwa, 2009). It is used externally for wounds (Gilca *et al.*, 2018). The European Medicines Agency recommends ash leaves for the treatment of minor articular pain, and urinary complaints (European Medicines Agency, 2012; Kiss *et al.*, 2020).

Fraxinus spp. are used as for their expectorant and sedative effects in cough (Bouguellid *et al.*, 2020). The leaves of *Fraxinus xanthoxyloides* (Afghan ash) are used to treat jaundice, malaria, and pneumonia (Younis *et al.*, 2016b).

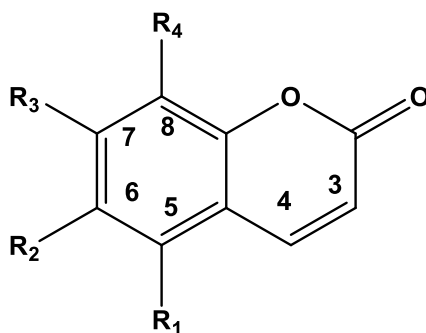
1.3.1.3 Previous phytochemical work

Ash bark, seeds and leaves contain coumarins, secoiridoids and phenylethanoids. Secoiridoids, present as simple secoiridoids, glucosides, and esters of hydroxyphenyl ethyl alcohol, are the major class of NPs in *Fraxinus* and the Oleaceae family (Table 1.5). The genus *Fraxinus* is distinguished from other genera in the Oleaceae family by the presence of coumarins which have been the main focus of the phytochemical investigations to date. Flavonoids, lignans, and simple phenolic derivatives are also common in this species (Kostova and lossifova, 2007).

Coumarins

Various hydroxycoumarins have been reported from different parts of *F. excelsior*. Several 6,7 dihydroxy-, 6,7,8 trihydroxy-, and 5,6,7 trihydroxycoumarins have been isolated from *F. excelsior* bark and leaves (Jensen and Nielsen, 1976; Kostova and lossifova, 2007; Poukens-Renwart *et al.*, 1992). The coumarins present in *F. excelsior* are listed in Table 1.4.

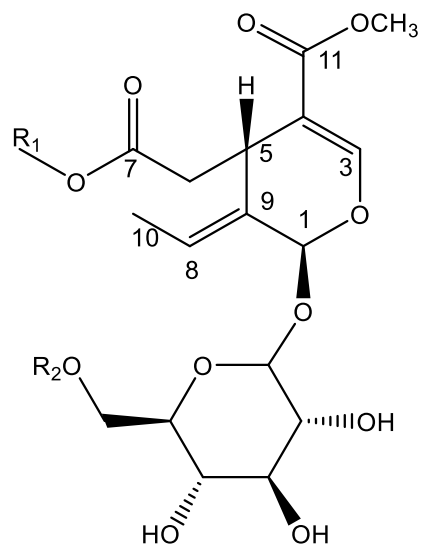
Table 1.4 Coumarins previously isolated from *F. excelsior*



Compound	R ₁	R ₂	R ₃	R ₄	Plant parts*
Esculetin	H	OH	OH	H	B, L
Esculin	H	OGlc	OH	H	B, L
Cichoriin	H	OH	OGlc	H	
Scopoletin	H	OMe	OH	H	B
Isoscopoletin	H	OH	OMe	H	B
7-Methylesculin	H	OGlc	OMe	H	B, L
Fraxetin	H	OMe	OH	OH	B, L
Fraxin	H	OMe	OH	OGlc	B, L
Fraxidin	H	OMe	OMe	OH	B
Fraxidin-O-β-D-glucoside	H	OMe	OMe	OGlc	B
Isofraxidin	H	OMe	OH	OMe	B
Calyncantoside	H	OMe	OGlc	OMe	B
Fraxinol	OMe	OH	OMe	H	B

* Studied plant parts; (B): bark, (L): leaves.

Table 1.5 Secoiridoids previously isolated from *F. excelsior*



Compound	R ₁	R ₂	Plant part*	Reference(s)
Simple secoiridoids				
Oleoside 11-methyl ester	H	H	S	(Bai <i>et al.</i> , 2010)
Oleoside-7,11-dimethylester	CH ₃	H	B, L, S	(Iossifova <i>et al.</i> , 1997; Bai <i>et al.</i> , 2010)
7-β-D-glucopyranosyl-11-methyloleoside	(1)- β-D-Glc	H	L	(Damtoft <i>et al.</i> , 1992)
Excelside A	CH ₃	OGlc	S	(Bai <i>et al.</i> , 2010)

Table 1.5 (Cont.) Secoiridoids previously isolated from *F. excelsior*

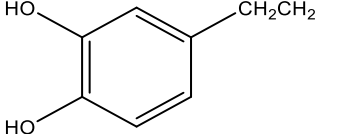
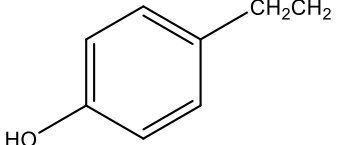
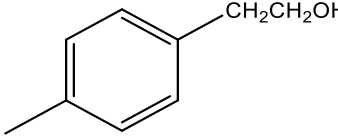
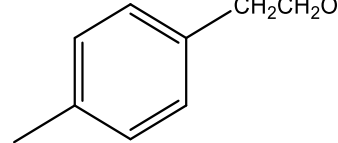
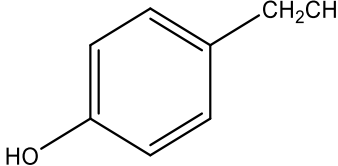
Conjugated secoiridoids: Aromatic-derivatives				
Compound	R₁	R₂	Plant part*	Reference(s)
Oleuropein		H	B, L	(Bai <i>et al.</i> , 2010; Egan <i>et al.</i> , 2004)
Ligstroside		H	B, S, L	(Egan <i>et al.</i> , 2004; Bai <i>et al.</i> , 2010; Damtoft <i>et al.</i> , 1992)
Excelsioside/ formoside		H	L	(Damtoft <i>et al.</i> , 1992; Egan <i>et al.</i> , 2004)
1'''-O-β-D-glucosylformoside		H	S	(Bai <i>et al.</i> , 2010)
Excelside B		OGlc	S	(Bai <i>et al.</i> , 2010)

Table 1.5 (Cont.) Secoiridoids previously isolated from *F. excelsior*

Conjugated secoiridoids: Sugar-derivatives			
Compound	Structure	Plant part*	Reference(s)
Nuzhenide		S	(Bai <i>et al.</i> , 2010)
10-Oxyderivative of oleoside secoiridoids: 10-Hydroxyligstroside		B, L	(Jensen and Nielsen, 1976)

Table 1.5 (Cont.) Secoiridoids previously isolated from *F. excelsior*

Dimeric secoiridoid glucoside which consisting of two oleoside moieties linked to glucose and/or tyrosol			
Compound	Structure	Plant part*	Reference(s)
GI-3		S	(Bai <i>et al.</i> , 2010)
GI-5		S, L	(Bai <i>et al.</i> , 2010; Egan <i>et al.</i> , 2004)

* Studied plant parts; (B): bark, (L): leaves, (S): seed.

Table 1.6 Phenylethanoids previously isolated from *F. excelsior*

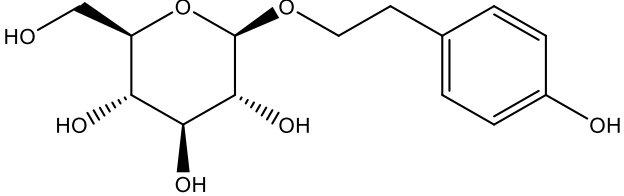
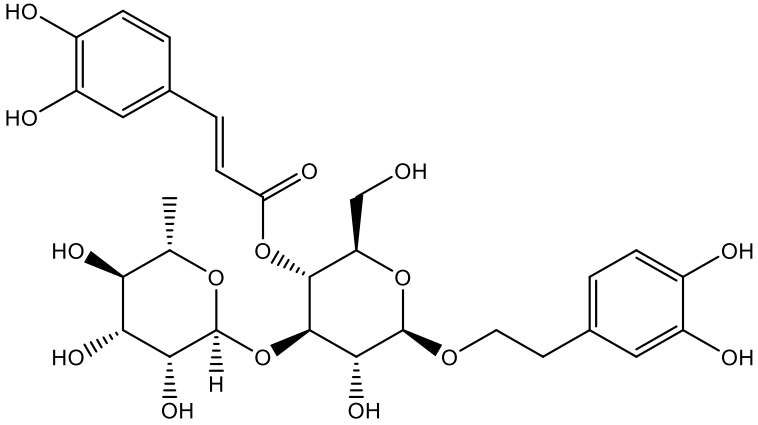
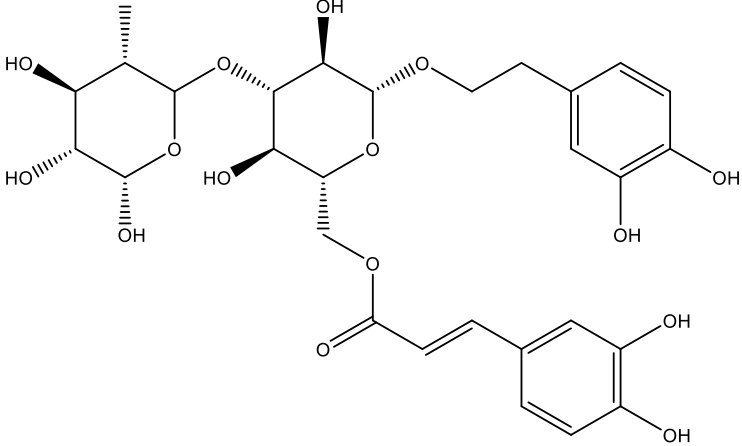
Compound	Structure	Plant part*	Reference(s)
Salidroside		S	(Bai <i>et al.</i> , 2010)
Verbascoside or acetoside		L	(Damtoft <i>et al.</i> , 1992)

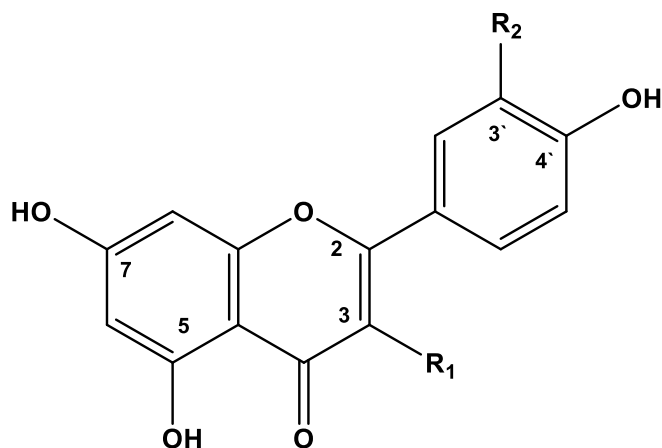
Table 1.6 (Cont.) Phenylethanoids previously isolated from *F. excelsior*

Compound	Structure	Plant part*	Reference(s)
Isoverbascoside	 <p>The structure of Isoverbascoside consists of two pyranose rings linked by a 1-6 glycosidic bond. The left ring is a galactopyranose unit with hydroxyl groups at C2 (dashed), C3 (wedged), and C4 (dashed). The right ring is a glucose unit with hydroxyl groups at C2 (wedged), C3 (dashed), and C6 (wedged). The C6 of the glucose unit is linked via an ether bond to a 2,4,6-trihydroxyphenyl group. The C4 of the glucose unit is linked via an ester bond to a 3,4,5-trihydroxyphenyl group.</p>	W	(Sanz <i>et al.</i> , 2012)

* Studied plant parts; (L): leaves, (S): seed, (W) wood.

Flavonoids

The structures of flavonoids reported from this plant species are shown in Figure 1.3 (Tissut and Egger, 1972; Kostova and Iossifova, 2007).



	R ₁	R ₂
Apigenin	H	H
Kaempferol	OH	H
Astragalin	O-Glc	H
Nicotiflorin	O-Glc-Rha	H
Quercetin	OH	OH
Rutin	O-Glc-Rha	OH
Isoquercetrin	O-Glc	OH
Quercetrin	O-Rha	OH

Figure 1.3 Structures of flavonoids reported in *F. excelsior*

Terpenoids and sterols

The triterpenes ursolic acid, betulinic acid, and betulin have been reported from *F. excelsior* leaves (Kowalczyk and Olechnowicz-Stepień, 1989). Abscisic acid, and gibberellins have been identified in *F. excelsior* seeds (Blake *et al.*, 2002). β -sitosterol has also been found in this species (Figure 1.4) (Kowalczyk and Olechnowicz-Stepień, 1989).

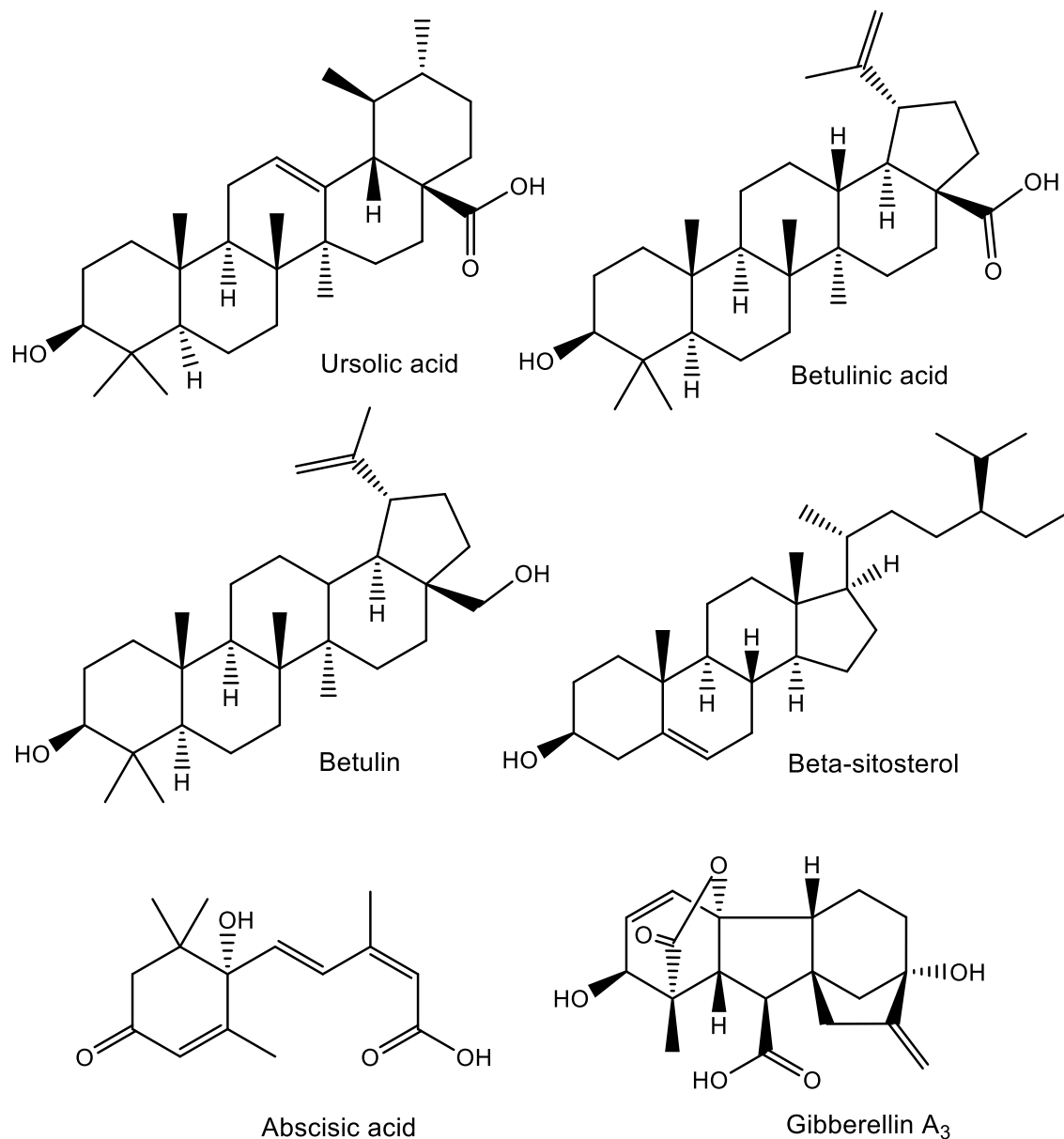
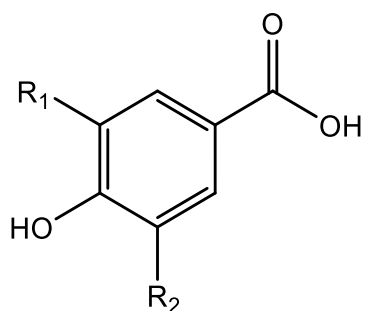


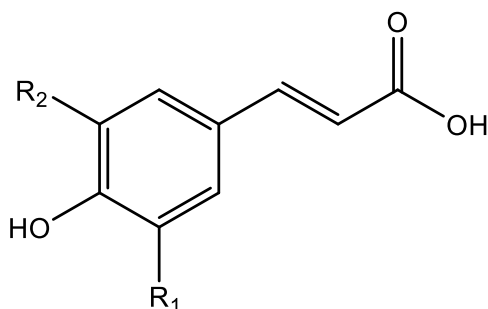
Figure 1.4 Structures of terpenoids and sterol isolated from *F. excelsior*

Phenolic acids and their derivatives

Various benzoic and cinnamic acid derivatives have been reported from *F. excelsior* (Figure 1. 5) (Méndez *et al.*, 1968; Kostova and Iossifova, 2007).



Benzoic acid derivatives		
Compound	R ₁	R ₂
<i>p</i> -hydroxybenzoic acid	H	H
protocatechuic acid	H	OH
Vanillic acid	H	OMe
Syringic acid	OMe	OMe
Gallic acid	OH	OH



Cinnamic acid derivatives		
Compound	R ₁	R ₂
<i>p</i> -coumaric acid	H	H
Caffeic acid	OH	H
Ferulic acid	OMe	H
Sinapic acid	OMe	OMe

Figure 1.5 Structures of phenolic acids and their derivatives isolated from *F. excelsior*

Other phytochemicals

Indole-3-acetic acid, jasmonic acid, and methyl jasmonate have been identified in *F. excelsior* seeds (Figure 1.6) (Blake *et al.*, 2002).

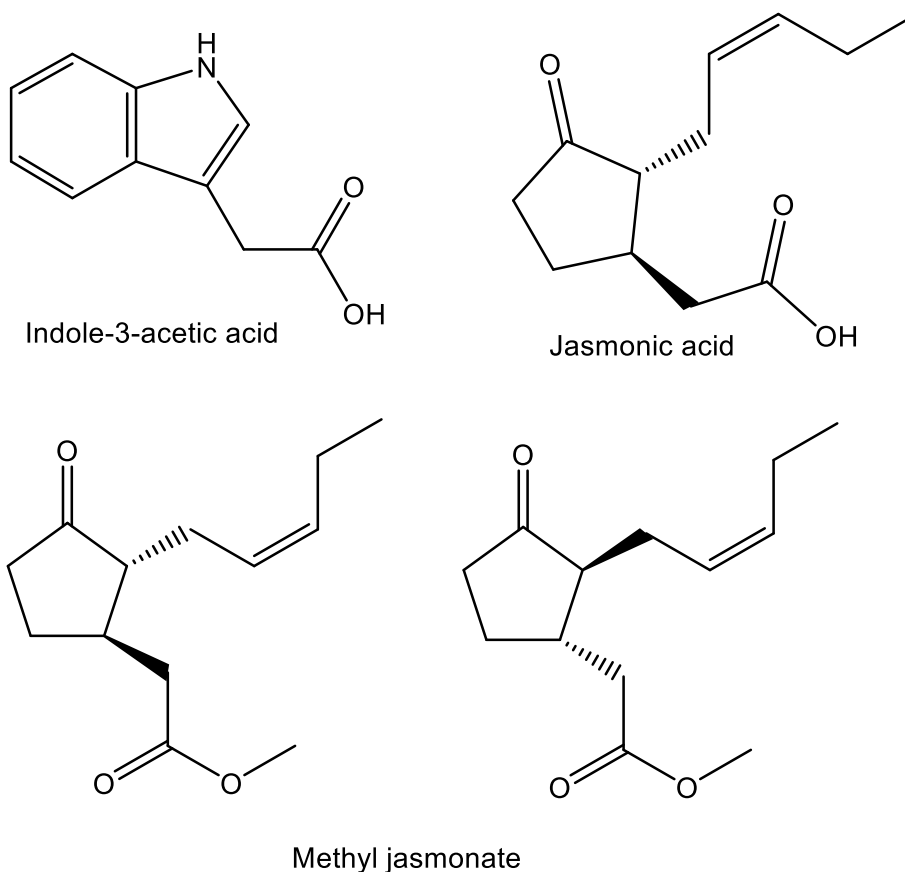


Figure 1.6 Structures of other phytochemicals isolated from *F. excelsior*

1.3.1.4 Previous biological work

Biological studies on the aqueous extract of *F. excelsior* seed have revealed antihyperglycemic and anti-obesity activity (Ibarra *et al.*, 2011; Eddouks and Maghrani, 2004). The aqueous seed extract has also showed hypotensive and diuretic activity (Eddouks *et al.*, 2005; Wright *et al.*, 2007). The *n*-hexane and DCM extracts of *F. excelsior* leaves have displayed activity against *Citrobacter freundii* (NCTC 9750), *Escherichia coli* (NCIMB 8110 and NCIMB 4174), *Klebsiella aerogenes* (NCTC 9528), *Lactobacillus plantarum* (NCIMB 6376), *Pseudomonas aeruginosa* (NCTC 6750), *Staphylococcus aureus* (10755) with MIC values in the range of 0.125

to 1.00 mg/mL. It has also shown activity against methicillin-resistant *Staphylococcus aureus* (MRSA) (MIC of 0.5 mg/mL) (Middleton *et al.*, 2010). The bark of *F. excelsior* (Ash) showed *in vitro* antimalarial activity (Aydin-Schmidt *et al.*, 2010). *F. excelsior* extract has demonstrated activity against *Mycobacterium tuberculosis* (Lucas *et al.*, 1951; Eshbakova and Kamoldinov, 2014).

Fraxinus species are a rich source of interesting phytochemicals. To date, there is little information in the literature about *F. excelsior* leaves, specifically regarding phytochemical and biological investigations to support the usefulness of this plant in traditional medicine (Kostova and Iossifova, 2007; European Medicines Agency, 2012; Sarfraz *et al.*, 2017; Kiss *et al.*, 2020). Conducting a phytochemical and biological investigations on *F. excelsior* leaves will contribute to advancing knowledge of this species and may provide scientific evidence to validate its traditional uses.

1.3.2 *Stachys arabica* Hornem (Lamiaceae)

1.3.2.1 Botanical description

Stachys (Lamiaceae) is a genus of about 300 species spread throughout the world (Evans, 2009). *Stachys arabica* is commonly known as Arabian woundwort (Figure 1.7). It is an annual herb distributed throughout the Mediterranean region. Its stems are 40-50 cm high, with opposite, rosette; entire; dentate or serrate margin leaves. The flowers are hermaphrodite with lilac petals. The flowering time starts from March until May ([Flora of Israel Online 2019](#)).



Figure 1.7. Aerial parts of *Stachys arabica* Hornem
(Picture provided by Dr. Mohammad Al-Garaibah, Al-mughayer)

1.3.2.2 Traditional uses

Stachys arabica is a medicinal herb used by traditional healers in the Mediterranean region to relieve cough, and pain associated with respiratory and gastrointestinal disorders. Infusions and decoctions prepared from *Stachys* species are used in traditional European, Iranian, and Mediterranean medicine to relieve cough, and symptoms associated with the common cold and respiratory infections. They also alleviate the symptoms of asthma. Moreover, the extracts are used externally to treat wounds and internally to treat gastrointestinal diseases, reduce anxiety, fever, rheumatic pain, gout, and other inflammatory disorders (Háznagy-Radnai *et al.*, 2012; Tundis *et al.*, 2014; Habib-Allah *et al.*, 2016; Tomou *et al.*, 2020). Dioscorides mentioned the use of *Stachys officinalis* with honey for tuberculosis and for internal abscesses (Tobyn *et al.*, 2011). In traditional Chinese medicine (TCM), *S. affinis* (*S. sieboldii*) are used to treat urinary tract infection, colds, and tuberculosis (Feng *et al.*, 2015).

1.3.2.3 Previous phytochemical work

Phytochemical investigations of *Stachys* species have revealed the presence of phenolic acids, flavonoids (Delazar *et al.*, 2005; El-Ansari *et al.*, 1991), phenethyl alcohol glycosides (Ahmad *et al.*, 2006; Delazar *et al.*, 2011; Miyase *et al.*, 1996; Nishimura *et al.*, 1991), diterpenoids (Farooq *et al.*, 2015; Fazio *et al.*, 1994; Mohamed Ael and Mohamed, 2014), iridoids (Munoz *et al.*, 2001; Murata *et al.*, 2008), and saponins (Ahmad *et al.*, 2008). The phytochemical composition of *Stachys arabica* has yet to be investigated.

1.3.2.4 Previous biological work

Stachys species have demonstrated antispasmodic (Gharib Naseri *et al.*, 2011), anti-oxidant, antimicrobial (Iscan *et al.*, 2012; Jassbi *et al.*, 2014), anti-inflammatory (Khanavi *et al.*, 2005), cytotoxic (Háznagy-Radnai *et al.*, 2008; Khanavi *et al.*, 2012; Venditti *et al.*, 2014), anxiolytic (Kumar *et al.*, 2012), antimycobacterial (Tosun *et al.*, 2004), anti-diabetic, anti-Alzheimer, and wound healing properties (Tomou *et al.*, 2020). This broad range of interesting pharmacological effects has been attributed to

the presence of wide range of bioactive phytochemicals (Kartsev *et al.*, 1994; Tundis *et al.*, 2014; Tomou *et al.*, 2020).

In this study, we conducted a phytochemical and biological investigation of *Stachys arabica* to provide some scientific evidence for the ethnobotanical uses of this species.

1.3.3 *Pelargonium sidoides* DC and *Pelargonium reniforme* Curt. (Geraniaceae)

1.3.3.1 Botanical description

Pelargonium sidoides and *Pelargonium reniforme* (Geraniaceae) are two perennial plant species indigenous to South Africa. They are distinguished by the shape of their leaves, the colour of their flowers, and the characteristics of their pollen. *P. sidoides* DC is characterised by dark red to almost black flowers, heart-shaped leaves, and yellowish pollen. The flowers heads of *P. reniforme* Curt. are magenta red with two distinctive stripes on the upper two petals. Its pollen is whitish-green, and its reniform leaves represent a characteristic feature that is reflected in its botanical name '*reniforme*'. In *P. sidoides*, the root wood is dark brown, while in *P. reniforme* it is markedly lighter or appears yellow. The geographical distribution of *P. sidoides* overlaps with that of *P. reniforme* but is wider. The former species occurs throughout eastern Cape, Lesotho, Free State and southern Gauteng (Kayser and Kolodziej, 1997; Brendler and Van Wyk, 2008; Bladt and Wagner, 2007; Kolodziej, 2008).

1.3.3.2 Traditional uses: Historical and modern uses

The root extract of *P. sidoides* and *P. reniforme* is known as '*Umckaloabo*', a herbal remedy used for persistent cough and respiratory tract infections, including TB. It is also employed in the treatment of gastrointestinal disorders such as diarrhoea and dysentery. The aerial parts of these species are used to treat wounds (Kolodziej, 2000; Bladt and Wagner, 2007).

A number of reviews have been published on the history of '*Umckaloabo*', from its status as a 'mystery drug' used in South Africa to its commercial development in Europe (Helmstaedter, 1996; Newsom, 2002; Bladt and Wagner, 2007; Brendler and

Van Wyk, 2008; Kolodziej, 2003; Kolodziej, 2000). 'Umckaloabo' was discovered in the late 19th century by an Englishman (Charles Stevens) who claimed that he recovered from TB during a trip to South Africa after being treated with Umckaloabo roots. Back in England, Stevens marketed this natural anti-TB remedy as 'Stevens Consumption Cure' or 'Umckaloabo', but here was some controversy about the actual identity of the roots used for the preparation of the remedy (Helmstaedter, 1996; Newsom, 2002). In 1920, a Swiss physician treated around 800 TB patients with Stevens' cure, and suggested that this remedy might cause 'neutralisation or destruction of the TB toxins' rather than exert a direct anti-Mtb activity (Newsom, 2002; Bladt and Wagner, 2007; Sechehaye, 1930; "An English Physician" 1931).

The true botanical origin of 'Umckaloabo' remained unidentified until 1974 when it was identified as *P. reniforme*. In 1998, it was announced that the true origin could also be *P. sidoides*. Various studies on the pharmacological activity and the clinical efficacy of 'Umckaloabo' on a range of respiratory conditions have been published (Kolodziej, 2000; Kolodziej, 2007). 'Umckaloabo' was later developed into a fully licensed herbal medicinal product (EPs® 7630 'Umckaloabo'), approved for the treatment of upper respiratory tract infections. Several clinical trials approved its efficacy and safety. *P. sidoides* and/or *P. reniforme* appear in the European Pharmacopoeia (Kolodziej, 2007; Brendler and Van Wyk, 2008; European Medicines Agency, 2018).

1.3.3.3 Previous phytochemical work

Several studies have been published on the phytochemical composition of the roots and the aerial parts of *P. sidoides* and *P. reniforme* (Kolodziej, 2007; Bladt and Wagner, 2007). Both *Pelargonium* species contain simple phenols, coumarins, flavonoids, and tannins (Table 1.7, Appendix I). The roots of both species contain coumarins. *P. sidoides* roots, unlike *P. reniforme*, are rich in highly oxygenated coumarins, coumarin sulphates, and coumarin glucosides. The coumarin umckalin, in *P. sidoides* roots and aerial parts, is used as a chemical marker to identify this species (without harvesting) as it is absent from *P. reniforme*. On the other hand, the diterpene reniformin is only present in the roots of *P. reniforme*, and has never been reported from *P. sidoides*. The aerial parts of both species are rich in flavonoids, including flavonols, flavanones, dihydroflavonols, and flavones. Noteworthy, is the presence of

a unique series of 2"-O-galloyl derivatives of C-glycosylflavones such as orientin, isoorientin, vitexin and isovitexin (Kolodziej, 2007; Brendler and Van Wyk, 2008; Hauer *et al.*, 2010).

Table 1.7 Number and types of phytochemicals previously isolated from *P. sidoides*/*P. reniforme* roots and aerial parts.

	<i>P. sidoides</i>		<i>P. reniforme</i>	
	Roots	Aerial parts	Roots	Aerial parts
Marker compound	umckalin	umckalin	reniformin	-
Phenolic acids, phenylpropanoids derivatives	3	6	10	15
Simple coumarins	10	4	6	1
Coumarin glycosides	3	2	-	-
Coumarin sulfates	11	1	-	-
Flavonoids	-	13	4	15
Flavanols/ proanthocyanidins	3	-	4	-
Hydrolysable tannins	-	-	-	13
Miscellaneous	1	3	3	-

1.3.3.4 Previous biological work

The aqueous ethanolic extract of *P. sidoides* roots has showed antibacterial, antiviral, and immunomodulatory properties. This helps support its therapeutic use in acute bronchitis, tonsillopharyngitis, sinusitis, and the common cold. Several clinical trials have approved its efficacy and safety. The presence of tannins in the aerial parts may explain the traditional use in wound healing (Kolodziej, 2008; Brendler and Van Wyk, 2008; Kolodziej, 2011).

Although the roots of the *Pelargonium* species are used in traditional medicine, several reports have showed that both the aerial parts and the roots of *P. sidoides* and/or *P. reniforme* have antibacterial and antifungal activity with no significant differences between MIC values from the two parts (Kayser and Kolodziej, 1997; Lewu *et al.*, 2006). The selection of *Pelargonium* roots over its aerial parts by traditional healers might be attributed to an easier collection but may also be

arbitrary. The medicinal use of *Pelargonium* aerial parts may be as valid as the use of its roots in the treatment of tuberculosis and bronchitis (Lewu *et al.*, 2006).

The crude extract of *P. reniforme* has showed activity against Mtb (96% inhibition at 12.5 µg/mL) with an MIC of 100 µg/mL. Neither *P. sidoides* extract nor any of the phenols and coumarins tested exhibited antimycobacterial activity. Rifampicin (control) showed an MIC of 0.06 µg/mL (Kolodziej, 2000). Bioassay-guided fractionation of the *n*-hexane extracts of *P. reniforme* and *P. sidoides* roots has led to the identification of mixtures of fatty acids with activity against rapidly growing mycobacteria. Oleic and linoleic acids were identified as the most active compounds (MICs of 2 mg/L) against *Mycobacterium aurum* (Seidel and Taylor, 2004).

Kim *et al* conducted a study to determine the capacity of extracts of *P. reniforme* and *P. sidoides* to stimulate the uptake and killing of Mtb and *Mycobacterium fortuitum*-infected murine peritoneal macrophages, and to identify the active compounds. A bioassay-guided fractionation of *P. reniforme* aqueous extract has showed that gallic acid, methyl gallate, quercetin-3-O-β-glucoside, and myricetin had immunomodulatory activity (Kim *et al.*, 2009).

Although *P. reniforme* and *P. sidoides* are traditional anti-TB cures, no compound from these spp. has demonstrated *in vitro* activity against Mtb. Previous studies have been performed on extracts and/or report on the isolation of NPs tested against mycobacteria other than Mtb. The anti-Mtb active principle(s) of *Pelargonium* remains to be identified. The traditional use of *Pelargonium* extracts in TB patients might be related to an indirect effect that could be linked to the modulation of the immune system rather than a direct action on Mtb (Mativandlela *et al.*, 2007; Kolodziej, 2011).

In this study, a combined ethno-guided approach with *in silico* screening was used to predict the anti-Mtb potential of both *Pelargoniums* aerial parts and roots.

1.4 The immune system

1.4.1 Innate and adaptive immunity

Immunity can be regarded as a state of resistance to infection. The immune system consists of a network of cells, molecules, organs, and tissues working together to fight harmful stimuli/infection. Different immunological strategies are required to tackle extra- and intracellular pathogens. The immune system consists of the innate immune system and adaptive immunity system (Marshall *et al.*, 2018).

Innate immunity is characterised as non-specific, first-line immunological defence for fighting against noxious stimuli. This immune response is rapid and is mediated by numerous cells such as macrophages, circulating monocytes, natural killer cells (NK), and neutrophils. The adaptive immunity operates in cooperation with the innate immunity to eradicate harmful stimuli. It depends on interaction between T cells, and B cells. The development of an “immunologic memory” is the interesting feature of adaptive immunity leading to effective immune responses upon subsequent exposure to the same or similar stimuli (Marshall *et al.*, 2018).

The innate immune system involves cellular defences, physical (skin), and chemical barriers (stomach acidity) (Bennett *et al.*, 2018). Innate immune cells residing in tissues, like macrophages, circulating monocytes and neutrophils, recognise pathogens or cell damage via intracellular or surface-expressed pattern recognition receptors (PRRs). These receptors detect, either directly or indirectly, pathogen-associated molecular patterns (PAMPs), or damage-associated molecular patterns (DAMPs) released from infected cells. Following this, activated PRRs initiate signalling pathways/cascades which trigger the release of mediators (like lipid mediators, cytokines, and proteolytic enzymes) that promote the inflammatory response (Newton and Dixit, 2012).

The immune response against Mtb is complex and involves various components of innate and adaptive immune system. The adaptive immune response mediated by CD4⁺ T cells is essential to control Mtb infection, cytokines released by CD4⁺ T helper cells (e.g., IFN γ) are important for the outcome of immune response against Mtb. Moreover, the importance of CD4⁺ T cells have been established because human infected with HIV are more susceptible to developing TB disease (Sakai *et al.*, 2014; Jasenosky *et al.*, 2015; Morgan *et al.*, 2021).

1.4.2 The innate immune response against Mtb

Macrophages (M_{ϕ}), dendritic cells (DCs), neutrophils, and natural killer cells (NK) are the major innate immune cells classically involved during Mtb infection. Airway epithelial cells (AECs), which are considered to be in the frontline against Mtb since they act as a physical barrier, and mast cells contribute to the early immune response against Mtb as “non-professional” immune cells. During Mtb infection, various components of the immune system collaborate effectively with overlapping roles at different times in their battle to eliminate Mtb. However, unfortunately Mtb interferes with their function. Dealing with such a “great manipulator” requires a very rapid immune response at the onset of infection (Liu *et al.*, 2017a; De Martino *et al.*, 2019).

The first step in the activation of the innate immune response during Mtb infection starts with pathogen recognition. During phagocytosis, Mtb interacts with innate immune cells and binds to receptors on their cell surface. These receptors include Toll like receptors TLRs (i.e., TLR2 binds lipomannan (LM), and lipoarabinomannan (LAM), TLR4 recognise acylated LM, and heat shock protein 65 (HSP65)), NOD-Like receptors (NLRs), complement receptors (i.e., CR3), mannose receptor, scavenger receptors, surfactant protein A receptor, and the dendritic cell-specific intercellular adhesion molecule grabbing nonintegrin. The interaction between Mtb and various immune cells induces an inflammatory response that can lead to clearance of Mtb or drive granuloma formation (Hossain and Norazmi, 2013; Liu *et al.*, 2017a).

Following Mtb infection, most individuals contain Mtb in a latent form because of an immunological equilibrium between the innate and the adaptive immune responses. The granuloma, the hallmark of TB, is a collection of inflammatory cells, and represent the host’s protective structure as an immunologic and physical barrier to contain infection and prevent dissemination. Maintenance of the granulomas is a dynamic process of continual immunologic control of bacterial replication (Vyas and Goswami, 2017).

According to the literature, the optimal control of outcomes of the Mtb infection depends on a complex balance between a pro- and an anti-inflammatory immune response that contain Mtb infection in a latent form for prolonged periods without causing tissue damage and Mtb dissemination . This balance fluctuates during the course of infection, between individuals, and even within the same host’s granulomas (Lin and Flynn, 2010; Vyas and Goswami, 2017).

1.5 Inflammation

Inflammation is a complicated physiological process and considered as the first response of the immune system to protect from noxious stimuli, such as pathogens, toxic compounds, or damaged cells, and to initiate the healing process. Controlled and successful inflammatory responses result in the efficient clearance of noxious stimuli and contributes to re-establishing tissue homeostasis. However, unsuccessful acute inflammatory responses lead to pathological consequences that contribute to a wide range of chronic inflammatory diseases (Medzhitov, 2008; Chen *et al.*, 2017b; Liu *et al.*, 2017b) including diabetes mellitus (Tsalamandris *et al.*, 2019; Wellen and Hotamisligil, 2005), rheumatoid arthritis (Choy and Panayi, 2001; Demoruelle *et al.*, 2014), osteoarthritis, inflammatory bowel disease (Fiocchi, 1998; Zhang and Li, 2014), atherosclerosis (Chávez-Sánchez *et al.*, 2014), hypertension cardiovascular disease (myocardial infarction and chronic heart failure) (Libby, 2006; De Miguel *et al.*, 2015), Alzheimer's disease (Akiyama *et al.*, 2000; Kinney *et al.*, 2018), and Parkinson's disease (Tufekci *et al.*, 2012; Caggiu *et al.*, 2019).

TB is an infectious disease caused by Mtb, which mainly affects the lung, where it infects and activates macrophages, NK, DCs and neutrophils and causes localised acute inflammation and granuloma formation. Failure to eliminate this infectious pathogen means that Mtb remains for an extended period of time, leading to inflammatory tissue damage and immunopathology. Thus, TB is considered as a chronic inflammatory condition. Cytokines (i.e., TNF- α and interleukins) and immune cells (i.e., M Φ s and Th₁ cells) are the main host components that are engaged in TB inflammation. Sequentially, these components have dual effects, either suppressing or triggering the events of inflammation (Medzhitov, 2010; Jnawali *et al.*, 2016).

Medzhitov (2010) mentioned that in Guido Majno's book "*The healing hand: Man and wound in the ancient world, 1975*" the first description of inflammation which was in the 1st century by the Roman doctor Celsus. The symptoms of inflammation described by four cardinal signs rubor, tumor, calor and dolore referring to redness and swelling with heat and pain respectively. However, the fifth cardinal sign "functio laesa" refers to disturbance of function, which was added later by Rudolph Virchow in 1858 in his book *Cellular Pathologie* establish the cellular basis of chronic inflammation. Individual inflammatory responses are dependent on the origin of the initial stimulus and its location in the body. However, they all share common aspects such as cell

surface pattern receptors which recognise stimuli, the inflammatory signalling pathways that are activated, the mediators produced, and the type of inflammatory cells that participate (Chen *et al.*, 2017b).

1.5.1 Pattern recognition receptors (PRRs)

Innate immune cells recognise pathogens or cell damage with intracellular or surface-expressed pattern recognition receptors (PRRs). These receptors detect, either directly or indirectly, pathogen-specific molecular signatures known as pathogen-associated molecular patterns (PAMPs), or damage-associated molecular patterns (DAMPs) released from infected cells. After that, activated PRRs initiate signalling pathways/cascades which in turn trigger the release of mediators (like lipid mediators, cytokines, and proteolytic enzymes) that promote the inflammatory responses (Newton and Dixit, 2012). These responses are considered critical for the pathogens clearance and can also orchestrate antigen-specific adaptive immune responses. Pattern recognition receptors (PRRs) include; Toll-like receptors (TLRs), Nod-like receptors (NLRs) and C-type lectin receptors (CLRs). Among these, TLRs are the most extensively characterized (Takeuchi and Akira, 2010).

1.5.2 Toll-like receptors (TLRs)

The TLRs family includes 10 members (TLR1–TLR10) in humans and 12 members (TLR1–TLR13 except TLR10) in mice. TLRs are a family of transmembrane proteins that contain Leucine rich repeats which recognise PAMPs (conserved features present in the pathogens). Examples of these PAMPs include; bacterial cell surface lipopolysaccharide (LPS) on Gram negative bacteria, lipoarabinomannan (LAM) a lipoglycan/glycolipid and major virulence factor from *Mycobacterium* spp., lipoprotein, and nucleic acid). These PAMPs lead to immune activation. Upon the recognition of PAMPs, TLRs recruit TIR domain-containing adaptor proteins (proteins that mediate other protein-protein interaction like MyD88 and TRIF), which initiate signal transduction pathways (STP). These pathways result in the activation of NF- κ B, or MAP kinases to regulate the expression of cytokines and chemokines which in turn participate in immune responses in the host during microbial infection (Kawasaki and Kawai, 2014; Federico *et al.*, 2020)

TLRs are classified into two subfamilies based on their localization (Table 1.8), cell surface TLRs and intracellular TLRs. TLRs 1, 2, 4, 5 and 6 are cell surface TLRs that have their receptors on the cell surface and bind to their ligands which derived from bacteria, fungi, and protozoa. Whereas TLRs 3, 7, 8 and 9 are considered intracellular receptors (endosome, lysosome) that bind to viruses or intracellular bacteria derived ligands. Functional TLRs consist of two dimers, a homodimer like in TLR4 and hetero dimers like TLR 1&2. TLRs have two structural domains; extracellular domain or Receptor domain, which is responsible for ligand binding and recognition, comprises of leucine rich repeats (LRRs) that fold into horseshoe like structure for binding and recognition. The other domain is the conserved cytoplasmic signalling domain known as Toll-Interleukin 1 receptor (TIR) domain (Takeda and Akira, 2005; Savva and Roger, 2013; Kawasaki and Kawai, 2014). Among the TLR family, TLR2, TLR4, and TLR9 play a role in host recognition of Mtb (O'garra et al., 2013) .

TLRs may also depend on other co-receptors for full ligand sensitivity, for example TLR4's recognition of LPS, which requires MD-2, CD14 and LPS-Binding Protein (LBP) are known to facilitate the presentation of LPS to MD-2 (O'Neill *et al.*, 2009; Vaure and Liu, 2014). As a result, the lipid A of LPS bind with LPS-binding protein (LBP) to form LPS-LBP complex which in turn bind with CD14 on cell surface and activate TLR4. The activated TLR4 binds with myeloid differentiation factor 88 (MyD88) which in turn initiates downstream signal transduction and activate NF- κ B or MAPK which regulate inflammatory cytokines release (Pålsson-Mcdermott and O'Neill, 2004; Ciesielska *et al.*, 2021).

Targeting TLRs offers a promising potential for sepsis management and the control of infectious diseases (O'Neill *et al.*, 2009; Savva and Roger, 2013). It is possible that compounds or drugs that demonstrate the ability to block TLR activation and their consequent TLR-dependent inflammatory responses, can provide new treatment approaches for inflammatory diseases (Mcinturff *et al.*, 2005). TLR4, in both the agonistic and antagonist aspects, has been extensively evaluated in several clinical trials. Eritoran (a TLR4 antagonist, phase 2) is of interest as a target of insulin resistance and as an anti-inflammatory agent (Anwar *et al.*, 2019). According to a recent perspective by Federico *et al* (2020). They outlined recent findings on TLR modulators and their therapeutic potential to treat a wide range of pathological conditions including infections, inflammatory, neurodegenerative, autoimmune diseases, metabolic disorders (diabetes), and cancer.

Table 1.8 : Examples of Human Toll-Like Receptors (TLRs) and their ligands

Receptor	Ligands	Origin
Surface located		
TLR1 withTLR2 heterodimer	Lipopeptides, glycosylphosphatidylinositol- anchored lipids	Bacteria Parasites (<i>Trypanosoma cruzi</i>)
TLR2 withTLR6 heterodimer	Lipoteichoic acid (LTA) Zymosan	Gram positive bacteria Fungi
TLR2	Lipoarabinomannan (LAM)	Mycobacteria
TLR 4 homodimer	LPS Paclitaxel HSP70, fibronectin, fibrinogen	Gram-negative bacteria NPs (<i>Taxus brevifolia</i>) Host -derived molecules
TLR 5 homodimer	Flagellin	bacteria
Intracellular		
TLR 3 homodimer	Double-stranded RNA (dsRNA)	Viruses
TLR 7 & 8 homodimer	Single-stranded RNA (ssRNA) Imidazoquinoline	Viruses Synthetic compounds
TLR 9	Unmethylated CpG DNA	bacteria

Adapted from (Mcinturff *et al.*, 2005; Savva and Roger, 2013; Anwar *et al.*, 2019)

1.5.3 The TLR signalling pathways

All TLRs except TLR3 utilize MyD88 to activate NF- κ B and MAPK which regulate inflammatory cytokines release, and this pathway is called the MyD88-dependent pathway. However, TLR4 initiates two major signalling pathways; the MyD88-dependent pathway, which regulates NF- κ B activation and related inflammatory cytokine production (TNF- α , IL-1 and IL-12), and the MyD88-independent (TRIF - dependent) pathway, which activates type I interferons and co-stimulatory molecules.

LPS binding to TLR4 on the cell surface activate MyD88 signalling leading to activation of IL-1 receptor associated kinase (IRAK) family members, which in turn activate tumour necrosis factor receptor-associated factor (TRAF6). Following this the IRAK-TRAF6 complex dissociates and forms a further complex in the cytosol with transforming growth factor- β -activated kinase (TAK1). Once activated, TAK1 modulates two different pathways that lead to activation of the nuclear factor kappa B (NF- κ B) pathway and mitogen-activated protein kinase (MAPK) pathway. NF- κ B is kept inactive in the cytoplasm by an inhibitor of κ B (I κ B), which can be phosphorylated by I κ B kinase α (IKK α) and IKK β , resulting in I κ B disengagement and subsequent degradation by the proteasome. The activated NF- κ B translocate into the nucleus. Another pathway of TAK1 activation also results in signalling activation of mitogen-activated protein kinases (MAPK) family members (such as ERK1/2, p38 and JNK), which mediate activation of the Activator protein-1 (AP-1) family transcription factors and regulate inflammatory responses. Both transcription factors (NF- κ B & AP-1) translocate to the nucleus and modulate/ promote inflammatory cytokine expression (Figure 1.8) (Takeda and Akira, 2005; Kawai and Akira, 2010; Vaure and Liu, 2014; Kawasaki and Kawai, 2014; Federico *et al.*, 2020).

NF- κ B regulates host inflammatory and immune responses. As deregulated NF- κ B activation contributes to the pathogenic processes of various inflammatory diseases, targeting NF- κ B signalling pathway by blocking different steps of the NF- κ B pathway (such as IKK inhibitors, Proteasome inhibitors, and Inhibitors that block nuclear translocation of different NF- κ B subunits) may represent an attractive therapeutic potential in the treatment of inflammation related diseases (Liu *et al.*, 2017b).

Natural products that inhibit the NF- κ B pathway could have therapeutic potential in the treatment of inflammation related diseases (Yamamoto and Gaynor, 2001). Several anti-LPS or anti-cytokine effects have been reported, N⁶-(2-

hydroxyethyl)adenosine (HEA) isolated from the medicinal mushroom *Cordyceps cicadae* attenuated LPS-induced TNF- α and PGE2 production of RAW 264.7 macrophages by down regulation of the activation of TLR4 mediated NF- κ B signalling (Lu *et al.*, 2015). Parthenolide, a sesquiterpene lactone, isolated from the shoots of feverfew (*Tanacetum parthenium*), inhibited LPS-induced inflammatory cytokines through TLR4 signal pathway in THP-1 cells (Li *et al.*, 2015b). Hesperetin, a flavanone isolated from *Citrus* plants attenuated TLR4 and phosphorylation of NF- κ B and could be a potential therapeutic agent to treat Alzheimer's disease-like neurodegenerative disorders (Ikram *et al.*, 2019).

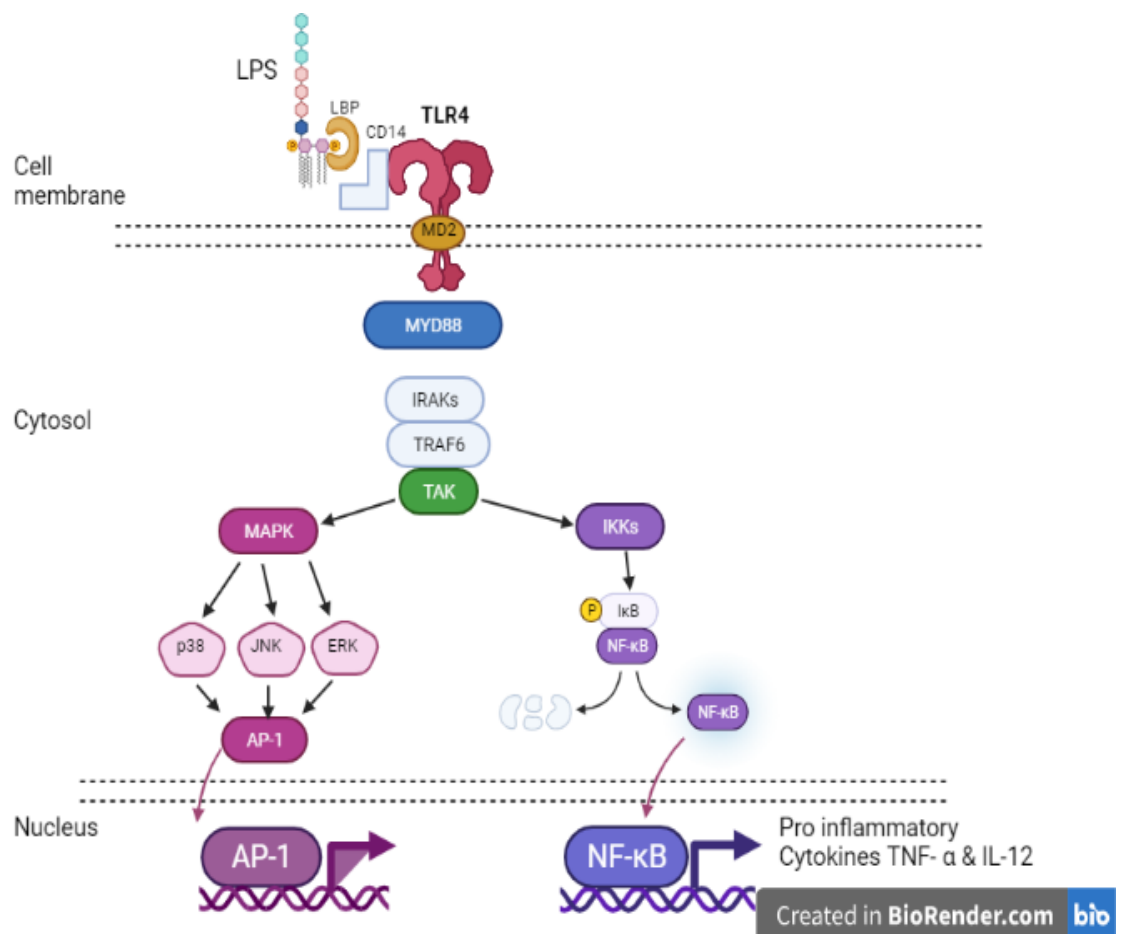


Figure 1.8 Simplified diagram of MyD88-dependent pathway following TLR4 activation by LPS (created in BioRender.com).

1.6 Cytokines

Cytokines are small cell signalling protein molecules released by immune cells and involved in cellular communication, immune response, inflammation, and haematopoiesis (Kany *et al.*, 2019). Cytokine is a general name; other nomenclature includes lymphokine (cytokines made by lymphocytes), monokine (cytokines made by monocytes), chemokine (cytokines with chemotactic activities), and interleukin (cytokines made by one leukocyte and acting on other leukocytes) (Zhang and An, 2007). Cytokines can be classified as pro- or anti-inflammatory according to their functional role during inflammatory responses (Arango Duque and Descoteaux, 2014). Cytokines are a cornerstone of any *in vitro* or *in vivo* model that deals with inflammation since there can be described as network in the infection, injury, and the disease process (Chiswick *et al.*, 2012). Cytokines can be pleiotropic with various effects on different cell types. Cytokines can act synergistically. Cytokine release can result in cascading expression of subsequent cytokines in other cells and can activate the production of other mediators of inflammation (Ramani *et al.*, 2015).

Mtb orchestrates a complex set of immune responses in humans. Several cytokines, including IFN- γ , TNF- α , IL-1 β , IL-12 contribute to the host response to *Mtb*, this has a critical role in controlling TB (Hossain and Norazmi, 2013). Toll-like receptors (TLRs) play a crucial role in immune recognition of *Mtb*, and the subsequent inflammatory response is regulated by production of pro- and anti-inflammatory cytokines and chemokines (Etna *et al.*, 2014). Cytokines, released in response to *Mtb* infection, are not always necessarily favourable to host protection; some of these mediators serve the pathogen. Studies showed that cytokines, in response to a particular pathogen, produce beneficial as well as damaging effects to the host (Hossain and Norazmi, 2013). This fact was supported by Domingo-Gonzalez *et al* (2016) who demonstrated that in TB, the role of any cytokine cannot be designated either “good” or “bad” but rather that cytokines can produce/generate both protective and pathologic consequences according to the situation. The balance of pro- and anti-inflammatory immune responses at the site of infection (mainly the granuloma) is crucial to control TB infection and predict clinical outcomes.

Taken together, in most inflammatory conditions, there is a high degree of overlap between the role of pro-inflammatory cytokines, the ability of a drug to suppress associated pro-inflammatory pathways could be desirable. In addition, treatment

leads to the inhibition of certain cytokine like TNF- α / IL-12, in some cases, is correlated by enhanced anti-inflammatory effects. However, there is a possibility that the non-selective suppression of pro-inflammatory pathways could be harmful in some pathophysiological conditions, such as, when a chronic autoimmune disorder is accompanied by an infectious disease. Sometimes, to maintain certain immune functions may be critical and selective pharmacological interventions to inhibit the production of certain, but not all cytokines should be applied. In general, these approaches could afford novel ways for the treatment of pathophysiological disorders (Haskó and Szabó, 1999).

1.6.1 Tumour Necrosis Factor-alpha (TNF- α)

TNF- α is represent a major pro-inflammatory cytokine produced upon activation by the immune system, released primarily from monocytes and macrophages and exhibit a multiple biological effects. TNF- α is responsible for a wide range of signalling events and in the inflammatory response. Although TNF- α has various valuable roles in immune regulation, it has been involved in the pathogenesis of acute and chronic inflammatory disorders (Wajant *et al.*, 2003; Chu, 2013).

Earlier studies revealed that during mycobacterial infection, TNF- α seems to have a crucial role in both the physiopathology and in protective immunity to TB (Cavalcanti *et al.*, 2012; Domingo-Gonzalez *et al.*, 2016). One piece of evidence of the protective effects of TNF- α is provided by the observation that patients with rheumatoid arthritis (RA), inflammatory bowel disease (IBD) and psoriasis undergoing treatment with TNF- α antagonists show a significant increased risk of reactivating latent TB (Solovic *et al.*, 2010; Stallmach *et al.*, 2010; Chu, 2013). These findings support the view that TNF- α is critical for the initiation and co-ordination of cellular immune responses in the early stages of Mtb infection (Domingo-Gonzalez *et al.*, 2016). However, other reports demonstrated that TNF- α might be related to immunopathological responses in TB patients, including the destruction of pulmonary tissue. Also, high levels of TNF- α are associated with an excessive inflammation with necrosis and cachexia (wasting syndrome) (Bekker *et al.*, 2000; Flynn *et al.*, 2011; Chu, 2013). High TNF- α levels may be associated with clinical deterioration observed early in the treatment of severe TB (Bekker *et al.*, 1998). Patients with pulmonary TB disease tend to have increased levels of TNF- α (Zumla *et al.*, 2015). TNF- α has a dual role in TB pathogenesis.

It is worth mentioning that in a clinical investigation conducted by Júnior *et al* (2008) to verify the correlation between serum level of TNF- α and several TB clinical patterns, the research team found a positive correlation between higher TNF- α levels and worse clinical outcomes in TB patients including weight loss, abnormal chest X-ray, and tissue destruction. The investigators proposed that a suppression of TNF- α serum level may reduce tissue destruction with clinical improvement especially when TNF- α remains elevated for a long time. It is interesting to note that in the same study, the authors suggested that TNF- α immune modulation should be taken into consideration in TB treatment particularly in cases having very high TNF- α serum levels. Another reports emphasises that before treatment, serum TNF- α levels are elevated in active pulmonary TB patients compared to inactive pulmonary TB patients and controls, after successful treatment with standard anti-TB chemotherapy serum TNF- α levels decrease significantly (Ameglio *et al.*, 2005; Deveci *et al.*, 2005; Kumar *et al.*, 2019).

1.6.2 Interleukin 12 (IL-12)

Interleukin-12 is a 70-kDa heterodimeric cytokine composed of covalently linked p35 and p40 subunit/chain. IL-12 is an early pro-inflammatory cytokine as well as immunomodulator, produced by activated monocytes, macrophages, antigen-presenting cells, dendritic cells, and B cells in response to bacterial products (LPS) and maintain cell -mediate immune responses. The most important positive regulators of IL-12 production are IFN- γ and TNF- α . IL-12 represents a bridge between innate and adaptive immune response. This cytokine has an important role in driving the immune system toward T helper 1 (Th1) cells and preventing a Th2 type immune profile as part of the normal immune response. Overproduction of IL-12 is involved in the pathology of several inflammatory and autoimmune disease; therefore, this cytokine can serve as an ideal target for shaping the immune response during inflammatory diseases as well as autoimmune diseases (Trinchieri, 1995; Haskó and Szabó, 1999). Overexpression of IL-12 can elicit immunopathological and chronic inflammatory disorders including inflammatory bowel diseases (IBD: ulcerative colitis & Crohn's disease), psoriasis, diabetes mellitus (DM), multiple sclerosis (MS), rheumatoid arthritis (RA) and septic shock. On the other hand, IL-12 deficiency may contribute to asthma, tumour growth, and cancer. IL-12 treatment can be used to

control chronic hepatitis and ADIS (Haskó and Szabó, 1999; Zundler and Neurath, 2015).

It is interesting to note that in an earlier study by Cooper *et al* (1997) it was demonstrated that mice deficient in IL-12 are highly susceptible to Mtb infection. Thus, IL-12 is essential to the generation of a protective immune response to Mtb. Its main functions are to induce IFN- γ expression and to create a protective granuloma. Another study reported that IL-12p70 is the critical cytokine that activates the generation of IFN γ -producing T cells that are believed to be vital for Mtb control (Cooper *et al.*, 2007). Deficiencies in the IL-12 or IFN- γ signalling pathways have been associated with human susceptibility to TB (Filipe-Santos *et al.*, 2006).

Domingo-Gonzalez *et al.* (2016) indicated that IL-12 is essential for survival following Mtb infection and mediates early T cell activation, polarisation, and survival. Over production of IL-12 is toxic during Mtb infection. Another study illustrated that the relative balance of each IL-12 family member (including IL-12) could have an important role for controlling Mtb infection as well as determining pathological consequences (Torrado and Cooper, 2013). A recent study showed a significant increase in the serum level of IL-12 in TB patients compared with healthy subjects (Mankhi *et al.*, 2018). Patients with pulmonary TB disease tend to have increased levels of TNF- α (Zumla *et al.*, 2015) and IL-12 (Djoba Siawaya *et al.*, 2009; Wang *et al.*, 2018). It might be that one of the suggested/successful approaches in TB treatment is to suppress the raised levels of TNF α - and IL-12 in TB patients.

1.7 Host-Directed Therapies (HDT) and Pathogen-Directed Therapy (PDT) to tackle TB infection

1.7.1 Adjunct host-directed therapies (HDTs)

The treatment of TB remains challenging mainly due to the long course of treatment with complex drug regimens showing a high toxicity potential. An interesting report by Barnes (2003) suggested three options for immunotherapeutic strategies for tackling TB. The first one is an immune activation-based therapy through

administration of cytokines (like IL-2, IFN- γ) to facilitate bacillary clearance and improve cure rate in patients with MDR- TB. The second one is immunotherapy to downregulate the inflammatory response (over production of cytokines like TNF- α) in severe TB cases. The third one is the potential use of immunotherapy to shorten the duration of treatment for DS-TB. Pyrazinamide (PZA) is one of the standard anti-TB drugs. Manca *et al* (2013) reported that PZA treatment of Mtb-infected human and mice monocytes could significantly decrease the production of pro-inflammatory cytokines (TNF- α , IL-1 β , and IL-6) and based on that the researchers suggested that PZA administration could modulate the host's immune response to Mtb infection by suppressing pro-inflammatory cytokine production, probably through an NF-kB dependent pathway (Manca *et al.*, 2013).

According to several reports, attention has been drawn to an emerging approach of adjunct host-directed therapies (HDTs) in the hope that this approach might overcome many of the challenges faced by TB-standard treatment and open new avenues to treat TB. These HDTs are commonly used with the standard anti-TB drugs to shorten their duration and improve their therapeutic efficacy, minimise the number of drugs required, support the host's immune response by targeting host pathways to regulate Mtb pathogenesis and prevent excessive inflammation. Corticosteroids (dexamethasone) for example have been useful as immune- adjunct to standard TB treatment (Hawn *et al.*, 2013; Tobin, 2015; Rayasam and Balganes, 2015; Palucci and Delogu, 2018; Young *et al.*, 2020; Vyas and Goswami, 2017). In addition, Mtb clearance could be achieved by two potential strategies; i) by improving the immune response to eliminate Mtb, and ii) by suppression inflammation through a 'target organ-saving strategy' (Zumla *et al.*, 2015).

Several reports have demonstrated the potential use of the antidiabetic agent metformin as a repurposed host-directed therapeutic adjuvant to antitubercular treatment. Metformin was able to decrease inflammation and lung damage, improve immune response, and shorten the standard anti-TB regimen (Singhal *et al.*, 2014; Degner *et al.*, 2017; Naicker *et al.*, 2020). Another interesting example of HDTs is cytokine modulation, particularly administering anti-TNF therapies including etanercept (a soluble TNF receptor) (Young *et al.*, 2020) which demonstrated that TNF inhibition could lead to rapid clearance of Mtb from the lung and alter the balance of inflammation to benefit the host (Wallis *et al.*, 2004; Wallis *et al.*, 2009). TNF- α

inhibitor etanercept in combination with first-line TB- drugs enhanced bacterial clearance in a murine model (Skerry *et al.*, 2012; Bourigault *et al.*, 2013).

Plant extracts and/or their constituents could be used as adjuncts HDTs in TB treatment. Adhvaryu *et al* (2008) evaluated the effect of *Curcuma longa* in combination with *Tinospora cordifolia* in anti-TB drug-induced hepatotoxicity in TB-patients. The group that received combination therapy showed a decrease in the incidence and severity of hepatotoxicity, as well as a decrease in serum levels of aspartate transaminase, alanine transaminase, and serum bilirubin when compared to the control group. The researchers suggested that this combination could be an adjunct to standard TB treatment in TB patients.

Curcumin is a polyphenol responsible for the bright yellow-orange colour of *Curcuma longa*. Singha *et al* (2012) reported on the protective effect of curcumin and silymarin (from *Silybum marianum*) on antitubercular drug-induced hepatotoxicity using an *in vitro* model of the human hepatocellular carcinoma cell line (HepG2). The presence of curcumin/silymarin during treatment of HepG2 cells with anti-TB drugs lowered the hepatotoxic effect of the drugs. This was observed in terms of increased cell viability, healthier-looking cell morphology. Curcumin has also been shown to enhance the clearance of Mtb in differentiated THP-1 human monocytes, and in primary human alveolar macrophages. Curcumin also inhibits NFκB activation (Bai *et al.*, 2016). Such results suggest that curcumin as well as other phytochemicals need to be further investigated as potential adjunct therapies to anti-TB regimens.

1.7.2 Adjunct pathogen-directed therapies (PDTs): Protein kinase G from *M. tuberculosis* (MtPknG) as a target for new antitubercular agents

Virulence factors that are essential for pathogenicity or virulence of Mtb have been proposed as potential drug targets for the development of novel TB drugs. Promising candidates are mycobacterial virulence factors mainly involved in the interaction of Mtb with the host macrophages, particularly protein kinases such as protein kinase G (PknG) (Forrellad *et al.*, 2013).

As Mtb enters the body *via* the respiratory route, alveolar macrophages in the lungs are the first line of defence for the host to combat this pathogen by phagocytosis. Normally, bacterial infections are resolved by innate immune cells such as neutrophils

and macrophages which take up bacteria by phagocytosis leading to digestion by the lysosomal enzyme system. This results in the elimination of bacteria and the resolution of infection. The challenge with tuberculosis infection arises from the fact that the host's immune system is not able to eliminate Mtb as it is for other bacteria. Instead, Mtb is able to survive within alveolar macrophages, and to tolerate the intracellular environment where it remains metabolically inert and enters a clinically silent status known as the latent state of infection, from which the bacteria can be constantly re-activated (Ernst, 2012; O'garra *et al.*, 2013).

Eleven different serine/threonine kinases have been reported in mycobacteria. These enzymes, including protein kinase G (*MtPknG*), play important roles in several pathways essential for Mtb's survival and pathogenesis (Av-Gay and Everett, 2000). Protein kinase G is secreted when Mtb is within macrophages. It can inhibit phagosome-lysosome fusion and mediate the intracellular survival of mycobacteria. Mycobacteria overexpressing a kinase mutant of PknG are transferred to lysosomes and killed. This illustrates that PknG activity is important for mycobacterial survival within macrophages. Inactivation of PknG by gene disruption or chemical inhibition of PknG activity results in bacteria which are more susceptible to intracellular degradation (Walburger *et al.*, 2004b). As PknG is essential to mycobacterial virulence by blocking phagosome–lysosome fusion, it is an attractive drug target.

Once inside the host's macrophages, Mtb is able to develop multiple strategies to successfully evade degradative pathways (Ernst, 2012). One strategy of the Mtb is to inhibit the fusion of the lysosome with phagosomes *via* the expression and the release of the *MtPknG* enzyme. Indeed, blocking PknG activity triggers phagosolysosomal fusion and results in the elimination of Mtb from macrophages. This has been observed for a tetrahydrobenzothiophene derivative (AX20017) that has been identified as a novel PknG inhibitor but that has limited usefulness as a drug candidate due to its cytotoxicity toward host cells. The discovery of new potent and selective PknG-inhibitors could lead to the development of novel anti-TB drugs (Szekely *et al.*, 2008; Sundaramurthy and Pieters, 2007; Janssen *et al.*, 2012; Walburger *et al.*, 2004a).

With the continuous increase in the number of drug-resistant TB cases, it is important to develop new drugs that have the ability to selectively inhibit novel bacterial targets. To avoid toxicity, it would be desirable if the target of inhibition is present in Mtb but

not in the host. As shown above, *MtPKnG* is a virulence *Mtb* factor which has been identified as druggable target for the development of novel anti-TB drugs.

In this study, a guided molecular docking approach using Vina was used to predict the binding affinity (and molecular interactions) of selected phytochemicals isolated from four plants (*Pelargonium sidoides*, *Pelargonium reniforme* , *Fraxinus excelsior*, and *Stachys arabica*) with *MtPKnG*.

1.8 Aims and objectives

The purpose of this study was to evaluate some phytochemicals isolated from a European plant (*Fraxinus excelsior*), a Jordanian plant (*Stachys arabica*), and two South African plants (*Pelargonium sidoides* and *Pelargonium reniforme*) for their potential as templates for new anti-TB drugs, as well as to assess their immunomodulatory effects that may be relevant to combat TB. This was achieved through a combination of experimental (phytochemical/biological) laboratory work, and virtual screening (molecular docking). The investigated plants were selected using ethno-guided and/or chemotaxonomical approaches.

The objectives of the work were to;

- Carry out a detailed phytochemical investigation of *Fraxinus excelsior* leaves, and *Stachys arabica* aerial parts
- Screen *Fraxinus excelsior*/*Stachys arabica* extracts, and selected isolated phytochemicals, for *in-vitro* activity as follows;
 - THP-1 and/or K562 cell viability using an MTT assay
 - Immunomodulatory activity: production of pro-inflammatory cytokines involved in the control of Mtb infection (TNF- α , IL-12) from LPS stimulated THP-1 cells using ELISA
- Perform molecular docking studies of selected phytochemicals from *Fraxinus excelsior*, *Stachys arabica*, and *Pelargonium sidoides/reniforme* towards M ϕ PknG

CHAPTER TWO:

MATERIALS AND METHODS

2. Materials and Methods

2.1 General

2.1.1 Solvents, chemicals and consumables used in phytochemical work

The solvents listed below were used in the extraction procedure of the plant material, chromatographic separation, and TLC. They were obtained in 2.5 L amber glass bottles from Fisher Scientific UK or VWR (UK). All the solvents were stored at room temperature and transferred to 500 mL solvent bottles for regular use

Solvents- extraction and chromatographic analyses

- Acetone (HPLC grade)
- Acetic acid glacial (laboratory reagent grade)
- Ethyl acetate (laboratory reagent grade)
- Ethanol, analytical reagent grade > 99.8%
- *n*-Hexane (HPLC grade)
- Methanol ((laboratory reagent grade)
- Dichloromethane (laboratory reagent grade)
- Petroleum ether (laboratory reagent grade)
- Sulfuric acid (ACS reagent, Sigma-Aldrich, UK)

Solvent- NMR analysis:

- Chloroform-d, CDCl₃ (99.9 % purity) from Sigma- Aldrich

Chemicals, reagents, and consumables

- *p*-Anisaldehyde (Sigma-Aldrich, UK)
- Lipophilic Sephadex® LH20100; (Sigma-Aldrich, UK)
- Silica gel 60 (0.063-0.200 mm; for column chromatography, 70-230 mesh ASTM, Merck, Germany)
- Silica gel 60 H (for TLC;200-300 mesh; Merck, Germany)
- TLC silica gel 60 F₂₅₄ Aluminium sheets (20 x 20 cm; Analytical chromatography, Merck, Germany)
- Filter paper QL 100 (qualitative, 125 mm diameter; Fisher, UK).

2.1.2 Solvents, chemicals and consumables used in biology work

Solvents

- Dimethyl Sulfoxide (DMSO), Sigma-Aldrich (UK)
- Ethanol, analytical reagent grade > 99.8%, Fisher Scientific (UK)

Chemicals and reagents

- Foetal Bovine Serum (FBS), Biosera (UK)
- L-Glutamine solution, Sigma-Aldrich (UK)
- MTT (Thiazolyl Blue Tetrazolium Bromide), Sigma-Aldrich (USA)
- Phosphate buffered saline (PBS), Lonza (Belgium)
- RPMI-1640 culture medium 1X, Corning (USA)
- RPMI-1640 culture medium without phenol red, 1X, Gibco (UK)
- Sodium Dodecyl sulphate (SDS), Sigma-Aldrich (USA)
- Triton X-100, 100 mL, Fisher Scientific (USA)
- Trypan blue solution (0.4%), Sigma-Aldrich (UK)

- Pure compounds: Oleanolic acid and Ursolic acid were obtained from Fisher Scientific (UK). Pinocembrin was obtained from Sigma-Aldrich (UK)

Consumables

- Cell culture flasks (75 cm²), Corning (USA)
- Cryo tube vials, Nunc(Denmark)
- Eppendorf -Microcentrifuge tubes (1.5ml), Star Lab (UK)
- F 16 Maxisorp loose Nunc- Immuno modules, Thermo Fisher Scientific (Denmark)
- Graduated tips (200 µL yellow tips, 1000 µL blue tips), Tip one, Star Lab (USA)
- Serological Pipettes (5, 10 & 25 mL), SARSTEDT (France).
- Sterile centrifuge tubes (15 & 50 ml), Corning (Mexico).
- Sterile universal tubes (30ml), Elkay Lab Products (UK).
- Tissue culture plates (24 and 96 well), Techno Plastic Products; TPP (Switzerland, Europe)

2.1.3 Cell lines and modulator

- Human myeloid leukaemic cell line K-562 Cells, European Collection of Authenticated Cell Cultures; (ECACC 89121407).
- Human Monocyte leukaemia cell line THP-1 Cells, European Collection of Authenticated Cell Cultures; (ECACC 88081201)
- Lipopolysaccharide (LPS; from *E.coli*), Sigma-Aldrich

2.1.4 Enzyme-linked immunosorbent assay (ELISA) materials

- Bovine serum albumin (BSA), Boehringer Mannheim GmbH (Germany).
- Disodium hydrogen orthophosphate anhydrous (Na_2HPO_4), Laboratory reagent grade >99%, Fisher Scientific (UK).
- Potassium chloride (KCL), Laboratory reagent grade >99%, Sigma-Aldrich (UK).
- Potassium dihydrogen orthophosphate (KH_2PO_4), Analytical grade, Fisher Scientific (UK).
- Sodium chloride (NaCl), >99.5%, Fisher Scientific (UK).
- Streptavidin-HRP conjugate, ELISA grade, Invitrogen (USA).
- Sulphuric acid (H_2SO_4), Sigma-Aldrich (UK).
- TMB stabilized chromogen, Invitrogen (USA).
- Tween-20, for molecular biology, Sigma-Aldrich (USA)

Immunoassay kits:

- Human IL-12p40 CytoSet™ (CHC1563) Invitrogen, by Thermo Fisher Scientific (USA)
- Human TNF- α CytoSet™ (CHC1753) Invitrogen, by Thermo Fisher Scientific (USA)

2.1.5 Equipment and Instruments

- Balance, Sartorius basic and portable BA210S (Germany, Europe).
- Centrifuge, Heraeus Multifuge 3S-R, Thermo Electron Corporation (Germany).
- Distilled water (D.H₂O) machine, Purite, Select, Neptune, Water Purification Systems. Life science (UK).
- Haemocytometer, Neubauer Improved B.S.748, 0.100 mm (Germany).
- Incubator (Carbon dioxide (CO₂)), Galaxy S, Sanyo (UK) and Function line, Thermo Scientific
- Incubator (37°C), Heraeus, thermo Scientific.
- Microscope, Nikon TMS (UK).
- pH- meter, Mettler Toledo (UK).
- Plate Reader, Spectra Max 119, Molecular Devices (USA).
- Rota mixer, Hook & Tucker Whirlimixer (UK).
- Pipetman P-20, P-200, and P-1000, Gilson (France).
- Vortex mixer, Fisons Whirlimixer (UK)

2.1.6 Software packages and databases used in the molecular docking study

2.1.6.1 SciFinder or SciFINDER

SciFinder: (<https://www.cas.org/products/scifinder>) is a web-based search engine which helps users to easily search the Chemical Abstracts Databases. Searches can be done by topics, author names, substances, and chemical identification such as structure, reactions, molecular formula. Moreover, this database allows the user to analysis, refine, and categorise their search results as well as saving, printing, and exporting the desired results. This database is produced by CAS, a division of the American Chemical Society. It is a core research tool for scientific disciplines.

2.1.6.2 BIOVIA Discovery Studio Visualizer v.4.5 (Dassault Systèmes, formerly Accelrys)

BIOVIA Discovery Studio Visualizer <http://accelrys.com/products/collaborative-science/biovia-discovery-studio/>) is a software which includes many tools for viewing and editing molecular structures, analysing docking results, understanding ligand–protein interactions, and generating 2D protein-ligand interaction plots.

2.1.6.3 ChemOffice

ChemOffice is a software that contains ChemDraw Professional 16.0 (a tool to draw chemical structures), and Chem 3D 16.0 (a tool to visualize and analyse 3D models of chemical structures, and to run/calculate MM2 energy minimisation for ligand geometry optimisation).

2.1.6.4 MGL Tools

MGLTools (<http://mgltools.scripps.edu/>) is a software developed by the Molecular Graphics Laboratory (MGL) of The Scripps Research Institute (USA) to visualise and analyse molecular structures. This package consists of three main applications. One of these applications is Auto Dock Tools v.1.5.6.

AutoDock Tools (ADT 1.5.6) is a graphical user interface (GUI) for AutoDock that allows the user to add hydrogen atoms, assign partial atomic (Gasteiger) charges, make rotatable bonds non-rotatable, set up AutoGrid Parameter File (GPF) using a visual representation of the grid box, prepare the ligand and the macromolecule as pdbqt files for further docking application. AutoDock is a molecular modelling simulation software (<http://autodock.scripps.edu/>). It consists of two generation of software: AutoDock 4 and an improved version called Auto Dock Vina.

AutoDock Vina (also known as Vina, web site: <http://vina.scripps.edu/>) is part of a relatively new generation of docking software developed by MGL. It is faster, easier to use and generally gives better performance and accuracy than AutoDock 4

2.1.6.5 Protein Data Bank

The Protein Data Bank (PDB) (<http://www.rcsb.org>) is a free crystallographic database that provides information (typically obtained by X-ray or NMR spectroscopy) about the 3D structures of large biological molecules, such as proteins and nucleic acids.

2.2 Plant material

Fraxinus excelsior leaves were purchased from the herbal supplier G. Baldwin & Co, UK. The dried leaves were ground to a fine powder using a grinder (IKA model A 11 basic, analytical mill) prior to extraction.

Stachys arabica was collected from the Al-mughayer and Rahoob regions of Irbid (Jordan) in April 2018 by Dr Mohammad Al-Garaibah (plant taxonomist at the Department of Natural Resources & Environment, Jordan University of Science and Technology). The fresh plant material was left to dry at 25 °C, and then ground to a fine powder using an analytical mill. All plant material was packed in paper bags. A voucher specimen has been deposited at the Herbarium of the Faculty of Pharmacy at Jordan University of Science and Technology.

Part A: Phytochemical study

2.3 Extraction

All plants subjected to phytochemical investigation were given a serial code number as illustrated in Table 2.1.

Table 2.1 Plant material used for the phytochemical investigation

Plant material	Code given	Part used	Dry weight (g)
<i>Fraxinus excelsior</i>	370	Leaves	500
<i>Stachys arabica</i>	390	Aerial parts	500

The dried plant material was sonicated using a Decon® sonicator for 1h at room temperature, using solvents of increasing polarity (starting with *n*-hexane followed by ethyl acetate and methanol).

All extracts obtained were filtered using a qualitative filter paper (240 mm; Fisher brand Fisher Scientific UK,) then evaporated at <40°C under vacuum using a rotary evaporator (BÜCHI R-205). All dried extracts were kept in sealed glass vials and stored at -20 °C before further analysis.

2.4 Chromatographic techniques

2.4.1 Vacuum liquid chromatography (VLC)

The set up used in VLC consisted of a glass vacuum filter funnel with a sintered disc (porosity 3) connected to an appropriate receiving flask and a vacuum pump. Silica gel 60 H was packed into a sintered glass funnel of a suitable size and tapped manually to eliminate any major air pockets. The silica surface was pressed gently under vacuum to obtain a uniform level for a well-compacted column (around 5 cm in height). The column was then eluted with *n*-hexane to check for voids and channels and to ensure packing had been done correctly, then the silica was allowed to dry under vacuum.

The plant extract was re-dissolved in a minimum volume of a suitable solvent. Silica gel 60 (mesh size 0.063-0.200 mm) was added to the extract and this mixture was left

to dry at room temperature until a dried powdered extract was obtained. This was transferred into a clean evaporating dish and ground to a free-flowing fine powder using a glass mortar. This powder was loaded carefully onto the column, spread evenly as a thin uniform layer on top of the silica and covered with cotton wool. Elution was started with *n*-hexane followed by ethyl acetate/*n*-hexane mixtures of increasing polarity (0-100% EtOAc in hexane (v/v) with increments of 5 – 10%) and finally with mixtures of ethyl acetate and methanol (up to 50% methanol in ethyl acetate). The column was allowed to dry completely between fractions to improve resolution and the separation of compounds. The collected fractions were evaporated to dryness at <40 °C under reduced pressure using a rotary evaporator. After that, the fractions were checked by thin layer chromatography (TLC) and pooled according to similar chemical profiles (Targett *et al.*, 1979; Coll and Bowden, 1986; Pedersen and Rosenbohm, 2001).

2.4.2 Thin layer chromatography (TLC)

TLC was used to screen the plant extracts for the presence of phytochemicals. TLC analyses were performed using aluminium-supported silica gel 60 F₂₅₄ TLC plates (Merck). Samples were dissolved in an appropriate solvent. A small amount of the sample to be examined was spotted using a capillary spotter about 1.5 cm above the bottom edge of a TLC plate. The samples were spotted away from the TLC plate edges and from each other to minimise any overlapping. The spotting pattern was as narrow bands to achieve an accurate and easy visualisation of compounds and to prevent tailing (Bele and Khale, 2011).

The TLC plate was immersed into a shallow pool of solvent (mobile phase) in a developing chamber. A filter paper was placed inside the chamber to help develop a uniform rise of the mobile phase on the plate. When the mobile phase reached the top of the plate, the plate was removed from the developing chamber, and the solvent was allowed to evaporate. Solvent systems such as *n*-hexane/ethyl acetate, dichloromethane/ethyl acetate in different ratios were used as mobile phases.

The plates were visualised under a UV light (Mineral light® lamp, multiband UV 254/366 nm, USA) under short and long wavelength ($\lambda = 254$ nm and $\lambda = 366$ nm, respectively). Short UV is useful for the detection of aromatic compounds while

compounds with conjugated double bonds are visible under long UV light. Then, plates were sprayed with the anisaldehyde-sulfuric acid reagent which allows the visualisation of a range of compounds including phenols, terpenes, sterols, pigments and sugars. This was done using a spraying vessel which dispersed the reagent solution through a fine mist. The TLC plate was placed vertically inside a spraying chamber in a fume hood, and evenly sprayed from a convenient distance with the spraying solution. Heating to 110 °C for approximately 5 minutes using a drying oven was done to accelerate the colour formation. It is good practice to perform two visualisation techniques, such as UV detection and reagent spraying, to maximise the detection of as many compounds as possible (Gibbons, 2012; Matysik *et al.*, 2016).

2.4.3 Column chromatography (CC)

2.4.3.1 Size exclusion chromatography (SEC)

The following protocol was followed:

- i. Column preparation: For non-polar fractions, Sephadex LH-20 was soaked in a solution of 5% *n*-hexane in dichloromethane, or 100% dichloromethane for medium-polarity extracts, and left overnight to allow the Sephadex LH-20 to swell. Once ready, the slurry was poured and packed in a glass column of appropriate size.
- ii. Sample application: Plant extracts were dissolved in a small volume of 5% *n*-hexane in dichloromethane or dichloromethane. The concentrated sample was loaded carefully at the top of the column by using a long Pasteur pipette taking care not to disturb the surface.
- iii. Elution and fractions collection: For non-polar fractions, elution was started with 5% *n*-hexane in dichloromethane. Dichloromethane only was used for medium-polar fractions. If needed, elution was continued with 100% dichloromethane or 5-10% methanol in dichloromethane, respectively. Eluents were collected in glass vials in a small volume (2-3 mL) and concentrated under vacuum. Upon completion, Sephadex LH-20 was washed with methanol several times and kept dried for further use.

2.4.3.2 Silica gel column chromatography (SiCC)

The following protocol was followed:

- i. Column preparation: Silica gel 60 (mesh size 0.063~0.200 mm) was used. The column was prepared using the wet method of packing using *n*-hexane to make a slurry. The slurry was then poured and packed in a glass column of appropriate size with tapping and opening the outlet valve. Excess hexane was added, and the stationary phase was allowed to settle down to ensure good packing of the column. The bottom of the column had a sintered glass frit or a cotton wool plug to support the stationary phase.
- ii. Sample application: Samples were dissolved in a minimum volume of mobile phase (hexane or other suitable solvent) and adsorbed on a small amount of silica gel 60 and, once a free-flowing powder, were loaded at the top of the column. A piece of cotton wool or filter paper was applied over the sample to ensure good separation and to prevent any damage to the surface of the column.
- iii. Elution and fraction collection: The elution was carried out with solvent systems of increasing polarity: (hexane/DCM) or hexane/EtOAc. For a non-polar extract (e.g., hexane extract): we used an initial mobile phase of 100% *n*-hexane, followed by 1%, 2% and 5% EtOAc in hexane, 10–100% EtOAc in hexane (increment of 10% in each), and 5–20% MeOH in EtOAc (increment of 5%). The eluted fractions were collected in glass vials, analysed by TLC, and pooled according to similar chemical profiles.

2.4.4 Flash chromatography (FC)

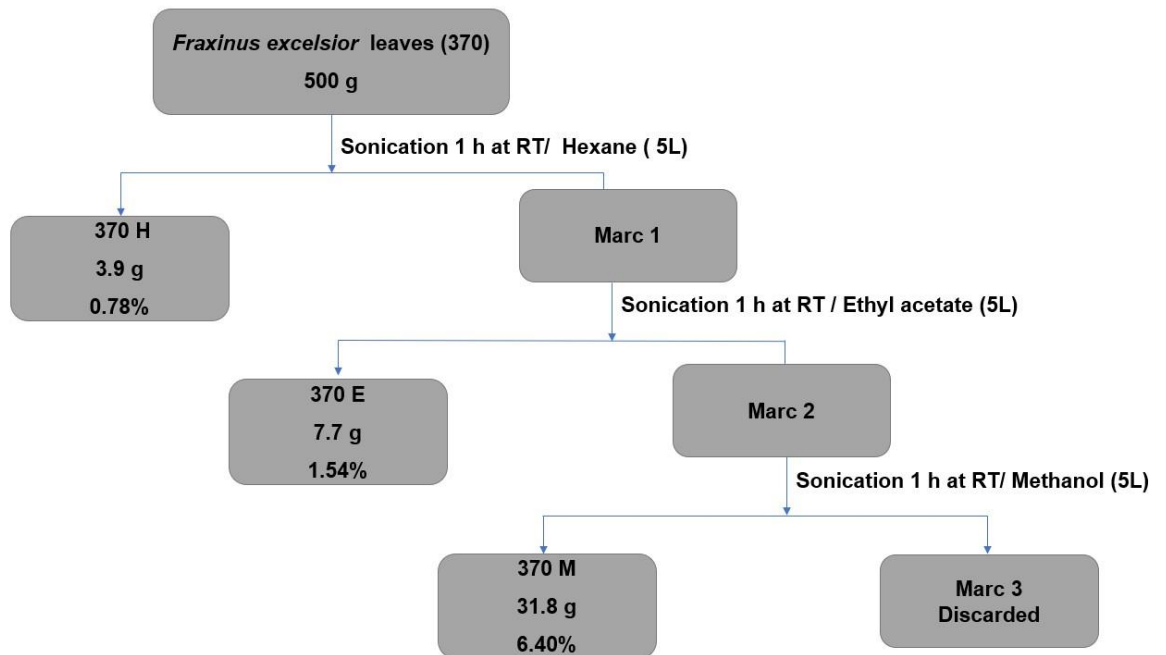
FC was performed on a SP4 Biotage® and the sample was loaded onto SNAP 50g prepacked cartridge. The elution was achieved at flow rate 40 mL/min (gradient elution of petroleum ether and ethyl acetate) as shown in table 2.2. The eluent was collected and monitored through UV-visible wavelength detector (254 and 319 nm, respectively).

Table 2.2 Gradient elution used in FC

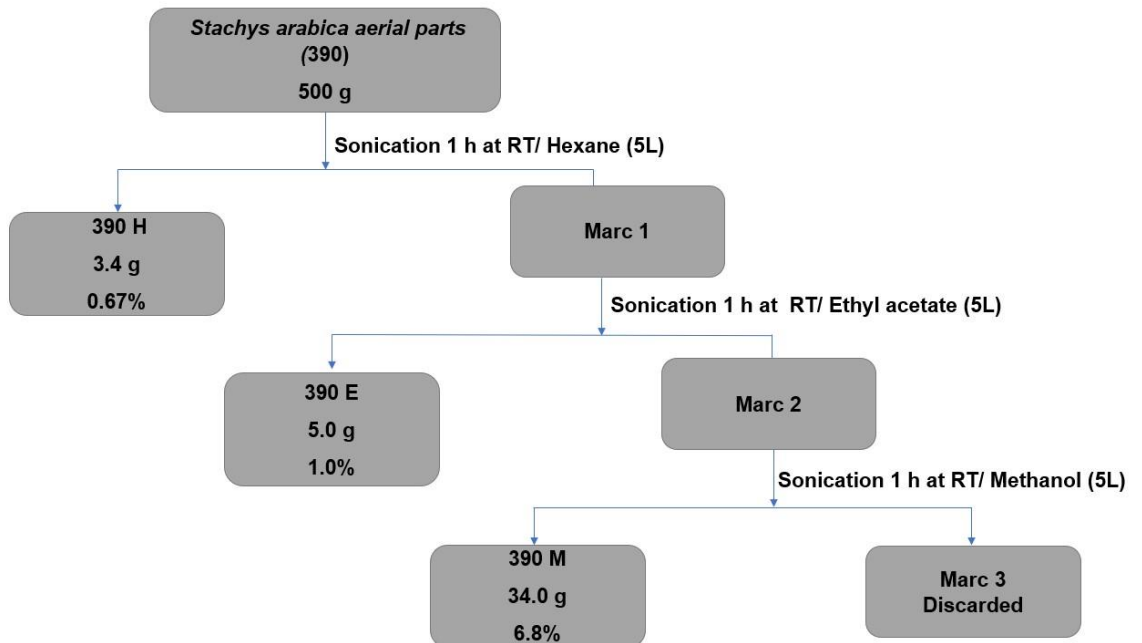
% Petroleum ether	% Ethyl acetate	Column Volume (CV)
100	0	2CV
100-50	0-50	21CV
50	50	5CV
50	50	7CV

2.5 Extraction and isolation protocols

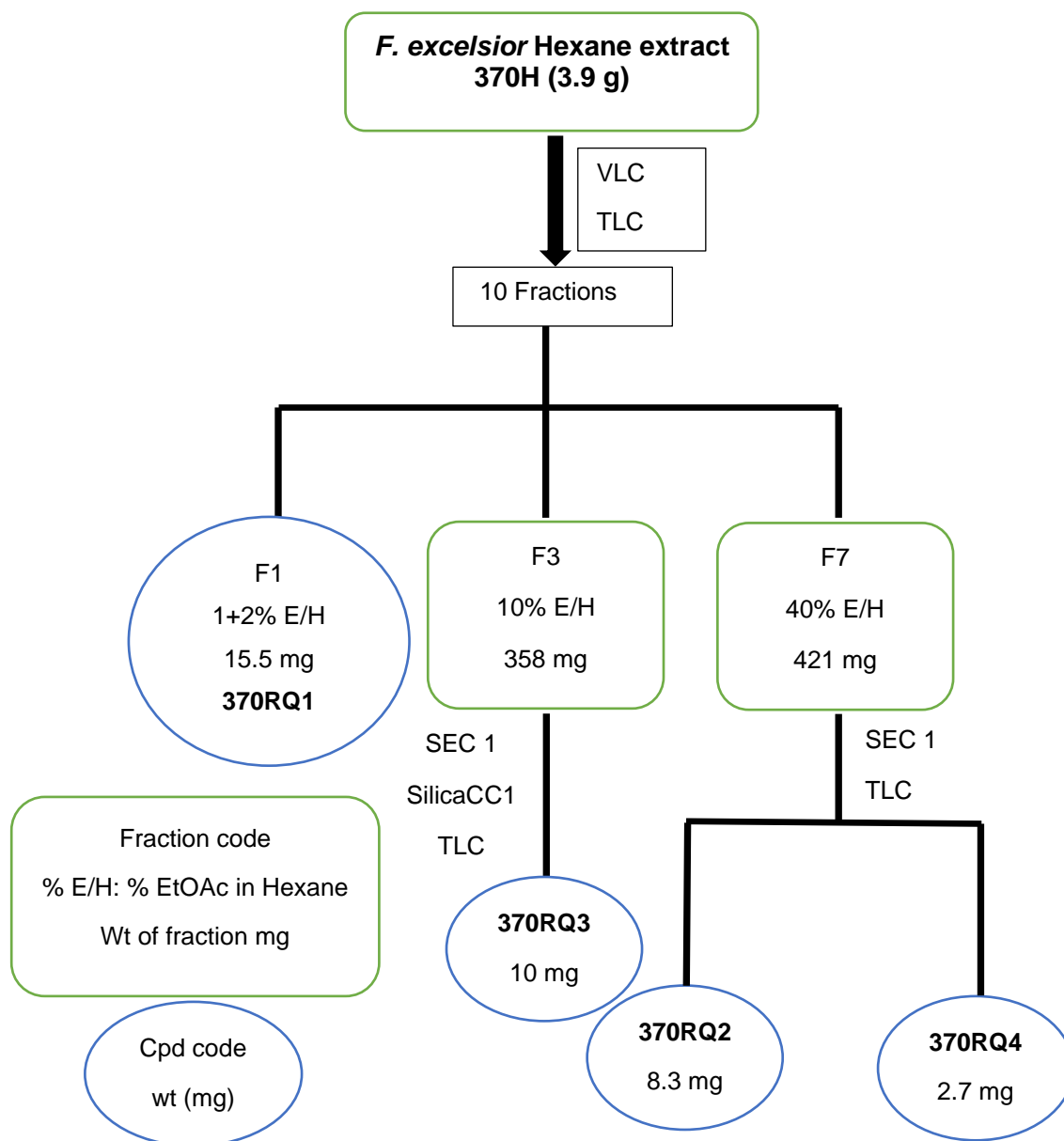
a-



b-

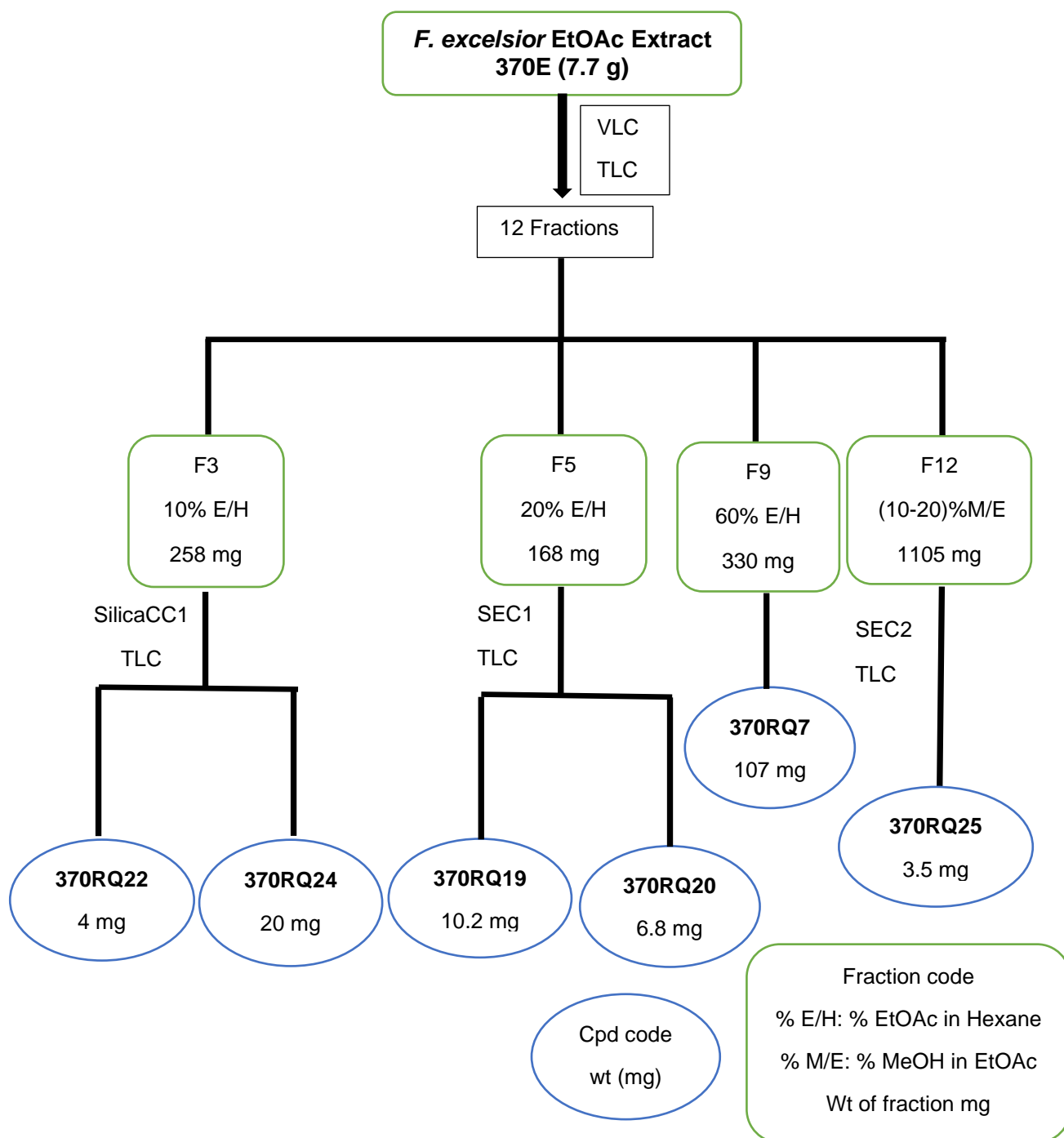


Protocol 1: Large-scale extraction of a- *Fraxinus excelsior* leaves (370), b- *Stachys arabica* aerial leaves (390)



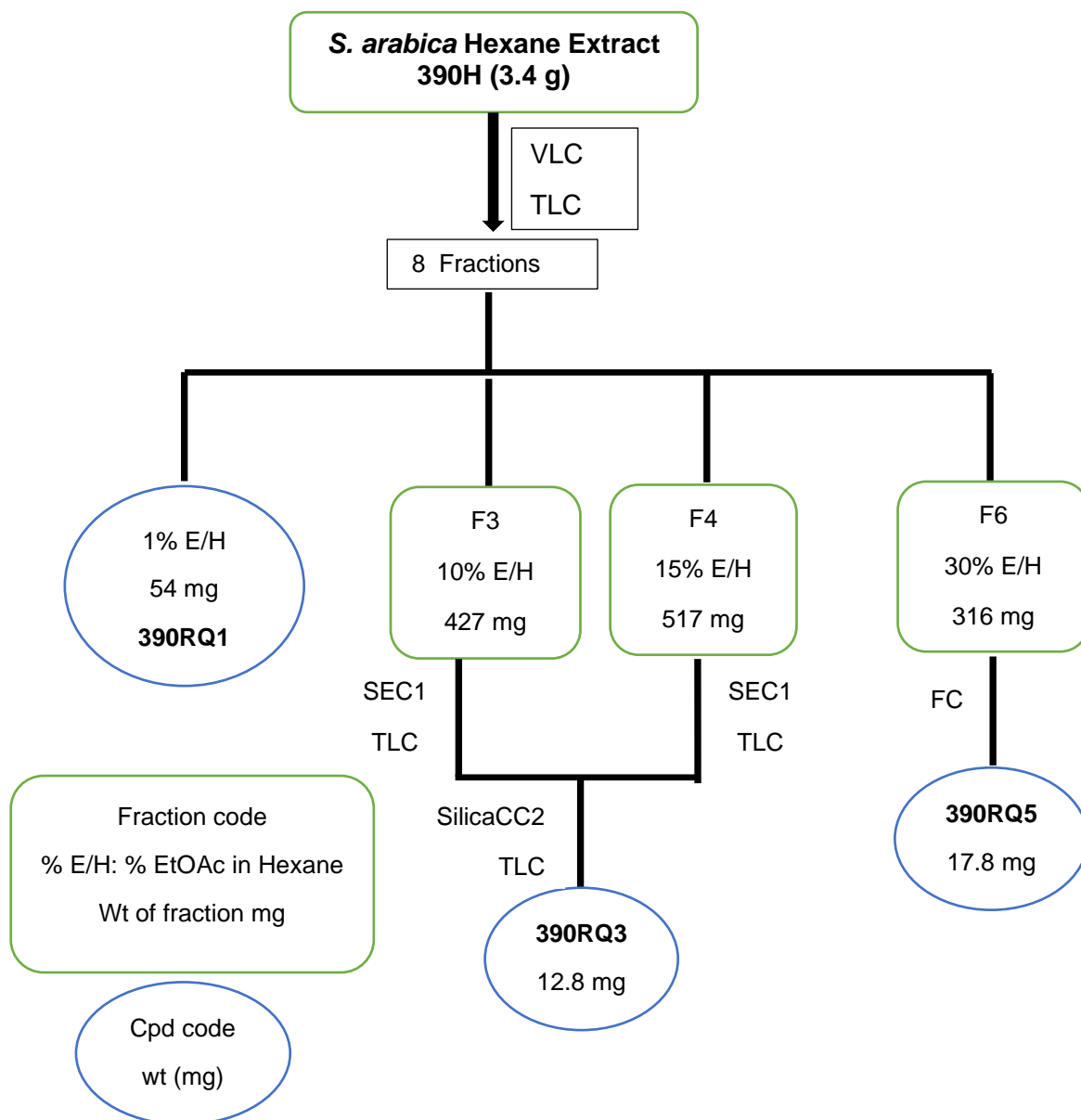
VLC: elution with 100% *n*-hexane, followed by *n*-hexane- EtOAc mixtures of increasing polarity (200 mL used for each solvent fraction), column size 7 cm (ø) ×10 cm. SEC1: elution with 5% *n*-hexane in DCM, followed by 100% DCM. Silica CC1: elution with 100% *n*-hexane, followed by *n*-hexane- EtOAc mixtures of increasing polarity.

Protocol 2: Fractionation and isolation of phytochemicals from the *n*-hexane extract of *Fraxinus excelsior* leaves (370H)



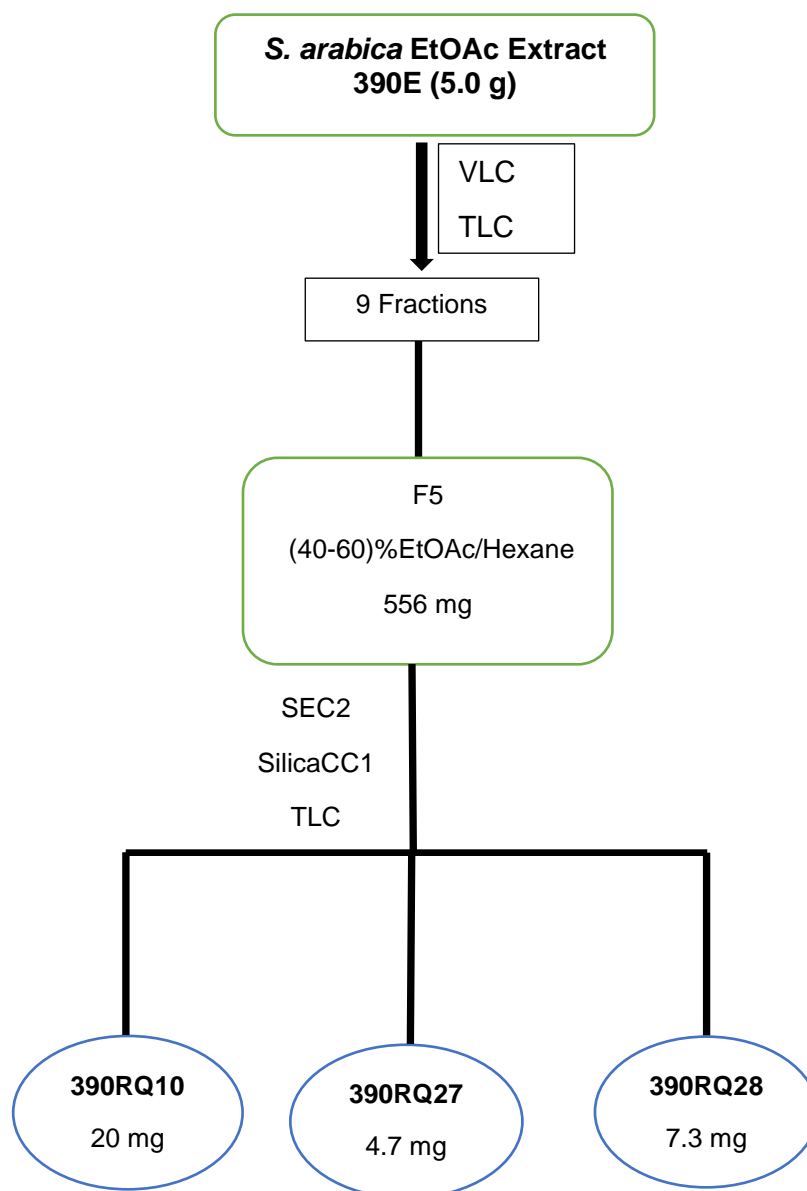
VLC: elution with 100% *n*-hexane, followed by *n*-hexane- EtOAc and then EtOAc-MeOH mixtures of increasing polarity (300 mL used for each solvent mixture), column size 7 cm (ø) ×13 cm. SEC1: elution with 5% *n*-hexane in DCM, followed by 100% DCM. SEC2: elution with 100% DCM, followed by 5 & 10% MeOH in DCM. Silica CC1: elution with 100% *n*-hexane, followed by *n*-hexane- EtOAc mixtures of increasing polarity.

Protocol 3: Fractionation and isolation of phytochemicals from the ethyl acetate extract of *Fraxinus excelsior* leaves (370E)



VLC: elution with 100% *n*-hexane, followed by *n*-hexane- EtOAc of increasing polarity (200 mL used for each fraction), column size 7 cm (\varnothing) \times 10 cm. SEC1: elution with 5% *n*-hexane in DCM, followed by 100% DCM. Silica CC2: elution with 100% *n*-hexane, followed by *n*-hexane-DCM mixtures of increasing polarity. FC: gradient elution of petroleum ether and EtOAc.

Protocol 4: Fractionation and isolation of phytochemicals from the *n*-hexane extract of *Stachys arabica* aerial parts (390H)



VLC: elution with 100% *n*-hexane, followed by *n*-hexane- EtOAc and then EtOAc-MeOH mixtures of increasing polarity (300 mL used for each solvent mixture), column size 7 cm (ø) ×13 cm. SEC2: elution with DCM. Silica CC1: elution with 100% *n*-hexane, followed by *n*-hexane- EtOAc mixtures of increasing polarity.

Protocol 5: Fractionation and isolation of phytochemicals from the ethyl acetate extract of *Stachys arabica* aerial parts (390E)

2.6 Structure elucidation

2.6.1 NMR spectroscopy

All NMR spectra were recorded at the Department of Pure and Applied Chemistry (University of Strathclyde) using either a Bruker Avance III AV500 NMR spectrometer operating at 500MHz for ^1H NMR and 125 MHz for ^{13}C NMR, or a Bruker Avance AV400 NMR spectrometer operating at 400MHz for ^1H NMR and 100 MHz for ^{13}C NMR. A Bruker Avance III AV600 instrument was also used in some cases (600 MHz for ^1H NMR and 150 MHz for ^{13}C NMR).

Norell® NMR tubes (5 mm), purchased from Sigma-Aldrich, were used for regular NMR analyses. The samples were dissolved in 0.6-0.75 mL of deuterated chloroform (CDCl_3) and placed in NMR tubes. NMR experiments of low weight samples (< 5 mg) were carried out using Shigemi NMR tubes (Sigma-Aldrich) and Norell® microbore NMR tube (Sigma-Aldrich). The samples were dissolved in 0.3 mL of deuterated chloroform (CDCl_3) and placed in Shigemi/Norell® microbore tubes. The solvent CDCl_3 was used as an internal standard, and its signals were used for calibration (δ_{H} 7.27 & δ_{C} 77.23). All spectral data were processed using the MestReNova® software (version 14). The spectra of all known compounds were identified by comparing with previously published data.

2.6.2 Mass spectrometry (MS)

High resolution accurate mass spectra were recorded at the National Mass Spectrometry Facility (NMSF) at Swansea University (UK) (Appendix II). Positive and negative ion mode nano-electrospray experiments were carried out on an Orbitrap (LTQ Orbitrap XL). Atmospheric solids analysis probe (ASAP) analyses were conducted using a Time-of-flight (TOF) mass spectrometer on Waters Xevo G2-S. GC/EI-MS analysis was carried out on Waters GCT Premier (TOF).

Preliminary GC-MS analysis for 390RQ5 was done at the Department of Pure and Applied Chemistry (University of Strathclyde). The sample was identified by matching its mass spectra with reference spectra using the NIST08 MS database. Further analysis was carried out at NMSF where the sample was derivatized to trimethylsilyl (TMS) ethers followed by HR-GC-EI-MS on Waters GCT Premier (TOF-MS).

Part B: Biological studies

2.7 Cell viability assessment using colorimetric MTT assay

The *n*-hexane, ethyl acetate (EtOAc) and methanol (MeOH) crude extract of both *F. excelsior* leaves and *S. arabica* aerial parts were evaluated for their effects on the viability of two cancer cell lines: the K562 human myeloid leukemic cell line (ECACC 89121407) and the THP-1 human monocytic leukemic cell line (ECACC 88081201) using an MTT-based cell viability assay. In addition to that, selected isolated phytochemicals were also examined on THP-1 cells to evaluate their effect on cell viability using the MTT assay. Measurements were carried out 24 hours after adding the treatments, then the cell viability was assessed and IC₅₀ values were determined.

2.7.1 Cell culture

All cell culture work was performed in a laminar airflow cabinet following strict aseptic technique.

2.7.1.1 Preparation of culture medium

The growth medium (known as culture or complete medium) for both cell lines was prepared in a sterile flow hood and stored at 4°C until required. Both cell lines were grown in RPMI 1640 medium supplemented with 10% (v/v) FBS, and 1% (v/v) L-glutamine (as medium was supplied glutamine-free to prevent degradation).

2.7.1.2 Preparation of K562 cells for experimental use

K562 cells were incubated in 75 cm² culture flasks containing growth medium at 37°C, 5% (v/v) CO₂ and 100% humidity, and the growth media replaced every 5-7 days. When the cells reached ≈ 80% confluence, they were collected for experimental work by transferring them into 30 mL sterile universal tubes, and centrifuged at 400 g x 6 minutes at 22°C. The media was discarded, leaving the pellet. The pellet was resuspended in appropriate volumes of PBS. K562 cells were counted using a haemocytometer for seeding density of approximate 5 × 10⁶ cells/mL for experimental use.

2.7.1.3 Preparation of THP-1 cells for experimental use

THP-1 cells were incubated in 75 cm² culture flasks containing growth medium at 37°C, 5% (v/v) CO₂, and 100% humidity, and the growth media replaced every 2- 3 days. When the cells reached ≈ 80% confluence, they were collected for experimental work by transferring them into a 30 mL sterile universal tubes and centrifuged at 400 g x 6 minutes at 22°C. The media was discarded, leaving the pellet. The pellet was resuspended in an appropriate volume of RPMI-1640 culture medium without phenol red. THP-1 cells were counted using a haemocytometer for seeding density of approximate 5 × 10⁵ cells/mL for experimental use.

2.7.1.4 Storage and recovery of THP-1 cells

When THP-1 cells reached 80% confluence, and not required directly for experimentation, the cells were centrifuged at 400 g x 6 minutes at 22°C. The supernatant was discarded, and the cells resuspended in cryopreservation medium which was prepared as 5% DMSO and 95% foetal bovine serum (FBS) and stored in a Cryo tube at -80°C until further recovery use.

Each vial of cells stored at -80°C was thawed rapidly in a water bath at 37°C and transferred into 10 mL of growth medium in a 15 mL centrifuge tube and centrifuged at 400 g x 6 minutes at 22°C. The supernatant was discarded, and the cells resuspended in 10 mL fresh growth medium. The suspension was then transferred into 75 cm² flask containing 20 mL fresh growth medium and incubated in humidified air at 37°C containing 5% CO₂ and the growth media replaced every 2- 3 days.

2.7.2 Plant extracts and phytochemicals - sample preparation

Crude plant extracts were dissolved in DMSO to give a stock solution of 10 mg/200µL and were kept at -20°C. Further dilution to the required starting concentration (250,125, 62.5, 31.25, and 15.6 µg/mL) was carried out using sterile PBS for K562 cells -MTT assay and RPMI1640 medium without phenol red for THP-1 cells - MTT assay. Making sure that the concentration of DMSO in the tested dilutions was ≤ 0.5%. All the dilutions were carried out in a laminar airflow cabinet under sterile conditions.

Isolated phytochemicals and pure compounds were dissolved in DMSO to give a stock solution of 5.0 mg /100µL DMSO and were stored at -20°C. Further dilution to the required starting concentration (250,125, 62.5, 31.25, and 15.6 µg/mL) was carried out using RPMI1640 medium without phenol red for THP-1 cell - MTT assay. Making sure that the concentration of DMSO in the tested dilutions was ≤ 0.5%. All the dilutions were carried out in a laminar airflow cabinet under sterile conditions

2.7.3 Preparation of MTT assay solutions

5 mg/mL MTT solution: 75 mg of MTT (Thiazolyl Blue Tetrazolium Bromide) was dissolved in 15 mL phosphate buffered saline (PBS, pH 7.4). the solution was vortex vigorously and stored at 4°C.

10% SDS: 25.0 g of Sodium dodecyl sulphate (SDS) was dissolved in 250 mL distilled water and stored at room temperature.

2.7.4 Protocol used

2.7.4.1 K562 MTT assay protocol

K562 cells (70 µL) were placed in 96-well plates at a density of 5×10^6 cells/mL. The cells were exposed to 10 µL crude extracts in a concentration range of 0-250 µg/mL. Sterile PBS was added to each well to adjust the final volume to 100 µL in each well (Each concentration was tested in triplicates in a single experiment). The negative controls were prepared by incubating cells with PBS alone without extract (untreated cells with 0 and 0.5% DMSO). TX-100 (0.5%) was used as a positive control. Blank samples were carried out at same time/ experiment, where 10 µL crude extracts in a concentration range of 0-250 µg/mL were added to sterile 90-100 µL PBS in each well without cells. The plate was incubated at 37°C in a CO₂ environment for 22 h. Then the cells were treated with 12 µL of MTT (5 mg/mL) and incubated for 2-3 hours. Then, 150 µL of 10% SDS was added to each well to solubilize the purple formazan and incubated for 24h/ overnight at 37°C. Absorbance was measured at λ 570 nm using a plate reader.

2.7.4.2 THP-1 MTT assay protocol

THP-1 cells (70 μL) were placed in 96-well plates at a density of 5×10^5 cells/mL. The cells were exposed to 10 μL crude extracts/ isolated phytochemicals in a concentration range of 0-250 $\mu\text{g}/\text{mL}$. RPMI-1640 culture medium without phenol red was added to each well to adjust the final volume to 100 μL in each well (Each sample was carried out in a minimum of triplicates). The negative controls were prepared by using RPMI-1640 culture medium without phenol red alone (untreated cells with 0 and 0.5% DMSO). TX-100 (0.5%) was used as the positive control. Blank samples were carried out at same time/experiment, where 10 μL of crude extracts/ isolated phytochemicals in a concentration range of 0-250 $\mu\text{g}/\text{mL}$ were added to sterile 90-100 μL RPMI-1640 culture medium w/o phenol red in each well without cells. The plate was incubated at 37°C in a CO_2 environment for 22 h. Then the cells were treated with 12 μL of MTT (5 mg/mL) and incubated for 2-3 hours. After that, 150 μL of 10% SDS was added to each well to solubilize purple formazan and incubated for 24h/ over the night at 37°C. Absorbance was measured at λ 570 nm using a plate reader. At least three independent experiments were conducted

2.8 Measurement of Cytokine production using ELISA

Sandwich ELISA (Enzyme Linked Immunosorbent Assay) experiments were conducted to determine the concentration of pro-inflammatory cytokines (TNF- α and IL-12) in THP-1 cells following incubation with different treatments (various plant extracts and isolated phytochemicals) with and without LPS.

2.8.1 Preparation of THP-1 cells

THP-1 cells were incubated in 75 cm² culture flasks containing growth medium at 37°C, 5% (v/v) CO₂ and 100% humidity and the growth media replaced every 2- 3 days. When the cells reached \approx 80% confluence, they were collected for experimental work by transferring them into a 50 mL sterile universal tubes and centrifuged at 400 g x 6 minutes at 22°C. The media was discarded, leaving the pellet. The pellet was resuspended in an appropriate volume of RPMI-1640 culture medium. THP-1 cells were counted using a haemocytometer for seeding density of approximate 1×10^6 cells/mL for experimental use.

2.8.2 THP-1 cell incubation protocol

THP-1 cells were prepared in a volume of 300 μ L and placed into sterile 24-well cell culture plates. Where LPS (10 μ g/mL) was added this was in a 50 μ L volume. Solutions of different treatments of various concentration of plant extracts and pure compound (0-250 μ g/mL) were added in volumes of 50 μ L. RPMI-1640 medium was added to yield an adjusted final volume of 500 μ L in each well, Control samples consisted of THP-1 cells (300 μ L) with 50 μ L of LPS with 150 μ L RPMI-1640 medium (Each sample treatment was prepared in triplicate). The same experiment was also conducted without adding LPS, where the unstimulated control consisted of THP-1 cells (300 μ L) in RPMI-1640 medium (200 μ L) without any treatments and the samples consisted of 300 μ L THP-1 cells, 50 μ L of the treatment and RPMI was added to yield a final volume of 500 μ L in each well. The plates were incubated at 37°C, 5% CO₂ with 100% humidified air for 20-22 hours. Following incubation, supernatants were collected and transferred into sterile labelled 1.5mL Eppendorf tubes for further analysis. If not used immediately, the samples were stored at -20°C until required.

2.8.3 Preparation of plant extracts and isolated phytochemicals for experimental use

The plant extracts were dissolved in DMSO to give a stock solution of 10 mg/200 μ L and were stored at -20°C . Further dilution to the required starting concentration (250, 125, 62.5, 31.25, and 15.6 $\mu\text{g}/\text{mL}$) was carried out using RPMI1640 medium. The concentration of DMSO in the tested dilutions was always $\leq 0.5\%$. All dilutions were carried out in a laminar airflow cabinet under sterile conditions.

The isolated phytochemicals and pure compounds were dissolved in DMSO to give a stock solution of 5.0 mg /100 μ L DMSO, and were stored at -20°C . Further dilution to the required starting concentrations (250, 125, 62.5, 31.25, and 15.6 $\mu\text{g}/\text{mL}$) was carried out using RPMI1640 medium. The concentration of DMSO in the tested dilutions was always $\leq 0.5\%$. All dilutions were carried out in a laminar airflow cabinet under sterile conditions.

Different sample dilutions with assay buffer were carried out for the IL-12 ELISA experiments in order to have analyte levels within the range of the conducted assay.

2.8.4 Preparation of ELISA buffers and solutions

ELISA buffers and solutions were prepared as following:

Coating buffer (10X): 40.0 g of NaCl, 5.6 g of Na_2HPO_4 , 1.0 g of KH_2PO_4 and 1.0 g of KCl were dissolved in 500 mL of distilled water.

Coating buffer (1X): 50.0 mL of coating buffer (10X) added to 450 mL distilled water (pH 7.4)

Wash buffer: 0.5ml of Tween-20 added to 500 mL of coating buffer (1X).

Assay buffer/ Standard diluent: 1.0 g of bovine serum albumin (BSA), 200 μL of Tween- 20 were dissolved in 200 mL of the coating buffer (1X).

Blocking buffer: 1.0 g of bovine serum albumin (BSA) dissolved in 200 mL of coating buffer (1X)

Streptavidin-HRP conjugate: prepared as 2.0 μl in 10.0 mL assay buffer (1 in 5000).

TMB substrate/stabilised chromogen: prepared as 1 volume of TMB to 1 volume of distilled water (1 in 2).

Stop solution (1M of H₂SO₄): prepared from conc. H₂SO₄ in distilled water

Coating buffer (10X) was stored at room temperature. Coating buffer (1X), blocking buffer, assay buffer and washing buffer were stored at 4°C.

Both Streptavidin-HRP conjugate and TMB stabilised chromogen were prepared immediately before use.

2.8.5 Preparation of ELISA antibody solutions

2.8.5.1 Preparation of TNF- α ELISA coating and detection antibody solutions

Both of coating antibody and detection antibody were prepared immediately before use as following:

Coating antibody solution (Primary antibody, anti-human TNF-α): stock coating antibody (0.250mg/0.125 mL) was diluted 1:1000 with coating buffer (1X) to obtain 2.0 µg/mL.

Detection antibody solution (Biotinylated secondary antibody, anti-human TNF-α Biotin): Stock detection antibody (0.025 mg/0.125 mL) was diluted 1:625 with assay buffer to achieve a concentration of 0.32 µg/mL

2.8.5.2 Preparation of IL-12 ELISA coating and detection antibody solutions

Both of coating antibody and detection antibody were prepared immediately before use as following:

Coating antibody solution (Primary antibody, anti-human IL-12+p40): stock coating antibody (0.125 mg/0.125 mL) was diluted 1:1000 with coating buffer (1X) to obtained 1.0 µg/mL.

Detection antibody solution (Biotinylated secondary antibody, anti-human IL-12+p40 Biotin): Stock detection antibody (0.025 mg/0.125 mL) was diluted 1:1250 with assay buffer to achieve a concentration of 0.16 µg/mL

2.8.6 Preparation of ELISA standards solutions

2.8.6.1 Preparation of TNF- α standards

Recombinant Human TNF- α was reconstituted with assay buffer to achieve a standard stock solution of 10000 pg/mL. After 10 minutes of rehydration, this stock solution was immediately distributed in aliquots of 50 μ L into polypropylene tubes and stored at -20°C until required. Aliquots (50 μ L) of standard stock solution were diluted with 450 μ L of assay buffer to give a final concentration of 1000pg/mL then, serial dilutions were carried out in order to prepare different concentrations of TNF- α standard solution ranging from 1000 pg/mL to 15.6 pg/mL. Assay buffer alone represented the zero-standard solution. New TNF- α standards were prepared for each ELISA experiment to generate a standard calibration curve in order to determine TNF- α concentrations for the different treatments/ samples

2.8.6.2 Preparation of IL-12 standards

Recombinant Human IL-12+p40 was reconstituted with assay buffer to yield a standard stock solution of 10000 pg/mL. After 10 minutes of rehydration, this stock solution was immediately distributed in aliquots of 120 μ L into polypropylene tubes and stored at -20°C until required. Aliquots (120 μ L) of standard stock solution was diluted with 480 μ L of assay buffer to give a final concentration of 2000pg/mL. then, a serial dilutions were carried out in order to prepare different concentrations of IL-12 standard solution ranging from 2000 pg/mL to 15.6 pg/mL. Assay buffer alone represented the zero-standard solution. New IL-12 standards were prepared for each ELISA experiment to generate a standard calibration curve in order to determine IL-12 concentrations for the different treatments/ samples

2.8.7 ELISA protocol

Sandwich ELISA a sensitive, simple, rapid technique was used for the determination of cytokines. A simplified diagram of ELISA protocol used in this study is shown in Figure 2.1.

Nunc immunosorbent modules (referred to later as wells) were arranged in a microplate frame and coated with 100 μ L of capture/coating antibody solution (2 μ g/mL) (**section 2.8.5**). Then, the plate was sealed with cling film and foil and incubated for minimum of 18 h or overnight at 4°C. Then the coating antibody solution was discarded, and the plate was washed four times using wash buffer (PBS pH 7.4 containing 0.1% v/v Tween-20). After the final wash step, excess washing solution was removed as follows; the plate was placed inverted and tapped upside down on an absorbent paper to remove excess liquid. Then, 300 μ L of blocking buffer (PBS pH 7.4 containing 0.5% v/v BSA) was added into the wells to block free binding sites on the wells and the plate was sealed with cling film and foil and incubated at room temperature for a minimum 2 h or at 4°C (or a maximum of one week).

The blocking solution was discarded, and the plate was washed 3 times using wash buffer. The prepared samples were thawed and the TNF- α / IL-12 standards were prepared as described (**section 2.8.6**). Aliquots (100 μ L) of either TNF- α / IL-12 standards (in duplicate) or samples (in triplicate) were added to designated wells. Following this 50 μ L of biotinylated detection antibody solution (0.32 μ g/mL) (**section 2.8.5**) was added to each well then, the plate was incubated for 2 hours at room temperature. Next, the plate was washed 3 times with washing buffer and 100 μ L of Streptavidin-HRP Conjugate (diluted 1:5000 with assay buffer) was added to each well, and the plate was incubated at room temperature for 30 minutes.

The plate was washed a further 4 times with wash buffer as before. 100 μ L of TMB stabilised chromogen (**see section 2.8.4**) was added to each well. The plate was incubated in the dark for a further 30 minutes at room temperature until standards/samples had turned blue. Once the top standard had turned blue, 100 μ L of sulfuric acid (1 M) was added to terminate the reaction. The absorbance was measured immediately (within 30 minutes of adding stop solution) at λ = 450nm using a plate reader.

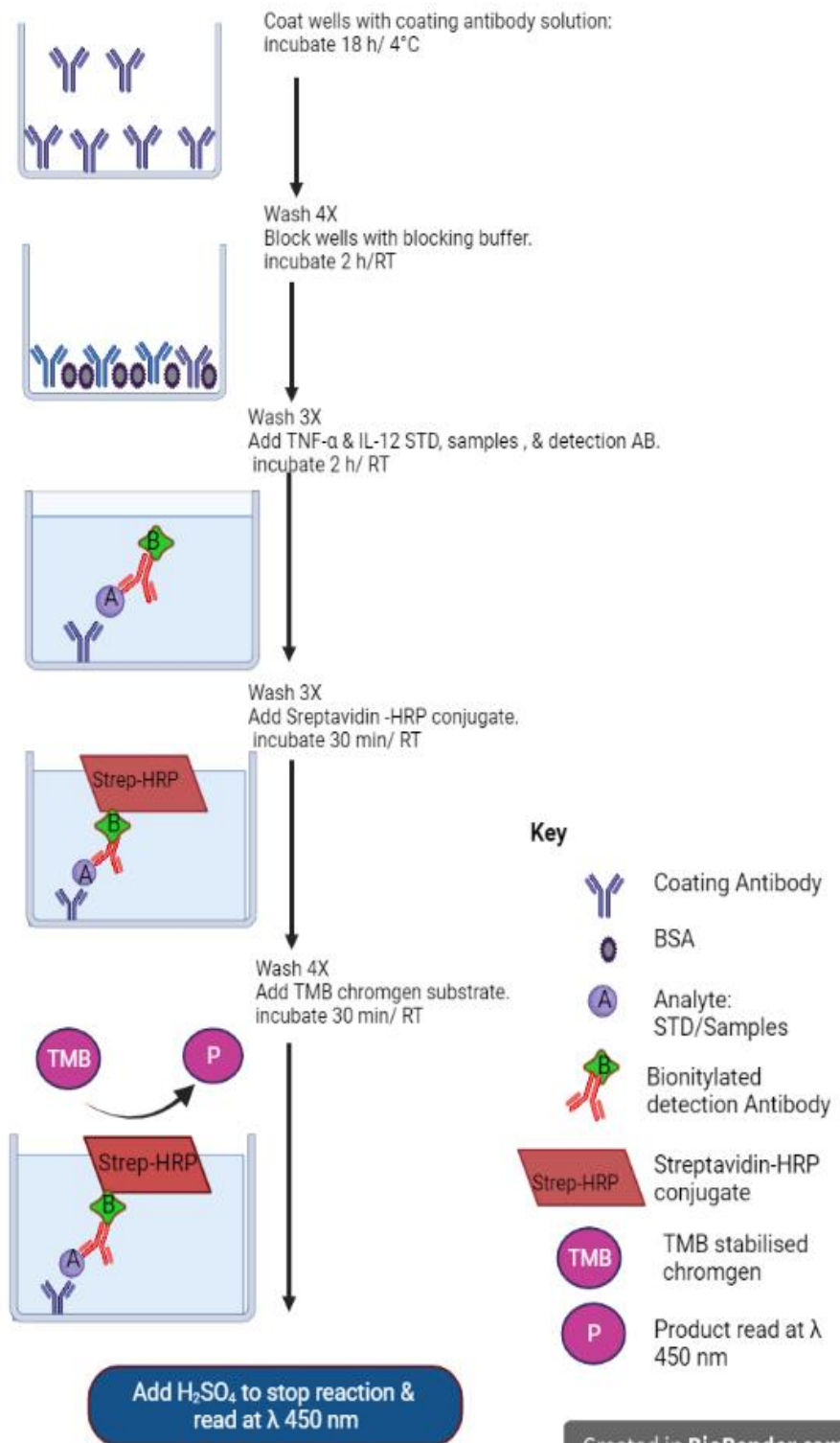


Figure 2.1 Simplified diagram of ELISA procedure steps followed in this study

2.9 Data analysis and statistical analysis

The effect of various plant extracts and/or the selected isolated phytochemicals on cell viability was evaluated based on a comparison with untreated cells (negative control) by using two separate graphical methods. In the first approach the percentage of cell viability was calculated using Microsoft Excel and the graphical representation was performed on GraphPad Prism v.6 using the following formula:

%Cell viability

$$= \frac{\text{Average absorbance of treated cells (a)} - \text{corresponding blank absorbance (b')}}{\text{Average absorbance of untreated cells (c)} - \text{corresponding blank absorbance (b')}} \times 100$$

In the second approach, the effect of extracts was evaluated by determination of the half-maximal inhibitory concentration IC_{50} values, defined as the concentration required for 50% inhibition of the cell viability with respect to untreated cells (negative control). IC_{50} was calculated using nonlinear regression analysis using GraphPad prism software v.6.

The effect of various plant extracts and/or the selected isolated phytochemicals on cytokine (TNF- α and IL-12) production by LPS stimulated THP-1 cells were analysed using GraphPad Prism software v.6. A standard calibration curves for the cytokines (TNF- α / IL-12) were generated for each ELISA experiment (Figure 2.2 and Figure 2.3) using third order polynomial regression analysis. The cytokine concentrations (TNF- α / IL-12 in ng/mL) within each sample were interpolate/ calculated from their absorbance values according to their corresponding standard calibration curves. In some assays the final values presented were adjusted for an appropriate dilution factors.

All the experimental data were presented as mean \pm standard deviation (s.d.); at least three independent experiments were conducted. All measurements were carried out in triplicates or quadruplicate. Statistical analysis of the data using one-way analysis of variance (ANOVA) followed by *Fisher's PLSD* test to compare each concentration (treatment) versus control were carried out using GraphPad Prism v.6 software. The differences between control and different treatments were considered to be significant when P value below 0.05 (P <0.05).

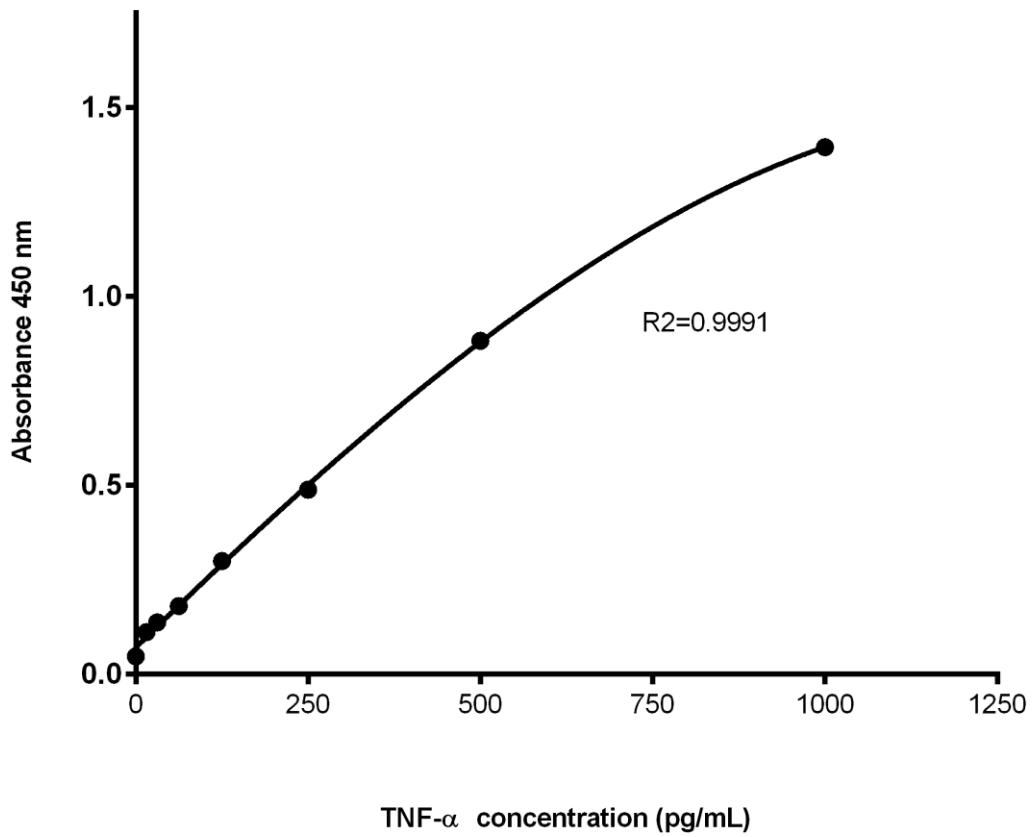


Figure 2.2: Typical TNF- α standard curve for ELISA assay

A standard curve for TNF- α was generated for each experiment using the TNF- α standards run along with the samples. The interpolation of the standard calibration curve was achieved using third order polynomial regression analysis (GraphPad Prism v.6 software) and was used to determine TNF- α concentrations in samples from the absorbance values.

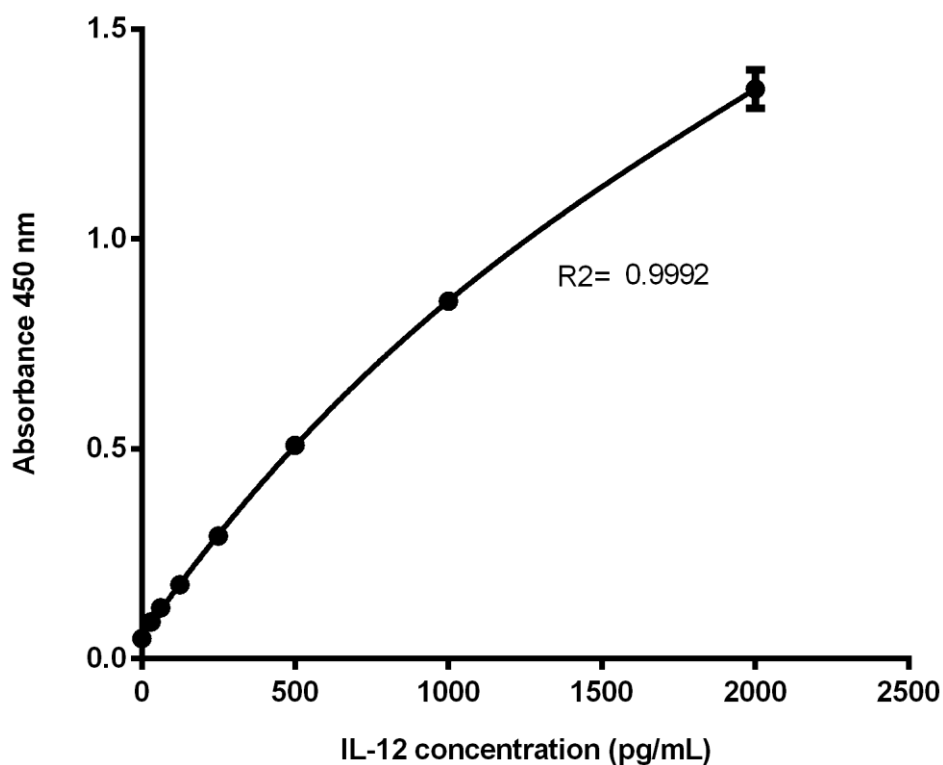


Figure 2.3: Typical IL-12 standard curve for ELISA assay

A standard curve for IL-12 was generated for each experiment using the IL-12 standards run along with the samples. The interpolation of the standard calibration curve was achieved using third order polynomial regression analysis (GraphPad Prism v.6 software) and was used to determine IL-12 concentrations in samples from the absorbance values.

Part C: Molecular docking studies

2.10 Molecular docking protocol

The protocol that was followed for the molecular docking work is illustrated in Figure 2.4

2.10.1 Ligand selection and preparation before docking

Two sets of phytochemicals were chosen for the screening. The first set consisted of eighty-four phytochemicals previously reported from *Pelargonium reniforme/sidoides*. The second set consisted of seven phytochemicals identified through phytochemical work (pinocembrin, oleanolic acid, ursolic acid, pheophytin a, 13² (S/R)-hydroxy-pheophytin a, and pheophytin b). All chemical structures were retrieved from SciFinder. The structure of the ligand inhibitor (AX20017) was retrieved from its corresponding complex with the *MtPknG* protein (PDB ID:2PZI) using BIOVIA Discovery Studio Visualizer v.4.5. Each ligand structure was drawn using ChemOffice as 2D and 3D structures, and geometry-optimised using MM2 energy minimisation. Docking files for all ligands were prepared using AutoDock Tools v. 1.5.6. All rotatable bonds present on the ligands were treated as non-rotatable. This allowed to perform rigid docking and minimise standard errors (approximate of 2.85 kcal/mol) likely due to ligands with many active rotatable bonds (Trott and Olson, 2010). The Gasteiger charge calculation method was used and partial charges were added to the ligand atoms prior to docking (Bikadi and Hazai, 2009). Each ligand was saved as a separate file in a pdbqt format in preparation for docking (Morris *et al.*, 2009).

2.10.2 Target protein preparation before docking

The three-dimensional crystal structure of the *MtPknG* protein (PDB ID:2PZI) in complex with its ligand inhibitor (AX20017) was retrieved from the RCSB Protein Data Bank (PDB) in a pdb format. The protein was used as a rigid structure and all water molecules, and hetero atoms were removed using BIOVIA Discovery Studio Visualizer v.4.5. A pdbqt file of the target protein, with added polar hydrogen atoms, was subsequently prepared using AutoDock Tools v.1.5.6 (Morris *et al.*, 2009).

2.10.3 Docking preparation

The grid box parameters were defined using AutoDock Tools v.1.5.6 to determine the size of the searching space around the *MtPknG* binding site residues. The centre of the grid box was set to $x = 19.234$, $y = -9.412$, $z = -3.495$ in the x , y , z dimensions. The size of the grid box was $22 \times 20 \times 20$ points in the x , y , z dimensions. The grid spacing was fixed to 1 Å. The exhaustiveness value was set up at 9 in all cases.

2.10.4 Docking experiment and visualisation of results

Molecular docking was performed using the AutoDock Vina v.1.1.2 software (as part of the MGLTools software) (Trott and Olson, 2010). The docking scores were calculated as the predicted free energies of binding (ΔG in kcal/mol). The lowest binding free energy (output ligand 1) showing the best score of the docking pose with the least root mean square deviation (RMSD) indicated the highest predictive ligand/protein affinity.

To validate the accuracy of the docking and to allow a comparison between docking scores, AX20017, the co-crystallised inhibitory ligand, was re-docked into *MtPknG*. Different orientations of the ligands were searched and ranked based on their energy scores. The docking protocol was able to produce a similar docking pose for the control ligand with respect to its biological conformation in the co-crystallised protein-ligand complex. We further visually inspected all binding poses for a given ligand and only poses with the lowest value of RMSD were considered to have a high accuracy of docking.

Ligand efficiencies (LEs) were calculated for all ligands. LE1 was calculated as the predicted free energy of binding (ΔG) divided by the number of heavy atoms in the ligand (NHA) ($LE1 = -\Delta G/NHA$). LE2 was calculated as the free energy of binding (ΔG) divided by molecular weight ($LE2 = -(\Delta G)/MW$) (Garcia-Sosa *et al.*, 2009). LE 3 or size-independent ligand efficiency (SILE) was calculated as $LE3 = -\Delta G/NHA^{(0.3)}$ (Nissink, 2009).

2.10.5 Protein-Ligand interactions and identification of binding site residues

Specific amino acids and intermolecular interactions (mainly hydrogen bonds and hydrophobic interactions) involved between the best ligand docking poses and the binding site of the target protein were further visualised using BIOVIA Discovery Studio Visualizer.

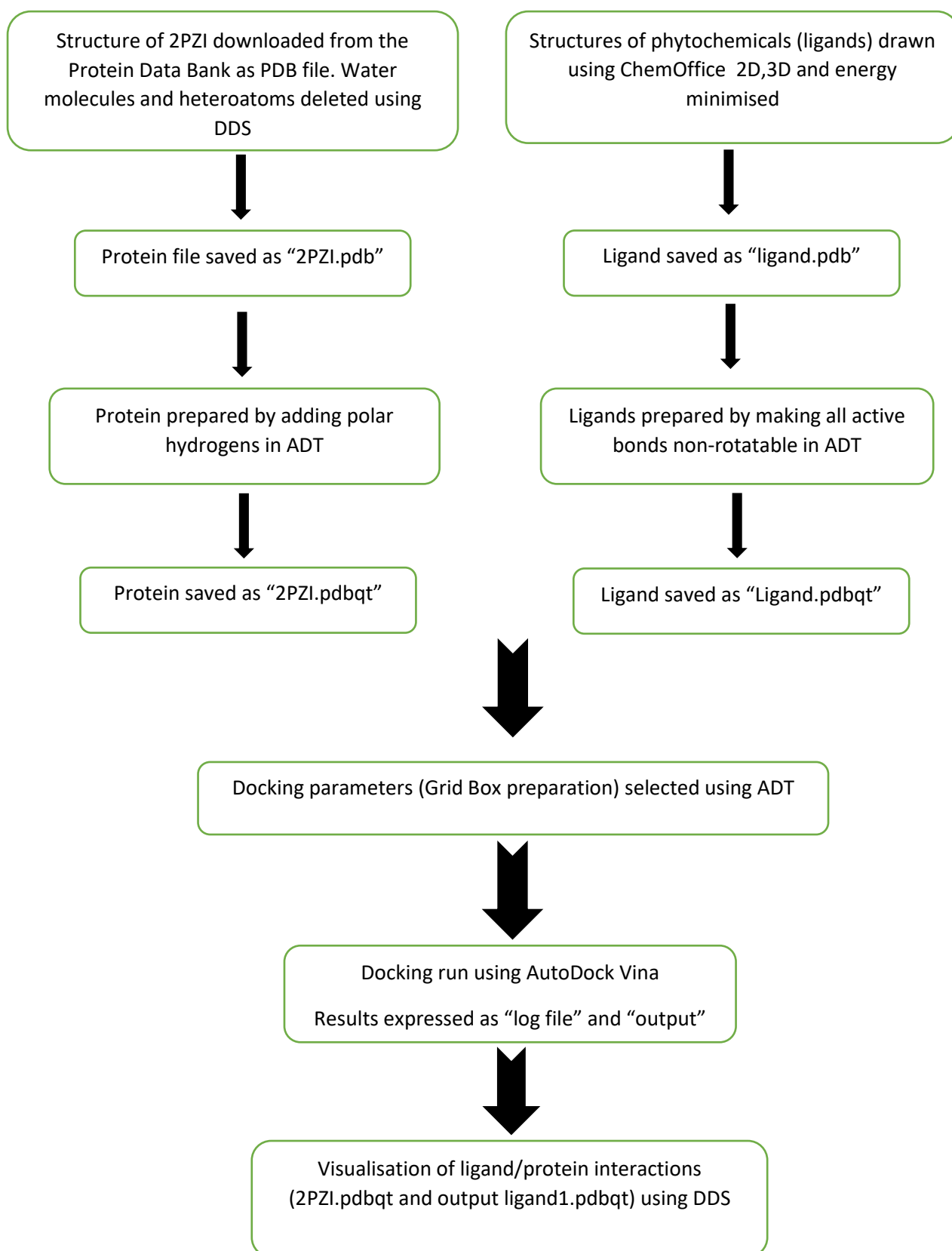


Figure 2.4 Protocol used for the molecular docking study

CHAPTER THREE

RESULTS AND DISCUSSION

PART A:

PHYTOCHEMICAL STUDY

3. Results and Discussion: Part A Phytochemical study

3.1 Characterisation of isolated phytochemicals

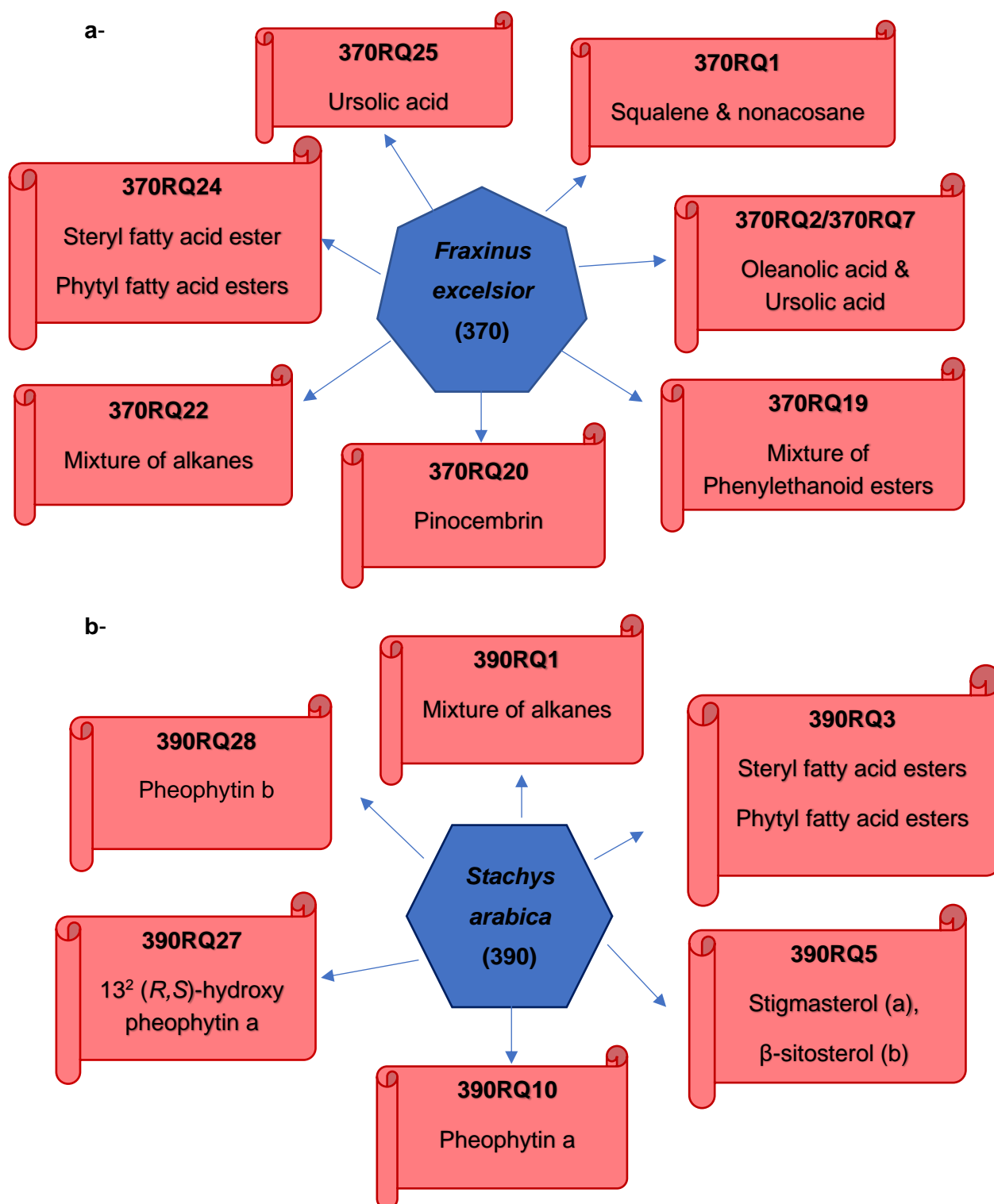


Figure 3.1 Summary of the isolated phytochemicals identified in a- *Fraxinus excelsior* leaves (370), and b- *Stachys arabica* aerial parts (390).

3.1.1 Terpenoids and phytosterols

3.1.1.1 Characterisation of 370RQ7/370RQ2 as a mixture of oleanolic acid (a) and ursolic acid (b)

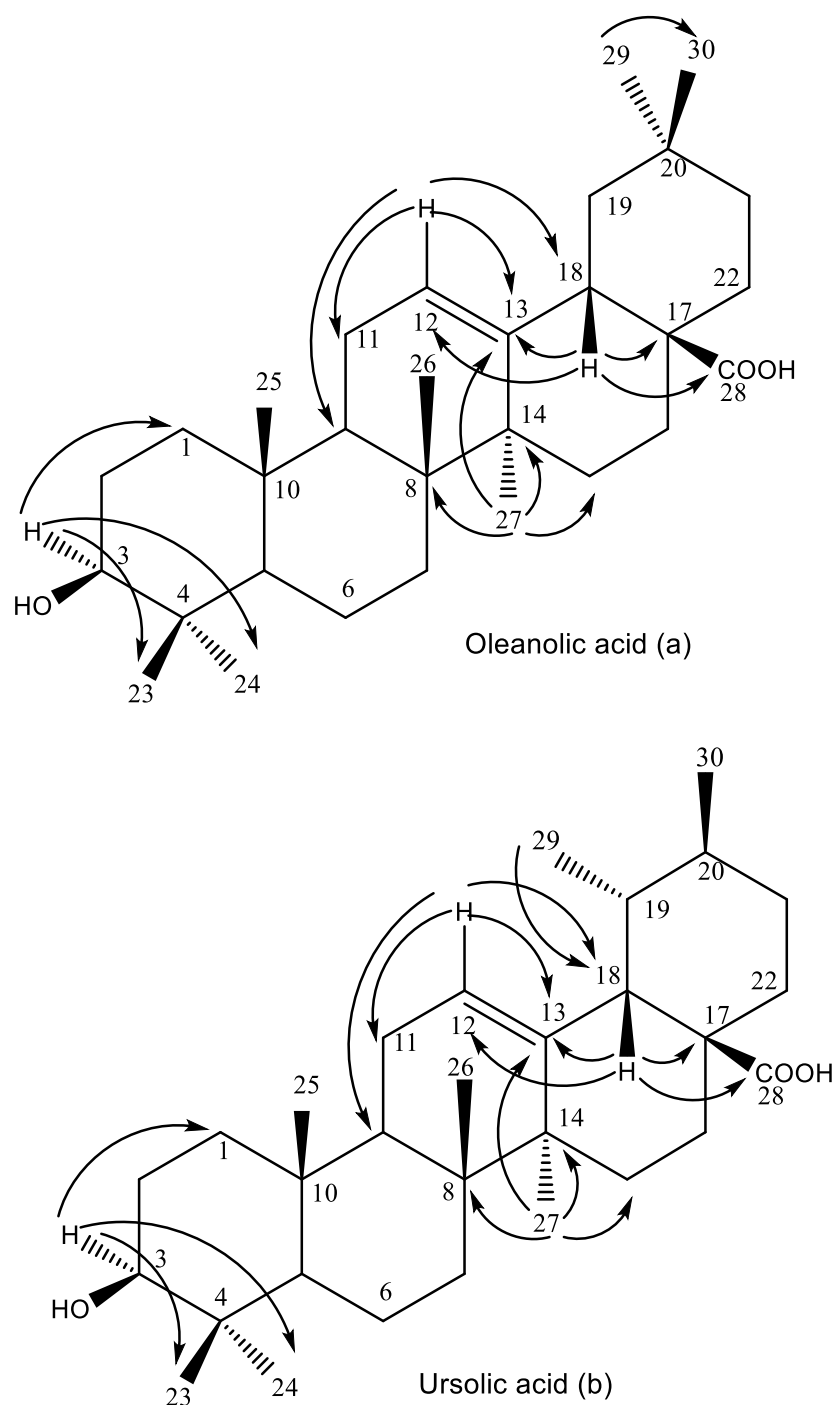


Figure 3.2 Structures of 370RQ2/370RQ7 or oleanolic acid (a) and ursolic acid (b) with selected HMBC correlations.

370RQ7 (107 mg) and 370RQ2 (8.3 mg) were isolated from the ethyl acetate and the *n*-hexane extracts of *F. excelsior*, respectively (Figure 3.2).

On TLC, 370RQ7 and 370RQ2 gave a quenching spot, and a red fluorescence under short (254 nm) and long wave UV light (366 nm), respectively. A purple spot was observed after treatment with anisaldehyde- sulphuric acid reagent and heating.

The negative ion mode HR-nanoESI-MS data of 370RQ7 and 370RQ2 showed a quasi-molecular ion peak $[M-H]^-$ at m/z 455.3530 and 455.3528, respectively (theoretical m/z 455.3531) suggesting for a molecular formula of $C_{30}H_{48}O_3$. A molecular ion peak $[2M-H]^-$ at m/z 911.7117 indicative of a dimer species was observed in the case of 370RQ7.

The 1H NMR spectrum of 370RQ7 (Figure 3.3, Tables 3.1 and 3.2) showed a signal for an oxymethine proton at δ_H 3.23 (dd, $J = 4.3, 11.7$ Hz, H-3 α) with an α -configuration (axial position), and a β -hydroxyl group. Two distinct triplets at δ_H 5.29 and 5.26 were characteristic of olefinic protons. The presence of a signal at δ_H 2.83 (1H, dd, $J = 12$ Hz) and another at δ_H 2.20 (1H, dd, $J = 11.4$ Hz) was typical for the H-18 of olean-12-ene and urs-12-ene type pentacyclic triterpenes, respectively (Migas *et al.*, 2005; Dais *et al.*, 2017). The spectrum showed seven singlets corresponding to seven methyl groups of oleanolic acid (a), and five singlets together with two doublets corresponding to seven methyl groups of ursolic acid (b) (Dais *et al.*, 2017).

The ^{13}C DEPTQ NMR spectrum of 370RQ7 (Figure 3.4, Tables 1.3 and 3.2) confirmed the presence of olean-12-ene and urs-12-ene type pentacyclic triterpenes with olefinic carbons. Characteristic signals of C-12 and C-13 for an olean-12-ene skeleton (δ_C 122.9 and 143.8, respectively) and urs-12-ene skeleton (δ_C 126.1 and 138.2, respectively) were observed. The presence of OH group at C-3 in both the olean-12-ene and the urs-12-ene structures was detected at δ_C 79.3. The most downfield signal appeared at δ_C 182.2, indicating the presence of a carboxylic group at C-17 (Mahato and Kundu, 1994; Dais *et al.*, 2017). The spectrum exhibited thirty carbon peaks for oleanolic acid (OA), consisting of eight quaternary carbons, ten methylenes, seven methyls, and five methines. Further confirmation of the presence of UA was confirmed with the presence of thirty carbon signals distinguished into seven methyls, nine methylenes, seven methines, and seven quaternary carbons.

The hydroxyl group at C-3 in 370RQ7 was in β or equatorial position. This made the chemical shift of the oxymethine carbon less shielded (≈ 79 ppm) than if OH had been in axial position (≈ 76 ppm). Moreover, the chemical shift of C-1 and Me-24 (≈ 38.6 & 15.7 ppm, respectively) were in good agreement with those expected for 3 β -OH triterpenes due to γ -gauche interaction (Mahato and Kundu, 1994).

Selected HMBC correlations extracted from the HMBC spectrum of 370RQ7 (Figure 3.6) are presented in Figure 3.2. Two methyl singlets at δ_{H} 0.78 (Me-24) and 0.99 (Me-23) showed long range correlations to three common carbons at C-4 (2J), C-5 (3J) and C-3 (3J), which supported that the presence of geminal methyls neighbouring the oxymethine at C-3. The hydroxyl group was attached to C-3 (δ_{C} 79.3) because of 3J correlations between C-3 and H-23 (δ_{H} 0.99) and H-24 (δ_{H} 0.78). The signal at δ_{C} 55.5 (C-5) correlated to protons H-23, H-25, and H-24.

All ^1H and ^{13}C connectivities for 370RQ7 were verified by HSQC and HMBC. All long-range correlations observed were consistent with the presence of oleanolic acid and ursolic acid.

The complete assignment of ^1H NMR and ^{13}C NMR values of 370RQ7 in comparison with the literature data is provided in Tables 3.1 and 3.2.

The ^1H and ^{13}C DEPTQ NMR spectra of 370RQ2 (Figure 3.7 - 3.8) shared a high degree of similarity with those obtained for 370RQ7. The ^1H NMR of 370RQ2 (Figure 3.6, Table 3.3) exhibited a signal for an oxymethine proton at δ_{H} 3.23 (dd, $J = 4.2, 11.0$ Hz). The spectrum exhibited chemical shifts indicative of the presence of a mixture of compounds, with triplets at δ_{H} 5.29 (strong signal) and 5.25 (weak signal) characteristic of olefinic protons. A signal at δ_{H} 2.83 and another at δ_{H} 2.20 were typical for the H-18 of olean-12-ene and urs-12-ene type pentacyclic triterpenes, respectively (Migas *et al.*, 2005). The spectrum showed seven singlets corresponding to methyl groups of oleanolic acid (a). The weak signal at δ_{H} 1.09 was attributed to the presence of a methyl group at C-27 for ursolic acid (b).

The ^{13}C DEPTQ NMR spectrum of 370RQ2 (Figure 3.8, Table 3.3) confirmed the presence of olean-12-ene and urs-12-ene type pentacyclic triterpenes with olefinic carbons. Characteristic signals of C-12 and C-13 of an olean-12-ene skeleton at (δ_{C} 122.8 and 143.8, respectively) and urs-12-ene skeleton (δ_{C} 126.1 and 138.2, respectively) were observed. The presence of OH group at C-3 in both the olean-12-

ene and the urs-12- ene structures was detected at δ_c 79.3. The most downfield signal appeared at δ_c 183.3 corresponding to the presence of a carboxylic group at C-17 (Mahato and Kundu, 1994; Dais *et al.*, 2017).

The HMBC spectrum (Figure 3.10) exhibited similar correlations to those observed for 370RQ7. Selected HMBC correlations are shown in Figure 3.2.

All ^1H and ^{13}C connectivities for 370RQ2 were verified by HSQC and HMBC. All long-range correlations observed were consistent with the presence of oleanolic acid and ursolic acid.

The complete assignment of ^1H NMR and ^{13}C NMR values of 370RQ2 is provided in Table 3.3.

Based on the aforementioned spectral data and by comparison with the data reported in the literature (Mahato and Kundu, 1994; Ragasa and Lim, 2005; Dais *et al.*, 2017; Seebacher *et al.*, 2003), 370RQ7/370RQ2 was identified as a mixture of 3β -hydroxy-olea-12-en-28-oic acid or oleanolic acid (**a**) and 3β -hydroxy -urs12-en-28-oic acid or ursolic acid (**b**).

The relative ratio of oleanolic acid to ursolic acid (1:1) in 370RQ7 (Figure 3.3) and (1:0.2) in 370RQ2 (Figure 3.7) was determined from the integrations reported for the H-12 olefinic signals at δ_H 5.29 and 5.26, respectively.

Whilst ursolic acid has previously been isolated from *F. excelsior* leaves (Kowalczyk and Olechnowicz-Stepień, 1989), the presence of oleanolic acid in *F. excelsior* is reported here for the first time.

Oleanolic acid (OA) is abundant in plants belonging to the Oleaceae family (Pollier and Goossens, 2012). Ursolic acid (UA) occurs in a wide variety of plants, including apples, blueberry, cranberry, persimmon, and olive (Ikeda *et al.*, 2008). OA and UA have been reported as major phytochemicals from many plants widely used in traditional medicine (Jesus *et al.*, 2015).

The pharmacological activity of OA and UA has been extensively studied and various reports have demonstrated their use in the prevention and management of chronic diseases (Ayeleso *et al.*, 2017; Seo *et al.*, 2018; Khwaza *et al.*, 2020). OA and UA have multiple biological effects, including anti-diabetic (Sung *et al.*, 2010; Li *et al.*, 2015a; Wang *et al.*, 2013), hepatoprotective (Zhao *et al.*, 2013), anti-hypertensive

(Bachhav *et al.*, 2011; 2015) and anti-cancer (Žiberna *et al.*, 2017; Khwaza *et al.*, 2020). Furthermore, OA and UA have been identified as potent agents for neurodegenerative disorders like Alzheimer's disease, Parkinson's disease, and multiple sclerosis (Zang *et al.*, 2014; Rai *et al.*, 2019; Castellano *et al.*, 2019; Zhang *et al.*, 2020).

Previous investigations have demonstrated that OA, UA, and their derivatives, exhibit significant *in vivo*, *in vitro*, and *in silico* activity against Mtb (Tanachatchairatana *et al.*, 2008; Jiménez-Arellanes *et al.*, 2013; Jee *et al.*, 2018). OA isolated from the *n*-hexane extract of *Lantana hispida* aerial parts exhibited an MIC of 25 µg/mL against Mtb H37Rv strain by microdilution alamar blue assay (Jiménez-Arellanes *et al.*, 2007). UA isolated from *Artemisia capillaris* inhibited the growth of both susceptible and resistant strains of Mtb with MIC values of 12.5 µg/mL against the susceptible strains, and 12.5–25 µg/mL against MDR/XDR strains of Mtb (Jyoti *et al.*, 2016). Another study showed that UA and OA isolated from *Chamaedora tepejilote* and *Lantana hispida*, used in Mexican traditional medicine to treat TB, had *in vitro* and *in vivo* antimycobacterial and immunoregulatory activity (Jiménez-Arellanes *et al.*, 2013).

Hepatotoxicity has been identified as a major side effect of the standard anti-TB drug regimen (Yew and Leung, 2006; Tostmann *et al.*, 2008). A study showed that administration of 100 and 200 µg/mouse/day of OA and UA mixture prevented the steatosis induced by the anti-tubercular drugs. The same study showed that the mice which received the OA/UA mixture had significantly decreased aspartate transaminase and alanine aminotransferase levels and ameliorated the histopathological changes induced by the anti-TB drugs (Gutiérrez-Rebolledo *et al.*, 2016). OA showed synergistic effect against Mtb when administered in combination with isoniazid, rifampicin or ethambutol *in vitro* (Ge *et al.*, 2010). As shown above, OA and UA protect against damage caused by anti-TB drugs, and this indicates that OA and UA could be used as an adjunct host-directed immune therapy for TB.

In the present study, OA and UA were assessed for their effect on THP-1 cell viability, and their potential immunomodulatory effects on TNF-α and IL-12 production from LPS stimulated THP-1 cells (for further details see section 3.2.4, 3.3.4 and 3.3.8).

Table 3.1 ¹H (600 MHz) and ¹³C (150 MHz) NMR chemical shift values* for 370RQ7a (recorded in CDCl₃) in comparison with literature data.

Position	¹ H NMR δ experimental	¹³ C NMR δ experimental	¹ H NMR δ Literature ^a	¹³ C NMR δ Literature ^b
1		38.7 CH ₂		38.4-38.6
2		27.5 CH ₂		27.2-27.4
3	3.23 (1H, dd, <i>J</i> = 11.7, 4.3 Hz)	79.3 CH	3.20-3.22 (1H, dd, <i>J</i> = 4, 12 Hz)	79.0-79.3
4		39.0 C		38.7-38.9
5		55.5 CH		55.2-55.4
6		18.5 CH ₂		18.3-18.5
7		32.9 CH ₂		32.6-32.7
8		39.5 C		39.2-39.5
9		47.8 CH		47.6-47.8
10		37.3 C		37.1-37.3
11		23.6 CH ₂		23.4-23.8
12	5.29 (1H, t, <i>J</i> = 3.8 Hz)	122.9 =CH	5.28-5.30 (1H, t, <i>J</i> = 3.6 Hz)	122.6-122.9
13		143.8 C=		143.3-143.8
14		41.9 C		41.8-41.9
15		27.9 CH ₂		27.7-27.9
16		23.2 CH ₂		23.0-23.7
17		46.7 C		46.4-46.8
18	2.83 (1H, dd, <i>J</i> = 12 Hz)	41.3 CH	2.81-2.83 (1H, dd, <i>J</i> = 4, 14 Hz)	41.0-41.3
19		46.1 CH₂		45.9-46.6
20		30.9 C		30.7-31.0
21		33.8 CH ₂		33.8-34.3
22		32.7 CH ₂		32.4-32.9
23	0.99 (3H, s)	28.3 CH ₃	0.98-0.99	28.1-28.4
24	0.78 (3H, s)	15.6 CH ₃	0.75-0.77 (3H, s)	15.5-15.8
25	0.94 (3H, s)	15.8 CH ₃	0.91-0.94 (3H, s)	15.3-15.5
26	0.77 (3H, s)	17.2 CH ₃	0.77-0.78 (3H, s)	16.9-17.4

Table 3.1 (Cont.) ¹H (600 MHz) and ¹³C (150 MHz) NMR chemical shift values* for 370RQ7a (recorded in CDCl₃) in comparison with literature data.

Position	¹ H NMR δ experimental	¹³ C NMR δ experimental	¹ H NMR δ Literature ^a	¹³ C NMR δ Literature ^b
27	1.14 (3H, s)	26.1 CH₃	1.13-1.15 (3H, s)	25.9-26.2
28		182.2 C		180.3-183.5
29	0.91 (3H, s)	33.3 CH₃	0.91-0.92 (3H, s)	33.1-33.3
30	0.92 (3H, s)	23.8 CH₃	0.90-0.93 (3H, s)	23.5-23.8

* Chemical shifts values in ppm

^a (Migas *et al.*, 2005; Ragasa and Lim, 2005; Dais *et al.*, 2017)

^b (Mahato and Kundu, 1994; Migas *et al.*, 2005; Ragasa and Lim, 2005; Dais *et al.*, 2017)

Table 3.2 ^1H (600 MHz) and ^{13}C (150 MHz) NMR chemical shift values* for 370RQ7b (recorded in CDCl_3) in comparison with literature data.

Position	^1H NMR δ experimental	^{13}C NMR δ experimental	^1H NMR δ Literature ^a	^{13}C NMR δ Literature ^b
1		38.8 CH_2		38.4-39.0
2		27.5 CH_2		27.2-28.1
3	3.23 (1H, dd, $J = 11.7, 4.3$ Hz)	79.3 CH	3.20-3.22 (1H, dd, $J = 4.6, 11.6$ Hz)	78.1-79.1
4		39.0 C		38.4-39.6
5		55.5 CH		55.2-55.8
6		18.5 CH_2		18.3-18.8
7		33.2 CH_2		33.0-33.6
8		39.7 C		39.5-40.0
9		47.9 CH		47.5-48.0
10		37.2 C		36.9-37.4
11		23.5 CH_2		23.0-23.6
12	5.25 (1H, t, $J = 3.6$ Hz)	126.1 =CH	5.26 (1H, t, $J = 3.6$ Hz)	125.9-126.1
13		138.2 C=		137.8-138.7
14		42.2 C		42.1-42.5
15		28.2 CH_2		28.3-28.7
16		24.4 CH_2		23.8-24.9
17		48.2 C		48.1-48.2
18	2.20 (1H, dd, $J = 11.4$ Hz)	52.9 CH	2.19-2.20 (1H, dd, $J = 11.4$ Hz)	52.7-53.5
19		39.1 CH		39.0-39.5
20		39.3 CH		38.8-39.1
21		30.8 CH_2		30.6-31.1
22		36.9 CH_2		36.7-37.3
23	0.99 (3H, s)	28.4 CH_3	0.99 s	28.1-28.8
24	0.78 (3H, s)	15.7 CH_3	0.78 s	15.6-15.8

Table 3.2 (Cont.) ¹H (600 MHz) and ¹³C (150 MHz) NMR chemical shift values* for 370RQ7b (recorded in CDCl₃) in comparison with literature data.

Position	¹ H NMR δ experimental	¹³ C NMR δ experimental	¹ H NMR δ Literature ^a	¹³ C NMR δ Literature ^b
25	0.94 (3H, s)	15.8 CH ₃	0.93 s	15.5-16.6
26	0.79 (3H, s)	17.3 CH ₃	0.79 s	17.1-17.4
27	1.09 (3H, s)	23.8 CH₃	1.09 s	23.6-23.8
28		182.2 C		180.0-183.5
29	0.87 (d, J = 6.6Hz)	17.2 CH₃	0.86 (d, J = 6.4Hz)	17.0-17.5
30	0.95 (d, J = 6.2Hz)	21.4 CH₃	0.95 (d, J = 6.5Hz)	21.2-21.4

* Chemical shifts values in ppm.

^a (Migas *et al.*, 2005; Dais *et al.*, 2017)

^b (Mahato and Kundu, 1994; Migas *et al.*, 2005; Dais *et al.*, 2017)

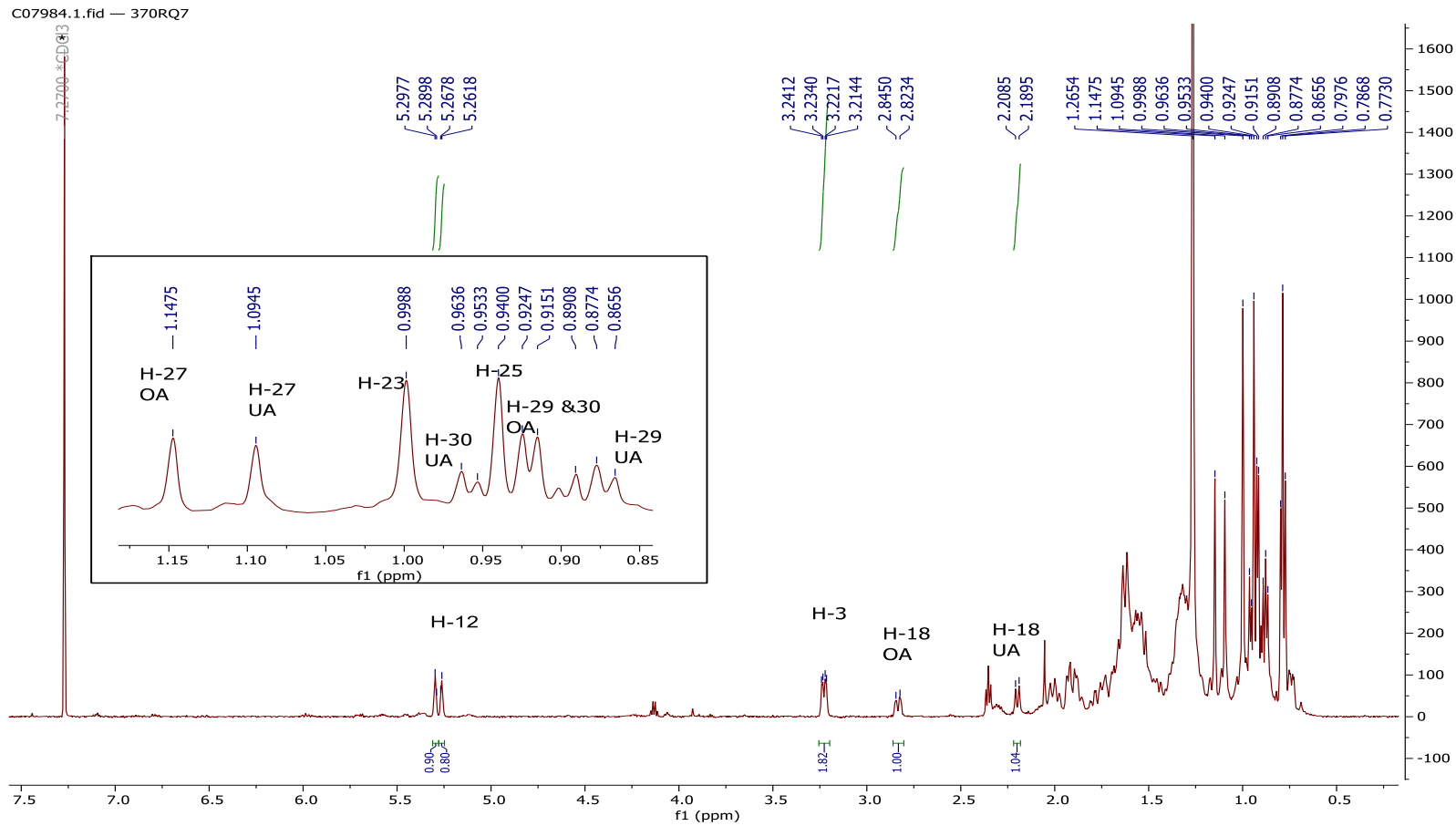


Figure 3.3 ^1H NMR spectrum (CDCl_3^* , 600 MHz) of 370RQ7

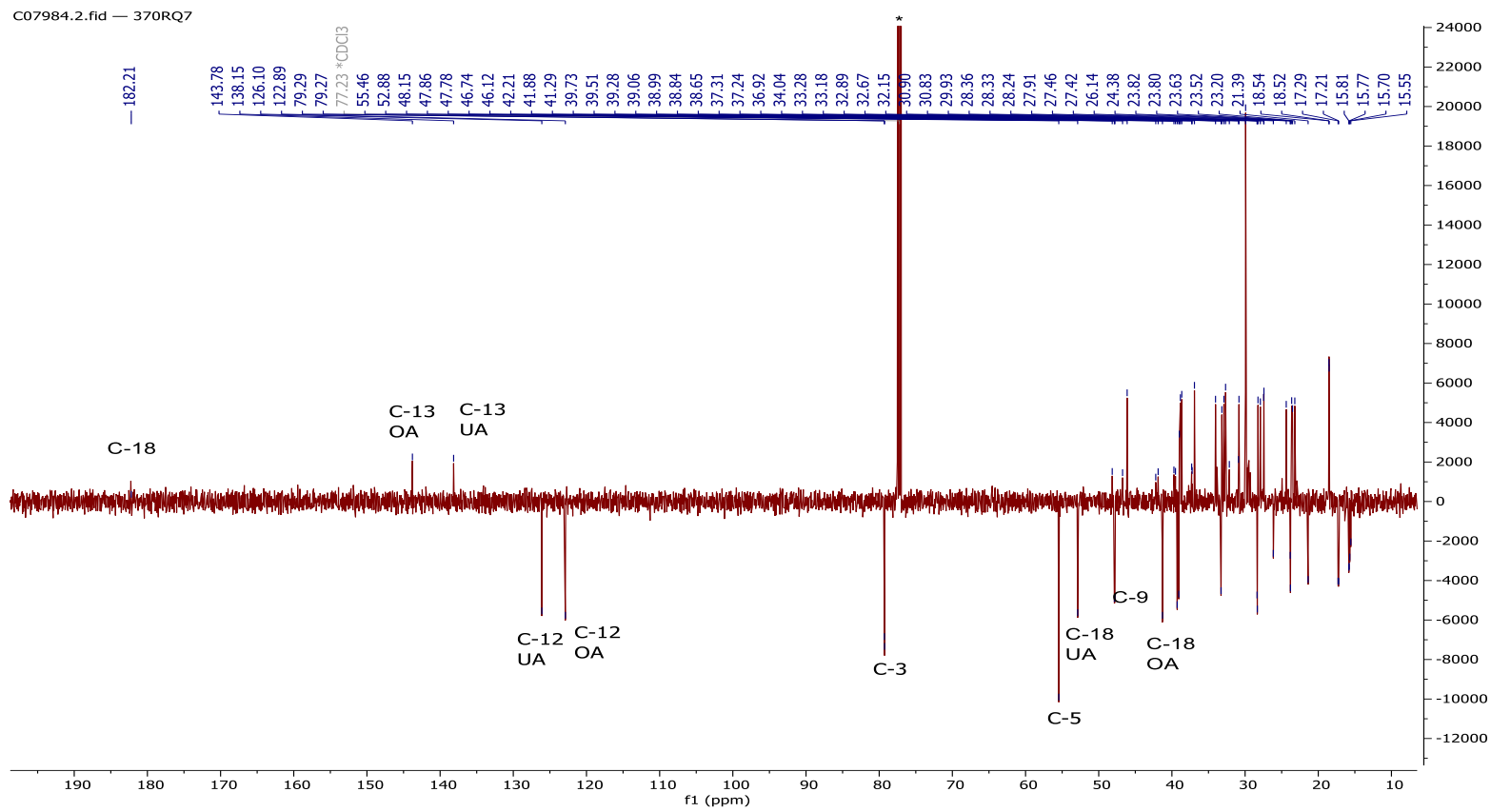
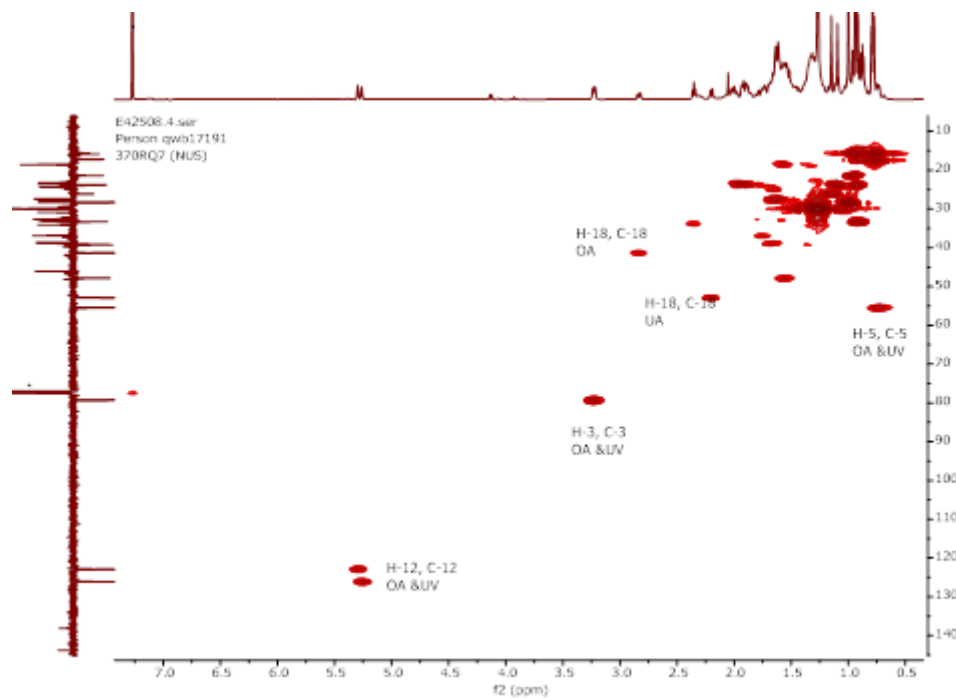
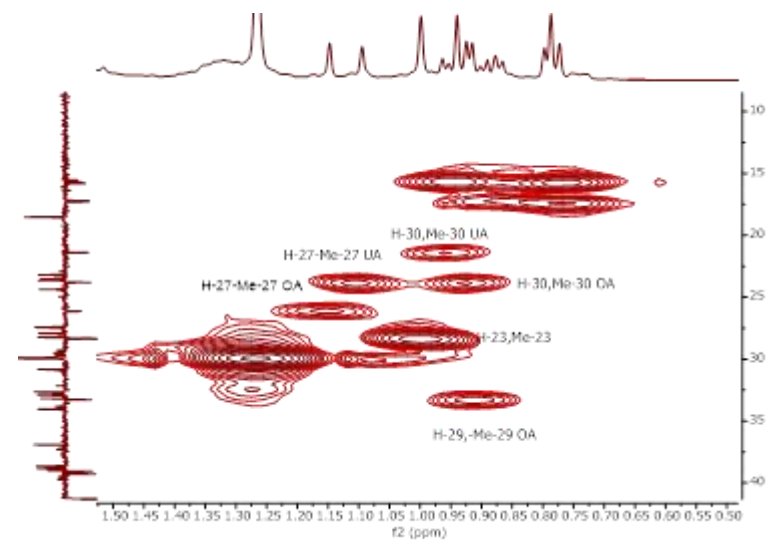


Figure 3.4 ^{13}C -DEPTQ NMR spectrum (CDCl_3^* , 150 MHz) of 370RQ7



A



B

Figure 3.5 HSQC spectrum (CDCl_3^* , 500 MHz) of 370RQ7
A: Full HSQC spectrum; B: Selected expansion of HSQC spectrum

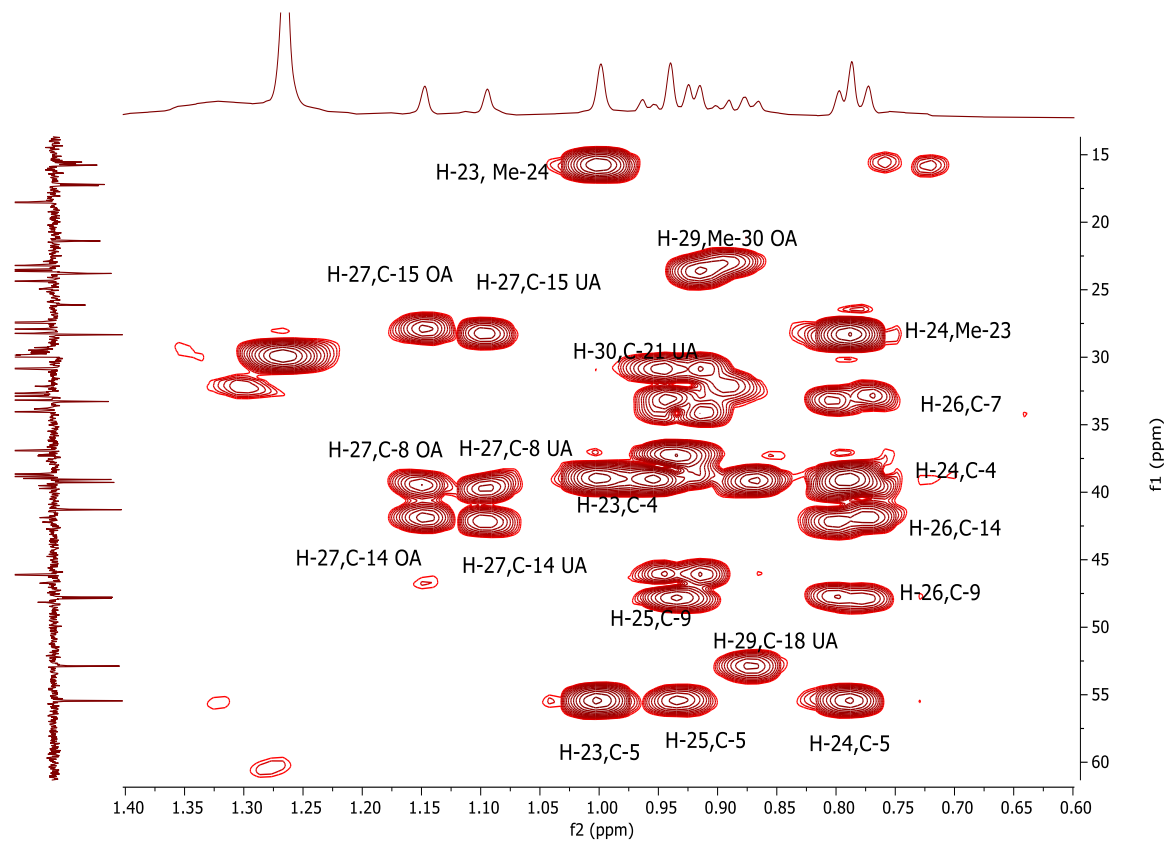


Figure 3.6 Selected expansion of HMBC spectrum (CDCl₃, 600 MHz) of 370RQ7

Table 3.3 ¹H (500 MHz) and ¹³C (125 MHz) NMR chemical shift values* for 370RQ2 (recorded in CDCl₃)

Position	370RQ2a (OA)		370RQ2b (UA)	
	¹ H δ	¹³ C δ	¹ H δ	¹³ C δ
1		38.6 CH ₂		38.8 CH ₂
2		27.4 CH ₂		27.4 CH ₂
3	3.23 (1H, dd, <i>J</i> = 4.2, 11.0 Hz)	79.3 CH	3.23 (1H, dd, <i>J</i> = 4.2, 11.0 Hz)	79.3 CH
4		38.96 C		38.8 C
5		55.4 CH		55.4 CH
6		18.5 CH ₂		18.5 CH ₂
7		32.6 CH ₂		--
8		39.5 C		39.6 C
9		47.8 CH		47.8
10		37.3 C		36.9 C
11		23.6 CH ₂		22.9
12	5.29 (1H, t, <i>J</i> = 3.7 Hz)	122.8 =CH	5.25 (1H, t, <i>J</i> = 3.4 Hz)	126.1 =CH
13		143.8 C		138.2 C=
14		41.8 C		42.1 C
15		27.9 CH ₂		--
16		23.2 CH ₂		24.3
17		46.7 C		48.1 C
18	2.83 (1H, dd, <i>J</i> = 4.8, 14 Hz)	41.2 CH	2.20 (1H, dd)	52.8 CH
19		46.1 CH₂		39.2 CH
20		30.9 C		39.0 CH
21		34.0 CH ₂		30.8
22		32.9 CH ₂		36.9
23	0.99 (3H, s)	28.3 CH ₃		--
24	0.76 (3H, s)	15.8 CH ₃		--
25	0.92 (3H, s)	15.5 CH ₃		--
26	0.78 (3H, s)	17.3 CH ₃		--
27	1.14 (3H, s)	26.2 CH₃	1.09 (3H, s)	23.8 CH₃

Table 3.3. (Cont.) ^1H (500 MHz) and ^{13}C (125 MHz) NMR chemical shift values* for 370RQ2 (recorded in CDCl_3)

Position	370RQ7a (OA)		370RQ7b (UA)	
	$^1\text{H } \delta$	$^{13}\text{C } \delta$	$^1\text{H } \delta$	$^{13}\text{C } \delta$
28		183.3 C		183.3 C
29	0.91 (3H, s)	33.3 CH₃		17.2 CH₃
30	0.93 (3H, s)	23.8 CH₃		21.4 CH₃

* Chemical shifts values in ppm

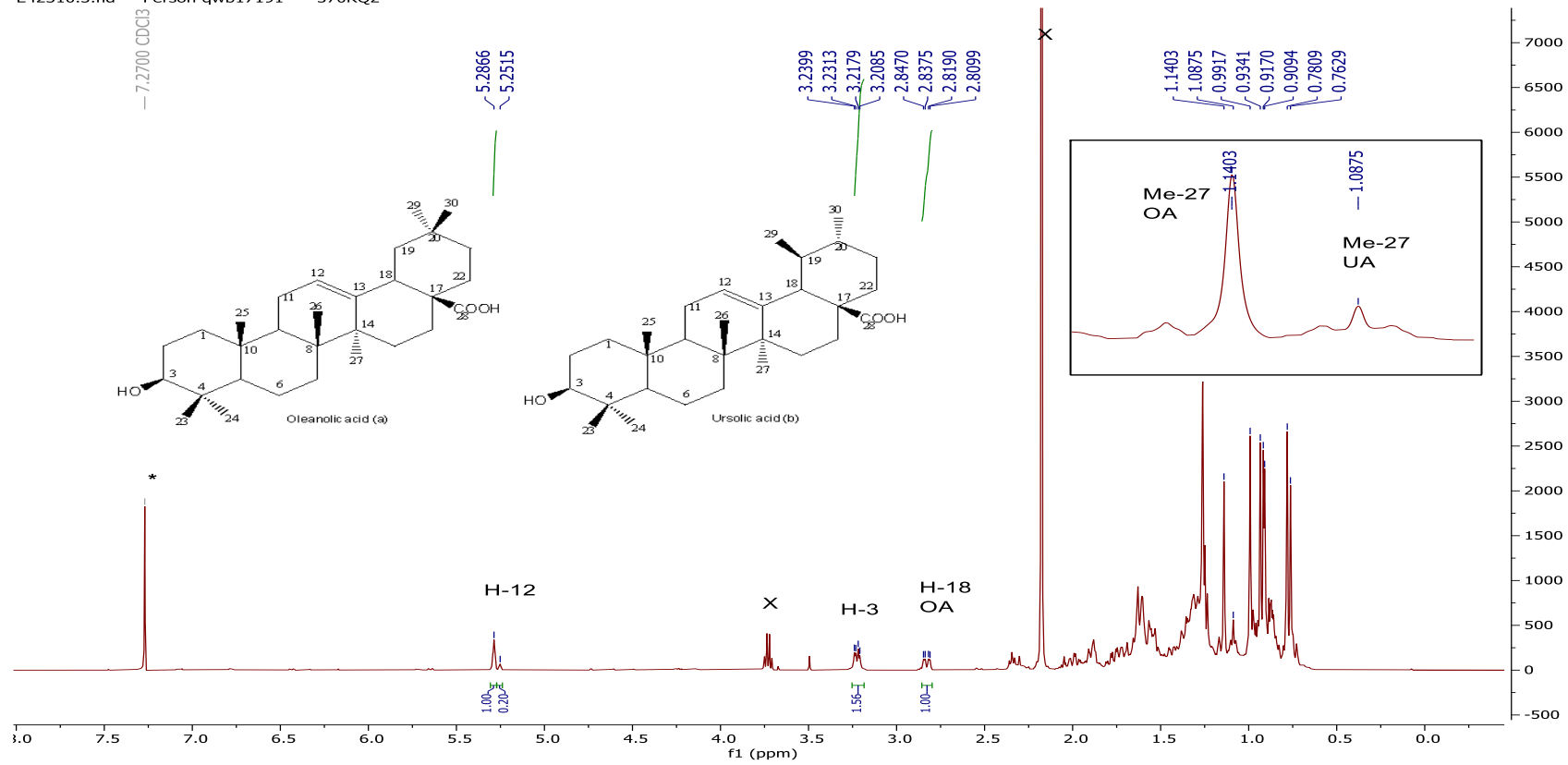


Figure 3.7 ¹H NMR spectrum (CDCl₃^{*}, 500 MHz) of 370RQ2

X refers to solvent impurities.

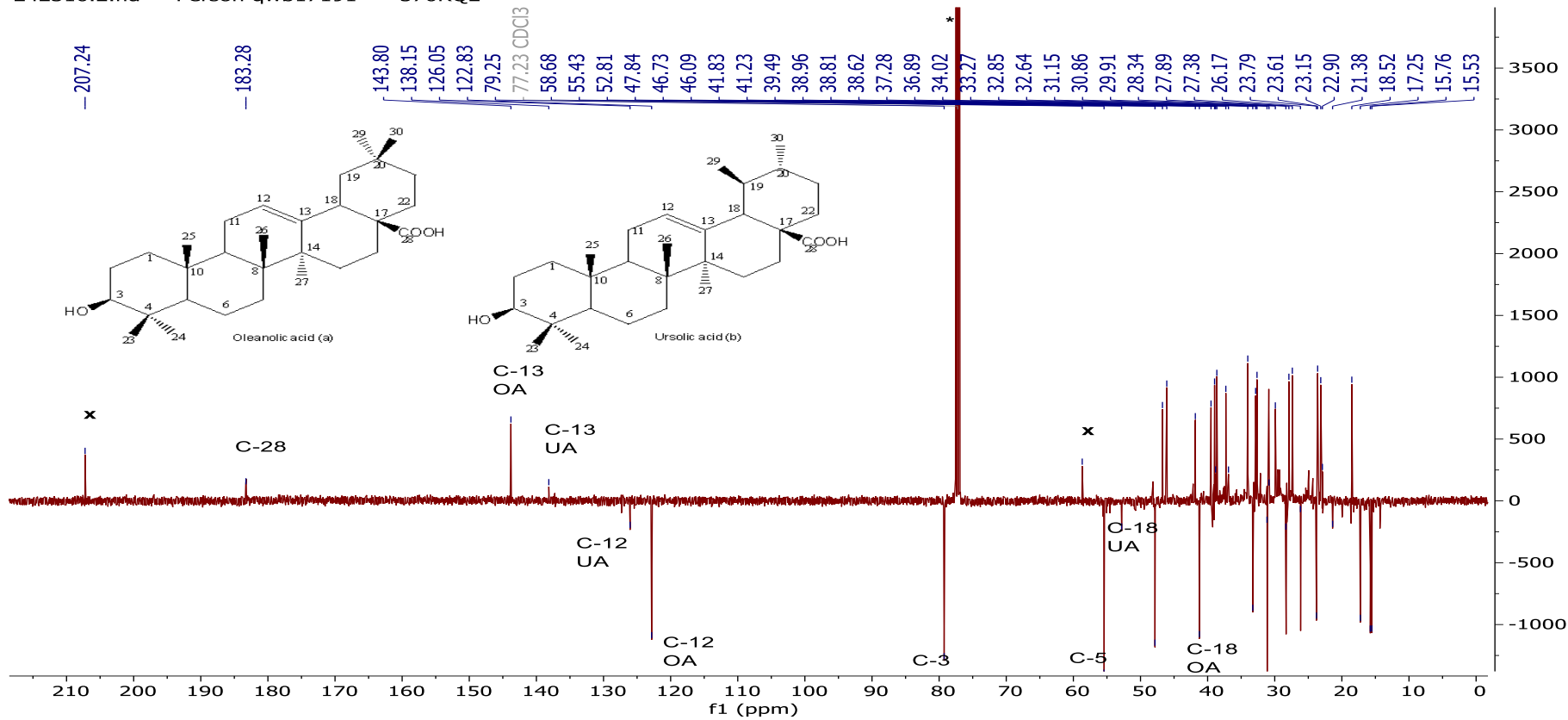


Figure 3.8 ¹³C-DEPTQ NMR spectrum (CDCl₃^{*}, 125 MHz) of 370RQ2

X refers to solvent impurities.

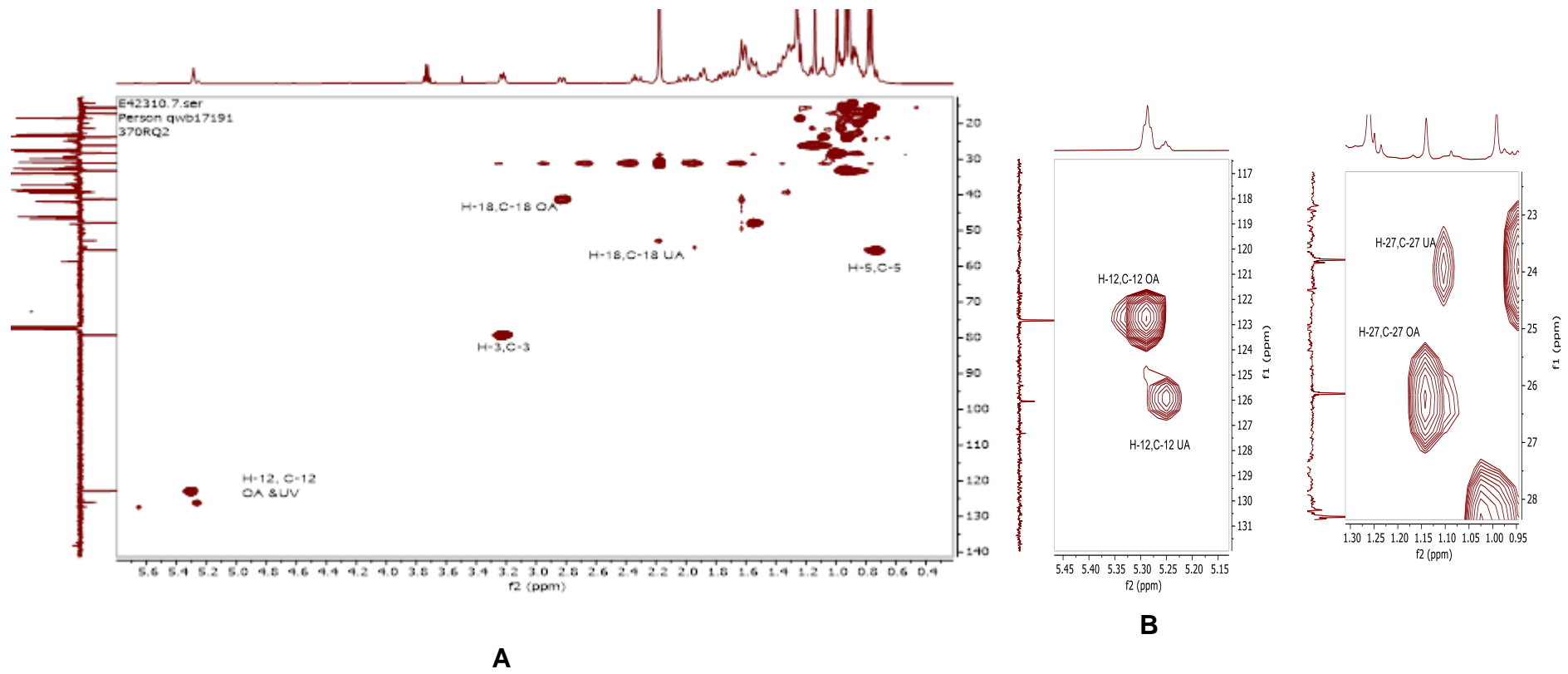
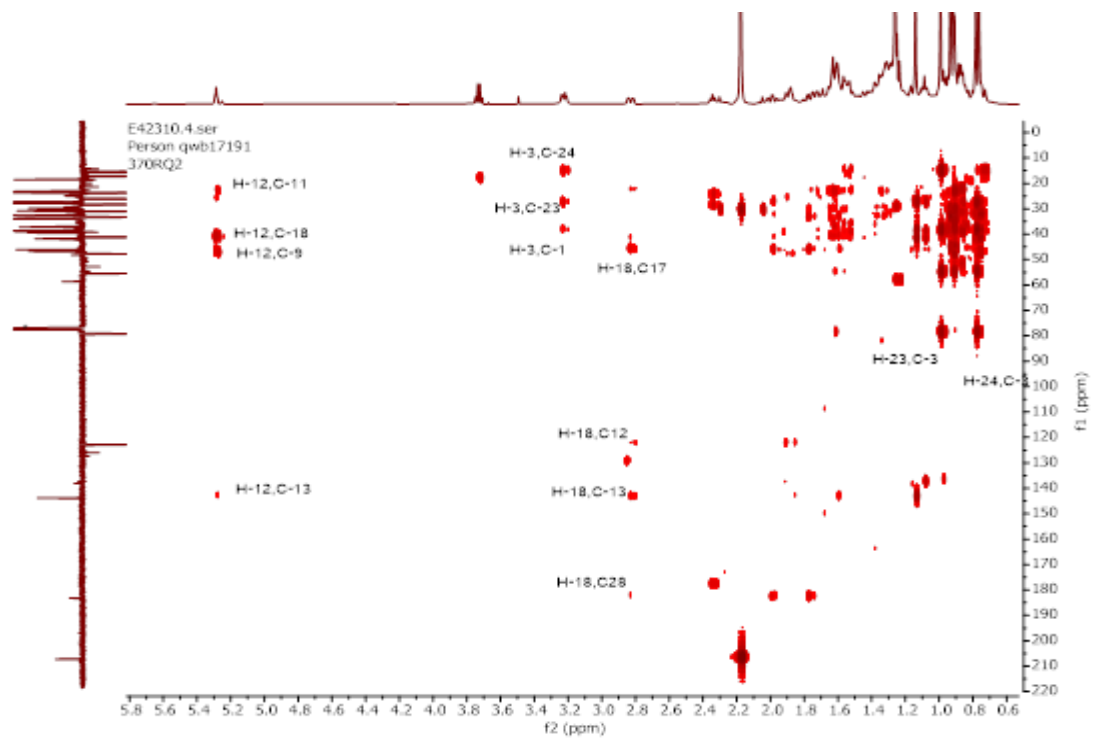
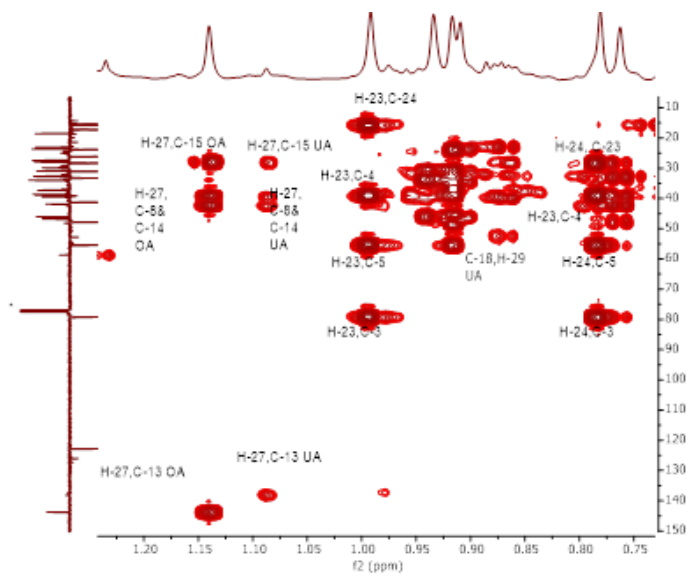


Figure 3.9 HSQC spectrum (CDCl_3 , 500 MHz) of 370RQ2
A: Full HSQC spectrum; B: Selected expansion of HSQC spectrum



A



B

Figure 3.10 HMBC spectrum (CDCl_3^* , 500 MHz) of 370RQ2

A: Full HMBC spectrum; B: Selected expansion of HMBC spectrum

3.1.1.2 Characterisation of 370RQ25 as ursolic acid

370RQ25 was isolated from the ethyl acetate extract of *F. excelsior* (3.5 mg) (Figure 3.2b). On TLC, 370RQ25 gave a quenching spot and a red fluorescence under short (254 nm) and long wave UV light (366 nm), respectively. A purple spot was observed after treatment with anisaldehyde- sulphuric acid reagent and heating.

The negative ion mode HR-nanoESI-MS data of 370RQ25 showed a quasi-molecular ion peak $[M-H]^-$ at m/z 455.3529 (theoretical m/z 455.3531) suggesting for a molecular formula of $C_{30}H_{48}O_3$. A molecular ion peak $[2M-H]^-$ at m/z 911.7119 indicated the presence of a dimer species.

The 1H NMR spectrum (Table 3.4, Figure 3.11) exhibited a signal for an olefinic proton at δ_H 5.26, an oxymethine proton at δ_H 3.23, five singlets (δ_H 0.78, 0.80, 0.94, 0.99 and 1.09) and two doublets (δ_H 0.87 and 0.95) for methyl groups, and a proton at δ_H 2.20 (dd) typical for H-18 of an urs-12-ene type triterpene (Migas *et al.*, 2005; Dais *et al.*, 2017).

The ^{13}C DEPTQ NMR (Table 3.4, Figure 3.12) confirmed the presence of C-12 and C-13 of an urs-12-ene skeleton (δ_C 126.1 and 138.2). The presence of a OH group at C-3 was detected at δ_C 79.3. There were 29 carbon signals distinguished into seven methyls (δ_C 15.7, 15.8, 17.2, 17.3, 21.4, 23.8, and 28.4), nine methylenes (δ_C 18.5, 23.5, 24.4, 27.0, 27.4, 30.8, 33.2, 36.9, and 38.8), seven methines (δ_C 39.1, 39.3, 47.8, 52.9, and 55.5), one carbons at δ_C 79.3 (oxymethine carbon C-3), and another at δ_C 126.1 (olefinic C-12). Six quaternary carbons appeared at δ_C 37.2, 39.0, 39.7, 42.2, 46.7, and 138.2. The C-28 (quaternary carbon) signal was not detected.

Selected HMBC correlations are shown in Table 3.4

The complete assignment of 1H NMR and ^{13}C NMR values of 370RQ25 in comparison with the literature data is provided in Table 3.4

Based on the spectral data obtained and by comparison with literature reports, 370RQ25 was characterised as 3- β -hydroxyurs-12-en-28-oic acid or ursolic acid (UA). The NMR and MS data were in good agreement with previous reports (Migas *et al.*, 2005; Dais *et al.*, 2017).

Table 3.4 ^1H (500 MHz) and ^{13}C (125 MHz) NMR chemical shift values* for 370RQ25 (recorded in CDCl_3) in comparison with literature data

Position	^1H NMR δ experimental	^{13}C NMR δ experimental	HMBC correlations	^1H NMR δ Literature ^a	^{13}C NMR δ Literature ^a
1		38.8 CH_2			38.4-39.0
2		27.5 CH_2			27.2-28.1
3	3.23 (1H, dd, $J = 4.4, 11.3$ Hz)	79.3 CH		3.20-3.22 (1H, dd, $J =$ 4.6, 11.6)	78.1-79.1
4		39.0 C			38.4-39.6
5		55.5 CH			55.2-55.8
6		18.5 CH_2			18.3-18.8
7		33.2 CH_2			33.0-33.6
8		39.7 C			39.5-40.0
9		47.9 CH			47.5-48.0
10		37.2 C			36.9-37.4
11		23.5 CH_2			23.0-23.6
12	5.26 (1H, t, J $= 3.8$ Hz)	126.1 =CH	C-11, C-18	5.26 (1H, t, $J = 3.6$ Hz)	125.9-126.1
13		138.2 C=			137.8-138.7
14		42.2 C			42.1-42.5
15		28.2 CH_2			28.3-28.7
16		24.4 CH_2			23.8-24.9
17		48.2 C			48.1-48.2
18	2.20 (1H, dd, $J = 10.9$ Hz)	52.9 CH	C-12, C-13, C-17	2.19-2.20 (1H, dd, $J =$ 11.4 Hz)	52.7-53.5
19		39.1 CH			39.0-39.5
20		39.3 CH			38.8-39.1
21		30.8 CH_2			30.6-31.1
22		36.9 CH_2			36.7-37.3
23	0.99 s	28.4 CH_3	C-3, C-4, C-5, Me-24	0.99 s	28.1-28.8

Table 3.4 (Cont.): ¹H (500 MHz) and ¹³C (125 MHz) NMR chemical shift values* for 370RQ25 (recorded in CDCl₃) in comparison with literature data

Position	¹ H NMR δ experimental	¹³ C NMR δ experimental	HMBC correlations	¹ H NMR δ Literature ^a	¹³ C NMR δ Literature ^a
24	0.78 s	15.7 CH ₃	C-3, C-4, C-5, Me-23	0.78 s	15.6-15.8
25	0.94 s	15.8 CH ₃	C-5, C-9	0.93 s	15.5-16.6
26	0.80 s	17.3 CH ₃	C-7, C-9, C- 14	0.79 s	17.1-17.4
27	1.09 s	23.8 CH ₃	C-8, C-13, C-14, C-15	1.09 s	23.6-23.8
28		not detected			180.0-181.7
29	0.87 (d, <i>J</i> = 6.4Hz)	17.2 CH ₃	C-18, C-20	0.86 (d, <i>J</i> = 6.4Hz)	17.0-17.5
30	0.95 (d, <i>J</i> = 6.4Hz)	21.4 CH ₃	C-19, C-21	0.95 (d, <i>J</i> = 6.5Hz)	21.2-21.4

* Chemical shifts values in ppm.

^a(Migas *et al.*, 2005; Dais *et al.*, 2017)

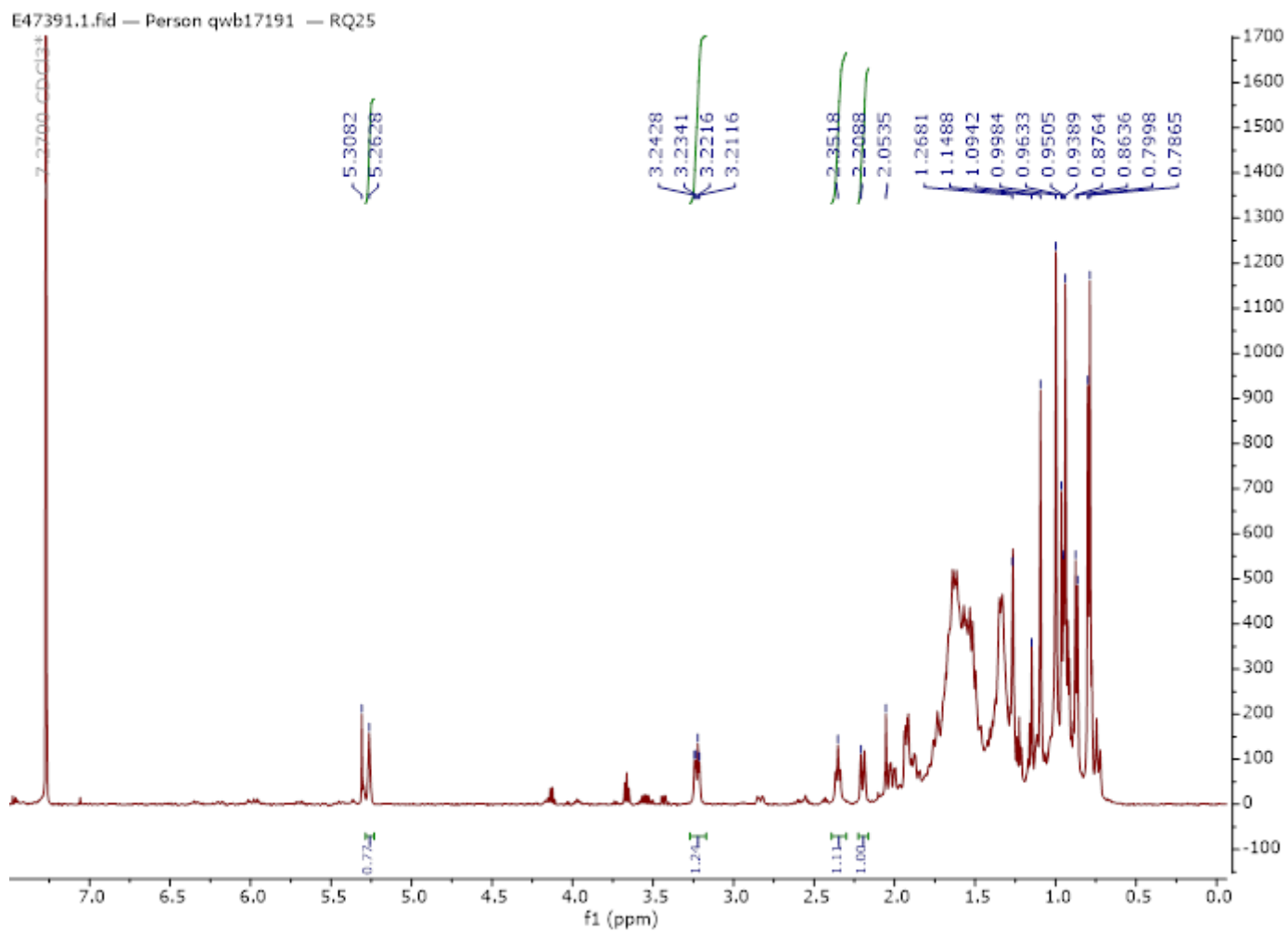


Figure 3.11 ^1H NMR spectrum (CDCl_3 , 500 MHz) of 370RQ25

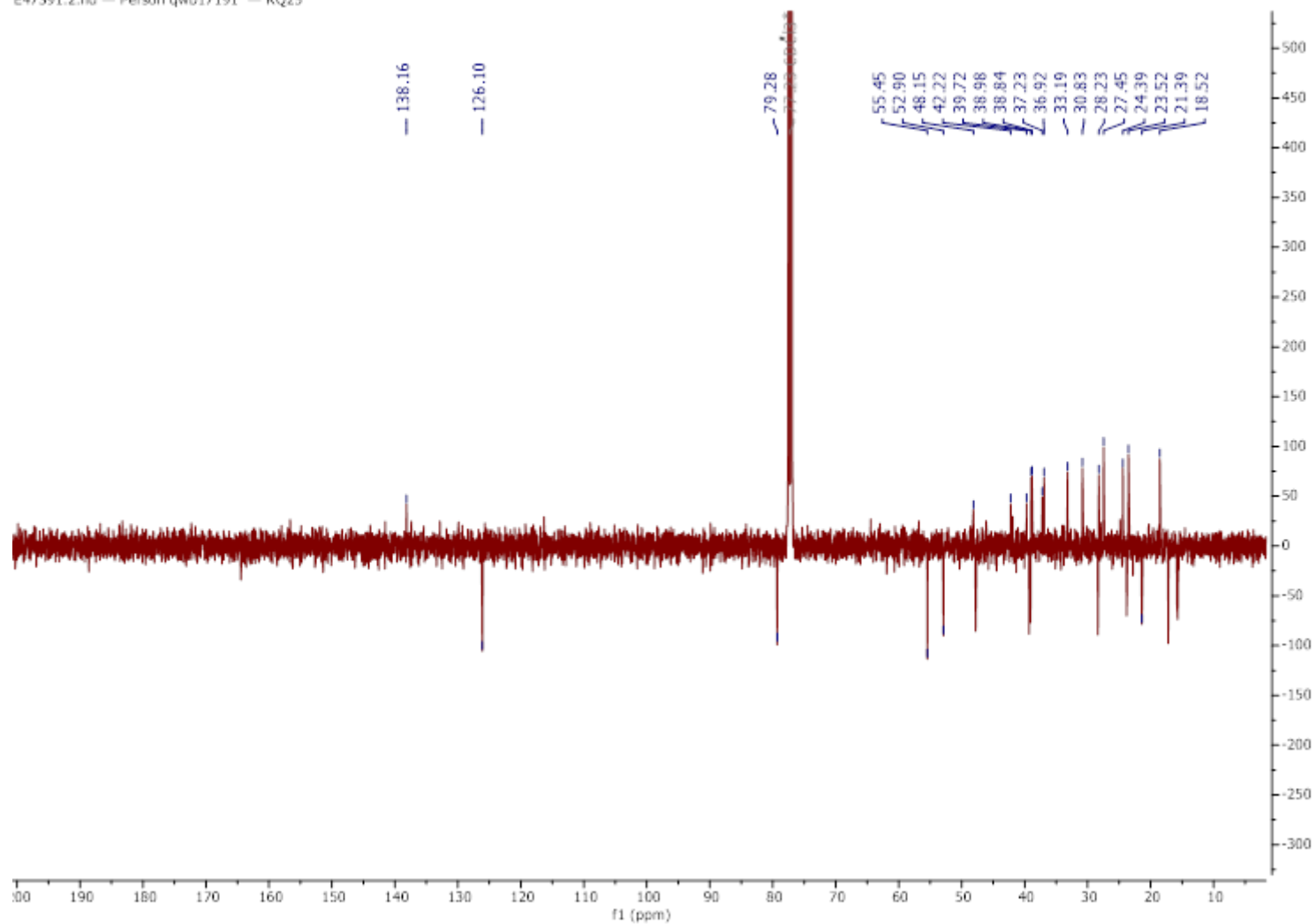


Figure 3.12 ^{13}C -DEPTQ NMR spectrum (CDCl_3 , 125 MHz) of 370RQ25

3.1.1.3 Characterisation of 390RQ5 as a mixture of stigmasterol (a), β -sitosterol (b) and campesterol (c)

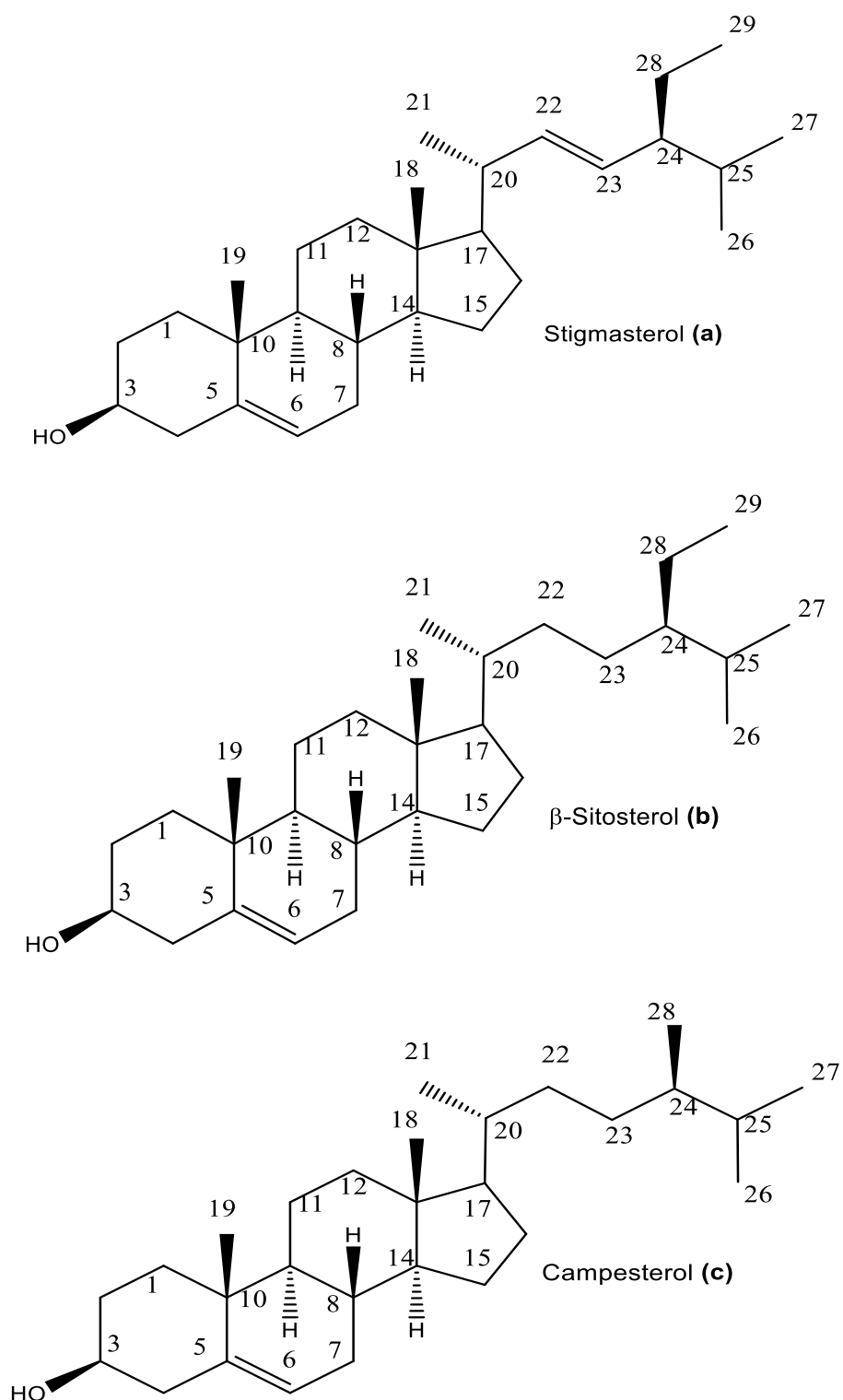


Figure 3.13 Structures of 390RQ5 or stigmasterol (a), β -sitosterol (b) and campesterol (c)

390RQ5 was isolated from the *n*-hexane extract of *S. arabica* as a white solid (17.8 mg) (Figure 3.13). A purple spot on TLC appeared after treatment with anisaldehyde-sulphuric acid reagent and heating.

Preliminary mass analysis was carried out using low resolution GC-EI- MS, the spectrum showed molecular ion peaks at 412 [M]⁺ and 414 [M]⁺, other peaks were also observed at *m/z* 394 and 396 for [M-H₂O]⁺, respectively. Comparison of this MS data with the NIST08 mass spectrometry database and a previous literature report (Suttiarporn *et al.*, 2015) suggested that 390RQ5 could be a mixture of stigmasterol (a) and β-sitosterol (b) with corresponding to the molecular formula C₂₉H₄₈O and C₂₉H₅₀O. Further analysis was carried out using HR-GC-EI-MS to confirm this data. The HR-GC-EI-MS spectrum of 390RQ5 showed three molecular ion adduct peaks as illustrated in Table 3.5.

Table 3.5. Molecular ions adduct peaks observed in the mass spectrum of 390RQ5

<i>m/z</i>	Theoretical mass	Formula	TMS derivative
486.4269	486.4257	C ₃₂ H ₅₈ OSi	β-sitosterol trimethylsilyl ether
484.4096	484.4100	C ₃₂ H ₅₆ OSi	Stigmasterol trimethylsilyl ether
472.4109	742.4100	C ₃₁ H ₅₆ OSi	Campesterol trimethylsilyl ether

Signals in the ¹H NMR spectrum of 390RQ5 (Figure 3.14) ranged between δ_H 0.69 to 5.36. The spectrum showed three signals at δ_H 5.36 (2H), 5.17 (1H, m), and 5.03 (1H, m) indicating the presence of olefinic protons. A multiplet at δ_H 3.53 (2H) was assigned to oxymethine protons. The appearance of sharp singlets at δ_H 0.69, 0.71, and 1.02 suggested the presence of methyl groups. These observations suggested the presence of more than one compound with a phytosterol skeleton, most likely a mixture of stigmasterol and β-sitosterol (Forgo and Kövér, 2004; Suttiarporn *et al.*, 2015). A characteristic cluster of overlapping signals was observed in the region of δ_H 0.5-2.5 and attributed to methylene and methine protons.

The DEPTQ ¹³C NMR (Figure 3.15) showed a signal at δ_C 72.0 assigned to the oxymethine carbon typical for C-3 of stigmasterol and β-sitosterol. Four distinctive signals at δ_C 140.9, 138.5, 129.5, and 121.9 corresponded to olefinic carbons. Signals at δ_C 140.9 and 121.9 were assigned to double bonds on the main skeleton at position

C5 and C6, other signals at δ_c 138.5 and 129.5 were assigned to the double bond in C-22 and C-23 of the side chain of stigmasterol. The signals for C-22 and C-23 on the side chain of β -sitosterol were observed at δ_c 34.2 and 26.3, respectively. Signals for methyl groups were observed in the range δ_c 12-22. Methylene and methine carbons typical for a saturated cyclic or linear hydrocarbon skeleton appeared in the range of δ_c 23-60.

The spectrum also showed a signal at δ_c 15.6 corresponding to the C-24 methyl of C_{28} sterols. Other weak signals appeared at δ_c 18.4 (Me-27), δ_c 20.4 (Me-26), δ_c 30.5 (C-23), δ_c 32.6 (C-25), δ_c 33.9 (C-22), δ_c 36.1 (C-20), and δ_c 39.0 (C-24) in agreement with the literature data reported for campesterol (C_{28} sterol/C-24 methyl sterol) (Wright *et al.*, 1978)

All 1H and ^{13}C connectivities for 390RQ5 (Table 3.6) were verified by HMBC. The HMBC experiment (Figure 3.16) showed long range correlations from the Me-19 at δ_H 1.02 to carbons at δ_c 37.5 (C-1, 3J), 141.0 (C-5, 3J), 50.4 (C-9, 3J), and 36.7 (C-10, 2J). The Me-18 at δ_H 0.69 and 0.71 showed 3J correlations to C-12, C-14, and C-17, as well as 2J correlations with C-13. The HMBC also revealed 3J correlations, between H-6 at δ_H 5.36 and C-4, C-8, and C-10. Another interesting correlation was for H-22 at δ_H 5.17 with C-17, C-20, Me-21, C-23, and C-24. The olefinic H-23 at δ_H 5.01 showed correlations with C-20, C-22, C-24, C-25, and C-28, which supported the presence of stigmasterol. All long-range correlations observed were consistent with the structure of stigmasterol (a) and β -sitosterol (b).

The complete assignment of 1H NMR and ^{13}C NMR values of 390RQ5 in comparison with the literature data is provided in Table 3.6.

Based on the above spectral data and by comparison with previous reports (Wright *et al.*, 1978; De-Eknamkul and Potduang, 2003; Pateh *et al.*, 2009; Edilu *et al.*, 2015), 390RQ5 was characterised as a mixture of stigmasterol (a), β -sitosterol (b), and campesterol (c) (Figure 3.4). Stigmasterol (a) and β -sitosterol (b) are two phytosterols commonly isolated from plants as a mixture (Pateh *et al.*, 2009). Although, stigmasterol (a) and β -sitosterol (b) have been previously isolated from other *Stachys* species (*S. spinosa* and *S. byzantina*) (Kotsos *et al.*, 2007; Khanavi *et al.*, 2005), this is the first report of their isolation from the aerial parts of *S. arabica*.

Previous reports have suggested that β -sitosterol may strengthen the immune system (Bouic *et al.*, 1999), and when tested in a randomised double-blind placebo-controlled

trial of 47 patients with pulmonary TB, patients who took β -sitosterol with anti-TB drugs showed improved weight gain and increased peripheral blood lymphocyte and eosinophil counts (Donald *et al.*, 1997). Another study revealed that stigmasterol and β -sitosterol isolated from a *Morinda citrifolia* leaf showed antimycobacterial activity with MIC values 32 and 128 $\mu\text{g/mL}$, respectively (Saludes *et al.*, 2002). Stigmasterol has also been reported to exhibit potent anti-inflammatory activity (Gabay *et al.*, 2010).

Table 3.6 ^1H (500MHz) and ^{13}C (125 MHz) NMR chemical shift values* for 390RQ5 (recorded in CDCl_3) in comparison with literature data

Position	Stigmasterol		β -sitosterol		Stigmasterol		β -sitosterol	
	^{13}C NMR δ Experimental	^{13}C NMR δ Literature ^a	^{13}C NMR δ Experimental	^{13}C NMR δ Literature ^a	^1H NMR δ Experimental	^1H NMR δ Literature ^b	^1H NMR δ Experimental	^1H NMR δ Literature ^b
1	37.5 CH ₂	37.1-37.6	37.5 CH ₂	37.1-37.6				
2	31.9 CH ₂	31.6-32.0	31.9 CH ₂	31.6-32				
3	72.1 CHOH	71.2-72.1	72.0 CHOH	71.2-72.1	3.53 (1H, m)	3.50-3.57 m	3.53 (1H, m)	3.51-3.57 m
4	42.6 CH ₂	42.2-42.5	42.4 CH ₂	42.2-42.5	2.21-2.32 m		2.21-2.32 m	
5	141.0 C	140.7-141.0	141.0 C	140.7-141				
6	121.9 CH	121.6-121.9	121.9 CH	121.3-121.9	5.36 (1H, br s)	5.3-5.36 br s	5.36 (1H, br s)	5.3-5.36 br s
7	32.1 CH ₂	31.9-32.1	32.1 CH ₂	31.9-32.1				
8	32.1 CH	31.9-32.1	32.1 CH	31.9-32.1				
9	50.4 CH	50-51	50.4 CH	50-51				
10	36.7 C	36.5-36.7	36.7 C	36.5-36.7				
11	21.3 CH ₂	21-21.7	21.3 CH ₂	21-21.7				
12	39.9 CH ₂	39.7-39.8	40.0 CH ₂	39.7-39.9				
13	42.6 C	42.3-42.5	42.6 C	42.3-42.5				
14	57.1 CH	56.9	57.0 CH	56.7-56.8				
15	24.6 CH ₂	24.4	24.5 CH ₂	24.3				

Table 3.6 (Cont.): ¹H (500MHz) and ¹³C (125 MHz) NMR chemical shift values* for 390RQ5 (recorded in CDCl₃) in comparison with literature data.

	Stigmasterol		β-sitosterol		Stigmasterol		β-sitosterol	
Position	¹³ C NMR δ Experimental	¹³ C NMR δ Literature ^a	¹³ C NMR δ Experimental	¹³ C NMR δ Literature ^a	¹ H NMR δ Experimental	¹ H NMR δ Literature ^b	¹ H NMR δ Experimental	¹ H NMR δ Literature ^b
16	29.1 CH ₂	28.4-29.3	28.5 CH ₂	28.2-28.5				
17	56.2 CH	55.9-56.1	56.3 CH	56.1-56.3				
18	12.3 CH ₃	12.1-12.3	12.1 CH ₃	11.9-12.1	0.71 (3H, s)	0.68-0.71 s	0.69 (3H, s)	0.68-0.71 s
19	19.6 CH ₃	19.4-19.8	19.6 CH ₃	19.4-19.8	1.02 (3H, s)	1.01-1.03 s	1.02 (3H, s)	1.01-1.03 s
20	40.7 CH	40.5-40.7	36.4 CH	36.2-36.3				
21	21.3 CH ₃	21.0-21.7	19.0 CH ₃	18.8-19.2	1.03 (3H, d)	1.02-1.04 d	0.93 (3H, d)	0.92-0.94
22	138.5 CH	138.1-138.7	34.2 CH₂	33.6-34.2	5.03 (1H, m)	4.98-5.07 m		
23	129.5 CH	128.9-129.6	26.3 CH₂	26.1-26.4	5.17 (1H, m)	5.14-5.20 m		
24	51.5 CH	51.0-51.3	46.1 CH	45.9-46.1				
25	32.1 CH	31.9-32.1	29.4 CH	29.1-29.4				
26	21.4 CH ₃	21.2-21.3	20.0 CH ₃	19.8-20.1	0.80-0.87**	0.80-0.90	0.80-0.87**	0.80-0.9
27	19.2 CH ₃	19.0-19.2	19.3 CH ₃	19.1-19.3	0.80-0.87**	0.80-0.90	0.80-0.87**	0.80-0.9
28	25.6 CH ₂	25.4-25.6	23.3 CH ₂	23.0-23.3				
29	12.5 CH ₃	12.1-12.4	12.2 CH ₃	12.0-12.3	0.80-0.87**	0.80-0.90	0.80-0.87**	0.80-0.9

* Chemical shift values are in ppm.

** overlapping peaks.

^a (Wright *et al.*, 1978; Pateh *et al.*, 2009; Edilu *et al.*, 2015)

^b (Pateh *et al.*, 2009; Edilu *et al.*, 2015)

E42315.1.fid — Person qwb17191 — 390HRQ5

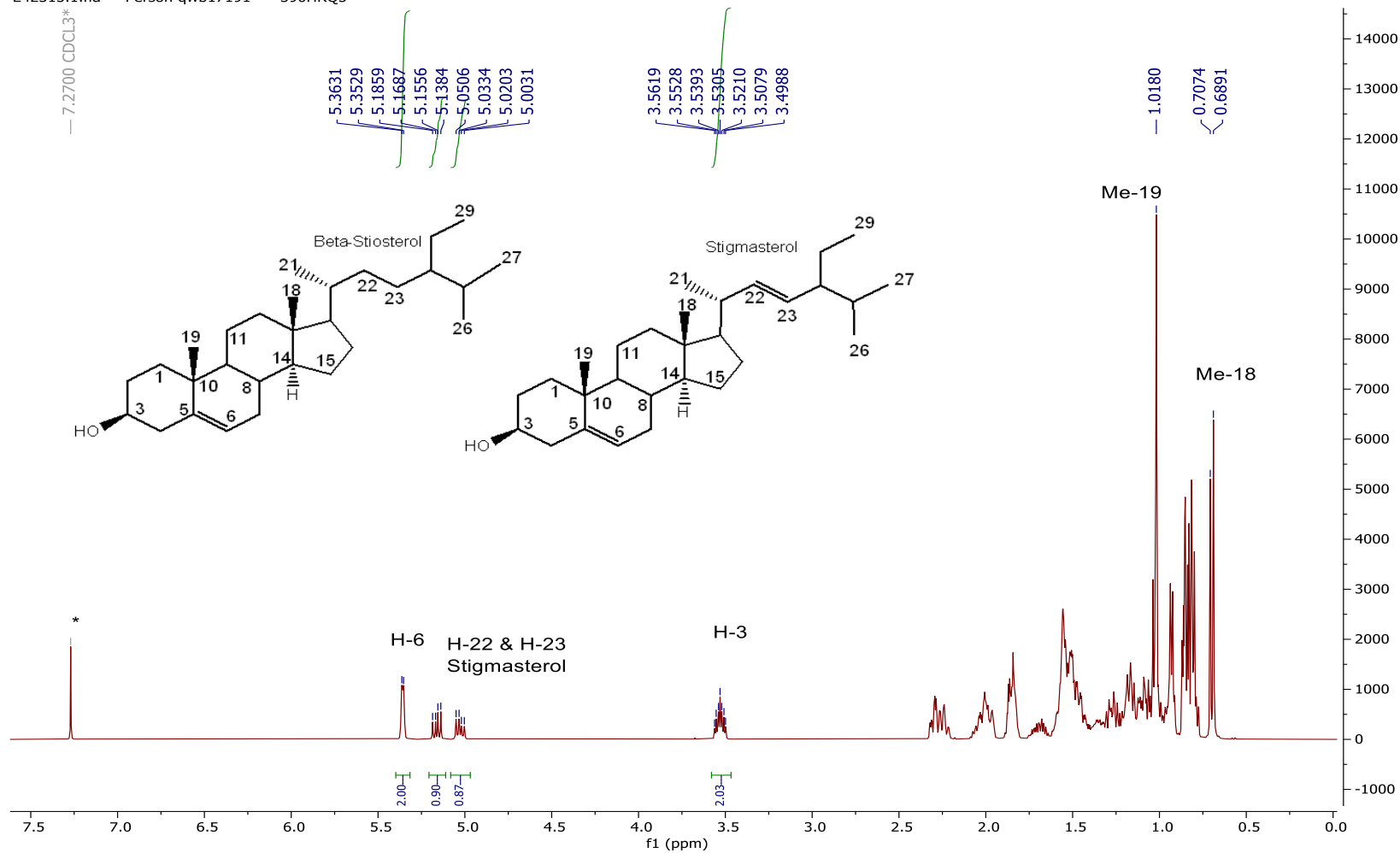


Figure 3.14 ¹H NMR spectrum (CDCl₃*, 500 MHz) of 390RQ5

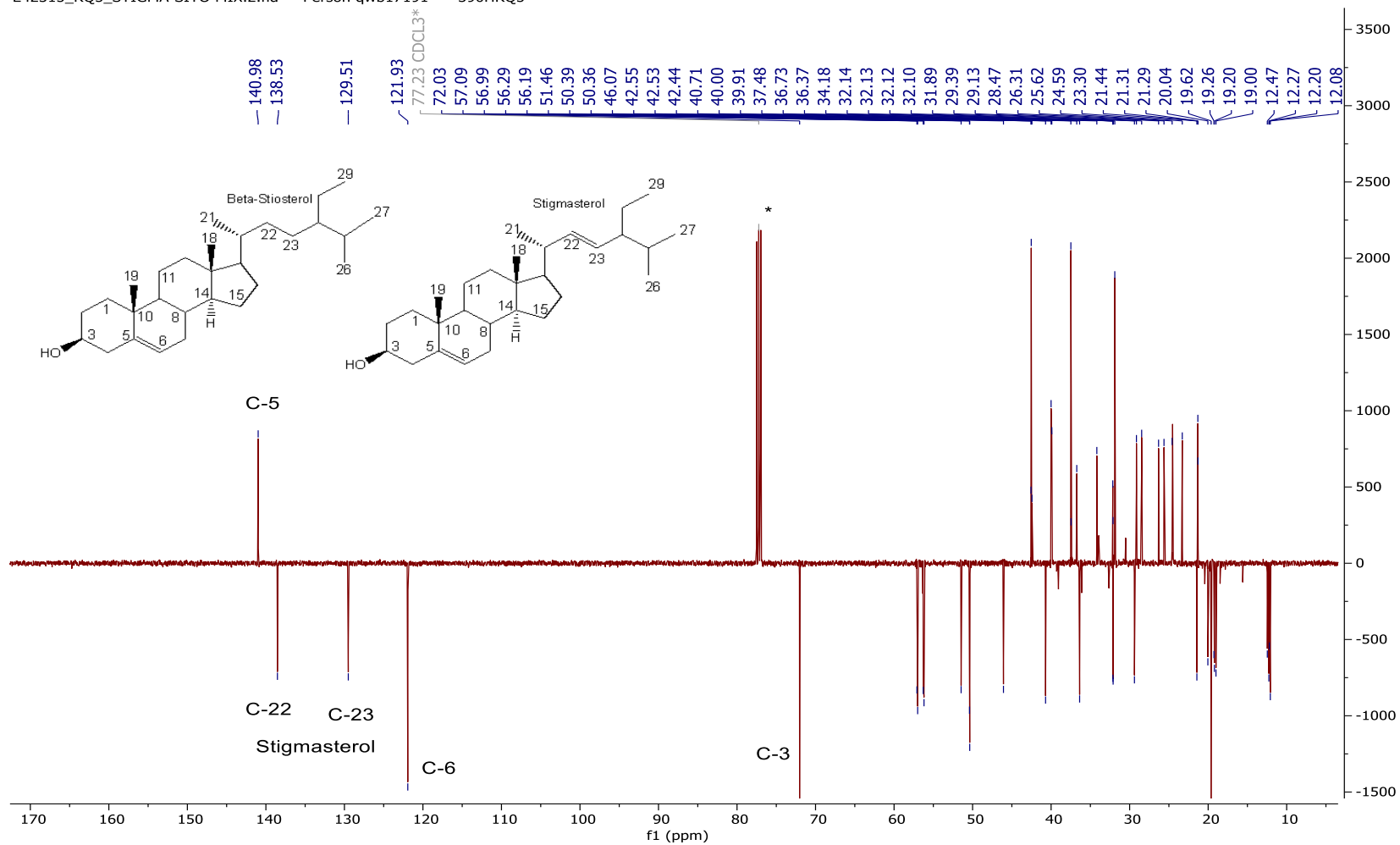


Figure 3.15 ¹³C-DEPTQ NMR spectrum (CDCl₃*, 125 MHz) of 390RQ5

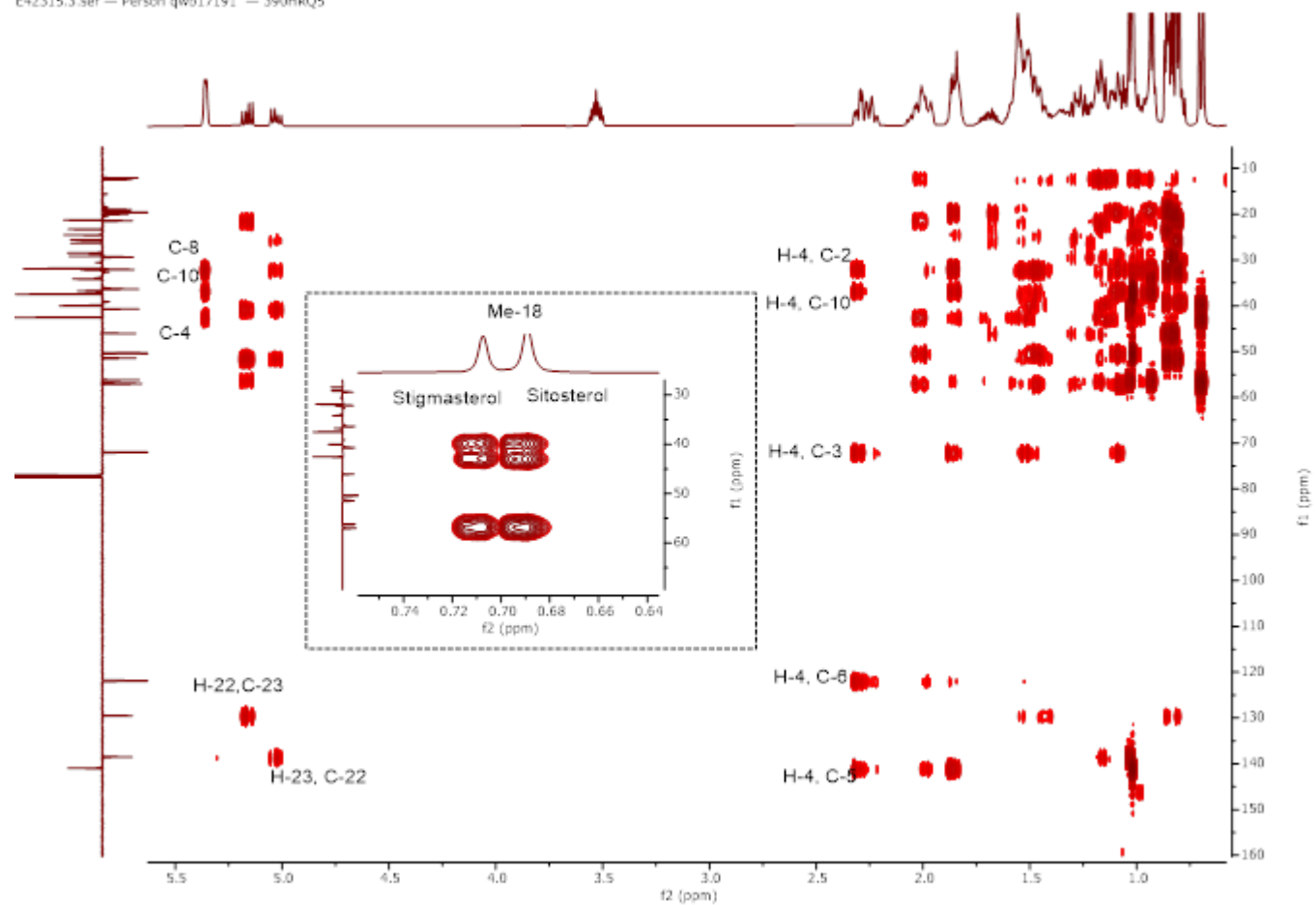


Figure 3.16 HMBC spectrum (CDCl₃^{*}, 500 MHz) of 390RQ5

3.1.1.4 Characterisation of 390RQ3/ 370RQ24 as a mixture of steryl fatty acid esters (a) and phytyl fatty acid esters (b)

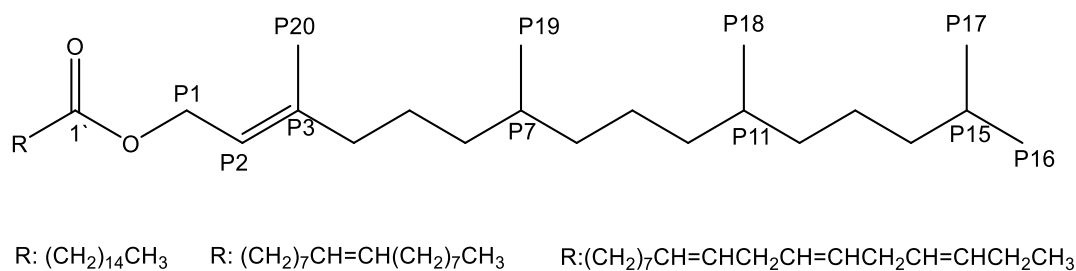
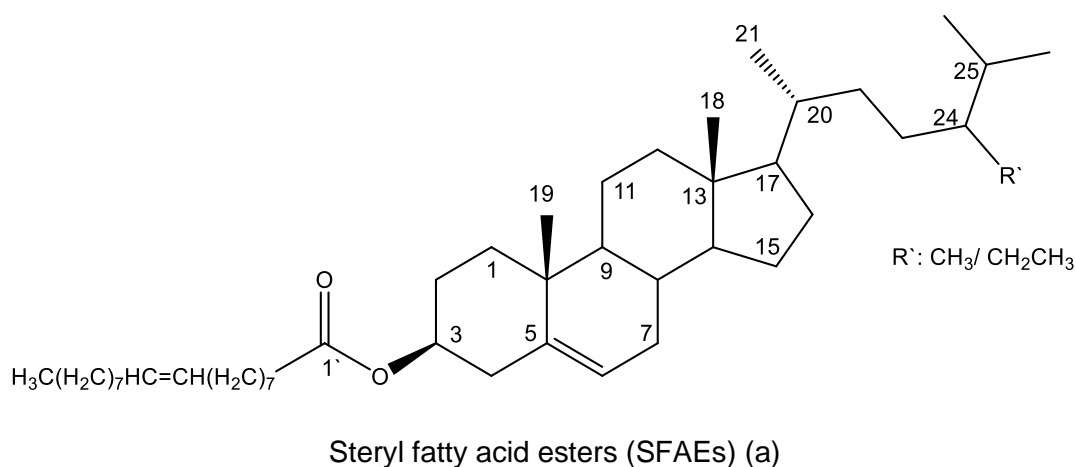


Figure 3.17 Structures of 390RQ3/370RQ24 or mixture of steryl fatty acid esters (SFAEs) (a) and a mixture of phytyl fatty acid esters (PFAEs) (b)

390RQ3 (12.8 mg) and 370RQ24 (20 mg) (Figure 3.17) were isolated from the *n*-hexane extract of *S. arabica* and the ethyl acetate extract of *F. excelsior* as white amorphous solids. No UV-active spot was observed on TLC plates under short UV light. Both revealed a purple spot on TLC after treatment with anisaldehyde-sulphuric acid reagent and heating.

The ^1H NMR spectra of 390RQ3/370RQ24 (Figure 3.18, Table 3.7) showed a signal (**A**) for olefinic protons at δ_{H} 5.35. Additional characteristic signals (**B**) at δ_{H} 4.59 could be assigned to protons attached to an esterified oxymethine. The spectra also showed two clear singlets (**J**) and (**K**) at δ_{H} 1.03 and δ_{H} 0.69 typical for methyl groups of a sterol moiety. These observations suggested the presence of an esterified sterol (Luo, 2006). Signals (**A**), (**B**), a multiplet (**D**) at δ_{H} 2.0, and the singlet (**E**) at δ_{H} 1.70 could be assigned to the presence of an esterified phytol. These signals correspond to P2, P1, P4, and the olefinic methyl (P-20) of a phytol moiety, respectively (Gilardoni *et al.*, 2011). Other signals (**C**) at δ_{H} 2.32 were typical for methylenes ($\alpha\text{-CH}_2$) adjacent to a carbonyl ester. A strong signal (**F**) at δ_{H} 1.27 (**F**) indicated the presence of a methylene envelope $(\text{CH}_2)_n$, suggesting the presence of a fatty acid moiety.

The ^{13}C DEPTQ NMR spectra (Figure 3.19) of 390RQ3/ 370RQ24 supported the presence of phytol and sterol moieties that were esterified with fatty acids. Signals for ester carbonyl groups were observed at δ_{C} 173.5-174.2 (C^1). Other distinctive signals at δ_{C} 140.0 and 122.8 were characteristic for the double bond of C-5 and C-6 of the sterol moiety. A signal at δ_{C} 73.9 was attributed to C-3 of the sterol moiety, this chemical shift was downshielded ($\Delta\delta \approx 2$ ppm) compared to sterol which confirmed that an ester function was present. The most upfield signals at δ 12.1 and 12.2 were assigned to Me-18 and Me-29 of the sterol moiety. The spectra showed signals at δ_{C} 142.8 and 118.4 which were assigned to the double bond P-3 and P-2, respectively of the phytol moiety. These chemical shifts were recorded with $\Delta\delta \approx 4.5$ ppm (P2) and $\Delta\delta \approx 2$ ppm (P3) when compared to phytol which confirmed the presence of an ester function. Signals observed at δ_{C} 61.4 and 16.6 were assigned to P-1 and P-20 of the phytol moiety, respectively. The presence of terminal methyls at δ_{C} 14.3 and 14.2 as well as other signals at δ_{C} 130.2 and 129.98 ($\text{CH}=\text{CH}$), δ_{C} 34 ($\alpha\text{-CH}_2$), 29-30 $(\text{CH}_2)_n$, 27.7 ($-\underline{\text{C}}\text{H}_2\text{CH}_3$), 24.7 ($\beta\text{-CH}_2$), and 22.7 confirmed the presence of fatty acid moieties.

The HMBC experiment of 390RQ3 (Figure 3.20) confirmed the esterification with fatty acids through a 3J correlation between δ_{H} 4.59 (P1, H-3) and carbonyl carbons at δ_{C} 173.6-174.3. In addition, a clear correlation between δ_{H} 2.33 ($\alpha\text{-CH}_2$ of the fatty acid side chain) with carbonyl carbons at δ_{C} 173.6-174.3 confirmed the esterification with fatty acid. Other correlations were observed between δ_{H} 4.59 (P1) and δ_{C} 142.7 (P3), 118.4 (P2). The methyl proton at δ_{C} 1.7 (P20-H) showed 2J correlations with δ_{C} 142.7 (P3), and 3J correlations with the methylene carbon at δ_{C} 40 (P4), and 2J correlations to methine at δ_{C} 118.4 (P2). The HMBC spectrum showed 3J correlations between the

methyl at δ_H 0.69 (Me-18 of steryl moiety) with C-12, C-14 & C-17, and 2J correlations with C-13. 3J correlations between the methyl at δ_H 1.03 (Me-19 of the steryl moiety) with C-5, C-9 C-1 were also observed.

All 1H and ^{13}C connectivities for 390RQ3 were verified by HMBC. All long-range correlations observed were consistent with the presence of a mixture of steryl fatty acid esters (SFAEs) (a) and phytol fatty acid esters (PFAEs) (b).

The combined spectral data confirmed that 390RQ3 and 370RQ24 were mixtures of steryl fatty acid esters (SFAEs) (a) and phytol fatty acid esters (PFAEs) (b). The NMR spectral data were in good agreement with previous reports (Gilardoni *et al.*, 2011; Pereira *et al.*, 2002; Ng *et al.*, 2015; Rathee *et al.*, 2012; Julien-David *et al.*, 2008; Rasool *et al.*, 1991).

The complete assignment of 1H NMR and ^{13}C NMR values of 390RQ3/ 370RQ24 is provided in Table 3.7.

The positive ion mode HR-nanoESI-MS spectrum of 390RQ3/ 370RQ24 showed the following molecular ion adducts peaks for 390RQ3 and 370RQ24 (Table 3.8).

Table 3.8 Molecular ions adduct peaks observed in the mass spectra of 390RQ3 & 370RQ24

[M+NH ₄] ⁺	<i>m/z</i> observed 390RQ3	<i>m/z</i> observed 370RQ24	Compound	Theoretical mass
SFAEs				
C ₄₇ H ₈₂ O ₂ NH ₄	696.6657	696.6657	β -Sitosterol oleate	696.6653
C ₄₆ H ₈₀ O ₂ NH ₄	682.6501		Campesterol oleate	682.6497
PFAEs				
C ₃₆ H ₇₀ O ₂ NH ₄	552.5711	552.5710	Phytol palmitate	552.5714
C ₃₈ H ₇₂ O ₂ NH ₄	578.5869	578.5867	Phytol oleate	578.5871
C ₃₈ H ₆₈ O ₂ NH ₄	--	574.5556	Phytol linolenate	574.5558

Table 3.7 ¹H (500 MHz) and ¹³C (125 MHz) NMR chemical shift values* for 390RQ3/ 370RQ 24 recorded in CDCl₃

390RQ3/ 370RQ24 (a)			390RQ3/ 370RQ24 (b)		
Position	¹³ C δ	¹ H δ	Position	¹³ C δ	¹ H δ
1	37.2		P1	61.4	4.59 d
2	28.1		P2	118.4	5.35 t
3	73.9	4.59	P3	142.8	
4	38.4		P4, P14	40.1, 39.6	
5	140.0		P5, P9, P13	25.4, 25.3, 25.0	
6	122.8	5.35	P6	36.9	
7	32.2		P7, P11	33.0, 32.9	
8	32.2		P8, P10, P12	37.6, 37.6, 37.5	
9	50.3		P15	28.2	
10	37.2		P16, P17	22.9, 22.8	
11	21.3		P18, P19	20.0, 19.9	
12	40.0		P20	16.6	1.70 s
13	42.6				
14, 16	56.9, 56.3		Fatty acid moiety		
15	24.5		Position	¹³ C δ	¹ H δ
16	28.5		C1'	173.6-174.3	
18	12.1	0.69 s	α- CH ₂	34.6	2.33 t
19,21,27	19.5, 19.0, 19.3,	H-19: 1.03 s	β-CH ₂	24.7	1.55-1.65 m
20	36.4/ 36.1		CH=CH	129.9-130.2	5.35
22	34.4/ 34.1		(CH ₂) _n	29-30	1.25-1.27
23	26.3		(-CH ₂ CH ₃)	22.7	
24	46.1		CH ₃	14.3	0.85-0.95 t
25	32.1				
26	20.0				
28	15.4/ 23.3				
29	12.2				

* Chemical shifts values in ppm

Although phytyl nonadecanoate has previously been reported in *S. byzantina* (Khanavi *et al.*, 2005), this is the first report of the isolation of phytyl oleate and phytyl palmitate from the genus *Stachys*. This is also the first report of the isolation of β -sitosterol oleate and campesterol oleate from *Stachys*.

Steryl fatty acid esters (a) and phytyl fatty acid esters (b) including phytyl stearate, phytyl linolenate and phytyl docosanoate have been previously detected in *F. excelsior leaves* (Van Bergen *et al.*, 1997). As far as we know, this is the first time that the isolation of β -sitosterol oleate, phytyl palmitate, and phytyl oleate are reported.

Plant sterols occur either free or as conjugates with fatty acids (steryl fatty acid ester; SFAEs), hydroxycinnamic acids, glycosides, or with glycosides and fatty acids (acylated steryl glycosides) (Moreau *et al.*, 2002; Moreau *et al.*, 2018). The occurrence of sterol fatty esters is common in plants. The fatty acid moieties range between C₁₂-C₂₂, with palmitic, stearic, oleic, linoleic, and linolenic being predominant. Their role in plants remain unclear (Dyas and Goad, 1993; Kawanishi and Hashimoto, 1987; Luo *et al.*, 2006). β -sitosterol laurate and β -Sitosterol myristate have been isolated from *Punica granatum* (Bagri *et al.*, 2009). β -Sitosterol triacontanoate isolated from *Capparis decidua* has showed cytotoxicity on A549 human lung cancer cells (Rathee *et al.*, 2012).

Phytyl fatty acid esters (PFAEs) have been found in mosses, marine organisms, and plants (Pereira *et al.*, 2002; Krauß and Vetter, 2018). PFAEs are present in olive oil (Biedermann *et al.*, 2008) . According to various reports, PFAEs represent a safe storage form for free phytol and free fatty acids. It has been suggested that the free phytol resulted from the degradation of chlorophyll and galactolipids during plant senescence, fruit ripening, and stress factors (like frost, drought, or nitrogen deficiency) (Anderson *et al.*, 1984; Lippold *et al.*, 2012). Interestingly, PFAEs have been found in ripe red, yellow bell peppers, and unripe green olives. But not detected in ripe black olives and ripe tomatoes, which might lead to another assumption not related to fruit ripening and unknown factor may be involved in the formation of PFAEs (Krauß *et al.*, 2017).

In recent years, phytosterols have attracted attention due to their cholesterol-lowering properties. For this reason, phytosterols, as free and esterified forms, are added to food products. Clinical studies showed that phytosterols and their esters reduce cholesterol levels at similar rates (Moreau *et al.*, 2002; Moreau *et al.*, 2018).

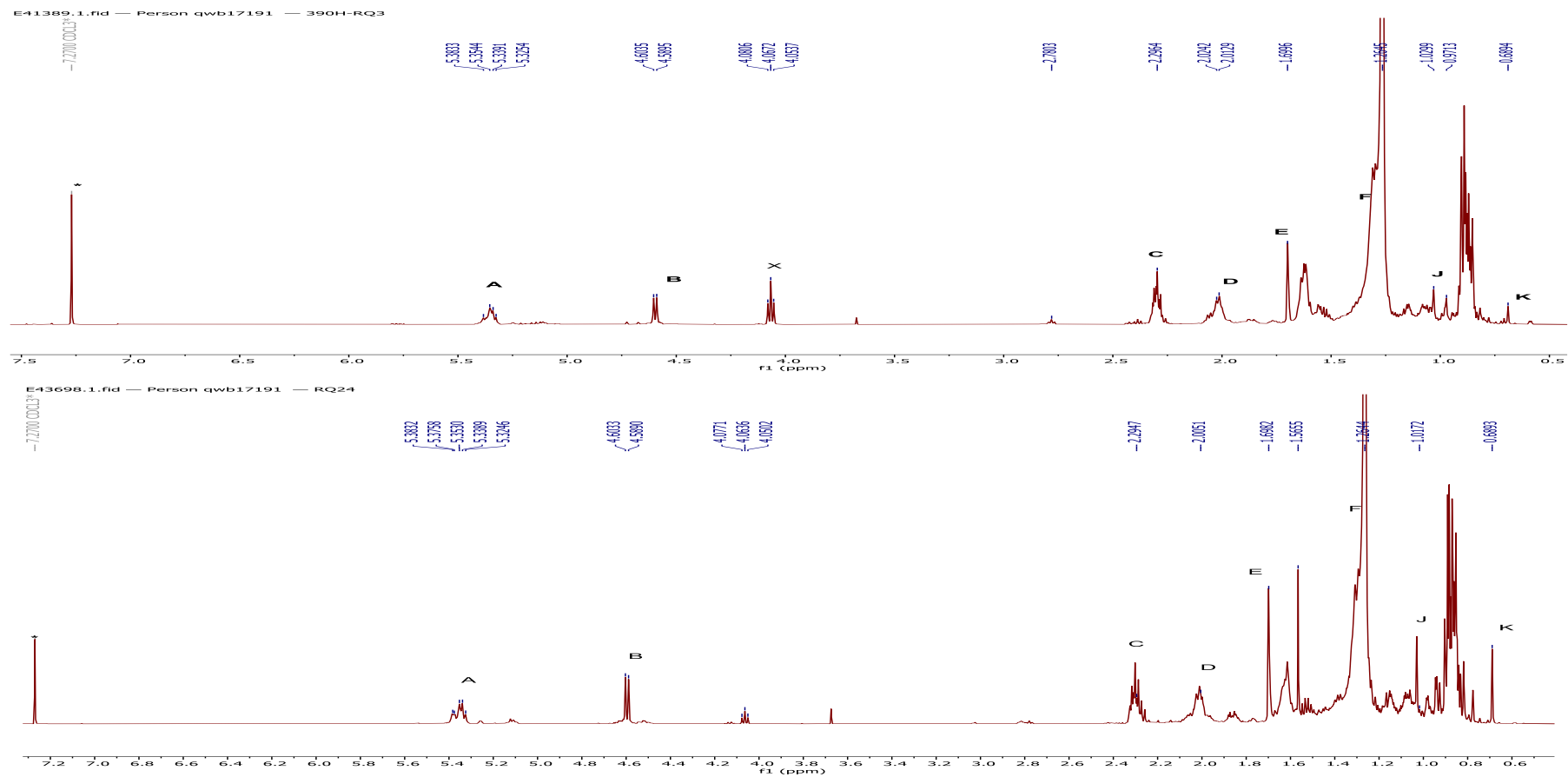


Figure 3.18 ¹H NMR spectra (CDCl₃*, 500 MHz) of 390RQ3 and 370RQ24

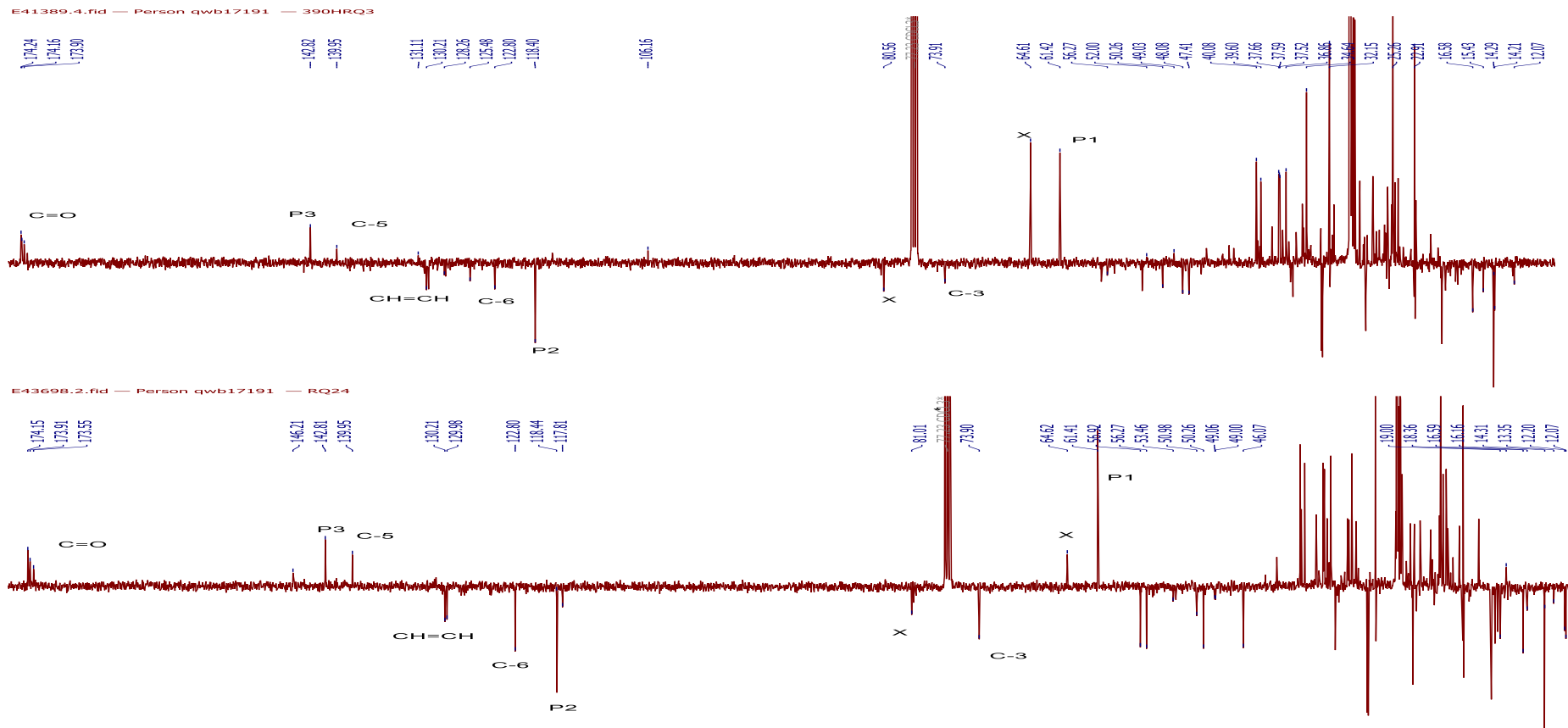


Figure 3.19 ¹³C DEPTQ NMR spectra (CDCl₃*, 125 MHz) of 390RQ3 and 370RQ24

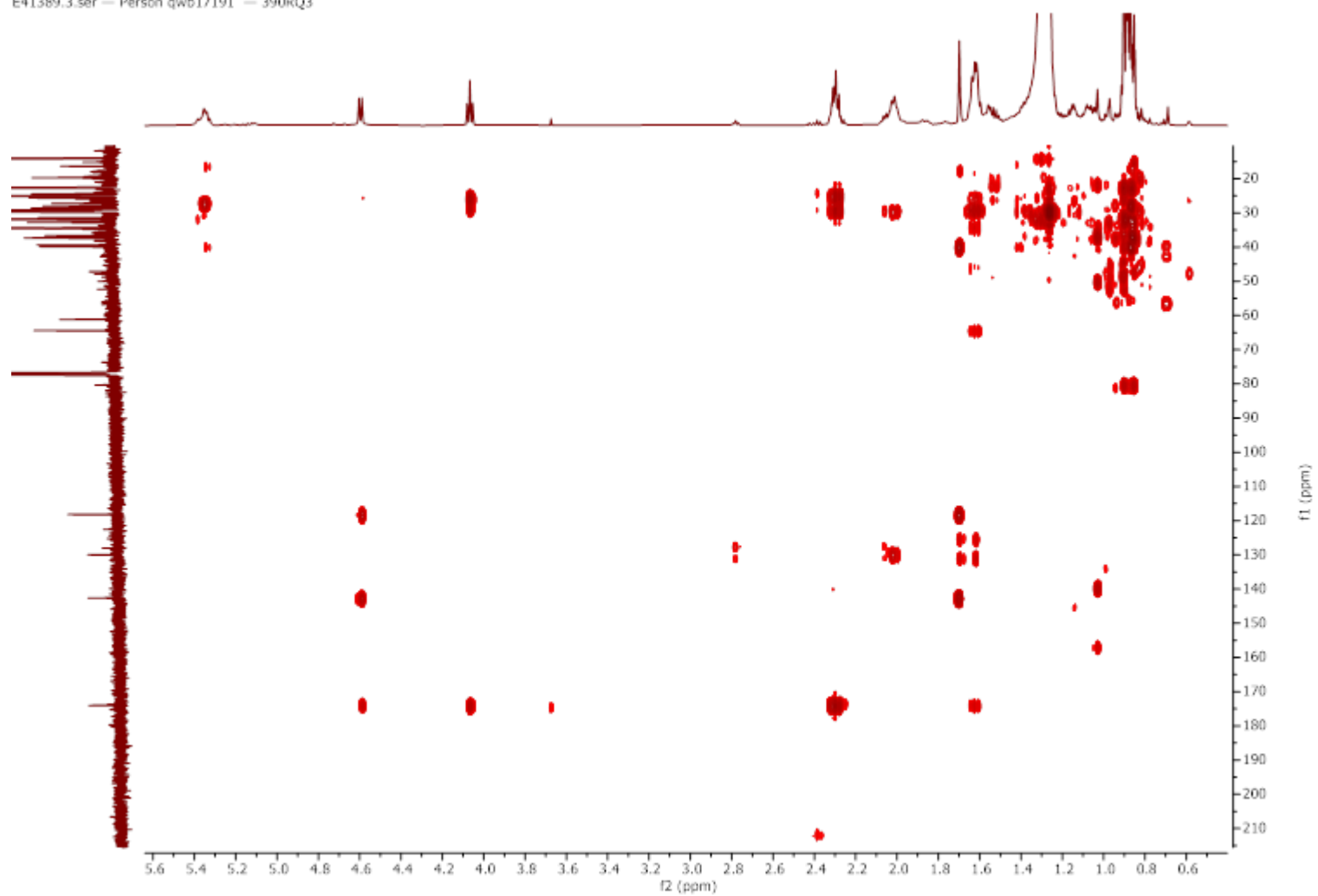


Figure 3.20 HMBC spectrum (CDCl_3 , 500 MHz) of 390RQ3

3.1.2 Pheophytins

390RQ10, 390RQ27 and 390RQ28 were isolated from the ethyl acetate extract of *S. arabica* as dark green solids (20, 4.7 and 7.3 mg, respectively) (Figure 3.21). On TLC plates, they gave a quenching spot and a red fluorescence under short (254 nm) and long UV light (366 nm), respectively.

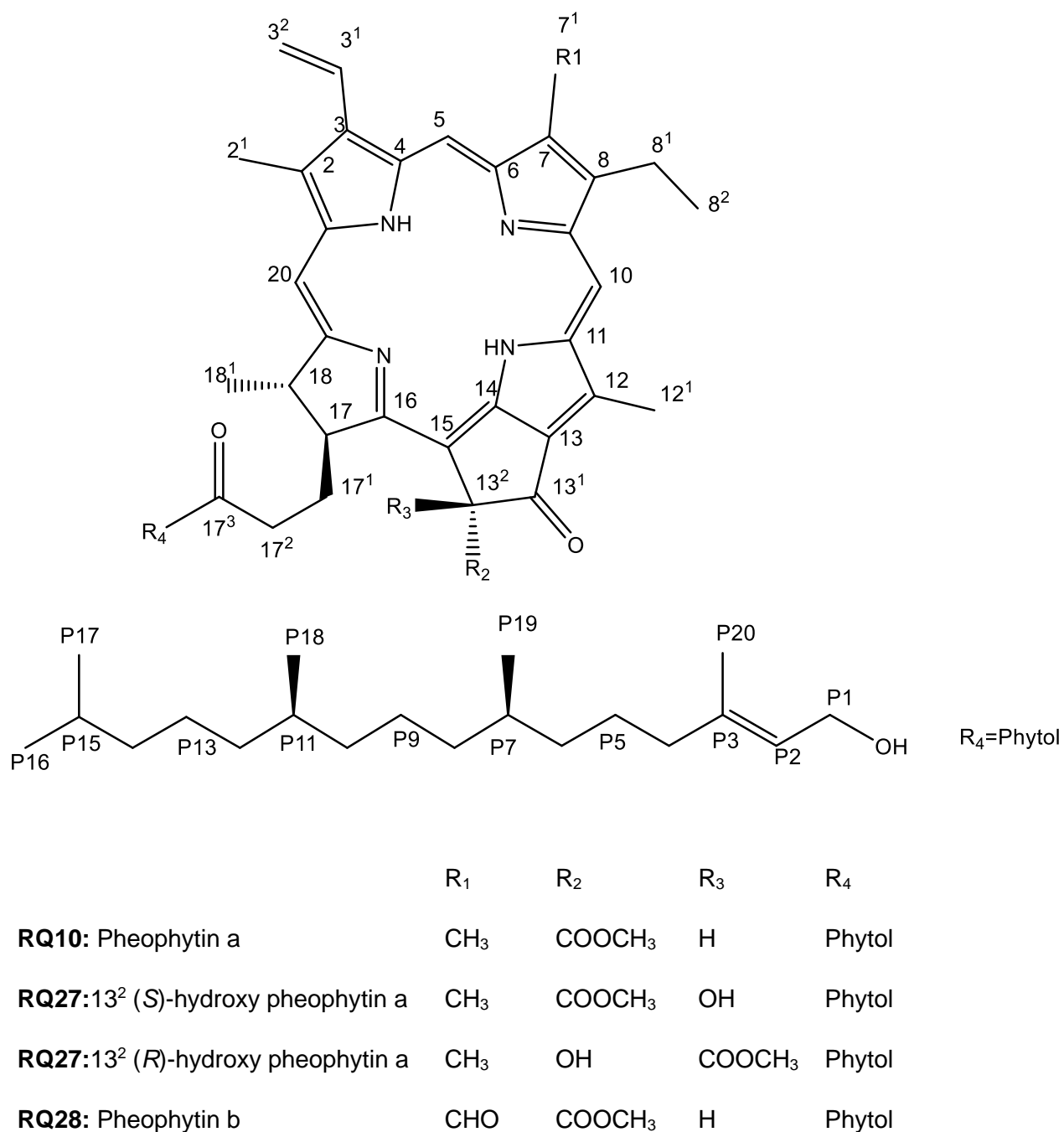


Figure 3.21 Structures of 390RQ10, 390RQ27, and 390RQ28

3.1.2.1 General NMR assignments

The ^1H NMR spectra (Table 3.9-3.11, Figure 3.23, 3.26, and 3.29) showed proton signals distributed over a wide range of chemical shifts. This included signals typical for three downfield singlets in the region of δ_{H} 8.5-11.0. A multiplet at around δ_{H} 8.0, and two doublet of doublets between δ_{H} 6.15 and 6.40 were assigned to vinyl groups ($-\text{CH}=\text{CH}_2$). In the region of δ_{H} 3.0-4.0 sharp singlets were attributed for methyl or methoxy groups.

The DEPTQ- ^{13}C NMR spectra (Table 3.9-3.11, Figure 3.24, 3.27, and 3.30) showed carbonyl carbons in the downfield region of δ_{C} 169-193. Four olefinic methines ($=\text{CH}-$) appeared between δ_{C} 93 and 130, and exomethylenes ($=\text{CH}_2$) at around δ_{C} 123. The spectra displayed some methine and methoxy carbons between δ_{C} 50-55. Methyl groups in the region of δ_{C} 11-24 were also observed. This is typical for the ^{13}C spectra of pheophytins.

390RQ10, RQ27, RQ28 were substituted with a phytol ester at C-17³ which was clearly seen in all ^1H and ^{13}C NMR spectra with the following diagnostic features: an oxymethylene multiplet at around δ_{H} 4.47 corresponding to (P1), a triplet near δ_{H} 5.15 corresponding to (P2), a multiplet at about δ_{H} 1.9 (P4), a singlet at around δ_{H} 1.60 (P20), and signals in the region of δ_{H} 0.79-0.89 suggesting the presence of aliphatic methyl groups of a phytol moiety. Peaks close to δ_{C} 117.9 and 61.8 corresponded to (P2) and (P1). The methyl groups P-20, P-18 and P-19 of phytol appeared near δ_{C} 16.5 and 19.9, respectively. These spectral data are in good agreement with a previous report (Brito Filho *et al.*, 2014).

3.1.2.2 Characterisation of 390RQ10 as pheophytin a

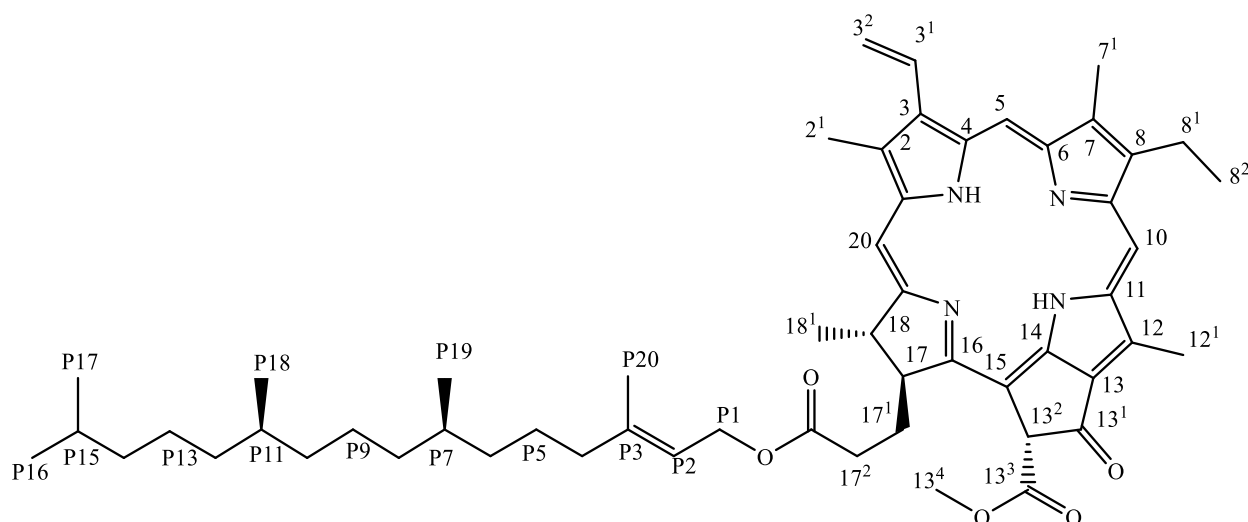


Figure 3.22 Structure of 390RQ10 or pheophytin a

390RQ10 was isolated from the ethyl acetate extract of *S. arabica* as a dark green solid (20 mg) (Figure 3.22). Under short UV light (254 nm), it gave a quenching spot and under long UV light (366 nm) a red fluorescence on the TLC plate. A green spot was observed after treatment with anisaldehyde- sulphuric acid reagent and heating.

The positive ion mode HR-nanoESI-MS spectral data of 390RQ10 showed a quasi-molecular ion $[M+H]^+$ at m/z 871.5740 (theoretical m/z 871.5732) suggesting for a molecular formula of $C_{55}H_{74}N_4O_5$. A molecular ion peak $2[M+H]^+$ at m/z 1743.1425 indicated the presence of a dimer species.

The 1H NMR (Figure 3.23, Table 3.9) showed typical signals for the presence of a pheophytin skeleton with three highly deshielded sharp proton singlets for olefinic protons at δ_H 9.39 (H-5), 9.49 (H-10), and 8.75 (H-20). A multiplet at δ_H 7.97 was assigned to the vinyl group at C-3¹ ($CH=CH_2$). The signals for H-3² appeared as doublet of doublets at δ_H 6.18 and 6.28. The three olefinic methyls for 7¹, 2¹, and 12¹ appeared as sharp singlets at δ_H 3.2, 3.4, and 3.69, respectively. An ethyl group at C-8 appeared as a multiplet at δ_H 3.66 (2H-8¹) and as a triplet at δ_H 1.69 (3H-8²), respectively. Singlets at δ_H 6.29 and 3.91 were assigned to H-13² and methoxy in H-13⁴. A signal of four multiplets in the region of δ_H 2-2.8 corresponded to H-17¹, H-17²,

and a doublet at δ_H 1.83 for H-18¹. The ¹H NMR spectrum also revealed an oxymethylene multiplet at δ_H 4.47 (2H, P1), a triplet at δ_H 5.16 (1H, P2), a multiplet at δ_H 1.9 (2H, P4), a singlet at δ_H 1.60 (3H, P20) and signals in the region of δ_H 0.78-0.88 suggesting the presence of aliphatic methyl groups of a phytol moiety in good agreement with a previous report (Brown, 1994).

The DEPTQ NMR spectrum (Table 3.9, Figure 3.23) showed the presence of 55 carbons, including 33 quaternary carbons/CH₂, and 22 CH₃/CH. This included three carbonyls with signals at δ_C 189.7, 173.9, and 169.6 revealing the presence of one ketone at C-13¹, and two carbonyl esters at C-17³ and C-13³, respectively. The presence of one methoxy group at C-13⁴ was confirmed with a peak at δ_C 52.9. Other signals at δ_C 11.2 and 12.1 were assigned to methyls in C-7¹, 2¹, and 12¹, respectively. Peaks for the ethyl side chain appeared at δ_C 17.4 (CH₃ at 8²) and δ_C 19.4 (CH₂ at 8¹). Peaks at δ_C 16.3 and 19.7 corresponded to the methyl groups P-20, P-19 and P-19 of phytol, respectively.

The complete assignment of ¹H NMR and ¹³C NMR values of 390RQ10 in comparison with the literature data is provided in Table 3.9.

Comparison of the above spectral data with MS and NMR data from the literature (Tomaz *et al.*, 2008; Hargus *et al.*, 2007; Schwikkard *et al.*, 1998; Droupadi and Krishnan, 1984; Abraham and Rowan, 1991; Brown, 1994; Goodman *et al.*, 1973; Yaacob *et al.*, 2015) confirmed the identification of 390RQ10 as pheophytin a. This is the first report of pheophytin a in *S. arabica* aerial parts.

Pheophytin a has previously showed anti-inflammatory properties (Lin *et al.*, 2014). Another study demonstrated that pheophytin a isolated from *Lonicera hypoglauca* had potent activity against hepatitis C virus by inhibiting viral protease (Wang *et al.*, 2009). Investigation of the anti-HIV activity of an extract of *Ocimum labiatum* led to the identification of pheophytin a as a potent anti-HIV compound targeting HIV-1 protease (Kapewangolo *et al.*, 2017). Pheophytin a has showed antibacterial activity against *E. coli* and *B. subtilis* (Matsuo *et al.*, 1996), antifungal activity against *C. albicans* (ATCC 90028 & 76615) (Gomes *et al.*, 2015). Pheophytin a has also shown *in vitro* antioxidant activity (Subramoniam *et al.*, 2012; Higashi-Okai *et al.*, 2001).

The acyclic diterpene phytol is found in plants as the esterified side chain of chlorophyll a/b and pheophytin a/b (Ludwiczuk *et al.*, 2017). Phytol, isolated from *Lucas volkensis*, has previously demonstrated antimycobacterial activity against Mtb with a MIC of 2 µg/mL (Rajab *et al.*, 1998).

In the present study, pheophytin a was assessed for its effect on THP-1 cell viability, and its potential immunomodulatory effects on TNF-α and IL-12 production by LPS-stimulated THP-1 cells (for further details see section 3.2.5, 3.3.5 and 3.3.9).

Table 3.9: ¹H (500 MHz) and ¹³C (125 MHz) NMR chemical shift values* for 390RQ10 recorded in CDCl₃ in comparison to literature data

position	¹ H NMR δ Experimental	¹ H NMR δ Literature ^a	¹³ C NMR δ Experimental	¹³ C NMR δ Literature ^a	Carbon type
1			142.8	142.3-142.9	C
2			132.0	131.1-131.8	C
2 ¹	3.40 (3H, s)	3.39-3.41 (3H, s)	12.1	12.1-12.3	CH ₃
3			136.5	136.5-136.8	C
3 ¹	7.97 (1H, dd, <i>J</i> = 17, 11.5 Hz)	7.95-8.02 (1H, dd <i>J</i> = 17, 11 Hz)	129.0	129.0-129.2	CH
3 ^{2E}	6.28 (1H, d, <i>J</i> = 18 Hz)	6.27-6.29 (1H, d, <i>J</i> = 18 Hz)	122.7	122.7-123.1	CH ₂
3 ^{2Z}	6.17 (1H, d, <i>J</i> = 11.5 Hz)	6.16-6.18 (1H, d, <i>J</i> = 11.5 Hz)			
4			136.2	136.2-136.5	C
5	9.34 (1H, s)	9.35-40 (1H, s)	97.5	97.3-97.7	CH
6			155.6	155.5-155.6	C
7			136.1	136.1-136.2	C
7 ¹	3.20 (3H, s)	3.19-3.25 (3H, s)	11.2	11.2-11.4	CH ₃
8			145.2	145.2-145.3	C
8 ¹	3.66 (2H, m)	3.6-3.7 (2H, m)	19.4	19.6-19.7	CH ₂
8 ²	1.69 (3H, t, <i>J</i> = 7.2 Hz)	1.66-1.70 (3H, t, <i>J</i> = 7.6 Hz)	17.4	16.3-17.5	CH ₃
9			150.9	150.9-151.0	C
10	9.49 (1H, s)	9.49-9.52 (1H, s)	104.4	104.4-104.6	CH
11			137.9	137.9-138.1	C
12			129.0	129.0-129.1	C
12 ¹	3.69 (3H, s)	3.64-3.70 (3H, s)	12.1	12.2-12.3	CH ₃
13			129.0	129-129.2	C
13 ¹			189.7	189.6-189.8	C
13 ²	6.29 (1H, s)	6.26-6.30 (1H, s)	64.7	64.7-64.9	CH
13 ³			169.6	169.6-173.0	C
13 ⁴	3.91 (3H, s)	3.88-3.91 (3H, s)	52.9	52.9-53.1	CH ₃

Table 3.9 (Cont.): ¹H (500 MHz) and ¹³C (125 MHz) NMR chemical shift values* for 390RQ10 recorded in CDCl₃ in comparison to literature data

position	¹ H NMR δ Experimental	¹ H NMR δ Literature ^a	¹³ C NMR δ Experimental	¹³ C NMR δ Literature ^a	Carbon type
14			149.7	149.6-150.2	C
15			105.2	105.1-105.2	C
16			161.3	161.2-161.3	C
17	4.25 (1H, m)	4.15-4.4 (1H, m)	51.3	51.1-51.4	CH
17 ¹			29.8	29.8-29.9	CH ₂
17 ²			31.2	31.2-31.4	CH ₂
17 ³			173.9	172.0-173.2	C
18	4.47 (1H, m)	4.2-4.49 (1H, m)	50.2	50.1-50.4	CH
18 ¹	1.83 (3H, d)	1.8-1.84 (3H, d)	23.1	22.7-23.3	CH ₃
19			172.2	170.0-172.6	C
20	8.57 (1H, s)	8.55-8.60 (1H, s)	93.1	93.1-93.7	CH
Phytol					
P1	4.47 (2H, m)	4.45-4.5 (2H, m)	61.5	59.40-61.5	CH ₂
P2	5.16 (1H, t, <i>J</i> = 7.0 Hz)	5.1-5.14 (1H, t, <i>J</i> = 7.0 Hz)	117.8	117.6-118.1	CH
P3			142.0	141.9-142.9	C
P4	1.9 (2H, m)	1.86-1.98 (2H, m)	39.8	39.8-40.0	CH ₂
P20	1.6 (3H, s)	1.25-1.67 (3H, s)	16.3	16.3-16.8	CH ₃
P16, P17	0.78-0.88 m	0.71-0.87 (6H, m)	22.6 & 22.7	22.6-22.8	CH ₃
P18, P19	0.78-0.88 m	0.71-0.87 (6H, m)	19.7	19.6-19.8	CH ₃
P5, P9, P13	1.00-1.55** Overlapping peaks	1.00-1.55 (19H, m)	24.4-24.9	24.5-25.3	CH ₂
P6			36.7	36.4-36.8	CH ₂
P7, P11			32.7 & 32.8	32.7-32.9	CH
P8, P10, P12			37.3-37.4	37.4-37.5	CH ₂
P14			39.3	39.0-39.5	CH ₂
P15			28.0	27.9-28.1	CH

*Chemical shift values are in δ ppm ^a (Abraham and Rowan, 1991; Schwikkard *et al.*, 1998; Tomaz *et al.*, 2008; Yaacob *et al.*, 2015).

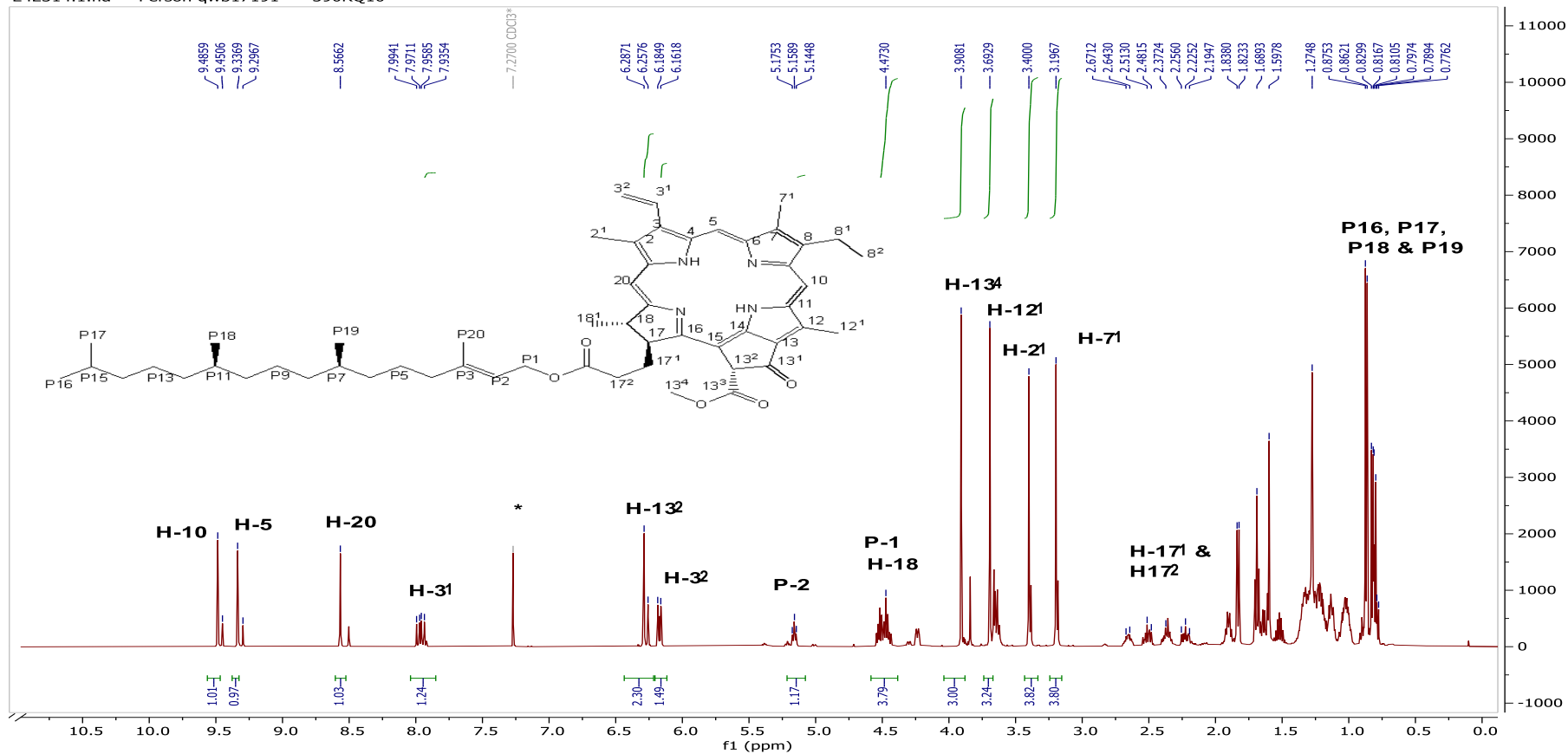


Figure 3.23 ¹H NMR spectrum (CDCl₃*, 500 MHz) of 390RQ10

E42314_RQ10.2.fid — Person eas03133 — 390RQ10

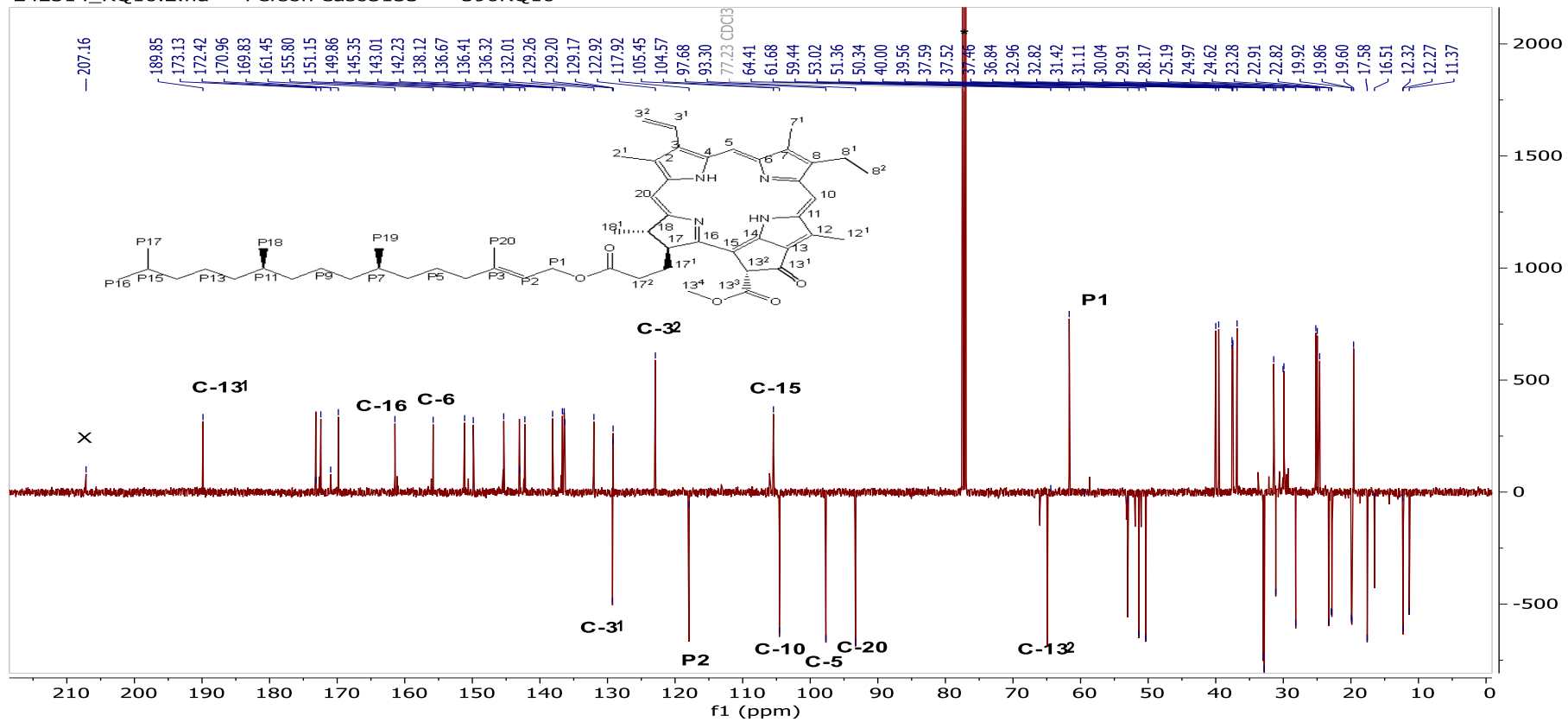


Figure 3.24 ¹³C-DEPTQ NMR spectrum (CDCl₃^{*}, 125 MHz) of 390RQ10

X refers to solvent impurities.

3.1.2.3 Characterisation of 390RQ27 as a mixture of 13²(S)-hydroxy pheophytin a and 13² (R)-hydroxy pheophytin a

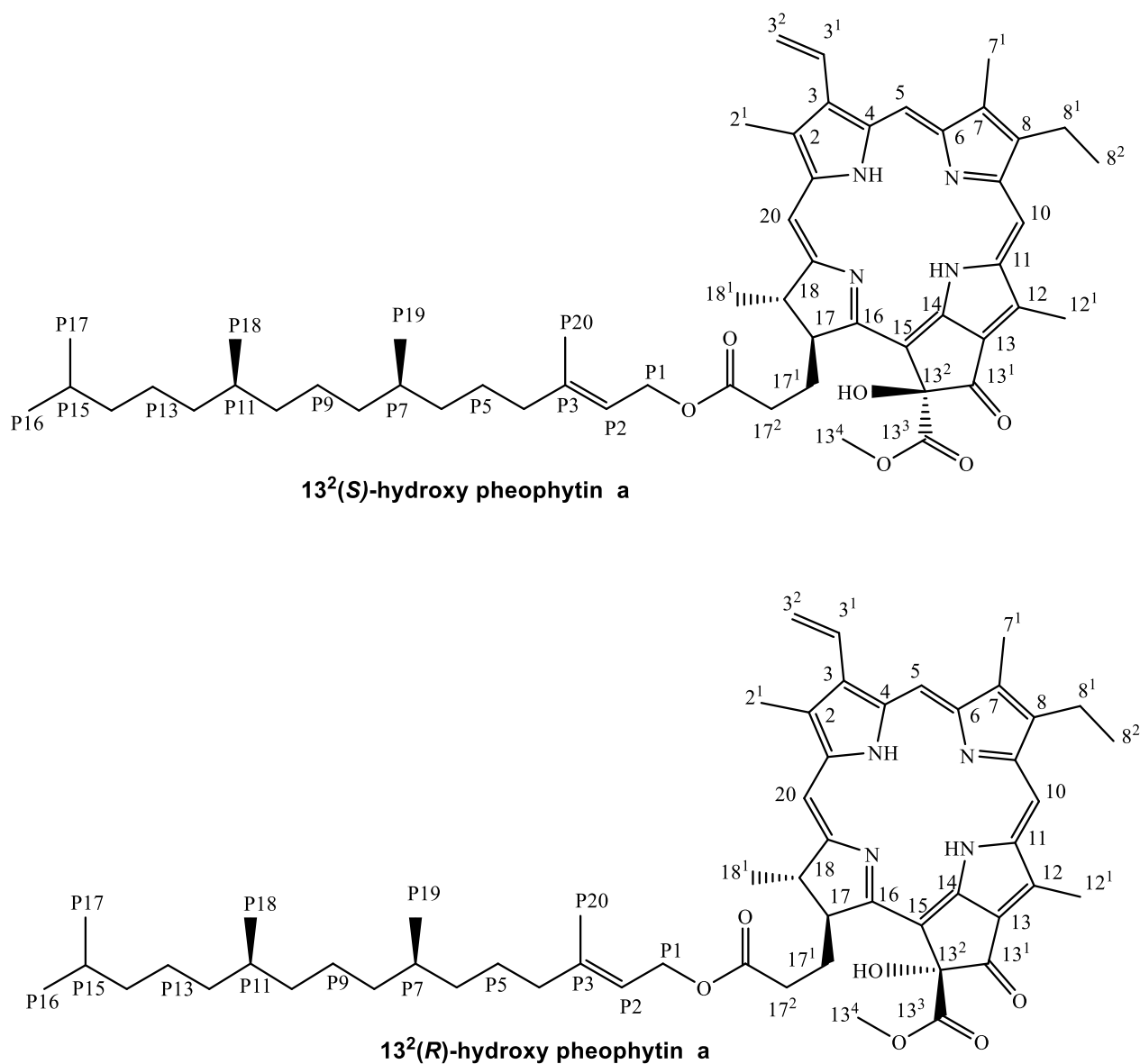


Figure 3.25 Structure of 390RQ27 or 13²(S,R)-hydroxy pheophytin a

390RQ27 was isolated from the ethyl acetate extract of *S. arabica* as a green solid (4.7 mg) (Figure 3.25). Under short UV light (254 nm), it gave a quenching spot and under long UV light (366 nm) a red fluorescence on the TLC plate. An olive-green spot was observed after treatment with anisaldehyde- sulphuric acid reagent and heating.

The positive ion mode HR-nanoESI-MS data of 390RQ27 showed a quasi-molecular ion $[M+H]^+$ at m/z 887.5688 (theoretical m/z 887.5681) suggesting a molecular formula of $C_{55}H_{74}N_4O_6$. A molecular ion peak $2[M+H]^+$ at m/z 1775.1312 indicative for a dimer species was also observed.

The 1H and ^{13}C DEPTQ-NMR spectra of 390RQ27 (Figure 3.26, Figure 3.27, and Table 3.10) showed similar peaks as 390RQ10 except for the absence of signals at δ_H 6.29 (H-13², s) in the 1H -NMR and δ_C 64.7 (C-13²) in the ^{13}C NMR spectrum and the presence of a new signal at δ_C 192.3 which was assigned to a keto group (C-13¹) and a signal at δ_C 89.2 which was assigned to a quaternary carbon (C13²-OH).

The three olefinic methyls in 7¹, 2¹, and 12¹ appeared as sharp singlets (six singlet appeared in the spectrum due to (S) and (R) isomers at δ_H 3.25 and 3.26 (for H-7¹), δ_H 3.42 and 3.43 (for H-2¹) and δ_H 3.72 and 3.73 (for H-7¹), respectively. Two very close singlets at δ_H 3.62 and 3.63 were assigned to H-13⁴ (methoxy groups).

The DEPTQ NMR spectrum (Table 3.10, Figure 3.27) showed a signal at δ_C 192.3 assigned to a keto group at C-13¹. The signals at δ_C 89.2 and 89.3 were assigned to 13²-OH (R & S). The methyl in C-13⁴ appeared at δ_C 53.6 and 54. Peaks at δ_C 51.0 and 52.1 corresponded to C-17, and at δ_C 162.1 and 162.7 corresponded to C-16. The peaks at δ_C 172.7 -173.8 were assigned to C-17³, C-19, C-13³. Other signals at δ_C 11.5 & 12.3 and 12.5 were assigned to methyl groups in C-7¹, 2¹, and 12¹, respectively. Peaks for the ethyl side chain appeared at δ 17.7 (CH₃ at 8²) and δ 19.7 (CH₂ at 8¹).

Comparison of the δ_H and δ_C -values between 13² (S)-hydroxy pheophytin a and 13² (R)- hydroxy pheophytin a showed that differences occurred for δ_H of 17-CH and δ_C of C-16, C-17 and C-13⁴. These differences might be connected to the steric interaction between the bulky substituents at C-17 (the propionate phytyl ester side-chain) and configuration at C-13². Small differences were also detected in the δ_H of the 5-CH and 10-CH protons, as well as the 13² -COH protons. These observations were in good agreement with previous reports on the difference in δ_H values between 13² (S)- hydroxy-chlorophyll a and 13² (R)- hydroxy-chlorophyll a as well as those between 13² (S)- hydroxy-chlorophyll b and 13² (R)- hydroxy-chlorophyll b (Hynninen *et al.*, 2006)

The complete assignment of 1H NMR and ^{13}C NMR values of 390RQ27 in comparison with the literature data is provided in Table 3.10

Comparison of the above spectral data with the literature (Kobayashi *et al.*, 1991; Matsuo *et al.*, 1996; Jerz *et al.*, 2007; Yaacob *et al.*, 2015) confirmed the identification of 390RQ27 as the *S/R* unresolved mixture of 13²-hydroxy pheophytin a. This is the first report of the presence of 13² (*S,R*)-hydroxy pheophytin a in *S. arabica* aerial parts.

13² (*S,R*)-hydroxy pheophytin a has previously showed activity against *E.coli* and *B. subtilis* (Matsuo *et al.*, 1996), as well as anti-herpes simplex activity (Sakdarat *et al.*, 2009), and lipid-reducing activity (Freitas *et al.*, 2019).

In the present study, 13² (*S,R*)-hydroxy pheophytin a was assessed for its effect on THP-1 cell viability, and its potential immunomodulatory effects on TNF- α and IL-12 production from LPS-stimulated THP-1 cells (for further details see section 3.2.5, 3.3.5 and 3.3.9).

Table 3.10 ^1H (400 MHz) and ^{13}C (100 MHz) NMR chemical shift values* for 390RQ27 recorded in CDCl_3 in comparison with literature data

position	^1H NMR δ Experimental	^1H NMR δ Literature ^a	^{13}C NMR δ Experimental	^{13}C NMR δ Literature ^a	Carbon type
1			142.9, 143	142.0-142.9	C
2			132.0, 132.1	131.8-132.6	C
2 ¹	3.42, 3.43 (3H, s)	3.37-3.45 (3H, s)	12.3	12.1-12.4	CH ₃
3			136.5	136.3-137.0	C
3 ¹	8.01 (1H, m)	7.9-8.04 (1H, m)	129.3	129.1-129.4	CH
3 ^{2E}	6.30 (1H, d, <i>J</i> = 17.8 Hz)	6.30-6.32 (1H, d, <i>J</i> = 17.5 Hz)	123.1	122.9-123.6	CH ₂
3 ^{2Z}	6.19 (1H, d <i>J</i> = 11.6 Hz)	6.17-6.23 (1H, d, <i>J</i> = 11.5 Hz)			
4			136.5	136.2-136.4	C
5	9.44, 9.47 (1H, s)	9.30-9.60 (1H, s)	98.1, 98.2	97.9-98.4	CH
6			155.6, 155.8	155.4-155.9	C
7			136.7	136.2-136.6	C
7 ¹	3.25, 3.26 (3H, s)	3.10-3.30 (3H, s)	11.5	11.3-11.6	CH ₃
8			145.4	145.2-145.8	C
8 ¹	3.66 (2H, m)	3.53-3.7 (2H, m)	19.7	19.5-19.9	CH ₂
8 ²	1.69 (3H, m)	1.60-1.70 (3H, t)	17.7	17.5-17.6	CH ₃
9			151.3	151.1-151.4	C
10	9.59, 9.61 (1H, s)	9.50-9.72 (1H, s)	104.5	104.2-104.7	CH
11			137.8	137.8-138.4	C
12			129.6, 129.7	129.3-129.4	C
12 ¹	3.72, 3.73 (3H, s)	3.61-3.77 (3H, s)	12.5	12.2-12.7	CH ₃
13			127.2	126.3-127.7	C
13 ¹			192.3	192.0-192.2	C

Table 3.10 (Cont.): ¹H (400 MHz) and ¹³C (100 MHz) NMR chemical shift values* for 390RQ27 recorded in CDCl₃ in comparison with literature data

position	¹ H NMR δ Experimental	¹ H NMR δ Literature ^a	¹³ C NMR δ Experimental	¹³ C NMR δ Literature ^a	Carbon type
13 ² -OH	5.35 (R) 5.50 (S)	5.34-5.35 (R) 5.47-5.53 (S)	89.2, 89.3	89.0-89.4	C
13 ³			173.0,173.2	172.8-173.3	C
13 ⁴	3.62, 3.63 (3H, s)	3.61-3.73 (3H, s)	53.6, 54.0	53.4-53.8	CH ₃
14			150.1	149.8-150.9	C
15			107.9	107.1-107.7	C
16			162.1 (R) 162.7 (S)	161.9-162 (R) 162.5-162.6 (S)	C
17	4.68 (R) 4.16 (S) (1H, m)	4.48-4.69 (R) 4.15-4.17 (S) (1H, m)	51.0 (R) 52.1 (S)	50.8-50.9 (R) 51.8-52 (S)	CH
17 ¹			31.4,31.4	31.1-31.6	CH ₂
17 ²			31.7,31.8	31.6-32	CH ₂
17 ³			173.7,173.8	172.4-173.8	C
18	4.47 m	4.2-4.49 (1H, m)	50.4,50.6	50.2-50.9	CH
18 ¹			22.8	22.6-22.9	CH ₃
19			172.7	172.4-174	C
20	8.61, 8.63 (1H, s)	8.60-8.65 (1H, s)	93.7, 93.9	93.4-95	CH
Phytol					
P1	4.56(2H, m)	4.45-4.6 (2H, m)	61.6,61.8	61.6-61.9	CH ₂
P2	5.16(1H, t)	5.1-5.24 (1H, t)	118.0,118.1	117.8-118.4	CH
P3			142.3	142.8-143.0	C
P4	1.9 (2H, m)	1.86-2.0 (2H, m)	40.1	39.8-40.2	CH ₂
P20	1.6 (3H, s)	1.3-1.7 (3H, s)	16.5,16.6	16.3-16.7	CH ₃

*Chemical shift values are in δ ppm

^a(Kobayashi *et al.*, 1991; Matsuo *et al.*, 1996; Jerz *et al.*, 2007; Yaacob *et al.*, 2015)

D324328.1.fid — Person qwb17191 — RQ27 — @proton CDCl3 {C:\NMRdata} VS 90

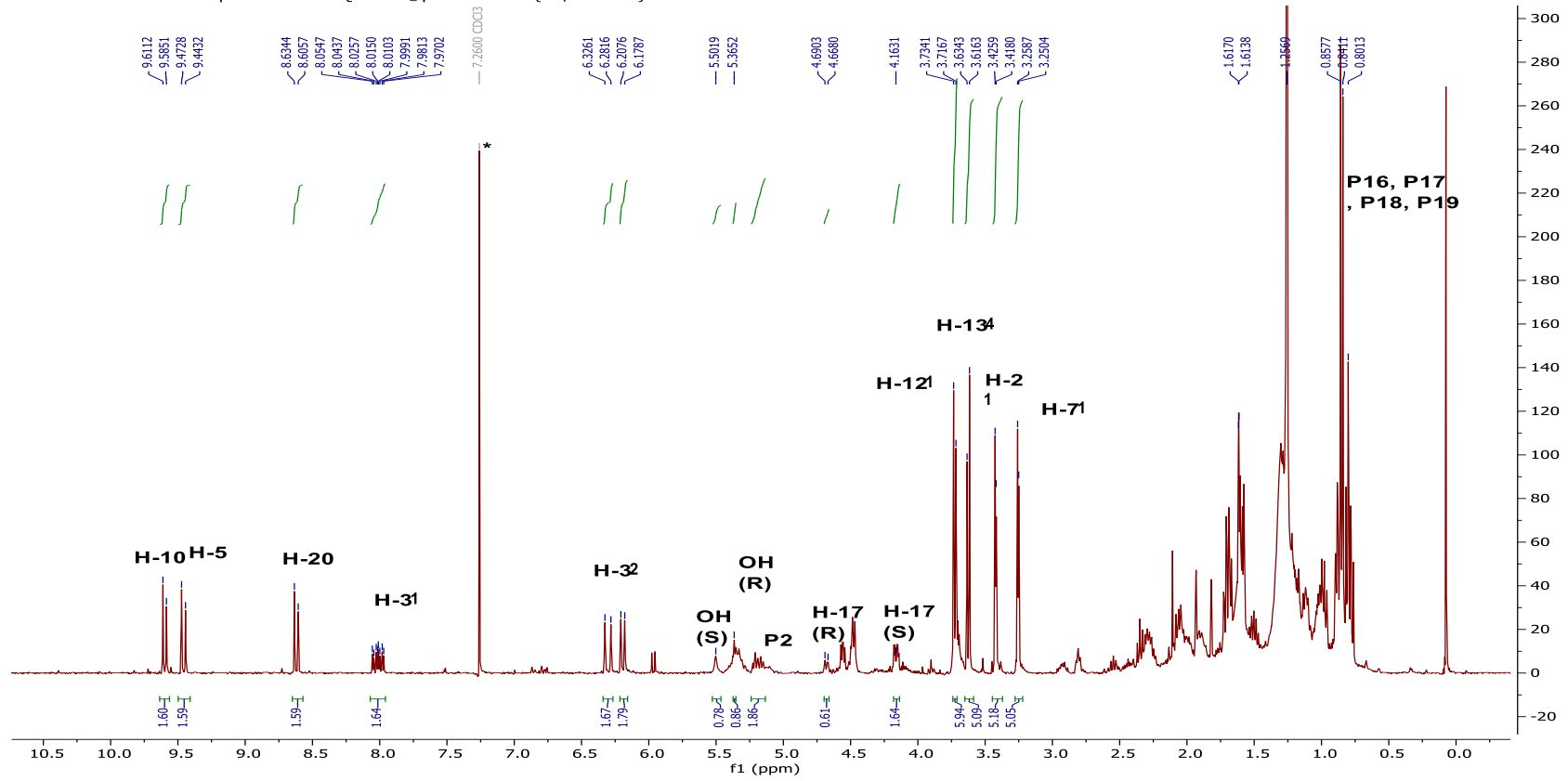


Figure 3.26 ^1H NMR spectrum (CDCl_3 , 400 MHz) of 390RQ27

D324328.3.fid — Person qwb17191 — RQ27 — @jmod CDCl3 {C:\NMRdata} VS 91

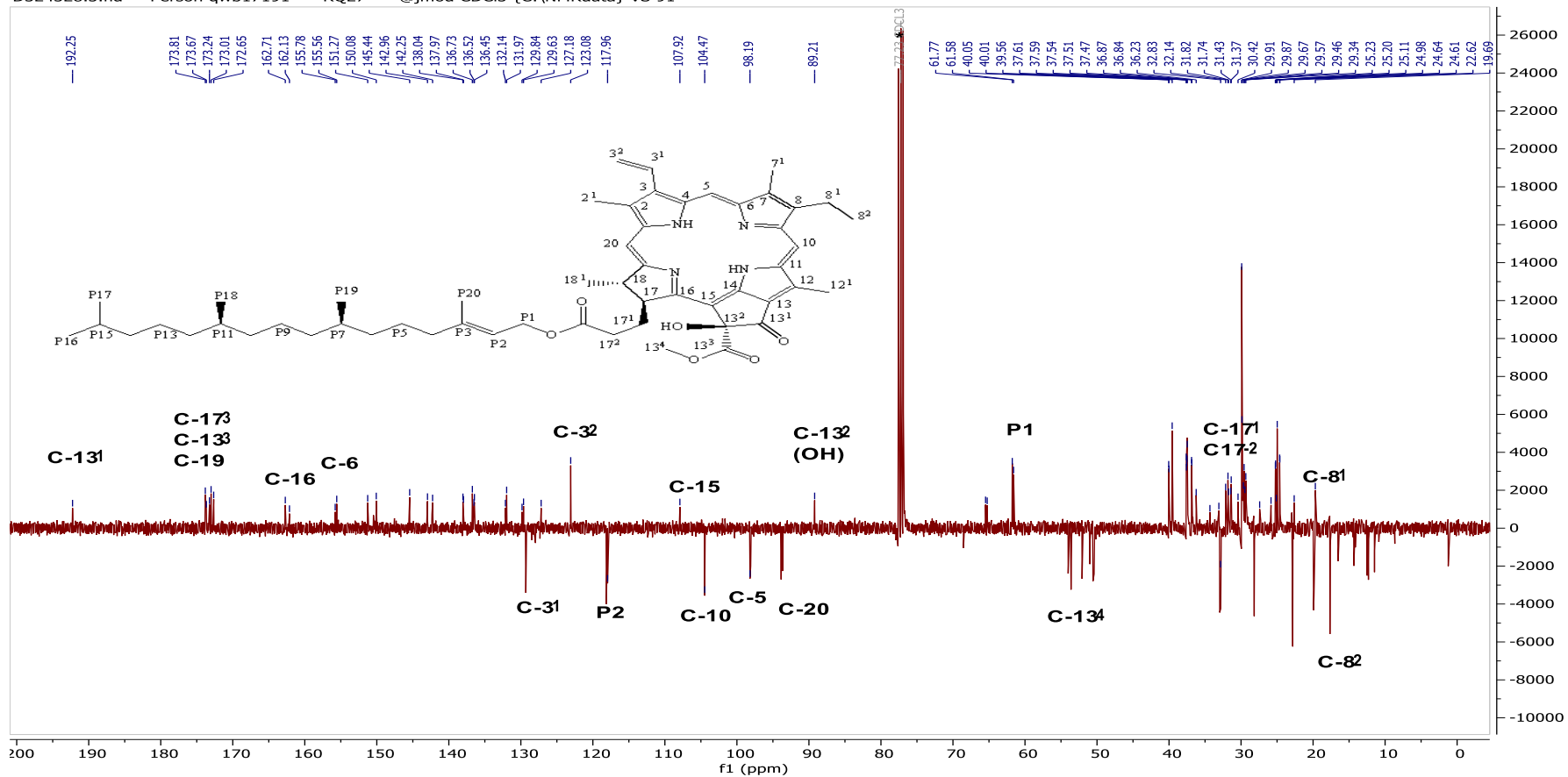


Figure 3.27 ¹³C-DEPTQ NMR spectrum (CDCl₃*, 100 MHz) of 390RQ27

3.1.2.4 Characterisation of 390RQ28 as pheophytin b

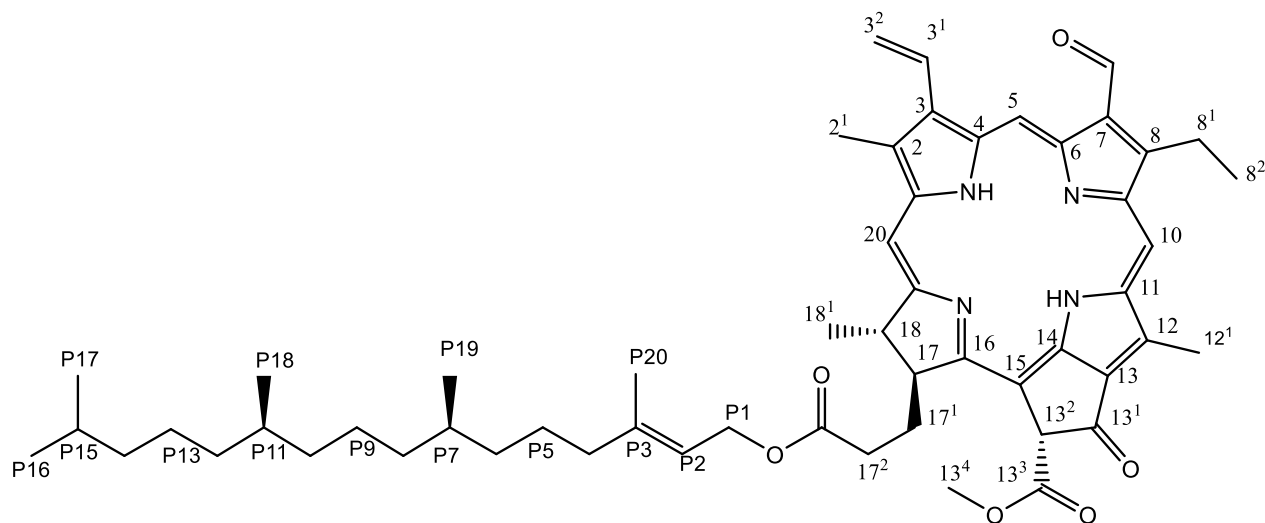


Figure 3.28 Structure of 390RQ28 or pheophytin b

390RQ28 was isolated from the ethyl acetate extract of *S. arabica* as a yellowish green solid (7.3 mg) (Figure 3.28). Under short UV light (254 nm), it gave a quenching spot and under long UV light (366 nm) a red fluorescence on the TLC plate. A yellowish spot was observed after treatment with anisaldehyde- sulphuric acid reagent and heating.

The positive ion mode HR-nanoESI-MS spectrum of 390RQ28 showed a quasi-molecular ion $[M+H]^+$ at m/z 885.5533 (theoretical m/z 885.5525) suggesting a molecular formula of $C_{55}H_{72}N_4O_6$, and an adduct at $[M+Na]^+$ at m/z 907.5357 suggesting a molecular formula of $C_{55}H_{72}N_4O_6Na$. A molecular ion peak $2[M+H]^+$ at m/z 1771.1000 indicated the presence of a dimer species.

The 1H NMR spectrum of 390RQ28 (Table 3.11, Figure 3.29) was similar to the NMR data observed for 390RQ10 suggesting a pheophytin derivative. However, it revealed a highly deshielded sharp proton singlet at δ_H 11.17 corresponding to an aldehyde at position C-7¹, instead of the methyl singlet at δ_H 3.20 observed for 390RQ10.

Comparing the chemical shifts of the meso protons at position H-5 and H-10 of 390RQ10 and 390RQ28, slight differences were observed, probably due to the presence of an aldehyde moiety at position C-7¹ (shifting from δ_{H} 9.34 to δ_{H} 10.39 and from δ_{H} 9.49 to δ_{H} 9.68 for H-5 and H-10, respectively).

The ¹³C DEPTQ NMR spectrum of 390RQ28 (Table 3.11, Figure 3.30) showed similar resonances to that of 390RQ10 (Table 3.9, Figure 3.24), except for the presence of a recognizable signal at δ_{C} 188.0, confirming the presence of an aldehydic carbonyl, and the absence of a methyl peak at δ_{C} 11.2. The rest of the NMR data were in good agreement with the literature data published for pheophytin b.

The complete assignment of ¹H NMR and ¹³C NMR values of 390RQ28 in comparison with the literature data is provided in Table 3.11

Comparison of the above spectral data with the literature (Nakatani *et al.*, 1981; Abraham and Rowan, 1991; Brito Filho *et al.*, 2014) confirmed the identification of 390RQ28 as pheophytin b. This is the first report of pheophytin b in *S. arabica*.

In the present study, pheophytin b was assessed for its effect on THP-1 cell viability, and its potential immunomodulatory effects on TNF- α and IL-12 production from LPS stimulated THP-1 cells (for further details see section 3.2.5, 3.3.5 and 3.3.9).

Table 3.11. ¹H (500 MHz) and ¹³C (125 MHz) NMR chemical shift values* for 390RQ28 recorded in CDCl₃ in comparison to literature

position	¹ H NMR δ Experimental	¹ H NMR δ Literature ^a	¹³ C NMR δ Experimental	¹³ C NMR δ Literature ^a	Carbon type
1			143.8	143.5-143.6	C
2			132.0	132.1-132.3	C
2 ¹	3.39 (3H, s)	3.37-3.40 (3H, s)	12.3	12.0-12.26	CH ₃
3			138.3	137.6-137.8	C
3 ¹	8.02 (1H, dd, <i>J</i> = 11.6, 17Hz)	8.00-8.02 (1H, dd, <i>J</i> = 11.5, 17 Hz)	128.9	128.6-128.8	CH
3 ^{2Z}	6.24 (1H, d <i>J</i> = 11.6 Hz)	6.22-6.29 (1H, d, <i>J</i> = 11.5 Hz)	123.8	123.3-123.6	CH ₂
3 ^{2E}	6.38 (1H, d <i>J</i> = 17 Hz)	6.37-6.38 (1H, d, <i>J</i> = 17 Hz)			
4			137.4	136.2-137.0	C
5	10.39 s	10.36-10.40 (1H, s)	101.8	101.3-101.7	CH
6			150.6	150.7-151.2	C
7			132.0	132.1-132.5	C
7 ¹	11.17 (3H, s)	11.13-11.20 (3H, s)	187.98	187.1-187.8	CHO
8			159.7	158.8-159.50	C
8 ¹			19.4	18.7-19.1	CH ₂
8 ²	1.70 (3H, t, <i>J</i> = 7.5 Hz)	1.67-1.70 (3H, t, <i>J</i> = 8 Hz)	19.6	16.1-19.4	CH ₃
9			147.5	146.8-147.2	C
10	9.68 (1H, s)	9.64-9.66 (1H, s)	107.2	106.5-107.1	CH
11			138.3	137.8-138.0	C
12			132.0	132.1-132.2	C

Table 3.11 (Cont.): ¹H (500 MHz) and ¹³C (125 MHz) NMR chemical shift values* for 390RQ28 recorded in CDCl₃ in comparison to literature

position	¹ H NMR δ Experimental	¹ H NMR δ Literature ^a	¹³ C NMR δ Experimental	¹³ C NMR δ Literature ^a	Carbon type
12 ¹	3.70 (3H, s)	3.68-3.70 (3H, s)	12.5	12.0-12.1	CH ₃
13			129.98	129.7-129.9	C
13 ¹			189.7	189.5-189.8	C
13 ²	6.24 (1H, s)	6.23-6.24 (1H, s)	64.8	64.5-64.8	CH
13 ³			169.7	169.3-169.5	C
13 ⁴	3.91 (3H, s)	3.90 (3H, s)	53.2	53-53.1	CH ₃
14			150.5	150.8	C
15			105.2	105.8-105.9	C
16			164.1	164.0-164.2	C
17			51.6	51.3-51.6	CH
17 ¹			31.4	31.2-31.4	CH ₂
17 ²			29.8	29.7-29.8	CH ₂
17 ³			173.0	173.1-174.1	C
18	4.52 (1H, m)	4.46-4.5 (1H, m)	50.3	50.1-50.3	CH
18 ¹	1.84 (3H, d, <i>J</i> = 7.5 Hz)	1.82-1.84 (3H, d)	23.3	23.1-23.3	CH ₃
19			174.2	172.8-174.0	C
20	8.55 (1H, s)	8.53-8.54 (1H, s)	93.5	93.3-93.4	CH

*Chemical shift values are δ ppm

^a (Nakatani *et al.*, 1981; Abraham and Rowan, 1991; Brito Filho *et al.*, 2014)

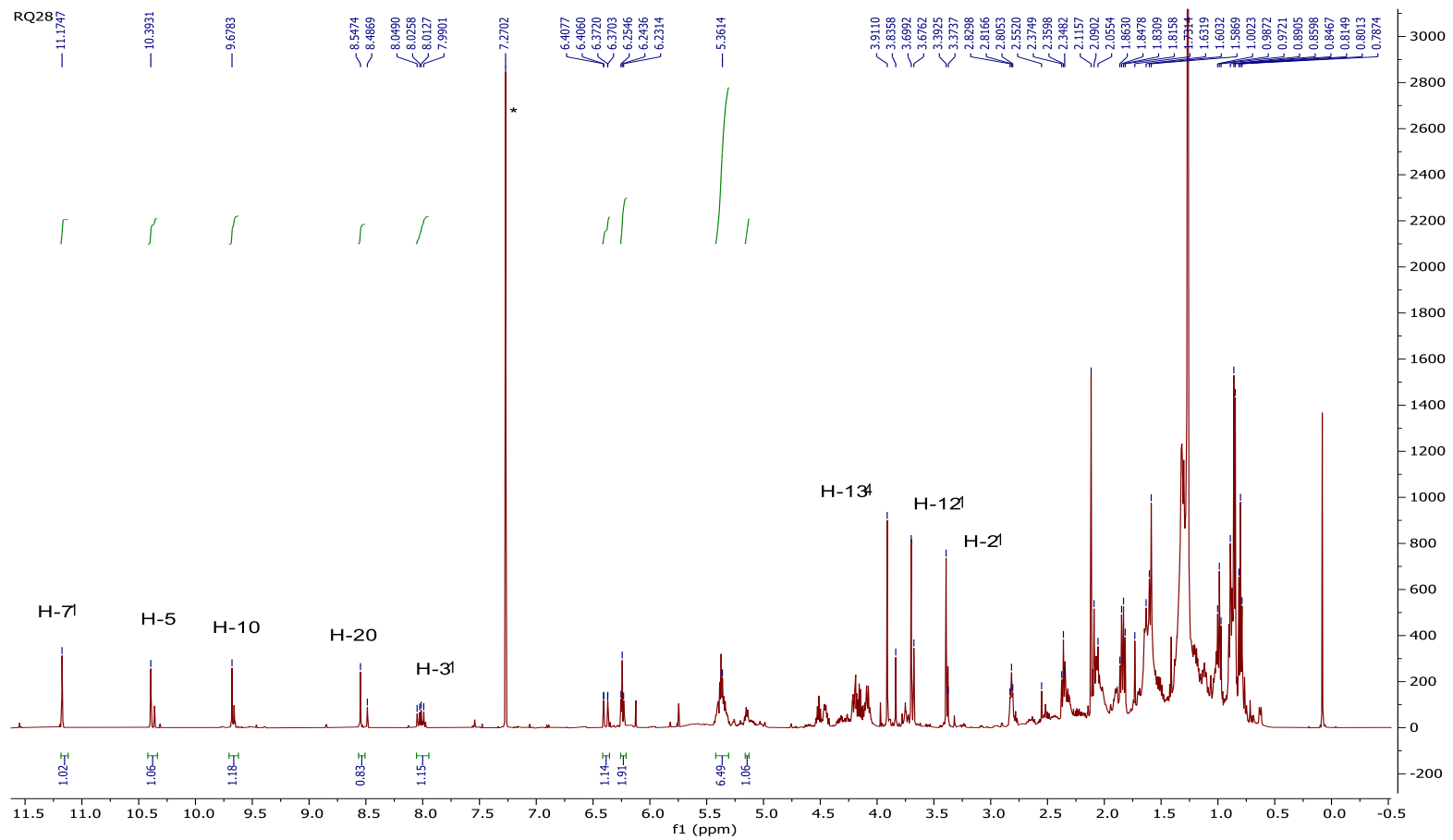


Figure 3.29 ^1H NMR spectrum (CDCl_3^* , 500 MHz) of 390RQ28

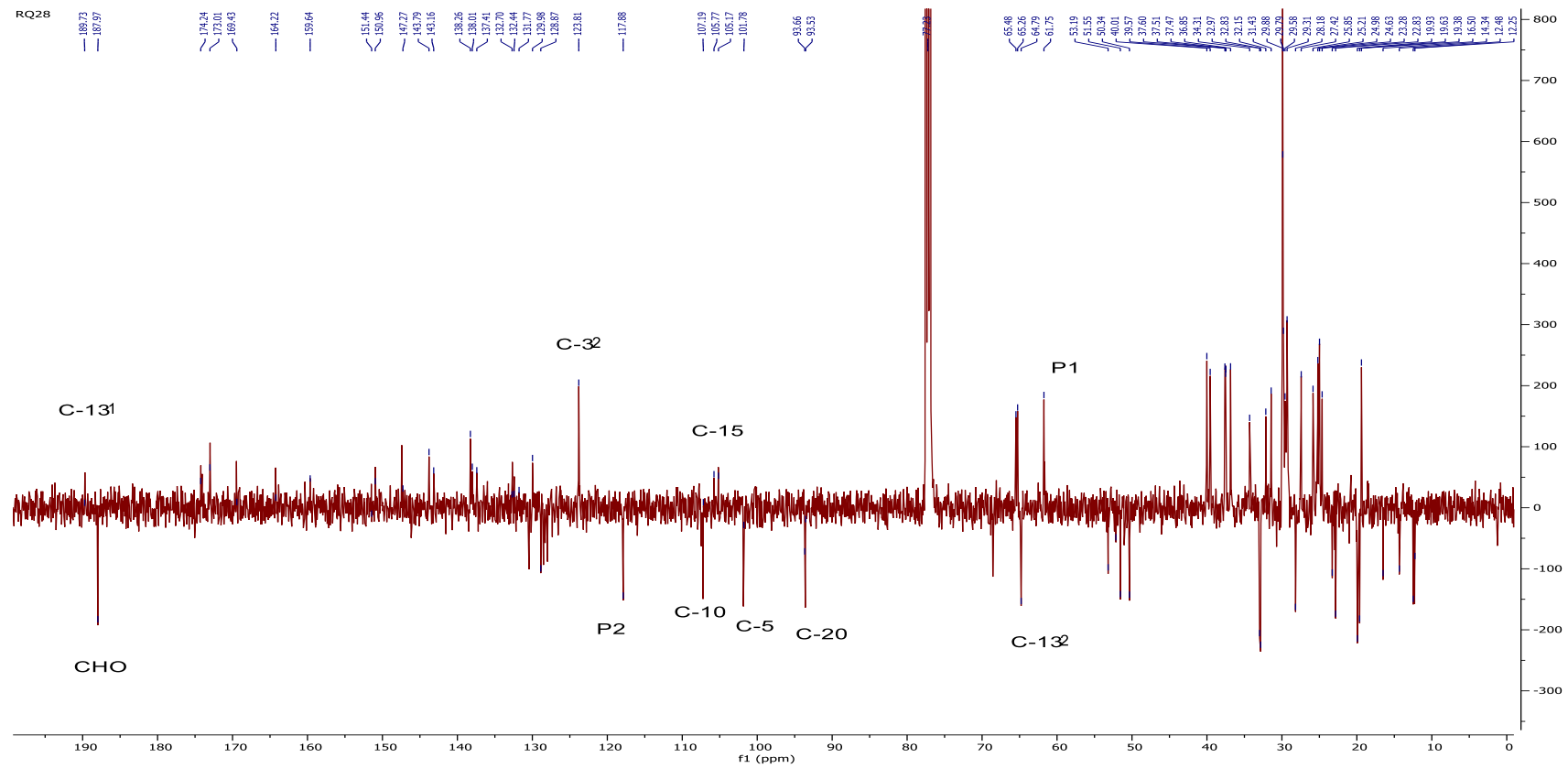


Figure 3.30 ^{13}C -DEPTQ NMR spectrum (CDCl_3^* , 125 MHz) of 390RQ28

3.1.3 Miscellaneous compounds

3.1.3.1 Characterization of 370RQ1 as a mixture of squalene (a) and nonacosane (b).

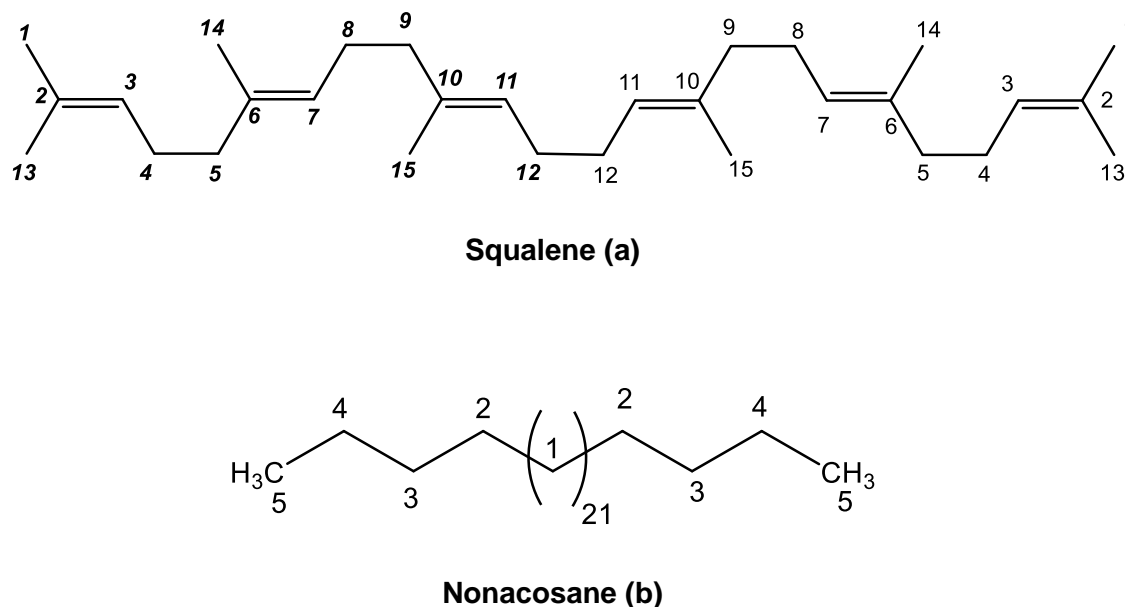


Figure 3.31 Structures of 370RQ1 or squalene (a) and nonacosane (b)

370RQ1 was isolated from the *n*-hexane extract of *F. excelsior* as a white amorphous solid (15.5 mg) (Figure 3.31). No UV-active spot was observed on TLC plates under UV light. A pink spot was observed after treatment with anisaldehyde-sulphuric acid reagent and heating.

The positive ion mode ASAP-MS data of 370RQ1 showed a quasi-molecular ion peak $[M+H]^+$ at m/z 411.3989 (theoretical m/z 411.3991) corresponding to a molecular formula of $C_{30}H_{50}$. A molecular ion peak $[M+H]^+$ at m/z 409.3831 corresponding to a molecular formula of $C_{29}H_{60}$ was also observed.

The 1H NMR spectrum (Figure 3.32, Table 3.12) showed signals for allylic methyl groups at δ_H 1.61 (s, 18H) assigned to Me -13, Me -14 and Me -15, as well as a signal

at δ_{H} 1.69 (s, 6H) assigned to Me-1. The spectrum also showed allylic methylene protons at δ_{H} 1.97-2.10 (m, 20H) and a multiplet at δ_{H} 5.11-5.13 corresponding to olefinic methines H-3, H-7, and H-11.

The ^{13}C DEPTQ- NMR spectrum (Figure 3.33, Table 3.12) displayed 15 signals belonging to three quaternary carbons at δ 135.3, 135.1 and 131.5 corresponding to C-10, C-6, and C-2 respectively, three olefinic methines at δ_{C} 124.6, 124.51, and 124.5 corresponding to C-3, C-7, and C-11, respectively, as well as five allylic methylenes at δ_{C} 39.98, 39.96, 28.5, 27.0, 26.9 (C-5, C-9, C-12, C-4, and C-8 respectively), and four methyls at δ_{C} 25.9, 17.9, 16.3 and 16.2 (C-1, C-13, C-14, and C-15, respectively).

Other signals in the ^1H and ^{13}C DEPTQ NMR spectra indicated the presence of an acyclic alkane in the sample. The ^1H NMR spectrum showed a signal at δ_{H} 1.27 and a triplet at δ_{H} 0.89 ($J = 7\text{Hz}$), integrating for 54 and 6 protons, respectively. This indicated that there were two methyls and 27 methylenes. In the DEPTQ NMR, there were signals at δ_{C} 14.3 (terminal methyl) and at δ_{C} 22.9, 29.6, 29.9 and 32.2 (CH_2) typical for a linear alkane which could be characterised as nonacosane $\text{CH}_3(\text{CH}_2)_{27}\text{CH}_3$ (Figure 3.31).

The complete assignment of ^1H NMR and ^{13}C NMR values of 370RQ1 (a) in comparison with the literature data is provided in Table 3.12.

Based on the above spectral data, 370RQ1 was identified as a mixture of 2,6,10,15,19,23-hexamethyl-2,6,10,14,18,22-tetracosahexaene or squalene (a) and nonacosane (b). The NMR and MS data obtained for squalene were in good agreement with the literature (Lee and Chang, 2000; Anne-Marie *et al.*, 2017; Inte *et al.*, 1998; He *et al.*, 2002; Pogliani *et al.*, 1994). This was also the case for nonacosane (Chen, 2008). Although nonacosane, has previously been isolated from *F. excelsior* leaves (Kowalczyk and Olechnowicz-Stepień, 1989), this is the first report of the isolation of squalene from *F. excelsior* leaves.

Squalene has previously been isolated from shark liver oil and other natural sources including amaranth oil, olive oil, and wheat germ (He *et al.*, 2002; Lou-Bonafonte *et al.*, 2018).

According to the literature, squalene has pharmacological, cosmetic, and nutritional potential. Its structure is similar to other isoprenoids like β -carotene, lycopene, and vitamin A and E that exhibit strong antioxidant activity. Squalene has also demonstrated cardioprotective, anticancer, detoxifying, skin hydrating, moisturising, and emollient effects (Kim and Karadeniz, 2012; Lou-Bonafonte *et al.*, 2018; Lozano-Grande *et al.*, 2018; Spanova and Daum, 2011). It has also previously shown reduction of the intracellular level of ROS, cytokines, and other inflammatory mediators on LPS-stimulated murine macrophages, human monocytes and neutrophils. This indicates that squalene has anti-inflammatory potential (Cárdeno *et al.*, 2015).

Table 3.12 ¹H (500 MHz) and ¹³C (125 MHz) NMR chemical shift values* for 370RQ1 (a) (recorded in CDCl₃) in comparison with literature data.

Position	¹ H NMR δ experimental	¹ H NMR δ literature ^a	¹³ C NMR δ experimental	¹³ C NMR δ literature ^b
1	1.69 (6H, s)	1.67-1.69 (6H, s)	25.9 CH ₃	25.6-25.8
2			131.5 C	131.1-131.3
3	5.11-5.13 (2H, m)	5.10-5.15 (2H, m)	124.6 CH	124.3-124.4
4	1.97-2.10 (4H, m)	1.9-2.10 (4H, m)	27.0 CH ₂	26.7-26.8
5	1.97-2.10 (4H, m)	1.9-2.10 (4H, m)	39.96 CH ₂	39.7-39.8
6			135.1 C	134.9-135.1
7	5.11-5.13 (2H, m)	5.10-5.15 (2H, m)	124.5 CH	124.3-124.4
8	1.97-2.10 (4H, m)	1.9-2.10 (4H, m)	26.9 CH ₂	26.7-26.8
9	1.97-2.10 (4H, m)	1.9-2.10 (4H, m)	39.98 CH ₂	39.8-39.9
10			135.3 C	134.9-135.1
11	5.11-5.13 (2H, m)	5.10-5.15 (2H, m)	124.5 CH	124.3-124.5
12	1.97-2.10 (4H, m)	1.9-2.10 (4H, m)	28.5 CH ₂	28.3-28.3
13	1.61 (6H, s)	1.59-1.62 (6H, s)	17.9 CH ₃	17.6-17.9
14	1.61 (6H, s)	1.59-1.62 (6H, s)	16.3 CH ₃	16.0-16.2
15	1.61 (6H, s)	1.59-1.62 (6H, s)	16.2 CH ₃	16.0-16.2

* Chemical shifts values in ppm

^a (Pogliani *et al.*, 1994; He *et al.*, 2002; Lee and Chang, 2000)

^b (Pogliani *et al.*, 1994; Lee and Chang, 2000; Anne-Marie *et al.*, 2017)

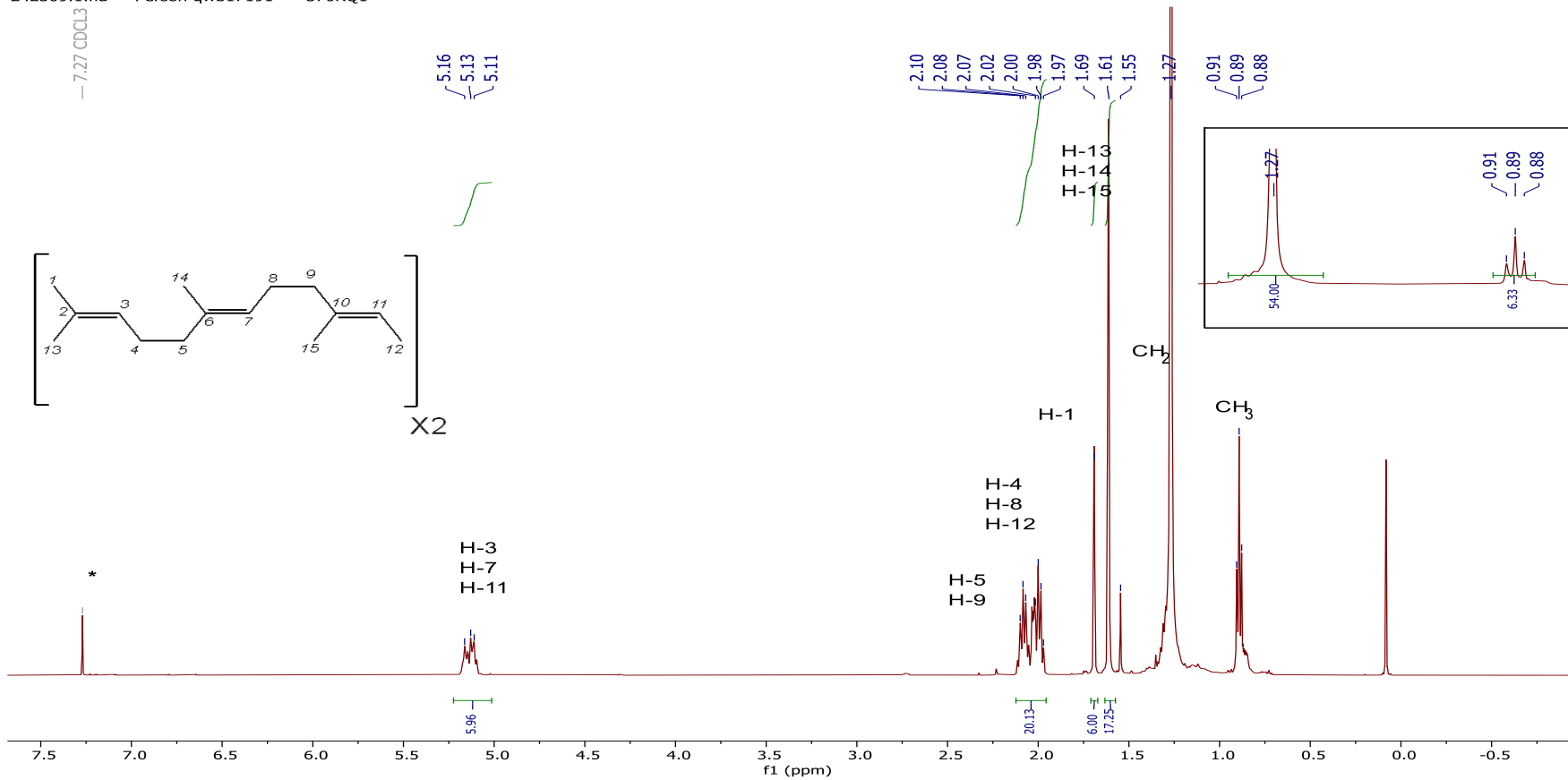


Figure 3.32 ¹H NMR spectrum (CDCl₃*, 500 MHz) of 370RQ1

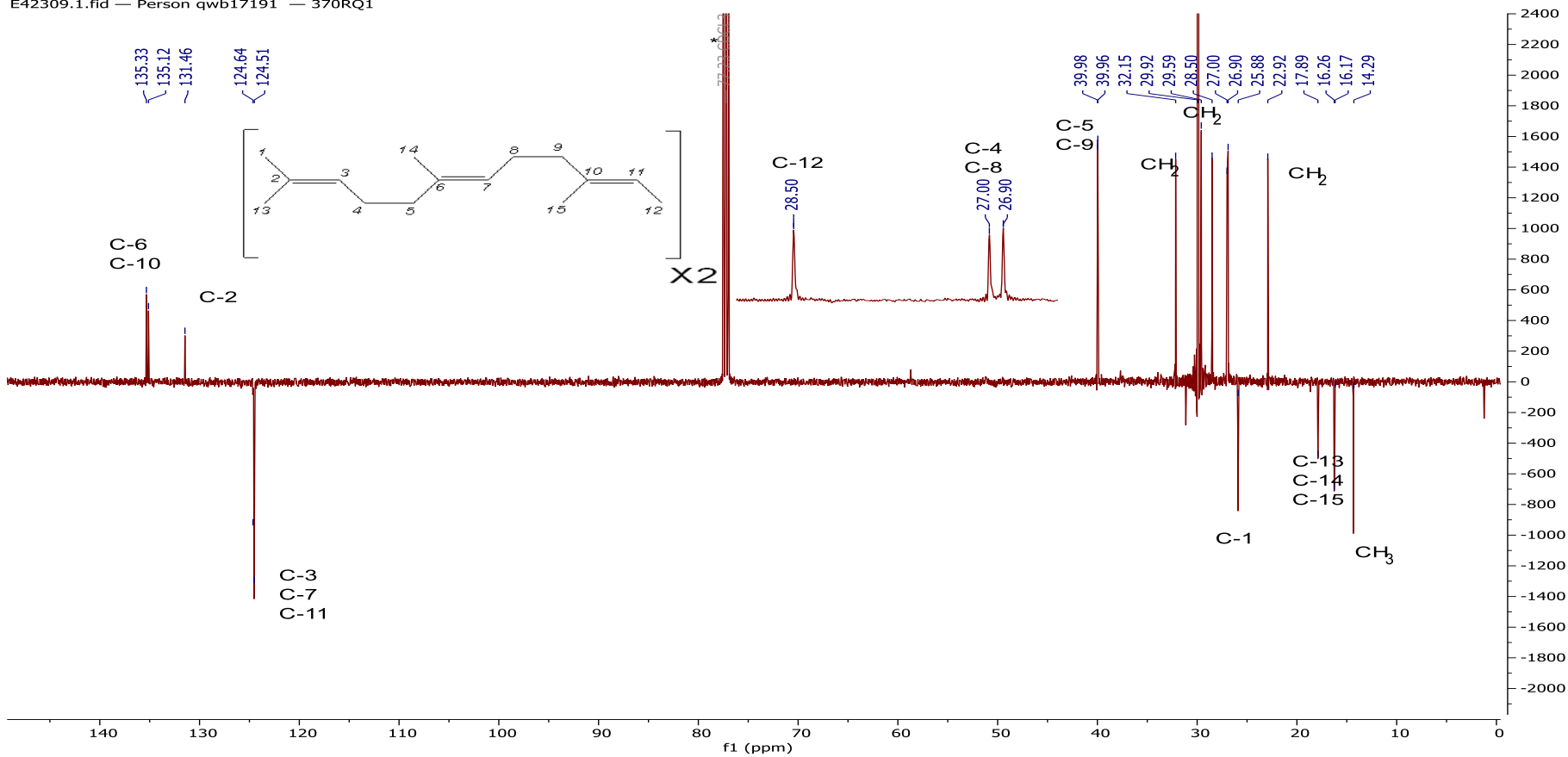


Figure 3.33 ¹³C-DEPTQ NMR spectrum (CDCl₃^{*}, 125 MHz) of 370RQ1

3.1.3.2 Characterisation of 370RQ20 as pinocembrin

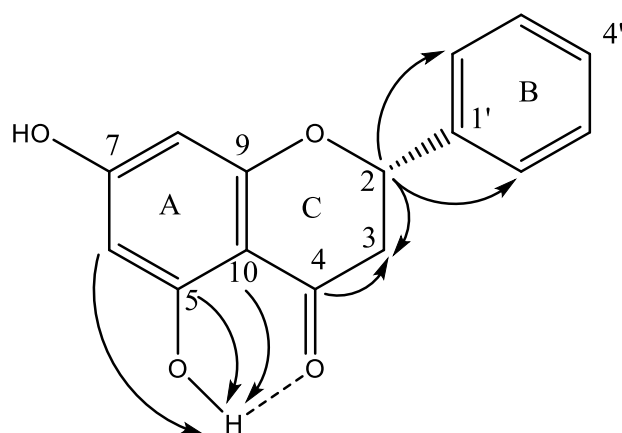


Figure 3.34 Structure of 370RQ20 or pinocembrin with key HMBC correlations.

370RQ20 was isolated from the ethyl acetate extract of *F. excelsior* (6.8 mg) (Figure 3.34). On TLC, 370RQ20 gave a quenching spot and a red fluorescence under short (254 nm) and long wave UV light (366 nm), respectively. An orange spot was observed after treatment with anisaldehyde-sulphuric acid reagent and heating.

The positive ion mode HR-ASAP-MS data of 370RQ20 showed a quasi-molecular ion $[M+H]^+$ at m/z 257.0814 (theoretical m/z 257.0814) suggesting for a molecular formula of $C_{15}H_{12}O_4$.

The 1H -NMR spectrum of 370RQ20 (Figure 3.35, Table 3.13) showed signals in both the aromatic (δ_H 6.0-7.5) and in the aliphatic regions (δ_H 2.8-5.5). Two overlapping signals appearing as doublets at δ_H 6.01 ($J_{8,6} = 2.4$ Hz) and 6.02 ($J_{6,8} = 2.3$ Hz) were assigned to *meta*-coupling protons of a 5,7 di-hydroxylated flavonoid ((Liu *et al.*, 1992). The aromatic region of the spectrum also showed a multiplet at δ_H 7.40-7.50 establishing the absence of substituents on the B-ring (Hammami *et al.*, 2004; Feng *et al.*, 2017). The aliphatic region revealed three double doublets at δ_H 2.83 ($J = 17.3$, 3.0 Hz, H-3 β), 3.09 ($J = 17.2$, 13 Hz, H-3 α), and 5.43 ($J = 13$, 3.0 Hz, H-2) suggesting the presence of a flavanone skeleton (Kang *et al.*, 2000). A sharp and strongly deshielded singlet at δ_H 12.05 was also observed. This was attributed to the C5-OH of flavonoids (due to intra-molecular hydrogen bonding between free 5-OH and the

oxygen of the C-4 carbonyl) (Jung and Mclaughlin, 1990; Charisiadis *et al.*, 2014). The above NMR data and comparison with the literature indicated that 370RQ20 was a flavanone.

The ^{13}C DEPTQ spectrum (Figures 3.36, Table 3.13) confirmed the presence of a 5,7-di-hydroxylated flavanone with fifteen carbon signals, including a carbonyl at δ_{C} 195.92, one methylene at δ_{C} 43.57, eight methines including an oxymethine at δ_{C} 79.4 and two upfield methines at δ_{C} 95.8 and 97.0, as well as six quaternary carbons.

Cross peaks in the HMBC spectrum (Figures 3.37, Table 3.13) further supported the presence of a flavanone skeleton. The C-5 hydroxy proton (δ_{H} 12.05) showed 3J correlations with C-6 and C-10, and 2J correlation with C-5. The H-2'/6' protons (δ_{H} 7.44) showed 3J correlations with C-2 (δ_{C} 79.0). The H-6 proton (δ_{H} 6.01) and the H-8 proton (δ_{H} 6.02) each showed correlations with C-5, C-7, and C-10. The proton at δ_{H} 3.09 (H-3 β) showed 2J correlations with the carbonyl carbon at δ_{C} 195.9 (C-4), and with C-2 (δ_{C} 79.0) as well as a 3J correlations with δ_{C} 138.6 (C-1'). The proton at δ_{H} 2.83 (H-3 α) correlated with C-4 and C-10. Cross peaks between H-2 (δ_{H} 5.43) with C-1', and C-2'/6' were also observed.

The complete assignment of ^1H NMR and ^{13}C NMR values of 370RQ20 in comparison with the literature data is provided in Table 3.13.

The above spectral data were in good agreement with the structure of pinocembrin (Figure 3.34). Comparison with literature data (Liu *et al.*, 1992; Tanjung *et al.*, 2013; Ching *et al.*, 2007; Jung and Mclaughlin, 1990; Nyokat *et al.*, 2017) confirmed the structure of 370RQ20 as 5,7-dihydroxyflavanone or pinocembrin Figure (3.34). This is the first report of the isolation of pinocembrin from the genus *Fraxinus*.

Pinocembrin (5,7-dihydroxyflavanone) has been reported in honey, propolis, and several plants. Previous studies have shown that pinocembrin has an interesting range of biological effects. This includes antibacterial, antifungal, anti-oxidant, anticancer, anti-inflammatory, neuroprotective, antidepressive effects (Rasul *et al.*, 2013; Lan *et al.*, 2016; Wang *et al.*, 2020). Researchers have also explored the effect of pinocembrin on Alzheimer's disease *in vitro* and *in vivo* (Liu *et al.*, 2012a; 2014b; Kang *et al.*, 2020), as well as on cardiovascular diseases, atherosclerosis (Sang *et al.*, 2012; Li *et al.*, 2013; Yang *et al.*, 2013; Su *et al.*, 2018), and osteoarthritis (Zhang *et al.*, 2015).

Pinocembrin isolated from *Dalbergia parviflora* stems exhibited antimycobacterial activity with a MIC value of 12.5 µg/mL. The activity was assessed against Mtb H37Ra using the Green Fluorescent Protein Microplate Assay where isoniazid and rifampicin were used as controls (Songsiang *et al.*, 2009). Another study showed that pinocembrin exhibited promising anti-TB activity against the dormant and active forms of Mtb H37Ra (Said *et al.*, 2015).

In the present study, pinocembrin was assessed for its effect on THP-1 cell viability, and potential immunomodulatory effects on TNF-α and IL-12 production from LPS stimulated THP-1 cells (for further details see section 3.2.4, 3.3.4 and 3.3.8).

Table 3.13 ^1H (500 MHz) and ^{13}C NMR (125 MHz) chemical shift values* for 370RQ20 (recorded in CDCl_3) in comparison with literature data

Position	^1H NMR δ Experimental	^1H NMR δ Literature ^a	HMBC	^{13}C δ Experimental	^{13}C δ Literature ^a
2	5.43 (1H, dd, $J = 13, 3$ Hz)	5.43 (1H, dd, $J = 13, 3$ Hz)	C-4, C-1', C-2', C-6'	79.4	79.2
3 β	2.83 (1H, dd, $J = 17, 3$ Hz)	2.86 (1H, dd, $J = 18, 3$ Hz)	C-4, C-10	43.6	43.4
3 α	3.09 (1H, dd, $J = 17, 13$ Hz)	3.10 (1H, dd, $J = 18, 13$ Hz)	C-2, C-4, C-1'		
4				195.9	195.7
5	12.05 (1H, s)	12.07 (1H, s)	C-5, C-6, C-10	164.5	164.3
6	6.01 (1H, d, $J = 2.4$ Hz)	6.03 (1H, d, $J = 2.2$ Hz)	C-5, C-8, C-10	97.0	96.8
7				165.2	
8	6.02 (1H, d, $J = 2.3$ Hz)	6.03 (1H, d, $J = 2.2$ Hz)	C-5, C-6, C-10	95.7	95.6
9				163.3	163.1
10				103.3	103.0
1'				138.6	138.4
2', 6'	7.4-7.47 m	7.41-7.49 m		126.4	126.2
3', 5'	7.4-7.47 m	7.41-7.55 m		129.1	128.9
4'	7.4-7.47 m	7.41-7.55 m		129.9	128.9

* Chemical shift values are in ppm

^a ^1H NMR and ^{13}C NMR were recorded in CDCl_3 , 400 MHz (Nyokat *et al.*, 2017)

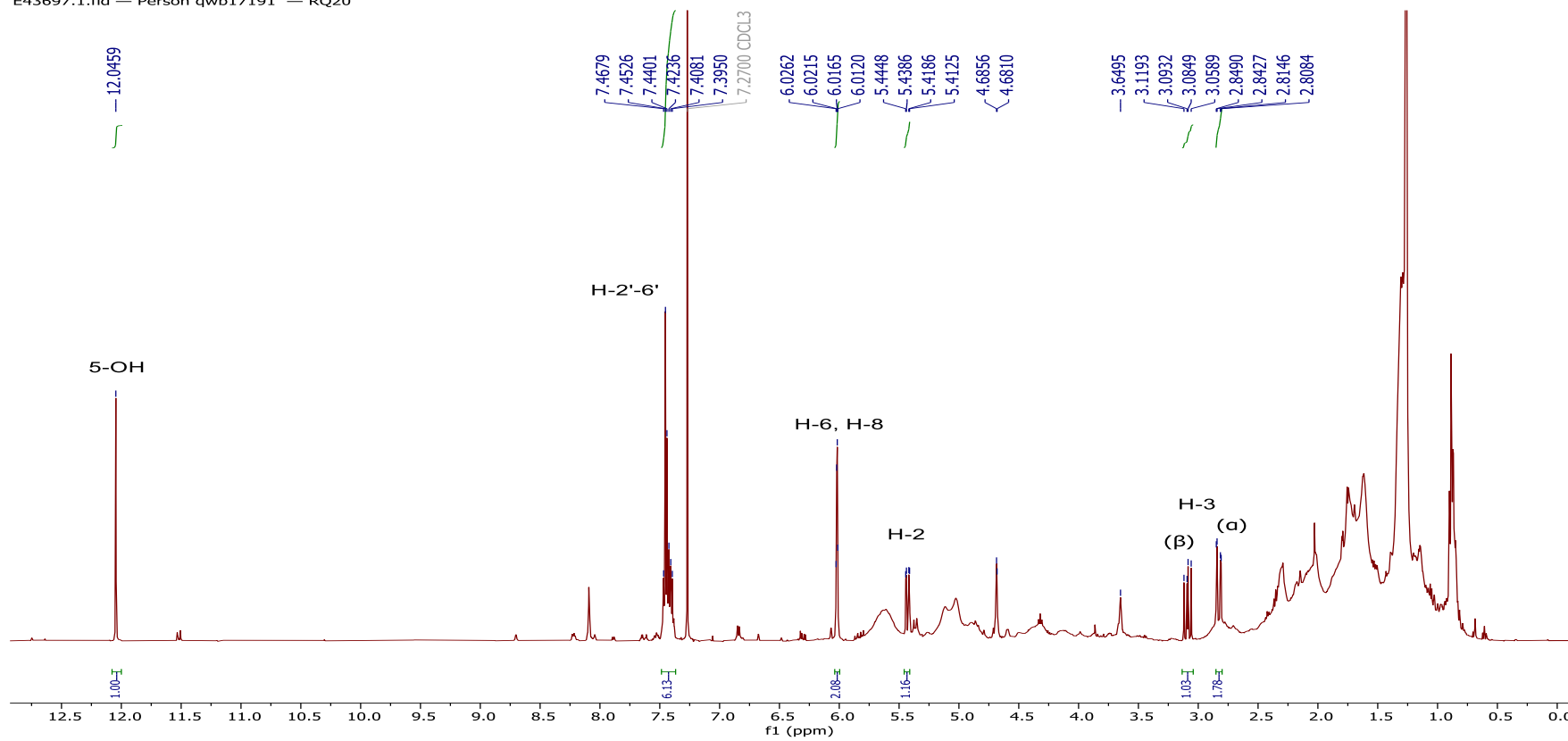


Figure 3.35 ¹H NMR spectrum (CDCl₃^{*}, 500 MHz) of 370RQ20

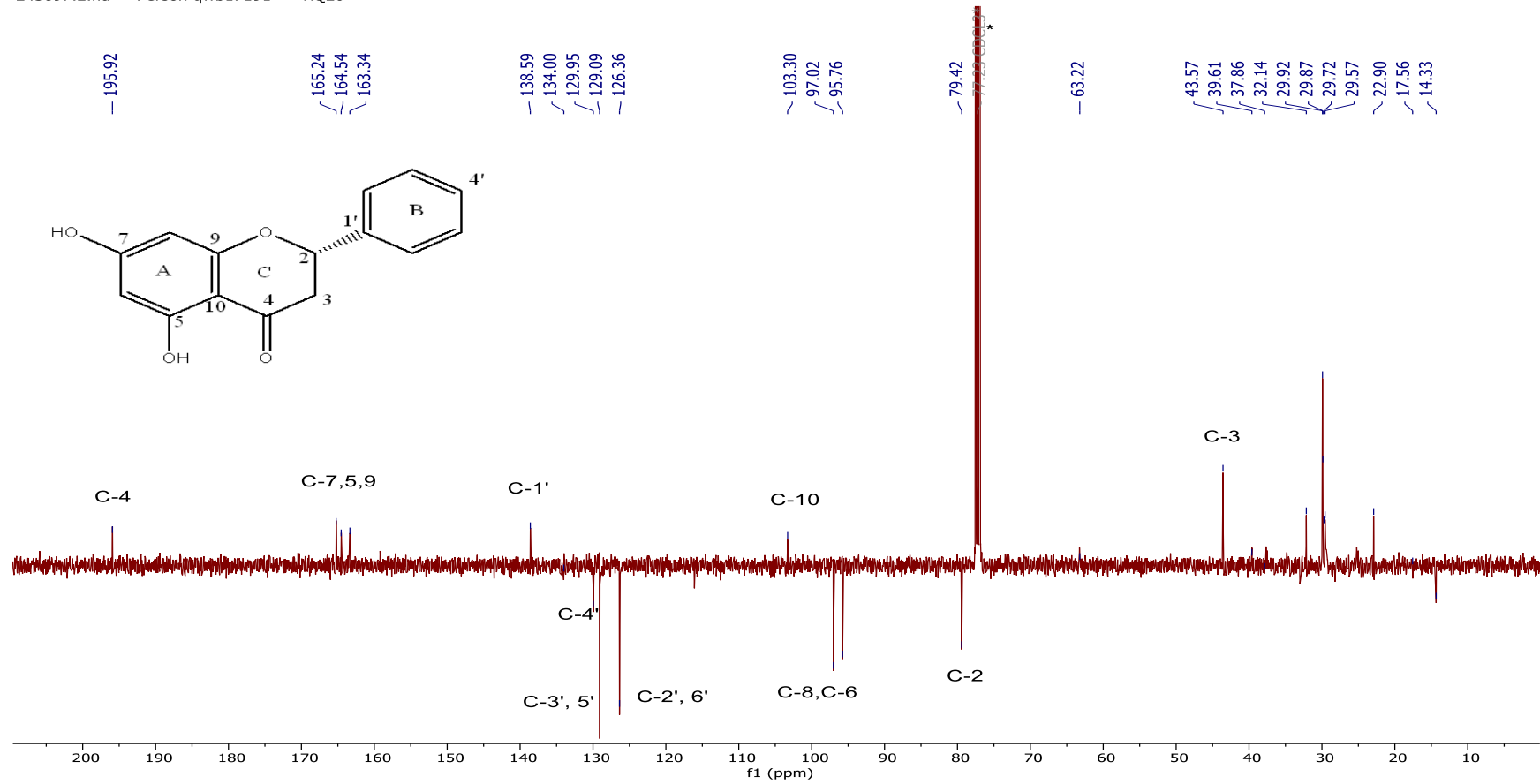


Figure 3.36 ¹³C-DEPTQ NMR spectrum (CDCl₃*, 125 MHz) of 370RQ20

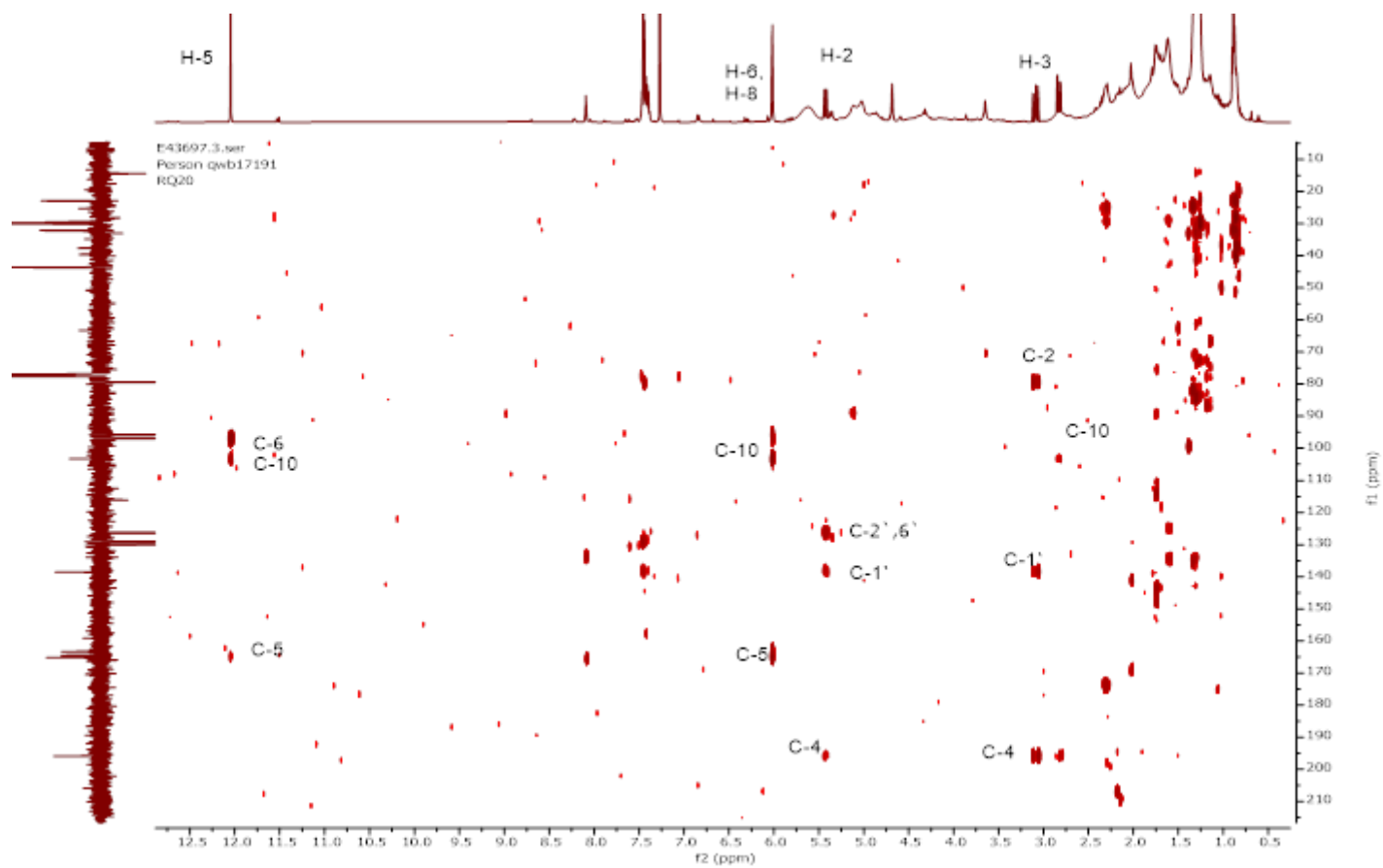
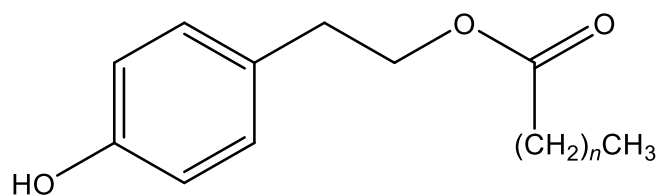


Figure 3.37 HMBC spectrum (CDCl_3 , 500 MHz) of 370RQ20

3.1.3.3 Characterisation of 370RQ19 as a mixture of phenylethanoid esters



Phenylethanoid esters

- $n = 30$ 4-hydroxyphenethyl dotriacontanoate
- $n = 28$ 4-hydroxyphenethyl triacontanoate
- $n = 26$ 4-hydroxyphenethyl octacosanoate
- $n = 24$ 4-hydroxyphenethyl hexacosanoate
- $n = 22$ 4-hydroxyphenethyl tetracosanoate

Figure 3.38 Structure of 370RQ19 or phenylethanoid esters

370RQ19 was isolated from the ethyl acetate extract of *F. excelsior* (10.2 mg) (Figure 3.38). On TLC, 370RQ19 gave a quenching spot and a red fluorescence under short (254 nm) and long wave UV light (366 nm), respectively. A purple spot was observed after treatment with anisaldehyde-sulphuric acid reagent and heating.

The ^1H NMR spectrum of 370RQ19 (Figure 3.39, Table 3.16) showed signals in both the aromatic (δ_{H} 6.5–7.5) and the aliphatic regions (δ_{H} 5.0–0.80). The aromatic region displayed a typical AA'XX' pattern for a *para*-disubstituted aromatic ring with doublets at δ_{H} 7.08 (2H, $J = 8.5$ Hz), and δ_{H} 6.76 (2H, $J = 8.5$ Hz) assigned to two sets of *ortho*-aromatic protons H2/6 and H3/5, respectively. The spectrum also showed a singlet at δ_{H} 4.80 most likely for a OH group at C-4 of the aromatic ring, three triplets at δ_{H} 4.25 (2H, $J = 7.1$ Hz) attributed to an oxymethylene proton (H-8), a benzylic methylene at δ_{H} 2.86 (2H, $J = 7.1$ Hz), and a methylene attached to a carbonyl ester proton (H-2') at δ 2.28 (2H, $J = 7.5$ Hz), respectively. There was also a triplet at δ 0.89 (3H, $J = 6.7$ Hz) indicating the presence of terminal methyl protons. Other signals at δ_{H} 1.59 and 1.27 were typical of methylenes of an aliphatic chain. These observations suggested the presence of a long chain fatty acid linked to a 4-hydroxyphenylethanol moiety (Acevedo *et al.*, 2000; Chen *et al.*, 2009)

The ^{13}C DEPTQ- NMR spectrum (Figure 3.40, Table 3.16) confirmed the presence of a phenylethanoid ester with signals for a carbonyl ester at δ_{C} 174.1 (C-1'), aromatic carbons between δ_{C} 154.43 and 115.5, an oxymethylene at δ_{C} 65.2 assigned to carbon C-8, and a terminal methyl at δ_{C} 14.3. Other signals between δ_{C} 35.0-22.0 were typical of methylene carbons in the aliphatic chain of a fatty acid.

Comparison of the above spectral data with the literature (Alfatafta *et al.*, 1989; Ali and Houghton, 1999; Acevedo *et al.*, 2000; Luo *et al.*, 2006; Mateos *et al.*, 2008; Aissa *et al.*, 2012; Nazreen *et al.*, 2019) suggested that 370RQ19 could be a phenylethanoid ester.

The GC-EI-MS of 370RQ19 did not yield any noticeable molecular ions, but it showed a prominent base peak at m/z 192.0978 corresponding to a TMS derivative of compounds containing phenylethanoid ($-\text{O}-\text{C}_8\text{H}_7$) (Angerosa *et al.*, 1995; Tasioula-Margari and Okogeri, 2001).

The positive ion mode HR-ASAP-MS data of 370RQ19 showed five quasi-molecular ions (Table 3.14) for $[\text{M}+\text{NH}_4]^+$ adducts at m/z 618.5826 ($\text{C}_{40}\text{H}_{72}\text{O}_3\text{NH}_4$), 590.5513 ($\text{C}_{38}\text{H}_{68}\text{O}_3\text{NH}_4$), 562.5200 ($\text{C}_{36}\text{H}_{64}\text{O}_3\text{NH}_4$), 534.4884 ($\text{C}_{34}\text{H}_{60}\text{O}_3\text{NH}_4$), and 506.4571 ($\text{C}_{32}\text{H}_{56}\text{O}_3\text{NH}_4$). A pseudo molecular ion peak $[\text{M}+\text{H}]^+$ at m/z 121.0645 established the presence of the 4-hydroxystyrene ($\text{C}_8\text{H}_8\text{O}$) moiety.

Table 3.14. Molecular ion peaks of ammonium adduct observed in the mass spectrum of 370RQ19

Peak	m/z $[\text{M}+\text{NH}_4]^+$	Formula $[\text{M}+\text{NH}_4]^+$	Phenylethanoid esters
A	618.5826	$\text{C}_{40}\text{H}_{72}\text{O}_3\text{NH}_4$	$\text{C}_{40}\text{H}_{72}\text{O}_3$
B	590.5513	$\text{C}_{38}\text{H}_{68}\text{O}_3\text{NH}_4$	$\text{C}_{38}\text{H}_{68}\text{O}_3$
C	562.5200	$\text{C}_{36}\text{H}_{64}\text{O}_3\text{NH}_4$	$\text{C}_{36}\text{H}_{64}\text{O}_3$
D	534.4884	$\text{C}_{34}\text{H}_{60}\text{O}_3\text{NH}_4$	$\text{C}_{34}\text{H}_{60}\text{O}_3$
E	506.4571	$\text{C}_{32}\text{H}_{56}\text{O}_3\text{NH}_4$	$\text{C}_{32}\text{H}_{56}\text{O}_3$

It is noteworthy to mention that the MS spectrum also revealed another five molecular ion peaks (Table 3.15) most likely attributable to methyl fatty acid esters corresponding to each phenylethanoid ester.

Table 3.15. Methyl fatty acid esters molecular ion peaks observed in the mass spectrum of 370RQ19

Peak	<i>m/z</i>	Methyl Fatty acid	Formula	Fatty Acid
A*	495.5141	C ₃₃ H ₆₇ O ₂	C ₃₂ H ₆₄ O ₂	Dotriacontanoic acid
B*	467.4828	C ₃₁ H ₆₃ O ₂	C ₃₀ H ₆₀ O ₂	Triacontanoic acid
C*	439.4515	C ₂₉ H ₅₉ O ₂	C ₂₈ H ₅₆ O ₂	Octacosanoic acid
D*	411.4202	C ₂₇ H ₅₅ O ₂	C ₂₆ H ₅₂ O ₂	Hexacosanoic acid
E*	383.3889	C ₂₅ H ₅₁ O ₂	C ₂₄ H ₄₈ O ₂	Tetracosanoic acid

In conclusion, HR-ASAP-MS analysis demonstrated that 370RQ19 was a mixture of five phenylethanoid esters, namely phenylethanoid esters, namely 4-hydroxyphenethyl dotriacontanoate, 4-hydroxyphenethyl triacontanoate, 4-hydroxyphenethyl octacosanoate, 4-hydroxyphenethyl hexacosanoate, and 4-hydroxyphenethyl tetracosanoate.

The complete assignment of ¹H NMR and ¹³C NMR values of 370RQ19 in comparison with the literature data is provided in Table 3.16

Whilst the presence of phenylethanoid esters has been reported from plants such as *Syringa komarowii* (Luo *et al.*, 2006) and *Olea europaea* (Bianco *et al.*, 2004) within the Oleaceae family, this is the first report of the presence of phenylethanoid esters in the genus *Fraxinus*.

Phenylethanoid esters have previously shown interesting biological activities. 4-hydroxyphenethyl tetracosanoate or 2-(4-hydroxyphenyl)-ethyl lignocerate isolated from the stem bark of *Buddleja cordata* has displayed moderate antibacterial activity in a radiorespirometric bioassay against Mtb (H37Rv) with MIC of 64 µg/mL (Acevedo *et al.*, 2000).

A mixture of phenylethanoid esters, comprised of 2-(4-hydroxyphenyl)ethyl docosanoate, 2-(4-hydroxyphenyl)ethyl tetracosanoate, 2-(4-hydroxyphenyl)ethyl hexacosanoate, 2-(4-hydroxyphenyl)ethyl octacosanoate, 2-(4-hydroxyphenyl)ethyl triacontanoate, isolated from the stem bark of *Spathodea campanulata* (4:19:40: 34:3 ratio) has shown activity against *Pseudomonas aeruginosa* and *Shigella flexneri* with MIC of 12.5 µg /mL (Mbosso *et al.*, 2008).

2-(4-hydroxyphenyl)ethyl dodecyloctadecanoate isolated from the stem of *Jacaranda filicifoia* has shown $\approx 3\%$ lipoxygenase inhibition (Ali and Houghton, 1999). phenylethanoid esters did not demonstrated antiviral activity against herpes simplex virus, and any cytotoxicity against breast, lung and nervous human cancer cell lines (Luo *et al.*, 2006).

In the present study, 370RQ19 was assessed for its effect on THP-1 cell viability, and potential immunomodulatory activity on TNF- α and IL-12 production from LPS-stimulated THP-1 cells (for further details see section 3.2.4, 3.3.4 and 3.3.8).

Table 3.16 ^1H (500 MHz) and ^{13}C (125 MHz) NMR chemical shift values* for 370RQ19 (recorded in CDCl_3) in comparison with literature data.

Position	^1H NMR δ experimental	^1H NMR δ literature ^a	^{13}C NMR δ experimental	^{13}C NMR δ literature ^a
1			130.2	130.0-130.2
2,6	7.09 (2H, d, J = 8.5 Hz)	7.0- 7.08 (2H, d, J = 8.5 Hz)	130.3	130.1-130.3
3,5	6.77 (2H, d, J = 8.5 Hz)	6.75- 6.77 (2H, d, J = 8.5 Hz)	115.5	115.2-115.5
4			154.4	154.2-155.4
7	2.86 (2H, t, J = 7.1 Hz)	2.85- 2.87 (2H, t, J = 7 Hz)	34.6	34.2-34.4
8	4.25 (2H, t, J = 7.1 Hz)	4.23- 4.26 (2H, t, J = 7Hz)	65.10	64.9-65.0
1'			174.1	173.9-174.1
2'	2.28 (2H, t, J = 7.5 Hz)	2.28- 2.30 (2H, t, J = 7.5 Hz)	34.5	34.4-34.9
3'	1.59 (2H, m)	1.57- 1.61 (2H, m)	25.3	24.8-25.2
(CH_2) _n	1.27 m	21.25- 1.29 m	29.4-29.9	29.2-31.8
Terminal Me	0.89 (3H, t, J = 6.7 Hz)	0.87- 0.90 (3H, t, J = 7.0 Hz)	14.3	14.0-14.3
OH	4.80 (s)	4.5- 4.87 (s)		

* Chemical shift values are in ppm

^a (Alfatafta *et al.*, 1989; Ali and Houghton, 1999; Acevedo *et al.*, 2000; Luo *et al.*, 2006)

E43696.1.fid — Person qwb17191 — RQ19

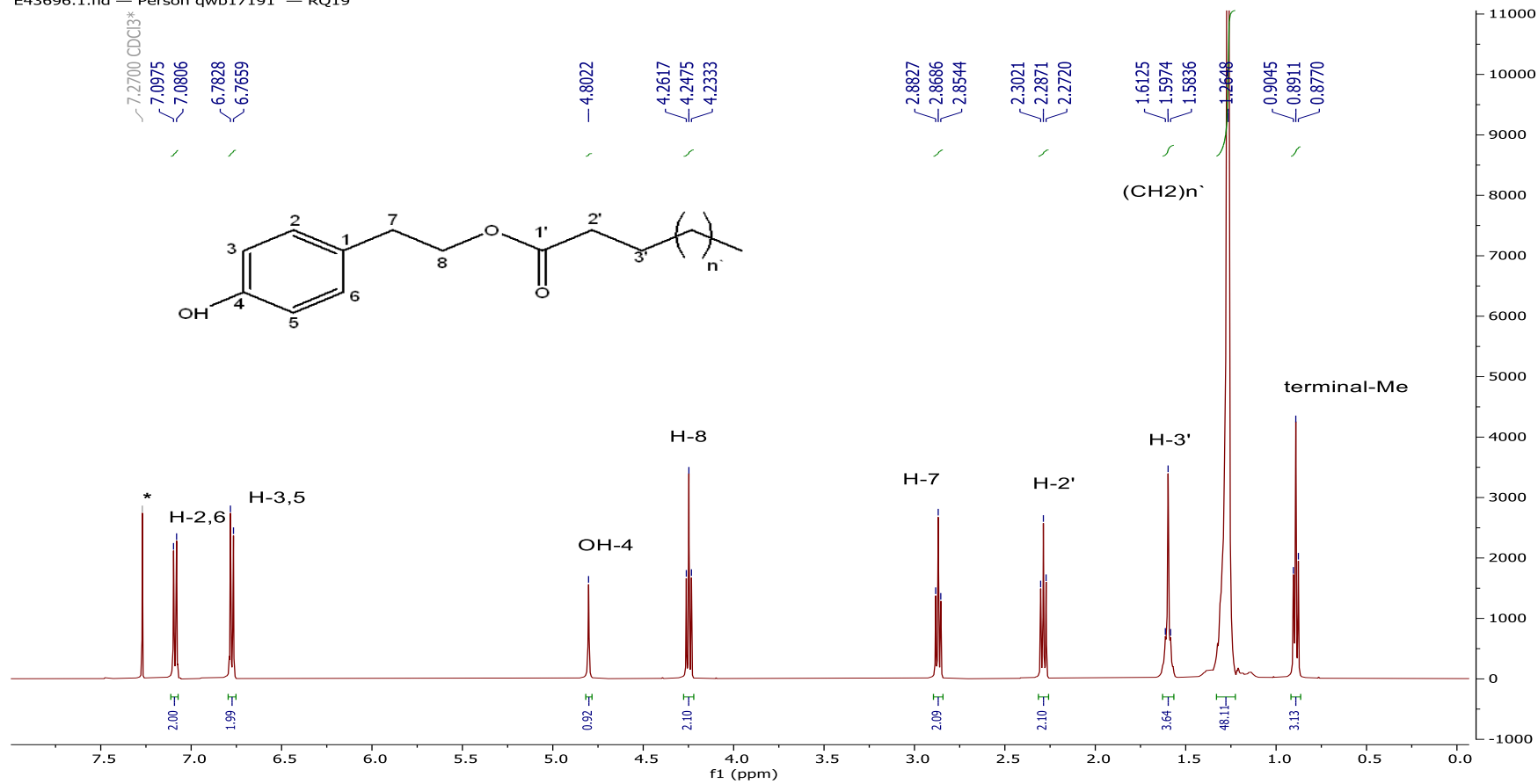


Figure 3.39 ¹H NMR spectrum (CDCl₃*, 500 MHz) of 370RQ19

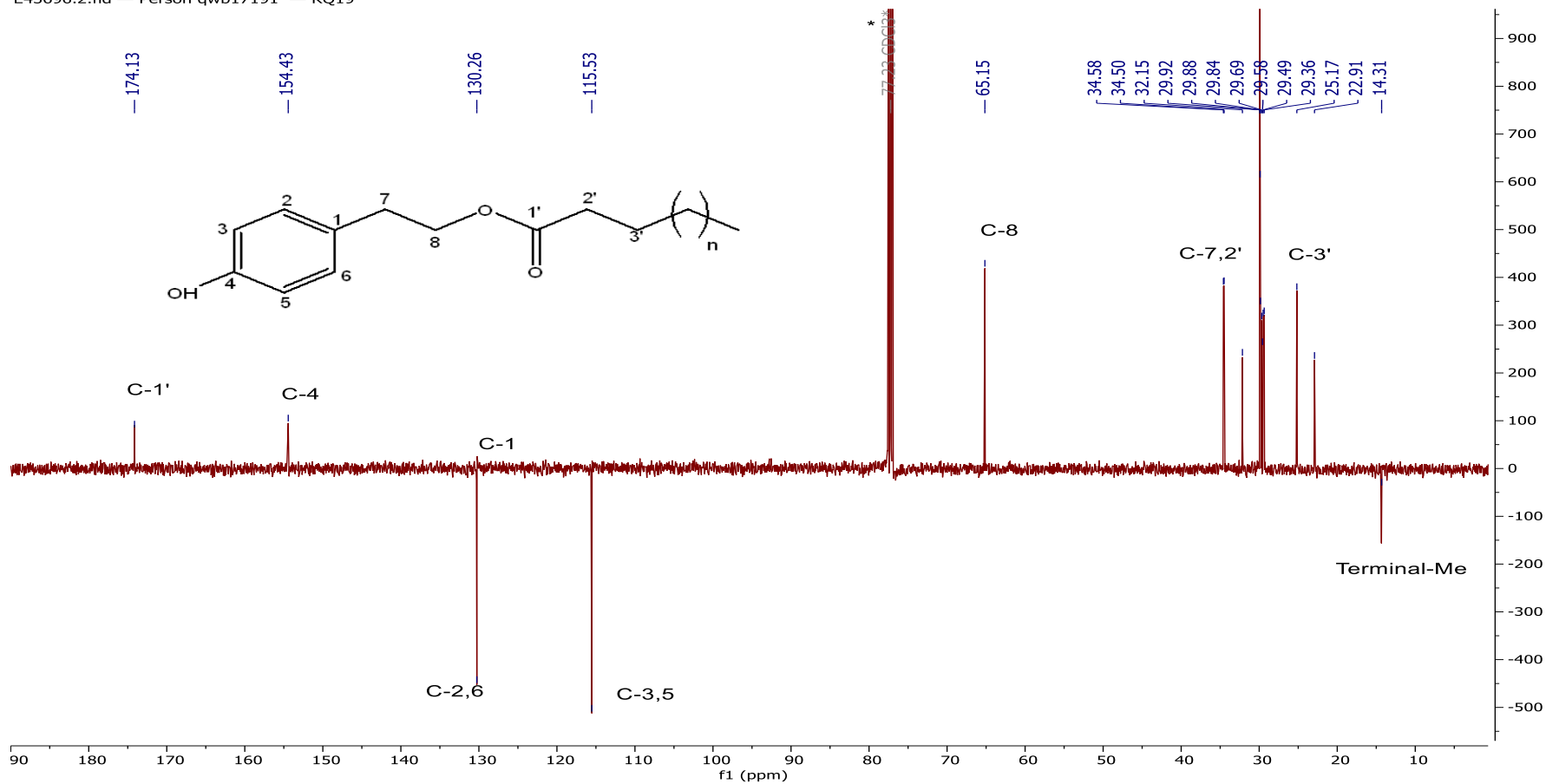
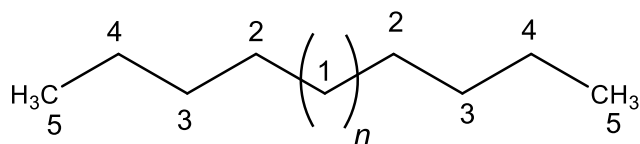


Figure 3.40 ¹³C-DEPTQ NMR spectrum (CDCl₃*, 125 MHz) of 370RQ19

3.1.3.4 Characterization of 390RQ1 and 370RQ22 as a mixture of acyclic alkanes



$n = 19$	$C_{27}H_{56}$	Heptacosane
$n = 20$	$C_{28}H_{58}$	Octacosane
$n = 21$	$C_{29}H_{60}$	Nonacosane
$n = 22$	$C_{30}H_{62}$	triacontane
$n = 23$	$C_{31}H_{64}$	hentriacontane
$n = 24$	$C_{32}H_{66}$	dotriacontane
$n = 25$	$C_{33}H_{68}$	tritriacontane

Figure 3.41 Structures of 390RQ1 / 370RQ22 or a mixture of acyclic alkanes

390RQ1 (54 mg) and 370RQ22 (4.0 mg) were isolated as white amorphous solids from the *n*-hexane extract of *S. arabica* and the ethyl acetate extract of *F. excelsior*, respectively (Figure 3.41). No UV-active spot was observed on TLC plates under short UV light (254 nm). A faint purple spot was observed after treatment with anisaldehyde-sulphuric acid reagent and heating.

The ^1H and ^{13}C NMR spectra of 390RQ1/ 370RQ22 (Figure 3.42 and Figure 3.43) showed signals typical for a long chain *n*-alkane with a triplet at δ_{H} 0.89 attributed to two methyl groups (6H, t, $J = 7\text{Hz}$). This was confirmed by signals for methyl carbons at δ_{C} 14.3. A signal at δ_{H} 1.27 was indicative for a methylene envelope $(\text{CH}_2)_n$, which correlated well with signals at δ_{C} 22.9-32.2.

The quasi-molecular peaks observed in the GC-EI-MS spectra of 370RQ22 and 390RQ1 are illustrated in Table 3.17.

GC-EI-MS analysis demonstrated that 390RQ1/ 370RQ22 were mixtures of acyclic alkanes.

Table 3.17 Molecular ions in the GC-EI-MS spectra of 370RQ22 and 390RQ1

[M]⁺	<i>m/z</i> observed 370RQ22	<i>m/z</i> observed 390RQ1	Formula	Theoretical mass
C ₂₇ H ₅₆	380.4385	380.4380	Heptacosane	380.4382
C ₂₈ H ₅₈	394.4547	394.4543	Octacosane	394.4539
C ₂₉ H ₆₀	408.4678	408.4690	Nonacosane	408.4695
C ₃₀ H ₆₂	422.4850	422.4857	triacontane	422.4852
C ₃₁ H ₆₄	436.5022	436.5011	Hentriacontane	436.5008
C ₃₂ H ₆₆	450.5173	nd [§]	Dotriacontane	450.5164
C ₃₃ H ₆₈	464.5320	464.5303	Tritriacontane	464.5321

[§]nd: not detected

Based on the above spectral data and by comparison with previous reports (Chen *et al.*, 2008) , 390RQ1 was characterised as a mixture of acyclic alkanes, namely heptacosane, octacosane, nonacosane, triacontane, hentriacontane and tritriacontane (Figure 3.41). This is the first report of the isolation of these alkanes from *S. arabica* aerial parts.

370RQ22 was characterised as a mixture of heptacosane, octacosane, nonacosane, triacontane, hentriacontane, dotriacontane and tritriacontane (Figure 3.41). Although nonacosane, hentriacontane, and teratriacontane have previously been isolated from *F. excelsior* leaves (Kowalczyk and Olechnowicz-Stepień, 1989), this is the first report of the isolation of the other alkanes from *F. excelsior* leaves.

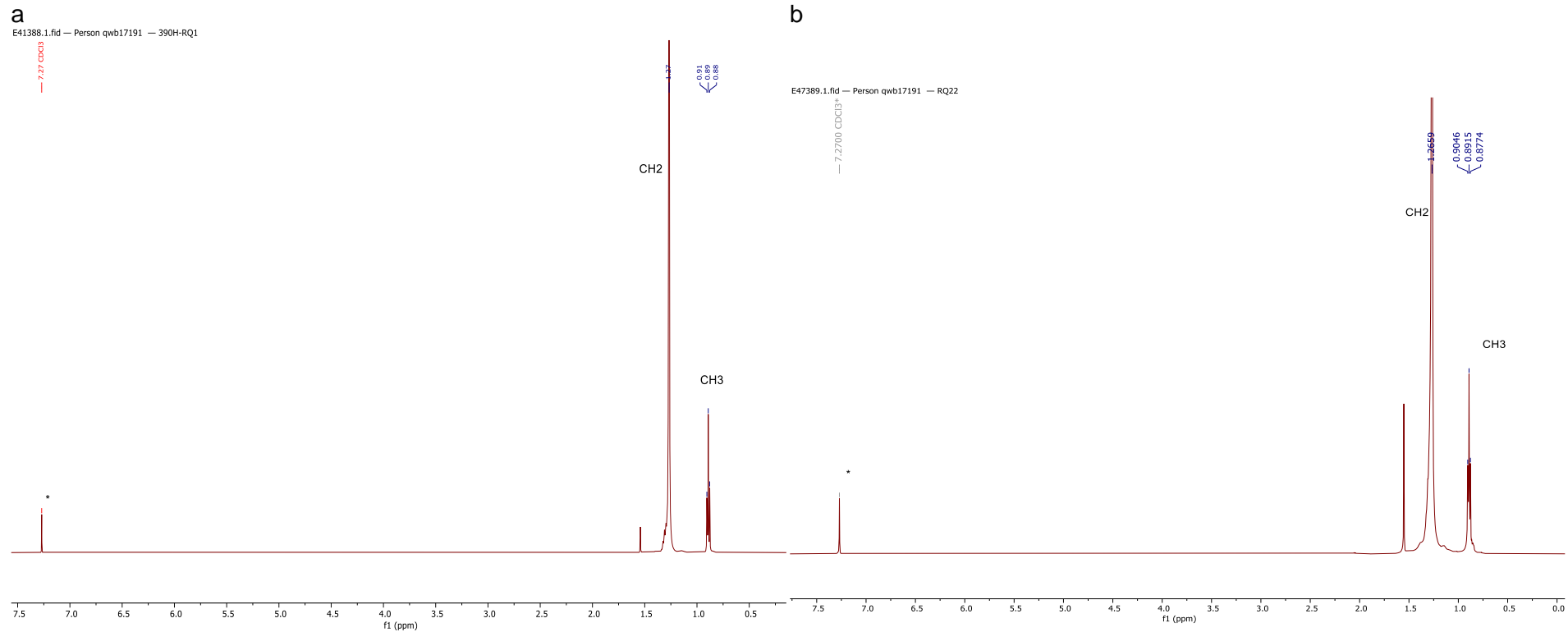


Figure 3.42 ¹H NMR spectrum (CDCl₃*, 500 MHz) spectra of 390RQ1/370RQ22

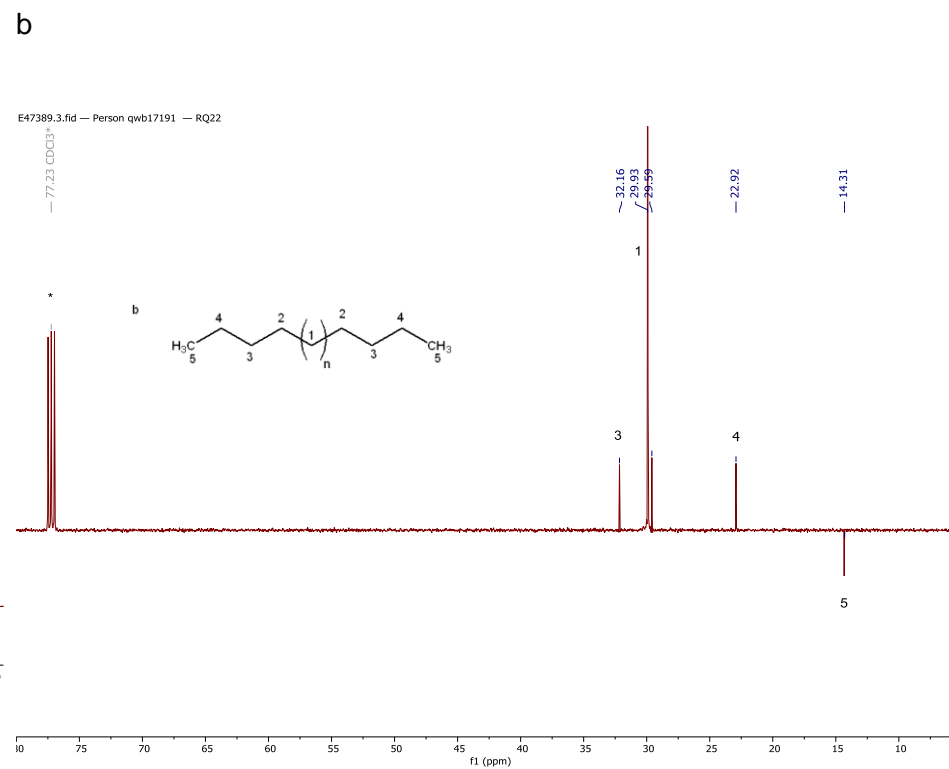
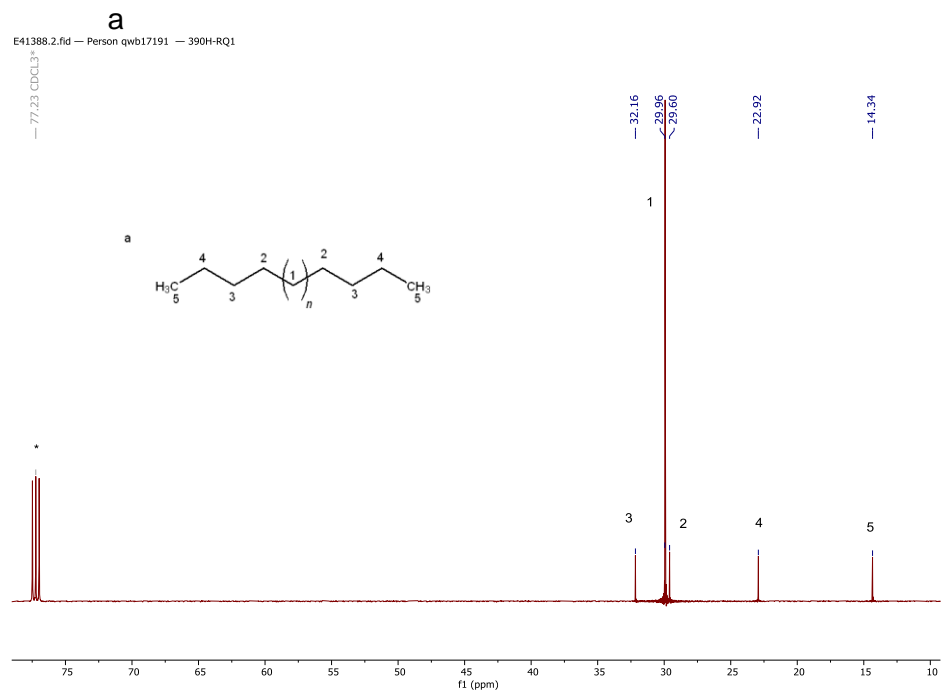


Figure 3.43 ¹³C NMR spectrum (CDCl₃*, 125 MHz) spectra of 390RQ1/ 370RQ22

3.1.3.5 Other compounds

Characterisation of 370RQ4 as dioctyl phthalate or bis(2-ethylhexyl)phthalate (BEHP)

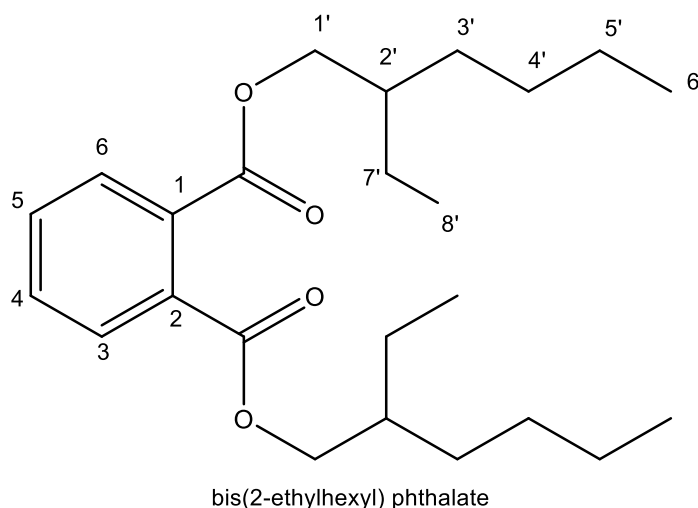


Figure 3.44: Structure of 370RQ4 or dioctyl phthalate (BEHP)

370RQ4 was isolated from the *n*-hexane extract of *F. excelsior* as a white solid (2.7mg) (Figure 3.44). On TLC, 370RQ4 was only active under long wave UV light (366 nm).

The positive ion mode HR-nanoESI-MS data of 370RQ4 showed a quasi-molecular ion peak $[M+Na]^+$ at m/z 413.2656 (theoretical m/z 413.2662) suggesting for a molecular formula of $C_{24}H_{38}O_4$. A molecular ion peak $[2M+Na]^+$ at m/z 803.5426 indicated the presence of a dimer species.

The 1H -NMR spectrum of 370RQ4 (Appendix III) showed signals at δ_H 7.71 (dd, 2H, $J = 5.7, 3.3$ Hz) and δ_H 7.53 (dd, 2H, $J = 5.7, 3.3$ Hz) for protons of an *ortho*-substituted aromatic ring. A signal at δ_H 4.23 (m, 4H) was assigned to a methylene group adjacent to an ester group (COO-CH₂). Two triplets at δ_H 0.89 and 0.93 indicated two terminal methyl groups. The spectrum also showed multiplets at about δ_H 1.2–1.7 for several methylenes.

The ^{13}C DEPTQ NMR spectrum (Appendix III) exhibited the presence of aromatic carbons at δ_{C} 133-129 (C1 and C2), δ_{C} 132.7 and δ_{C} 131.1 (C4 and C5), and δ_{C} 129 (C3 and C6). The presence of signal at δ_{C} 68.4 referred to a methylene group (C1') next to an ester group (COO). Another signal appeared at δ_{C} 39 assigned to a methine group (C2'). Two signals at δ_{C} 14.3 and 11.2 were assigned to two different terminal methyl groups (C6' and C8').

The carbonyl group was difficult to assign as it was not detected in the DEPTQ ^{13}C NMR spectrum, most probably due to the low yield of this sample. However, based on the mass spectral analysis which confirmed the presence of four oxygen atoms and by comparison with literature reports, 370RQ4 was characterised as dioctyl phthalate or bis(2-ethylhexyl)phthalate (BEHP). The NMR and MS data were in good agreement with previous reports (Rao *et al.*, 2000; Habib and Karim, 2009; Nair *et al.*, 2012)

The natural occurrence of phthalate in plants is reported in the literature. Dioctyl phthalate (BEHP) has been reported from *Cassia auriculata* leaves (Rao *et al.*, 2000), as well as from *Alchornea cordifolia* leaves and root bark (Mavar-Manga *et al.*, 2008), *Calotropis gigantea* flowers (Habib and Karim, 2009), and from a commercial South African 'Sejeso' herbal mixture (Ingwe®) (Nair *et al.*, 2012).

The plant material, subsequent extracts, and sub-fractions were not kept in plastic containers. Moreover, all solvents used in this study were kept in glass bottles. Having said that, it cannot be confirmed if the isolated dioctyl phthalate (BEHP) was a natural phytochemical from *F. excelsior* or if it was detected as a result of experimental/environmental contamination (Ortiz and Sansinenea, 2018).

Characterisation of 370RQ3 as triacyl glyceride (TAG)

370RQ3 was isolated from the *n*-hexane extract of *F. excelsior* as a white solid (10 mg). On TLC, 370RQ3 gave a purple spot after treatment with anisaldehyde-sulphuric acid reagent and heating. The ¹H NMR spectrum of 370RQ3 (Table 3.18, Appendix III) demonstrated nine characteristic peaks (A-I).

Table 3.18 ¹H (600 MHz) NMR chemical shift values* and proton assignments of 370RQ3 (recorded in CDCl₃)

Signal [§]	¹ H NMR δ experimental	Proton assignments & Functional group	
A	5.30-5.41 (m)	-CH=CH-	olefinic proton of unsaturated fatty acid
B	5.27 (m)	>CH-OCO-R	(TAG_sn2)
C	4.13-4.18 dd 4.27-4.32 dd	-CH ₂ -OCO-R	(TAG_sn1 & sn3)
D	2.75-2.83	-CH=CH-CH ₂ -CH=CH	Bisallylic (Di-unsaturated & polyunsaturated: linoleyl & linoenyl)
E	2.25-2.35	-OCO-CH ₂ -	α -methylene proton (α -CH ₂)
F	1.95-2.08	-CH ₂ -CH=CH-	(Allylic CH ₂)/ Unsaturated fatty acid
G	1.57-1.65	-OCO-CH ₂ -CH ₂ -	(β -CH ₂)
H	1.23-1.39	-(CH ₂) _n -	All acyl chain
I	0.85-0.92	CH ₂ -CH ₂ -CH ₃	Terminal methyl

* Chemical shift values are in ppm

[§]The signal letters agree with those given in (Figure 5, Appendix III)

Based on the spectral data obtained and by comparison with literature reports, 370RQ3 could be characterised as a mixture of TAGs. The NMR data were in good agreement with those reported for TAG in the literature (Salinero *et al.*, 2012; Nieva-Echevarría *et al.*, 2014; Garcia *et al.*, 2019; Thoss *et al.*, 2012).

Triacyl glycerides (TAGs) are tri-esters composed of a glycerol backbone esterified with three fatty acids. The determination of the exact TAGs profile offers the possibility to identify various combinations of fatty acids with different alkyl chain lengths, degrees of unsaturation (i.e., saturated, mono-, di-, and polyunsaturated), and positions of unsaturations (Buchgraber *et al.*, 2004; Salinero *et al.*, 2012). This was not within the scope of the present study.

PART B:

BIOLOGICAL STUDIES:

**Cell viability and
immunomodulatory
activity**

Part B: Biological studies

3.2 Evaluation of the effect of various crude extracts from *Fraxinus excelsior* leaves, *Stachys arabica* aerial parts, and selected isolated phytochemicals on cell viability using an MTT assay

The *n*-hexane, ethyl acetate (EtOAc) and methanol (MeOH) extracts of both *F. excelsior* leaves (370) and *S. arabica* aerial parts (390) were tested against K562 and THP-1 cell lines to evaluate their effect on the viability of these cell lines using an MTT assay. In addition to that, selected isolated phytochemicals/ pure compounds identified through the phytochemical work were also tested on THP-1 cell to evaluate their effect on the cell viability using MTT assay. Measurements were carried out as described in the Methods section (section 2.7) and IC₅₀ values were determined.

3.2.1 Effect of varying K562 and THP-1 cell concentrations on cell viability.

Cell concentration experiments were carried out before starting the subsequent assays, as it was necessary to determine the optimum cell concentration (cell density) for each cell line used.

Figure 3.45 and Figure 3.46, where various cell concentrations (10^6 /mL) were plotted versus their absorbance values at λ 570 nm, the optimal cell concentration for each cell line is the concentrations that yield an absorbance values in the range of 0.75 - 1.25. Based on this, the cell concentration used depend on the cell type, for K562, we use concentrations in the range of 7.0 - 8.0×10^6 cell /mL (approximate 5.0×10^6 cell/mL per well), and for THP-1 cell in the range of 7.0 - 8.0×10^5 cell /mL (approximate 5.0×10^5 cell/mL as final conc. per well)

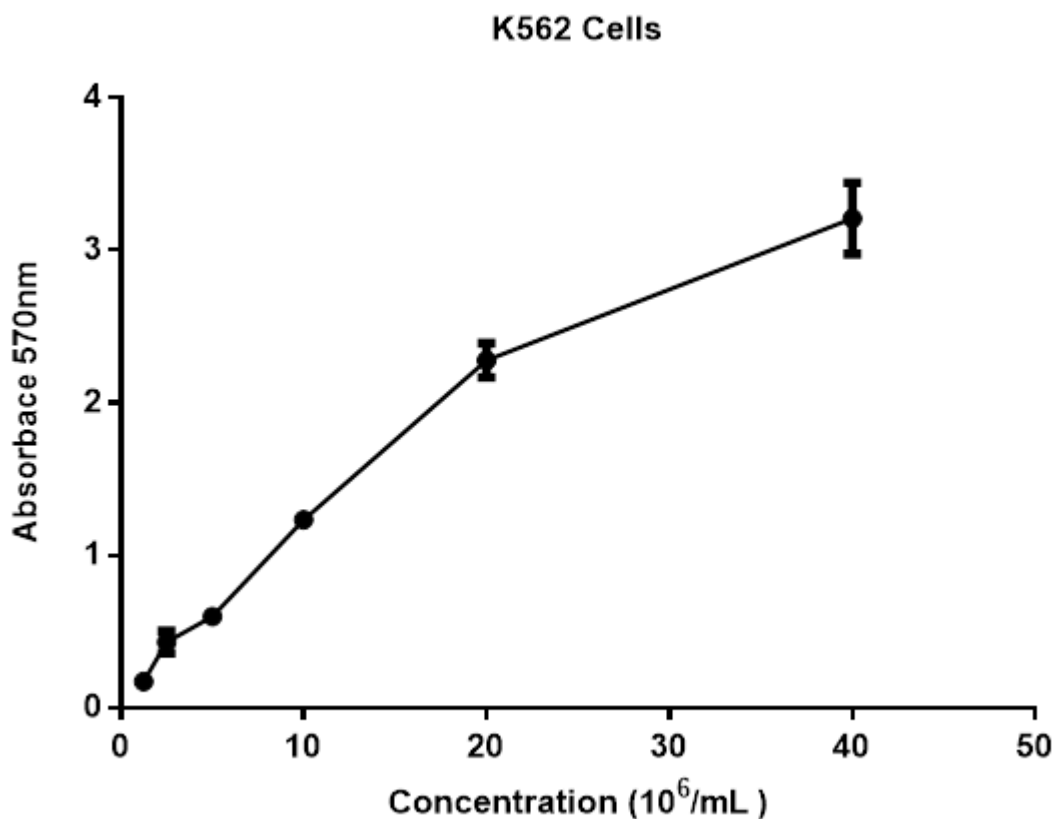


Figure 3.45 K562 cell viability with increasing cell numbers

K562 cell viability, at various cell concentrations, was examined by performing an MTT assay. Cells were serially diluted from a starting concentration of 40.0×10^6 cell /mL, transferred to sterile 96 well plates and incubated for 20 minutes, after which MTT was added and they were further incubated at 37°C , 5% CO_2 for two hours. SDS solution was added to wells and incubated at 37°C for 24 hours. Absorbance was measured at 570 nm. The values are presented as the means of $n = 4 \pm \text{s.d.}$ and are representative of two independent experiments.

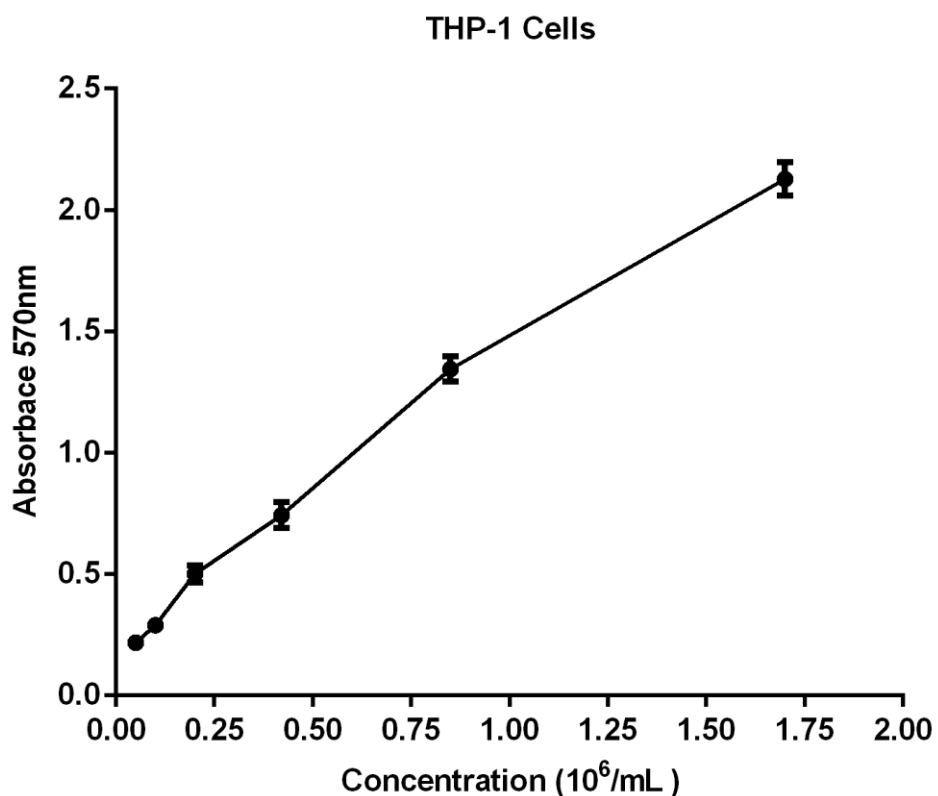


Figure 3.46 THP-1 cell viability with increasing cell numbers

THP-1 cell viability, at various cell concentrations, was examined by carrying out an MTT assay. Cells were serially diluted from a starting concentration of 1.7×10^6 cell/mL and transferred to a sterile 96 well plate and incubated for 20 minutes, after which MTT was added and they were further incubated at 37°C, 5% CO₂ for two hours. SDS solution was added to wells and incubated at 37°C for 24 hours. Absorbance was measured at 570 nm. The values are presented as the means of $n = 4 \pm$ s.d. and are representative of two independent experiments.

3.2.2 Effect of the various crude extracts of *Fraxinus excelsior* leaves (370) on cell viability

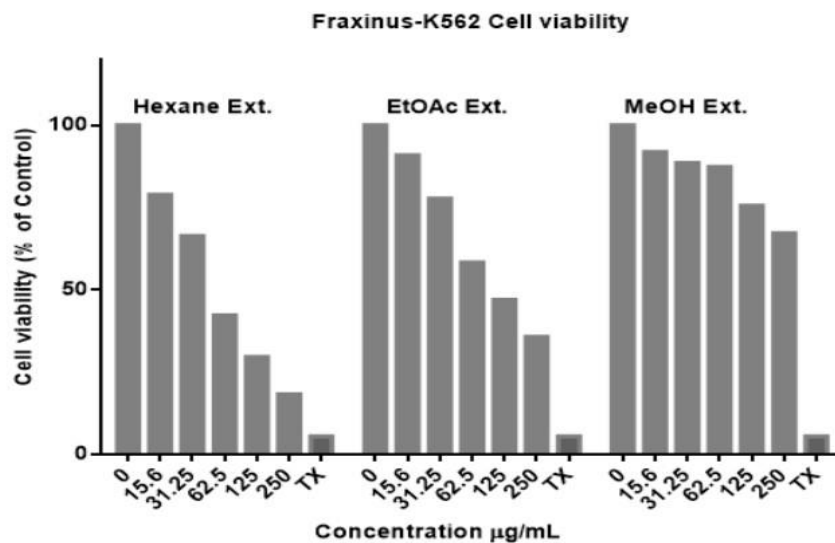
The purpose of these experiments was to evaluate the effect of MeOH (polar), EtOAc (semi-polar) and *n*-hexane (non-polar) extracts of *F. excelsior* leaves (370) on THP-1 and K562 cell viability using an MTT assay.

The effect of the *n*-hexane (370H) and ethyl acetate (370E) extracts on the viability of K562 cells is illustrated in Figure 3.47. The results showed that an increase in the concentrations of the extracts resulted in a decrease in K562 cell viability. Both extracts caused significant reduction in cell viability at concentrations > 31.25 µg/mL for (370H) and > 62.5 µg/mL for (370E). The IC₅₀ values obtained for 370H and 370E were 44.8 and 85.2 µg/mL, respectively (Figure 3.47b).

As shown in Figure 3.48, the results showed that an increase in the concentrations of *F. excelsior* extracts resulted in a decrease in THP-1 cell viability. The effect of the *n*-hexane (370H) and ethyl acetate (370E) extracts on the viability of THP-1 cells was observed at lower concentrations. Both extracts demonstrated a significant reduction in cell viability compared to the control at concentrations ≥ 31.25 µg/mL. 370H at 31.25 µg/mL maintained 87% cell viability compared to untreated cells, whereas 370E at the same concentration showed a significant reduction in cell viability (approximately 35% compared to untreated cells). According to the data presented in Figure 3.48b, the IC₅₀ values for 370H and 370E were 56.9 µg/mL and 39.9 µg/mL, respectively.

The methanol extract of *F. excelsior* leaves (370M) did not demonstrate any significant effect on the viability of K562 cell line at all concentrations tested. However, the same extract showed a significant reduction in cell viability of THP-1 cells at concentrations ≥ 125 µg/mL with an IC₅₀ value of 124.7 µg/mL.

a



b

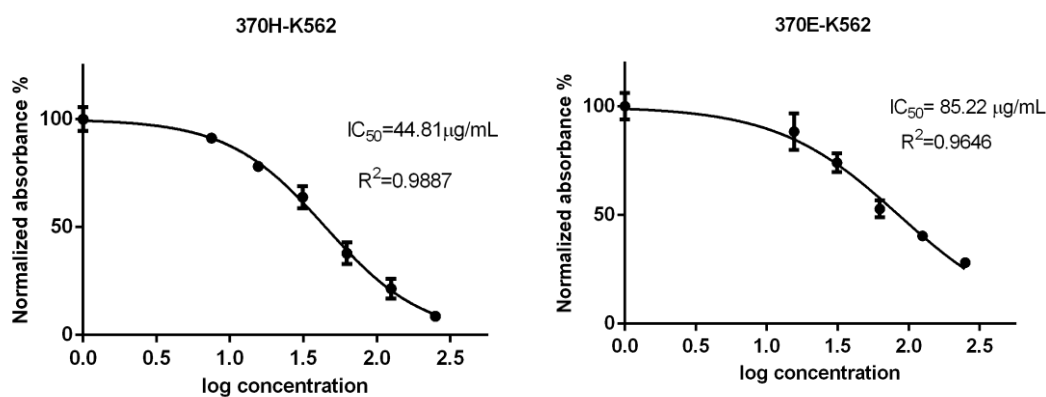
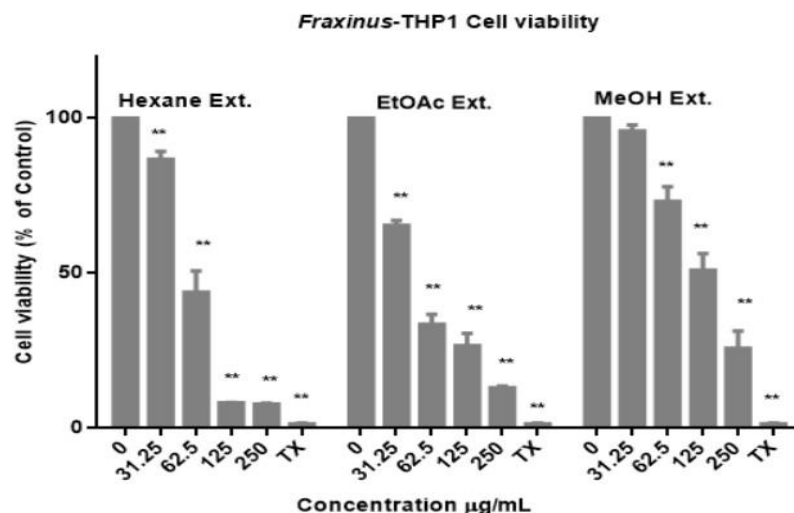


Figure 3.47 Effect of the various crude extracts of *Fraxinus excelsior* leaves (370) on the viability of K562 cells

a- The effect of the various crude extracts (*n*-hexane, EtOAc and MeOH) from *Fraxinus excelsior* leaves (370) on the viability of K562 cells using an MTT assay. K562 cells (5×10^6 cell/mL) were placed into 96-well plates then incubated at 37 °C in 5% CO₂ and 100 % humidity for 24 hours with various plant extracts. Untreated cells (0), and cells treated with Triton X-100 (0.5%), were used as negative and positive controls, respectively. Absorbance was measured at 570 nm. Values are the means of $n = 3$.

b- The effect of *n*-hexane and EtOAc crude extracts from *F. excelsior* leaves (370) on the viability of K562 cells was expressed as IC_{50} values. Experimental data were expressed as the means of $n = 3 \pm \text{s.d.}$ IC_{50} was calculated using nonlinear regression analysis.

a



b

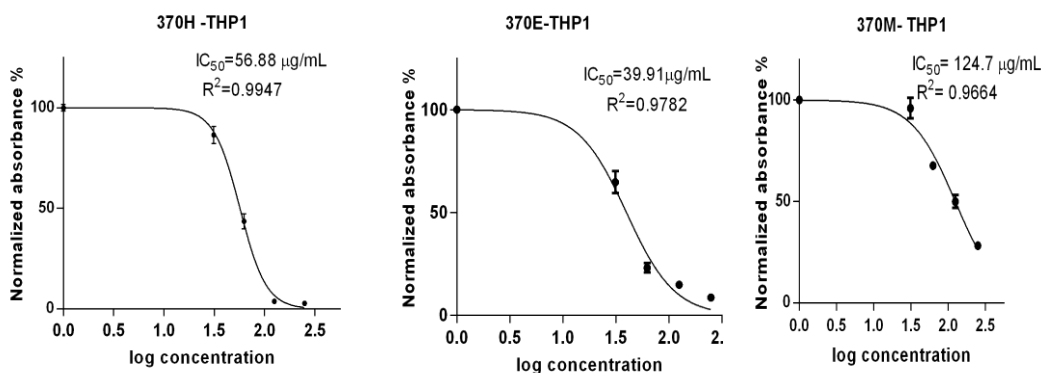


Figure 3.48 Effects of the various crude extracts of *Fraxinus excelsior* leaves (370) on the viability of THP-1 cells

a- The effect of the various crude extracts (*n*-hexane, EtOAc and MeOH) from *Fraxinus excelsior* leaves (370) on the viability of THP-1 cells using an MTT assay. THP-1 cells (5×10^5 cells/mL) were placed into 96-well plates then incubated at 37 °C in 5% CO₂ and 100% humidity for 24 hours with the various plant extracts. Untreated cells (0), and cells treated with Triton X-100 (0.5%), were used as negative and positive controls, respectively. Absorbance was measured at 570 nm. Values are the means of $n = 3 \pm$ s.d. from three independent experiments.

b- The effect of various crude extracts from *F. excelsior* leaves (370) on the viability of THP-1 cells was expressed as IC₅₀ values. Experimental data were expressed as the mean of $n = 4 \pm$ s.d., and are representative of three independent experiments. IC₅₀ was calculated using nonlinear regression analysis.

3.2.3 Effect of the various crude extracts of *Stachys arabica* aerial parts (390) on cell viability

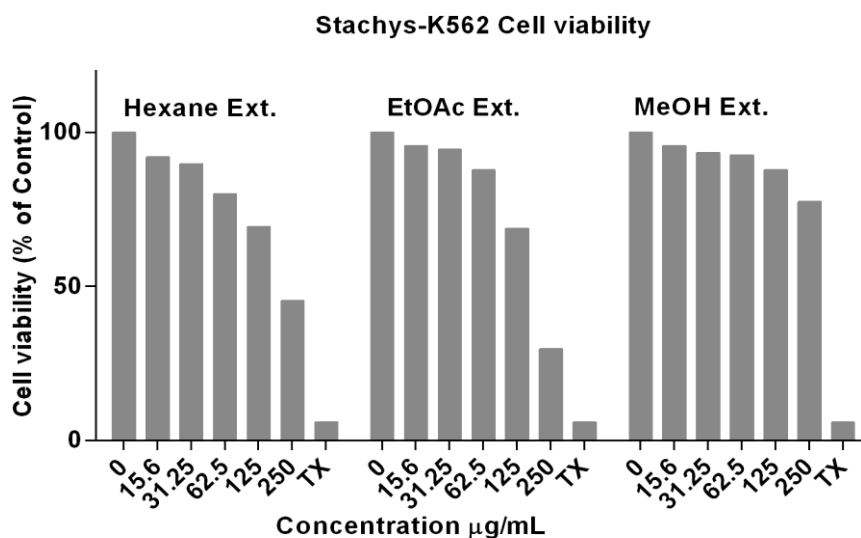
The purpose of this experiment was to evaluate the effect of MeOH (polar), EtOAc (semi-polar) and *n*-hexane (non-polar) extracts of *S. arabica* aerial parts (390) on THP-1 and K562 cell viability using an MTT assay.

The effect of *n*-hexane (390H) and ethyl acetate (390E) extracts on the viability of K562 cells was observed at higher concentrations only. Both extracts caused significant reduction in the cell viability at concentrations > 125 µg/mL (Figure 3.49). The IC₅₀ values for 390H and 390E were 207.9 and 161.2 µg/mL, respectively (Figure 3.49b).

As observed in Figure 3.50, The effect of *n*-hexane (390H) and ethyl acetate (390E) extracts on the viability of THP-1 cells was greater than their effect on the cell viability of K562, the results showed that an increase in the concentrations of *S. arabica* extracts resulted in a decreased in THP-1 cell viability. Both extracts demonstrated a significant reduction in cell viability compared to the control at concentrations > 62.5 for 390H and > 31.25µg/mL for 390E. 390H at 62.5 µg/mL maintained 80% cell viability compared to untreated cells, whereas 390E at the same concentration showed a significant reduction in cell viability (approximately 33% compared to untreated cells). Figure 3.50b shows the IC₅₀ values for (390H) at 86.9 µg/mL and for (390E) at 49.4 µg/mL, respectively.

The methanol extract of *S. arabica* (390M) did not show any significant effect on the viability of either THP-1 or K562 cell lines at all tested concentrations. The cell viability approximately ≥ 80%.

a



b

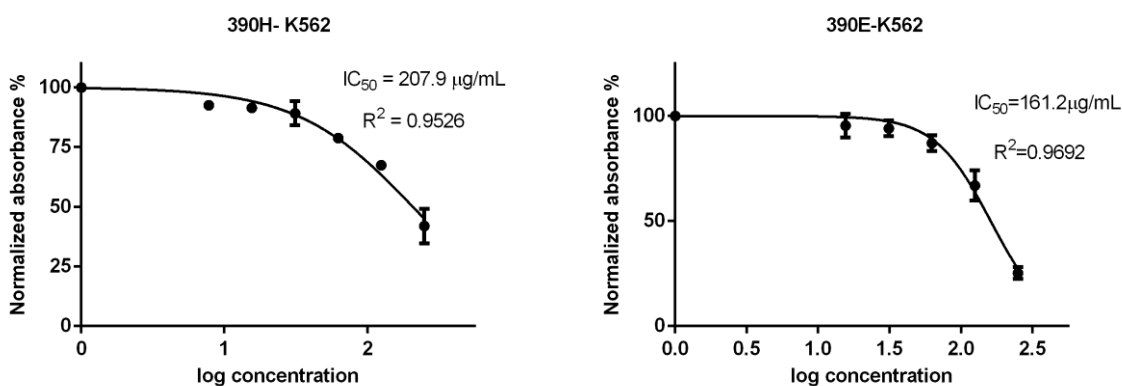
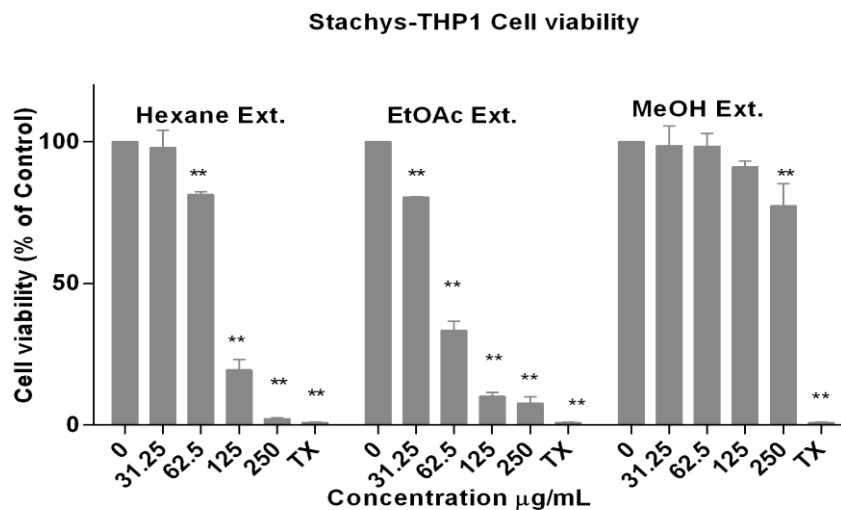


Figure 3.49 Effect of the various crude extracts of *Stachys arabica* aerial parts (390) on the viability of K562 cells

a- The effect of the various crude extracts (*n*-hexane, EtOAc and MeOH) from *Stachys arabica* aerial parts (390) on the viability of K562 cells using an MTT assay. K562 cells (5×10^6 cell/mL) were placed into 96-well plates then incubated at 37°C in 5% CO₂ and 100 % humidity for 24 hours with various plant extracts. Untreated cells (0), and cells treated with Triton X-100 (0.5%), were used as negative and positive controls, respectively. Absorbance was measured at 570 nm. Values are the means of $n = 3$.

b- The effect of *n*-hexane and EtOAc crude extract from *S. arabica* aerial parts (390) on the viability of K562 cells was expressed as IC₅₀ values. Experimental data were expressed as the means of $n = 3 \pm$ s.d. IC₅₀ was calculated using nonlinear regression analysis

a



b

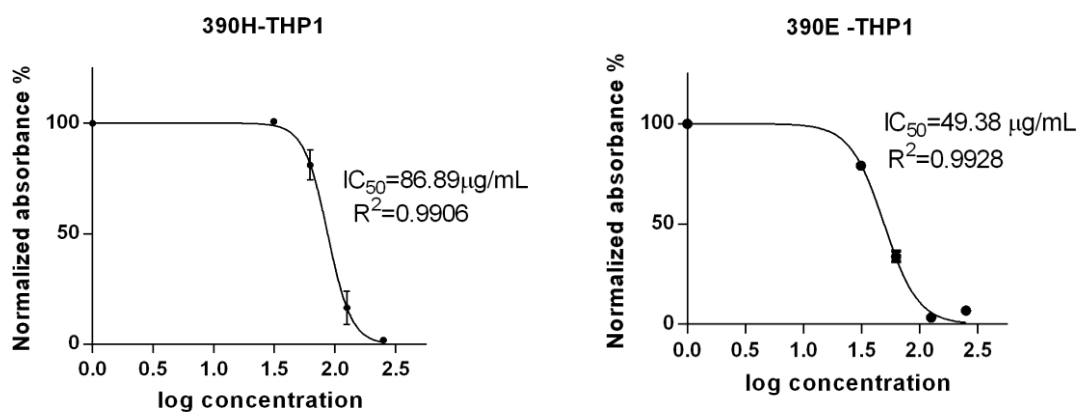


Figure 3.50 Effect of the various crude extracts of *Stachys arabica* aerial parts (390) on the viability of THP-1 cells

a- The effect of the various crude extracts (*n*-hexane, EtOAc and MeOH) from *Stachys arabica* aerial parts (390) on the viability of THP-1 cells using an MTT assay. THP-1 cells (5×10^5 cells/mL) were placed into 96-well plates then incubated at 37°C in 5% CO₂ and 100 % humidity for 24 hours with various plant extracts. Untreated cells (0), and cells treated with Triton X-100 (0.5%), were used as negative and positive controls, respectively. Absorbance was measured at 570 nm. Values are the means of $n = 3 \pm$ s.d. from three independent experiments.

b- The effect of *n*-hexane and EtOAc crude extract from *S. arabica* aerial parts (390) on the viability of THP-1 cells was expressed as IC₅₀ values. Experimental data were expressed as the means of $n = 4 \pm$ s.d. and are representative of three independent experiments. IC₅₀ was calculated using nonlinear regression analysis

3.2.4 Effect of selected phytochemicals isolated from EtOAc extract of *Fraxinus excelsior* leaves (370E) on THP-1 cell viability

Several phytochemicals were isolated from the EtOAc extract of *F. excelsior* leaves. This included two pentacyclic triterpenes (oleanolic acid (**OA**) and ursolic acid (**UA**); 370RQ7/370RQ25), one flavonoid pinocembrin (370RQ20), and mixture of phenylethanoid esters (370RQ19). OA, UA, and pinocembrin were purchased from a commercial suppliers (see section 2.1.2) and tested as pure compounds. The isolated sample of 370RQ19 was used since it was obtained in enough amount, and it is not commercially available. These phytochemicals were assessed on the viability of THP-1 cells and their effects are shown in the following Figures (3.51- 3.55).

As shown in Figure 3.51, pinocembrin demonstrated a significant decrease in the number of viable THP-1 cells compared to the control, at concentrations >122.0 μM (IC_{50} value of 178.6 μM). pinocembrin at 122.0 μM maintained approximately 86% of the THP-1 cell viability, whereas a concentration of 243.9 μM reduced cell viability to approximate 20% of the control level.

The cell viability in the presence of **UA** exceeded 94% at concentrations $\leq 34.2 \mu\text{M}$. However, at 68.4 μM it significantly decreased the number of viable THP-1 cells to approximately 40% compared to the control with an IC_{50} value of 61.5 μM (Figure 3.52). On the other hand, the cell viability exceeded 84% with **OA** concentrations $\leq 68.4 \mu\text{M}$, and only at concentration of 273.7 μM of **OA** did the reduction of cell viability exceed 50% compared to the control with an IC_{50} value of 199.8 μM (Figure 3.53).

Finally, the mixture of phenylethanoid esters was assessed on its effect on the cell viability of THP-1 cell line as shown in Figure 3.54. The results of this investigation demonstrated that the mixture of phenylethanoid esters had no significant effect on the number of viable THP-1 cells in all tested concentration compared to the control/untreated cells. The cell viability exceeded 87% at the higher concentration used (250 $\mu\text{g}/\text{mL}$). It might be concluded that this mixture of phenylethanoid esters was relatively non-toxic/ safe at all tested concentrations.

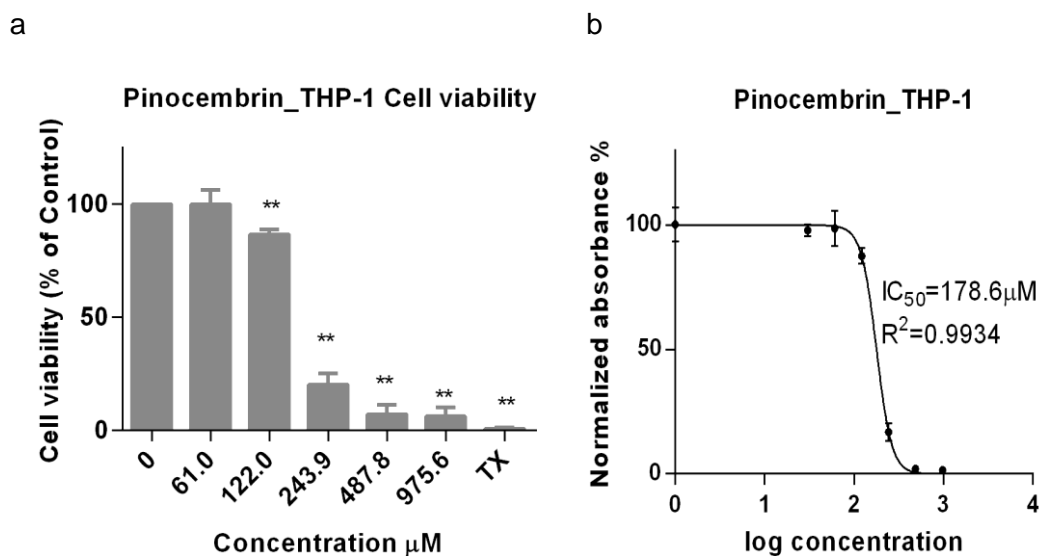


Figure 3.51 Effect of the various concentrations of pinocembrin on the viability of THP-1 cells

a- The effect of the various concentrations of pinocembrin on the viability of THP-1 cells using a MTT assay. THP-1 cells (5×10^5 cell/mL) were placed into 96-well plates then incubated at 37 °C in 5% CO₂ and 100% humidity for 24 hours with various concentrations. Untreated cells (0), and cells treated with Triton X-100 (0.5%), were used as negative and positive controls, respectively. Absorbance was measured at 570 nm. Values are the means of $n = 3 \pm$ s.d. from three independent experiments.

b- The effect of the various concentrations of pinocembrin on the viability of THP-1 cells was expressed as IC₅₀ values. Experimental data were expressed as the means of $n = 4 \pm$ s.d. and are representative of three independent experiments. IC₅₀ was calculated using nonlinear regression analysis

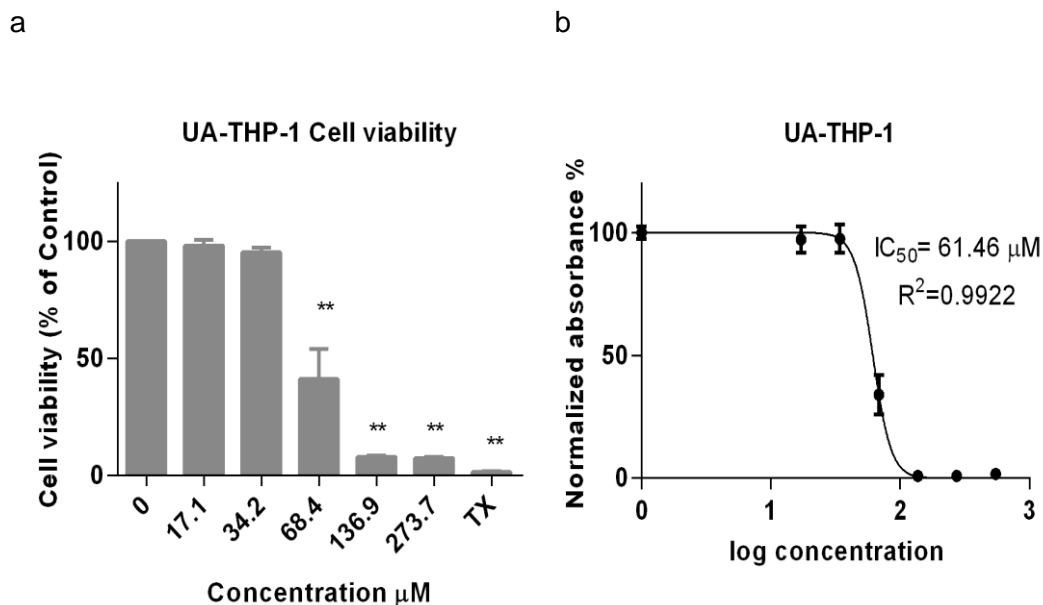


Figure 3.52 Effect of the various concentrations of UA on the viability of THP-1 cells

a- The effect of the various concentrations of UA on the viability of THP-1 cells using an MTT assay. THP-1 cells were (5×10^5 cell/mL) were placed into 96-well plates then incubated at 37 °C in 5% CO₂ and 100% humidity for 24 hours with various concentrations. Untreated cells (0), and cells treated with Triton X-100 (0.5%), were used as negative and positive controls, respectively. Absorbance was measured at 570 nm. Values are the means of $n = 3 \pm$ s.d. from three independent experiments.

b- The effect of the various concentrations of UA on the viability of THP-1 cells was expressed as IC₅₀ values. Experimental data were expressed as the mean of $n = 4 \pm$ s.d. and are representative of three independent experiments. IC₅₀ value was calculated using nonlinear regression analysis

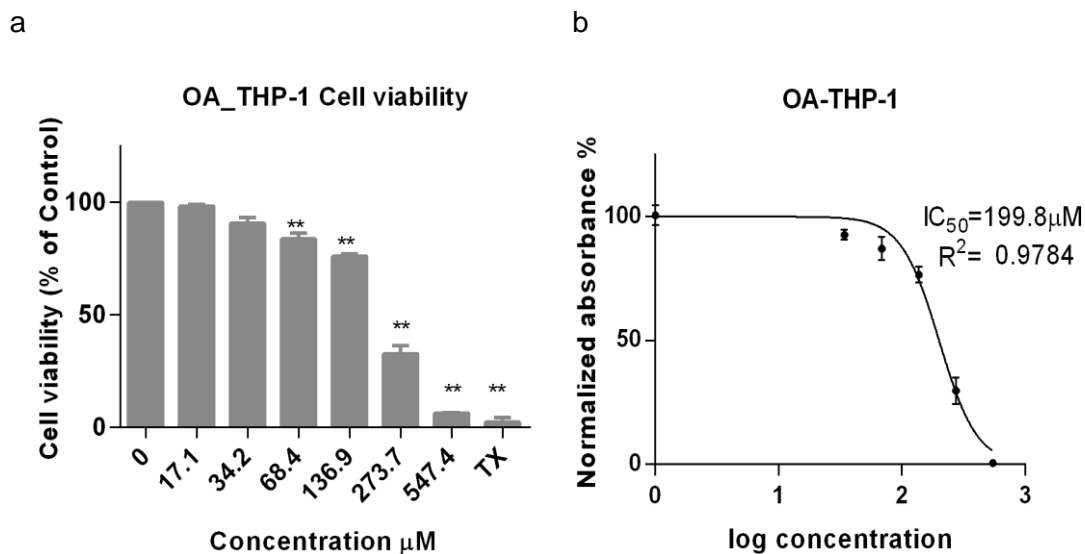


Figure 3.53 Effect of the various concentrations of OA on the viability of THP-1 cells

a- The effect of the various concentrations of OA on the viability of THP-1 cells using a MTT assay. THP-1 cells (5×10^5 cell/mL) were placed into 96-well plates then incubated at 37 °C in 5% CO₂ and 100% humidity for 24 hours with various concentrations. Untreated cells (0), and cells treated with Triton X-100 (0.5%), were used as negative and positive controls, respectively. Absorbance was measured at 570 nm. Values are the means of $n = 3 \pm$ s.d. from three independent experiments.

b- The effect of the various concentrations of OA on the viability of THP-1 cells was expressed as IC₅₀ values. Experimental data were expressed as the mean of $n = 4 \pm$ s.d. and are representative of three independent experiments. IC₅₀ value was calculated using nonlinear regression analysis

The mixture of phenylethanoid esters_THP-1 Cell viability

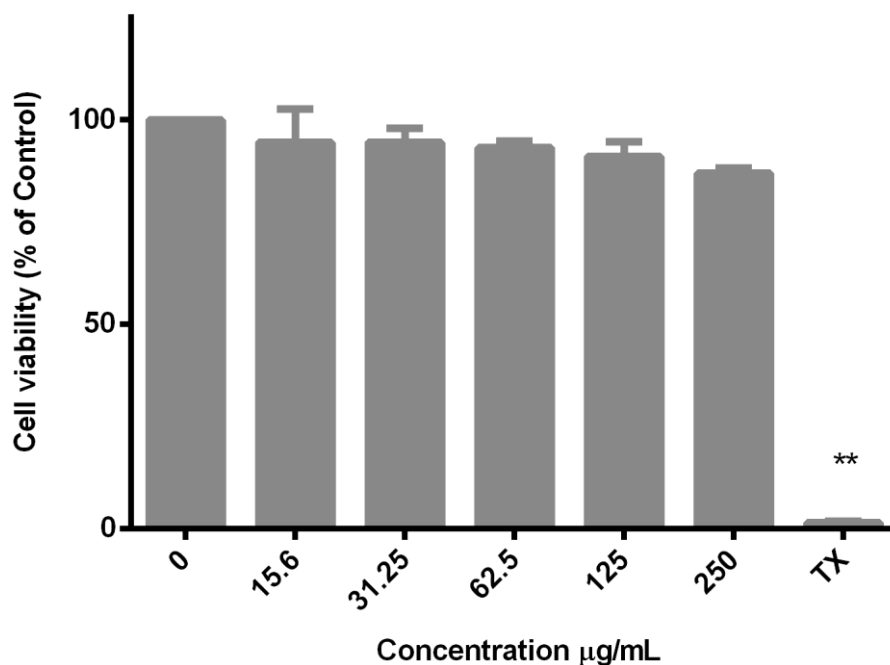


Figure 3.54 Effect of the various concentration of the mixture of phenylethanoid esters on the viability of THP-1 cells

The effect of the various concentration of the mixture of phenylethanoid esters on the viability of THP-1 cells using an MTT assay, THP-1 cells (5×10^5 cell/mL) were placed into 96-well plates then incubated at 37 °C in 5% CO₂ and 100% humidity for 24 hours with various concentrations. Untreated cells (0), and cells treated with Triton X-100 (0.5%), were used as negative and positive controls, respectively. Absorbance was measured at 570 nm. Values are the means of $n = 3 \pm$ s.d. from three independent experiments.

3.2.5 Effect of phytochemicals isolated from EtOAc extracts of *Stachys arabica* aerial parts (390E) on THP-1 cell viability

Three pheophytins were isolated from the EtOAc extract of *S. arabica* aerial parts, including pheophytin a (**390RQ10**), 13²(*R,S*)-hydroxy pheophytin a (**390RQ27**), and pheophytin b (**390RQ28**). These pheophytins were assessed on the viability of THP-1 cells, and their effects are illustrated in Figures 3.55-3.57.

A significant reduction in the number of viable THP-1 cells compared to the control was observed in the presence of pheophytin a, at a concentration of 143.5 μM (IC_{50} value of 186.4 μM). THP-1 cell viability was not affected by concentrations $\leq 71.7 \mu\text{M}$ as a viability of approximately 85% was maintained when compared to untreated cells (Figure 3.55).

As shown in Figure 3.56 and Figure 3.57, Both 13²(*R,S*)-hydroxy pheophytin a and pheophytin b demonstrated a potent effect on the cell viability of THP-1 compared to pheophytin a at all tested concentrations $> 35 \mu\text{M}$. 13²(*R,S*)-hydroxy pheophytin a (IC_{50} value of 42.2 μM) and pheophytin b (IC_{50} value of 40.4 μM) significantly decrease the number of viable THP-1 cells at a concentration $> 35 \mu\text{M}$ when compared to the control. 13²(*R,S*)-hydroxy pheophytin a at concentrations of 17.6 and 35.2 μM , the cell viability was circa 85% and 75%, respectively. Also, pheophytin b at concentrations of 17.7 & 35.3 μM , the cell viability was around 95% and 75%, respectively when compared to untreated cells.

According to these results, the concentrations that maintained cell viability $\geq 75\%$ compared to the control/untreated cells, and lower than the IC_{50} values, were considered non-toxic/safe to be used in subsequent experiments.

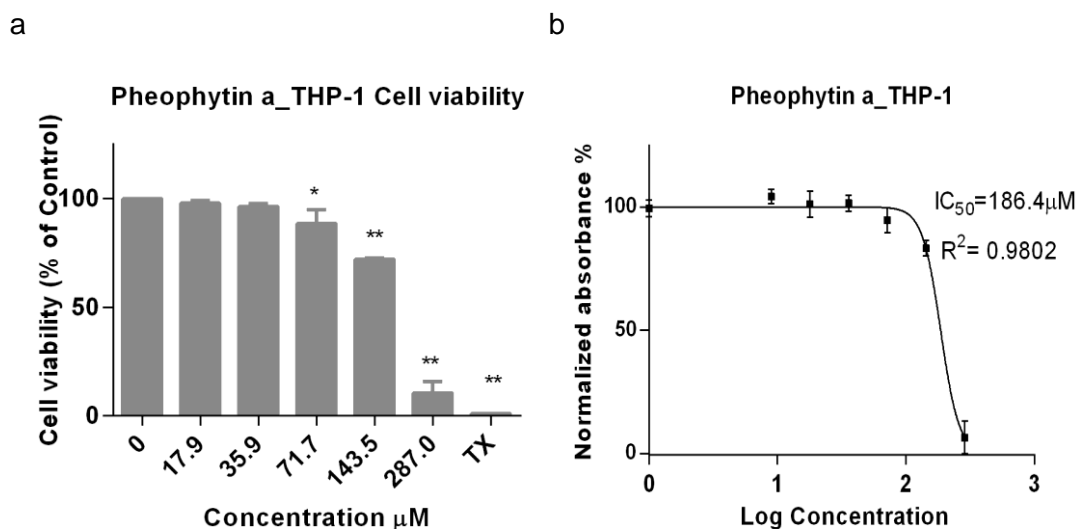


Figure 3.55 Effect of the various concentration of pheophytin a on the viability of THP-1 cells

a- The effect of the various concentration of pheophytin a on the viability of THP-1 cells using an MTT assay. THP-1 cells (5×10^5 cell/mL) were placed into 96-well plates then incubated at 37 °C in 5% CO₂ and 100% humidity for 24 hours with various concentrations. Untreated cells (0), and cells treated with Triton X-100 (0.5%), were used as negative and positive controls, respectively. Absorbance was measured at 570 nm. Values are the means of $n = 3 \pm$ s.d. from three independent experiments.

b- The effect of the various concentrations of pheophytin a on the viability of THP-1 cells was expressed as IC₅₀ values. Experimental data were expressed as the mean of $n = 4 \pm$ s.d. and are representative of three independent experiments. IC₅₀ value was calculated using nonlinear regression analysis

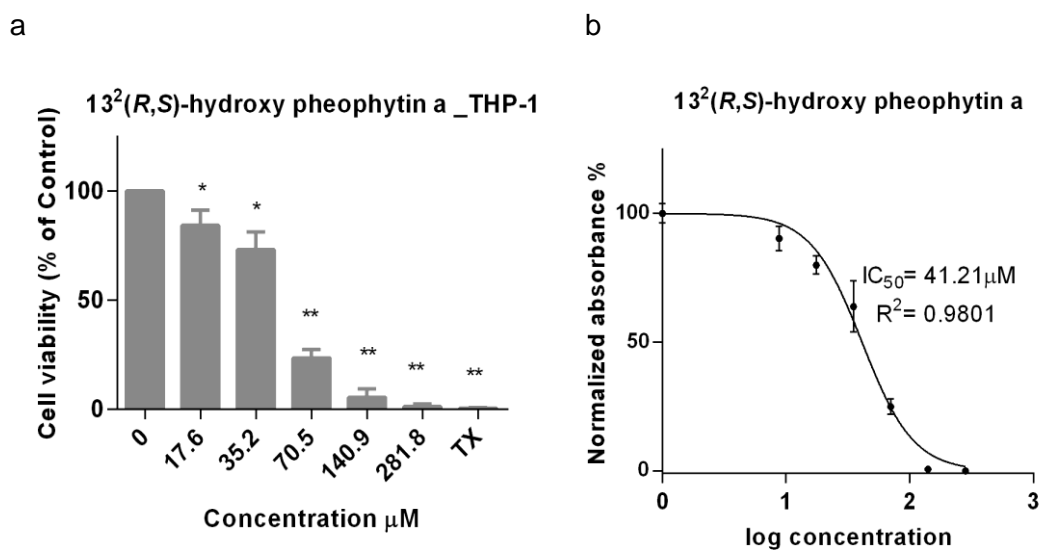


Figure 3.55 Effect of the various concentration of 13²(R,S)-hydroxy pheophytin a on the viability of THP-1 cells

a- The effect of the various concentration of 13²(R,S)-hydroxy pheophytin a on the viability of THP-1 cells using a MTT assay. THP-1 cells (5×10^5 cell/mL) were placed into 96-well plates then incubated at 37 °C in 5% CO₂ and 100% humidity for 24 hours with various concentrations. Untreated cells (0), and cells treated with Triton X-100 (0.5%), were used as negative and positive controls, respectively. Absorbance was measured at 570 nm. Values are the means of $n = 3 \pm$ s.d. from three independent experiments.

b- The effect of the various concentrations of 13²(R,S)-hydroxy pheophytin a on the viability of THP-1 cells was expressed as IC₅₀ values. Experimental data were expressed as the mean of $n = 4 \pm$ s.d. and are representative of three independent experiments. IC₅₀ value was calculated using nonlinear regression analysis

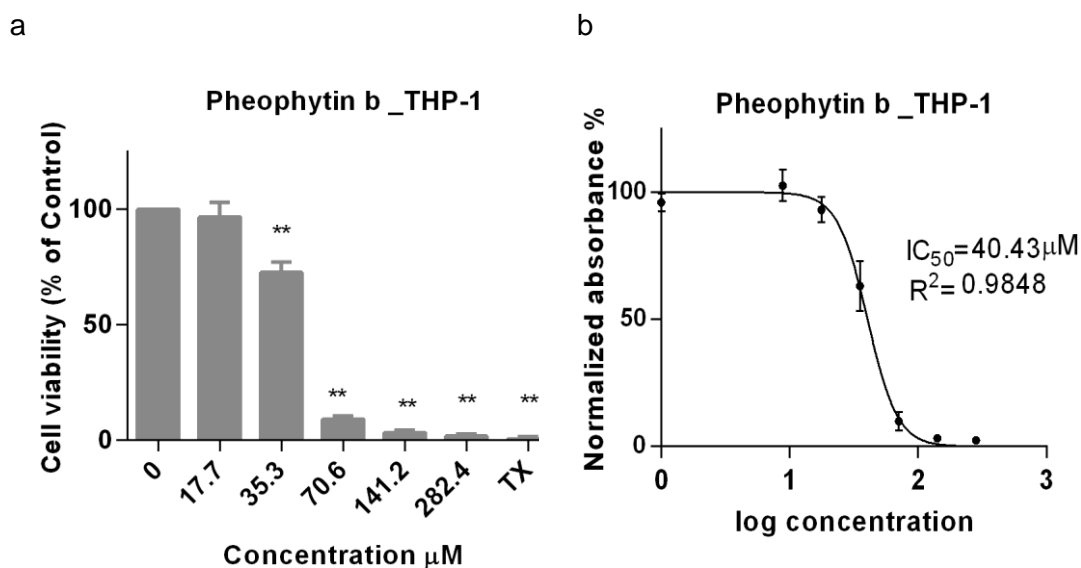


Figure 3.57 Effect of the various concentration of pheophytin b on the viability of THP-1 cells

a- The effect of the various concentration of pheophytin b on the viability of THP-1 cells using an MTT assay. THP-1 cells (5×10^5 cell/mL) were placed into 96-well plates then incubated at 37°C in 5% CO₂ and 100% humidity for 24 hours with various concentrations. Untreated cells (0), and cells treated with Triton X-100 (0.5%), were used as negative and positive controls, respectively. Absorbance was measured at 570 nm. Values are the means of $n = 3 \pm$ s.d. from three independent experiments.

b- The effect of the various concentrations of pheophytin b on the viability of THP-1 cells was expressed as IC₅₀ values. Experimental data were expressed as the mean of $n = 4 \pm$ s.d. and are representative of three independent experiments. IC₅₀ value was calculated using nonlinear regression analysis

3.3 Determination of the effect of various crude extracts from *F. excelsior* leaves, *S. arabica* aerial parts, and selected isolated phytochemicals on pro-inflammatory cytokines (TNF- α and IL-12) production by THP-1 cells

The purpose of this part of this research was to investigate the potential immunomodulatory effects of various extracts from *F. excelsior* leaves (370), *S. arabica* aerial parts (390), and selected phytochemicals isolated from these plants, on the pro-inflammatory cytokine profiles of LPS-stimulated THP-1 cells using ELISA.

All the experiments were performed using non-toxic concentrations of each tested extract or phytochemical ($< IC_{50}$ values) and exhibited a cell viability $\geq 70\%$ compared to untreated cells according to the previous MTT assay results. Aliquots of THP-1 cells were incubated with LPS (10 $\mu\text{g}/\text{mL}$) in the presence of various extracts/phytochemicals compared to the control (absence of extract/phytochemical) for 22 hours. The TNF- α /IL-12 levels were then measured using ELISA. At least three independent experiments were conducted, and all measurements were carried out in triplicate or quadruplicate.

3.3.1 The effect of LPS on TNF- α and IL-12 production from THP-1 Cells

Previous reports have demonstrated that lipopolysaccharide (LPS) significantly increased the output of pro-inflammatory cytokines, particularly TNF- α and IL-12. Preliminary experiments were carried out to evaluate the effect of various concentration of LPS on the TNF- α and IL-12 levels from THP-1 cells.

THP-1 cells were incubated with RPMI1640 medium in the absence of LPS (0) or with various concentration of LPS (0.1-50 $\mu\text{g}/\text{mL}$), following that, the supernatants were collected and the TNF- α and IL-12 levels were measured using Human TNF- α and Human IL-12 ELISA kits respectively as described previously in the Methods (section 2.8). As shown in Figures 3.58 and 3.59, the increase of LPS concentration leads to significant increase in both TNF- α and IL-12 production from THP-1 cells in concentration dependent manner. The maximal/ultimate TNF- α levels were in the range of 10 $\mu\text{g}/\text{mL}$ to 50 $\mu\text{g}/\text{mL}$. Based on this, the optimum concentration of LPS used in the subsequent experiments was determined to be 10 $\mu\text{g}/\text{mL}$.

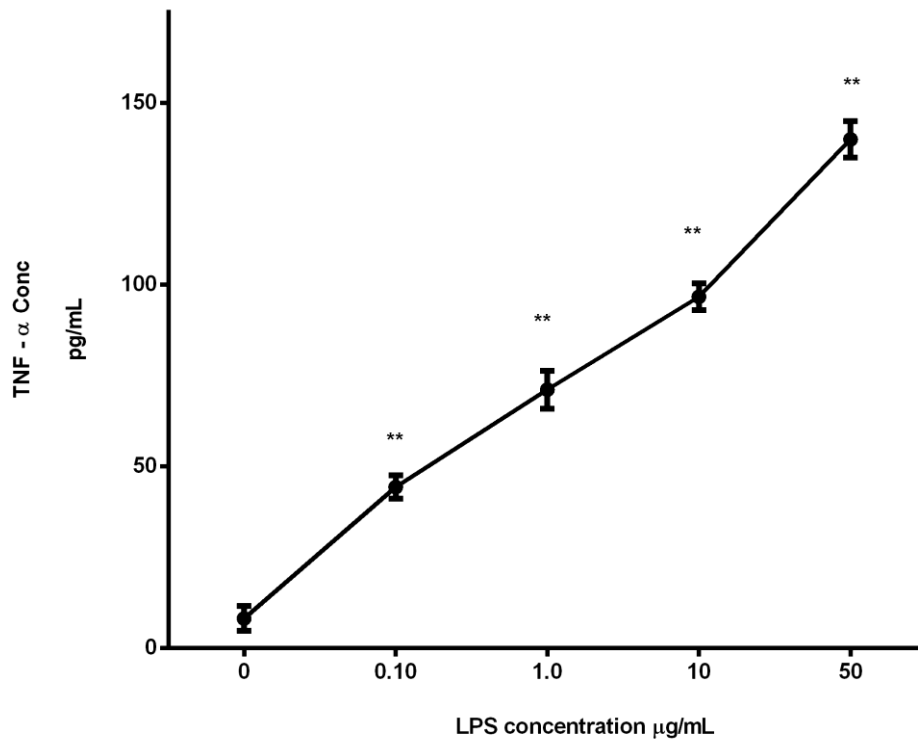


Figure 3.58 The effect of various concentrations of LPS on TNF- α production from THP-1 cells

THP-1 cells (1×10^6 cells/mL) were incubated with increasing concentrations of LPS (0.1-50 $\mu\text{g/mL}$) at 37°C with 5% CO_2 . After 22 hours, the supernatant was collected and TNF- α levels were measured by ELISA. Values are presented as the mean of $n = 3 \pm \text{s.d.}$ and are representative of two independent experiments. ** $P < 0.01$ vs. control (THP-1 cells incubated with RPMI-1640 medium alone; $0 \mu\text{g/mL}$ LPS).

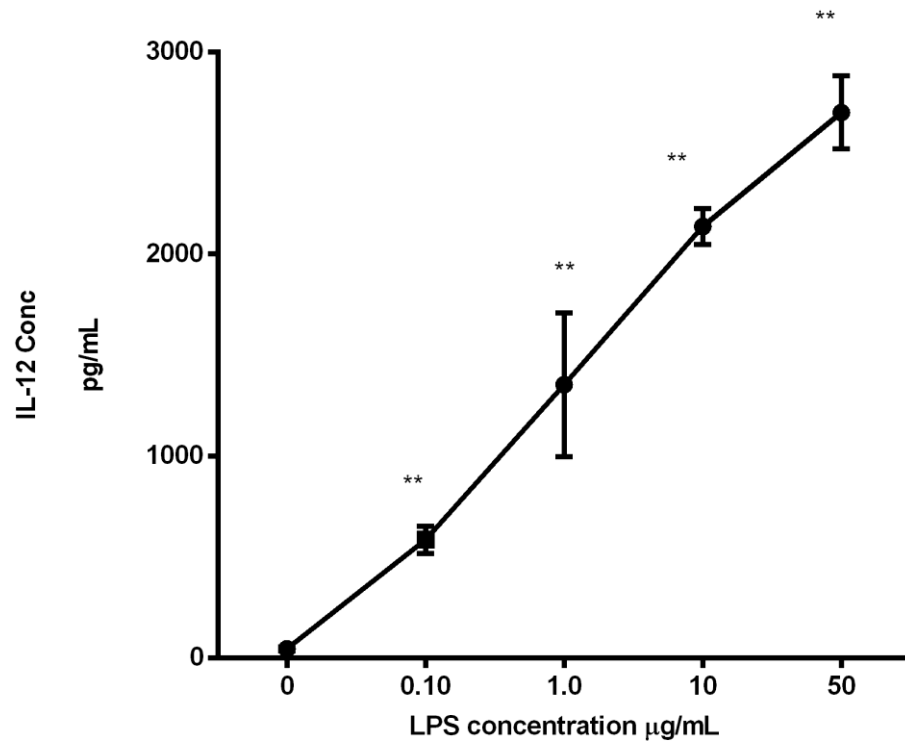


Figure 3.59 The effect of various concentrations of LPS on IL-12 production from THP-1 cells

THP-1 cells (1×10^6 cells/mL) were incubated with increasing concentrations of LPS (0.1-50 µg/mL) at 37°C with 5% CO₂. After 22 hours, the supernatant was collected, and IL-12 levels were measured by ELISA. Values are presented as the mean of $n = 3 \pm$ s.d. and are representative of two independent experiments. ** $P < 0.01$ vs. control (THP-1 cells incubated with RPMI-1640 medium alone; 0µg/mL LPS).

3.3.2 The effect of various crude extracts of *F. excelsior* leaves (370) on LPS-stimulated TNF- α production from THP-1 cells

The following experiment was carried out to investigate the potential immunomodulatory effects of various crude extracts from of *F. excelsior* leaves (370H-31.3, 370E-31.3, 370M-31.3 and 370M-62.5 $\mu\text{g}/\text{mL}$) on TNF- α production from LPS stimulated THP-1 cells.

As observed in Figure 3.60, THP-1 cells incubated with LPS alone in the absence of any *F. excelsior* extract (stimulated control) resulted in a significant increase in TNF- α levels when compared to the incubations without LPS (unstimulated control; RPMI-1640 medium alone). All *F. excelsior* extract incubations alone (without LPS) had no effect on TNF- α concentrations. However, when LPS was added to the culture, all the *F. excelsior* extracts at all tested concentrations significantly reduced TNF- α levels compared to the stimulated control (LPS alone). The most significant suppression in the TNF- α levels was observed with *n*-hexane extract of *F. excelsior* leaves (370H-31.3 $\mu\text{g}/\text{mL}$) which generated a 50% reduction in LPS-stimulated TNF- α production when compared with LPS alone. The TNF- α production was also reduced by EtOAc extract (370E-31.3 $\mu\text{g}/\text{mL}$) and the MeOH extract (370M-31.3 $\mu\text{g}/\text{mL}$) in a comparable way and resulted in a circa 30% decrease in LPS-stimulated TNF- α production. 370M-62.5 caused a significant reduction in TNF- α level. Vehicle stimulated control (0.125% DMSO with LPS) was carried and showed no statistical differences compared to the LPS-stimulated control (cells in RPMI without DMSO).

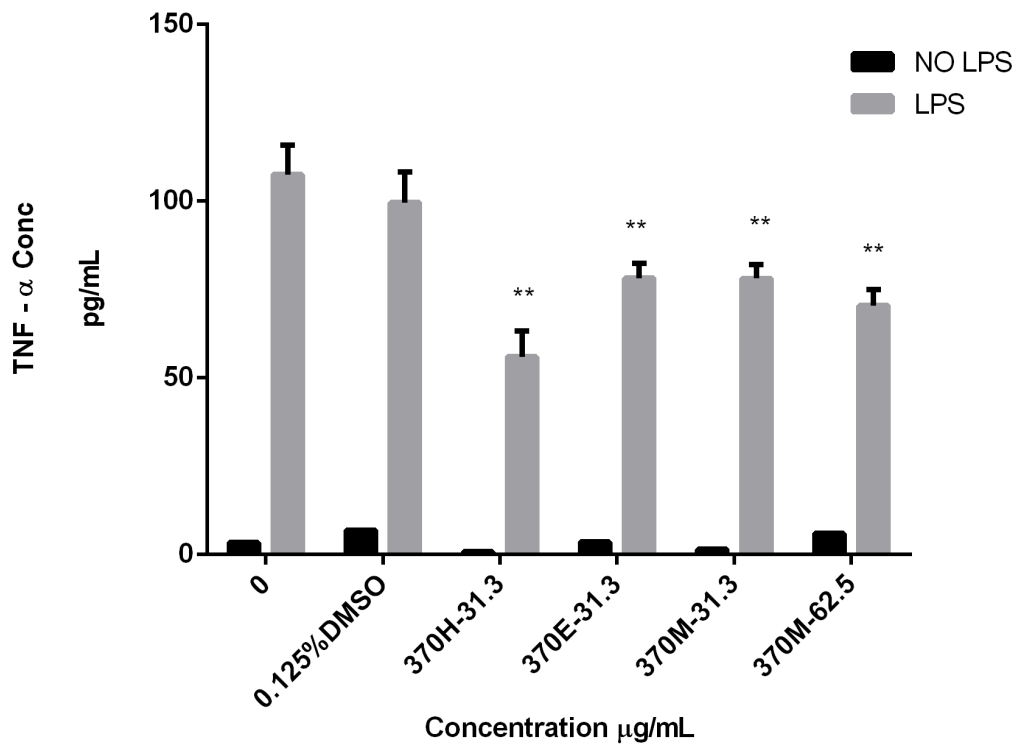


Figure 3.60 The effect of various crude extract of *F. excelsior* leaves (370) on LPS-stimulated TNF- α production from THP-1 cells

THP-1 cells (1×10^6 cells/mL) were incubated with different extract of *F. excelsior* leaves (0, 370H-31.3, 370E-31.3, 370M-31.3 & 370M-62.5 $\mu\text{g/mL}$) in the presence of LPS (10 $\mu\text{g/mL}$) (grey colour columns). Incubations without LPS are shown as black colour columns. Incubations were carried out for 22 hours at 37°C, 5%CO₂ and 100% humidity. After that, the supernatant was collected and TNF- α levels were measured by ELISA. Values are expressed as the means of $n = 3 \pm \text{s.d.}$. Asterisk shows level of significance (* $P < 0.05$, & ** $P < 0.01$) between the treated groups vs. stimulated control (THP-1 cells incubated with LPS alone) by ANOVA.

3.3.3 The effect of various crude extract of *S. arabica* aerial parts (390) on LPS-stimulated TNF- α production from THP-1 cells

The following experiments were carried out to investigate the potential immunomodulatory effects of various crude extracts from *S. arabica* aerial parts (390) on TNF- α production from LPS stimulated THP-1 cells.

As shown in Figure 3.61 and Figure 3.62, THP-1 cells incubated with LPS alone in the absence of any extract (stimulated control) showed a significant increase in TNF- α levels when compared to the incubation without LPS (unstimulated control; RPMI-1640 medium alone). All *S. arabica* extract incubations alone (without LPS) had no effect on TNF- α concentrations. However, when LPS was added to the culture, all the *S. arabica* extracts at all tested concentrations significantly reduced TNF- α levels compared to the stimulated control (LPS alone). Vehicle stimulated controls (0.125% & 0.5% DMSO with LPS) were carried out and showed no statistical differences compared to the LPS-stimulated control (cells in RPMI without DMSO).

Figure 3.61 demonstrated that TNF- α production was significantly suppressed by the *n*-hexane extract (390H-31.25 & 62.5 $\mu\text{g}/\text{mL}$) resulting in a concentration-dependent manner suppression in TNF- α levels and generated a reduction of approximately 50% and 80% respectively in TNF- α levels when compared with the stimulated control. Also, it was observed that the EtOAc extract (390E-31.25 $\mu\text{g}/\text{mL}$) resulted in a significant reduction in the TNF- α levels of circa 65% reduction in LPS-stimulated TNF- α production when compared with stimulated control.

As demonstrated in Figure 3.62, MeOH extract (390M-31.25 - 390M-250 $\mu\text{g}/\text{mL}$) suppressed TNF- α production from THP-1 cells stimulated with LPS resulting in a concentration-dependent decrease in TNF- α concentrations. MeOH extract in concentration of 31.25, 62.25, 125 and 250 $\mu\text{g}/\text{mL}$ generated a corresponding reduction of approximately 20, 30, 35 and 70% when compared to the stimulated control.

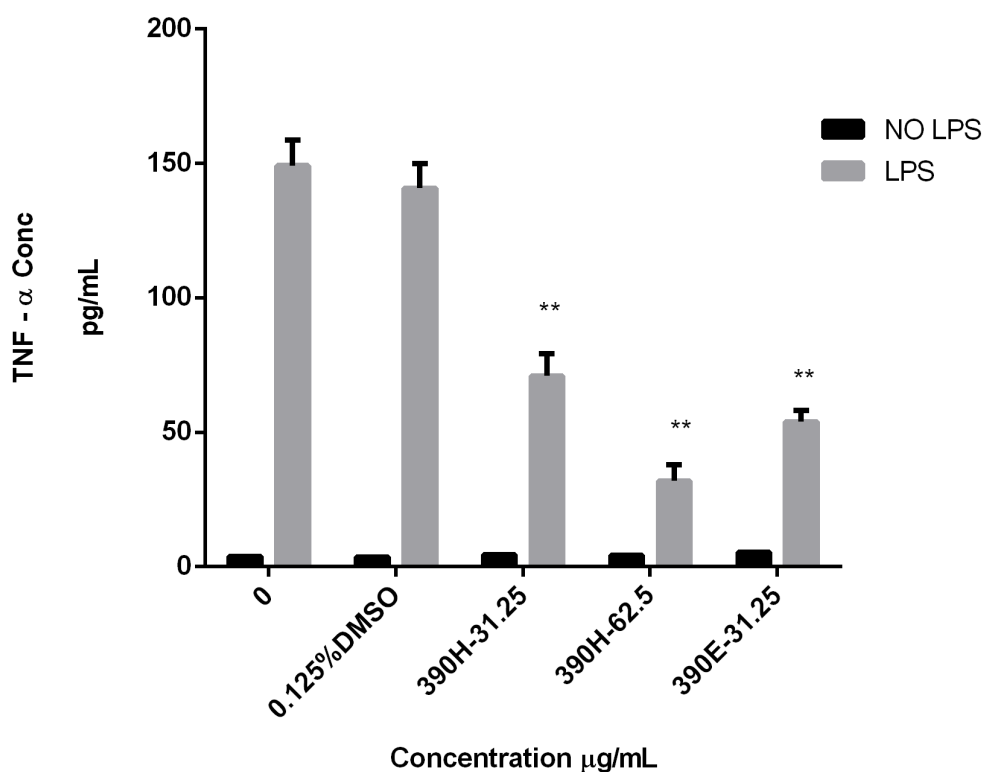


Figure 3.61 The effect of *n*-hexane and EtOAc crude extract of *S. arabica* aerial parts (390H & 390E) on LPS-stimulated TNF- α production from THP-1 cells

THP-1 cells (1×10^6 cells/mL) were incubated with different extract of *S. arabica* aerial parts (0, 390H-31.3, 390H-62.5 & 390E-31.3 $\mu\text{g/mL}$) in the presence of LPS (10 $\mu\text{g/mL}$) (grey colour columns). Incubations without LPS are shown as black colour columns. Incubations were carried out for 22 hours at 37°C, 5%CO₂ and 100% humidity. After that, the supernatant was collected and TNF- α levels were measured by ELISA. Values are expressed as the means of $n = 3 \pm \text{s.d.}$. Asterisk shows level of significance (** $P < 0.01$) between the treated groups vs. stimulated control (THP-1 cells incubated with LPS alone) by ANOVA.

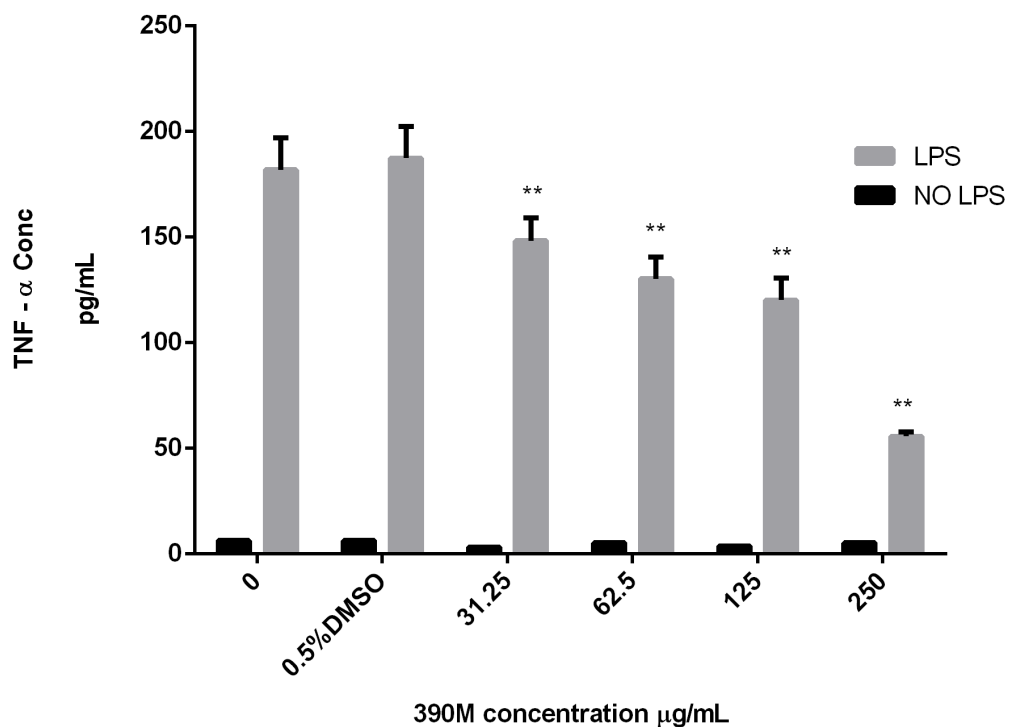


Figure 3.62 The effect of MeOH crude extract of *S. arabica* aerial parts (390M) on LPS-stimulated TNF- α production from THP-1 cells

THP-1 cells (1×10^6 cells/mL) were incubated with different concentration of MeOH extract of *S. arabica* aerial parts (0, 390M-31.3, 62.5, 125 and 250 $\mu\text{g/mL}$) in the presence of LPS (10 $\mu\text{g/mL}$) (grey colour columns). Incubations without LPS are shown as black colour columns. Incubations were carried out for 22 hours at 37°C , 5% CO_2 and 100% humidity. After that, the supernatant was collected and TNF- α levels were measured by ELISA. Values are expressed as the means of $n = 3 \pm \text{s.d.}$. Asterisk shows level of significance ($*P < 0.05$, & $**P < 0.01$) between the treated groups vs. stimulated control (THP-1 cells incubated with LPS alone) by ANOVA.

3.3.4 The effect of selected phytochemicals isolated from *F. excelsior* leaves (370E) on LPS-stimulated TNF- α production from THP-1 cells

The following experiments were carried out to investigate the potential immunomodulatory effects of phytochemicals (oleanolic acid (**OA**), ursolic acid (**UA**), Pinocebrin, and the mixture of phenylethanoid esters isolated from EtOAc extract of *F. excelsior* leaves (370E) on TNF- α production from LPS stimulated THP-1 cells.

As shown in Figure 3.63, THP-1 cells incubated with LPS in the absence of **UA/ Pinocebrin** (stimulated control, 0 μ M) produced a significant increase in TNF- α levels when compared to the incubation without LPS (unstimulated control, RPMI-1640 medium alone). **UA** and **Pinocebrin** incubations alone (without LPS) had no effect on TNF- α concentrations. **UA** significantly decreased TNF- α production from THP-1 cells stimulated with LPS by approximately 25% compared to the stimulated control (LPS alone). Also, it was observed that **Pinocebrin** had a potent significant decrease in TNF- α levels in THP-1 cells stimulated with LPS compared to the control in concentration dependent manner. **Pinocebrin** -61.0 and 122.0 μ M resulted in a reduction of approximately 40% and 50% respectively in TNF- α levels when compared with the stimulated control.

As shown in Figure 3.64, THP-1 cells incubated with LPS alone in the absence of **OA** (stimulated control) produced a significant increase in TNF- α levels when compared to the incubation without LPS (unstimulated control RPMI-1640 medium alone). **OA** incubations alone without LPS had no effect on TNF- α levels. However, **OA** suppressed LPS-stimulated TNF- α production from THP-1 cells resulting in a concentration dependent manner decrease in TNF- α levels which generated a reduction of approximately 10-15% compared to the stimulated control (LPS alone).

The mixture of phenylethanoid esters was assessed on its effect on TNF- α production from THP-1 cells. The results of this experiment illustrated in Figure 3.65; THP-1 cells incubated with LPS alone in the absence of mixture of phenylethanoid esters (stimulated control) produced a significant increase in TNF- α levels when compared to the incubation without LPS (unstimulated control). The mixture of phenylethanoid esters incubations alone without LPS had no effect on TNF- α levels. However, THP-1 cells incubated with LPS in the presence of the mixture of phenylethanoid esters at all the tested concentrations showed no statistically significant differences in TNF- α levels compared to the stimulated control were observed.

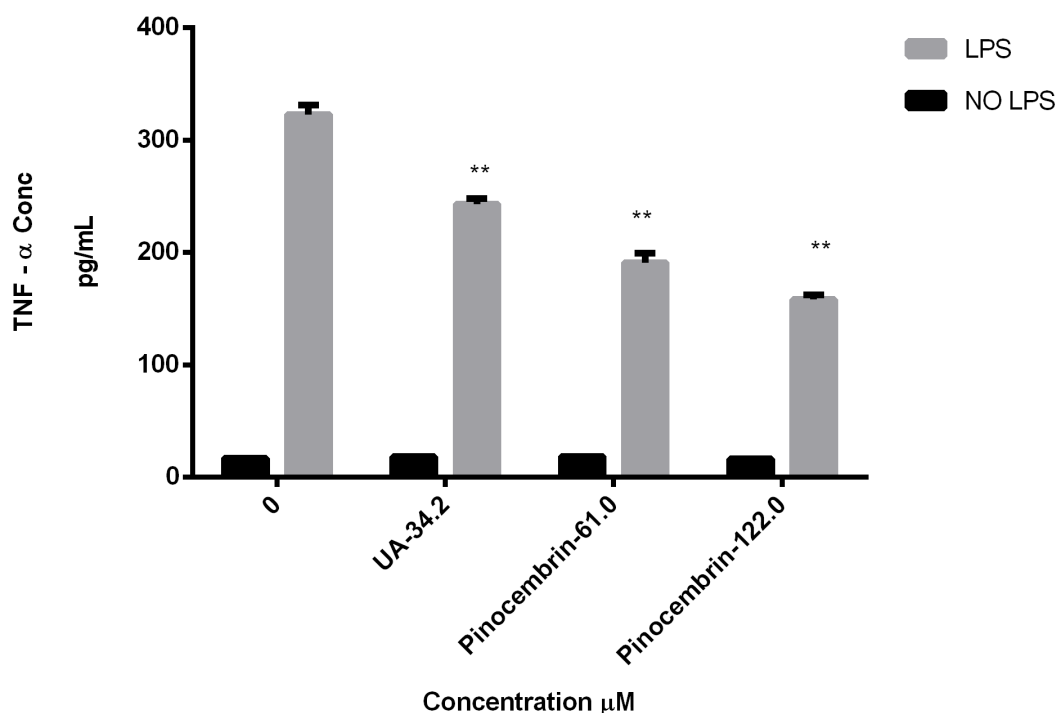


Figure 3.63 The effect of different concentrations of UA & Pinocembrin on LPS-stimulated TNF- α production from THP-1 cells

THP-1 cells (1×10^6 cells/mL) were incubated with different concentrations of UA & Pinocembrin (0, UA-34.2, Pinocembrin-61 & 122 μ M) in the presence of LPS (10 μ g/mL) (grey colour columns). Incubations without LPS are shown as black colour columns. Incubations were carried out for 22 hours at 37°C, 5%CO₂ and 100% humidity. After that, the supernatant was collected and TNF- α levels were measured by ELISA. Values are expressed as the means of $n = 3 \pm$ s.d. . Asterisk shows level of Significant **P < 0.01 between the treated groups vs. stimulated control (THP-1 cells incubated with LPS alone) by ANOVA.

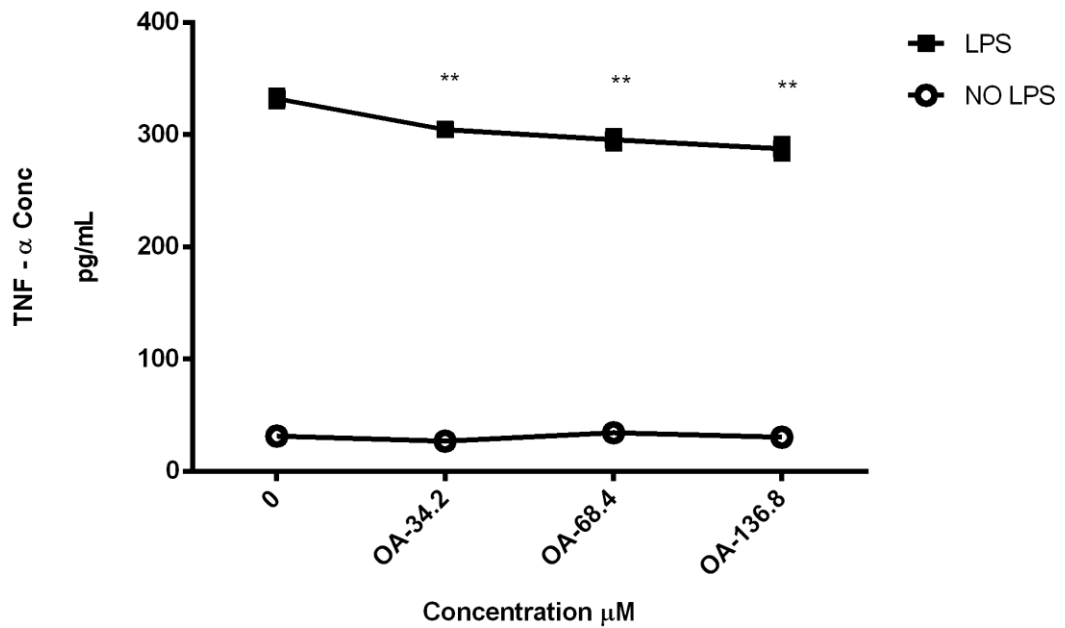


Figure 3.64 The effect of different concentrations of OA on LPS-stimulated TNF- α production from THP-1 cells

THP-1 cells (1×10^6 cells/mL) were incubated with different concentrations of OA (0-136.8 μ M) in the presence of LPS (10 μ g/mL) (square filled symbols). Incubations without LPS are shown as open circle. Incubations were carried out for 22 hours at 37°C, 5%CO₂ and 100% humidity. After that, the supernatant was collected and TNF- α levels were measured by ELISA. Values are expressed as the means of $n = 3 \pm$ s.d. . Asterisk shows level of significance (* $P < 0.05$, ** $P < 0.01$) between the treated groups vs. stimulated control (THP-1 cells incubated with LPS alone) by ANOVA.

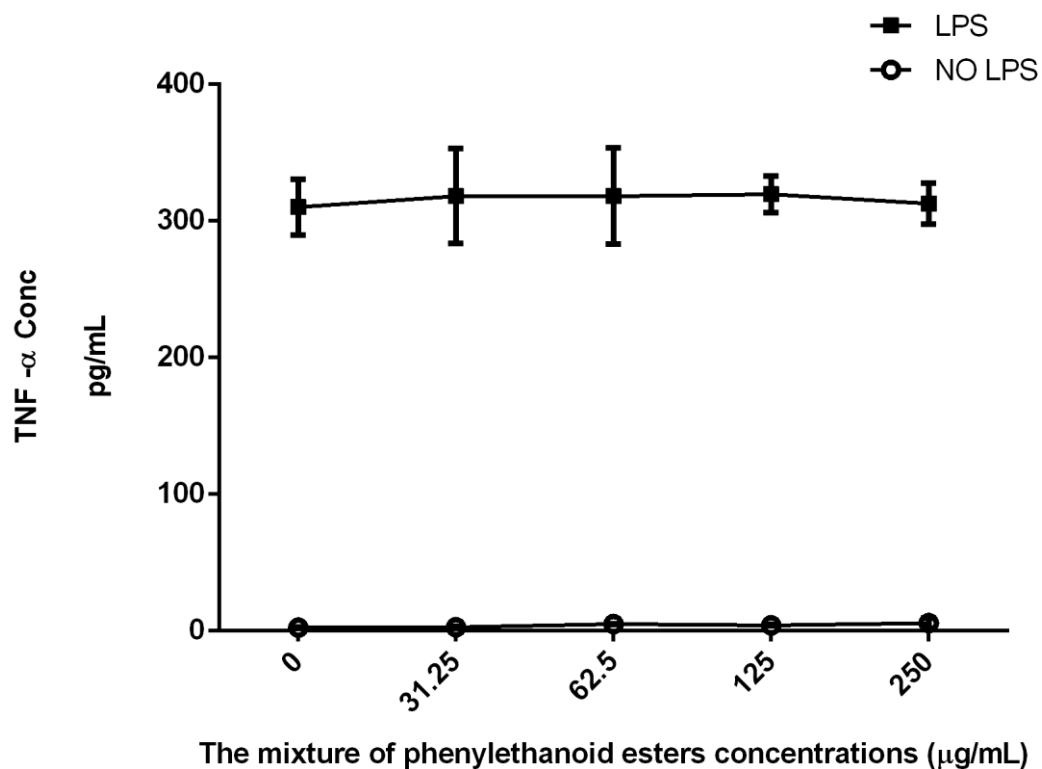


Figure 3.65 The effect of different concentrations of the mixture of phenylethanoid esters on LPS-stimulated TNF- α production from THP-1 cells

THP-1 cells (1×10^6 cells/mL) were incubated with different concentrations of the mixture of phenylethanoid esters (0- 250 $\mu\text{g/mL}$) in the presence of LPS (10 $\mu\text{g/mL}$) (square filled symbols). Incubations without LPS are shown as open circle. Incubations were carried out for 22 hours at 37°C, 5%CO₂ and 100% humidity. After that, the supernatant was collected and TNF- α levels were measured by ELISA. Values are expressed as the means of $n = 3 \pm \text{s.d.}$. *P < 0.05 vs. stimulated control (THP-1 cells incubated with LPS alone) by ANOVA.

3.3.5 The effect of selected phytochemicals isolated of *S. arabica* aerial parts (390E) on LPS-stimulated TNF- α production from THP-1 cells

The following experiments were carried out to investigate the potential immunomodulatory effects of three pheophytins (pheophytin a, 13² (R,S)-hydroxy pheophytin a, and pheophytin b) isolated from EtOAc extract of *S. arabica* aerial parts (390E) on TNF- α production from LPS stimulated THP-1 cells.

As shown in Figure 3.66 and Figure 3.67, THP-1 cells incubated with LPS in the absence of any pheophytin (stimulated control, 0 μ M) produced a significant increase in TNF- α levels when compared to the incubation without LPS (unstimulated control RPMI-1640 medium alone). Pheophytins incubations alone without LPS had no effect on TNF- α concentrations.

Pheophytin a (in concentration of 17.9 to 143.5 μ M) suppressed TNF- α production from LPS- stimulated THP-1 cells resulting in a concentration-dependent decrease in TNF- α levels as illustrated in Figure 3.66. **Pheophytin a** in concentration of 17.9, 35.9, 71.8 and 143.5 μ M generated a corresponding reduction of approximately 20, 27, 40 and 60% when compared to the stimulated control (LPS alone).

Figure 3.67 demonstrated that both of 13² (R,S)-hydroxy pheophytin a (**hydroxy pheo a** - 17.6 & 35.2 μ M) and pheophytin b (17.7 & 35.3 μ M) significantly suppressed TNF- α production from THP-1 cells stimulated with LPS compared to the stimulated control. **hydroxy pheo a** -17.6 & 35.2 μ M generated a reduction of approximately 60% and 75%, respectively in TNF- α levels when compared with the stimulated control (LPS alone), whereas **pheophytin b** -17.65 & 35.30 μ M generated a reduction of approximately 70% and 85% respectively in TNF- α levels when compared with the stimulated control (LPS alone).

For the lowest concentration (about 17.8 μ M) where the cell viability for all pheophytins is exceeded 90%, the most potent pheophytin in TNF- α suppression effect was observed with **pheophytin b**, then **hydroxy pheo a** followed by **pheophytin a**.

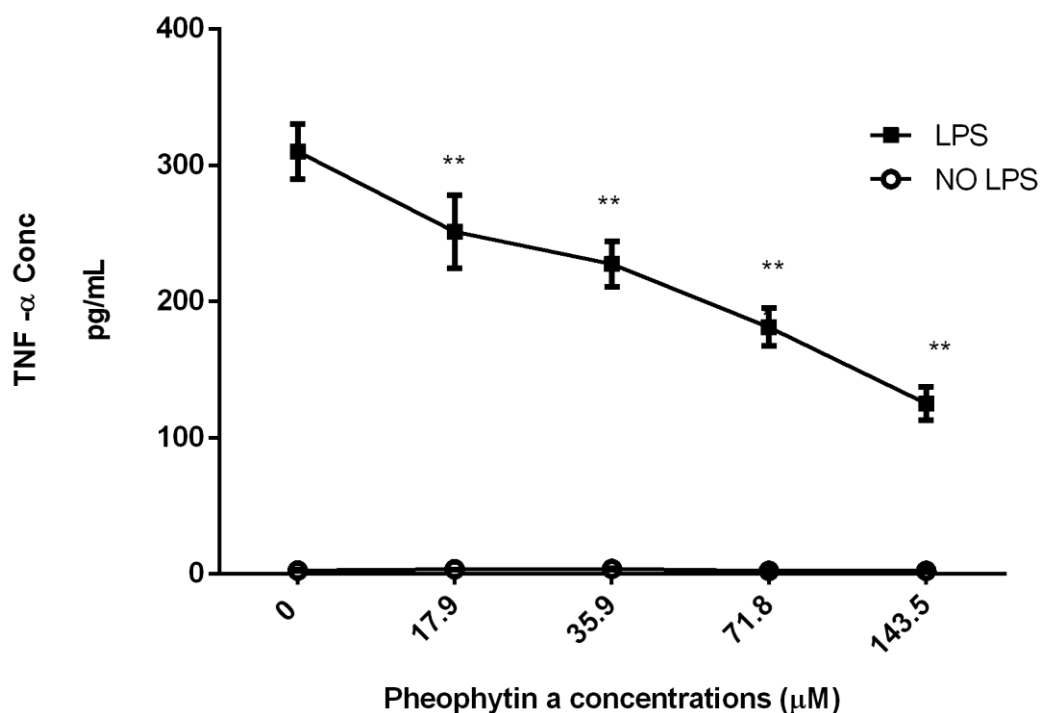


Figure 3.66 The effect of different concentrations of pheophytin a on LPS-stimulated TNF-α production from THP-1 cells

THP-1 cells (1×10^6 cells/mL) were incubated with different concentrations of pheophytin a (0- 143.5 μM) in the presence of LPS (10 μg/mL) (square filled symbols). Incubations without LPS are shown as open circle. Incubations were carried out for 22 hours at 37°C, 5%CO₂ and 100% humidity. After that, the supernatant was collected and TNF-α levels were measured by ELISA. Values are expressed as the means of $n = 3 \pm$ s.d. . Asterisk shows level of significance (*P < 0.05, & **P < 0.01) between the treated groups vs. stimulated control (THP-1 cells incubated with LPS alone,) by ANOVA.

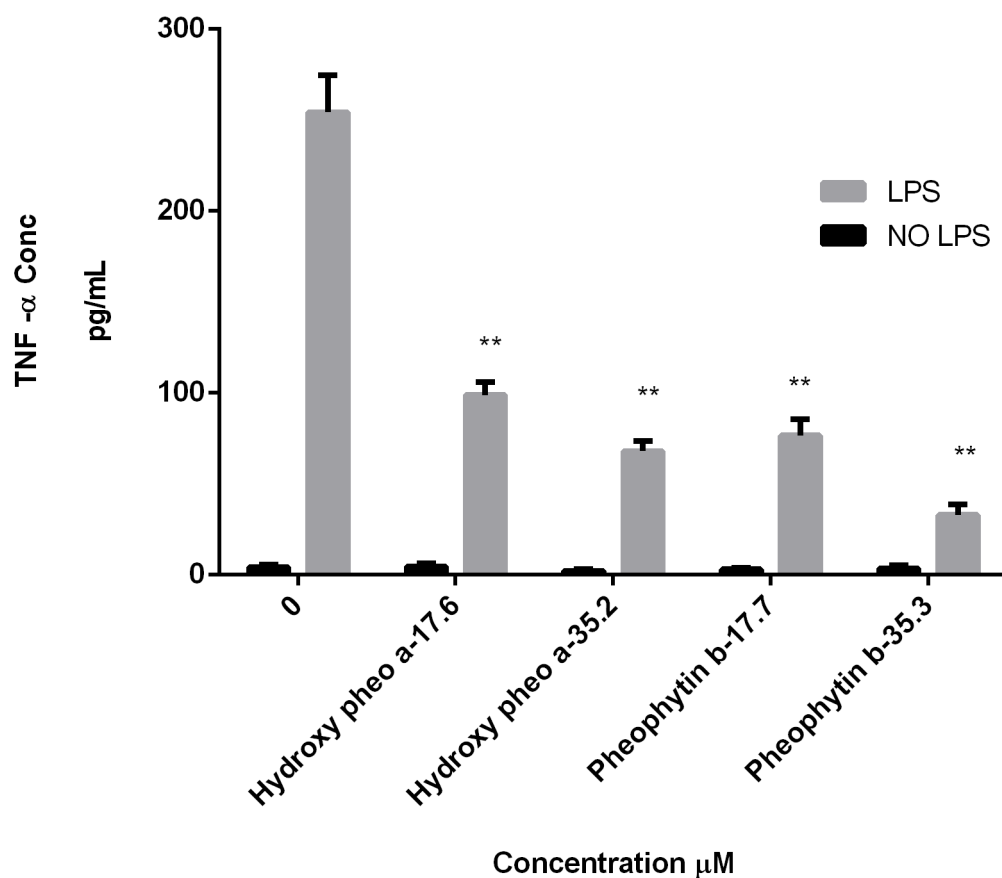


Figure 3.67 The effect of different concentrations of 13² (*R,S*)-hydroxy pheophytin a & pheophytin b on LPS-stimulated TNF- α production from THP-1 cells

THP-1 cells (1×10^6 cells/mL) were incubated with different concentrations of 13² (*R,S*)-hydroxy pheophytin a (hydroxy pheo a) & pheophytin b (0- 35.3 μ M) in the presence of LPS (10 μ g/mL) (grey colour columns). Incubations without LPS are shown as black colour columns. Incubations were carried out for 22 hours at 37°C, 5%CO₂ and 100% humidity. After that, the supernatant was collected and TNF- α levels were measured by ELISA. Values are expressed as the means of $n= 4 \pm$ s.d. . Asterisk shows level of Significant ** $P < 0.01$ between the treated groups vs. stimulated control (THP-1 cells incubated with LPS alone) by ANOVA.

3.3.6 The effect of various crude extract of *F. excelsior* leaves (370) on LPS-stimulated IL-12 production from THP-1 cells

Corresponding experiments were carried out to investigate the potential immunomodulatory effects of various crude extracts from *F. excelsior* leaves (370) on IL-12 production from LPS stimulated THP-1 cells.

As observed in the Figure 3.68, THP-1 cells incubated with LPS alone in the absence of any *F. excelsior* extracts (stimulated control) produced a significant increase in IL-12 levels when compared to the incubation without LPS (non-stimulated control; RPMI-1640 medium alone). All incubations with *F. excelsior* extract alone had no effect on IL-12 production. However, when LPS was added to the cultures, all the *F. excelsior* extracts at all tested concentrations significantly suppressed IL-12 levels compared to the stimulated control (LPS alone). The most significant suppression in the IL-12 levels was observed with *n*-hexane extract of *F. excelsior* leaves (370H-31.3 µg/mL) and EtOAc extract (370E-31.3 µg/mL) by with noticeable decrease close to 90% in IL-12 concentration when compared to the stimulated control. The IL-12 production was significantly reduced by the MeOH extract (370M-31.3 and 370M-62.5 µg/mL) in concentration dependent manner. 370M-31.3 generated a 60% reduction in IL-12 levels and 370M-62.5 caused around 85% reduction in IL-12 level when compared with stimulated control. Vehicle stimulated control (0.125% DMSO with LPS) was carried out and showed no statistical difference compared to the stimulated control (cells in RPMI without DMSO)

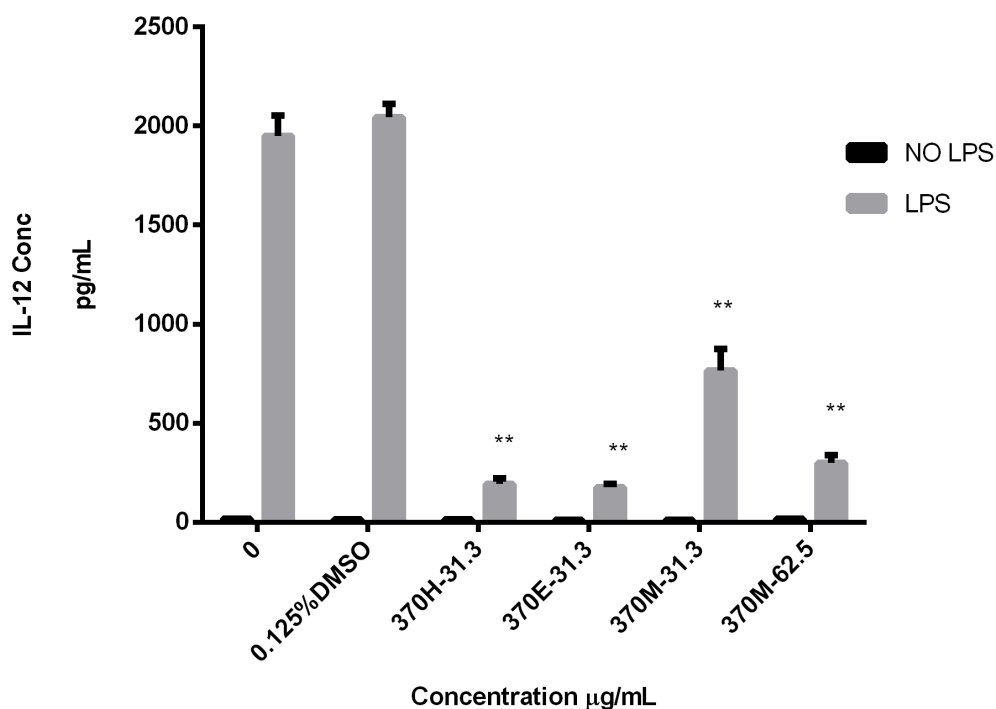


Figure 3.68 The effect of various crude extracts of *F. excelsior* leaves (370) on LPS-stimulated IL-12 production from THP-1 cells

THP-1 cells (1×10^6 cells/mL) were incubated with various extracts of *F. excelsior* leaves (0, 370H-31.3, 370E-31.3, 370M-31.3 & 370M-62.5 µg/mL) in the presence of LPS (10 µg/mL) (grey colour columns). Incubations without LPS are shown as black colour columns. Incubations were carried out for 22 hours at 37°C, 5%CO₂ and 100% humidity. After that, the supernatant was collected, and IL-12 levels were measured by ELISA. Values are expressed as the means of $n = 4 \pm$ s.d. Asterisk shows level of significance (**P < 0.01) between the treated groups vs. stimulated control (THP-1 cells incubated with LPS alone) by ANOVA.

3.3.7 The effect of various crude extracts of *S. arabica* aerial parts (390) on LPS-stimulated IL-12 production from THP-1 cells

Corresponding experiments were carried out to investigate the potential immunomodulatory effects of various crude extracts from *S. arabica* aerial parts (390M) on IL-12 production from LPS stimulated THP-1 cells.

As shown in Figure 3.69 and Figure 3.70, THP-1 cells incubated with LPS in the absence of any extract (stimulated control) produced a significant increase in IL-12 levels when compared to the incubation without LPS (unstimulated control RPMI-1640 medium alone). All *S. arabica* extract incubations alone (without LPS) had no effect on IL-12 production. However, when LPS was added to the culture, *S. arabica* extracts at all-tested concentrations suppressed IL-12 levels compared to the stimulated control (LPS alone). The most potent suppression effect was observed with 390H-62.5 and 390E-31.3 µg/mL with considerable decrease exceeded 85% in IL-12 levels when compared to the stimulated control (LPS alone).

Figure 3.69 demonstrated that IL-12 production was significantly reduced by the *n*-hexane extract (390H-31.3 & 62.5 µg/mL) resulting in a concentration-dependent manner and generated a considerable suppression of approximately 80% and 95% respectively in IL-12 levels when compared with the stimulated control. Also, it was observed that The EtOAc extract (390E-31.3 µg/mL) caused significant reduction in the IL-12 levels and generated a reduction of comparatively 85% in IL-12 concentration compared to stimulated control. Vehicle stimulated control (0.125% DMSO with LPS) was carried out and showed no statistical differences compared to the stimulated control (cells in RPMI without DMSO).

As demonstrated in Figure 3.70, MeOH extract of *S. arabica* (390M-31.25 - 390M-250 µg/mL) suppressed IL-12 production from THP-1 cells stimulated with LPS resulting in a concentration-dependent decrease in IL-12 levels. MeOH extract in concentration of 31.3, 62.25, 125 and 250 µg/mL generated a corresponding reduction of approximately 25, 40, 65 and 85% when compared to the stimulated control. Also, Vehicle stimulated control (cells in RPMI with 0.5% DMSO) was carried out and there no statistical differences compared to the stimulated control (cells in RPMI without DMSO) was observed.

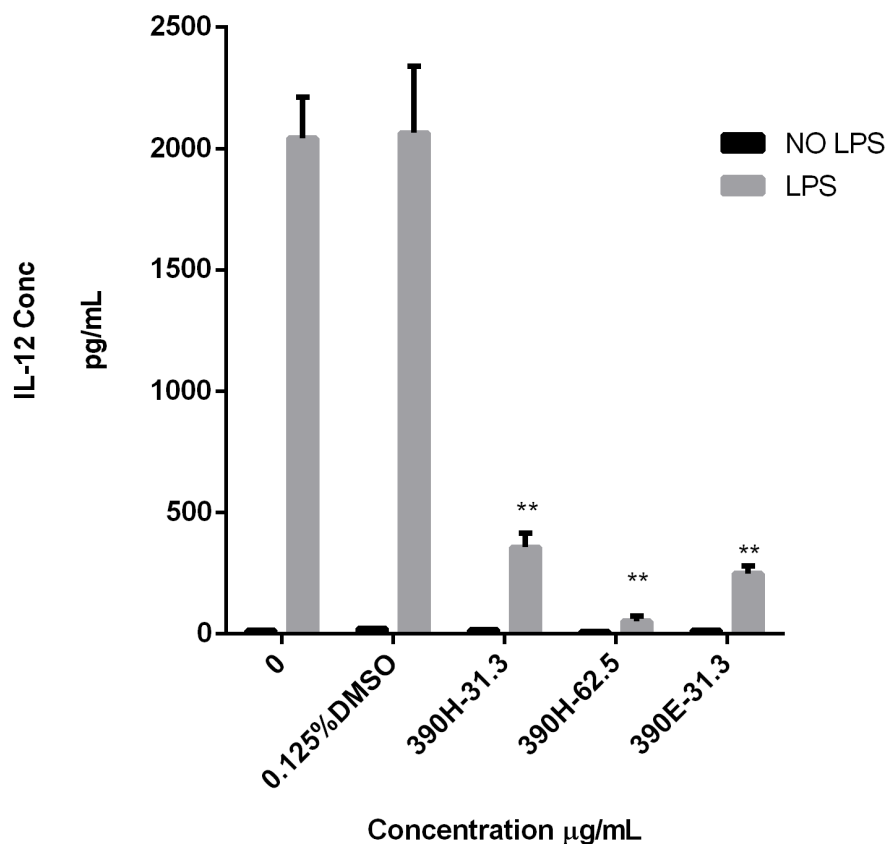


Figure 3.69 The effect of *n*-hexane and EtOAc crude extracts of *S. arabica* aerial parts (390H & 390E) on LPS-stimulated IL-12 production from THP-1 cells

THP-1 cells (1×10^6 cells/mL) were incubated with different extracts of *S. arabica* aerial parts (0, 390H-31.3, 390H-62.5 & 390E-31.3 µg/mL) in the presence of LPS (10 µg/mL) (grey colour columns). Incubations without LPS are shown as black colour columns. Incubations were carried out for 22 hours at 37°C, 5%CO₂ and 100% humidity. After that, the supernatant was collected, and IL-12 levels were measured by ELISA. Values are expressed as the means of $n = 3 \pm$ s.d. . Asterisk shows level of significance (**P < 0.01) between the treated groups vs. stimulated control (THP-1 cells incubated with LPS alone) by ANOVA.

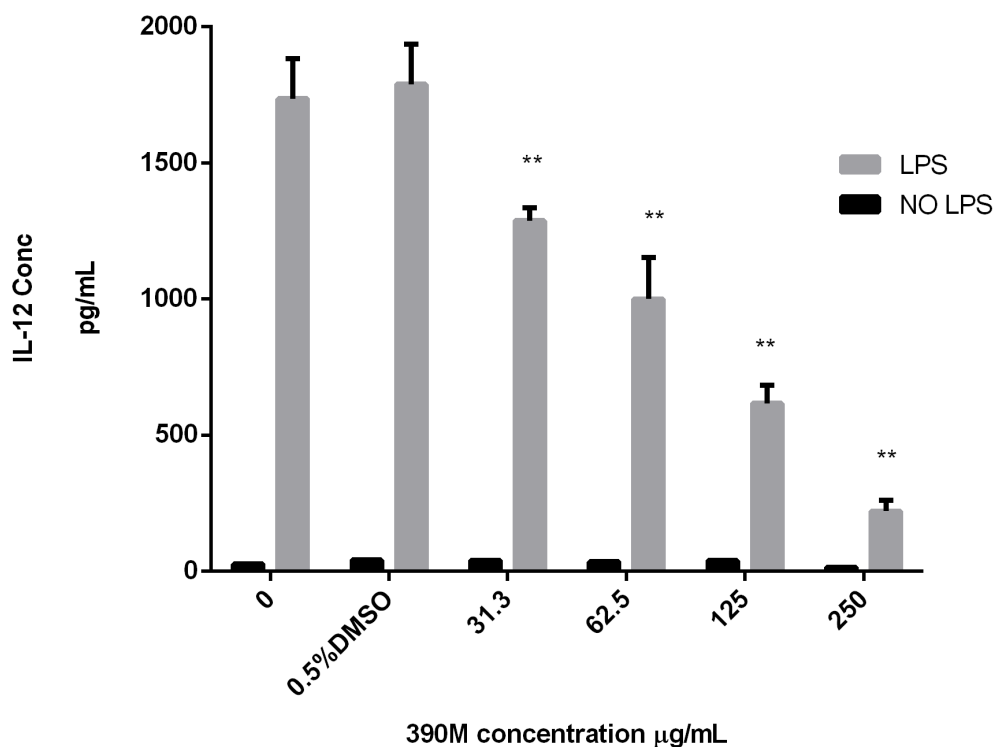


Figure 3.70 The effect of MeOH crude extract of *S. arabica* aerial parts (390M) on LPS-stimulated IL-12 production from THP-1 cells

THP-1 cells (1×10^6 cells/mL) were incubated with different concentration of MeOH extract of *S. arabica* aerial parts (0, 390M-31.3 – 390M-250 µg/mL) in the presence of LPS (10 µg/mL) (grey colour columns). Incubations without LPS are shown as black colour columns. Incubations were carried out for 22 hours at 37°C, 5%CO₂ and 100% humidity. After that, the supernatant was collected, and IL-12 levels were measured by ELISA. Values are expressed as the means of $n = 3 \pm$ s.d. Asterisk shows level of significance (** P<0.01) between the treated groups vs. stimulated control (THP-1 cells incubated with LPS alone) by ANOVA.

3.3.8 The effect of selected phytochemicals isolated from *F. excelsior* leaves (370E) on LPS-stimulated IL-12 production from THP-1 cells

Corresponding experiments were carried out to investigate the potential immunomodulatory effects of selected phytochemicals (**OA, UA, Pinocembrin, and the mixture of phenylethanoid esters**) isolated from EtOAc extract of *F. excelsior* leaves (370E) on IL-12 production of LPS stimulated THP-1 cells.

As shown in Figure 3.71, THP-1 cells incubated with LPS in the absence of **UA/Pinocembrin** (stimulated control) produced a significant increase in IL-12 levels when compared to the incubation without LPS (unstimulated control RPMI-1640 medium alone). **UA** and **Pinocembrin** incubations alone (without LPS) had no effect on IL-12 concentrations. **UA-34.2**, with this concentration significantly decreased the production of IL-12 in THP-1 cells stimulated with LPS by approximately 50% compared to the stimulated control. Also, it was observed that **Pinocembrin** had a potent significant decrease in IL-12 levels in THP-1 cells stimulated with LPS compared to the stimulated control in concentration dependent manner. Pinocembrin-61.0 and 122.0 μM generated a reduction of 75% and 90% respectively in IL-12 levels when compared with the stimulated control (LPS alone).

As demonstrated in Figure 3.72. THP-1 cells incubated with LPS in the absence of **OA** (stimulated control) produced a significant increase in IL-12 levels when compared to incubation without LPS (unstimulated control RPMI-1640 medium alone). OA incubations alone (without LPS) had no effect on IL-12 levels. However, **OA** was able to decrease LPS-stimulated IL-12 production from THP-1 cells in a concentration dependent manner resulting in a decrease in IL-12 levels, **OA** in concentration of 34.2, 68.4 and 136.9 μM generated a corresponding reduction of approximately 20, 40, and 70% when compared to the control (LPS alone).

The mixture of phenylethanoid esters was assessed on its effect on IL-12 production from THP-1 cells. The results of this experiment illustrated in Figure 3.73; THP-1 cells incubated with LPS alone (stimulated control) produced a significant increase in IL-12 levels when compared to the incubation without LPS (unstimulated control). The mixture of phenylethanoid esters incubations alone (without LPS) had no effect on IL-12 levels. However, THP-1 cells incubated with LPS in the presence of the mixture of phenylethanoid esters showed no statistically significant differences in IL-12 levels compared to the stimulated control at all the tested concentrations.

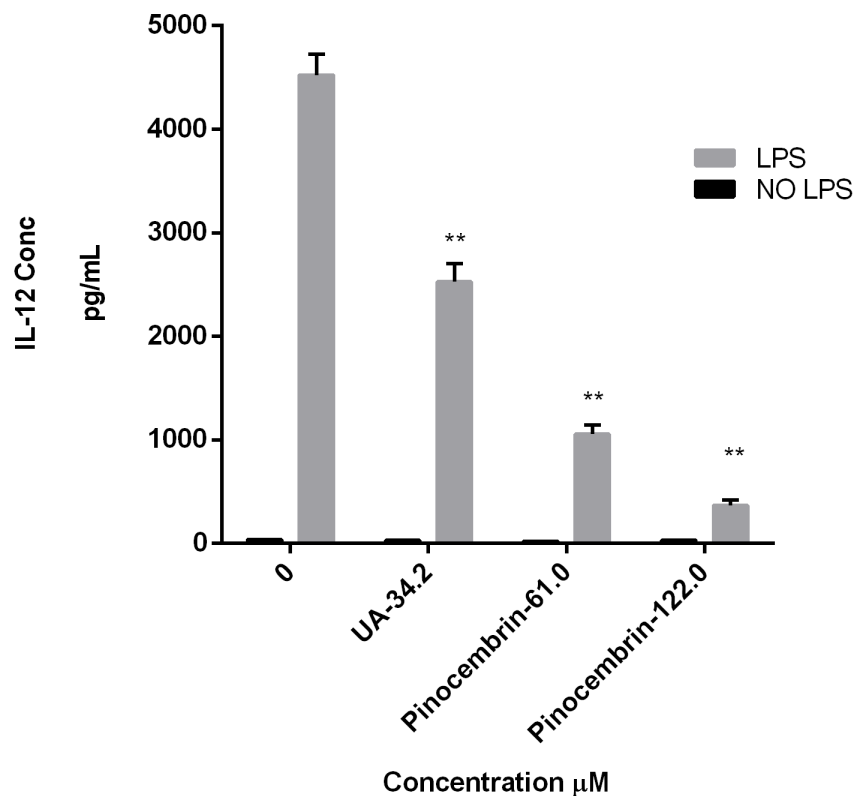


Figure 3.71 The effect of different concentrations of UA & Pinocembrin on LPS-stimulated IL-12 production from THP-1

THP-1 cells (1×10^6 cells/mL) were incubated with different concentrations of UA & Pinocembrin (0, UA-34.2, Pinocembrin-61 & 122 μ M) in the presence of LPS (10 μ g/mL) (grey colour columns). Incubations without LPS are shown as black colour columns. Incubations were carried out for 22 hours at 37°C, 5%CO₂ and 100% humidity. After that, the supernatant was collected, and IL-12 levels were measured by ELISA. Values are expressed as the means of $n = 3 \pm$ s.d. Asterisk shows level of Significant $**P < 0.01$ between the treated groups vs. stimulated control (THP-1 cells incubated with LPS alone) by ANOVA.

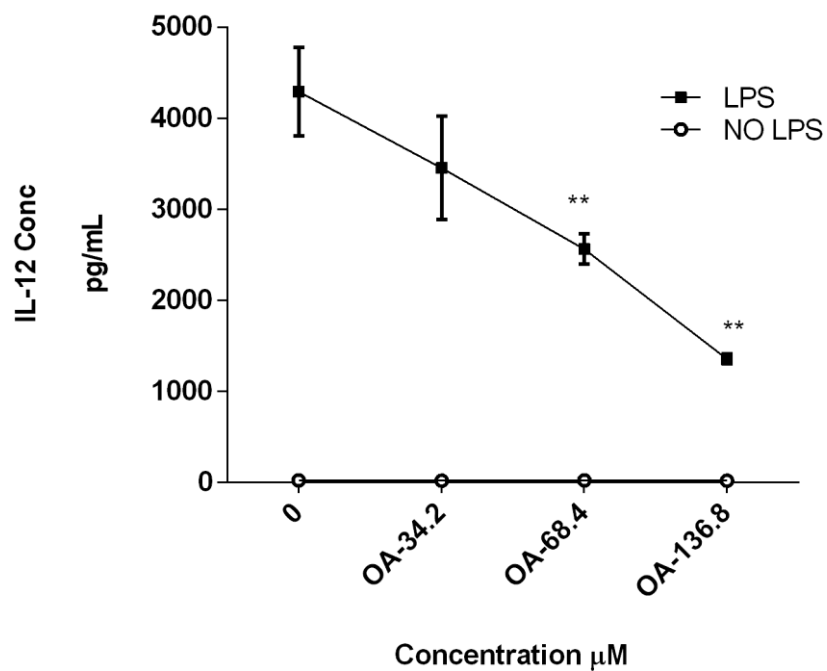


Figure 3.72 The effect of different concentrations of OA on LPS-stimulated IL-12 production from THP-1 cells

THP-1 cells (1×10^6 cells/mL) were incubated with different concentrations of OA (0-136.8 μ M) in the presence of LPS (10 μ g/mL) (square filled symbols). Incubations without LPS are shown as open circle. Incubations were carried out for 22 hours at 37°C, 5%CO₂ and 100% humidity. After that, the supernatant was collected, and IL-12 levels were measured by ELISA. Values are expressed as the means of $n = 3 \pm$ s.d. . Asterisk shows level of significance (* $P < 0.05$, & ** $P \leq 0.01$) between the treated groups vs. stimulated control (THP-1 cells incubated with LPS alone) by ANOVA.

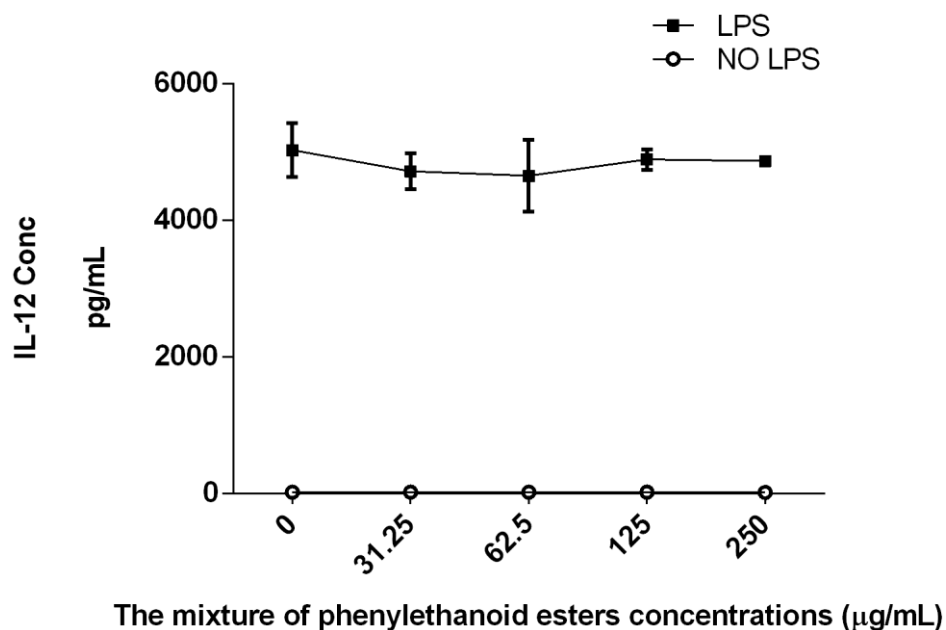


Figure 3.73 The effect of different concentrations of the mixture of phenylethanoid esters on LPS-stimulated IL-12 production from THP-1 cells

THP-1 cells (1×10^6 cells/mL) were incubated with different concentrations of the mixture of phenylethanoid esters (0- 250 µg/mL) in the presence of LPS (10 µg/mL) (square filled symbols). Incubations without LPS are shown as open circle. Incubations were carried out for 22 hours at 37°C, 5%CO₂ and 100% humidity. After that, the supernatant was collected, and IL-12 levels were measured by ELISA. Values are expressed as the means of $n = 3 \pm$ s.d . *P < 0.05 vs. stimulated control (THP-1 cells incubated with LPS alone) by ANOVA.

3.3.9 The effect of selected phytochemicals isolated from *S. arabica* aerial parts (390E) on LPS-stimulated IL-12 production from THP-1 cells

Corresponding experiments were carried out to investigate the potential immunomodulatory effects of pheophytins isolated from *S. arabica* aerial parts (390E) on IL-12 production of LPS stimulated THP-1 cells.

As shown in Figure 3.74 and Figure 3.74, THP-1 cells incubated with LPS alone in the absence of pheophytin (stimulated control) produced a significant increase in IL-12 levels when compared to the incubation without LPS (unstimulated control; RPMI-1640 medium alone). Pheophytins incubations alone (without LPS) had no effect on IL-12 concentrations.

Pheophytin a (at concentrations of 17.9 to 143.5 μM) decreased IL-12 production from LPS- stimulated THP-1 cells resulting in a concentration-dependent decrease in IL-12 levels as illustrated in Figure 3.74. **Pheophytin a** in concentration of 17.9, 35.9, 71.8 and 143.5 μM generated a corresponding reduction of approximately 30, 50, 60 and 75% when compared to the stimulated control (LPS alone).

Figure 3.75 demonstrated that both of 13² (*R,S*)-hydroxy pheophytin a (**hydroxy pheo a**-17.6 & 35.2 μM) and **pheophytin b** (17.7 & 35.3 μM) significantly suppressed IL-12 production from THP-1 cells stimulated with LPS compared to the stimulated control and their effects was more potent than **pheophytin a**. **Hydroxy pheo a**-17.6 & 35.2 μM generated a reduction of approximately 60% and 85% respectively in IL-12 levels when compared with the stimulated control, whereas **pheophytin b** -17.7 & 35.30 μM generated a reduction of approximately 70% and 90% respectively in IL-12 levels when compared with the stimulated control (LPS alone).

At the lowest concentration of (\approx 17.8 μM) where the cell viability for all pheophytins is very close to 90%, the most potent pheophytin in IL-12 suppression effect was observed with **pheophytin b**, then **hydroxy pheo a** followed by **pheophytin a**.

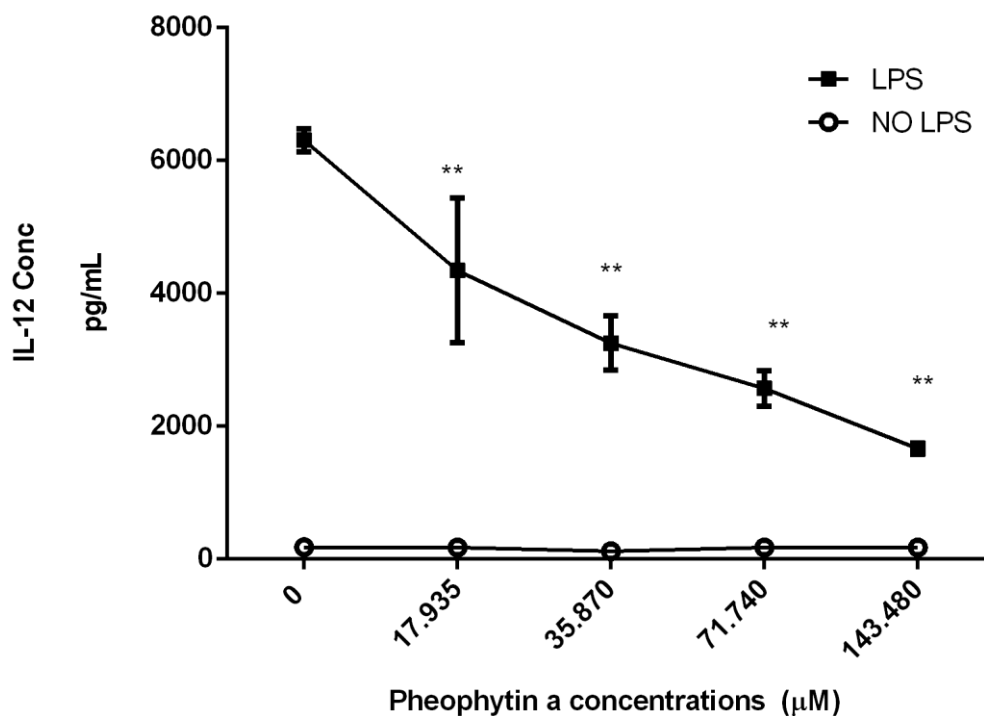


Figure 3.74: The effect of different concentrations of pheophytin a on LPS-stimulated IL-12 production from THP-1 cells

THP-1 cells (1×10^6 cells/mL) were incubated with different concentrations of pheophytin a (0- 143.5 µM) in the presence of LPS (10 µg/mL) (square filled symbols). Incubations without LPS are shown as open circle. Incubations were carried out for 22 hours at 37°C, 5%CO₂ and 100% humidity. After that, the supernatant was collected, and IL-12 levels were measured by ELISA. Values are expressed as the means of $n = 3 \pm$ s.d. Asterisk shows level of significance (** $P < 0.01$) between the treated groups vs. stimulated control (THP-1 cells incubated with LPS alone) by ANOVA.

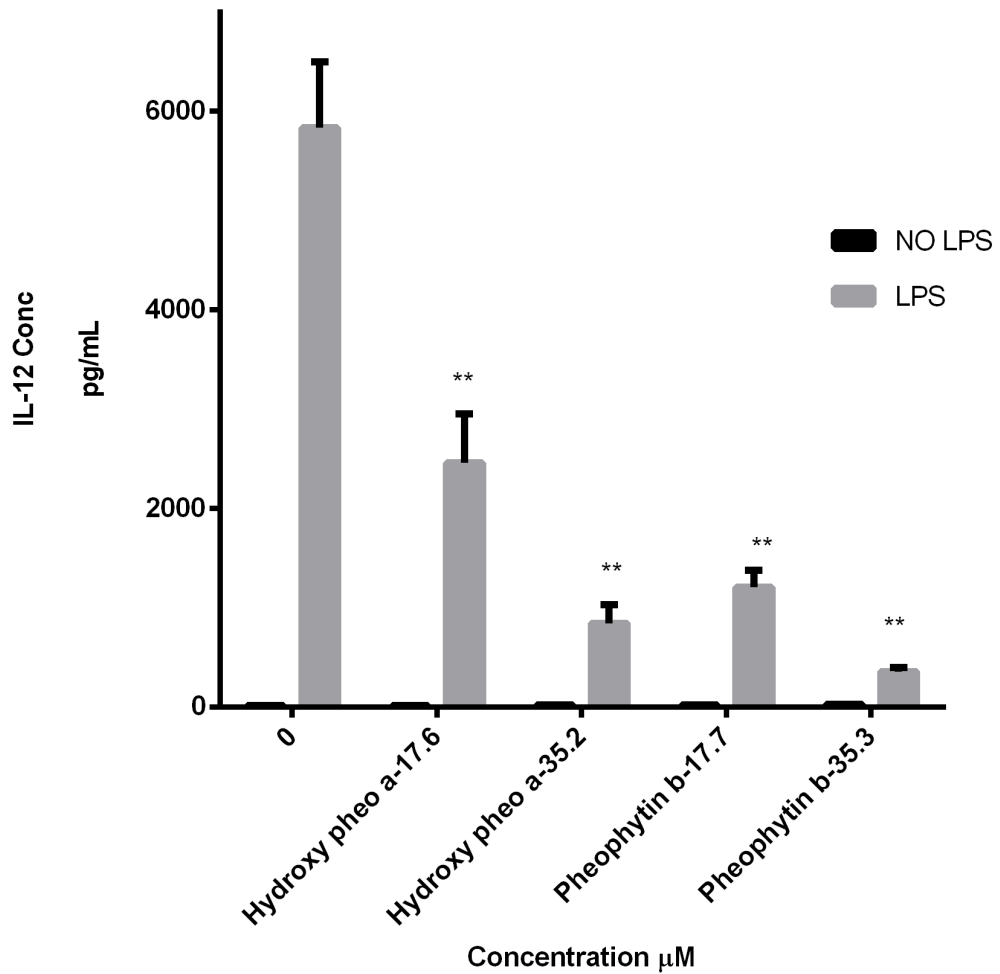


Figure 3.75 The effect of different concentrations of 13² (R,S)-hydroxy pheophytin a & pheophytin b on LPS-stimulated IL-12 production from THP-1 cells

THP-1 cells (1×10^6 cells/mL) were incubated with different concentrations of 13² (R,S) hydroxy pheophytin a (hydroxy pheo a) & pheophytin b (0- 35.30 μM) in the presence of LPS (10 μg/mL) (grey colour columns). Incubations without LPS are shown as black colour columns. Incubations were carried out for 22 hours at 37°C, 5%CO₂ and 100% humidity. After that, the supernatant was collected, and IL-12 levels were measured by ELISA. Values are expressed as the means of $n = 3 \pm$ s.d. Asterisk shows level of Significant **P < 0.01 between the treated groups vs. stimulated control (THP-1 cells incubated with LPS alone) by ANOVA.

3.4 Modulation of cell viability by various crude extracts and purified phytochemicals.

Many studies mentioned that THP-1 cells (Ayesh *et al.*, 2014; Kartini *et al.*, 2017; Garcia *et al.*, 2013) and K562 cells (Chueahongthong *et al.*, 2011; Fatemeh and Piri, 2011; Tayarani-Najaran *et al.*, 2017) are used generally to monitor cell viability/ cytotoxicity as well as safety assessment of plant extract and their phytochemicals.

Prior to the investigation of immunomodulatory effects, it was necessary to evaluate the effect of the six crude extracts and selected isolated phytochemicals from the two plants on cell viability. The potential effect on the cell viability was assessed against two cell lines, Human myeloid leukemic cell line K562 cells and/or human monocyte Leukaemia cell line THP-1 cells using colorimetric MTT assay to ensure that the effects observed on the production of pro-inflammatory cytokines (TNF- α and IL-12) were not influenced by alterations in cell viability. Based on the MTT assay results, all concentrations that were below IC₅₀ values and /or maintained cell viability of more than 75% when compared to untreated cell were considered safe and applied for subsequent experiments.

3.4.1 Modulation of cell viability by crude extracts of *F. excelsior* leaves (370) and their purified phytochemicals

In the preliminary evaluation of the three crude extracts on the cell viability. The *n*-hexane (370H) and EtOAc (370E) extracts of *F. excelsior* leaves (Figures 3.47 and 3.48) reduced the cell viability of both cell lines (THP-1 and K562) in a concentration dependent manner resulting in IC₅₀ values in the range of 45-85 and 40-60 μ g/mL for K562 and THP-1 cells respectively. These results might be explained because that these crude extracts contain certain phytochemicals like squalene and pentacyclic triterpenes like oleanonic acid (OA) and its isomer ursolic acid (UA) in (370H), and pinocembrin and pentacyclic triterpenes (OA and UA) in (370E) which in turn exhibited a significant reduction of the cell viability as illustrated in section 3.2.4. The methanolic extract (370M) (Figure 3.48), reduced the number of THP-1 viable cells at higher concentration. However, the same extract did not affect number of viable K562 cell even at higher concentrations

THP-1 cells incubated with **UA** and **OA** for 24 hours and assessed for their effect on the cell viability using MTT assay showed that **UA** (Figure 3.52) at concentration of

68 μM (31.3 $\mu\text{g/mL}$) significantly decreased the number of viable THP-1 cells compared to the control, whereas **OA** (Figure 3.53) significantly decreased the number of viable THP-1 cells compared to the control at higher concentration (200 μM / 90 $\mu\text{g/mL}$). The results obtained for UA but not for OA was in good agreement with the observation of Kartini *et al* (2017) whose finding showed THP-1 macrophages incubated with **UA** and **OA** (isolated from *Plantago major seeds*) for 48 hours and assessed for their cell viability using an MTT assay showed both **UA** and **OA** significantly reduced the number of viable cells at concentrations ≥ 30 $\mu\text{g/mL}$.

Pinocembrin demonstrated significant decrease in the number of viable THP-1 cells compared to the control at concentrations > 122 μM with IC_{50} value of 178.6 μM (Figure 3.51). Previous study found that pinocembrin, isolated from methanolic extract of *Polygonum glabrum*, showed potent antiproliferative effect with IC_{50} in the range of 1.88–11.00 $\mu\text{g/mL}$ against a panel of five human cancer lines: monocytic leukaemia cell line THP-1, lung A549 adenocarcinoma, pancreatic PANC-1 adenocarcinoma, cervix adenocarcinoma HeLa and MCF7 human mammary gland/breast adenocarcinoma epithelial cell line using MTT assay (Said *et al.*, 2015).

The mixture of phenylethanoid esters (Figure 3.54) , in all the tested concentrations, showed no effect on the number of viable THP-1 cell compared to that of untreated cells. This result was in good consensus with a previous report by Luo *et al* which showed that these esters did not demonstrate any cytotoxicity against breast, lung and nervous human cancer cell lines (Luo *et al.*, 2006)

3.4.2 Modulation of cell viability by crude extracts of *S. arabica* aerial parts (390) and their purified phytochemicals

The effect of *n*-hexane (390H) and EtOAc (390E) extracts of *S. arabica* aerial leaves on the viability of THP-1 cells (Figure 3.50) was greater than their effect on the cell viability of K562 (Figure 3.49). The results showed that increase in the concentrations of these extracts lead to the decrease the number of viable THP-1 and K562 cell. It could be assumed that the differences in the effects of *n*-hexane (390H) and EtOAc (390E) extracts of *S. arabica* on the cell viability of the two cell lines (THP-1 & K562) most likely be an indicator of the potential selectivity to different cancer cells.

These results might be justified as that these crude extracts, when subjected to further purification led to identified phytochemicals like β - sitosterol, stigmasterol from (390H) and pheophytins from (390E) which in turn exhibited a significant decrease of the number of viable cells as observed in section 3.2.5.

The methanolic extract (390M), did not affect the viability of both THP-1 or K562 cells at all examined concentrations. These results correlate well with those reported for other *Stachys spp.*, including a study by Venditti *et al.* (2017) who reported that the ethanolic extract of *S. affinis* did not show any cytotoxic effect on treated cells, even at the highest concentrations (1.0 mg/mL) against three human cell lines; SHSY-5Y (bone marrow neuroblastoma), Caco-2 (colorectal adenocarcinoma) and K562 (chronic myelogenous leukaemia) human cell lines using MTT assay. Similar results have been found using methanolic extract of *S. parviflora* collected from Iran against three cell lines, human ovarian carcinoma (A2780), human colon carcinoma (HCT) and mouse melanoma cell line (B16F10) and with the methanolic extract of *S. lavandifolia* collected from Iran against five cell lines human lung adenocarcinoma (A549), human breast adenocarcinoma (MCF7), bovine kidney cells (MDBK), hepatocellular carcinoma (HepG2) and human colon carcinoma (HT-29) where no cytotoxic effects using MTT assay were observed for both species (Shakeri *et al.*, 2019; Behzad *et al.*, 2014).

The isolated phytochemicals were also assessed for their effect on THP-1 cell viability, the results obtained from MTT assay indicate that THP-1 cell incubated with the three pheophytins (pheophytin a , 13² (*R,S*)-hydroxy pheophytin a and pheophytin b which isolated from EtOAc extract of *S. arabica*) for 24 hours were found to reduce

cell viability in concentration dependent manner (Figures 3.55- 3.57). Both of 13² (*R,S*)-hydroxy pheophytin a (Hydroxy pheo a) and pheophytin b exhibited a comparable potent effect ($IC_{50} \approx 41 \mu\text{M}/ 37 \mu\text{g/mL}$) on the number of viable cell, and more than pheophytin a which had a IC_{50} value of 186.4 μM . One possible explanation accounts for such difference in activity might be the presence of hydroxyl group at position C-13 (for hydroxy pheo a), and an aldehyde group at position C-7 (for pheophytin b) when compared to the structure of pheophytin a (Figure 3.21).

Searching the literature showed no previous study addressing the effects of pheophytins on THP-1 cell viability. However, 13² (*R,S*)-hydroxy pheophytin a and pheophytin b have an *in vitro* cytostatic activity (at conc. of 33 $\mu\text{g/mL}$) against hepatoma tissue culture (HTC) cells using Trypan Blue dye (Nakatani *et al.*, 1981) and this correlate well with the results obtained in this study.

Previous studies have reported the cytotoxicity of pheophytins against other cell lines. Pheophytin a was previously tested on the A549 (Human lung adenocarcinoma) cell line with IC_{50} value of $22.9 \pm 5.8 \mu\text{M}$, and on non-cancerous vero cell line with an IC_{50} of $183.6 \pm 1.9 \mu\text{M}$ (Shailaja *et al.*, 2019). Other study reported pheophytin a has cytotoxicity for RAW264.7 cells at 25 μM using the Alamar Blue assay (Lin *et al.*, 2014) . However, In another study pheophytin at a concentration of 30 μM did not influence the viability of RAW 264.7 murine macrophage cells (Islam *et al.*, 2013). Regarding pheophytin b, a concentration of 50 μM showed no significant change in the cell viability of RW264.7 murine macrophage cells, and human CD14+ monocyte-derived macrophages using an Alamar Blue Cell viability kit (Lin *et al.*, 2017). Inconsistency of some of these results might be explained due to different cell model used and the cell viability assay used (Jakštys *et al.*, 2015) .

3.5 Suppression of pro-inflammatory cytokines (TNF- α and IL-12) production from LPS- stimulated THP-1 cells

In this study, the immunomodulatory activity of *F. excelsior* (370), *S. arabica* (390) extracts and some of their purified phytochemicals was investigated on human THP-1 cells. The effects of the six crude plant extracts and selected isolated phytochemicals/ pure compounds (OA, UA, pinocembrin, the mixture of phenylethanoid esters, pheophytin a, 13² (*R,S*)-hydroxy pheophytin a and pheophytin b) on TNF- α and IL-12 production from LPS-stimulated THP-1 cells are illustrated in section 3.3. Collectively, all the six crude extracts and the selected purified phytochemicals/ pure compounds (except the phenylethanoid esters) were significantly suppressed the production of the pro-inflammatory cytokines (TNF- α and IL-12) in comparison to the stimulated control. Whereas the mixture of phenylethanoid esters did not appear to significantly influence the production of both cytokines examined.

3.5.1. Suppression of pro-inflammatory cytokines (TNF- α and IL-12) production from LPS- stimulated THP-1 cells by crude extracts of *F. excelsior* leaves (370) and their purified phytochemicals.

All the *F. excelsior* extracts in all tested concentrations (370H-31.3, 370E-31.3, 370M-31.3 and 370M-62.5 $\mu\text{g/mL}$) significantly reduced TNF- α and IL-12 production from LPS-stimulated THP-1 cells when compared to the stimulated control (Figure 3.60 & 3.68).

The *n*-hexane (370H) and ethyl acetate (370E) extracts of *F. excelsior* leaves exhibited a significant decrease effect on the TNF- α and IL-12 levels which could be linked to the fact that these crude extracts contain certain phytochemicals including squalene, OA and its isomer UA from (370H). While flavonoids like pinocembrin and pentacyclic triterpenes (OA and UA) presented in the (370E) which in turn exhibited a significant suppression of the examined cytokines TNF- α and IL-12 as illustrated in section 3.3.4 and 3.3.8

The scientific literature has very limited information about biological activities of *F. excelsior* leaves. No previous study addressed the effect of various crude extracts (with different polarity) of *F. excelsior* leaves on IL-12 production. Regarding the effect

of various crude extracts of *F. excelsior* leaves (with different polarity) on TNF-production, our findings namely for the polar MeOH extract (370M), appear to be well supported by a recent report illustrated that the aqueous infusion of *F. excelsior* leaves (from 5 different samples) at a concentration of 100 µg/mL was able to significantly suppress the release of reactive oxygen species (ROS), cytokines (TNF- α and IL-1 β), and chemokines (IL-8 and monocyte chemoattractant protein1 (MCP-1)) production on LPS-stimulated neutrophils. The research team suggested that these findings may provide a scientific support for the traditional use of *F. excelsior* leaves for minor articular pain and to increase the amount of urine for flushing minor urinary complaints, which in turn connected to the inflammatory state (Kiss *et al.*, 2020).

Phytodolor® (STW 1) is a standardized herbal combination including alcoholic extracts of *Populus tremula* (Poplar), *Fraxinus excelsior* (Ash) and *Solidago virgaurea* (goldenrod) in a ratio of (60:20:20). A recent study provide evidence for therapeutic use of Phytodolor® (STW 1) as phytopharmaceutical in inflammation and pain related disorders. The result of study showed the effect of Phytodolor® (STW 1) and its components on LPS-activated human monocytes by inhibiting TNF- α through the suppression of NF- κ B activation (Bonaterra *et al.*, 2019).

It is noteworthy to mention another interesting biological activity of *F. excelsior* seeds including diuretic, and hypoglycaemic activities (Eddouks and Maghrani, 2004; Eddouks *et al.*, 2005; Visen *et al.*, 2009; Bai *et al.*, 2010; López-Carreras *et al.*, 2013; 2014; Monto *et al.*, 2014). A clinical study conducted by Zulet *et al.* (2014) demonstrated administration of Glucevia® (natural extract of *F. excelsior* seed/fruit) in combination with moderate low caloric diet may be beneficial in metabolic disturbances associated with impaired glucose tolerance, insulin resistance, obesity, and inflammatory status in older adults.

According to a previous reports of other *Fraxinus* species, significant anti-inflammatory effects against carrageenan-induced acute inflammation in mice of the methanol extract of *F. micrantha* leaves (Kumar and Kashyap, 2015) and ethanol extract of *F. ornus* stem bark (Stefanova *et al.*, 1995) have been reported. Methanol extract of *F. xanthoxyloides* leaves showed anti-inflammatory effects by decreasing the inflammatory mediator levels of; IL-6, TNF- α , and PGE2 in rats and (TNF- α induced production of NF- κ B and NO) using *in vitro* models (Younis *et al.*, 2016a).

Fraxinus rhynchophylla extract showed an antidepressant effect on chronic stress-induced depression mouse model *via* electric foot shock, and the concentration of serum serotonin and cortisol returned to normal levels. The results illustrated that it exerts these effects by modulating the secretion of proinflammatory cytokines (including TNF- α and IL-12) and by controlling inflammation and neurogenesis-related signalling (Kim *et al.*, 2018). In this context, the suppression of TNF- α and IL-12 production by *F. excelsior* extracts could serve as an option for long term treatment against stress induced depression.

Overall, in the present study, we reported for the first time that *F. excelsior* leaves (370) showed a suppression effect on the production of TNF- α and IL-12 which in turn may contribute to the anti-inflammatory effect associated with their traditional uses.

According to the present study, pentacyclic triterpenes (OA and UA) suppressed TNF- α production in LPS-stimulated THP-1 cells when compared with stimulated control after 24 hours of treatment using ELISA (Figure 3.63 & 3.64). Our results showed that at concentration of 34 μ M (16 μ g/mL), UA exhibited a potent suppression effect more than OA for both examined cytokines. These findings are in good agreement with the observations of Kartini *et al* (2017) whose findings showed that OA and UA (isolated from *Plantago major* seeds) at concentration of 10 μ g/mL (21 μ M) were able to suppress the production of TNF- α , IL-1 β , and IFN- γ in LPS- stimulated THP-1 macrophages after 48 hours of incubation using MILLIPLEX[®] MAP kit. The same study showed that UA was more potent than OA in TNF- α suppression.

In the present study, when pentacyclic triterpenes (OA and UA) were assessed for their effect on IL-12 production in LPS-stimulated THP-1 cells, the results demonstrated that OA & UA had a significant suppressive effect (Figure 3.71 & 3.72). Also, at concentration of 34 μ M, UA exhibited a potent suppression effect more than OA. These findings of OA and UA are in line with previous reports conducted by using another *in vitro* model. OA, isolated from *Glossogyne tenuifolia*, inhibit the release of inflammatory mediators (NO, PGE2, TNF- α , IL-1 β , IL-6 and IL-12), as well as NF- κ B activation in LPS- stimulated RAW264.7 cells (Wu *et al.*, 2004). Also, OA isolated from *Kandelia candel* showed the inhibitory effects on IL-12 production in LPS-stimulated bone marrow-derived dendritic cells (BMDCs) (Le *et al.*, 2015). In case of

UA, the same result reported in LPS stimulated peritoneal macrophages (Chun *et al.*, 2014)

The anti-inflammatory activities of pentacyclic triterpenes (OA and its isomer UA) were intensively investigated previously. A previous report by Lee *et al* (2013) assessed the effect of OA on the inflammatory reaction triggered by LPS using *in vitro* and *in vivo models*. The study showed that OA suppressed the production of TNF- α and activation of NF- κ B responses in human umbilical vein endothelial cells (HUVECs) induced by LPS.

UA has been reported to show anti-inflammatory and immunomodulatory activities using *in vitro and in vivo* (Checker *et al.*, 2012). The results also suggest that UA inhibit LPS-stimulated inflammatory responses. UA, which was isolated from an ethanol extract of *Cornus officinalis* seed, inhibited the expression of pro-inflammatory cytokines (TNF- α and IL-1 β) and inflammatory enzymes (COX-2 and iNOS) in LPS stimulated peritoneal macrophages. UA inhibited activation of NF- κ B (via suppression of phosphorylation of interleukin 1 receptor-associated kinase (IRAK1), TAK1, IKK β , and I κ B α and by suppression translocation of NF- κ B into nuclei) in LPS- stimulated peritoneal macrophages. Also, UA inhibited activation of MAPKs (via suppression of phosphorylation of ERK, JNK and p38) in LPS-stimulated peritoneal macrophages. The same research team investigated the effect of oral administration of UA on TNBS-stimulated colitis in mice and found that UA inhibited the expression of pro-inflammatory cytokines (TNF- α and IL-1 β) and activation of transcription factor NF- κ B, and based on this, they suggested UA ameliorate colitis by regulating NF- κ B and MAPK signalling pathways and via the inhibition of LPS binding to TLR4 (Jang *et al.*, 2014). A study by Chen and co-authors (2013) showed that UA can attenuate LPS-induced acute lung injury and improve the survival time in a mouse model by increasing the survival rate of LPS + UA group (96 h) from 10 to 30% compared with the LPS group, they reported administration of UA inhibited TNF- α , IL-6, IL-1 β , and NO and attenuated NF- κ B in the lungs (Chen *et al.*, 2013). Another reported showed UA significantly decreased LPS-induced inflammatory cytokine (TNF- α , IL-6 and IL-1 β) release via TLR4/MyD88 pathway in RAW264.7 cells (Zhao *et al.*, 2019). UA has significant potential as an anti-inflammatory and neural repair drug for multiple sclerosis (MS) , particularly at the chronic-progressive stage. UA decrease TNF- α , CNS inflammation and promotes myelin repair (Zhang *et al.*, 2020).

A report by Zerin *et al* (2016) investigated the effect of UA on TNF- α , IL-1 β and IL-6 release from three cell lines: RAW 264.7 murine macrophages, A549 alveolar epithelial cells stimulated by Mtb H37Rv and in concanavalin A (Con A)-stimulated rat splenocytes, the three cytokines were upregulated by different stimuli in the different three cells. The results showed that UA significantly suppressed levels of the three cytokines in all stimulated cells and the researchers in same study, suggested that UA may be used as an adjunct host-directed therapy for TB, in addition to the standard TB regimen, to improve treatment efficacy and outcome due to their anti-inflammatory potential (Zerin *et al.*, 2016).

Taking everything into consideration, OA and UA are phytochemicals of interest in many aspects related to TB treatment. As adjunct therapy to standard TB drugs: i) suppressing overproduction of TNF- α and IL-12 which could be a strategy for targeting inflammation suppression in TB patients, ii) by showing synergistic effects against Mtb, iii) minimising their hepatotoxicity. In addition to have direct anti-Mtb activity against susceptible and resistance strains of Mtb.

Pinocembrin among the phytochemicals investigated in this study, the results obtained demonstrated that with pinocembrin significantly suppressed the production of TNF- α and IL-12 from LPS stimulated THP-1 cells (Figure 3.63 & 3.71). These results correlate well with those found in the literature using different *in vitro* cell model and/or *in vivo* model.

According to a previous reports, pinocembrin represents a novel candidate for the modulation of inflammatory responses. Pinocembrin reduced the production of TNF- α , IL-1 β , and IL-6 in a dose dependent manner in LPS-stimulated RAW 264.7 macrophages cells and significantly protect mice against endotoxin- induced acute lung injury. The results suggest that the suppression effects of pinocembrin on the production of inflammatory cytokines could occur through blocking of the p38/MAPK and NF- κ B signalling pathways in murine macrophage and endotoxin-induced acute lung injury model (Soromou *et al.*, 2012). Another study by Zhou *et al* (2015) showed that pinocembrin inhibited production of inflammatory mediators (TNF- α , IL-1 β , NO and PGE₂ production) from LPS-stimulated BV2 microglial cells by suppressing PI3K/Akt/NF- κ B signalling pathway.

An interesting study on the inflammatory effect of pinocembrin on fish immune cells was conducted by Giri *et al* (2016), the results showed that pinocembrin decreased LPS-induced TNF- α , IL-1 β , NO and PGE₂ in *Labeo rohita* macrophages via downregulation of the NF- κ B signalling pathway (Giri *et al.*, 2016).

Searching the literature showed a study of the potential immunomodulatory effect of pinocembrin on the production of IL-12. In this study, *in vivo* model of Atlantic salmon was used to examine the effect of pinocembrin and alpinone on the cytokines production by fish kidney. Pinocembrin decreased the expression of TNF- α , IL-1, and IL-12 in treated fish compared to untreated fish. Whereas alpinone increased the expression of same cytokines (Valenzuela *et al.*, 2018).

Pinocembrin has been shown to suppress inflammatory response by inhibiting NF- κ B pathway (Liu *et al.*, 2014a; Gu *et al.*, 2017) and/or by blocking TLR4 activation (Lan *et al.*, 2017).

Since there was no sufficient data has been reported previously regarding the effect of pinocembrin on the IL-12 release using *in vitro* model. The preliminary findings in present study regarding the immunomodulatory effects of pinocembrin on LPS-stimulated cytokines (TNF- α and IL-12) from THP-1 cells are first to be reported. Taking everything into account, pinocembrin suppresses production of TNF- α and IL-12 could be via inhibiting TLR4 activation and/or NF- κ B pathway.

Regarding the mixture of phenylethanoid esters, the obtained results demonstrated no effects were observed on the production of both cytokines (TNF- α and IL-12) from LPS-stimulated THP-1 cells compared to the stimulated control in all the tested concentrations (Figure 3.65 & 3.73). Given that the immunomodulatory effects of the mixture of phenylethanoid esters on LPS-stimulated cytokines (TNF- α and IL-12) from THP-1 cells have not been reported, these preliminary findings are first to be reported.

3.5.2 Suppression of pro-inflammatory cytokines (TNF- α and IL-12) production from LPS- stimulated THP-1 cells by crude extracts of *S. arabica* aerial parts (390) and their purified phytochemicals.

According to the results illustrated in section 3.3.3 and 3.3.7, *S. arabica* (390) extracts in all-tested concentrations suppressed TNF- α and IL-12 levels in LPS- stimulated THP-1 cells when compared to the stimulated control (Figures 3.61-3.62 and 3.69-3.70).

Although *S. arabica* (390) is an unexplored species and there is no report regarding any biological activity, there are many studies on the biological activities of other *Stachys* species in the literature centred on ethnomedicinal uses. Previous pharmacological studies have suggested that extracts or phytochemicals isolated from *Stachys* species showed anti-inflammatory and reducing pain (antinociception) activities. The aqueous extracts from the aerial parts of Hungarian *Stachys* species (*S. officinalis*, *S. alpina*, *S. germanica* and *S. recta*) showed a potent activity against carrageenan-induced inflammation in animal models (Háznagy-Radnai *et al.*, 2012). *S. lavandulifolia* essential oil significantly reduced the production of pro-inflammatory cytokines like TNF- α and IL-1 β in a carrageenan-induced pleurisy assay (an anti-inflammation assay) and the results of this study justify the use of this species in traditional medicine as an analgesic and anti-inflammatory (Barreto *et al.*, 2016). Dichloromethane extracts of *S. circinate* aerial parts exerted immunomodulatory and anti-arthritic effects in mouse models, it decreased the inflammation (the oedema size) when compared to the control group (Slimani *et al.*, 2020). Moreover, the anti-inflammatory and antinociception effects of (acetone, methanolic and hydroalcoholic crude extracts of several *Stachys* species (*S. chrysantha*, *S. candida*, *S. inflata*, *S. beckeana*, *S. anisochila*, *S. plumosa*, *S. alpine*, *S. athorecalyx*, and *S. byzanthina*) have been established in an animal models (Skaltsa *et al.*, 2000; Maleki *et al.*, 2001; Kukić *et al.*, 2007; Rezazadeh *et al.*, 2009; Khanavi *et al.*, 2005). An interesting study by Ramazanov *et al* (2017) demonstrated the effective wound healing activity of ecdysteroid-containing preparation from the extract of *S. hissarica* on rats, and the wound healing effect of *S. hissarica* extract exceeded methyl uracil, a stimulator of regenerative processes, especially in case of alloxan induced diabetic animals. This study in turn may validate the traditional use as wound healing.

It is noteworthy that searching the literature showed only two reports on the effect of *Stachys* species on TNF- α production and it was a suppressive effect which correlates well with the results obtained in this study. Interestingly, no report was found on the effect of *Stachys* species on IL-12 production. As there are no previous studies addressing the immunomodulatory activity of *S. arabica* in the literature; the preliminary findings described in this research are the first to be reported.

The crude *n*-hexane extract of *S. arabica* leaves (390H) considerably decrease the pro-inflammatory level of TNF- α and IL-12 and the reason for this might be to synergistic effects of purified bioactive phytosterols like β -sitosterol, stigmasterol (390RQ5). Phytosterol demonstrated a wide range of biological activities including immune modulating, anti-pyretic, and anti-inflammatory effects (Gupta *et al.*, 1980; Navarro *et al.*, 2001). Phytosterol (β -sitosterol, stigmasterol) alleviated the inflammatory reaction in LPS-stimulated RAW264.7 macrophage model through inhibition of TNF- α production, nitric acid (NO) production, and expression of cyclooxygenase-2 (Yuan *et al.*, 2019). Liao *et al.* (2018) study investigated the anti-inflammatory activity of β -sitosterol isolated from *Moringa oleifera* in two cell lines. This study proved that β -sitosterol was able to decrease TNF- α , IL-1 β , and IL-6 secretion in J774A.1 macrophages induced by LPS in a dose-dependency manner of the decrease through inhibition of NF- κ B in macrophages, also, β -sitosterol inhibit the generation of inflammatory cytokines in stimulated HaCaT cells (keratinocytes). β -sitosterol decreases the levels of TNF- α , IL-6, and IL-1 β in intestinal tissue of mice with experimental colitis in a concentration-dependent manner (Ding *et al.*, 2019). A study by Khan *et al.* (2020) evaluated the anti-inflammatory effect of stigmasterol in the treatment of Rheumatoid arthritis in collagen-induced arthritic (CIA) model of arthritis. the results showed that efficacy of stigmasterol against CIA induced inflammation in rats are significantly suppressed the expression of proinflammatory mediators (TNF- α , IL-6, IL-1 β , iNOS and COX-2). An investigation by Desai *et al.* (2009) on the effects of β -sitosterol treatment on cytokine release from peripheral blood mononuclear cells (PBMC) of multiple sclerosis (MS) patients showed that β -sitosterol decreased pro-inflammatory cytokines (TNF- α and IL-12) without strongly affecting anti-inflammatory cytokine IL-10 release from PBMC of MS patients.

Interestingly, the crude EtOAc extract of *S. arabica* leaves (390E-31.3 μ g/mL) significantly decrease the pro-inflammatory level of TNF- α and IL-12 levels in LPS-stimulated THP-1 cells when compared to the stimulated control. When the EtOAc

extract (390E) was subjected for further purification, three pheophytins (pheophytin a (390RQ10), 13²(*R,S*)-hydroxy pheophytin a (390RQ27) and pheophytin b (390RQ28)) were identified, which in turn, demonstrated a potent suppression of pro-inflammatory level of TNF- α and IL-12 levels in LPS- stimulated THP-1 cells when compared to the stimulated control as shown in Figures 3.66-3.67 and 3.74-3.75.

The results of previous reports conducted on *Stachys spp.* suggested that iridoids and flavonoids are the main constituents that might be responsible for the anti-inflammatory effects (Háznagy-Radnai *et al.*, 2012). However, the results of the present study showed that the potent suppression effects on TNF- α and IL-12 production by *S. arabica* most probably due to the synergistic effects of pheophytins and phytosterols.

Although, chlorophylls and their Mg-free derivatives (pheophytins) are considered among the most abundant pigments in nature, researchers did not widely investigate their biological activity. The biological studies about chlorophylls and their Mg-free derivatives (pheophytins) are limited due to the difficulty to obtain them as pure substances as well as the concern regarding their degradation and instability.

Pheophytin a and chlorophyll a inhibit TNF- α expression and showed anti-inflammatory activity against carrageenan-induced inflammation in mice. The researchers in this study established the scientific basis for the ethno-medicinal use of green leaves to treat inflammation (Subramoniam *et al.*, 2012). Pheophytin a and chlorophyll a suppressed expressions of proinflammatory cytokines (TNF- α , IL-1 β , and IL-6) in LPS- and IFN- γ - stimulated BV2 murine microglia cells and suppressed activation of NF- κ B and STAT-1 pathways. These results suggested that pheophytin a and chlorophyll a have a potential role as a neuroprotective and anti-inflammatory agent for microglia-mediated neuroinflammatory disorders (Park *et al.*, 2014).

Lin *et al* (2014; 2017) conducted two separate extensive investigations regarding the effect of pheophytin a and pheophytin b on cytokines, nitric oxide (NO), and PGE2 overproduction as potential therapeutic target in sepsis, and tried to clarify the anti-inflammatory molecular mechanisms of both pheophytin a and pheophytin b. According to the first report of Lin *et al* (2014), pheophytin a showed significant anti-inflammatory properties, it was able to attenuate IL-1 β , PGE2 and NO production in LPS-stimulated RAW 264.7 cell and modulate ERK and STAT-1 signalling pathways. In the second report by the same research team, Pheophytin b illustrated potent anti-

inflammatory activity and significantly decreased the overproduction of cytokines (TNF- α , IL-1 β , IL-6), NO, and PGE2 in LPS-stimulated murine macrophages (RAW264.7) and human CD14+ monocyte-derived macrophage via inhibition of STAT-1 and PI3K/Akt signalling pathways. the same study showed that pheophytin b had no effect on NF- κ B, MAKP and AP-1 signalling pathways (Lin *et al.*, 2017).

Pheophytin a & 13² hydroxy pheophytin a (isolated from *Tagetes minuta*) decreased LPS-stimulated transcriptional activation of NF- κ B in a dose-dependent manner using human stomach (Hs 746T), human small intestine (HIEC-6) and THP-1 cell lines (Apaza Ticona *et al.*, 2021). Another study showed that 13²-hydroxy pheophytin a and 13²-hydroxy pheophytin b exhibited moderate inhibition of TNF- α induced NF- κ B activation in HeLa cells (Huang *et al.*, 2007).

There do not appear to be any reports on the effect of pheophytins (pheophytin a, 13²(*R,S*)-hydroxy pheophytin a, and pheophytin b) on the release of IL-12 neither *in vitro* nor *in vivo* models, therefore, the aforementioned preliminary findings are the among the first to be reported and serve as promising findings for furthermore extensive investigation.

Taken together, the results of the present study would suggest that pheophytin a (390RQ10), 13²(*R,S*)-hydroxy pheophytin (390RQ27), and pheophytin b (390RQ28) exert potential anti-inflammatory activity and serve as potential phytochemicals to be used as immunomodulatory agents for inflammatory related diseases.

3.5.3 Putative mode(s) of action of the plant extracts/phytochemicals

Taken altogether our findings suggest that the examined six crude plant extracts and their purified phytochemicals (OA, UA, pinocembrin, pheophytin a, 13²(*R,S*)-hydroxy pheophytin a, and pheophytin b) have the potential to lower inflammation via reduction in the release of the pro-inflammatory cytokines TNF- α and IL-12 (Table 3.24). These results correlate well with those found in the literature using different *in vitro* and/or *in vivo* models.

Medicinal plants and their phytochemicals have already been reported to inhibit the production of TNF- α (Iqbal *et al.*, 2013; Di Gesso *et al.*, 2015), IL-12 (Kolehmainen *et al.*, 2012; Bui *et al.*, 2017) and as inhibitors of NF- κ B induced cytokine production (Karunaweera *et al.*, 2015; Jeong and Lee, 2018).

While treatment with LPS has been shown to increase the expression of TLR4 and NF- κ B in the BV2 murine microglia cells, OA (Li *et al.*, 2020), pinocembrin (Zhou *et al.*, 2015) and pheophytin a (Park *et al.*, 2014) suppressed the production of TNF- α and other inflammatory cytokines in LPS-stimulated BV2 murine microglia cells by blocking the TLR4-NF- κ B pathway. This indicates that these phytochemicals may have a promising role as neuroprotective and anti-inflammatory agents for microglia-mediated neuroinflammatory disorders. UA was able to inhibit the binding of LPS to TLR4, as well as the activation of NF- κ B and of MAPKs in LPS-stimulated peritoneal macrophages (Jang *et al.*, 2014). Previous reports have revealed that pheophytin a and 13²-hydroxy pheophytin a decreased LPS-stimulated transcriptional activation of NF- κ B from human stomach, human small intestine and THP-1 cell lines (Apaza Ticona *et al.*, 2021). Another study showed that 13²-hydroxy pheophytin a exhibited moderate inhibition of TNF- α induced NF- κ B activation in HeLa cells (Huang *et al.*, 2007).

Regarding IL-12, previous reports have highlighted the potential therapeutic use of targeted anti-(IL-12p40) may be beneficial in the treatment of psoriasis, rheumatoid arthritis (RA), Crohn's disease (CD), ulcerative colitis (UC), and multiple sclerosis (MS) (Rosmarin and Strober, 2005; Zundler and Neurath, 2015). This was similar to activities that reported for TNF- α (Victor and Gottlieb, 2002; Kallioli and Ivashkiv, 2016). Interestingly, both plants (*Fraxinus excelsior* and *Stachys arabica*) are used traditionally to treat gastrointestinal-related diseases, fever, rheumatic pain, gout and

other inflammatory diseases. Our findings validate to some extent some of these traditional uses.

Overall, these plant extracts and their phytochemicals (namely, OA, UA, pinocembrin, pheophytin a (390RQ10), 13² (*R,S*)-hydroxy pheophytin a (390RQ27), and pheophytin b (390RQ28) exhibited potential anti-inflammatory activity and could serve as potential immunomodulatory agents for inflammatory related diseases. The proposed mode of action could be through blocking NF- κ B activation cascade /signalling pathway at different steps, or via inhibition of LPS binding to TLR4. As consequence of that, pro-inflammatory cytokines (TNF- α and IL-12) production from LPS stimulated THP-1 cells would be suppressed (Figure 3.76). Further investigations are required to confirm the exact mode(s) of action of these extracts and phytochemicals.

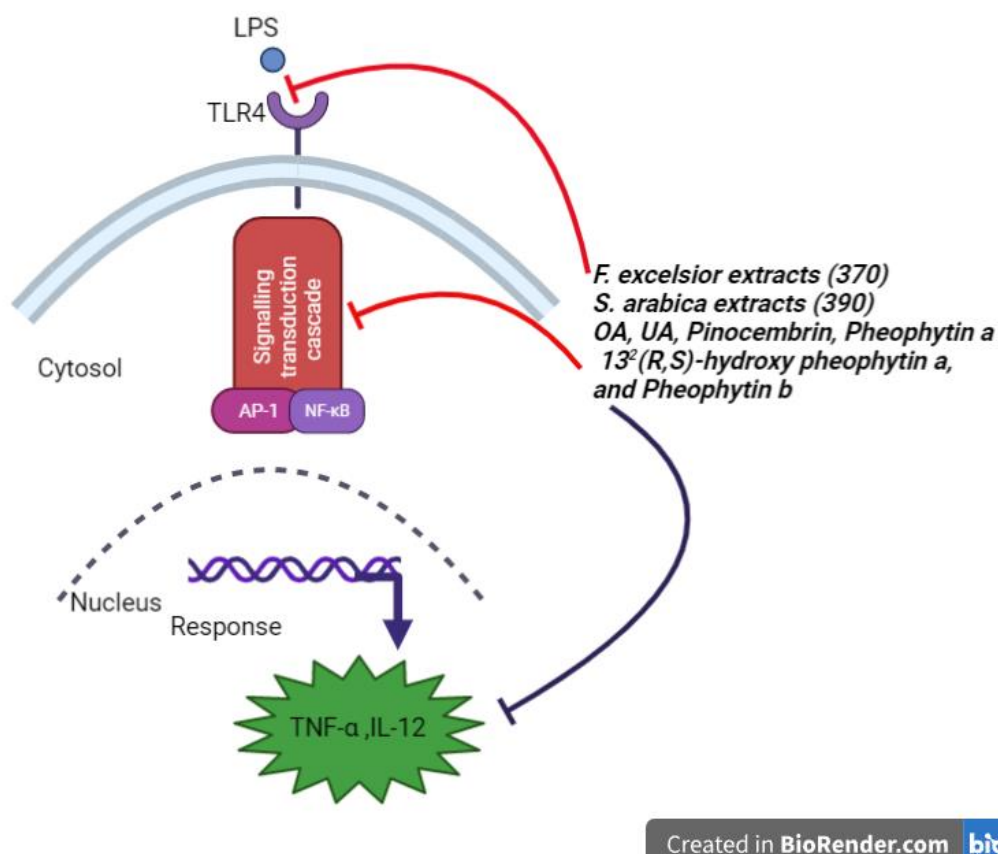


Figure 3.76 Proposed mechanisms representing the effect of *F. excelsior*, *S. arabica*, and selected phytochemicals on LPS-stimulated THP-1 cells.

The blue line indicates direct inhibition of what cytokines (TNF- α and IL-12) measured experimentally. The red lines indicate possible interactions with targets at the molecular level (created in BioRender.com).

PART C:
MOLECULAR *DOCKING*
STUDIES

Part C: Molecular docking studies

3.6 Molecular docking of ligands towards the protein kinase G enzyme of *Mycobacterium tuberculosis* (*MtPknG*)

3.6.1 *Phytochemicals from Pelargonium reniforme and Pelargonium sidoides*

Eighty-four phytochemicals from the roots and aerial parts of two *Pelargonium* spp. were selected for the molecular docking study. They were classified into four main groups: phenolics, coumarins (coumarin glycosides and coumarin sulfates), flavonoids, and other miscellaneous compounds as illustrated in Table 3.19 & 3.20. A guided docking approach using Autodock Vina was conducted to predict their binding free energies (ΔG in kcal/mol) towards *MtPknG*, with the best docking score indicating the highest predicted ligand/protein affinity (Table 3.19 & 3.20). The co-crystallized control inhibitor AX20017 was re-docked into the target protein structure to validate the docking.

The docking score obtained for each ligand was compared to the score of the re-docked control inhibitor (-7.9 kcal/mol). The scores for the eighty-four ligands ranged between -5.8 and -13.2 kcal/mol. A total of eleven ligands (10 of which were flavonoids) present in the aerial parts of *P. reniforme* and/or *P. sidoides* showed strong binding affinities towards *MtPknG* ranging from -10.7 to -13.2 kcal/mol. Three ligand efficiencies (LE1, LE2, and SILE) were calculated for all ligands and are presented in Table 3.19 & 3.20.

The docking score shows how strongly a ligand will interact with a given protein, the ranking of best ligands was on basis of the predicted binding affinity towards *MtPknG*. The ten ligands (flavonoids) yielding the best/ strong docking score are presented in Table 3.22.

The five flavonoids **60**, **61**, **74**, **77** and **79** (Figures 3.78a to 3.82a) were selected for further investigation as they showed the best docking and SILE scores (with values superior to those obtained for the re-docked AX20017) (Table 3.22).

The detailed molecular interactions (hydrogen and hydrophobic bonds) between the top ranked ligands and the amino acid residues of *MtPknG* involved in the binding are illustrated in Table 3.23 and Figures 3.78 to 3.82.

The re-docked control inhibitor (AX20017) (Figure 3.77) formed two hydrogen bonds with Val 235 and Met 283, as well as hydrophobic interactions with Ile165, Ile292, Ile157, Val179, and Ala 158. These interactions are consistent with a previous report (Scherr *et al.*, 2007).

The interactions between isoorientin 2''-O-gallate (**79**) and *MtPknG* showed that the sugar moiety formed strong hydrogen bonds with Ser239 and Lys241, while the para-hydroxyl group of the gallate moiety interacted with His159. Hydrophobic interactions with Ala158, Val179 and Ile292 were also seen (Figure 3.78). In the case of isovitexin 2''-O-gallate (**77**), the para hydroxyl group present on the B ring of the flavonoid and the gallate moiety formed hydrogen bonds with Lys241 and Met232. Hydrophobic interactions were also observed between (**77**) and Ala158, Val179, Val235 and Ile292 (Figure 3.79). Kaempferol 3-O- β -D-rutinoside (nicotiflorin) (**61**) exhibited several interactions with *MtPknG*, including strong hydrogen bonds (distances < 2.5 Å) with Glu233, Glu280, Gln238, Ser 239, and hydrophobic interactions with Ile292, Ile157, Ala91, Ala158, Ile165 and Val235 (Figure 3.80). The B-ring hydroxyl groups of orientin (**74**) showed three hydrogen bonds with Lys181, and one with Asp293, while the flavone backbone interacted via hydrophobic interactions with Ala158 and Ile157 (Figure 3.81). Kaempferol 7-O- β -D-glucoside (populnin) (**60**) interacted strongly via hydrogen bonds with Lys181, Asp 293 and Gln238 (<2.5 Å) and via hydrophobic interactions with Ala158, Ile165 and Ile157 (Figure 3.82).

3.6.2 Selected phytochemicals isolated from *Fraxinus excelsior* and *Stachys arabica*

The docking scores and ligand efficiencies (LEs) toward *MtPknG* of each phytochemical are illustrated in Table 3.21. The obtained docking scores ranged between 3 and -8.7 kcal/mol. There was no ligand showing a strong binding affinity towards *MtPknG* compared to the control inhibitor.

Table 3.19 Predicted binding free energies (docking scores (ΔG in kcal/mol) and ligand efficiencies* (LEs) of *P. reniforme* and *P. sidoides* root constituents and re-docked control inhibitor AX20017 towards *MtPknG*.**

Code	Compound	<i>P. reniforme</i>	<i>P. sidoides</i>	ΔG	LE1	LE2	SILE
Phenolic acid and phenylpropanoids derivatives							
1.	Gallic acid	+	+	-6.7	0.56	0.04	3.18
2.	Gallic acid methyl ester	+	+	-6.9	0.53	0.04	3.20
3.	<i>p</i> -hydroxybenzoic acid	+		-6.2	0.62	0.04	3.11
4.	Protocatechuic acid	+		-6.5	0.59	0.04	3.17
5.	Vanillic acid	+		-6.6	0.55	0.04	3.13
6.	Caffeic acid	+		-7.6	0.58	0.04	3.52
7.	Ferulic acid	+		-7.5	0.54	0.04	3.40
8.	<i>p</i> -coumaric acid	+		-7.4	0.62	0.05	3.51
9.	<i>p</i> -coumaraldehyde	+		-7.0	0.64	0.05	3.41
10.	Shikimic acid 3-O-gallate	+	+	-9.1	0.40	0.03	3.55
Coumarin, Coumarin glycosides and Coumarin sulfates							
11.	7-hydroxy-6-methoxycoumarin (Scopoletin)	+	+	-7.3	0.52	0.04	3.31
12.	7-hydroxy-5,6-dimethoxycoumarin (Umckalin)		+	-7.5	0.47	0.03	3.26
13.	7-acetoxy-5,6-dimethoxycoumarin		+	-7.6	0.40	0.03	3.14
14.	5,6,7-trimethoxycoumarin		+	-7.4	0.44	0.03	3.16

Table 3.19 (Cont.) Predicted binding free energies (docking scores (ΔG in kcal/mol) and ligand efficiencies* (LEs) of *P. reniforme* and *P. sidoides* root constituents and re-docked control inhibitor AX20017 towards MtPknG.**

Code	Compound	<i>P. reniforme</i>	<i>P. sidoides</i>	ΔG	LE1	LE2	SILE
15.	6-hydroxy-5,7-dimethoxycoumarin (Fraxinol)	+		-7.4	0.46	0.03	3.22
16.	5,6-dihydroxy-7-dimethoxycoumarin (Isofraxetin)	+		-7.9	0.53	0.04	3.51
17.	6,7,8-trihydroxycoumarin	+	+	-7.7	0.55	0.04	3.49
18.	6,8-dihydroxy-7-methoxycoumarin		+	-7.6	0.51	0.04	3.37
19.	8-hydroxy-6,7-dimethoxycoumarin (Fraxidin)	+		-7.5	0.47	0.03	3.26
20.	7,8-dihydroxy-6-methoxycoumarin (Fraxetin)		+	-7.7	0.51	0.04	3.42
21.	6,8-dihydroxy-5,7-dimehoxycoumarin		+	-7.5	0.44	0.03	3.20
22.	5,6,7,8-tetramethoxycoumarin (Artelin)		+	-8.2	0.43	0.03	3.39
23.	8-hydroxy-5,6,7-trimehtoxycoumarin	+	+	-7.7	0.43	0.03	3.24
24.	Magnolioside		+	-8.7	0.35	0.02	3.31
25.	Isofraxoside		+	-8.3	0.32	0.02	3.12
26.	Umckalin-7- β -D-glucoside		+	-7.5	0.28	0.02	2.80
27.	5,6-dimethoxycoumarin-7-sulfate		+	-8.7	0.44	0.04	3.54
28.	6,7-dihydroxycoumarin-8-sulfate		+	-8.3	0.46	0.03	3.49
29.	6-hydroxy-5,7-dimthoxycoumarin-8-sulfate		+	-8.5	0.41	0.04	3.41
30.	8-hydroxy-5,7-dimthoxycoumarin-6-sulfate		+	-8.8	0.42	0.04	3.53

Table 3.19 (Cont.) Predicted binding free energies (docking scores (ΔG in kcal/mol) and ligand efficiencies* (LEs) of *P. reniforme* and *P. sidoides* root constituents and re-docked control inhibitor AX20017 towards MtPknG.**

Code	Compound	<i>P. reniforme</i>	<i>P. sidoides</i>	ΔG	LE1	LE2	SILE
31.	6-methoxycoumarin-7-sulfate		+	-8.2	0.46	0.03	3.45
32.	7,8-dihydroxy-5,6-dimethoxycoumarin		+	-7.9	0.46	0.03	3.38
33.	7-hydroxy-5,6-dimethoxycoumarin-8-sulfate		+	-8.4	0.40	0.04	3.37
34.	7,8-dihydroxycoumarin-6-sulfate		+	-8.2	0.46	0.03	3.45
35.	7-hydroxycoumarin-6,8-bisulfate		+	-8.7	0.40	0.02	3.44
36.	7-hydroxy-6-methoxycoumarin-8-sulfate		+	-7.8	0.41	0.03	3.09
37.	8-hydroxy-7-methoxycoumarin-6-sulfate		+	-8.1	0.43	0.03	3.35
38.	7-methoxycoumarin-6,8-bisulfate		+	-8.7	0.38	0.02	3.40
Flavonoids and flavan-3-ols							
39.	Kaempferol-3-O- β -D-glucoside (Astragalín)	+		-10.3	0.32	0.02	3.64
40.	Kaempferol-3-O- β -D-galactoside (Trifolin)	+		-9.7	0.30	0.02	3.43
41.	Quercetin-3-O- β -D-glucoside (Isoquercetin)	+		-9.8	0.30	0.02	3.43
42.	Myricetin-3-O- β -D-glucoside (Isomericitrin)	+		-9.4	0.28	0.02	3.26
43.	Afzelechin	+		-8.1	0.41	0.03	3.30
44.	Catechin	+	+	-8.1	0.39	0.03	3.25
45.	Gallocatechin	+	+	-8.5	0.39	0.03	3.41

Table 3.19 (Cont.) Predicted binding free energies (docking scores (ΔG in kcal/mol) and ligand efficiencies* (LEs) of *P. reniforme* and *P. sidoides* root constituents and re-docked control inhibitor AX20017 towards *MtPknG*.**

Code	Compound	<i>P. reniforme</i>	<i>P. sidoides</i>	ΔG	LE1	LE2	SILE
Miscellaneous							
46.	Reniformin	+		-9.1	0.27	0.02	3.16
47.	β -sitosterol	+	+	-10.3	0.34	0.02	3.71
48.	β -sitosterol-3-O- β -D-glucoside	+		-8.4	0.20	0.01	2.76

+ = Present

* LE1 defines the ligand efficiency coefficient = $-(\Delta G/NHA)$. LE2 defines the ligand efficiency coefficient = $-(\Delta G/\text{molecular weight of the ligand})$. SILE defines a size-independent ligand efficiency coefficient = $-\Delta G/NHA^{(0.3)}$.

**The re-docked inhibitor AX20017 had a predicted binding energy of -7.9 kcal/mol towards *MtPknG* and ligand efficiencies LE1, LE2 and SILE of 0.44, 0.03 and 3.32, respectively.

The docking outputs better than the control inhibitor AX20017 (ΔG , LE1, LE2 and SILE) are shown in bold.

Table 3.20 Predicted binding free energies (docking scores (ΔG in kcal/mol) and ligand efficiencies* (LEs) of *P. reniforme* and *P. sidoides* aerial parts constituents and re-docked control inhibitor AX20017 towards MtPknG.**

Code	Compound	<i>P. reniforme</i>	<i>P. sidoides</i>	ΔG	LE1	LE2	SILE
Phenolic acid and phenylpropanoids derivatives							
49.	Gallic acid ethyl ester	+	+	-7.6	0.54	0.04	3.44
50.	Gallic acid butyl ester	+		-8.3	0.52	0.04	3.61
51.	Shikimic acid 3,5-di- <i>O</i> -gallate	+		-10.7	0.31	0.02	3.71
52.	<i>p</i> -Hydroxyphenyl ethanol	+		-5.8	0.58	0.04	2.9
53.	<i>p</i> -Hydroxyphenyl acetic acid	+		-6.9	0.63	0.05	3.36
54.	<i>p</i> -Hydroxybenzyl alcohol	+		-6.7	0.74	0.05	3.47
55.	<i>p</i> -coumaroyl-4- <i>O</i> - β -D-glucoside	+		-9.1	0.40	0.03	3.55
56.	Glycerol-1-gallate	+		-8.2	0.48	0.03	3.5
57.	Glucogallin	+	+	-9.3	0.40	0.03	3.63
58.	(α,β)-3,4-Di- <i>O</i> -galloylglucopyranoside	+		-10.6 (α) -10 (β)	0.31 0.29	0.02	3.47
59.	Salidroside-6''- <i>O</i> -gallate	+		-10.2	0.32	0.02	3.60
Flavonoids							
60.	Kaempferol 7- <i>O</i> - β -D-glucoside (Populnin)	+		-11.6	0.36	0.03	4.10
61.	Kaempferol 3- <i>O</i> - β -D-rutinoside (Nicotiflorin)	+		-12.2	0.29	0.02	3.98
62.	Quercetin		+	-9.9	0.45	0.03	3.92

Table 3.20 (Cont.) Predicted binding free energies (docking scores (ΔG in kcal/mol) and ligand efficiencies* (LEs) of *P. reniforme* and *P. sidoides* aerial parts constituents and re-docked control inhibitor AX20017 towards *MtPknG*.**

Code	Compound	<i>P. reniforme</i>	<i>P. sidoides</i>	ΔG	LE1	LE2	SILE
63.	Quercetin 3- <i>O</i> - β -D-rutinoside (Rutin)	+		-11.4	0.27	0.02	3.69
64.	Quercetin 7- <i>O</i> - β -D-glucoside (Quercimeritrin)	+		-11.2	0.39	0.02	3.92
65.	Dihydrokaempferol (Aromadendrin)	+		-7.9	0.38	0.03	3.17
66.	Dihydrokaempferol 3- <i>O</i> - β -D-glucoside		+	-9.2	0.29	0.02	3.25
67.	Dihydroquercetin (Taxifolin)	+		-8.0	0.36	0.03	3.16
68.	Taxifolin-7- <i>O</i> - β -D-glucoside	+		-9.2	0.28	0.02	3.22
69.	Taxifolin-3- <i>O</i> - β -D-glucoside		+	-9.7	0.29	0.02	3.40
70.	Narnigenin-7- <i>O</i> - β -D-glucoside (Prunin)	+		-9.8	0.32	0.02	3.50
71.	Luteolin-7- <i>O</i> - β -D-glucoside (Glucoluteolin)		+	-11.1	0.35	0.02	3.92
72.	Vitexin	+	+	-11.2	0.36	0.03	4.0
73.	Vitexin 2''- <i>O</i> -gallate		+	-9.7	0.23	0.02	3.16
74.	Orientin	+	+	-11.8	0.37	0.03	4.17
75.	Orientin 2''- <i>O</i> -gallate	+	+	-9.9	0.23	0.02	3.20
76.	Isovitexin	+	+	-10.4	0.34	0.02	3.71
77.	Isovitexin 2''- <i>O</i> -gallate		+	-12.6	0.30	0.02	4.11
78.	Isoorientin	+	+	-11.2	0.35	0.02	3.96
79.	Isoorientin 2''- <i>O</i> -gallate	+	+	-13.2	0.31	0.02	4.27

Table 3.20 (Cont.) Predicted binding free energies (docking scores (ΔG in kcal/mol) and ligand efficiencies* (LEs) of *P. reniforme* and *P. sidoides* aerial parts constituents and re-docked control inhibitor AX20017 towards *MtPknG*.**

Code	Compound	<i>P. reniforme</i>	<i>P. sidoides</i>	ΔG	LE1	LE2	SILE
80.	Epigallocatechin-3-O-gallate		+	-9.2	0.28	0.02	3.2
Hydrolysable tannins and miscellaneous							
81.	Brevifolin carboxylic acid	+		-10	0.48	0.03	4.01
82.	Phyllanthusiin E	+		-10.1	0.48	0.03	4.05
83.	Phyllanthusiin E O-methyl ester	+		-9.2	0.42	0.03	3.60
84.	4,6-Dihydroxyacteophenone 2-O- β -D-glucoside		+	-7.6	0.33	0.02	2.96

+ = Present

* LE1 defines the ligand efficiency coefficient = $-\Delta G/NHA$. LE2 defines the ligand efficiency coefficient = $-\Delta G/\text{molecular weight of the ligand}$. SILE defines a size-independent ligand efficiency coefficient = $-\Delta G/NHA^{(0.3)}$.

**The re-docked inhibitor AX20017 had a predicted binding energy of -7.9 kcal/mol towards *MtPknG* and ligand efficiencies LE1, LE2 and SILE of 0.44, 0.03 and 3.32, respectively.

The docking outputs better than the control inhibitor AX20017 (ΔG , LE1, LE2 and SILE) are shown in bold

Table 3.21 Predicted binding free energies (ΔG in kcal/mol) and ligand efficiencies* (LE) of selected phytochemicals isolated from *F. excelsior* and *S. arabica* and of the re-docked control inhibitor AX20017 towards *MtPknG*.**

Compound	<i>F. excelsior</i>	<i>S. arabica</i>	docking scores ΔG	LE1	LE2	SILE
Pinocembrin	+		-8.7	0.46	0.03	3.60
Oleanolic acid	+		-8.6	0.26	0.02	3.01
Ursolic acid	+		-8.4	0.25	0.02	2.94
Pheophytin a		+	3.1	0.05	0.004	0.90
Pheophytin b		+	3.4	0.05	0.004	0.97
13 ² (<i>R</i>) hydroxy pheophytin a		+	3.3	0.05	0.004	0.94
13 ² (<i>S</i>) hydroxy pheophytin a		+	-3.3	0.05	0.004	0.94

+ = Present

* LE1 defines the ligand efficiency coefficient = $-\Delta G/NHA$. LE2 defines the ligand efficiency coefficient = $-\Delta G/\text{molecular weight of the ligand}$. SILE defines a size-independent ligand efficiency coefficient = $-\Delta G/NHA^{(0.3)}$.

**The re-docked inhibitor AX20017 had a predicted binding energy of -7.9 kcal/mol towards *MtPknG* and ligand efficiencies LE1, LE2 and SILE of 0.44, 0.03 and 3.32, respectively.

Table 3.22 List of best ligands obtained in this study, ranked according to their predicted free binding energy (docking score) and SILE towards *MtPknG*

Ligand	docking scores (ΔG in kcal/mol)	SILE
Isoorientin 2''-O-gallate (79)	-13.2	4.27
Isovitexin 2''-O-gallate (77)	-12.6	4.11
Kaempferol 3-O- β -D-rutinoside (Nicotiflorin) (61)	-12.2	3.98
Orientin (74)	-11.8	4.17
Kaempferol 7-O- β -D-glucoside (Populnin) (60)	-11.6	4.10
Quercetin 3-O- β -D-rutinoside (Rutin) (63)	-11.4	3.69
Quercetin 7-O- β -D-glucoside (Quercimeritrin) (64)	-11.2	3.92
Vitexin (72)	-11.2	4.0
Isoorientin (78)	-11.2	3.96
Luteolin-7-O- β -D-glucoside (Glucoluteolin) (71)	-11.1	3.92

The re-docked inhibitor AX20017 had a predicted binding energy of -7.9 kcal/mol towards *MtPknG* and SILE value of 3.32.

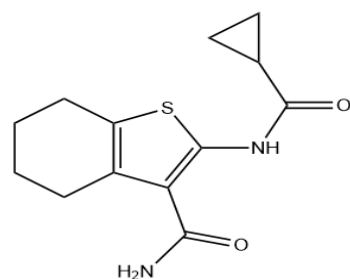
Table 3.23 Detailed molecular interactions between the top ranked ligands of *Pelargonium* spp. and MtPknG.

Ligand	Interacting residues	Distance (Å)	Category	Type
Isoorientin 2"-O-gallate (79) $\Delta G = -13.2$ SILE = 4.27	Lys241	2.650	H-Bond	Conventional
	Ser239	2.825	H-Bond	Conventional
	His159	3.063	H-Bond	Conventional
	Lys241	3.140	H-Bond	Carbon Hydrogen Bond
	Ser239	3.512	H-Bond	Carbon Hydrogen Bond
	Ile292	4.701	Hydrophobic	Alkyl
	Val179	4.893	Hydrophobic	Alkyl
	Ala158	4.195	Hydrophobic	Pi-Alkyl
Isovitexin 2"-O-gallate (77) $\Delta G = -12.6$ SILE = 4.11	Met232	2.903	H-Bond	Conventional
	Lys241	2.168	H-Bond	Conventional
	Ala158	3.898	Hydrophobic	Pi- Sigma
	Val179	4.317	Hydrophobic	Pi-Alkyl
	Ile292	4.811	Hydrophobic	Pi-Alkyl
Kaempferol 3-O- β -D- rutinoside (Nicotiflorin) (61) $\Delta G = -12.2$ SILE = 3.98	Glu233	2.119	H-Bond	Conventional
	Glu280	2.286	H-Bond	Conventional
	Gln238	2.293	H-Bond	Conventional
	Ser239	2.395	H-Bond	Conventional
	Ile292	3.806	Hydrophobic	Pi-Sigma
	Ile292	3.940	Hydrophobic	Pi-Sigma
	Ile157	4.593	Hydrophobic	Pi-Alkyl
	Ala91	4.573	Hydrophobic	Pi-Alkyl
	Ala158	4.830	Hydrophobic	Pi-Alkyl
	Ala158	5.256	Hydrophobic	Pi-Alkyl
	Ile165	5.270	Hydrophobic	Pi-Alkyl
	Val235	5.496	Hydrophobic	Pi-Alkyl

Table 3.23 (Cont.) Detailed molecular interaction between top ranked ligands of *Pelargonium* spp. and MtPknG

Ligand	Interacting residues	Distance (Å)	Category	Type
Orientin (74) $\Delta G = -11.8$ SILE = 4.17	Lys181	2.248	H-Bond	Conventional
	Lys181	2.668	H-Bond	Conventional
	Lys181	2.714	H-Bond	Conventional
	Asp293	2.728	H-Bond	Conventional
	Ala158	4.456	Hydrophobic	Pi-Alkyl
	Ala158	4.835	Hydrophobic	Pi-Alkyl
	Ile157	4.846	Hydrophobic	Pi-Alkyl
Kaempferol 7-O- β -D-glucoside (Populnin) (60) $\Delta G = -11.6$ SILE = 4.10	Asp293	2.205	H-Bond	Conventional
	Gln238	2.278	H-Bond	Conventional
	Lys181	2.498	H-Bond	Conventional
	Gln238	3.455	H-Bond	Carbon Hydrogen Bond
	Ile292	3.872	Hydrophobic	Pi-Sigma
	Ala158	4.526	Hydrophobic	Pi-Alkyl
	Ala158	4.719	Hydrophobic	Pi-Alkyl
	Ile165	4.817	Hydrophobic	Pi-Alkyl
	Ile165	5.160	Hydrophobic	Pi-Alkyl
Ile157	5.327	Hydrophobic	Pi-Alkyl	
Control inhibitor (AX20017) $\Delta G = -7.9$ SILE = 3.32	Val235	1.830	H-Bond	Conventional
	Met283	2.711	H-Bond	Conventional
	Ile292	3.700	Hydrophobic	Pi-Sigma
	Ile165	3.75	Hydrophobic	Pi-Sigma
	Ala158	4.300	Hydrophobic	Alkyl
	Ile157	4.364	Hydrophobic	Alkyl
	Ala158	5.182	Hydrophobic	Pi-Alkyl
	Ile165	5.127	Hydrophobic	Pi-Alkyl
	Val179	5.354	Hydrophobic	Pi-Alkyl
Ile292	4.852	Hydrophobic	Pi-Alkyl	

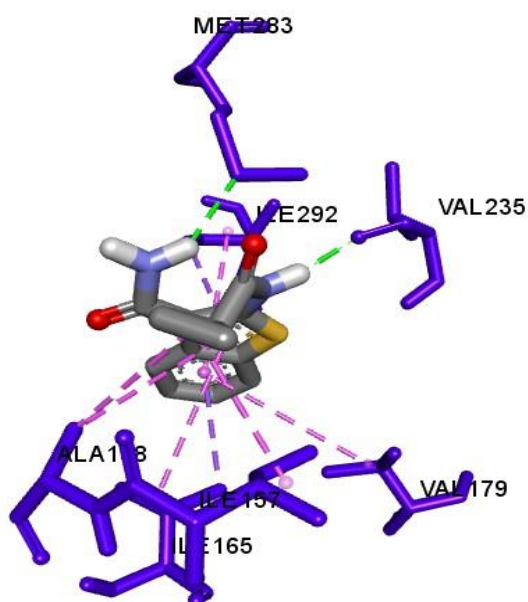
(a)



mode	affinity (kcal/mol)	dist from best mode rmsd l.b. rmsd u.b.
1	-7.9	0.000 0.000
2	-7.7	3.246 6.142
3	-7.6	2.513 4.837
4	-7.3	2.527 4.588
5	-7.3	3.565 6.061
6	-7.1	3.095 5.927
7	-7.0	2.968 4.768
8	-6.9	3.002 5.318
9	-6.9	3.615 5.012

Writing output ... done.

(b)



(c)

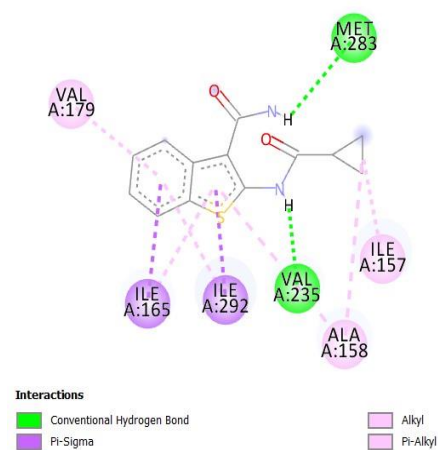
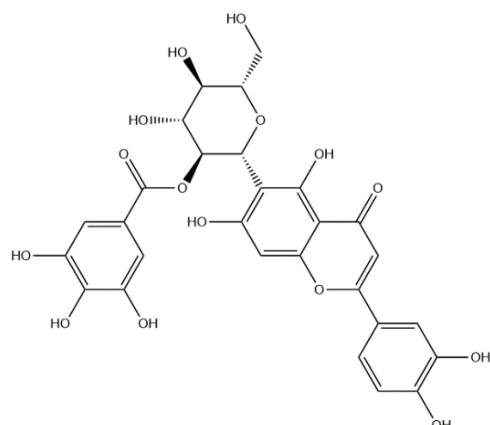


Figure 3.77 Predicted binding free energy (docking score) and detailed molecular interactions of the control inhibitor AX20017 within the active site of *MtPknG*.

(a) Structure and docking scores of the control inhibitor AX20017; predicted binding free energy of -7.9 kcal/mol. (b) Docked pose of the control inhibitor AX20017 in the *MtPknG* binding site showing molecular interactions; hydrogen and hydrophobic bonds as green and pink/ purple dashed lines, respectively; (c) 2D plot of interactions between control inhibitor AX20017 and key residues of *MtPknG* generated by BIOVIA Discovery Studio visualizer

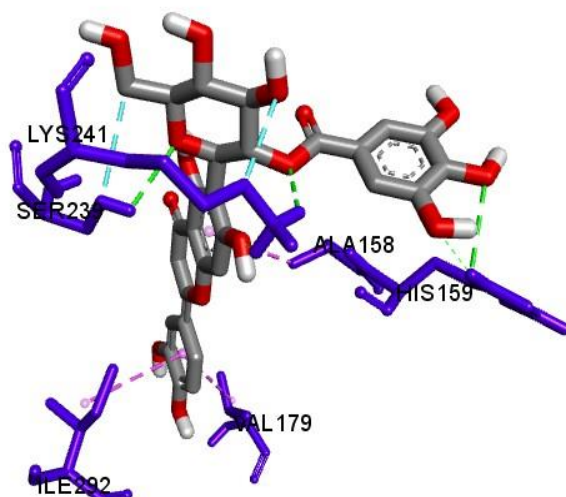
(a)



mode	affinity (kcal/mol)	dist from best mode rmsd l.b. rmsd u.b.
1	-13.2	0.000 0.000
2	-11.9	2.104 2.505
3	-11.5	1.719 2.144
4	-11.0	1.700 1.820
5	-10.8	2.545 3.388
6	-10.3	1.676 2.176

Writing output ... done.

(b)



(c)

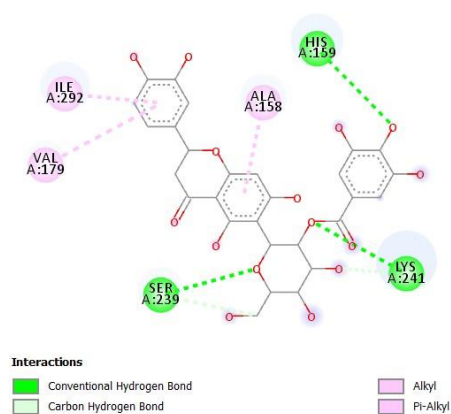
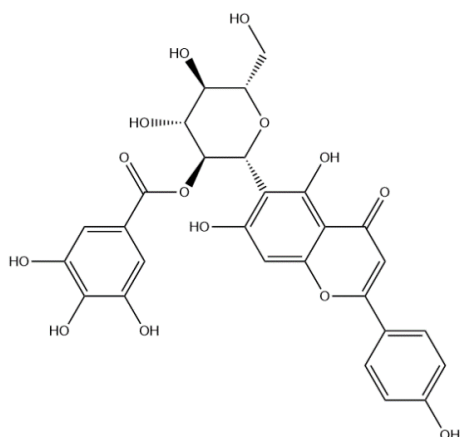


Figure 3.78 Predicted binding free energy (docking score) and detailed molecular interactions of isorientin 2''-O-gallate (79) within the active site of *MtPknG*.

(a) Structure and docking scores of isorientin 2''-O-gallate (79); predicted binding free energy of -13.2 kcal/mol). (b) Docked pose of (79) in the *MtPknG* binding site showing molecular interactions; hydrogen and hydrophobic bonds as green and pink/purple dashed lines, respectively; (c) 2D plot of interactions between (79) and key residues of *MtPknG* generated by BIOVIA Discovery Studio visualizer

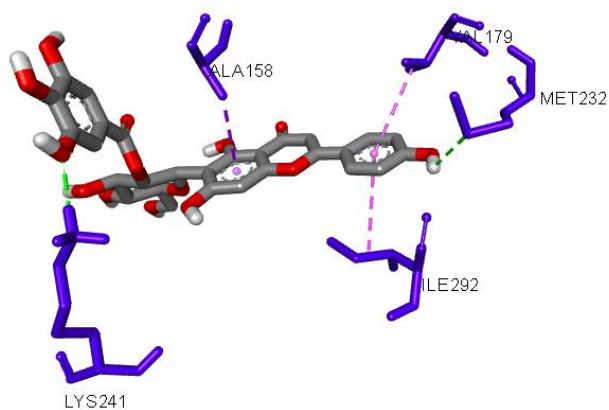
(a)



mode	affinity (kcal/mol)	dist from best mode rmsd l.b.	rmsd u.b.
1	-12.6	0.000	0.000
2	-12.6	2.237	2.722
3	-11.8	2.008	2.312
4	-11.4	2.441	3.174
5	-11.1	1.647	2.150
6	-10.9	4.095	9.419

Writing output ... done.

(b)



(c)

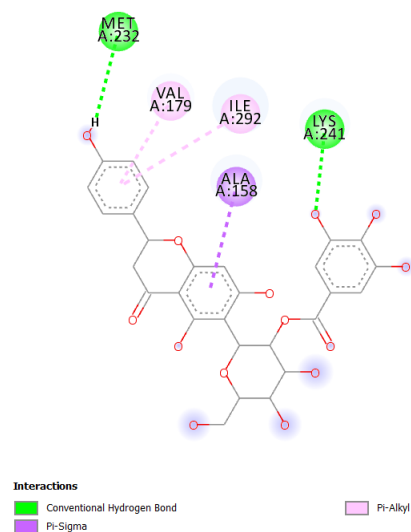


Figure 3.79 Predicted binding free energy (docking score) and detailed molecular interactions of isovitexin 2''-O-gallate (77) within the active site of *MtPknG*.

(a) Structure and docking scores of isovitexin 2''-O-gallate (77); predicted binding free energy of -12.6 kcal/mol. (b) Docked pose of (77) in the *MtPknG* binding site showing molecular interactions; hydrogen and hydrophobic bonds as green and pink/ purple dashed lines, respectively; (c) 2D plot of interactions between (77) and key residues of *MtPknG* generated by BIOVIA Discovery Studio visualizer

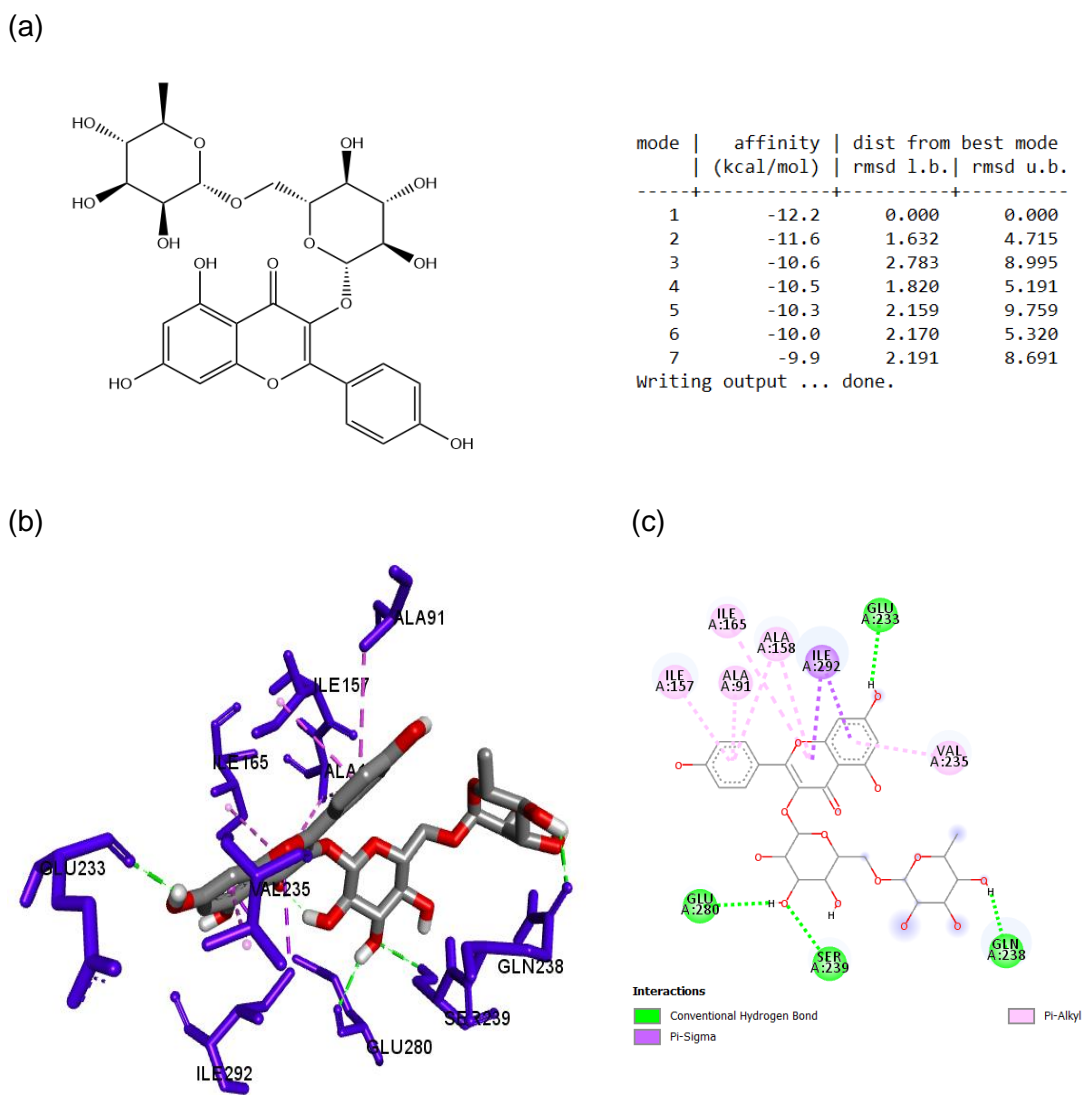
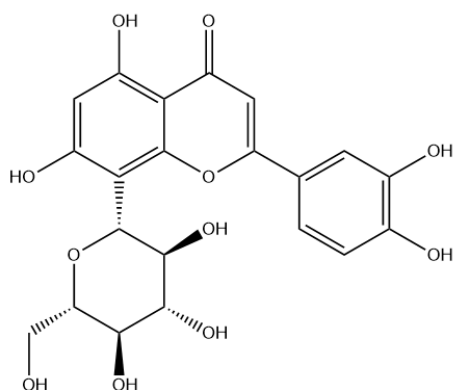


Figure 3.80 Predicted binding free energy (docking score) and detailed molecular interactions of kaempferol 3-O- β -D-rutinoside (nicotiflorin) (61**) within the active site of *MtPknG*.**

(a) Structure and docking scores of kaempferol 3-O- β -D-rutinoside (nicotiflorin) (**61**); predicted binding free energy of -12.2 kcal/mol. (b) Docked pose (**61**) in the *MtPknG* binding site showing molecular interactions; hydrogen and hydrophobic bonds as green and pink/ purple dashed lines, respectively; (c) 2D plot of interactions between (**61**) and key residues of *MtPknG* generated by BIOVIA Discovery Studio visualizer.

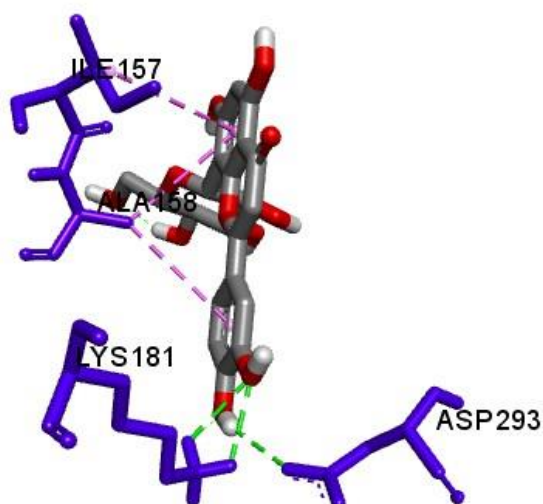
(a)



mode	affinity (kcal/mol)	dist from best mode rmsd l.b.	rmsd u.b.
1	-11.8	0.000	0.000
2	-11.2	1.847	2.735
3	-9.2	2.456	5.552
4	-9.2	2.578	4.152
5	-9.0	2.099	5.182
6	-9.0	2.406	2.866
7	-8.9	1.593	2.134

Writing output ... done.

(b)



(c)

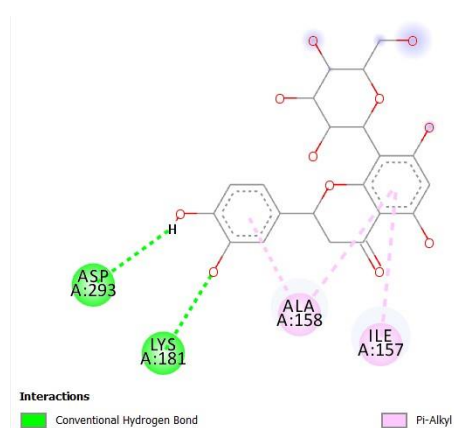


Figure 3.81 Predicted binding free energy (docking score) and detailed molecular interactions of orientin (74) within the active site of *MtPknG*.

(a) Structure and docking scores of orientin (74); predicted binding free energy of -11.8 kcal/mol. (b) Docked pose of (74) in the *MtPknG* binding site showing molecular interactions; hydrogen and hydrophobic bonds as green and pink/ purple dashed lines, respectively; (c) 2D plot of interactions between (74) and key residues of *MtPknG* generated by BIOVIA Discovery Studio visualizer

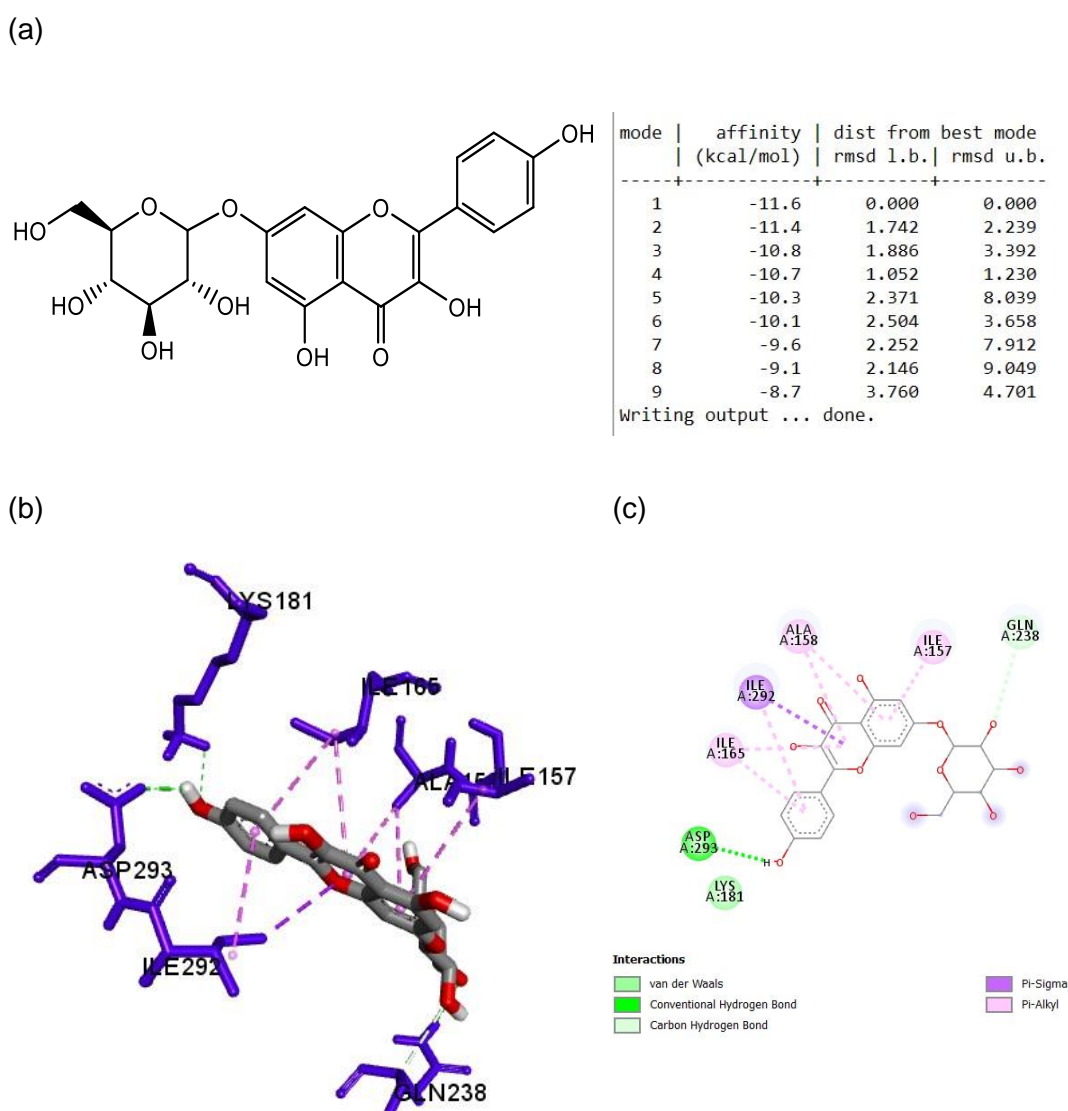


Figure 3.82 Predicted binding free energy (docking score) and detailed molecular interactions of kaempferol 7-O- β -D-glucoside (populnin) (60) within the active site of *MtPknG*.

(a) Structure and docking scores of kaempferol 7-O- β -D-glucoside (populnin) (60); predicted binding free energy of -11.6 kcal/mol. (b) Docked pose of (60) in the *MtPknG* binding site showing molecular interactions; hydrogen and hydrophobic bonds as green and pink/ purple dashed lines, respectively; (c) 2D plot of interactions between (60) and key residues of *MtPknG* generated by BIOVIA Discovery Studio visualizer.

3.7 Evaluation of the docking studies

Targeting the virulence factors of Mtb such as PKnG is an attractive strategy for the development of novel and effective drugs for the treatment of TB (Scherr *et al.*, 2009; Kanehiro *et al.*, 2018). Very few compounds have been reported as *MtPknG* inhibitors to date (Singh *et al.*, 2015). Only one molecular docking study targeting *MtPknG* (PDB ID: 2PZI) with plant natural products was found in the literature (Santhi and Aishwarya). This focussed on the molecular docking of forty withanolide derivatives from the medicinal plant *Withania somnifera* towards *MtPknG* with the identification of three potential withanolides (D, E and F) which showed best G-Score value of -7.86, -7.69, and -7.63, respectively in comparison with AX20017 (G-Score value of -5.63). These withanolides (D,E and F) formed hydrogen bonding with the residues Glu233, Val235, Gly237, Gln238, Ser239, Lys241, Ile292 and Ser293 of *MtPknG*, and hydrophobic interactions with Ala158, Ile165, Val179, Lys181, Met232, Ile292 and Asp293 (Santhi and Aishwarya, 2011). Another study reported on the marine-derived compound sclerotiorin, identified as an inhibitor of *MtPknG* (PDB ID: 4Y0X). It also reduced mycobacterial growth inside macrophages (IC₅₀ value of 76.5 μ M), showing no toxicity on mammalian cells (Chen *et al.*, 2017a).

Apart from natural products, another study evaluated a set of 2- aminopyrimidines as potential inhibitors of *MtPknG* based on the combination of pharmacophore-based virtual screening (docking using Surlex, Flex-X, and Autodock 4.2), molecular dynamics simulations, and biological evaluation. The compound NRB04248 was able to inhibit *MtPknG* by ADP-Glo kinase assay. It also inhibited the growth of *M. bovis* BCG and was nontoxic against the host's macrophages. NRB04248 was proposed to be explored for the further development of new and more potent inhibitors of *MtPknG* (Singh *et al.*, 2015).

In the present work, a molecular docking study, using Auto dock Vina, was conducted to evaluate the interactions between *MtPknG* and a range of phytochemicals isolated from two *Pelargonium* spp., *F. excelsior* and *S. arabica* in an attempt to discover some potential *MtPknG* inhibitors.

Vina is a popular docking program widely used to predict protein–ligand binding affinities and poses (Gaillard, 2018; Nguyen *et al.*, 2020). It is generally accepted that in virtual screening, once docking is completed, the resulting ligand binding pose is evaluated by scoring functions (here in vina; the predicted binding free energy), and

candidate ligands are ranked according to their predicted binding affinities. It should be noted that the ligand-target affinity prediction distinguishes active (strong-binding) ligands from inactive (weak-binding) ones (Park *et al.*, 2011; Jiang *et al.*, 2020; Pantsar and Poso, 2018; Li *et al.*, 2016).

Ligand efficiencies (LEs) were introduced to improve the outcome of docking scoring functions. In the present study, LE1 and LE2 were calculated as they were among the first ligand efficiency coefficients introduced to improve optimisation and lead selection in the drug discovery process. Size-independent LE (SILE) is preferred when a comparison across wide size ranges is required (Cavalluzzi *et al.*, 2017). However, great care should be taken when considering and applying these metrics, and in the interpretation of their values. For example, the relevance of LE1 as a metric has been challenged as it has some limitations, all non-hydrogen atoms (carbon; CH₃, nitrogen; NH₂, oxygen; OH, sulphur; S, and halogen: Cl or Br) are counted the same and treated equally without taking in consideration the differences in sizes and binding properties. Also, as mentioned earlier, it has been observed that the averaged values of LE1 are higher for small ligands compared to large ligands. These observations highlight that there is *not one* metric that correlates successfully without taking in consideration other metrics in the decision-making process (Murray *et al.*, 2014; Kenny *et al.*, 2014).

Drug discovery and development are complex processes. Researchers in this field are faced with challenges to establish parameters for better optimization and result validation. A common criticism against drug discovery and development rules and metrics is that they could limit the possibility of choices, and this might restrict the opportunities of finding out a new drug beyond the classical drug-likeness area (Kell, 2013).

In this study, the criteria for selection the top ranked ligands were based on giving the binding affinity the priority, taking into consideration SILE as the applicable ligand efficiency metric (because the examined phytochemicals showed a wide range of size (see appendix I). Being mindful of the fact that if there is no good affinity toward the target protein, it is worthless to go further even a superior values of LE1 and or LE2 were obtained compared to the control inhibitor.

It is worth mentioning that phytochemicals from the aerial parts of *Pelargonium reniforme/sidoides* showed promising docking scores. This in good agreement with

a previous report finding which reported that the medicinal use of *Pelargonium* aerial parts may be used as an alternative for its roots in the treatment of tuberculosis and other bacterial infections even though that the roots of the *Pelargonium* are traditionally used (Lewu *et al.*, 2006). Flavonoids showed better binding affinities towards MtPKnG than other phytochemicals. Coumarins, coumarin derivatives, and other phenolic compounds did not show any interesting binding affinity towards MtPKnG (Table 3.19 and 3.20).

Flavonoids are a large group of bioactive phytochemicals. They are able to target several enzymes essential for mycobacterium survival (Brown *et al.*, 2007; Yadav *et al.*, 2013; Zheng *et al.*, 2014; Sasikumar *et al.*, 2018), and have been reported as potential adjuvants in anti-TB therapy (Lechner *et al.*, 2008). Flavonoids also have the potential to overcome antimicrobial resistance as they exhibit antimicrobial activity via different mechanisms to conventional antibiotics. This includes by inhibiting virulence factors, efflux pumps, biofilm formation, bacterial motility, and by disrupting microbial cell membranes, cell wall and nucleic acid synthesis (Biharee *et al.*, 2020).

Several studies conducted on *Pelargonium* have revealed that the anti-TB potential of this herbal remedy is probably related to an indirect immunomodulatory effect (Kolodziej, 2011; Mativandlela *et al.*, 2007; Seidel and Taylor, 2004). One interesting finding is that it has been previously observed that the flavonoid quercetin-3-O- β -glucoside (**41**) from *P. reniforme* aqueous extract showed immunomodulatory activity and increased the intracellular killing of Mtb-infected macrophages (Kim *et al.*, 2009). In the present study, this flavonoid had a binding affinity of -9.8 kcal/mol and a SILE of 3.43. It has also previously been reported that quercetin (**62**) could effectively dock with the subunit B of DNA gyrase in *M. tuberculosis* and *M. smegmatis* using *in silico* analysis and effectively inhibited the bacilli *in vitro* (MIC = 100 μ g/mL) (Suriyanarayanan *et al.*, 2013).

Kaempferol 3-O-rutinoside (**61**) and quercetin 3-O-rutinoside (**63**) are among the top ranked ligands (Table 3.22). It is interesting to note that quercetin 3-O-rutinoside (**63**), kaempferol 3-O-rutinoside (**61**), and isorhamnetin 3-O-glucoside, three flavonoid glycosides from *Urtica dioica* (traditional plant used for the treatment of TB) also previously showed high intracellular Mtb killing activity (Akabay *et al.*, 2003).

Altogether, the results described in this study would suggest the possibility of exploring flavonoids further as they may represent an attractive class of plant NPs that warrant further biological investigation as potential *MtPKnG* inhibitors.

The analysis of the interaction pattern of selected docking poses indicated that the top ranked Ligands interacted via hydrogen bonding with amino acid residues of *MtPKnG* active site, including Val235, Ser239, Glu233, Glu280, Gln238, Gly237, Asp293, Lys181, Lys241, Ala158, Ile292, Met 232, and His 159. In addition, hydrophobic interactions with side chains of Ile165, Ile292, Ile157, Val 179, Val235 and Ala158, Ala91 of *MtPKnG* were also observed for all the examined ligands as illustrated in detailed Table 3.23 and Figure 3.76 to 3.81. Overall, the observed interactions shared a number of similarities with previously published findings (Santhi and Aishwarya, 2011). Intermolecular interactions such as hydrogen bond and hydrophobic interactions with amino acid residues play an important role for the ligand- protein complex stability (Pace *et al.*, 2011; De Freitas and Schapira, 2017; Hariono *et al.*, 2016; Patil *et al.*, 2010). The presence of hydrogen bond and hydrophobic interactions in the top ranked docked flavonoids with *MtPKnG* might contribute to the higher binding affinities compared to the control inhibitor AX20017. It remains to be confirmed whether any of these potential candidates will exert the any *in vitro/in vivo* activity.

When selected isolated phytochemicals (OA, UA, pinocembrin, and pheophytins,) were investigated for their interactions towards *MtPKnG* using Vina, the results were below expectations. Even though OA and UA were reported to successfully docked into potential Mtb target proteins other than *MtPKnG* (Jee *et al.*, 2018; Kataev *et al.*, 2018). Further investigations (*in vitro* and *in vivo* experiments) are still needed to validate these *in silico* results.

CHAPTER FOUR :
CONCLUSION AND FUTURE
WORK

4.0 CONCLUSION AND FUTURE WORK

4.1 Conclusion

This study was an attempt to discover some phytochemicals from a European plant (*Fraxinus excelsior*), a Jordanian plant (*Stachys arabica*), and two South African plants (*Pelargonium sidoides*/*Pelargonium reniforme*) as potential candidates for the design of new anti-TB drugs, and to assess their immunomodulatory effects that may be relevant to anti-TB activity. This was achieved through a combination of experimental (phytochemical and *in vitro* biological) and *in silico* screening (molecular docking) studies. The investigated plants were selected using ethno-guided and/or chemotaxonomical approaches.

Inflammation is considered as an essential element of the innate immune system to protect against inflammatory stimuli including pathogens. LPS induces the production of pro-inflammatory cytokines (TNF- α and IL-12) in monocytes, macrophages, and other immune cells. Pro-inflammatory cytokines (TNF- α and IL-12) are essential for an effective immune response against bacterial infections and have a crucial role in controlling TB in the early stage of infection. High and sustained levels of TNF- α and IL-12, however, are detrimental for the host and could lead to severe complications including tissue damage in TB patients. This emphasises the importance of the proper balance of pro-inflammatory cytokines (TNF- α and IL-12) production and well-regulated immune response against *Mtb*. Thus, it was decided in this study to investigate the effect of two plant (*Fraxinus excelsior* and *Stachys arabica*) extracts and selected isolated phytochemicals (oleanolic acid, ursolic acid, pinocembrin, pheophytin a (390RQ10), 13² (*R,S*)-hydroxy pheophytin a (390RQ27), and pheophytin b (390RQ28)) directly on the production of pro-inflammatory cytokines (TNF- α and IL-12) from LPS-stimulated THP-1 cells.

Plant material (*Fraxinus excelsior* leaves and *Stachys arabica* aerial parts) were extracted using solvent of increasing polarity (*n*-hexane, ethyl acetate, and methanol). The fractionation of the resulting extracts and subsequent purification using different chromatographic techniques led to the isolation of one flavonoid, two pentacyclic triterpenoids, squalene, three phytosterols, steryl fatty acid esters, phytyl fatty acid esters, three pheophytins, phenylethanoid esters, and a mixture of acyclic alkanes.

The structures of all isolated phytochemicals were established using a combination of MS and NMR techniques including 1D NMR (^1H , ^{13}C , DEPTQ) and 2D NMR (HSQC, HMBC).

A total of 28 phytochemicals were isolated and characterized from both plants (Figure 3.83). The phytochemical investigation of the *n*-hexane and ethyl acetate extracts of *F. excelsior* leaves (370) revealed the presence of 20 phytochemicals. Although they are all known compounds, sixteen phytochemicals are reported for the first time in the leaves of *F. excelsior* including oleanolic acid, squalene, pinocembrin, phenylethanoid esters include (4-hydroxyphenethyl dotriacontanoate, 4-hydroxyphenethyl triacontanoate, 4-hydroxyphenethyl octacosanoate, 4-hydroxyphenethyl hexacosanoate, and 4-hydroxyphenethyl tetracosanoate), phytol fatty acid esters (phytol palmitate and phytol oleate), β -sitosterol oleate and mixture of acyclic alkanes (heptacosane, octacosane, triacontane, dotriacontane and tritriacontane). Other phytochemicals including ursolic acid, phytol linolenate, nonacosane, and hentriacontane have been previously isolated from *F. excelsior* leaves.

Stachys arabica (390), which has not been previously phytochemically nor biologically investigated, contained seventeen known phytochemicals including pheophytins (pheophytin a, 13^2 (*R,S*)-hydroxy-pheophytin a, and pheophytin b), mixture of phytosterols (stigmasterol, β -sitosterol and campesterol), mixture of sterol fatty acid esters (β -sitosterol oleate & campesterol oleate), mixture of phytol fatty acid esters (phytol palmitate, phytol oleate) and mixture of acyclic alkanes (heptacosane, octacosane, nonacosane, triacontane, hentriacontane and tritriacontane). This is the first report of their isolation from *S. arabica*.

The results of the present study showed that two plant extracts (*Fraxinus excelsior* leaves and *Stachys arabica*) and selected isolated phytochemicals (oleanolic acid, ursolic acid, pinocembrin, pheophytin a (390RQ10), 13^2 (*R,S*)-hydroxy pheophytin a (390RQ27), and pheophytin b (390RQ28)) were able to suppress the production of pro-inflammatory cytokines (namely TNF- α and IL-12) from LPS-stimulated THP-1 cells (Table 3.24). Based on previous reports discussed earlier, the possible mechanism of action might involve blocking signalling pathways (NF- κ B and MAPK) and/or inhibiting LPS binding to toll like receptor (TLR4). Further experiments are still required to confirm the exact mode of action.

F. excelsior leaves and *S. arabica* aerial parts showed *in vitro* anti-inflammatory activity by suppressing the production of pro-inflammatory cytokines (TNF- and IL-12) from LPS-stimulated THP-1 cells. These preliminary findings support to some extent the therapeutic potential of these plants for complications associated with inflammation including TB as adjunct host therapy.

The PknG enzyme, produced by *Mycobacterium tuberculosis*, is known to block phagosome lysosome fusion in the host's macrophages. This has been identified as an effective survival strategy for this pathogen. Targeting *MtPknG* could be a promising strategy in screening of anti-TB drugs and tackle *Mtb* infection. In this study, a molecular docking approach was used to predict the binding affinity and the molecular interactions of phytochemicals from the roots and aerial parts of *Pelargonium reniforme* and *Pelargonium sidoides* with *MtPknG*. The results revealed that flavonoids such as isorientin 2"-O-gallate (**79**), isovitexin 2"-O-gallate (**77**), nicotiflorin (**61**), orientin (**74**) and populnin (**60**) were able to bind to the active site of *MtPknG* and displayed highest binding affinities towards *MtPknG* compared to the re-docked control inhibitor AX20017. However, further *invitro* and *in vivo* experiments are required to validate these *in silico* results for the development and design of new *MtPknG* inhibitors as anti-TB drugs.

Graphical summary of the present study was illustrated in Figure 3.83

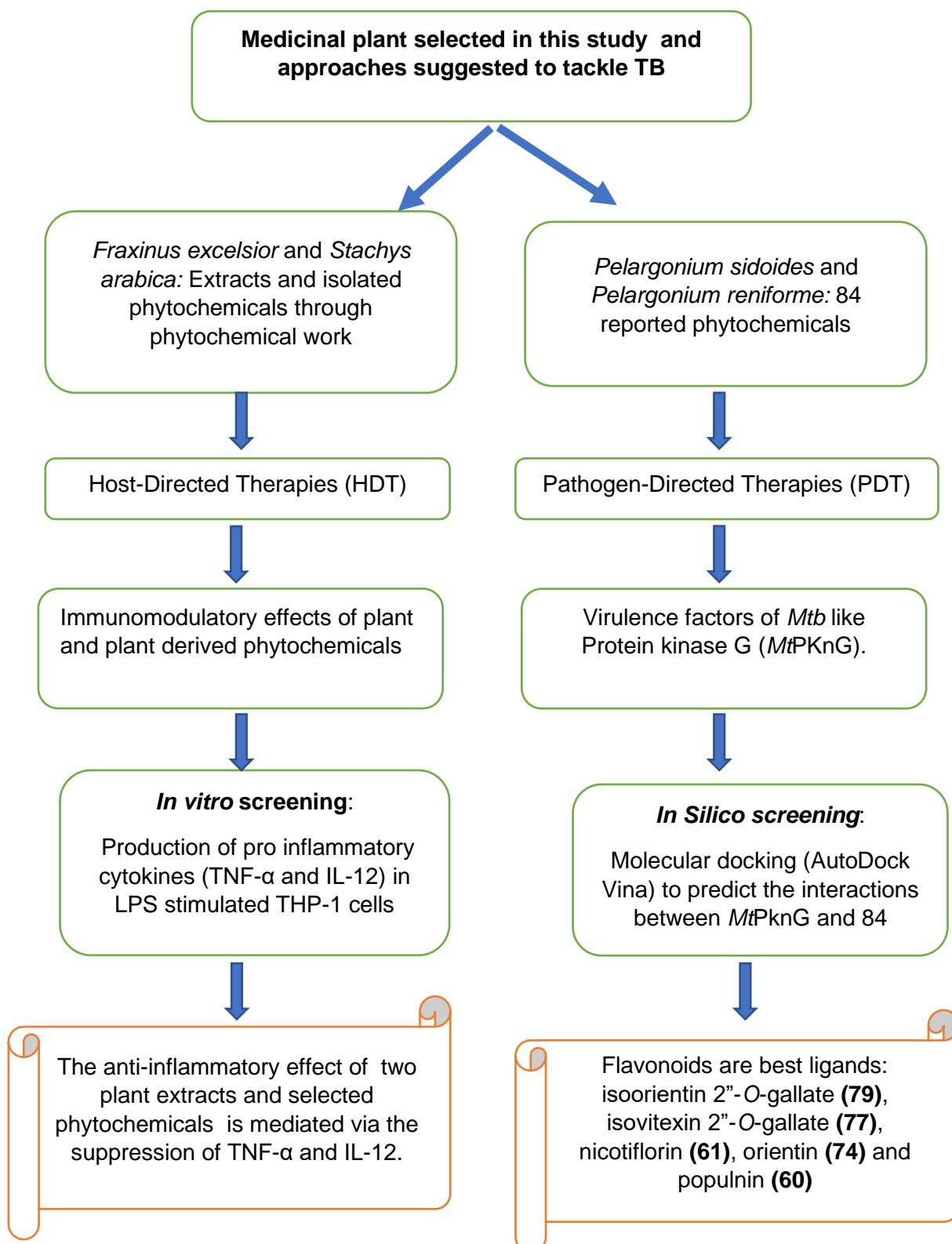


Figure 3.83 Graphical summary of the present study.

Table 3.24 Summary of biology results (IC₅₀ values & observed effect on cytokines production from LPS stimulated THP-1 cells)

Code	Sample/Treatment used	IC₅₀ (µg/mL)	TNF- α	IL-12
370H	Hexane extract of <i>F. excelsior</i>	57µg/mL	↓	↓
370E	Ethyl acetate extract of <i>F. excelsior</i>	40 µg/mL	↓	↓
370M	Methanol extract of <i>F. excelsior</i>	125 µg/mL	↓	↓
390H	Hexane extract of <i>S. arabica</i>	87 µg/mL	↓	↓
390E	Ethyl acetate extract <i>S. arabica</i>	50 µg/mL	↓	↓
390M	Methanol extract of <i>S. arabica</i>	>250 µg/mL	↓	↓
370RQ19	Mixture of phenylethanoid esters	>250 µg/mL	<i>No effect</i>	<i>No effect</i>
OA	Oleanolic acid	200 µM	↓	↓
UA	Ursolic acid	62 µM	↓	↓
370RQ20	Pinocebrin	179 µM	↓	↓
390RQ10	Pheophytin a	187 µM	↓	↓
390RQ27	13 ² (<i>R,S</i>)-hydroxy pheophytin a	41 µM	↓	↓
390RQ28	Pheophytin b	40 µM	↓	↓

4.2 Recommendations for future work

The present study revealed some promising outcomes in the field of plant-derived natural product chemistry. This study suggests future investigations which deserve further consideration including:

- Conducting a phytochemical investigation on the methanolic extract of *Fraxinus excelsior* and *Stachys arabica* to characterise the isolated phytochemicals and evaluate their immunomodulatory effect on cytokine production in LPS-stimulated THP-1 cells.
- Performing *in vitro* kinase assays to evaluate the inhibitory activity of the identified *Pelargonium* flavonoids and validate the results of the docking study.
- Screening *Fraxinus excelsior* and *Stachys arabica* extracts and phytochemicals (oleanolic acid, ursolic acid, pinocembrin, pheophytins, and phytochemicals identified from the methanolic extracts) using *in vitro* kinase assays to evaluate their inhibitory activity against *MtPknG*.

APPENDICES

APPENDICES

Appendix I:

List of natural products isolated from the roots of *Pelargonium reniforme* and *Pelargonium sidoides*

Code	Compound	CAS ID	Molecular formula	M.wt
Phenolic acid and phenylpropanoids derivatives				
1	Gallic acid	149-91-7	C ₇ H ₆ O ₅	170.1
2	Gallic acid methyl ester	99-24-1	C ₈ H ₈ O ₅	184.1
3	<i>p</i> -hydroxybenzoic acid	99-96-7	C ₇ H ₆ O ₃	142.1
4	Protocatechuic acid	99-50-3	C ₇ H ₆ O ₄	154.1
5	Vanillic acid	121-34-6	C ₈ H ₈ O ₄	168.1
6	Caffeic acid	501-16-6	C ₉ H ₈ O ₄	180.2
7	Ferulic acid	1135-24-6	C ₁₀ H ₁₀ O ₄	194.2
8	<i>p</i> -coumaric acid	7400-08-0	C ₉ H ₈ O ₃	164.2
9	<i>p</i> -coumaraldehyde	2538-87-6	C ₉ H ₈ O ₂	148.2
10	Shikimic acid 3-O-gallate	95719-51-0	C ₁₄ H ₁₄ O ₉	326.3
Coumarin, Coumarin glycosides and Coumarin sulfates				
11	7-hydroxy-6-methoxycoumarin (Scopoletin)	92-61-5	C ₁₀ H ₈ O ₄	192.2
12	7-hydroxy-5,6-dimethoxycoumarin (Umckalin)	43053-62-9	C ₁₁ H ₁₀ O ₅	222.2
13	7-acetoxy-5,6-dimethoxycoumarin	43053-61-8	C ₁₃ H ₁₂ O ₆	264.2
14	5,6,7-trimethoxycoumarin	55085-47-7	C ₁₂ H ₁₂ O ₅	236.2
15	6-hydroxy-5,7-dimethoxycoumarin (Fraxinol)	486-28-2	C ₁₁ H ₁₀ O ₅	222.2
16	5,6-dihydroxy-7-dimethoxycoumarin (Isofraxetin)	50656-75-2	C ₁₀ H ₈ O ₅	208.2
17	6,7,8-trihydroxycoumarin	114371-80-1	C ₉ H ₆ O ₅	194.1
18	6,8-dihydroxy-7-methoxycoumarin	167105-91-1	C ₁₀ H ₈ O ₅	208.2

(Cont). List of natural products isolated from the roots of *Pelargonium reniforme* and *Pelargonium sidoides*

Code	Compound	CAS ID	Molecular formula	M.wt
19	8-hydroxy-6,7-dimethoxycoumarin (Fraxidin)	525-21-3	C ₁₁ H ₁₀ O ₅	222.2
20	7,8-dihydroxy-6-methoxycoumarin (Fraxetin)	574-84-5	C ₁₀ H ₈ O ₅	208.2
21	6,8-dihydroxy-5,7-dimethoxycoumarin	167105-92-2	C ₁₁ H ₁₀ O ₆	238.2
22	5,6,7,8-tetramethoxycoumarin (Artelin)	66173-52-2	C ₁₅ H ₁₈ O ₅	278.3
23	8-hydroxy-5,6,7-trimethoxycoumarin	309751-57-3	C ₁₂ H ₁₂ O ₆	252.2
24	Magnolioside	20186-29-2	C ₁₆ H ₁₈ O ₉	354.3
25	Isofraxoside	24778-11-8	C ₁₆ H ₁₈ O ₁₀	370.3
26	Umckalin-7-β -D-glucoside	--	C ₁₇ H ₁₅ O ₁₀	379.0
27	5,6-dimethoxycoumarin-7-sulfate	309751-58-4	C ₁₁ H ₁₀ O ₈ S	302.3
28	6,7-dihydroxycoumarin-8-sulfate	866630-10-6	C ₉ H ₆ O ₈ S	274.2
29	6-hydroxy-5,7-dimethoxycoumarin-8-sulfate	309751-60-8	C ₁₁ H ₁₀ O ₉ S	318.3
30	8-hydroxy-5,7-dimethoxycoumarin-6-sulfate	309751-62-0	C ₁₁ H ₁₀ O ₉ S	318.3
31	6-methoxycoumarin-7-sulfate	116532-46-8	C ₁₀ H ₈ O ₇ S	272.2
32	7,8-dihydroxy-5,6-dimethoxycoumarin	1116055-84-5	C ₁₁ H ₁₀ O ₆	238.2
33	7-hydroxy-5,6-dimethoxycoumarin-8-sulfate	1071422-88-2	C ₁₁ H ₁₀ O ₉ S	318.3
34	7,8-dihydroxycoumarin-6-sulfate	873188-79-5	C ₉ H ₆ O ₈ S	274.2

(Cont). List of natural products isolated from the roots of *Pelargonium reniforme* and *Pelargonium sidoides*

Code	Compound	CAS ID	Molecular formula	M.wt
35	7-hydroxycoumarin-6,8-bisulfate	873188-78-4	C ₉ H ₆ O ₁₁ S ₂	354.3
36	7-hydroxy-6-methoxycoumarin-8-sulfate	1232043-09-2	C ₁₀ H ₈ O ₈ S	288.2
37	8-hydroxy-7-methoxycoumarin-6-sulfate	1232043-12-7	C ₁₀ H ₈ O ₈ S	288.2
38	7-methoxycoumarin-6,8-bisulfate	1232043-14-9	C ₁₀ H ₈ O ₁₀ S ₂	352.3
Flavonoids and flavan-3-ols				
39	Kaempferol-3-O-β-D-glucoside (Astragalin)	480-10-4	C ₂₁ H ₂₀ O ₁₁	448.4
40	Kaempferol-3-O-β-D-galactoside (Trifolin)	23627-87-4	C ₂₁ H ₂₀ O ₁₁	448.4
41	Quercetin-3-O-β-D-glucoside (Isoquercetin)	482-35-9	C ₂₁ H ₂₀ O ₁₂	464.4
42	Myricetin-3-O-β-D-glucoside (Isomericitrin)	19833-12-6	C ₂₁ H ₂₀ O ₁₃	480.4
43	Afzelechin	2545-00-8	C ₁₅ H ₁₄ O ₅	274.3
44	Catechin	154-23-4	C ₁₅ H ₁₄ O ₆	290.3
45	Gallocatechin	970-73-0	C ₁₅ H ₁₄ O ₇	306.3
Miscellaneous				
46	Reniformin	1006039-05-9	C ₂₈ H ₄₀ O ₆ S	504.7
47	β-sitosterol	83-46-5	C ₂₉ H ₅₀ O	414.7
48	β-sitosterol-3-O-β-D-glucoside	474-58-8	C ₃₅ H ₆₀ O ₆	576.9

List of natural products isolated from the aerial parts of *Pelargonium reniforme* and *Pelargonium sidoides*

Code	Compound	CAS ID	Molecular formula	M.wt
Phenolic acid and phenylpropanoids derivatives				
49	Gallic acid ethyl ester	831-61-8	C ₉ H ₁₀ O ₅	198.2
50	Gallic acid butyl ester	1083-41-6	C ₁₁ H ₁₄ O ₅	226.2
51	Shikimic acid 3,5-di- <i>O</i> -gallate	95753-52-9	C ₂₁ H ₁₈ O ₁₃	478.4
52	<i>p</i> -Hydroxyphenyl ethanol	501-94-0	C ₈ H ₁₀ O ₂	138.2
53	<i>p</i> -Hydroxyphenyl acetic acid	156-38-7	C ₈ H ₈ O ₃	152.2
54	<i>p</i> -Hydroxybenzyl alcohol	623-05-2	C ₇ H ₈ O ₂	124.2
55	<i>p</i> -coumaroyl-4- <i>O</i> - β -D-glucoside	7139-64-2	C ₁₅ H ₁₈ O ₈	326.3
56	Glycerol-1-gallate	59634-75-2	C ₁₀ H ₁₂ O ₇	244.2
57	Glucogallin	554-37-0	C ₁₃ H ₁₆ O ₁₀	332.3
58	(α,β)-3,4-Di- <i>O</i> -galloylglucopyranoside	23363-08-8	C ₂₀ H ₂₀ O ₁₄	484.4
59	Salidroside-6"- <i>O</i> -gallate	83013-86-9	C ₂₁ H ₂₄ O ₁₁	452.4
Flavonoids				
60	Kaempferol 7- <i>O</i> - β -D-glucoside (Populnin)	16290-07-6	C ₂₁ H ₂₀ O ₁₁	448.1
61	Kaempferol 3- <i>O</i> - β -D-rutinoside (Nicotiflorin)	17650-84-9	C ₂₇ H ₃₀ O ₁₅	594.1
62	Quercetin	117-39-5	C ₁₅ H ₁₀ O ₇	302.0
63	Quercetin 3- <i>O</i> - β -D-rutinoside (Rutin)	153-18-4	C ₂₇ H ₃₀ O ₁₆	610.2
64	Quercetin 7- <i>O</i> - β -D-glucoside (Quercimeritrin)	491-50-9	C ₂₁ H ₂₀ O ₁₂	464.1
65	Dihydrokaempferol (Aromadendrin)	480-20-6	C ₁₅ H ₁₂ O ₆	288.1
66	Dihydrokaempferol 3- <i>O</i> - β -D-glucoside	31049-08-8	C ₂₁ H ₂₂ O ₁₁	450.4
67	Dihydroquercetin (Taxifolin)	480-18-2	C ₁₅ H ₁₂ O ₇	304.1
68	Taxifolin-7- <i>O</i> - β -D-glucoside	14292-40-1	C ₂₁ H ₂₂ O ₁₂	466.1

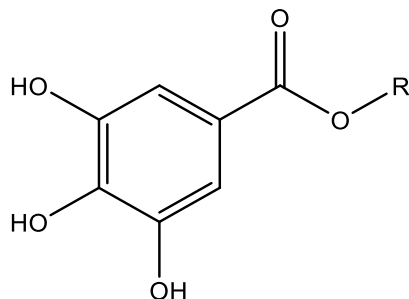
Cont. List of Natural products isolated from the aerial parts of *Pelargonium reniforme* and *Pelargonium sidoides*

Code	Compound	CAS ID	Molecular formula	M.wt
69	Taxifolin-3-O-β-D-glucoside	27297-45-6	C ₂₁ H ₂₂ O ₁₂	466.1
70	Narnigenin-7-O-β-D-glucoside (Prunin)	529-55-5	C ₂₁ H ₂₂ O ₁₀	434.1
71	Luteolin-7-O-β-D-glucoside (Glucoluteolin)	5373-11-5	C ₂₁ H ₂₀ O ₁₁	448.4
72	Vitexin	3681-93-4	C ₂₁ H ₂₀ O ₁₀	432.1
73	Vitexin 2"-O-gallate	267883-59-0	C ₂₈ H ₂₄ O ₁₄	584.1
74	Orientin	28608-75-5	C ₂₁ H ₂₀ O ₁₁	448.1
75	Orientin 2"-O-gallate	438000-12-5	C ₂₈ H ₂₄ O ₁₅	600.1
76	Isovitexin	38953-85-4	C ₂₁ H ₂₀ O ₁₀	432.1
77	Isovitexin 2"-O-gallate	267883-58-9	C ₂₈ H ₂₄ O ₁₄	584.1
78	Isoorientin	4261-42-1	C ₂₁ H ₂₀ O ₁₁	448.1
79	Isoorientin 2"-O-gallate	438000-11-4	C ₂₈ H ₂₄ O ₁₅	600.1
80	Epigallocatechin-3-O-gallate	989-51-5	C ₂₂ H ₁₈ O ₁₁	458.4
Miscellaneous				
81	Brevifolin carboxylic acid	18490-95-4	C ₁₃ H ₈ O ₈	292.2
82	Phyllanthusiin E	142674-53-1	C ₁₃ H ₈ O ₈	292.2
83	Phyllanthusiin E O-methyl ester	PubChem CID 102509857	C ₁₄ H ₁₀ O ₈	306.2
84	4,6-Dihydroxyacetophenone 2-O-β-D-glucoside	26089-54-3	C ₁₄ H ₁₈ O ₉	330.3

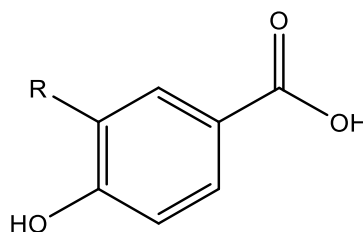
All the data are extracted from SciFinder (<https://www.cas.org/products/scifinder>), PubChem (<http://www.pubchem.ncbi.nlm.nih.gov>), (Hauer *et al.*, 2010; Kolodziej *et al.*, 2002; Kolodziej, 2007).

Chemical structures of natural products Isolated from *P. reniforme* and *P. sidoides*

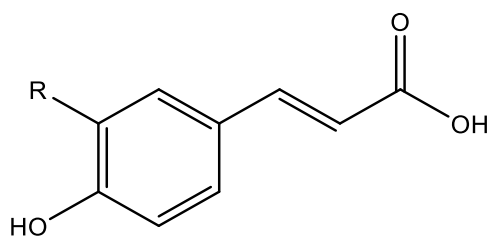
Chemical structures of phenolic acid and phenylpropanoid derivatives present in *P. reniforme/sidoides* roots (1-10) and aerial parts (49 -59)



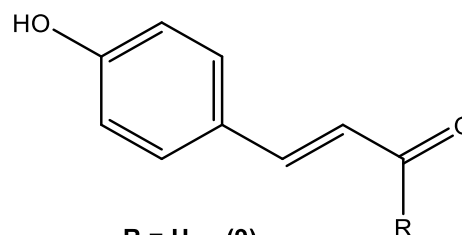
R = H (1)
R = Methyl (2)
R = Ethyl (49)
R = Butyl (50)



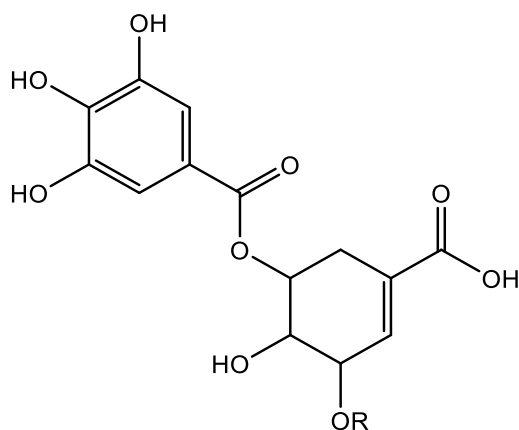
R = H (3)
R = OH (4)
R = OCH₃ (5)



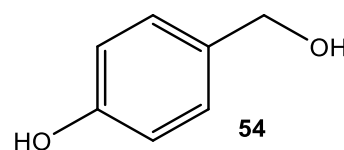
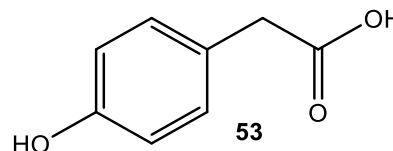
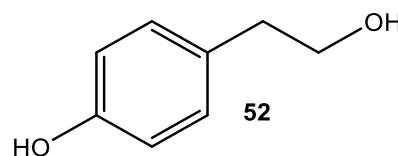
R = H (8)
R = OH (6)
R = OCH₃ (7)

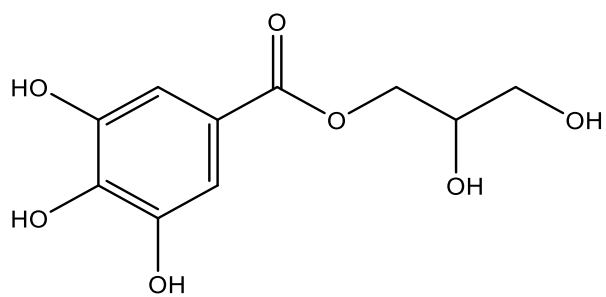


R = H (9)
R = OGlu (55)

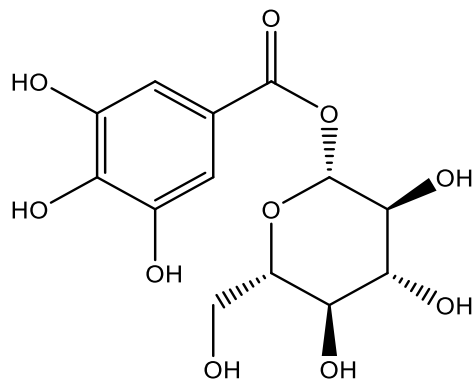


R = H (10)
R = Gallate (51)

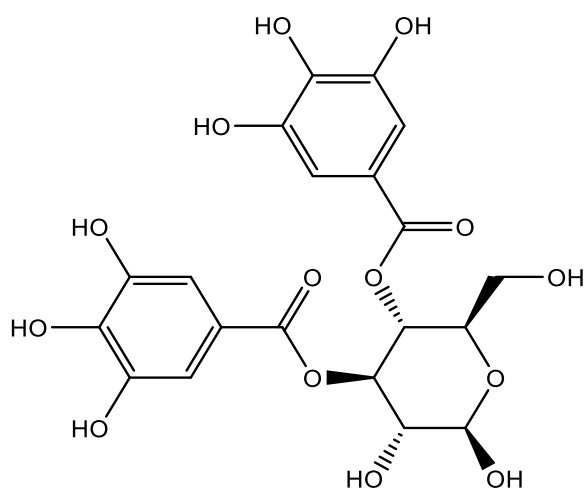




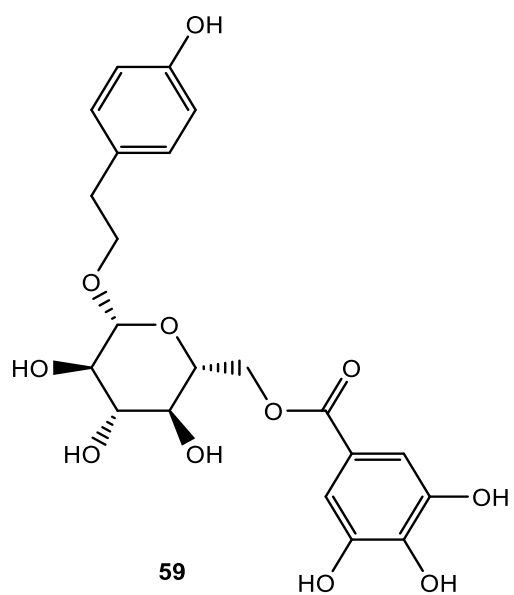
56



57

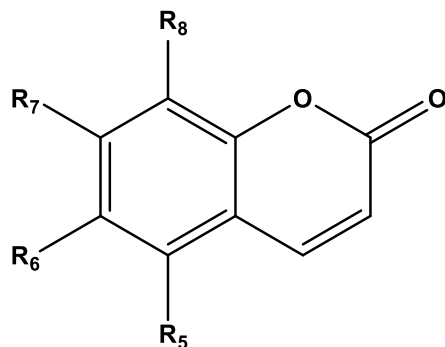


58



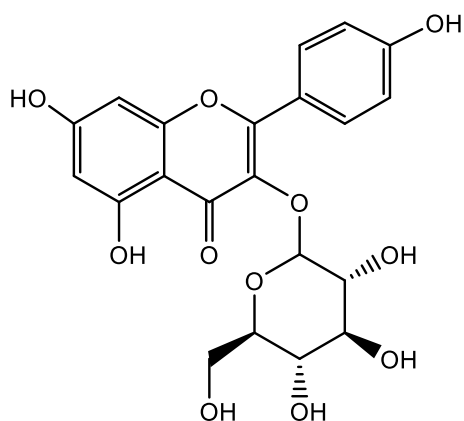
59

Chemical structures of coumarins and derivatives present in *P. reniforme/sidooides* roots (11) to (38)

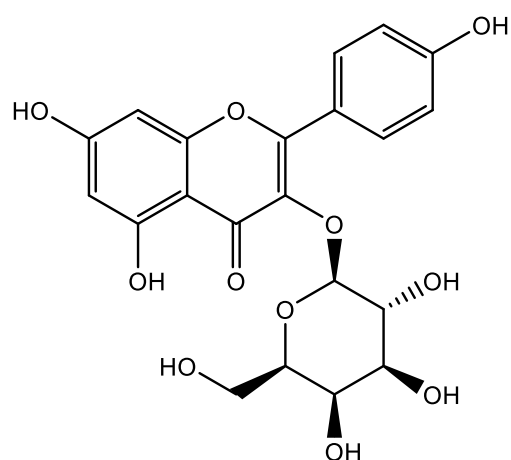


Compound	R ₅	R ₆	R ₇	R ₈
Coumarin				
11	H	OCH ₃	OH	H
12	OCH ₃	OCH ₃	OH	H
13	OCH ₃	OCH ₃	OAC	H
14	OCH ₃	OCH ₃	OCH ₃	H
15	OCH ₃	OH	OCH ₃	H
16	OH	OH	OCH ₃	H
17	H	OH	OH	OH
18	H	OH	OCH ₃	OH
19	H	OCH ₃	OCH ₃	OH
20	H	OCH ₃	OH	OH
21	OCH ₃	OH	OCH ₃	OH
22	OCH ₃	OCH ₃	OCH ₃	OCH ₃
23	OCH ₃	OCH ₃	OCH ₃	OH
Coumarin glycosides				
24	H	OGlc	OCH ₃	H
25	OH	OCH ₃	OGlc	OH
26	OCH ₃	OCH ₃	OGlc	H
Coumarin sulfates				
27	OCH ₃	OCH ₃	OSO ₃ H	H
28	H	OH	OH	OSO ₃ H
29	OCH ₃	OH	OCH ₃	OSO ₃ H
30	OCH ₃	OSO ₃ H	OCH ₃	OH
31	H	OCH ₃	OSO ₃ H	H
32	OCH ₃	OCH ₃	OH	OH
33	OCH ₃	OCH ₃	OH	OSO ₃ H
34	H	OSO ₃ H	OH	OH
35	H	OSO ₃ H	OH	OSO ₃ H
36	H	OCH ₃	OH	OSO ₃ H
37	H	OSO ₃ H	OCH ₃	OH
38	H	OSO ₃ H	OCH ₃	OSO ₃ H

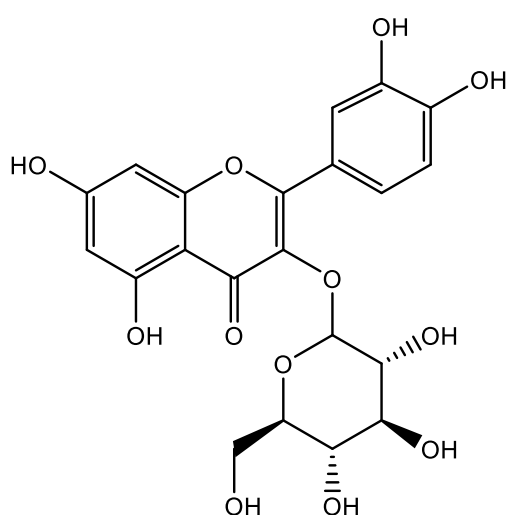
Chemical structures of flavonoids present in *P. reniforme/sidoides* roots (39-45) and aerial parts (60 -80)



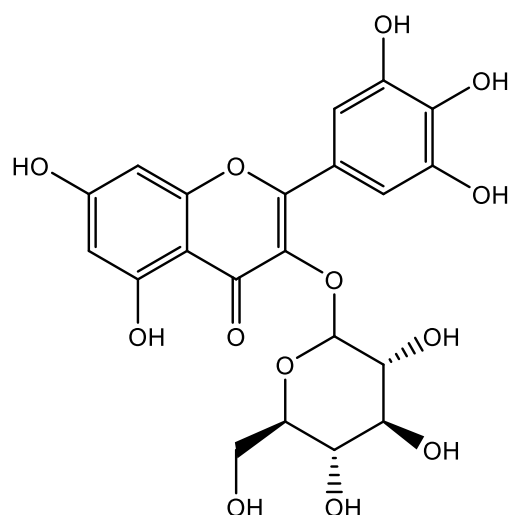
39



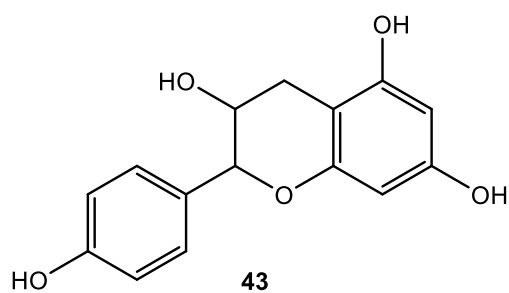
40



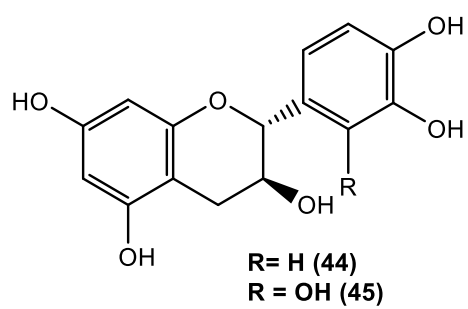
41

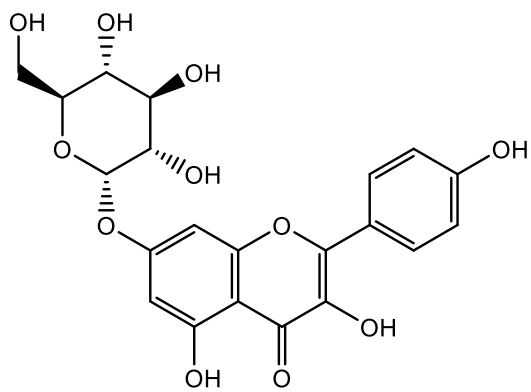


42

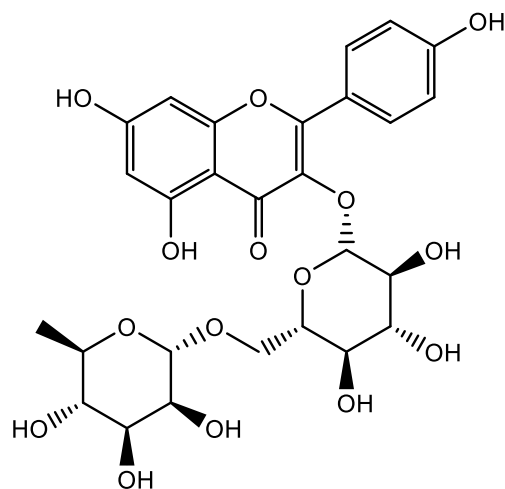


43

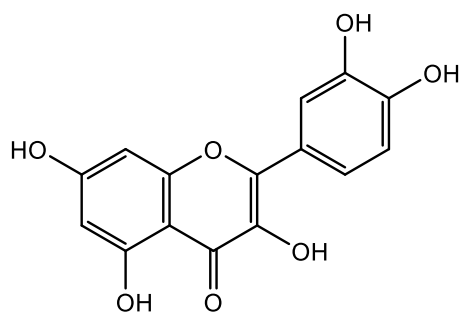




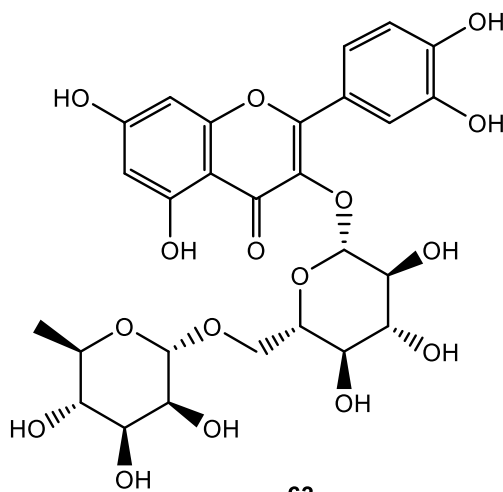
60



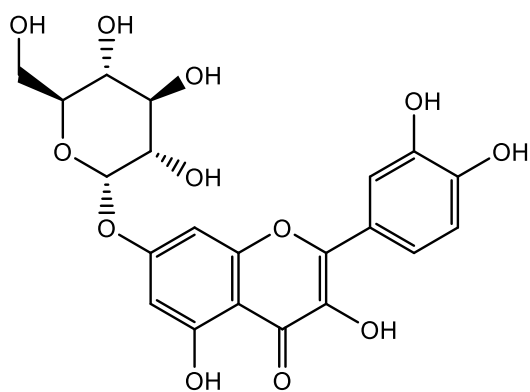
61



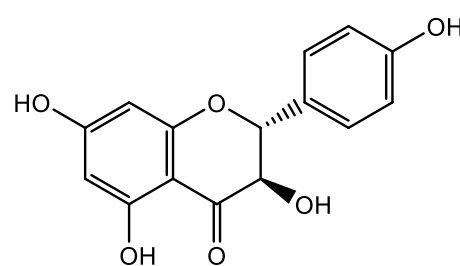
62



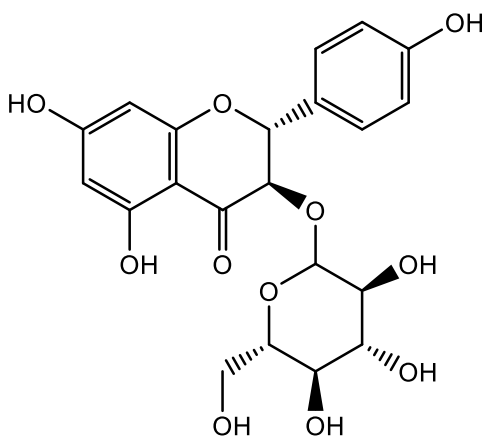
63



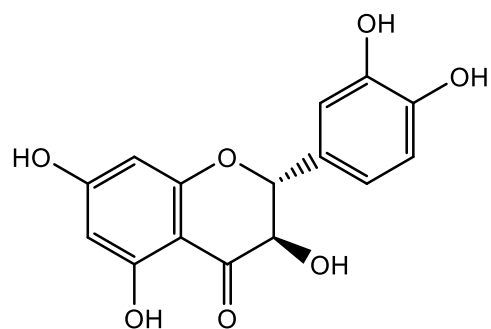
64



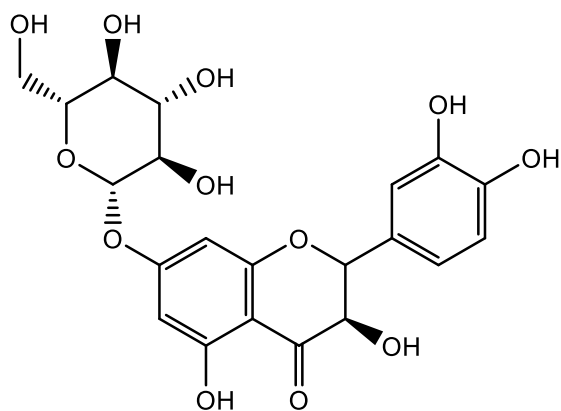
65



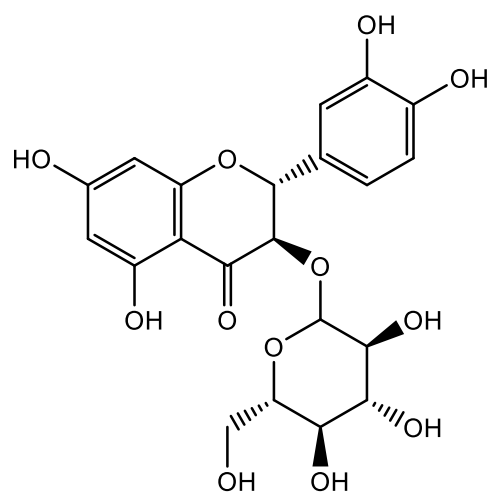
66



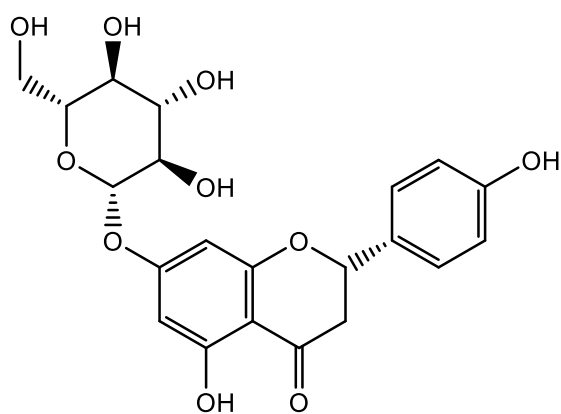
67



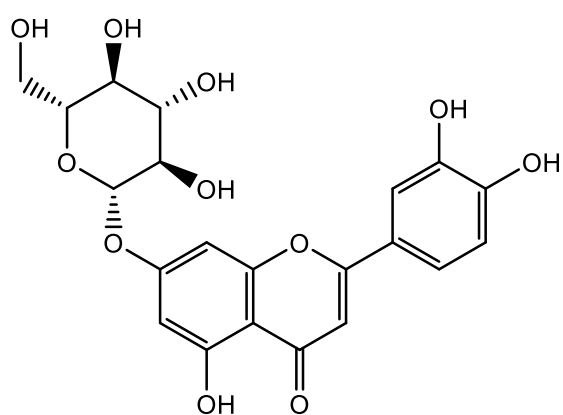
68



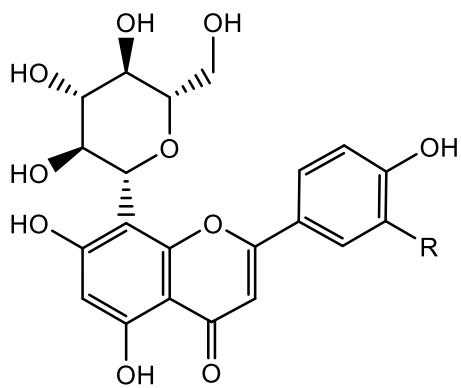
69



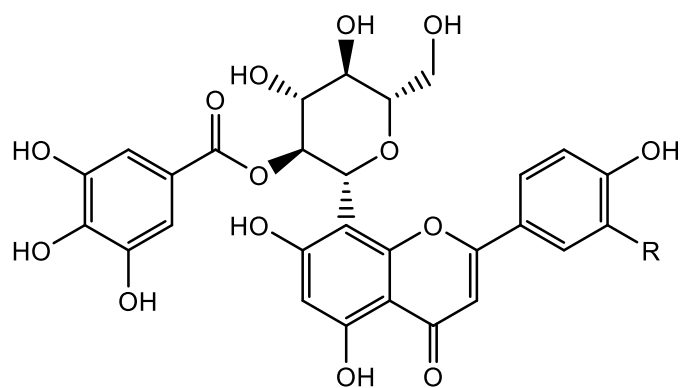
70



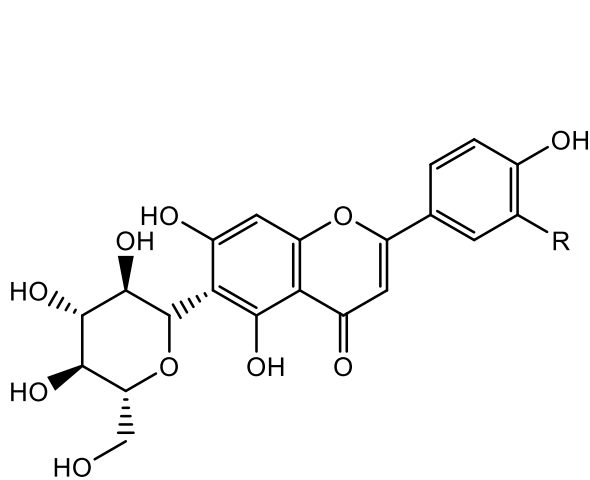
71



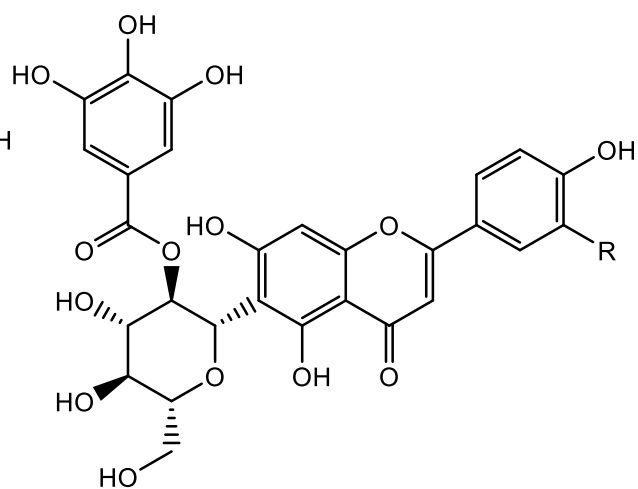
R=H (72)
R= OH (74)



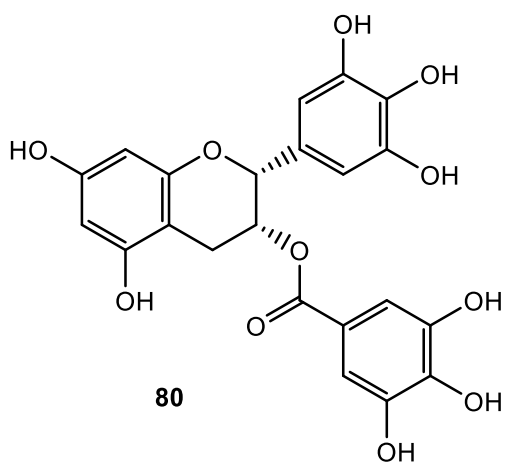
R=H (73)
R= OH (75)



R=H (76)
R= OH (78)

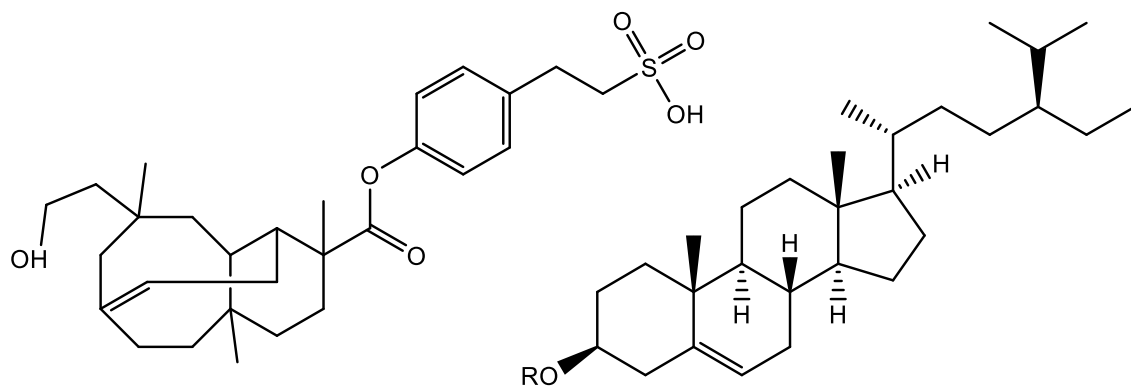


R=H (77)
R= OH (79)



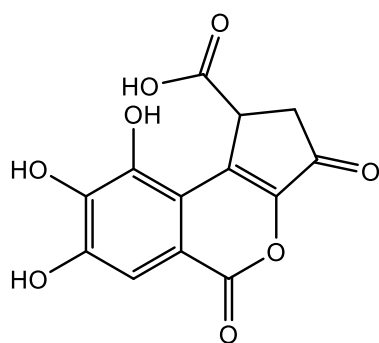
80

Chemical structures of miscellaneous NPs present in *P. reniforme/sidoides* roots (46-48) and aerial parts (81 -84)

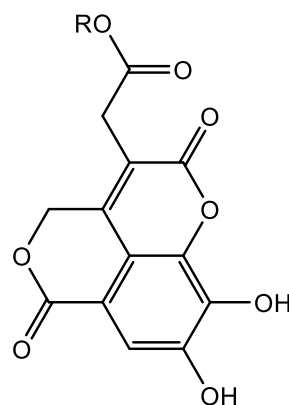


46

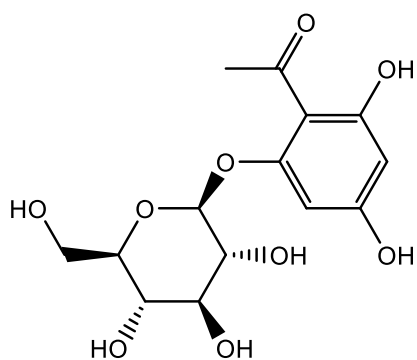
**R = H (47)
R = Glu (48)**



81



**R = H (82)
R = Me (83)**



84

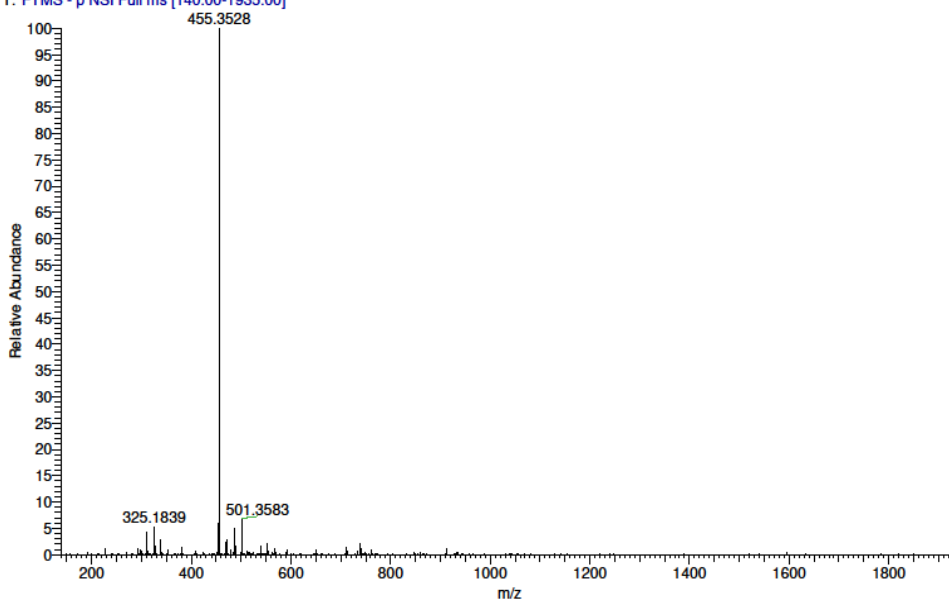
Appendix II: Mass Spectrometry Results

370RQ2 MW=456? C30H48O3
(DCM)/MeOH+DEA

NMSF, Swansea
LTQ Orbitrap XL

Veronique Seidel
16/11/2020 12:34:49

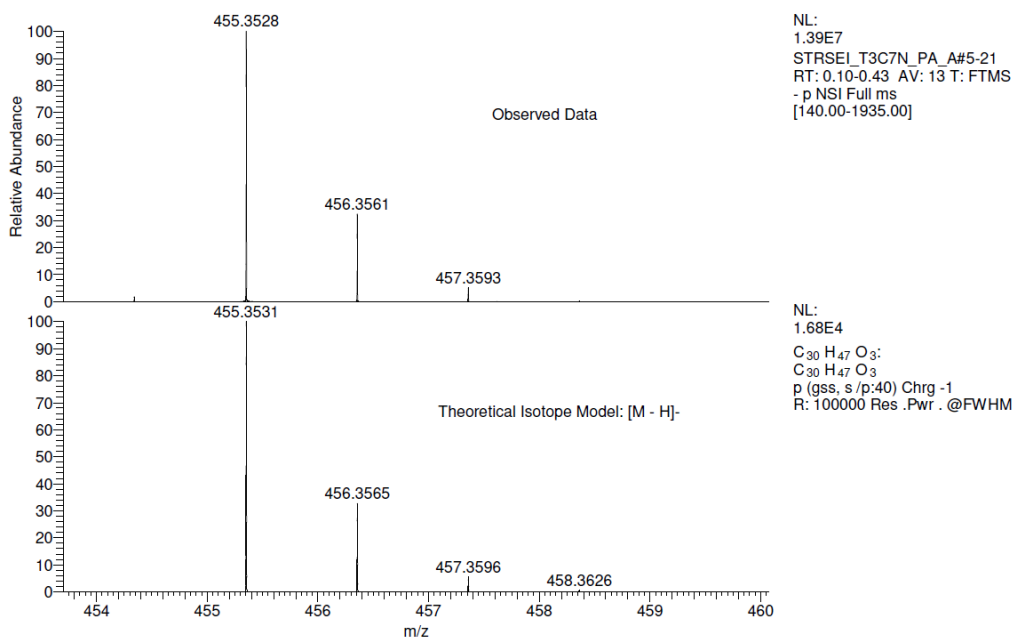
STRSEL_T3C7N_PA_A#5-21 RT: 0.10-0.43 AV: 13 NL: 1.39E7
T: FTMS - p NSI Full ms [140.00-1935.00]



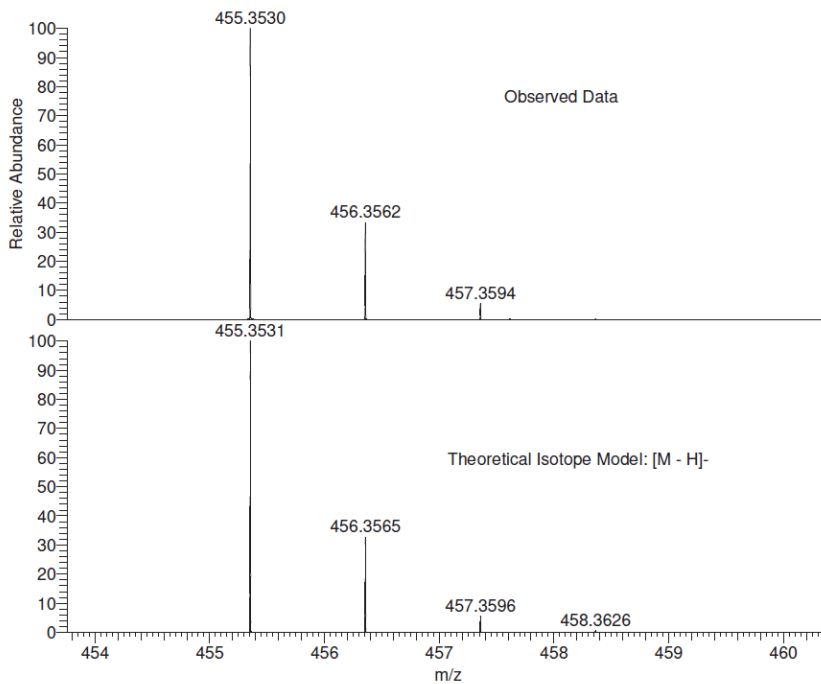
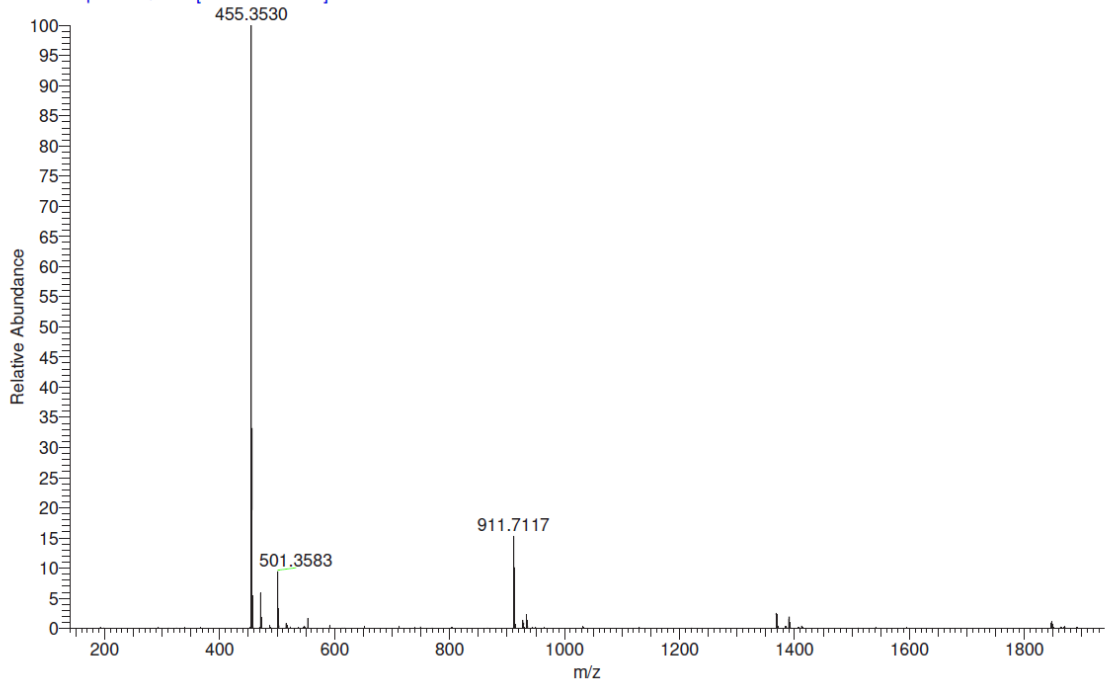
370RQ2 MW=456? C30H48O3
(DCM)/MeOH+DEA

NMSF, Swansea
LTQ Orbitrap XL

Veronique Seidel
16/11/2020 12:34:49



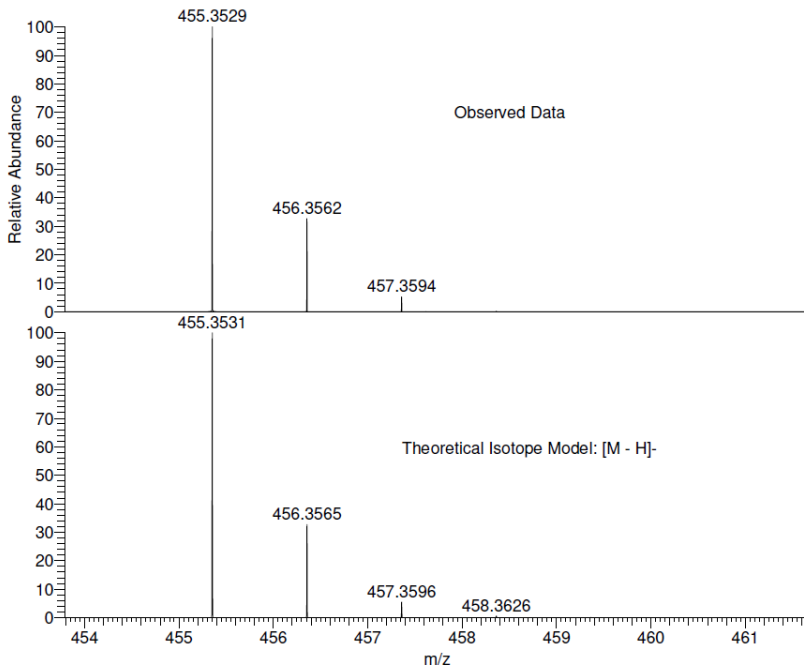
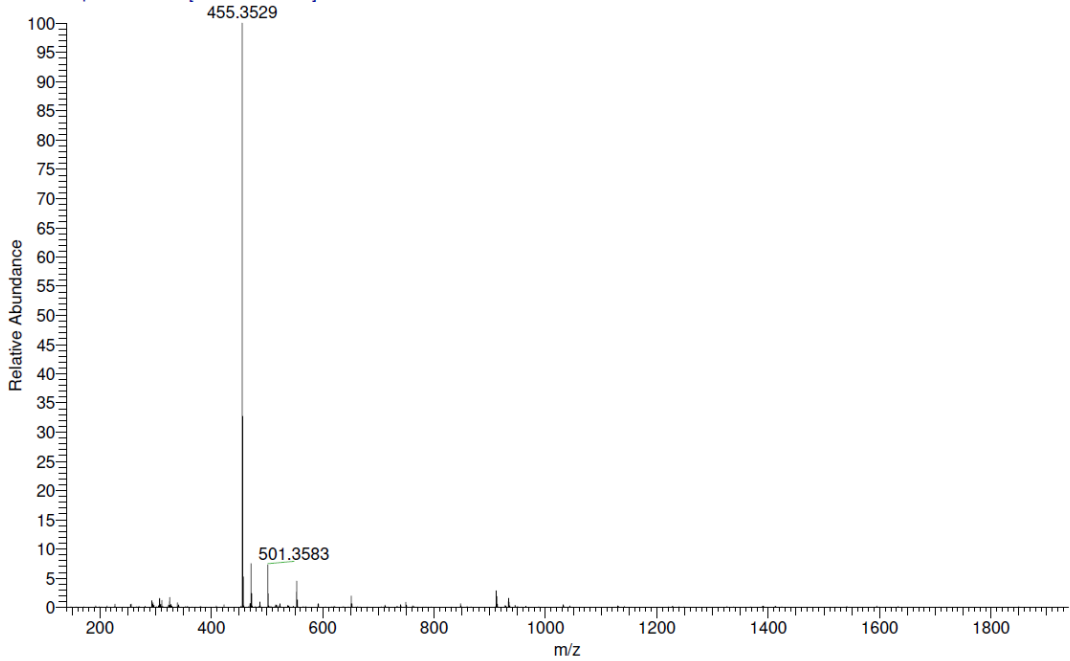
STRSEI_T3C3A_PA_A#4-20 RT: 0.07-0.43 AV: 13 NL: 6.69E7
T: FTMS - p NSI Full ms [140.00-1935.00]



NL:
6.69E7
STRSEI_T3C3A_PA_A#4-20
RT: 0.07-0.43 AV: 13 T: FTMS
- p NSI Full ms
[140.00-1935.00]

NL:
1.68E4
C₃₀H₄₇O₃:
C₃₀H₄₇O₃
p (gss, s/p:40) Chrg -1
R: 100000 Res .Pwr . @FWHM

STRSEI_T3CEY_PA_A #5-20 RT: 0.10-0.43 AV: 13 NL: 9.83E6
T: FTMS - p NSI Full ms [140.00-1935.00]



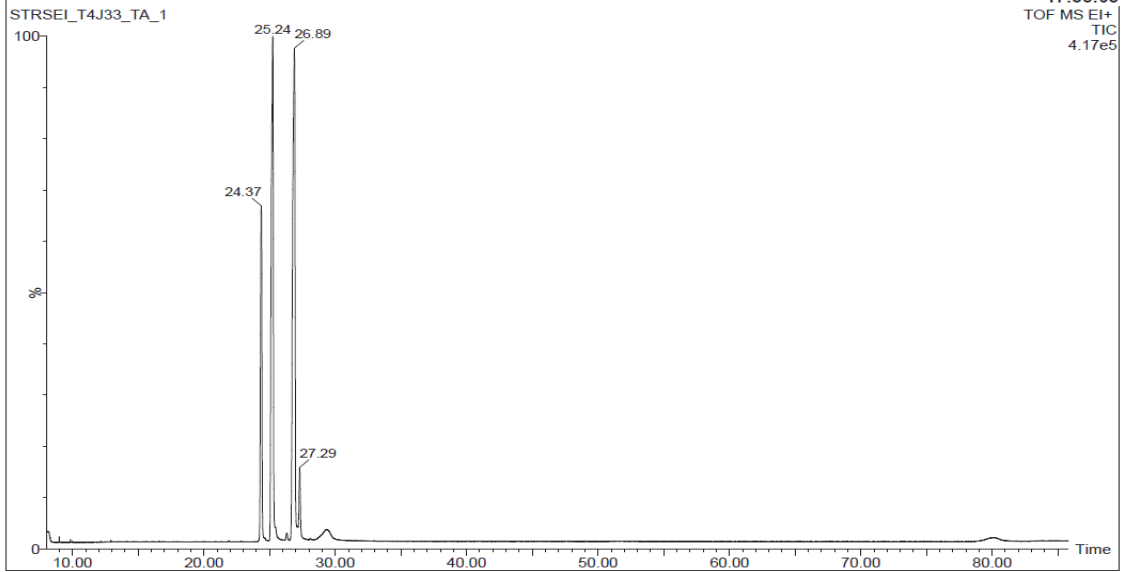
NL:
9.83E6
STRSEI_T3CEY_PA_A#5-20
RT: 0.10-0.43 AV: 13 T: FTMS
- p NSI Full ms
[140.00-1935.00]

NL:
1.68E4
C₃₀ H₄₇ O₃:
C₃₀ H₄₇ O₃
p (gss, s /p:40) Chrg -1
R: 100000 Res .Pwr . @FWHM

390RQ5 MW=414?
C29H50O

National Mass Spectrometry Facility, Swansea
Waters GCT Premier

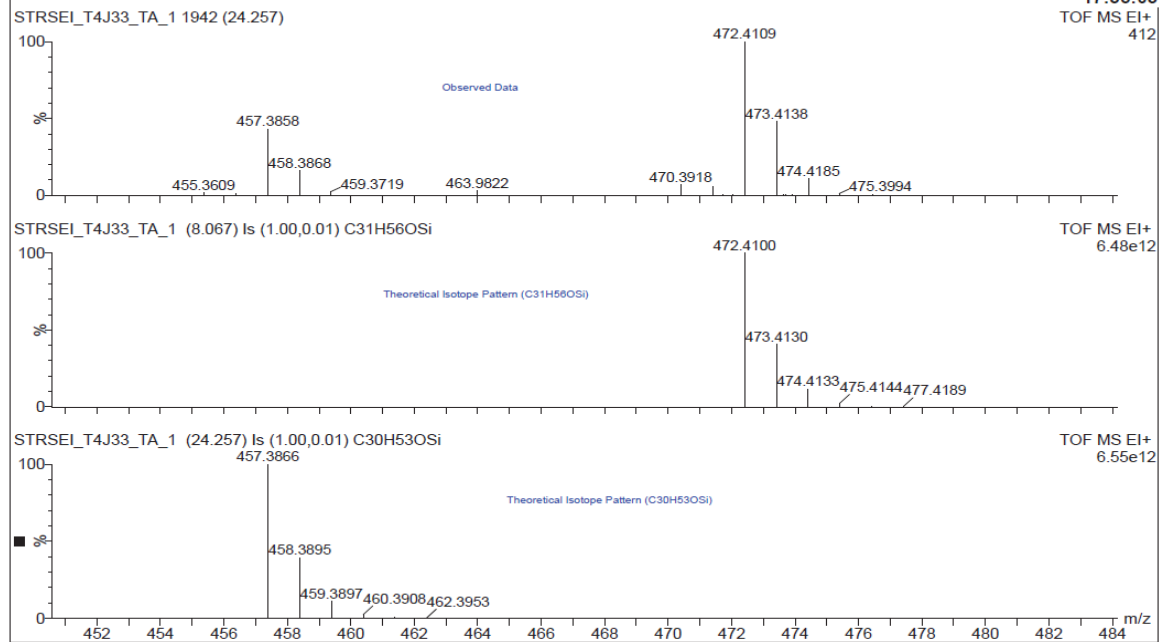
Veronique Seidel
13-Jan-2021
17:35:03
TOF MS EI+
TIC
4.17e5

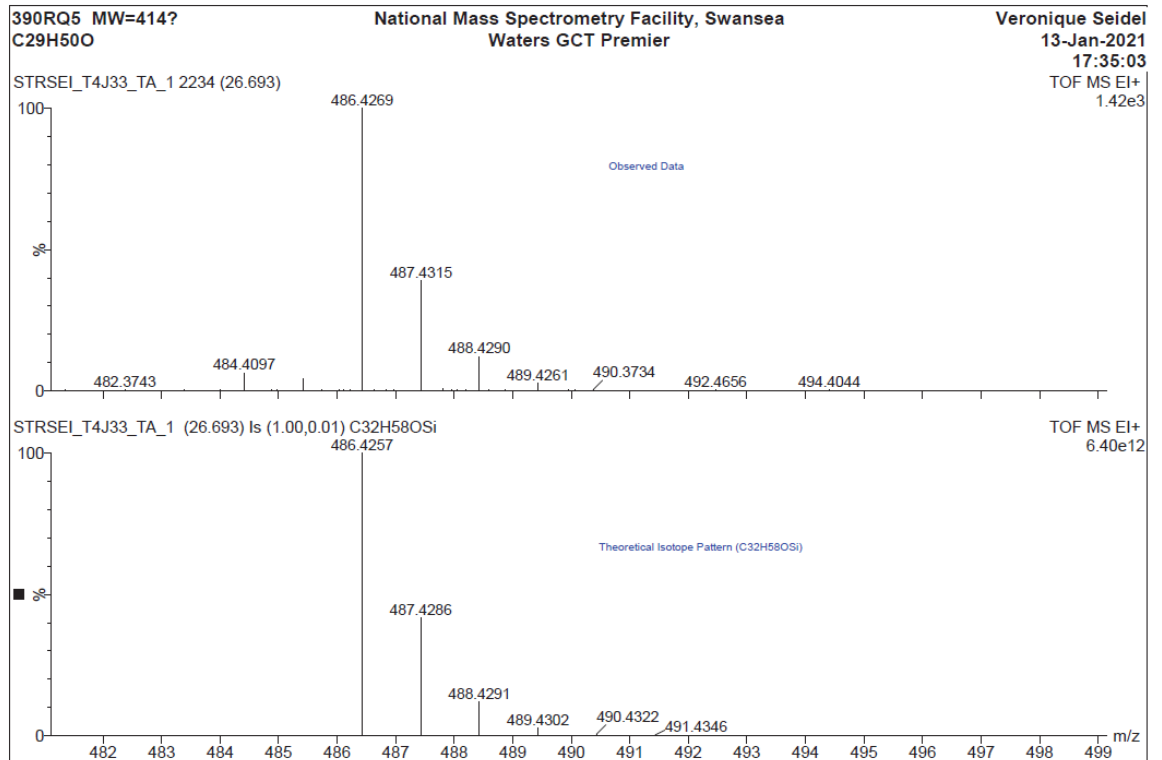
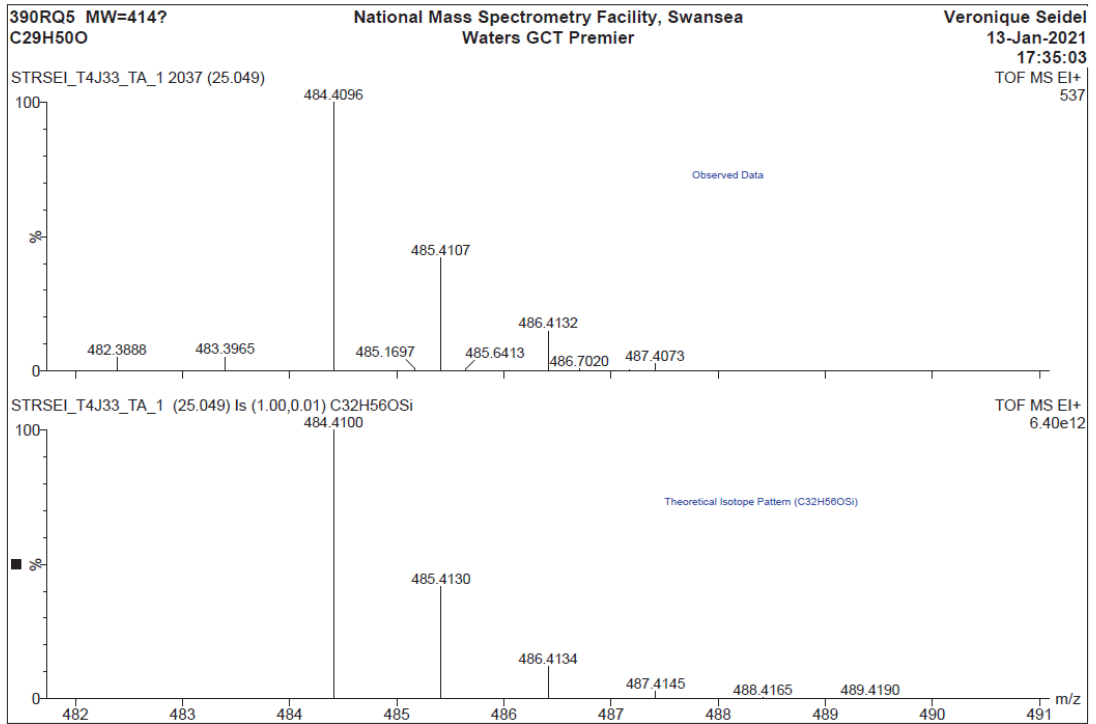


390RQ5 MW=414?
C29H50O

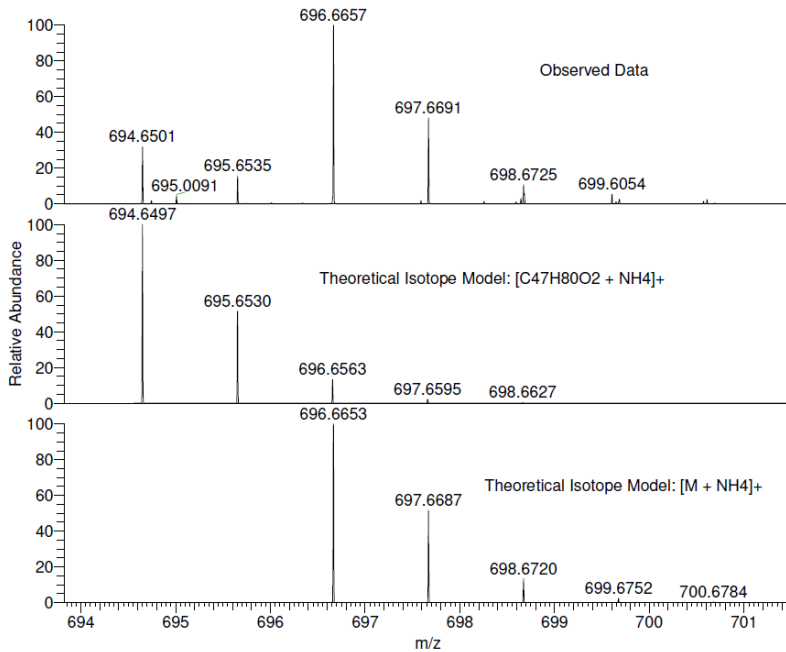
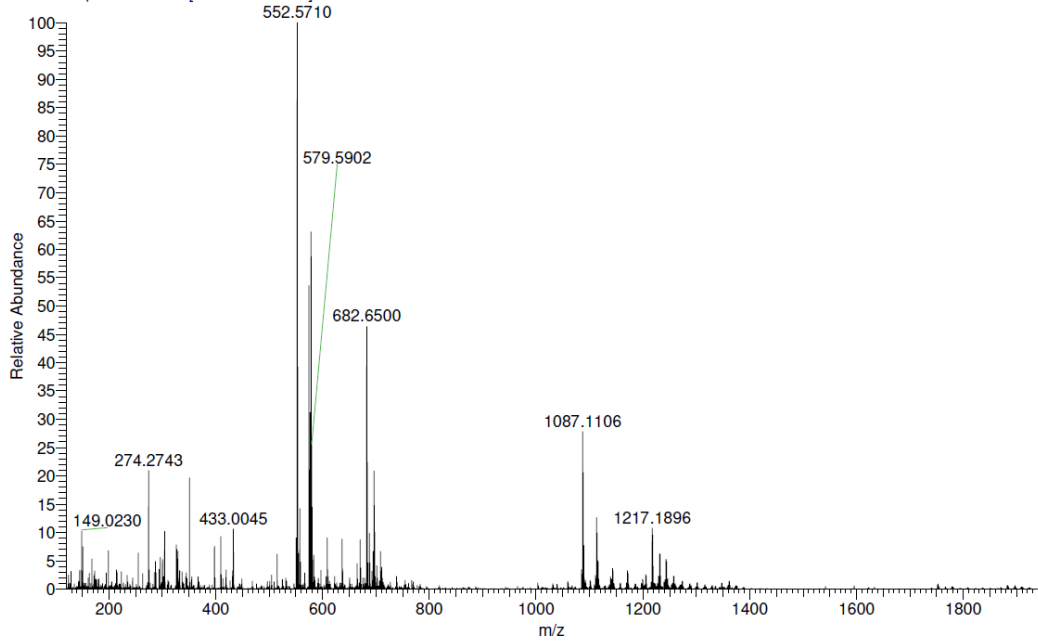
National Mass Spectrometry Facility, Swansea
Waters GCT Premier

Veronique Seidel
13-Jan-2021
17:35:03
TOF MS EI+
412





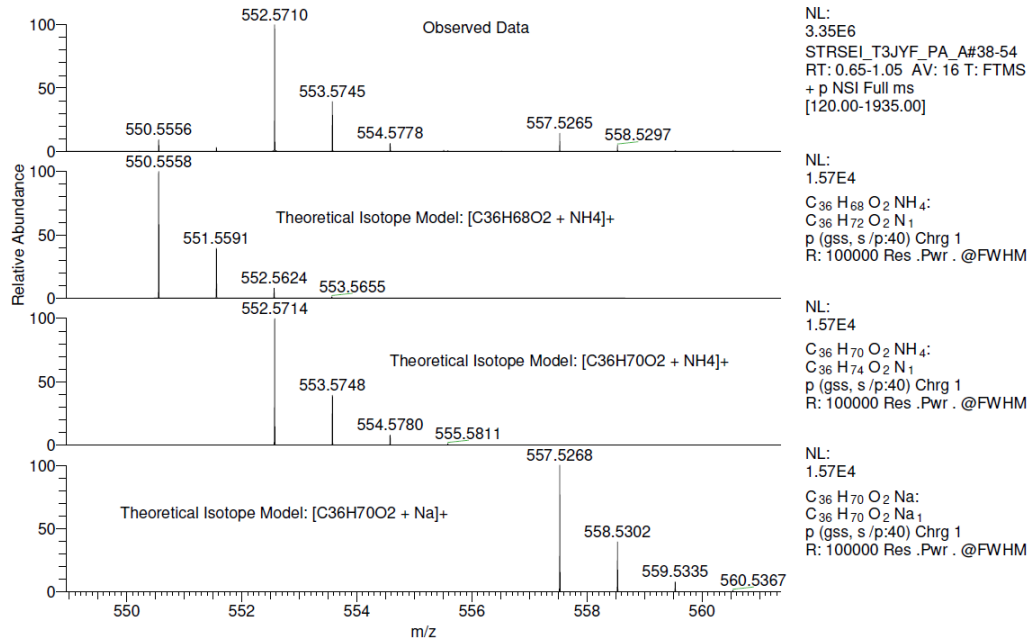
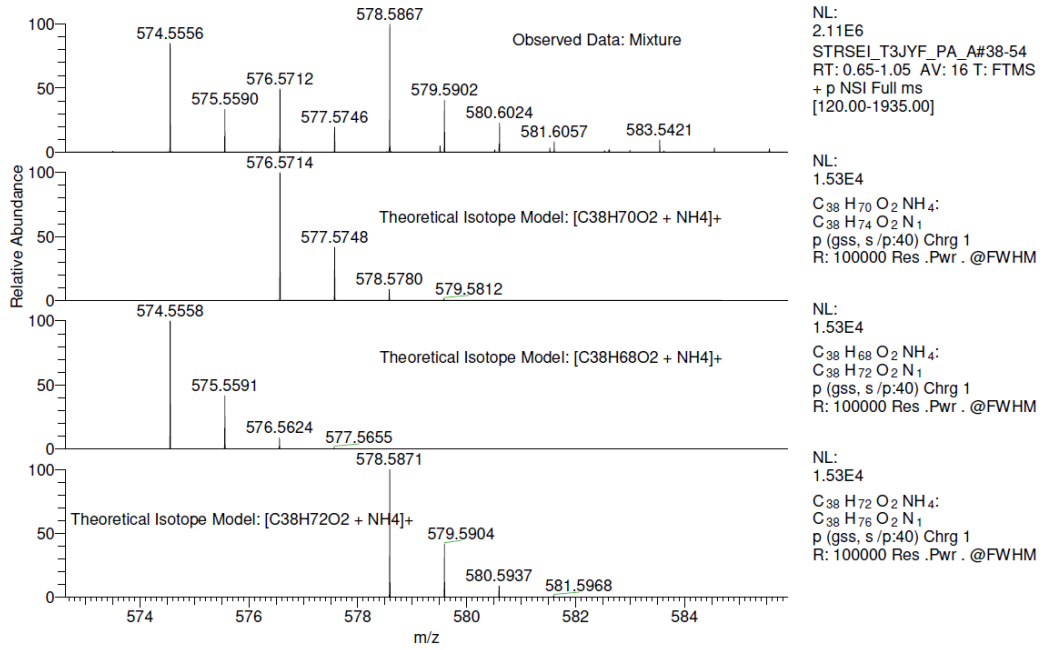
STRSEI_T3JYF_PA_A #38-54 RT: 0.65-1.05 AV: 16 NL: 3.35E6
T: FTMS + p NSI Full ms [120.00-1935.00]



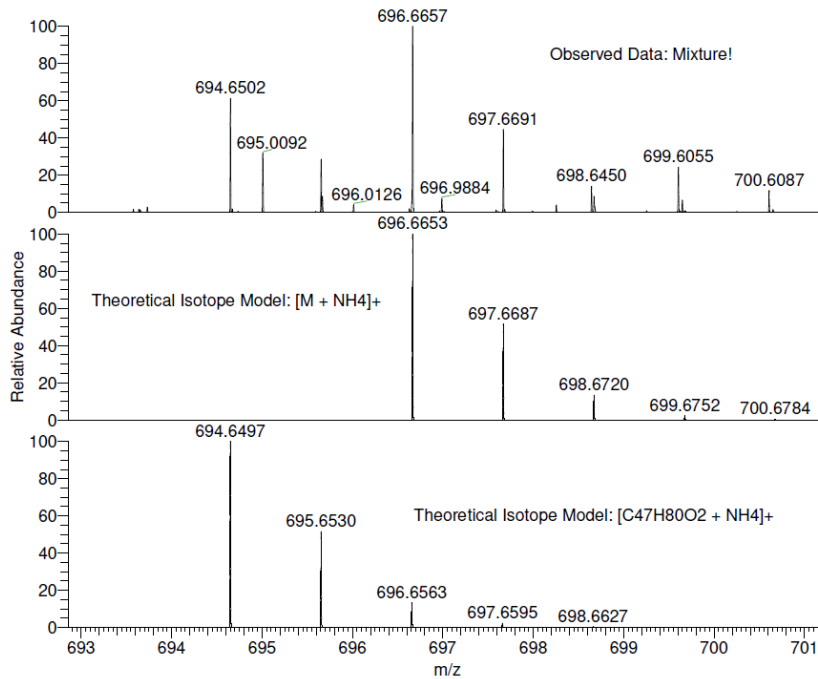
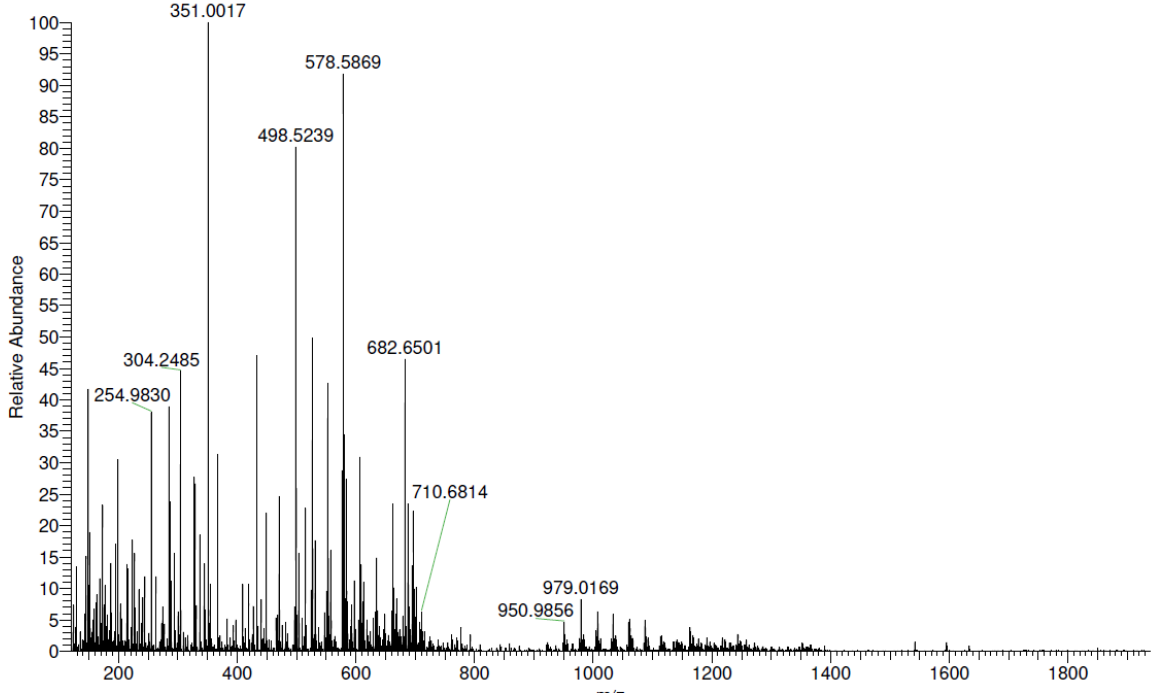
NL:
6.99E5
STRSEI_T3JYF_PA_A#38-54
RT: 0.65-1.05 AV: 16 T: FTMS
+ p NSI Full ms
[120.00-1935.00]

NL:
1.39E4
C₄₇H₈₀O₂NH₄⁺
C₄₇H₈₄O₂N₁
p (gss, s/p:40) Chrg 1
R: 100000 Res .Pwr . @FWHM

NL:
1.39E4
C₄₇H₈₂O₂NH₄⁺
C₄₇H₈₆O₂N₁
p (gss, s/p:40) Chrg 1
R: 100000 Res .Pwr . @FWHM



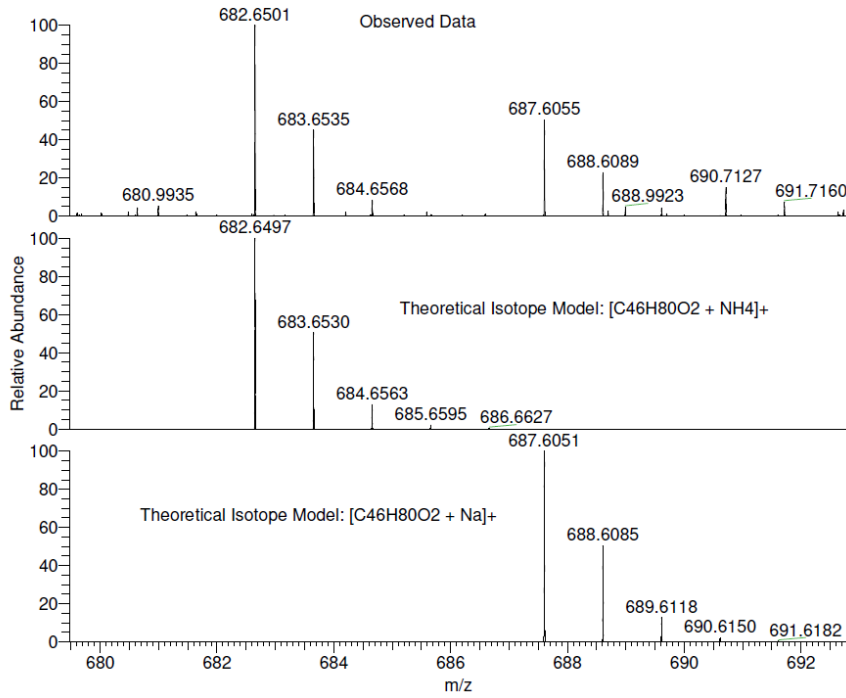
STRSEI_T4LVW_PA_A #37-53 RT: 0.66-1.03 AV: 15 NL: 9.47E5
T: FTMS + p NSI Full ms [120.00-1935.00]



NL:
2.11E5
STRSEI_T4LVW_PA_A#37-53
RT: 0.66-1.03 AV: 15 T:
FTMS + p NSI Full ms
[120.00-1935.00]

NL:
1.39E4
C₄₇H₈₂O₂NH₄⁺
C₄₇H₈₆O₂N₁
p (gss, s/p:40) Chrg 1
R: 100000 Res .Pwr . @FWHM

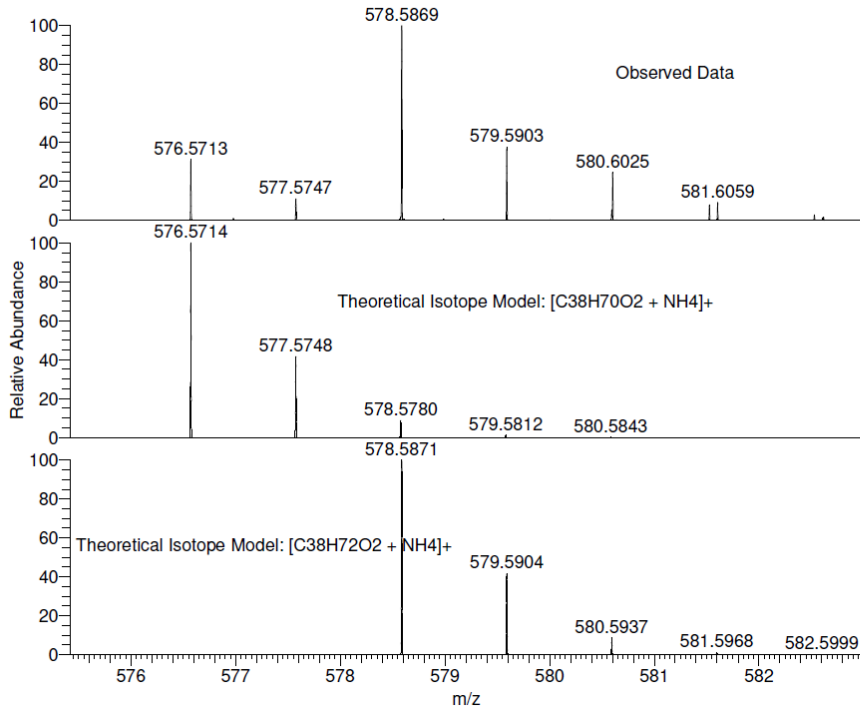
NL:
1.39E4
C₄₇H₈₀O₂NH₄⁺
C₄₇H₈₄O₂N₁
p (gss, s/p:40) Chrg 1
R: 100000 Res .Pwr . @FWHM



NL:
4.40E5
STRSEI_T4LVW_PA_A#37-53
RT: 0.66-1.03 AV: 15 T:
FTMS + p NSI Full ms
[120.00-1935.00]

NL:
1.40E4
C46 H80 O2 NH4:
C46 H84 O2 N1
p (gss, s/p:40) Chrg 1
R: 100000 Res .Pwr . @FWHM

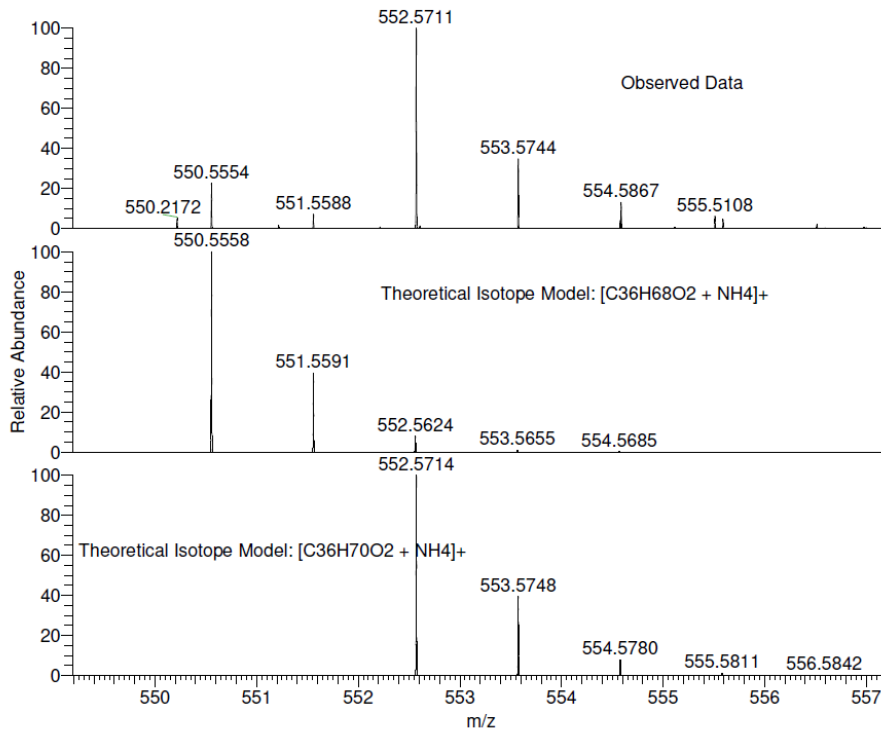
NL:
1.41E4
C46 H80 O2 Na:
C46 H80 O2 Na1
p (gss, s/p:40) Chrg 1
R: 100000 Res .Pwr . @FWHM



NL:
8.70E5
STRSEI_T4LVW_PA_A#37-53
RT: 0.66-1.03 AV: 15 T:
FTMS + p NSI Full ms
[120.00-1935.00]

NL:
1.53E4
C38 H70 O2 NH4:
C38 H74 O2 N1
p (gss, s/p:40) Chrg 1
R: 100000 Res .Pwr . @FWHM

NL:
1.53E4
C38 H72 O2 NH4:
C38 H76 O2 N1
p (gss, s/p:40) Chrg 1
R: 100000 Res .Pwr . @FWHM

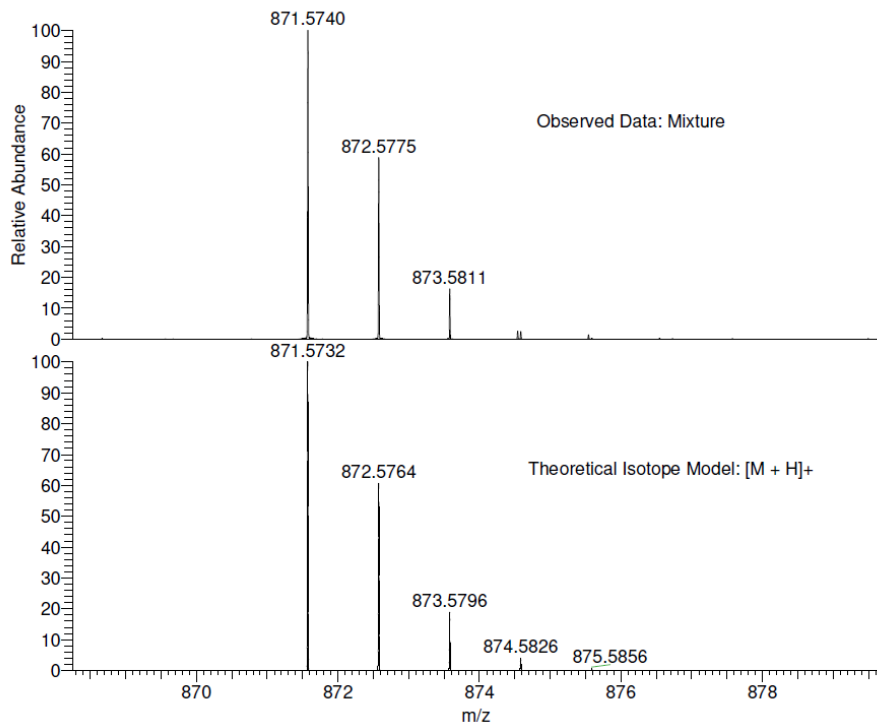
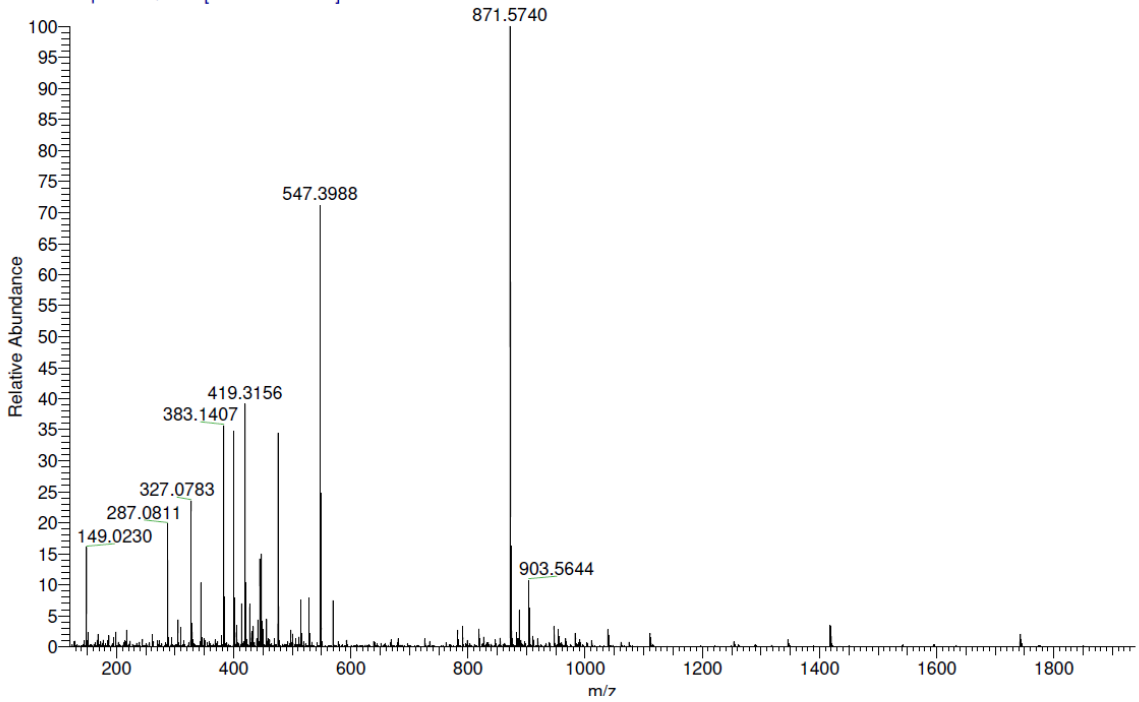


NL:
4.04E5
STRSEI_T4LVW_PA_A#37-53
RT: 0.66-1.03 AV: 15 T:
FTMS + p NSI Full ms
[120.00-1935.00]

NL:
1.57E4
 $C_{36}H_{68}O_2NH_4$:
 $C_{36}H_{72}O_2N_1$
p (gss, s /p:40) Chrg 1
R: 100000 Res .Pwr . @FWHM

NL:
1.57E4
 $C_{36}H_{70}O_2NH_4$:
 $C_{36}H_{74}O_2N_1$
p (gss, s /p:40) Chrg 1
R: 100000 Res .Pwr . @FWHM

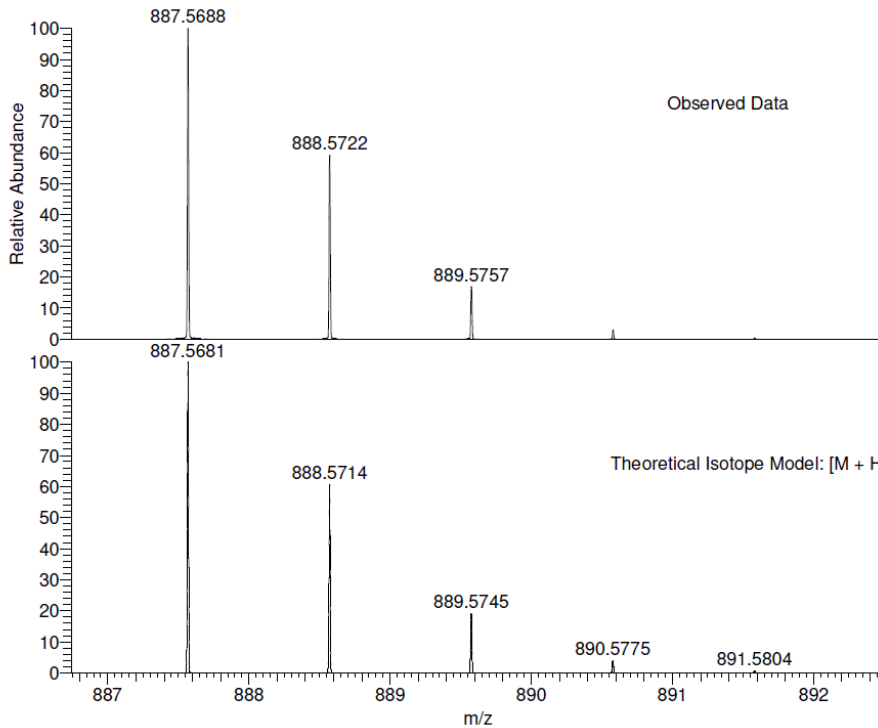
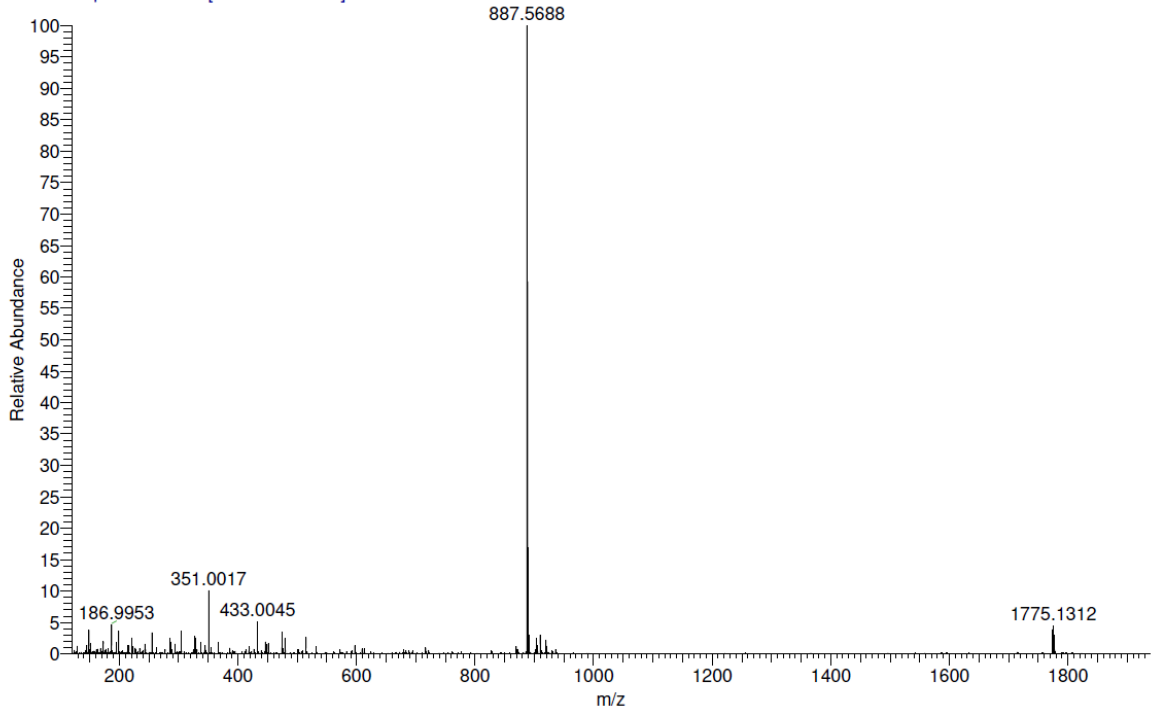
STRSEL T4PVT_PA_A #39-55 RT: 0.65-1.04 AV: 16 NL: 8.59E6
T: FTMS + p NSI Full ms [120.00-1935.00]



NL:
8.59E6
STRSEL T4PVT_PA_A #39-55
RT: 0.65-1.04 AV: 16 T: FTMS
+ p NSI Full ms
[120.00-1935.00]

NL:
1.25E4
C₅₅H₇₄N₄O₅H:
C₅₅H₇₅N₄O₅
p (gss, s/p:40) Chrg 1
R: 100000 Res .Pwr . @FWHM

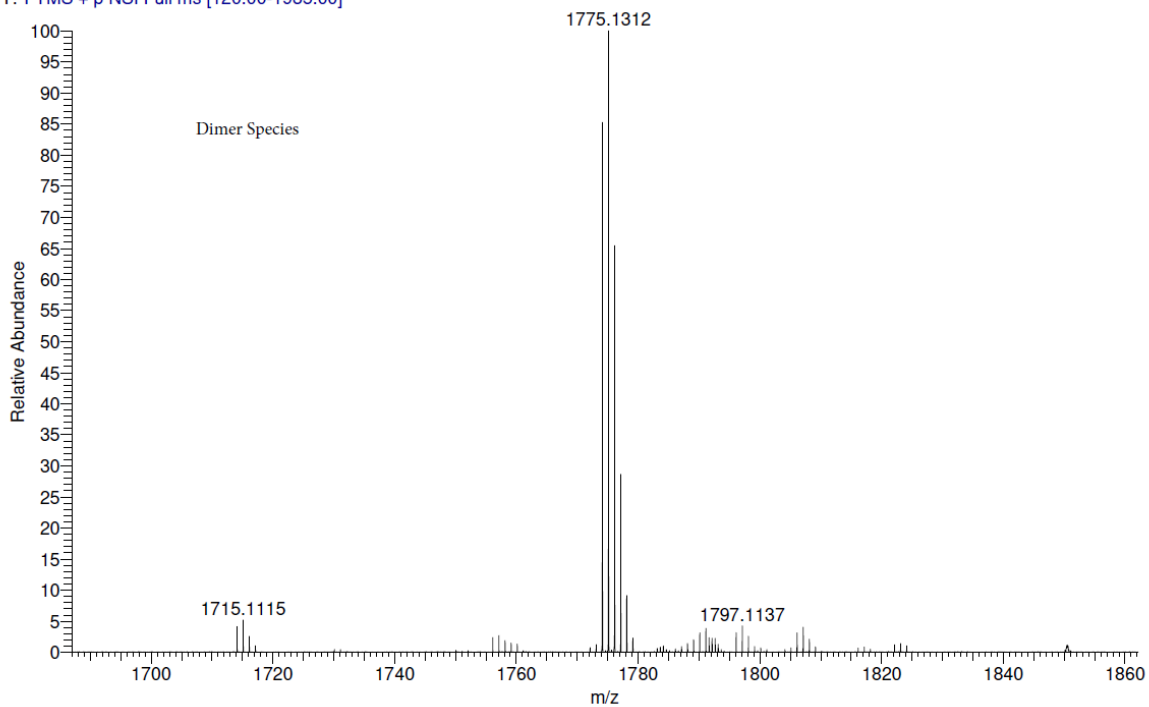
STRSEL T4N9F_PA_A #38-55 RT: 0.66-1.03 AV: 15 NL: 9.93E6
T: FTMS + p NSI Full ms [120.00-1935.00]



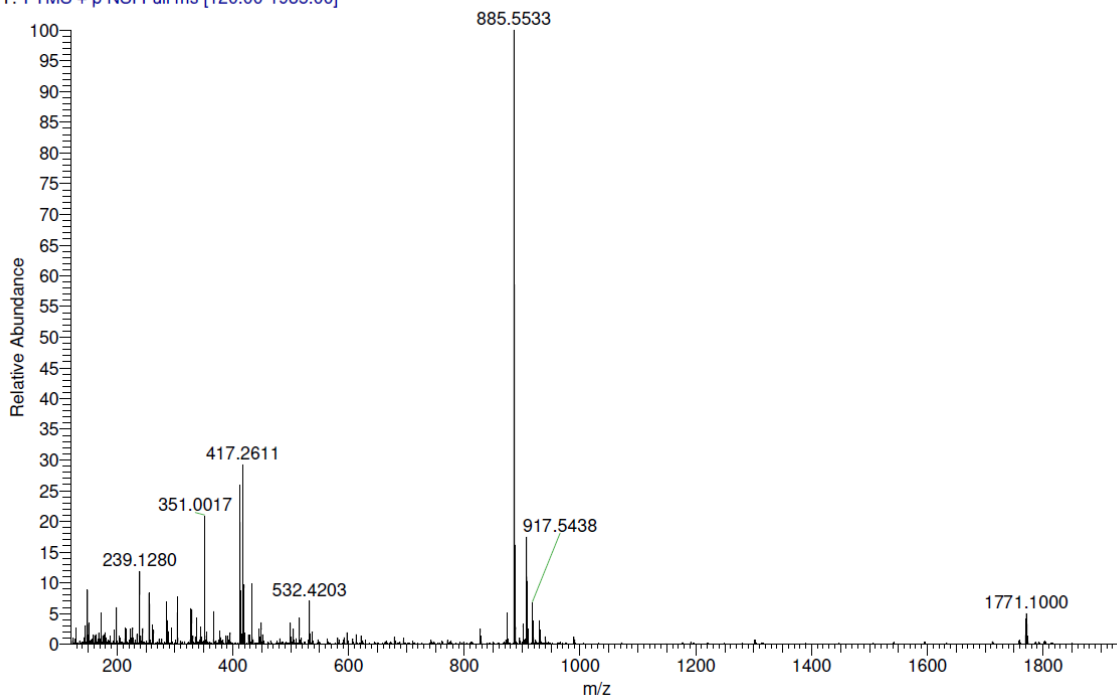
NL:
9.93E6
STRSEL T4N9F_PA_A#38-55
RT: 0.66-1.03 AV: 15 T: FTMS
+ p NSI Full ms
[120.00-1935.00]

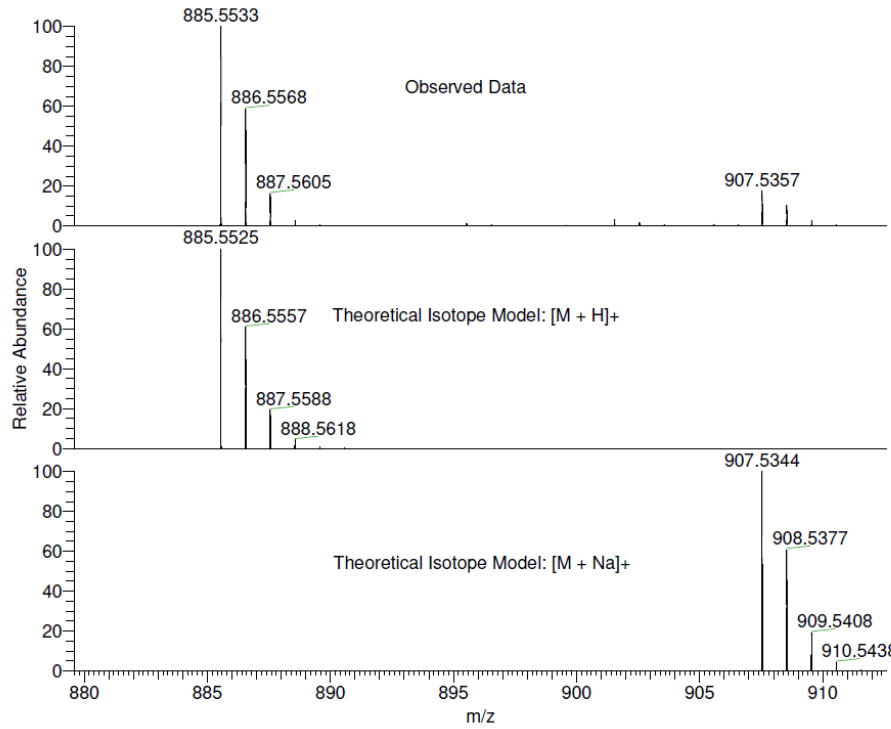
NL:
1.25E4
C₅₅H₇₄N₄O₆h:
C₅₅H₇₅N₄O₆
p (gss, s/p:40) Chrg 1
R: 100000 Res .Pwr . @FWHM

STRSEI_T4N9F_PA_A #38-55 RT: 0.66-1.03 AV: 15 NL: 4.42E5
T: FTMS + p NSI Full ms [120.00-1935.00]



STRSEI_T4RCC_PA_A #38-53 RT: 0.65-1.05 AV: 16 NL: 4.39E5
T: FTMS + p NSI Full ms [120.00-1935.00]



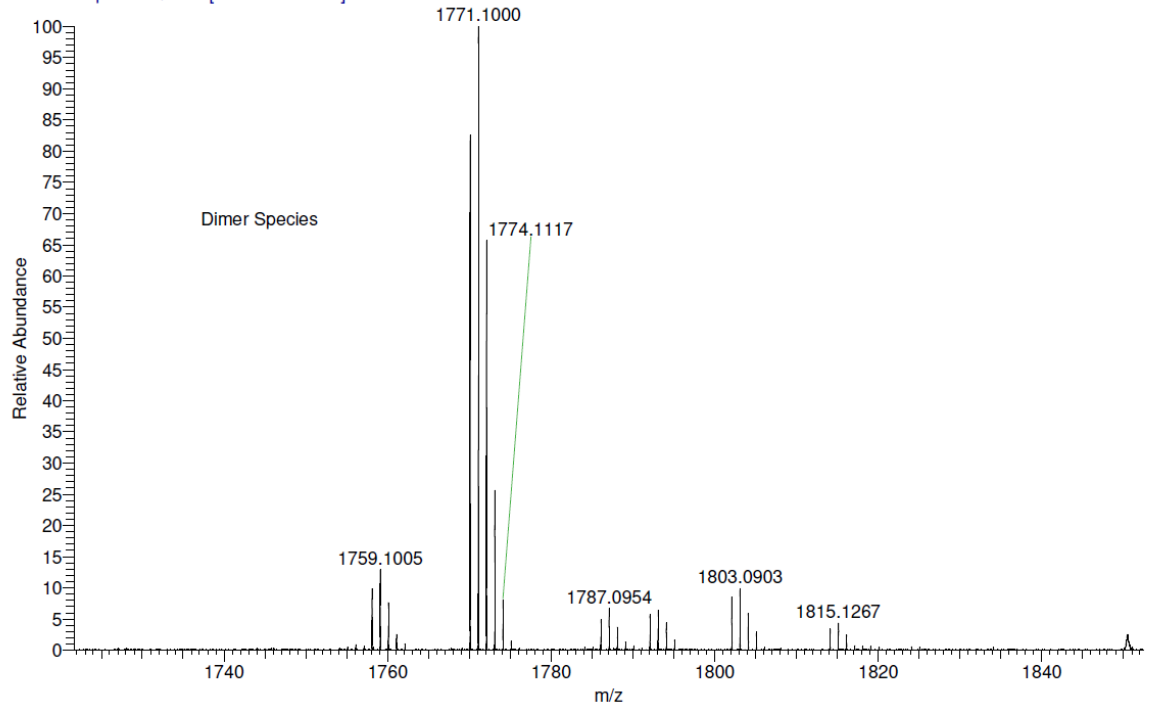


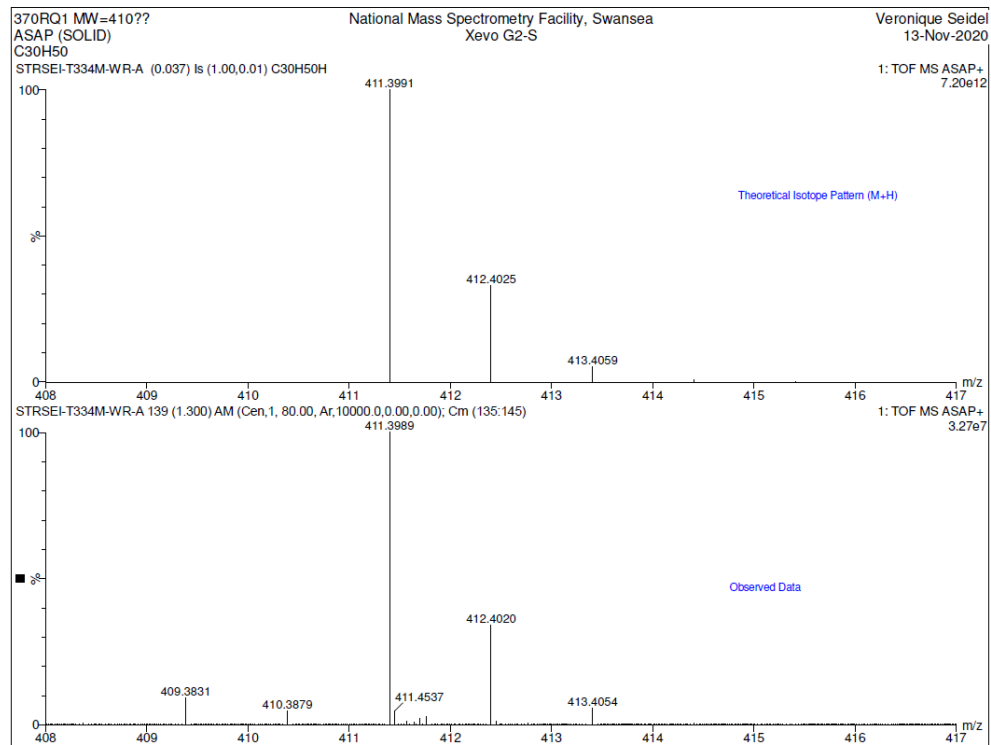
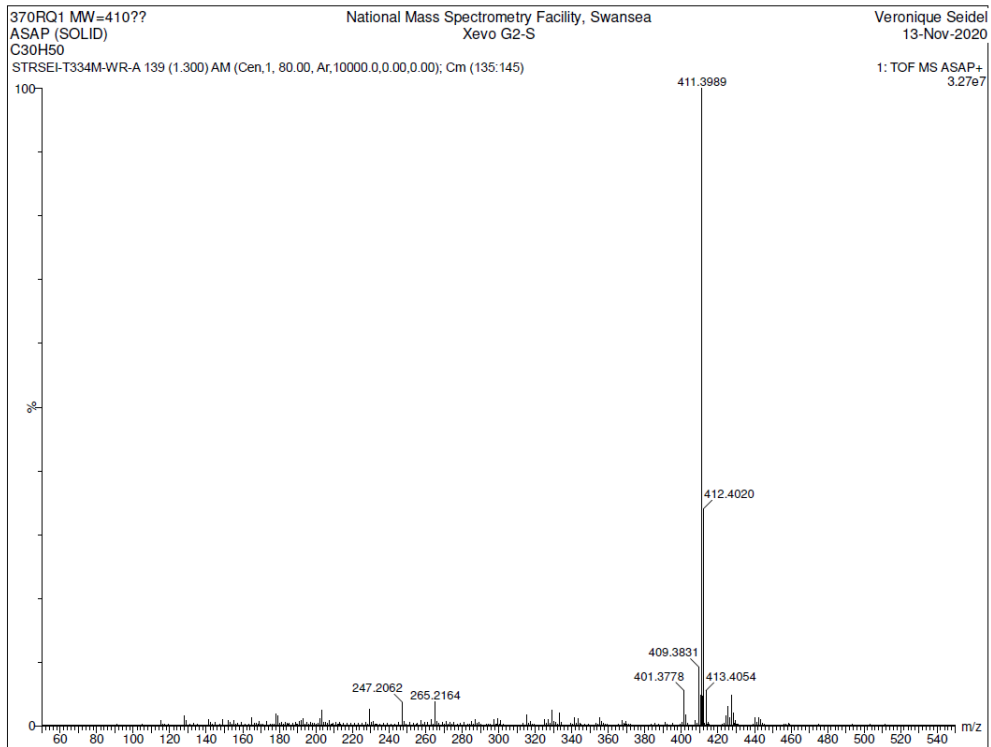
NL:
4.39E6
STRSEI_T4RCC_PA_A#38-53
RT: 0.65-1.05 AV: 16 T: FTMS
+ p NSI Full ms
[120.00-1935.00]

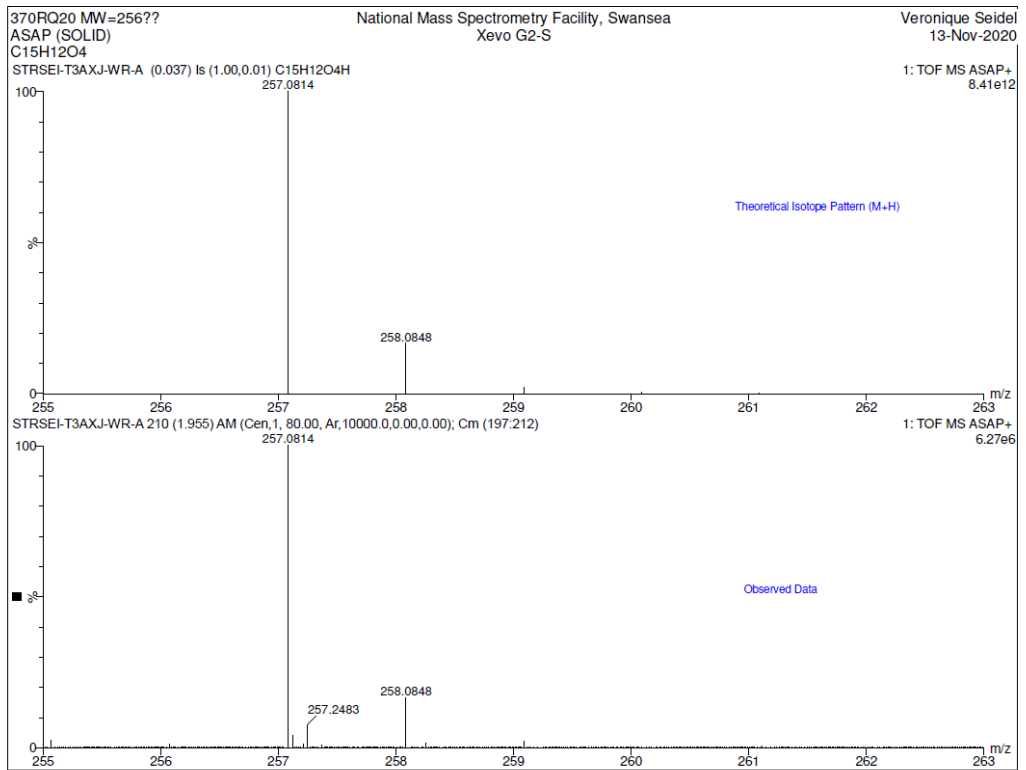
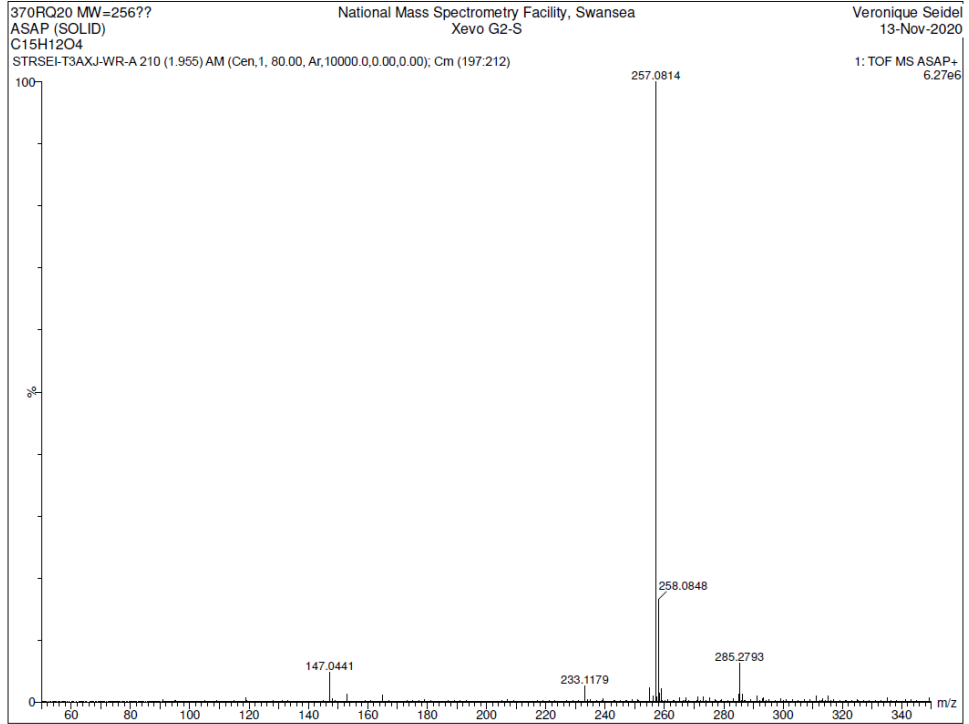
NL:
1.25E4
C₅₅H₇₂N₄O₆H:
C₅₅H₇₃N₄O₆
p (gss, s /p:40) Chrg 1
R: 100000 Res .Pwr . @FWHM

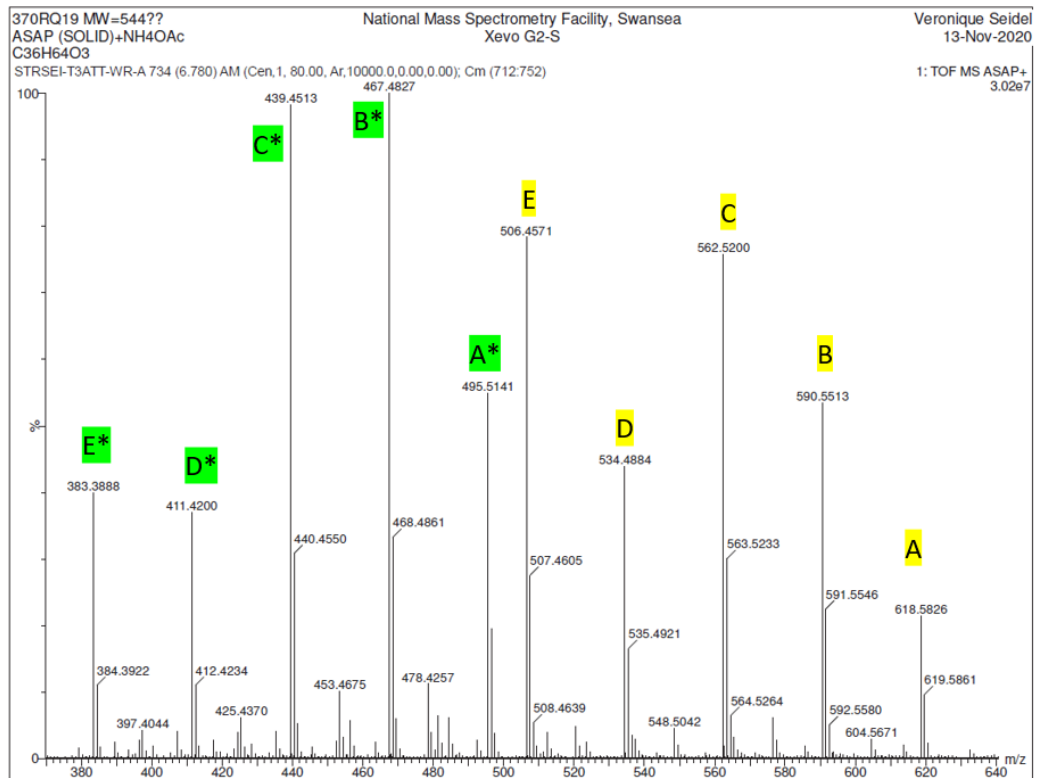
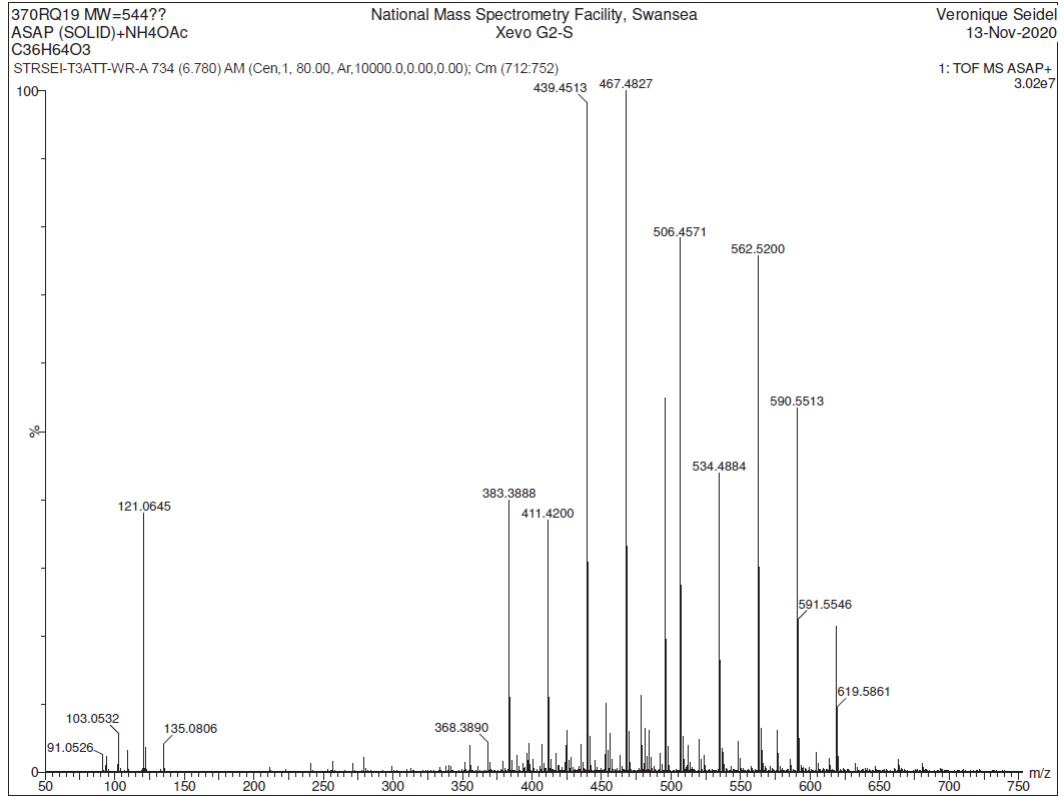
NL:
1.25E4
C₅₅H₇₂N₄O₆Na:
C₅₅H₇₂N₄O₆Na₁
p (gss, s /p:40) Chrg 1
R: 100000 Res .Pwr . @FWHM

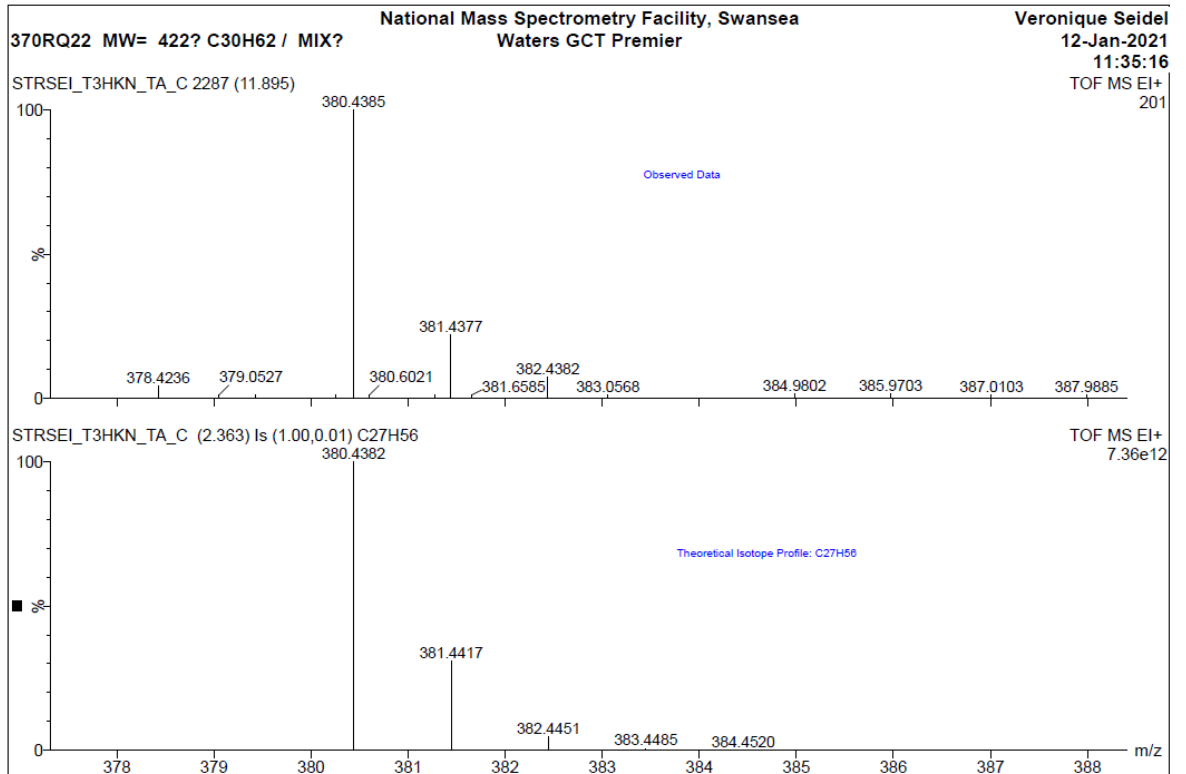
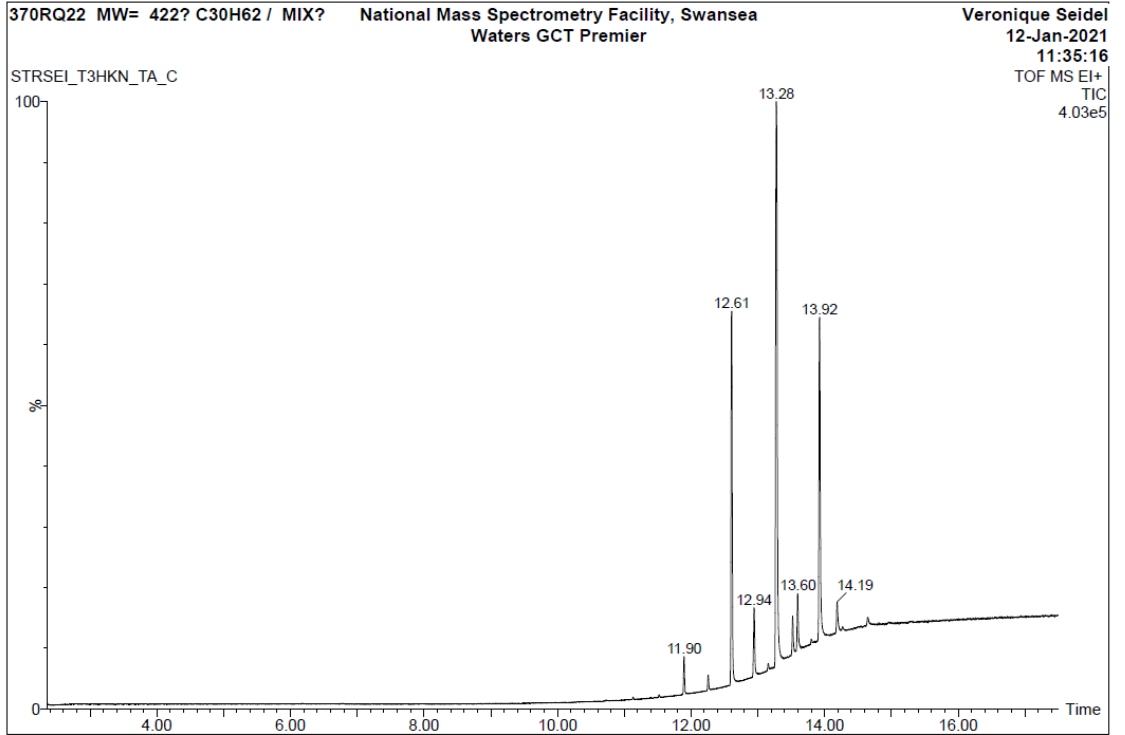
STRSEI_T4RCC_PA_A #38-53 RT: 0.65-1.05 AV: 16 NL: 2.19E5
T: FTMS + p NSI Full ms [120.00-1935.00]

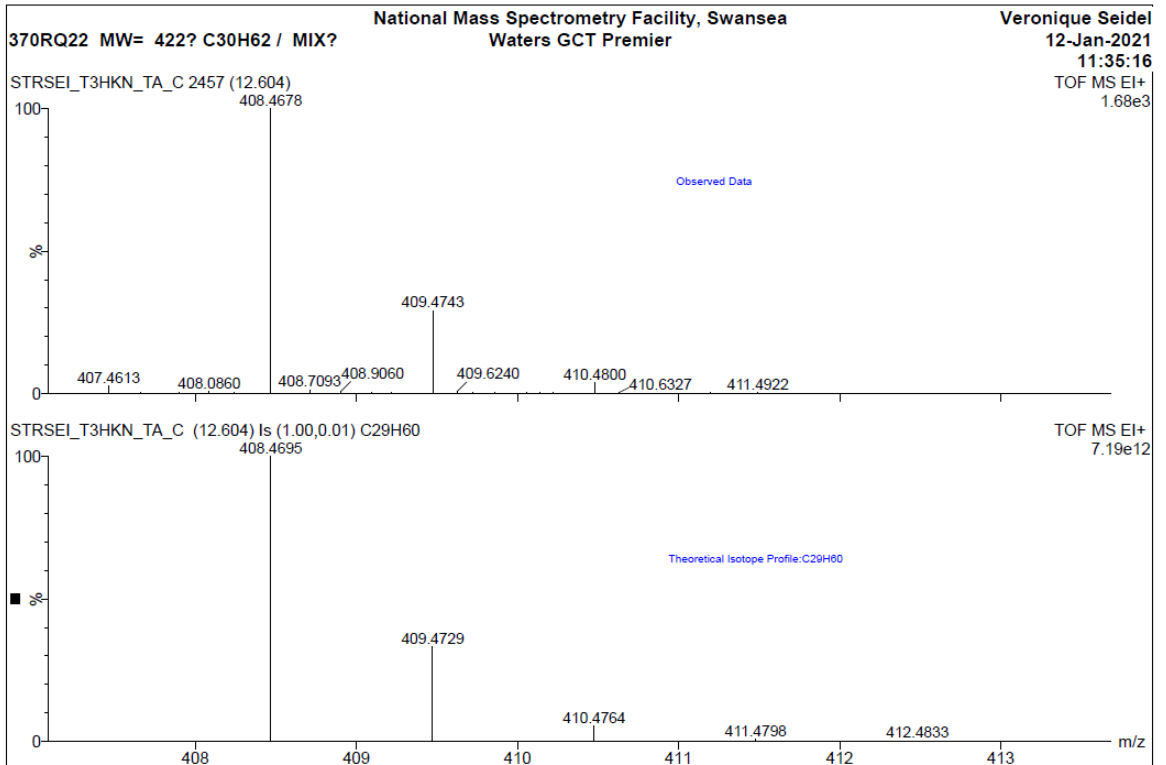
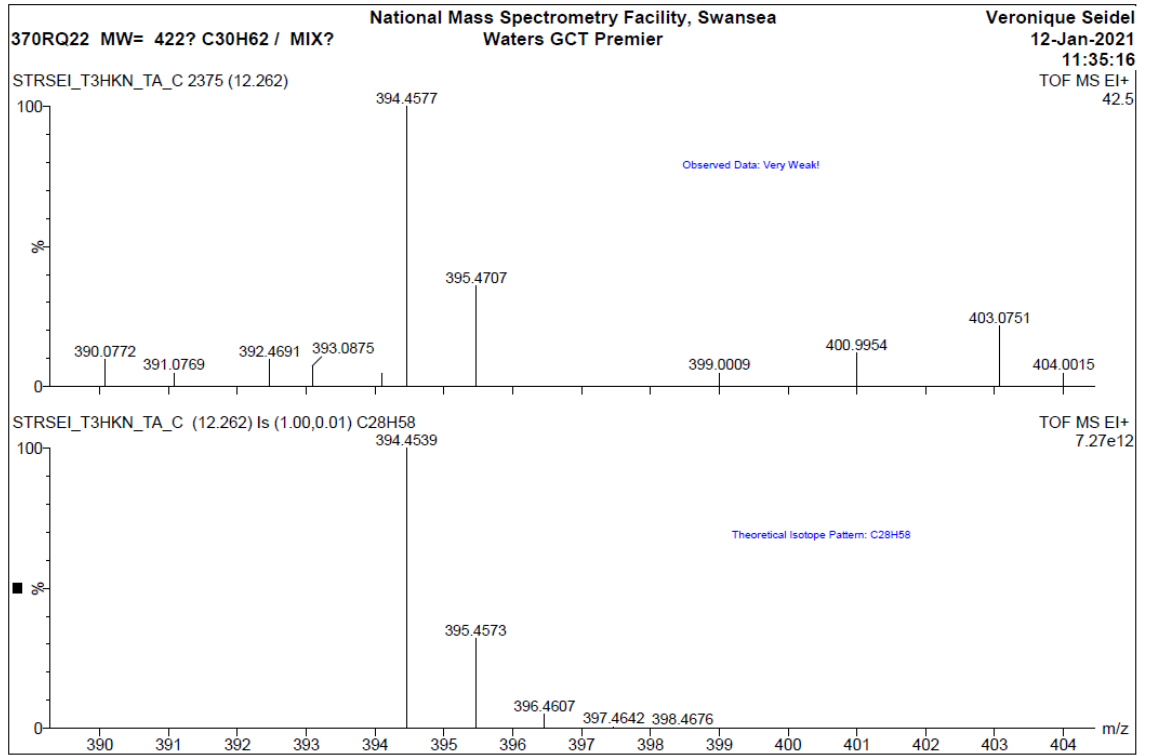


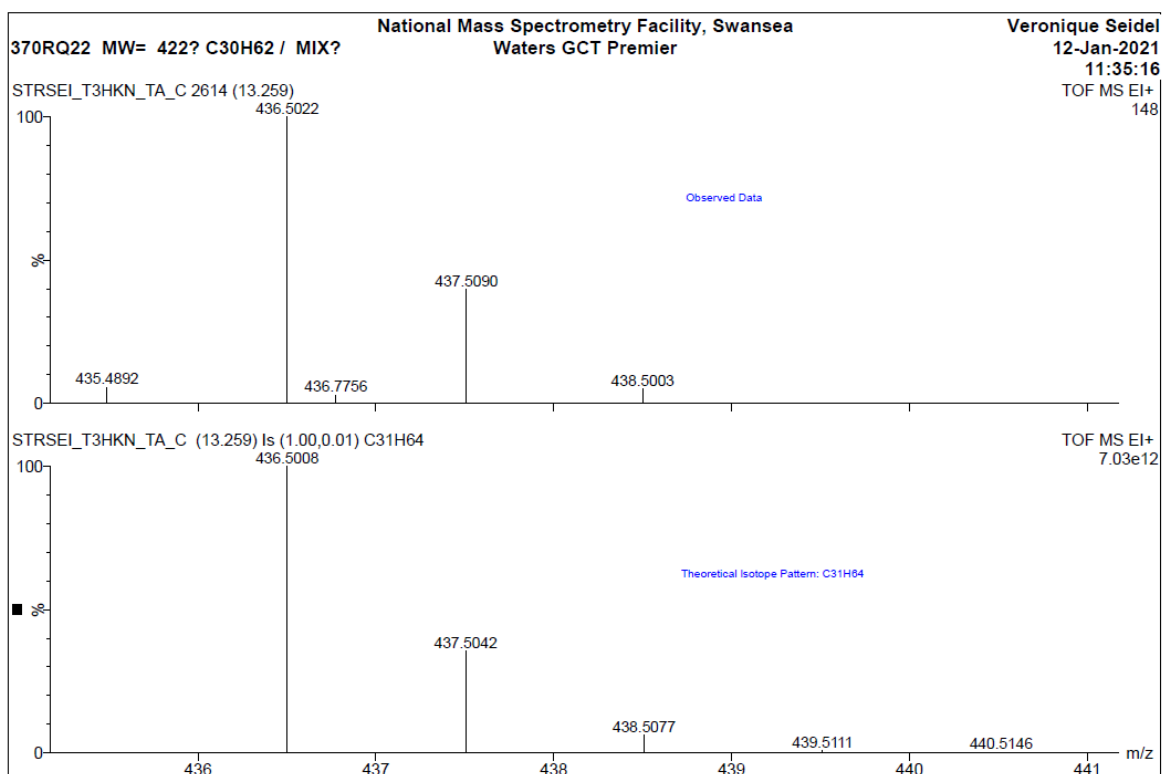
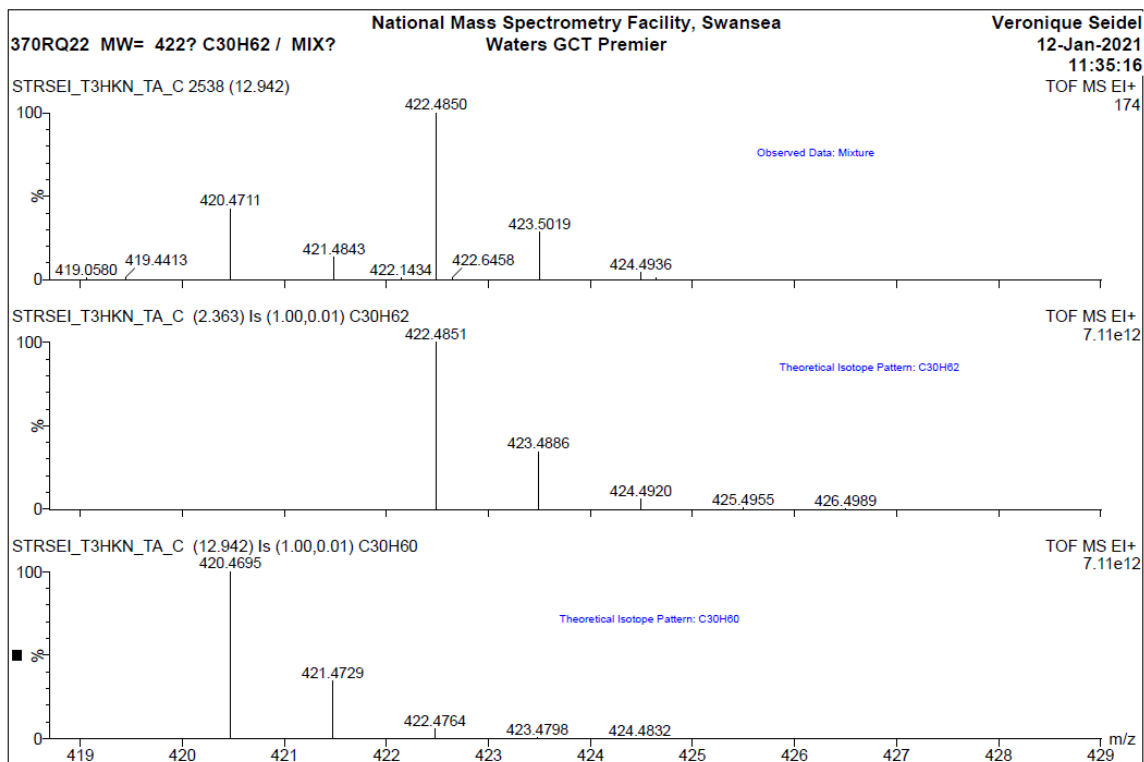


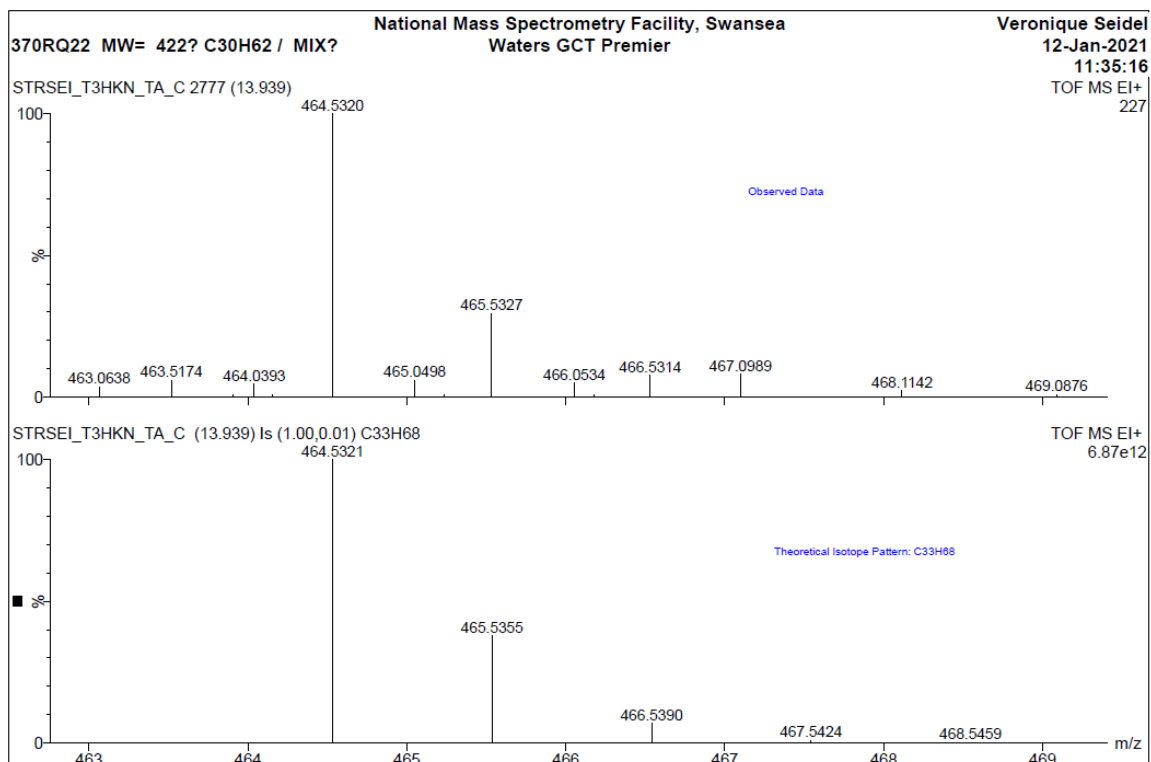
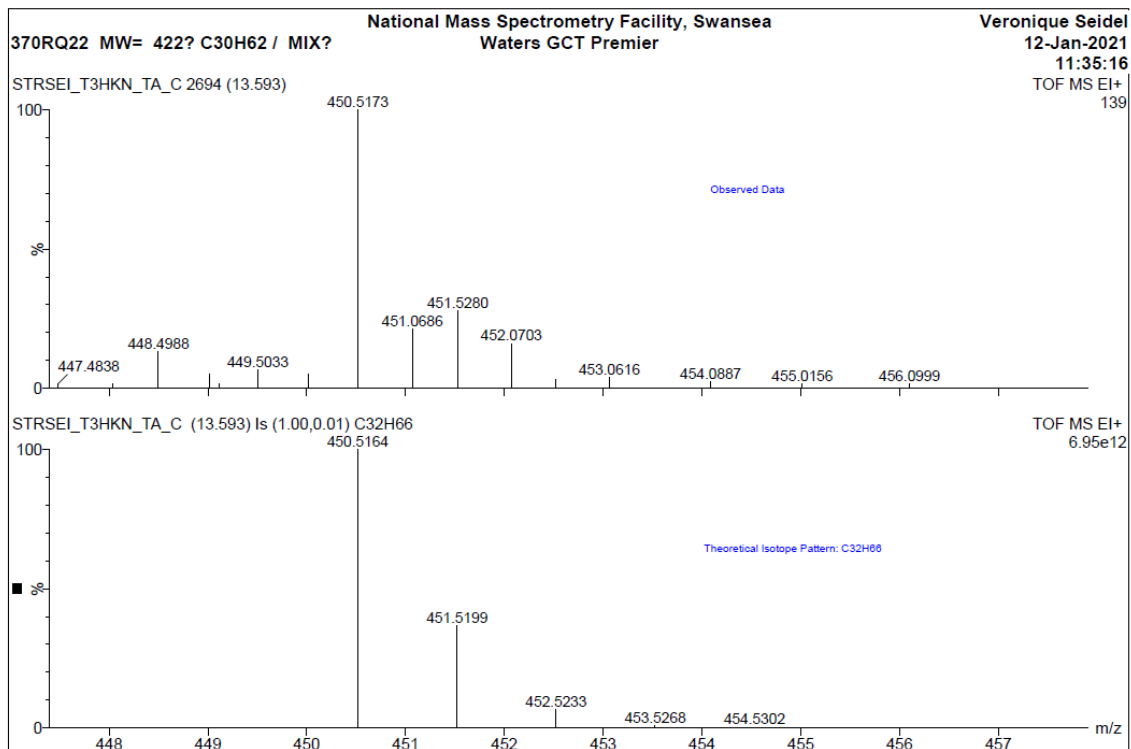


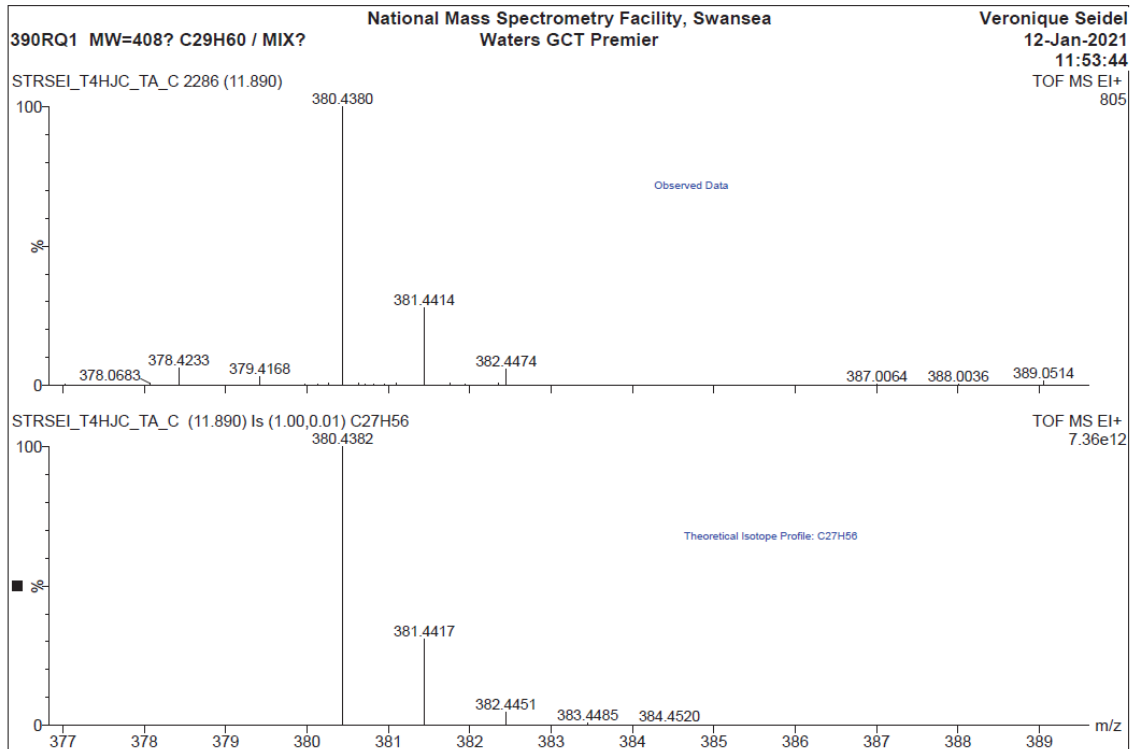
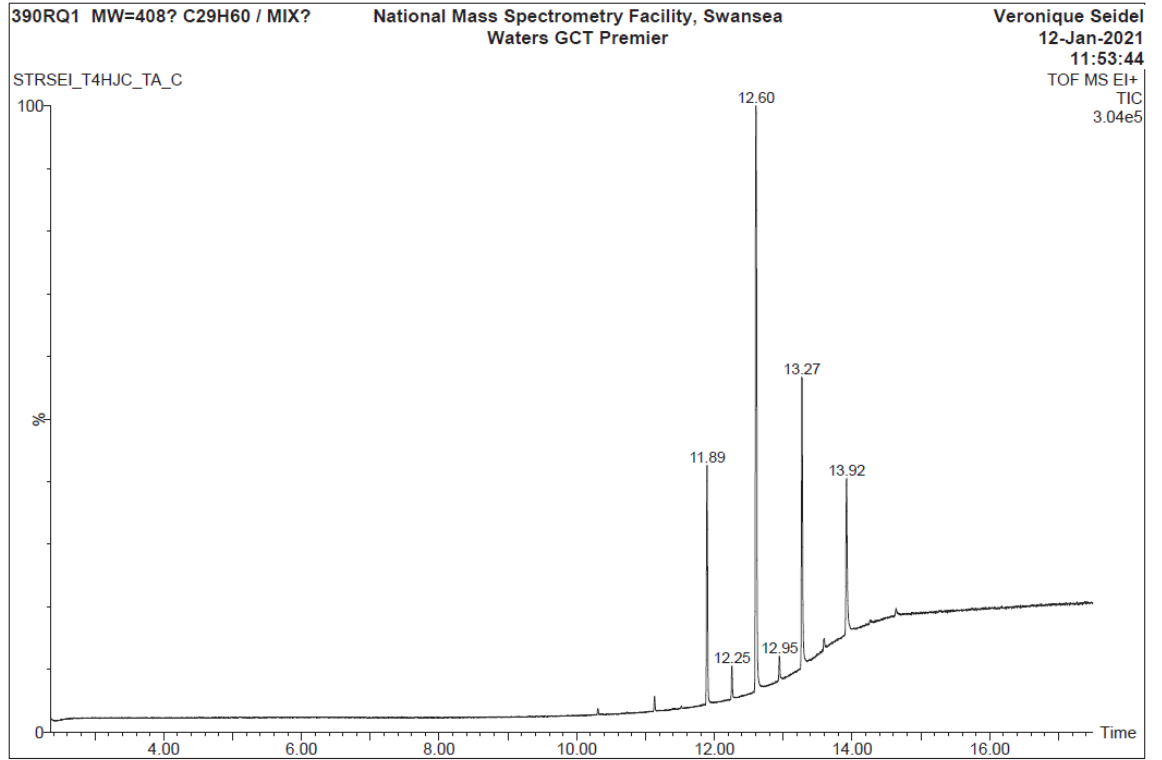


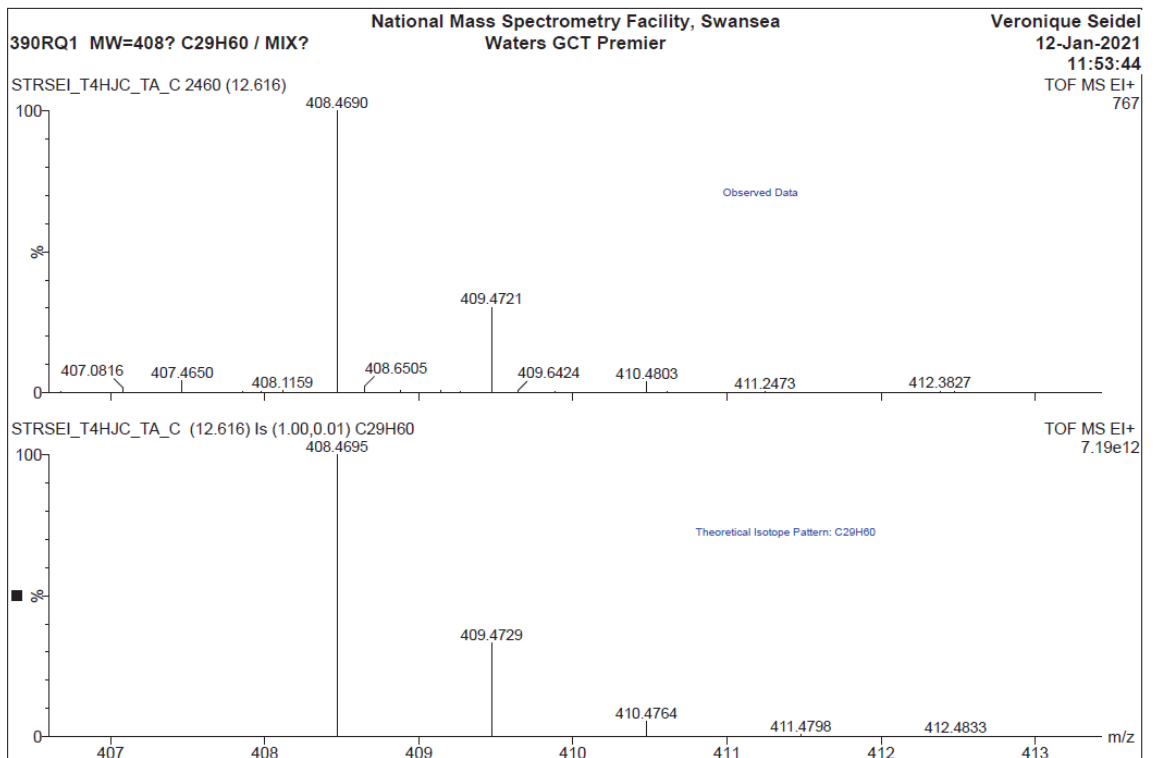
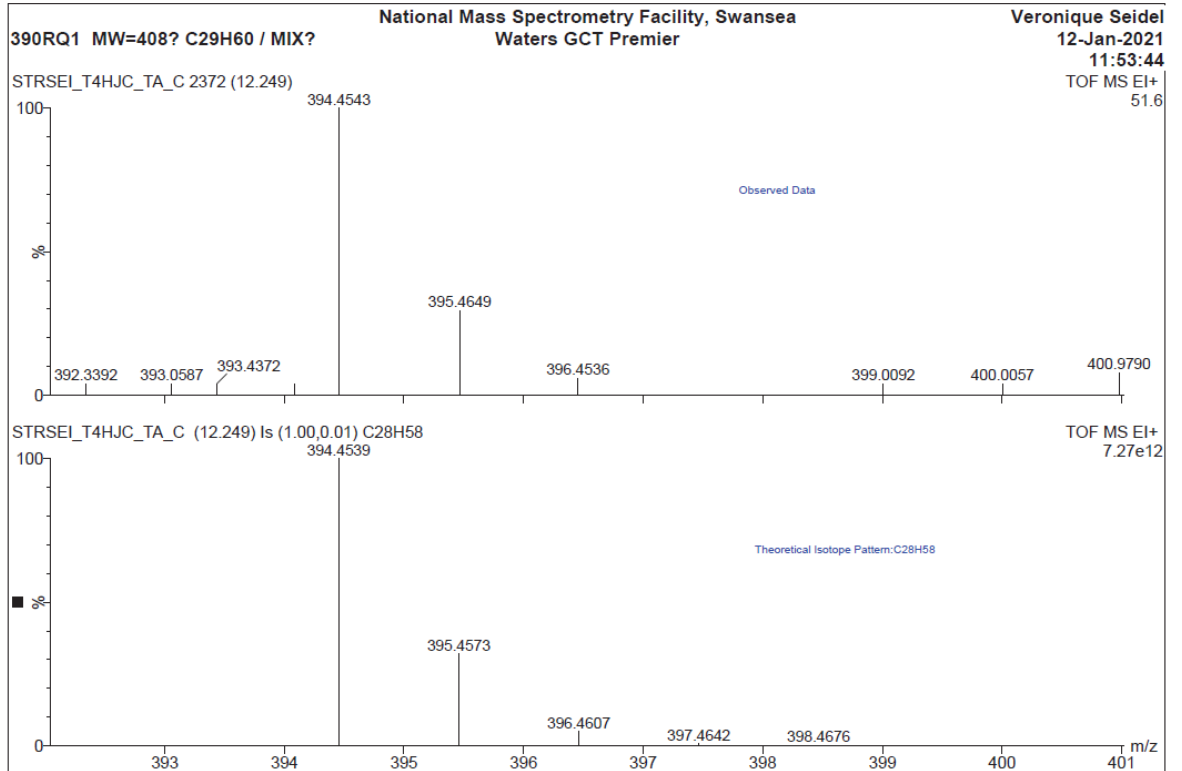


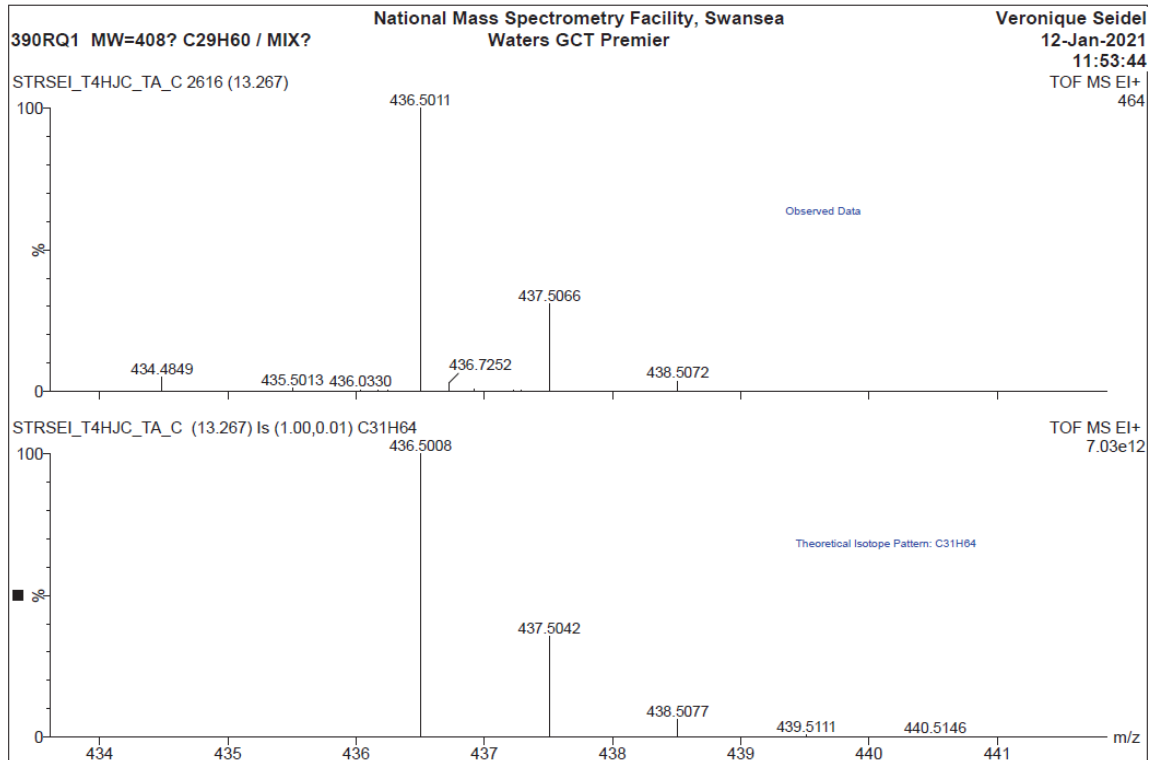
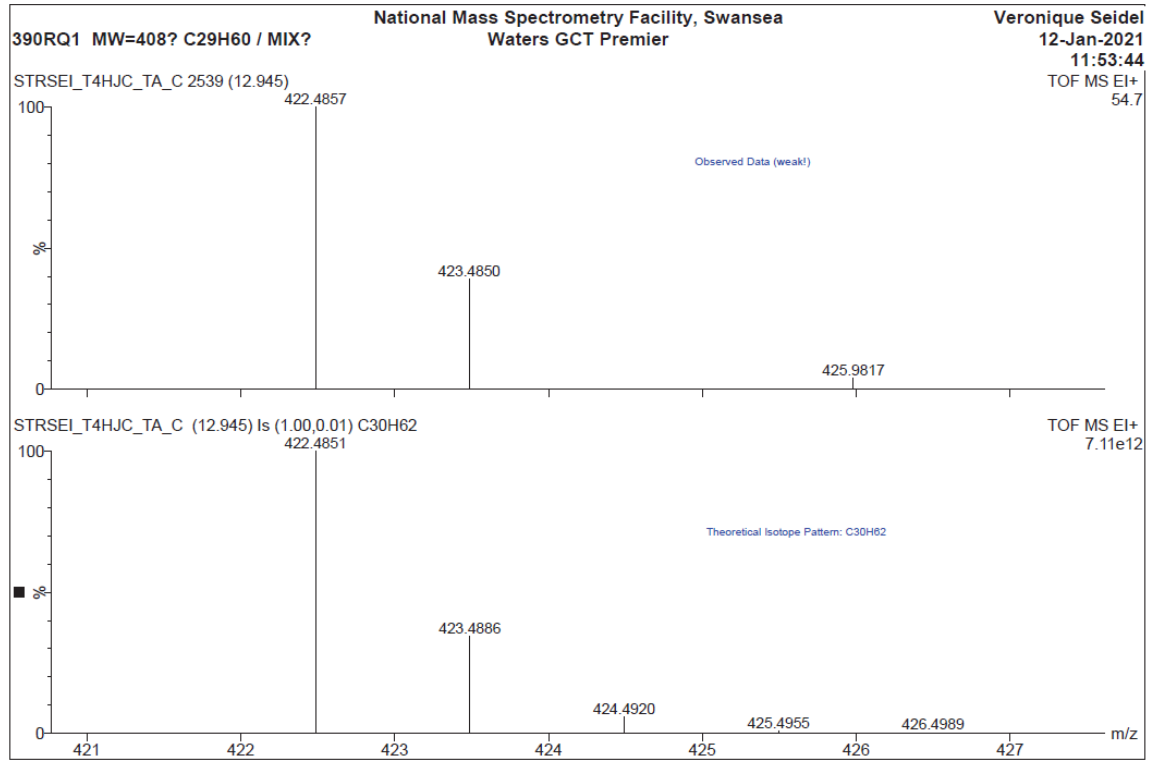


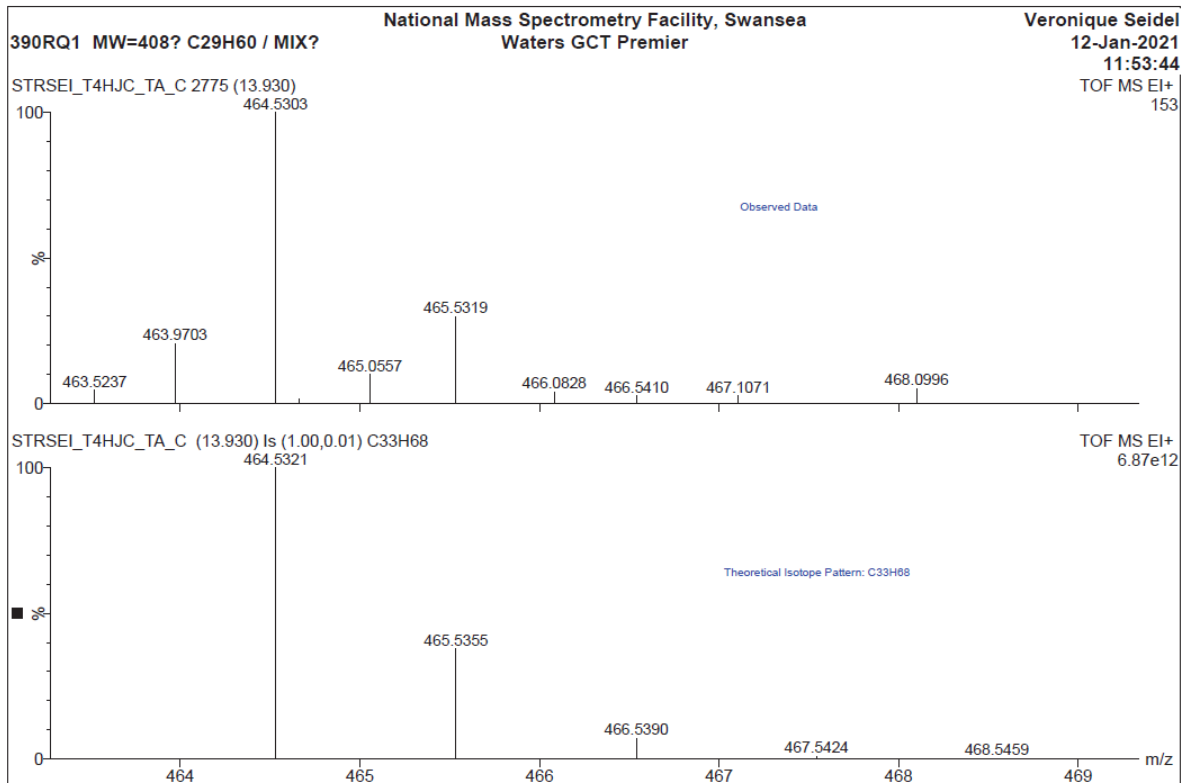




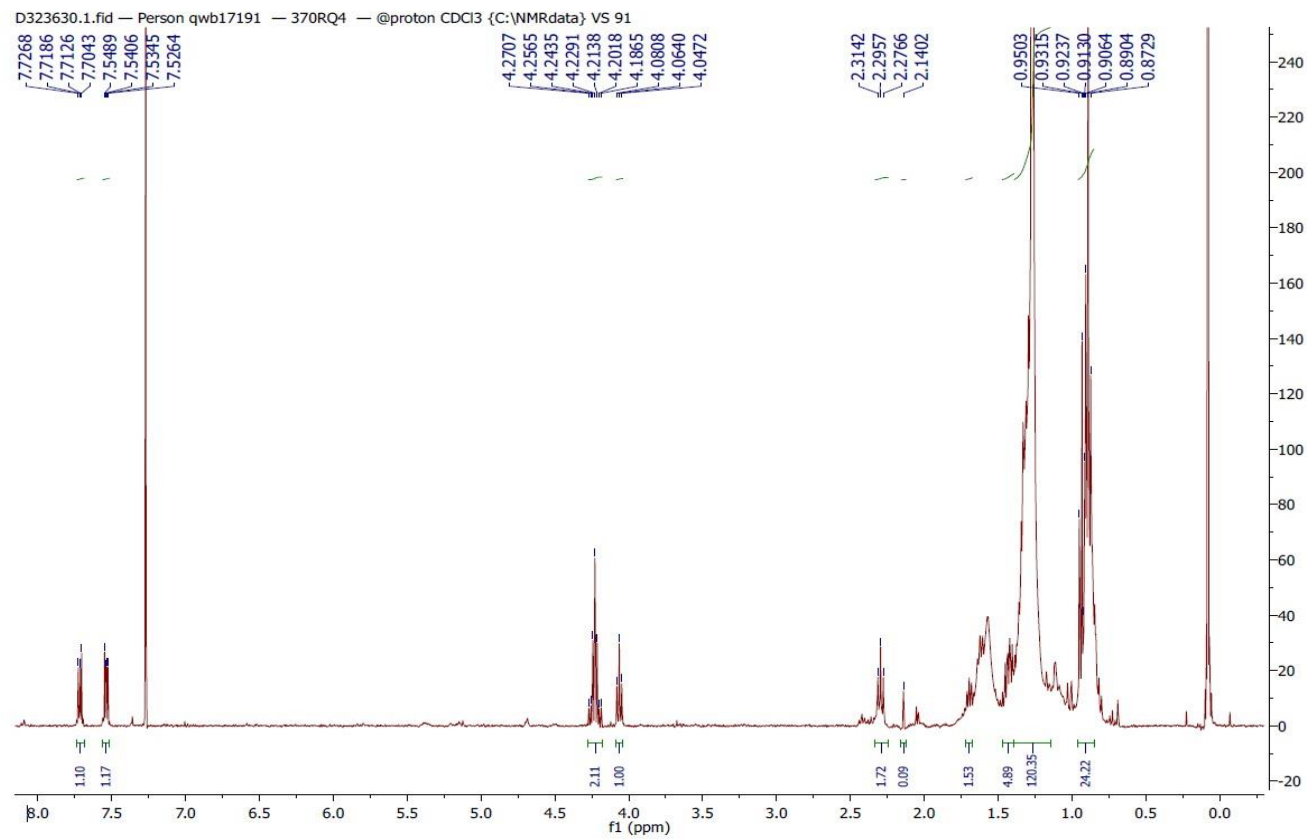






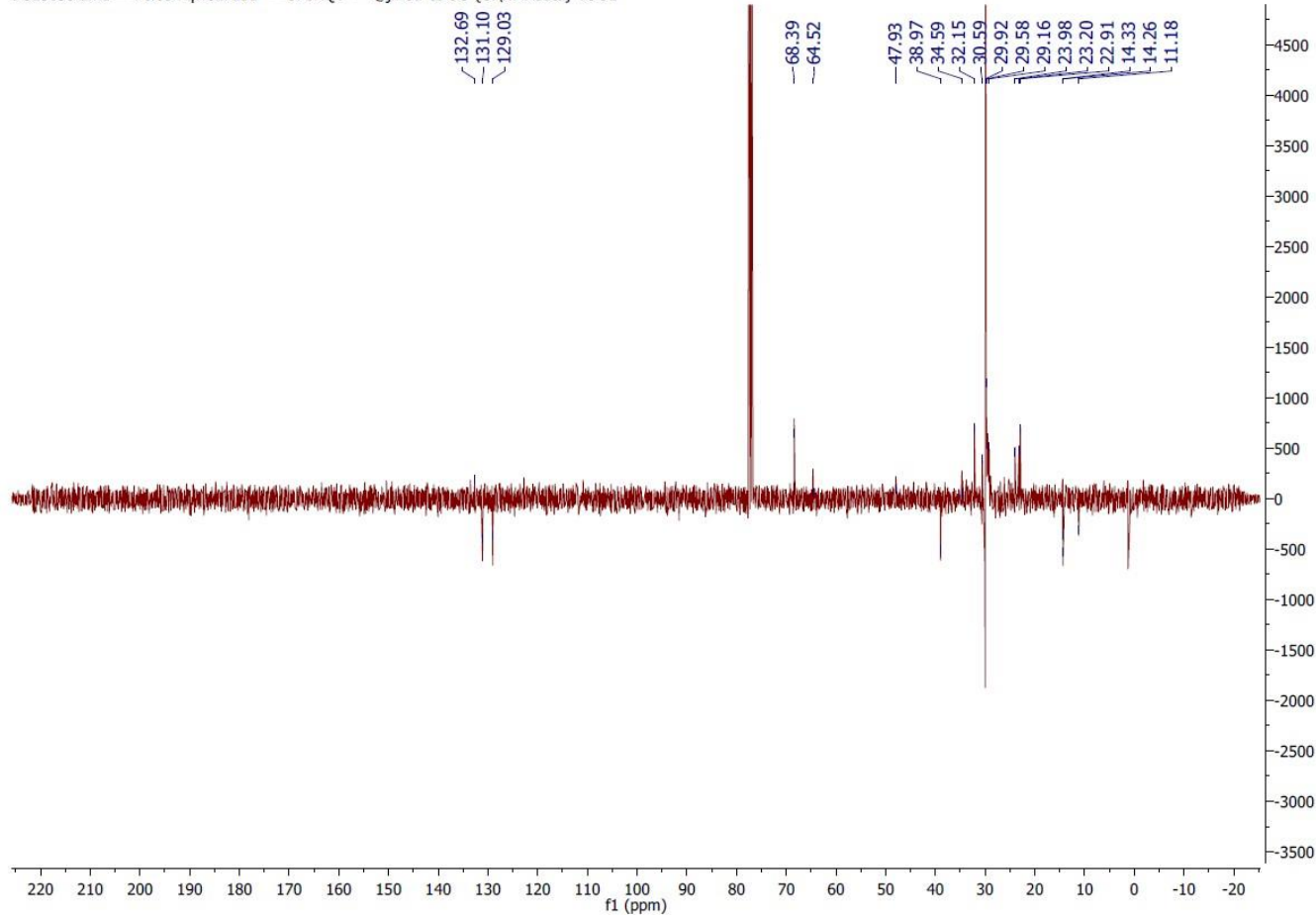


Appendix III: Others



^1H NMR spectrum (CDCl_3^* , 400 MHz) of 370RQ4.

D323630.2.fid — Person qwb17191 — 370RQ4 — @jmod CDCl3 {C:\NMRdata} VS 91



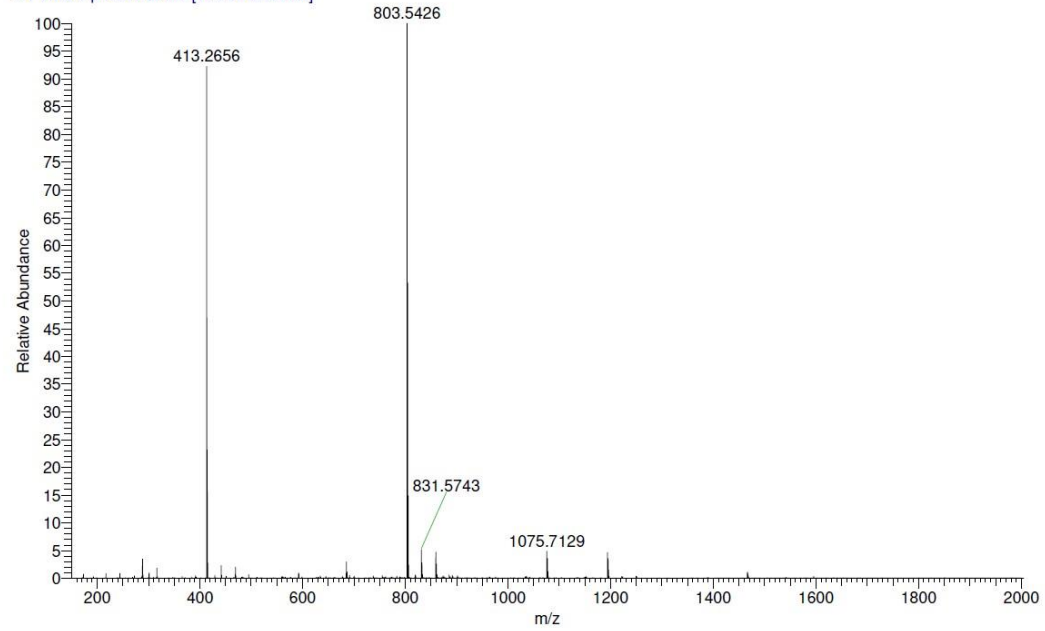
^{13}C DEPTQ NMR spectrum (CDCl_3^* , 100 MHz) of 370RQ4.

370RQ4 MW=278? C16H22O4
(DCM)/MeOH

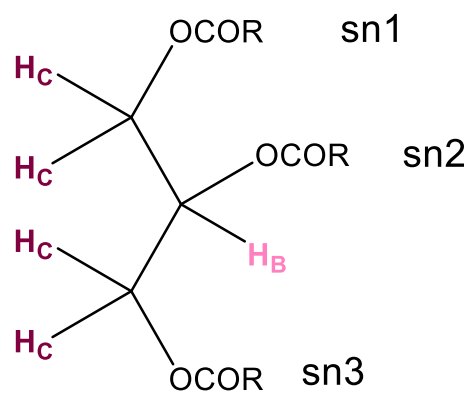
National Mass Spectrometry Facility, Swansea
LTQ Orbitrap XL

Veronique Seidel
16/11/2020 08:17:33

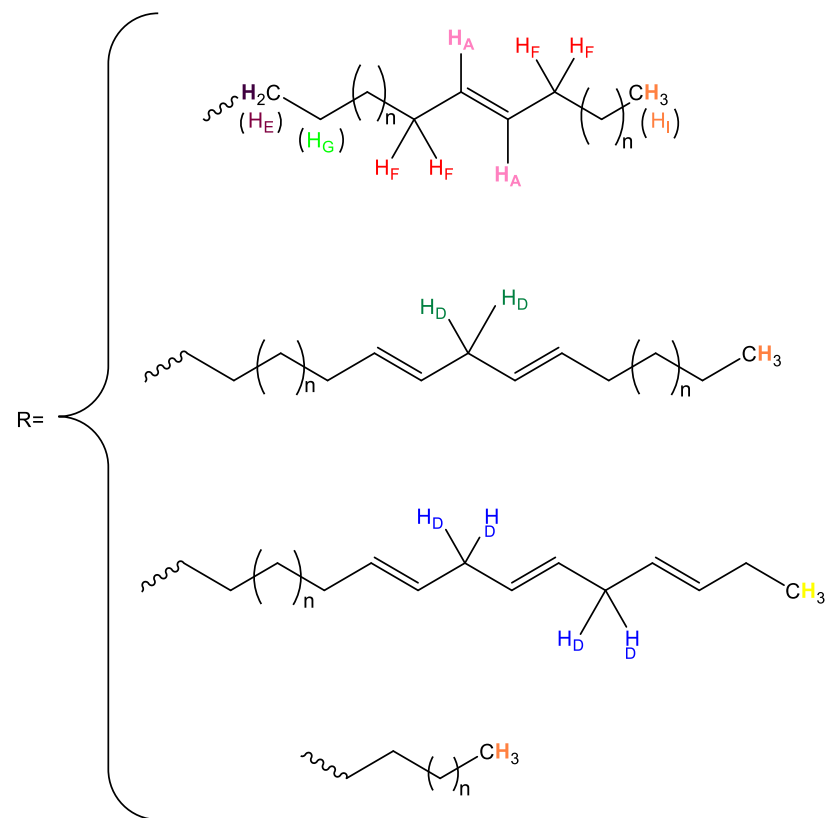
STRSEL_T3ANV_PA_B #26-35 RT: 0.96-1.28 AV: 10 NL: 7.32E5
T: FTMS + p NSI Full ms [150.00-2000.00]



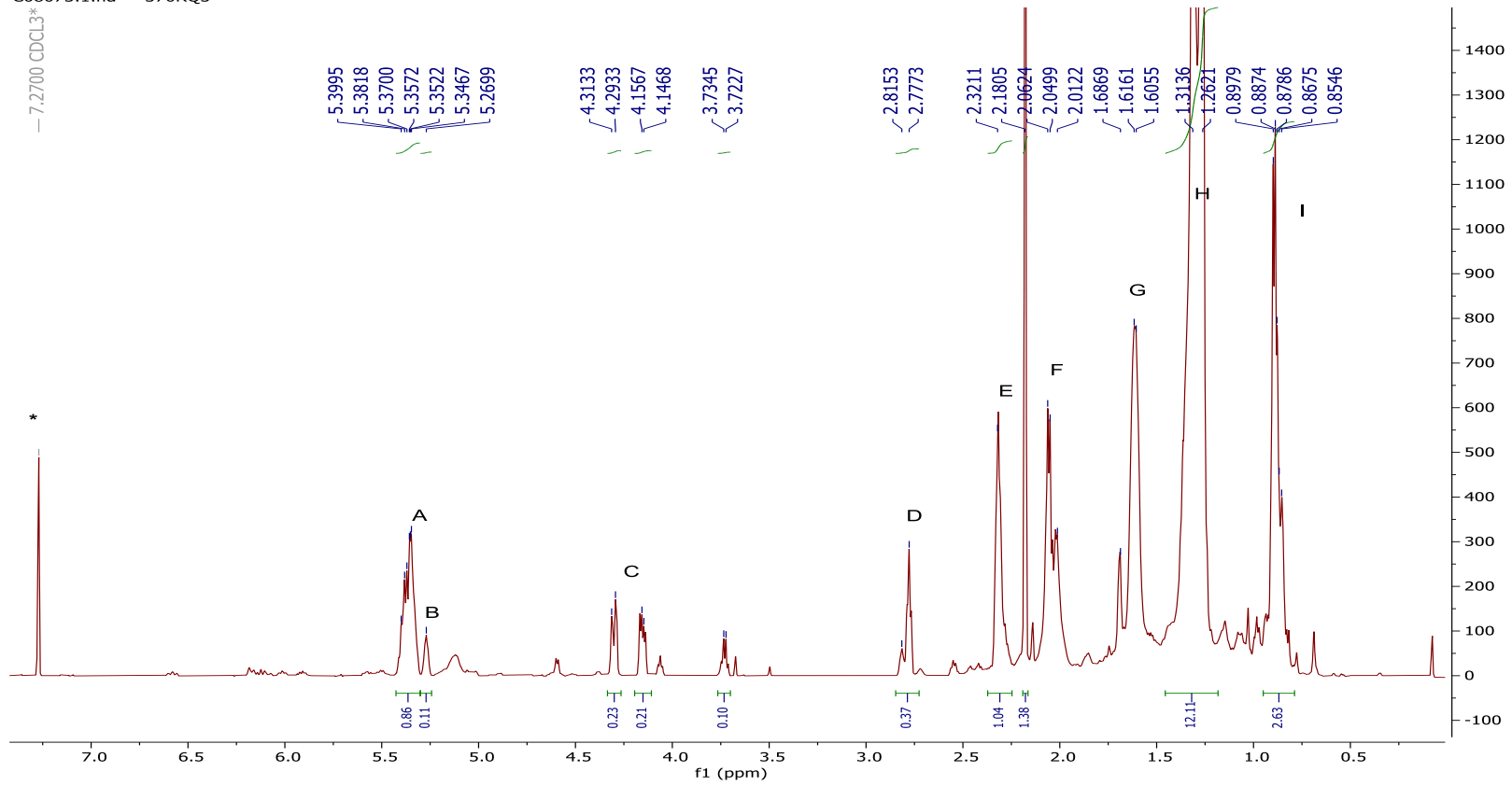
Mass spectrum of 370RQ4



Structure of 370RQ3 or TAG



C08073.1.fid — 370RQ3



^1H NMR spectrum (CDCl_3^* , 600 MHz) of 370RQ3.

REFERENCES

- Abraham, RJ and Rowan, A (1991) 'Nuclear magnetic resonance spectroscopy of chlorophyll'. In: Scheer, H. (ed.) *Chlorophylls*. CRC Press: 797-834.
- Acevedo, L *et al.* (2000) 'New Phenylethanoids from *Buddleja cordata* subsp. *cordata*'. *Planta Medica*, 66: 257-261.
- Adhvaryu, MR, Reddy, N and Vakharia, BC (2008) 'Prevention of hepatotoxicity due to anti tuberculosis treatment: a novel integrative approach'. *World Journal of Gastroenterology*, 14: 4753-4762.
- Ahmad Khan, M *et al.* (2020) 'Stigmasterol protects rats from collagen induced arthritis by inhibiting proinflammatory cytokines'. *International Immunopharmacology*, 85: 106642.
- Ahmad, VU *et al.* (2006) 'New phenethyl alcohol glycosides from *Stachys parviflora*'. *Journal of Asian Natural Products Research*, 8: 105-111.
- Ahmad, VU *et al.* (2008) 'New terpenoids from *Stachys parviflora* Benth'. *Magnetic Resonance in Chemistry*, 46: 986-989.
- Aissa, I *et al.* (2012) 'Synthesis of lipophilic tyrosyl esters derivatives and assessment of their antimicrobial and antileishmania activities'. *Lipids in Health and Disease*, 11: 13.
- Akbay, P *et al.* (2003) 'In vitro immunomodulatory activity of flavonoid glycosides from *Urtica dioica* L'. *Phytotherapy Research*, 17: 34-37.
- Akiyama, H *et al.* (2000) 'Inflammation and Alzheimer's disease'. *Neurobiology of Aging*, 21: 383-421.
- Alfatafta, AA *et al.* (1989) 'An investigation of *Bongardia chrysogonum*'. *Journal of Natural Products*, 52: 818-821.
- Ali, RM and Houghton, PJ (1999) 'A new phenolic fatty acid ester with lipoxygenase inhibitory activity from *Jacaranda filicifolia*'. *Planta Medica*, 65: 455-457.
- Ameglio, F *et al.* (2005) 'Post-treatment changes of six cytokines in active pulmonary tuberculosis: differences between patients with stable or increased fibrosis'. *International Journal of Tuberculosis and Lung Disease*, 9: 98-104.
- Anderson, WH, Gellerman, JL and Schlenk, H (1984) 'Effect of drought on phytol wax esters in *Phaseolus* leaves'. *Phytochemistry*, 23: 2695-2696.
- Andrade Júnior, DR *et al.* (2008) 'Correlation between serum tumor necrosis factor alpha levels and clinical severity of tuberculosis'. *Brazilian Journal of Infectious Diseases*, 12: 226-233.

- Angerosa, F *et al.* (1995) 'GC-MS Evaluation of Phenolic Compounds in Virgin Olive Oil'. *Journal of Agricultural and Food Chemistry*, 43: 1802-1807.
- Anne-marie, N *et al.* (2017) 'Quantification of Squalene in Olive Oil Using ¹³C Nuclear Magnetic Resonance Spectroscopy'. *Magnetochemistry*, 3: 34.
- Anwar, MA *et al.* (2019) 'Recent clinical trends in Toll-like receptor targeting therapeutics'. *Medicinal Research Reviews*, 39: 1053-1090.
- Apaza Ticona, L *et al.* (2021) 'Hydroalcoholic extract of *Tagetes minuta* L. inhibits inflammatory bowel disease through the activity of pheophytins on the NF-κB signalling pathway'. *Journal of Ethnopharmacology*, 268: 113603.
- Arango Duque, G and Descoteaux, A (2014) 'Macrophage Cytokines: Involvement in Immunity and Infectious Diseases'. *Frontiers in Immunology*, 5.
- Atanasov, AG *et al.* (2015) 'Discovery and resupply of pharmacologically active plant-derived natural products: A review'. *Biotechnology Advances*, 33: 1582-1614.
- Av-Gay, Y and Everett, M (2000) 'The eukaryotic-like Ser/Thr protein kinases of *Mycobacterium tuberculosis*'. *Trends in Microbiology*, 8: 238-244.
- Aydin-Schmidt, B, Thorsell, W and Wahlgren, M (2010) 'Carolus Linnaeus, the ash, worm-wood and other anti-malarial plants'. *Scandinavian Journal of Infectious Diseases*, 42: 941-942.
- Ayeleso, TB, Matumba, MG and Mukwevho, E (2017) 'Oleanolic Acid and Its Derivatives: Biological Activities and Therapeutic Potential in Chronic Diseases'. *Molecules (Basel, Switzerland)*, 22: 1915.
- Ayesh, BM, Abed, A and Faris, DM (2014) 'In vitro inhibition of human leukemia THP-1 cells by *Origanum syriacum* L. and *Thymus vulgaris* L. extracts'. *BMC Research Notes*, 7: 612.
- Bachhav, S *et al.* (2015) 'Oleanolic acid prevents increase in blood pressure and nephrotoxicity in nitric oxide dependent type of hypertension in rats'. *Pharmacognosy Research*, 7: 385.
- Bachhav, S *et al.* (2011) 'Oleanolic acid prevents glucocorticoid-induced hypertension in rats'. *Phytotherapy Research*, 25: 1435-1439.
- Bagri, P *et al.* (2009) 'New sterol esters from the flowers of *Punica granatum* Linn'. *Journal of Asian Natural Products Research*, 11: 710-715.
- Bahuguna, A and Rawat, DS (2020) 'An overview of new antitubercular drugs, drug candidates, and their targets'. *Medicinal Research Reviews*, 40: 263-292.
- Bai, N *et al.* (2010) 'Iridoids from *Fraxinus excelsior* with adipocyte differentiation-inhibitory and PPARα activation activity'. *Journal of Natural Products*, 73: 2-6.
- Bai, X *et al.* (2016) 'Curcumin enhances human macrophage control of *Mycobacterium tuberculosis* infection'. *Respirology*, 21: 951-957.

- Balunas, MJ and Kinghorn, AD (2005) 'Drug discovery from medicinal plants'. *Life Sciences*, 78: 431-441.
- Barberis, I *et al.* (2017) 'The history of tuberculosis: from the first historical records to the isolation of Koch's bacillus'. *Journal of Preventive Medicine and Hygiene*, 58: E9-E12.
- Barnes, PF (2003) 'Immunotherapy for Tuberculosis'. *American Journal of Respiratory and Critical Care Medicine*, 168: 142-143.
- Barreto, RSS *et al.* (2016) 'Evidence for the involvement of TNF- α and IL-1 β in the antinociceptive and anti-inflammatory activity of *Stachys lavandulifolia* Vahl. (Lamiaceae) essential oil and (-)- α -bisabolol, its main compound, in mice'. *Journal of Ethnopharmacology*, 191: 9-18.
- Behzad, S, Pirani, A and Mosaddegh, M (2014) 'Cytotoxic activity of some medicinal plants from hamedan district of iran'. *Iranian journal of pharmaceutical research : IJPR*, 13: 199-205.
- Bekker, L-G *et al.* (2000) 'Immunopathologic Effects of Tumor Necrosis Factor Alpha in Murine Mycobacterial Infection Are Dose Dependent'. *Infection and Immunity*, 68: 6954.
- Bekker, LG *et al.* (1998) 'Selective increase in plasma tumor necrosis factor-alpha and concomitant clinical deterioration after initiating therapy in patients with severe tuberculosis'. *Journal of Infectious Diseases*, 178: 580-584.
- Bele, A and Khale, A (2011) 'An overview on thin layer chromatography'. *International Journal of Pharmaceutical Sciences and Research*, 2: 256-267
- Bennett, JM *et al.* (2018) 'Inflammation-Nature's Way to Efficiently Respond to All Types of Challenges: Implications for Understanding and Managing "the Epidemic" of Chronic Diseases'. *Frontiers in medicine*, 5: 316-316.
- Bianco, A *et al.* (2004) 'Phenolic components of *Olea europaea*--isolation of tyrosol derivatives'. *Natural Product Research*, 18: 29-32.
- Biedermann, M *et al.* (2008) 'Fatty acid methyl and ethyl esters as well as wax esters for evaluating the quality of olive oils'. *European Food Research and Technology*, 228: 65-74.
- Biharee, A *et al.* (2020) 'Antimicrobial flavonoids as a potential substitute for overcoming antimicrobial resistance'. *Fitoterapia*, 146: 104720.
- Bikadi, Z and Hazai, E (2009) 'Application of the PM6 semi-empirical method to modeling proteins enhances docking accuracy of AutoDock'. *Journal of Cheminformatics*, 1: 15.
- Bladt, S and Wagner, H (2007) 'From the Zulu medicine to the European phytomedicine Umckaloabo®'. *Phytomedicine*, 14: 2-4.

- Blake, PS, Taylor, JM and Finch-Savage, WE (2002) 'Identification of abscisic acid, indole-3-acetic acid, jasmonic acid, indole-3-acetonitrile, methyl jasmonate and gibberellins in developing, dormant and stratified seeds of ash (*Fraxinus excelsior*)'. *Plant Growth Regulation*, 37: 119-125.
- Bloom, BR and Murray, CJ (1992) 'Tuberculosis: commentary on a reemergent killer'. *Science*, 257: 1055-1064.
- Bonaterra, GA *et al.* (2019) 'Anti-inflammatory effects of Phytodolor® (STW 1) and components (poplar, ash and goldenrod) on human monocytes/macrophages'. *Phytomedicine*, 58: 152868.
- Bouguellid, G *et al.* (2020) 'Antimutagenic, antigenotoxic and antiproliferative activities of *Fraxinus angustifolia* Vahl. leaves and stem bark extracts and their phytochemical composition'. *PLoS One*, 15: e0230690.
- Bouic, P *et al.* (1999) 'The effects of B-sitosterol (BSS) and B-sitosterol glucoside (BSSG) mixture on selected immune parameters of marathon runners: inhibition of post marathon immune suppression and inflammation'. *International Journal of Sports Medicine*, 20: 258-262.
- Bourigault, ML *et al.* (2013) 'Tumor necrosis factor neutralization combined with chemotherapy enhances *Mycobacterium tuberculosis* clearance and reduces lung pathology'. *Am J Clin Exp Immunol*, 2: 124-134.
- Brendler, T and van Wyk, BE (2008) 'A historical, scientific and commercial perspective on the medicinal use of *Pelargonium sidoides* (Geraniaceae)'. *Journal of Ethnopharmacology*, 119: 420-433.
- Brito Filho, SGd *et al.* (2014) 'Chemical constituents isolated from *turnera subulata* Sm. and electrochemical characterization of phaeophytin b'. *Química Nova*, 37: 603-609.
- Brown, AK *et al.* (2007) 'Flavonoid inhibitors as novel antimycobacterial agents targeting Rv0636, a putative dehydratase enzyme involved in *Mycobacterium tuberculosis* fatty acid synthase II'. *Microbiology (Reading)*, 153: 3314-3322.
- Brown, GD (1994) 'Phytene-1,2-diol from *Artemisia annua*'. *Phytochemistry*, 36: 1553-1554.
- Buchgraber, M *et al.* (2004) 'Triacylglycerol profiling by using chromatographic techniques'. *European Journal of Lipid Science and Technology*, 106: 621-648.
- Bui, TT *et al.* (2017) '*Citrus tachibana* Leaves Ethanol Extract Alleviates Airway Inflammation by the Modulation of Th1/Th2 Imbalance via Inhibiting NF-κB Signaling and Histamine Secretion in a Mouse Model of Allergic Asthma'. *Journal of Medicinal Food*, 20: 676-684.
- Caggiu, E *et al.* (2019) 'Inflammation, Infectious Triggers, and Parkinson's Disease'. *Frontiers in Neurology*, 10.

- Cantrell, CL *et al.* (1996) 'Antimycobacterial Cycloartanes from *Borrighia frutescens*'. *Journal of Natural Products*, 59: 1131-1136.
- Cárdeno, A *et al.* (2015) 'Squalene targets pro- and anti-inflammatory mediators and pathways to modulate over-activation of neutrophils, monocytes and macrophages'. *Journal of Functional Foods*, 14: 779-790.
- Castellano, JM *et al.* (2019) 'Oleanolic Acid Exerts a Neuroprotective Effect Against Microglial Cell Activation by Modulating Cytokine Release and Antioxidant Defense Systems'. *Biomolecules*, 9.
- Cavalcanti, YVN *et al.* (2012) 'Role of TNF-Alpha, IFN-Gamma, and IL-10 in the Development of Pulmonary Tuberculosis'. *Pulmonary Medicine*, 2012: 745483.
- Cavalluzzi, MM *et al.* (2017) 'Ligand efficiency metrics in drug discovery: the pros and cons from a practical perspective'. *Expert Opinion on Drug Discovery*, 12: 1087-1104.
- Cavero, RY and Calvo, MI (2015) 'Medicinal plants used for musculoskeletal disorders in Navarra and their pharmacological validation'. *Journal of Ethnopharmacology*, 168: 255-259.
- Chan, ED and Iseman, MD (2002) 'Current medical treatment for tuberculosis'. *BMJ : British Medical Journal*, 325: 1282-1286.
- Charisiadis, P *et al.* (2014) '¹H-NMR as a structural and analytical tool of intra- and intermolecular hydrogen bonds of phenol-containing natural products and model compounds'. *Molecules (Basel, Switzerland)*, 19: 13643-13682.
- Chávez-Sánchez, L *et al.* (2014) 'Innate Immune System Cells in Atherosclerosis'. *Archives of Medical Research*, 45: 1-14.
- Checker, R *et al.* (2012) 'Potent Anti-Inflammatory Activity of Ursolic Acid, a Triterpenoid Antioxidant, Is Mediated through Suppression of NF-κB, AP-1 and NF-AT'. *PloS One*, 7: e31318.
- Chen, D *et al.* (2017a) 'Sclerotiorin inhibits protein kinase G from *Mycobacterium tuberculosis* and impairs mycobacterial growth in macrophages'. *Tuberculosis (Edinb)*, 103: 37-43.
- Chen, JJ *et al.* (2009) 'seco-Abietane diterpenoids, a phenylethanoid derivative, and antitubercular constituents from *Callicarpa pilosissima*'. *Journal of Natural Products*, 72: 223-228.
- Chen, L *et al.* (2017b) 'Inflammatory responses and inflammation-associated diseases in organs'. *Oncotarget*, 9: 7204-7218.
- Chen, X *et al.* (2013) 'Ursolic acid attenuates lipopolysaccharide-induced acute lung injury in a mouse model'. *Immunotherapy*, 5: 39-47.
- Chen, YC (2015) 'Beware of docking!'. *Trends in Pharmacological Sciences*, 36: 78-95.

- Chen, Z *et al.* (2008) 'Studies on the chemical constituents and anticancer activity of *Saxifraga stolonifera* (L) Meeb'. *Bioorganic and Medicinal Chemistry*, 16: 1337-1344.
- Ching, A *et al.* (2007) 'Characterization of flavonoid derivatives from *Boesenbergia rotunda* (L.)'. *The Malaysian Journal of Analytical Sciences*, 11.
- Chinsembu, KC (2016) 'Tuberculosis and nature's pharmacy of putative anti-tuberculosis agents'. *Acta Tropica*, 153: 46-56.
- Chiswick, EL *et al.* (2012) 'Detection and quantification of cytokines and other biomarkers'. *Methods in Molecular Biology*, 844: 15-30.
- Choy, EH and Panayi, GS (2001) 'Cytokine pathways and joint inflammation in rheumatoid arthritis'. *New England Journal of Medicine*, 344: 907-916.
- Chu, W-M (2013) 'Tumor necrosis factor'. *Cancer Letters*, 328: 222-225.
- Chueahongthong, F *et al.* (2011) 'Cytotoxic effects of crude kaffir lime (*Citrus Hystrix*, DC.) leaf fractional extracts on leukemic cell lines'. *Journal of Medicinal Plants Research*, 5: 3097-3105.
- Chun, J *et al.* (2014) 'Ursolic acid inhibits nuclear factor- κ B signaling in intestinal epithelial cells and macrophages, and attenuates experimental colitis in mice'. *Life Sciences*, 110: 23-34.
- Ciesielska, A, Matyjek, M and Kwiatkowska, K (2021) 'TLR4 and CD14 trafficking and its influence on LPS-induced pro-inflammatory signaling'. *Cellular and Molecular Life Sciences*, 78: 1233-1261.
- Coll, JC and Bowden, BF (1986) 'The Application of Vacuum Liquid Chromatography to the Separation of Terpene Mixtures'. *Journal of Natural Products*, 49: 934-936.
- Cooper, AM *et al.* (1997) 'Interleukin 12 (IL-12) Is Crucial to the Development of Protective Immunity in Mice Intravenously Infected with *Mycobacterium tuberculosis*'. *Journal of Experimental Medicine*, 186: 39-45.
- Cooper, AM, Solache, A and Khader, SA (2007) 'Interleukin-12 and tuberculosis: an old story revisited'. *Current Opinion in Immunology*, 19: 441-447.
- Dais, P *et al.* (2017) 'Complete ^1H and ^{13}C NMR assignment and ^{31}P NMR determination of pentacyclic triterpenic acids'. *Analytical Methods*, 9: 949-957.
- Damtoft, S, Franzyk, H and Jensen, SR (1992) 'Excelsioside, a secoiridoid glucoside from *Fraxinus excelsior*'. *Phytochemistry*, 31: 4197-4201.
- Daniel, TM (2006) 'The history of tuberculosis'. *Respiratory Medicine*, 100: 1862-1870.
- De-Eknamkul, W and Potduang, B (2003) 'Biosynthesis of β -sitosterol and stigmasterol in *Croton sublyratus* proceeds via a mixed origin of isoprene units'. *Phytochemistry*, 62: 389-398.

- De Freitas, RF and Schapira, M (2017) 'A systematic analysis of atomic protein–ligand interactions in the PDB'. *MedChemComm*, 8: 1970-1981.
- De Martino, M *et al.* (2019) 'Immune Response to *Mycobacterium tuberculosis*: A Narrative Review'. *Frontiers in Pediatrics*, 7.
- De Miguel, C *et al.* (2015) 'Inflammation and hypertension: new understandings and potential therapeutic targets'. *Current Hypertension Reports*, 17: 507.
- Degner, NR *et al.* (2017) 'Metformin Use Reverses the Increased Mortality Associated With Diabetes Mellitus During Tuberculosis Treatment'. *Clinical Infectious Diseases*, 66: 198-205.
- Delazar, A *et al.* (2005) 'Two acylated flavonoid glycosides from *Stachys bombycina*, and their free radical scavenging activity'. *Pharmazie*, 60: 878-880.
- Delazar, A *et al.* (2011) 'Lavandulifolioside B: a new phenylethanoid glycoside from the aerial parts of *Stachys lavandulifolia* Vahl'. *Natural Product Research*, 25: 8-16.
- Demoruelle, MK, Deane, KD and Holers, VM (2014) 'When and where does inflammation begin in rheumatoid arthritis?'. *Current Opinion in Rheumatology*, 26: 64-71.
- Desai, F *et al.* (2009) 'Comparison of the immunomodulatory effects of the plant sterol β -sitosterol to simvastatin in peripheral blood cells from multiple sclerosis patients'. *International Immunopharmacology*, 9: 153-157.
- Deveci, F *et al.* (2005) 'Changes in serum cytokine levels in active tuberculosis with treatment'. *Mediators of Inflammation*, 2005: 256-262.
- Dewick, PM (2009) *Medicinal Natural Products: A Biosynthetic Approach*. third Edition edn. John Wiley & Sons Ltd Baffins Lane, Chichester, , pp.214.
- Dheda, K, Barry, CE, 3rd and Maartens, G (2016) 'Tuberculosis'. *The Lancet*, 387: 1211-1226.
- Di Gesso, JL *et al.* (2015) 'Flavonoid metabolites reduce tumor necrosis factor- α secretion to a greater extent than their precursor compounds in human THP-1 monocytes'. *Molecular Nutrition & Food Research*, 59: 1143-1154.
- Dias, DA, Urban, S and Roessner, U (2012) 'A Historical Overview of Natural Products in Drug Discovery'. *Metabolites*, 2: 303.
- Ding, K *et al.* (2019) ' β -Sitosterol improves experimental colitis in mice with a target against pathogenic bacteria'. *Journal of Cellular Biochemistry*, 120: 5687-5694.
- Djoba Siawaya, JF *et al.* (2009) 'Differential cytokine/chemokines and KL-6 profiles in patients with different forms of tuberculosis'. *Cytokine*, 47: 132-136.
- Domingo-Gonzalez, R *et al.* (2016) 'Cytokines and Chemokines in *Mycobacterium tuberculosis* Infection'. *Microbiology spectrum*, 4: 10.1128/microbiolspec.TB1122-0018-2016.

- Donald, P *et al.* (1997) 'A randomised placebo-controlled trial of the efficacy of beta-sitosterol and its glucoside as adjuvants in the treatment of pulmonary tuberculosis'. *The International Journal of Tuberculosis and Lung Disease*, 1: 518-522.
- Dong, M, Pfeiffer, B and Altmann, K-H (2017) 'Recent developments in natural product-based drug discovery for tuberculosis'. *Drug Discovery Today*, 22: 585-591.
- Dookie, N *et al.* (2018) 'Evolution of drug resistance in *Mycobacterium tuberculosis*: a review on the molecular determinants of resistance and implications for personalized care'. *Journal of Antimicrobial Chemotherapy*, 73: 1138-1151.
- Droupadi, PR and Krishnan, V (1984) 'An efficient method of preparation of pheophytina—Divalent metal pheophytinates'. *Proceedings of the Indian Academy of Sciences - Chemical Sciences*, 93: 117-124.
- Duke, JA (2008) *Duke's handbook of medicinal plants of Latin America*. Boca Raton: Boca Raton : Taylor & Francis.
- Dyas, L and Goad, LJ (1993) 'Steryl fatty acyl esters in plants'. *Phytochemistry*, 34: 17-29.
- Eddouks, M and Maghrani, M (2004) 'Phlorizin-like effect of *Fraxinus excelsior* in normal and diabetic rats'. *Journal of Ethnopharmacology*, 94: 149-154.
- Eddouks, M *et al.* (2005) '*Fraxinus excelsior* L. evokes a hypotensive action in normal and spontaneously hypertensive rats'. *Journal of Ethnopharmacology*, 99: 49-54.
- Edilu, A, Adane, L and Woyessa, D (2015) 'In vitro antibacterial activities of compounds isolated from roots of *Caylusea abyssinica*'. *Annals of Clinical Microbiology and Antimicrobials*, 14: 15.
- Egan, P *et al.* (2004) 'GI 5, a dimer of oleoside, from *Fraxinus excelsior* (Oleaceae)'. *Biochemical Systematics and Ecology*, 32: 1069-1071.
- El-Ansari, MA *et al.* (1991) 'Flavonoid constituents of *Stachys aegyptiaca*'. *Phytochemistry*, 30: 1169-1173.
- Ernst, JD (2012) 'The immunological life cycle of tuberculosis'. *Nature Reviews Immunology*, 12: 581.
- Eshbakova, K and Kamoldinov, KS (2014) 'CHEMICAL CONSTITUENTS OF *FRAXINUS SYRIACA*'. *International Journal of Pharmacy & Therapeutics*, , 5: 181-184.
- Etna, MP *et al.* (2014) 'Pro- and anti-inflammatory cytokines in tuberculosis: A two-edged sword in TB pathogenesis'. *Seminars in Immunology*, 26: 543-551.
- European Medicines Agency (2012) *Assessment report on Assessment report on *Fraxinus excelsior* L. or *Fraxinus angustifolia* Vahl, folium*. . Available at: https://www.ema.europa.eu/en/documents/herbal-report/final-assessment-report-fraxinus-excelsior-l-fraxinus-angustifolia-vahl-folium_en.pdf.

European Medicines Agency (2018) *Assessment report on Pelargonium sidoides DC and/or Pelargonium reniforme Curt., radix.* Available at: https://www.ema.europa.eu/en/documents/herbal-report/final-assessment-report-pelargonium-sidoides-dc/pelargonium-reniforme-curt-radix-revision-1_en.pdf.

Evans, WC (2009) *Trease and Evans pharmacognosy*. 16th ed. / rev. with the assistance of Daphne Evans.. edn., pp.37.

Fabricant, DS and Farnsworth, NR (2001) 'The value of plants used in traditional medicine for drug discovery'. *Environmental Health Perspectives*, 109 Suppl 1: 69-75.

Farooq, U *et al.* (2015) 'A new rosane-type diterpenoid from *Stachys parviflora* and its density functional theory studies'. *Natural Product Research*, 29: 813-819.

Fatemeh, K and Piri, K (2011) 'In vitro cytotoxic activity of aqueous root extract of *Althea kurdica* against endothelial human bone marrow cells (line K562) and human lymphocytes'. *Bull Environ Pharmacol Life Sci*, 26: 23-29.

Fazio, C *et al.* (1994) 'Diterpenoids from *Stachys mucronata*'. *Planta Medica*, 60: 499.

Federico, S *et al.* (2020) 'Modulation of the Innate Immune Response by Targeting Toll-like Receptors: A Perspective on Their Agonists and Antagonists'. *Journal of Medicinal Chemistry*, 63: 13466-13513.

Feng, K *et al.* (2015) 'Optimization extraction, preliminary characterization and antioxidant activity in vitro of polysaccharides from *Stachys sieboldii* Miq. tubers'. *Carbohydrate Polymers*, 125: 45-52.

Feng, W, Hao, Z and Li, M (2017) 'Isolation and structure identification of flavonoids'. *Flavonoids, from biosynthesis to human health/Ed. by Justino GC Intech Open*: 17-43.

Ferenczy, GG and Keserű, GM (2010) 'Thermodynamics guided lead discovery and optimization'. *Drug Discovery Today*, 15: 919-932.

Ferenczy, GG and Keserű, GM (2013) 'How Are Fragments Optimized? A Retrospective Analysis of 145 Fragment Optimizations'. *Journal of Medicinal Chemistry*, 56: 2478-2486.

Filipe-Santos, O *et al.* (2006) 'Inborn errors of IL-12/23- and IFN-gamma-mediated immunity: molecular, cellular, and clinical features'. *Seminars in Immunology*, 18: 347-361.

Fiocchi, C (1998) 'Inflammatory bowel disease: etiology and pathogenesis'. *Gastroenterology*, 115: 182-205.

Flynn, JL, Chan, J and Lin, PL (2011) 'Macrophages and control of granulomatous inflammation in tuberculosis'. *Mucosal Immunology*, 4: 271-278.

Forgo, P and Kövér, KE (2004) 'Gradient enhanced selective experiments in the 1H NMR chemical shift assignment of the skeleton and side-chain resonances of stigmasterol, a phytosterol derivative'. *Steroids*, 69: 43-50.

- Forrellad, MA *et al.* (2013) 'Virulence factors of the *Mycobacterium tuberculosis* complex'. *Virulence*, 4: 3-66.
- Freitas, S *et al.* (2019) 'Chlorophyll Derivatives from Marine *Cyanobacteria* with Lipid-Reducing Activities'. *Marine Drugs*, 17: 229.
- Gabay, O *et al.* (2010) 'Stigmasterol: a phytosterol with potential anti-osteoarthritic properties'. *Osteoarthritis and Cartilage*, 18: 106-116.
- Gaillard, T (2018) 'Evaluation of AutoDock and AutoDock Vina on the CASF-2013 Benchmark'. *Journal of Chemical Information and Modeling*, 58: 1697-1706.
- Garcia-Sosa, A, Hetényi, C and Maran, U (2009) 'Drug Efficiency Indices for Improvement of Molecular Docking Scoring Functions'. *Journal of Computational Chemistry*, 31: 174-184.
- García, A *et al.* (2012) 'Recent advances in antitubercular natural products'. *European Journal of Medicinal Chemistry*, 49: 1-23.
- Garcia, I *et al.* (2013) 'Evaluation of THP-1 cell line as an in vitro model for long-term safety assessment of new molecules'. *International Journal of Cosmetic Science*, 35: 568-574.
- Garcia, R *et al.* (2019) 'Assessment of the triacylglycerol fraction of olive oil by 1D-NMR spectroscopy: exploring the usefulness of DEPT tool on the peak assignments of 13C NMR spectra'. *European Food Research and Technology*, 245: 2479-2488.
- Gautam, R, Saklani, A and Jachak, SM (2007) 'Indian medicinal plants as a source of antimycobacterial agents'. *Journal of Ethnopharmacology*, 110: 200-234.
- Ge, F *et al.* (2010) 'In vitro synergistic interactions of oleanolic acid in combination with isoniazid, rifampicin or ethambutol against *Mycobacterium tuberculosis*'. *Journal of Medical Microbiology*, 59: 567-572.
- Gharib Naseri, MK *et al.* (2011) 'Spasmolytic effect of *Stachys lavandulifolia* vahl. Crude methanolic extract and fractions on rat ileum'. *Iran J Pharm Res*, 10: 307-312.
- Gibbons, S (2012) 'An Introduction to Planar Chromatography and Its Application to Natural Products Isolation'. In: Sarker, S.D. and Nahar, L. (eds.) *Natural Products Isolation*. Totowa, NJ: Humana Press: 117-153.
- Gilardoni, G *et al.* (2011) 'Lipophilic components from the Ecuadorian plant *Schistocarpha eupatorioides*'. *Natural Product Communications*, 6: 767-772.
- Gilca, M, Tiplica, GS and Salavastru, CM (2018) 'Traditional and ethnobotanical dermatology practices in Romania and other Eastern European countries'. *Clinics in Dermatology*, 36: 338-352.
- Giri, SS *et al.* (2016) 'Pinocembrin attenuates lipopolysaccharide-induced inflammatory responses in *Labeo rohita* macrophages via the suppression of the NF- κ B signalling pathway'. *Fish & Shellfish Immunology*, 56: 459-466.

Goodman, RA, Oldfield, E and Allerhand, A (1973) 'Assignments in the natural-abundance carbon-13 nuclear magnetic resonance spectrum of chlorophyll a and a study of segmental motion in neat phytol'. *Journal of the American Chemical Society*, 95: 7553-7558.

Gordien, AY *et al.* (2009) 'Antimycobacterial terpenoids from *Juniperus communis* L. (Cupressaceae)'. *Journal of Ethnopharmacology*, 126: 500-505.

Grange, JM and Davey, RW (1990) 'Detection of antituberculous activity in plant extracts'. *Journal of Applied Bacteriology*, 68: 587-591.

Gu, X *et al.* (2017) 'Pinocembrin attenuates allergic airway inflammation via inhibition of NF- κ B pathway in mice'. *International Immunopharmacology*, 53: 90-95.

Gupta, MB *et al.* (1980) 'Anti-Inflammatory and Antipyretic Activities of β -Sitosterol'. *Planta Medica*, 39: 157-163.

Gupta, VK *et al.* (2017) 'Plants in our combating strategies against *Mycobacterium tuberculosis*: progress made and obstacles met'. *Pharmaceutical Biology*, 55: 1536-1544.

Gutiérrez-Rebolledo, GA *et al.* (2016) 'Hepatoprotective properties of oleanolic and ursolic acids in antitubercular drug-induced liver damage'. *Asian Pacific Journal of Tropical Medicine*, 9: 644-651.

Gyllenhaal, C *et al.* (2012) 'Ethnobotanical approach versus random approach in the search for new bioactive compounds: support of a hypothesis'. *Pharmaceutical Biology*, 50: 30-41.

Habib-Allah, M *et al.* (2016) 'Collection and assessment of traditional medicinal plants used by the indigenous people of Dastena in Iran'. *Journal of HerbMed Pharmacology*, 5: 54-60.

Habib, MR and Karim, MR (2009) 'Antimicrobial and Cytotoxic Activity of Di-(2-ethylhexyl) Phthalate and Anhydrosophoradiol-3-acetate Isolated from *Calotropis gigantea* (Linn.) Flower'. *Mycobiology*, 37: 31-36.

Hammami, S *et al.* (2004) 'Isolation and structure elucidation of a flavanone, a flavanone glycoside and vomifoliol from *Echiochilon fruticosum* growing in Tunisia'. *Molecules (Basel, Switzerland)*, 9: 602-608.

Hargus, JA *et al.* (2007) 'Mono-(l)-aspartylchlorin-e6'. *Photochemistry and Photobiology*, 83: 1006-1015.

Hariono, M *et al.* (2016) 'Potential New H1N1 Neuraminidase Inhibitors from Ferulic Acid and Vanillin: Molecular Modelling, Synthesis and in Vitro Assay'. *Scientific Reports*, 6: 38692-38692.

Haskó, G and Szabó, C (1999) 'IL-12 as a therapeutic target for pharmacological modulation in immune-mediated and inflammatory diseases: regulation of T helper 1/T helper 2 responses'. *British Journal of Pharmacology*, 127: 1295-1304.

- Hauer, H *et al.* (2010) 'Benzopyranones and their sulfate esters from *Pelargonium sidoides*'. *Planta Medica*, 76: 350-352.
- Hawn, TR *et al.* (2013) 'Host-directed therapeutics for tuberculosis: can we harness the host?'. *Microbiology and Molecular Biology Reviews*, 77: 608-627.
- Háznagy-Radnai, E *et al.* (2012) 'Antiinflammatory Activities of Hungarian *Stachys* species and Their Iridoids'. *Phytotherapy Research*, 26: 505-509.
- Haznagy-Radnai, E *et al.* (2008) 'Cytotoxic activities of *Stachys* species'. *Fitoterapia*, 79: 595-597.
- He, H-P *et al.* (2002) 'Extraction and Purification of Squalene from *Amaranthus* Grain'. *Journal of Agricultural and Food Chemistry*, 50: 368-372.
- Heinrich, M (2010) 'Ethnopharmacology in the 21st century - grand challenges'. *Frontiers in Pharmacology*, 1: 8-8.
- Heinrich, M and Gibbons, S (2001) 'Ethnopharmacology in drug discovery: an analysis of its role and potential contribution'. *Journal of Pharmacy and Pharmacology*, 53: 425-432.
- Helmstaedter, A (1996) *Umckaloabo – Late vindication of a secret remedy*.
- Higashi-Okai, K *et al.* (2001) 'Identification and antioxidant activity of several pigments from the residual green tea (*Camellia sinensis*) after hot water extraction'. *Journal of University of Occupational and Environmental Health*, 23: 335-344.
- Hopkins, AL, Groom, CR and Alex, A (2004) 'Ligand efficiency: a useful metric for lead selection'. *Drug Discovery Today*, 9: 430-431.
- Hopkins, AL *et al.* (2014) 'The role of ligand efficiency metrics in drug discovery'. *Nature Reviews Drug Discovery*, 13: 105-121.
- Hossain, MM and Norazmi, M-N (2013) 'Pattern Recognition Receptors and Cytokines in *Mycobacterium tuberculosis* Infection—The Double-Edged Sword?'. *BioMed Research International*, 2013: 179174.
- Huang, X *et al.* (2007) 'Proteasome and NF-kappaB inhibiting phaeophytins from the green alga *Cladophora fascicularis*'. *Molecules (Basel, Switzerland)*, 12: 582-592.
- Humphries, C (1981) *Hamlyn guide to trees of Britain & Europe*. Hamlyn, pp.288-289.
- Hynninen, PH, Leppäkases, TS and Mesilaakso, M (2006) 'The enolate anions of chlorophylls a and b as ambident nucleophiles in oxidations with (-)- or (+)-(10-camphorsulfonyl)oxaziridine. Synthesis of 132(S/R)-hydroxychlorophylls a and b'. *Tetrahedron*, 62: 3412-3422.
- Ibarra, A *et al.* (2011) '*Fraxinus excelsior* seed extract FraxiPure™ limits weight gains and hyperglycemia in high-fat diet-induced obese mice'. *Phytomedicine*, 18: 479-485.

Ikeda, Y, Murakami, A and Ohigashi, H (2008) 'Ursolic acid: an anti- and pro-inflammatory triterpenoid'. *Molecular Nutrition & Food Research*, 52: 26-42.

Ikram, M *et al.* (2019) 'Hesperetin Confers Neuroprotection by Regulating Nrf2/TLR4/NF- κ B Signaling in an A β Mouse Model'. *Molecular Neurobiology*, 56: 6293-6309.

Inte, V, Ragasa, C and Rideout, J (1998) 'Triterpenes, hydrocarbons and an antimutagenic alkaloid from *Catharanthus roseus*'. *Asia life sciences*, 7: 11-12.

Iossifova, T, Kostova, I and Evstatieva, LN (1997) 'Secoiridoids and hydroxycoumarins in Bulgarian *Fraxinus* species'. *Biochemical Systematics and Ecology*, 25: 271-274.

Iqbal, M *et al.* (2013) 'Phytochemicals as a potential source for TNF- α inhibitors'. *Phytochemistry Reviews*, 12: 65-93.

Iscan, G *et al.* (2012) 'Antimicrobial and antioxidant activities of *Stachys lavandulifolia* subsp. *lavandulifolia* essential oil and its infusion'. *Natural Product Communications*, 7: 1241-1244.

Islam, MN *et al.* (2013) 'Anti-inflammatory activity of edible brown alga *Saccharina japonica* and its constituents pheophorbide a and pheophytin a in LPS-stimulated RAW 264.7 macrophage cells'. *Food and Chemical Toxicology*, 55: 541-548.

Jakštys, B *et al.* (2015) 'Different Cell Viability Assays Reveal Inconsistent Results After Bleomycin Electrotransfer In Vitro'. *Journal of Membrane Biology*, 248: 857-863.

Jang, S-E *et al.* (2014) 'Ursolic Acid Isolated from the Seed of *Cornus officinalis* Ameliorates Colitis in Mice by Inhibiting the Binding of Lipopolysaccharide to Toll-like Receptor 4 on Macrophages'. *Journal of Agricultural and Food Chemistry*, 62: 9711-9721.

Janssen, S *et al.* (2012) 'Exploring prospects of novel drugs for tuberculosis'. *Drug Design, Development and Therapy*, 6: 217-224.

Jasenosky, LD *et al.* (2015) 'T cells and adaptive immunity to *Mycobacterium tuberculosis* in humans'. *Immunological Reviews*, 264: 74-87.

Jassbi, AR *et al.* (2014) 'Cytotoxic, antioxidant and antimicrobial effects of nine species of woundwort (*Stachys*) plants'. *Pharmaceutical Biology*, 52: 62-67.

Jee, B *et al.* (2018) 'Ursolic acid and carvacrol may be potential inhibitors of dormancy protein small heat shock protein16.3 of *Mycobacterium tuberculosis*'. *Journal of Biomolecular Structure and Dynamics*, 36: 3434-3443.

Jensen, SR and Nielsen, BJ (1976) 'A new coumarin fraxidin 8-O- β -d-glucoside and 10-hydroxylogstroside from bark of *Fraxinus exelsior*'. *Phytochemistry*, 15: 221-223.

Jeong, YE and Lee, M-Y (2018) 'Anti-Inflammatory Activity of *Populus deltoides* Leaf Extract via Modulating NF- κ B and p38/JNK Pathways'. *International Journal of Molecular Sciences*, 19: 3746.

- Jerz, G *et al.* (2007) 'Structural characterization of 13²-hydroxy-(13²-S)-phaeophytin-a from leaves and stems of *Amaranthus tricolor* isolated by high-speed countercurrent chromatography'. *Innovative Food Science & Emerging Technologies*, 8: 413-418.
- Jesus, JA *et al.* (2015) 'Antimicrobial Activity of Oleanolic and Ursolic Acids: An Update'. *Evidence-Based Complementary and Alternative Medicine*, 2015: 620472.
- Jiang, M *et al.* (2020) 'Drug–target affinity prediction using graph neural network and contact maps'. *RSC Advances*, 10: 20701-20712.
- Jiménez-Arellanes, A *et al.* (2013) 'Ursolic and oleanolic acids as antimicrobial and immunomodulatory compounds for tuberculosis treatment'. *BMC Complementary and Alternative Medicine*, 13: 258-258.
- Jnawali, HN *et al.* (2016) 'Antituberculosis Activity of a Naturally Occurring Flavonoid, Isorhamnetin'. *Journal of Natural Products*, 79: 961-969.
- Julien-David, D *et al.* (2008) 'Synthesis of highly pure oxyphytosterols and (oxy)phytosterol esters. Part II. (Oxy)-sitosterol esters derived from oleic acid and from 9,10-dihydroxystearic acid [1]'. *Steroids*, 73: 1098-1109.
- Jung, JH and McLaughlin, JL (1990) '¹³C-¹H NMR Long-range coupling and deuterium isotope effects of flavanones'. *Phytochemistry*, 29: 1271-1275.
- Jyoti, MA *et al.* (2016) 'Antimycobacterial activity of methanolic plant extract of *Artemisia capillaris* containing ursolic acid and hydroquinone against *Mycobacterium tuberculosis*'. *Journal of Infection and Chemotherapy*, 22: 200-208.
- Kallioliias, GD and Ivashkiv, LB (2016) 'TNF biology, pathogenic mechanisms and emerging therapeutic strategies'. *Nature reviews. Rheumatology*, 12: 49-62.
- Kanehiro, Y *et al.* (2018) 'Identification of Novel Mycobacterial Inhibitors Against Mycobacterial Protein Kinase G'. *Frontiers in Microbiology*, 9: 1517-1517.
- Kang, T-H *et al.* (2000) 'Cytotoxic Lavandulyl Flavanones from *Sophora flavescens*'. *Journal of Natural Products*, 63: 680-681.
- Kang, ZC *et al.* (2020) 'Pinocembrin Ameliorates Cognitive Impairment Induced by Vascular Dementia: Contribution of Reelin-dab1 Signaling Pathway'. *Drug Design, Development and Therapy*, 14: 3577-3587.
- Kany, S, Vollrath, JT and Relja, B (2019) 'Cytokines in Inflammatory Disease'. *International Journal of Molecular Sciences*, 20: 6008.
- Kapewangolo, P, Kandawa-Schulz, M and Meyer, D (2017) 'Anti-HIV Activity of *Ocimum labiatum* Extract and Isolated Pheophytin-a'. *Molecules*, 22: 1763.
- Kartini *et al.* (2017) 'Effects of *Plantago major* Extracts and Its Chemical Compounds on Proliferation of Cancer Cells and Cytokines Production of Lipopolysaccharide-activated THP-1 Macrophages'. *Pharmacognosy Magazine*, 13: 393-399.

- Kartsev, VG, Stepanichenko, NN and Auelbekov, SA (1994) 'Chemical composition and pharmacological properties of plants of the genus *Stachys*'. *Chemistry of Natural Compounds*, 30: 645-654.
- Karunaweera, N *et al.* (2015) 'Plant polyphenols as inhibitors of NF- κ B induced cytokine production-a potential anti-inflammatory treatment for Alzheimer's disease?'. *Frontiers in Molecular Neuroscience*, 8: 24-24.
- Kataev, V *et al.* (2018) 'New Targets for Growth Inhibition of *Mycobacterium tuberculosis*: Why Do Natural Terpenoids Exhibit Antitubercular Activity?'. *Russian Journal of Bioorganic Chemistry*, 44: 438-452.
- Kawai, T and Akira, S (2010) 'The role of pattern-recognition receptors in innate immunity: update on Toll-like receptors'. *Nature Immunology*, 11: 373-384.
- Kawanishi, K and Hashimoto, Y (1987) 'Long chain esters of *Viola* species'. *Phytochemistry*, 26: 749-752.
- Kawasaki, T and Kawai, T (2014) 'Toll-Like Receptor Signaling Pathways'. *Frontiers in Immunology*, 5.
- Kayani, S *et al.* (2014) 'Ethnobotanical uses of medicinal plants for respiratory disorders among the inhabitants of Gallies - Abbottabad, Northern Pakistan'. *Journal of Ethnopharmacology*, 156: 47-60.
- Kayser, O and Kolodziej, H (1997) 'Antibacterial activity of extracts and constituents of *Pelargonium sidoides* and *Pelargonium reniforme*'. *Planta Medica*, 63: 508-510.
- Kell, DB (2013) 'Finding novel pharmaceuticals in the systems biology era using multiple effective drug targets, phenotypic screening and knowledge of transporters: where drug discovery went wrong and how to fix it'. *FEBS Journal*, 280: 5957-5980.
- Kenny, PW, Leitão, A and Montanari, CA (2014) 'Ligand efficiency metrics considered harmful'. *Journal of Computer-Aided Molecular Design*, 28: 699-710.
- Khamis, MA, Gomaa, W and Ahmed, WF (2015) 'Machine learning in computational docking'. *Artificial Intelligence in Medicine*, 63: 135-152.
- Khanavi, M *et al.* (2012) 'Investigation of cytotoxic activity in four *Stachys* species from iran'. *Iran J Pharm Res*, 11: 589-593.
- Khanavi, M *et al.* (2005) 'Phytochemical investigation and anti-inflammatory activity of aerial parts of *Stachys byzanthina* C. Koch'. *Journal of Ethnopharmacology*, 97: 463-468.
- Khwaza, V, Oyedeji, OO and Aderibigbe, BA (2020) 'Ursolic Acid-Based Derivatives as Potential Anti-Cancer Agents: An Update'. *International Journal of Molecular Sciences*, 21: 5920.
- Kim, C, Griffiths, W and Taylor, P (2009) 'Components derived from *Pelargonium* stimulate macrophage killing of *Mycobacterium* species'. *Journal of Applied Microbiology*, 106: 1184-1193.

Kim, SK and Karadeniz, F (2012) 'Biological importance and applications of squalene and squalane'. *Advances in Food and Nutrition Research*, 65: 223-233.

Kim, YR *et al.* (2018) 'Antidepressant Effect of *Fraxinus rhynchophylla* Hance Extract in a Mouse Model of Chronic Stress-Induced Depression'. *BioMed research international*, 2018: 8249563-8249563.

Kinney, JW *et al.* (2018) 'Inflammation as a central mechanism in Alzheimer's disease'. *Alzheimer's & dementia (New York, N. Y.)*, 4: 575-590.

Kiss, AK *et al.* (2020) 'UHPLC-DAD-ESI-MS/MS and HPTLC profiling of ash leaf samples from different commercial and natural sources and their in vitro effects on mediators of inflammation'. *Phytochemical Analysis*, 31: 57-67.

Kobayashi, M *et al.* (1991) '10-Hydroxypheophytins and a New Norlabdane Diterpene from the Leaves of *Cupressus funebris* ENDL'. *Chemical & Pharmaceutical Bulletin*, 39: 3348-3349.

Kolehmainen, M *et al.* (2012) 'Bilberries reduce low-grade inflammation in individuals with features of metabolic syndrome'. *Molecular Nutrition & Food Research*, 56: 1501-1510.

Kolodziej, H (2000) *Traditionally used Pelargonium species: Chemistry and biological activity of umckaloabo extracts and their constituents.*

Kolodziej, H (2003) '*Pelargonium reniforme* and *Pelargonium sidoides*: their botany, chemistry and medicinal use'. *Geranium and Pelargonium, Series: Medicinal and Aromatic Plants-Industrial Profiles. Lis-Balchin M*, 27: 262-290.

Kolodziej, H (2007) 'Fascinating metabolic pools of *Pelargonium sidoides* and *Pelargonium reniforme*, traditional and phytomedicinal sources of the herbal medicine Umckaloabo'. *Phytomedicine*, 14 Suppl 6: 9-17.

Kolodziej, H (2008) 'Aqueous Ethanolic Extract of the Roots of *Pelargonium sidoides* - New Scientific Evidence for an Old Anti-Infective Phytopharmaceutical'. *Planta Medica*, 74: 661-666.

Kolodziej, H (2011) 'Antimicrobial, Antiviral and Immunomodulatory Activity Studies of *Pelargonium sidoides* (EPs® 7630) in the Context of Health Promotion'. *Pharmaceuticals*, 4: 1295.

Kolodziej, H, Kayser, O and Tan, N (2002) 'Novel Coumarin Sulfates from *Pelargonium sidoides*'. 59-64.

Kostova, I and Iossifova, T (2007) 'Chemical components of *Fraxinus* species'. *Fitoterapia*, 78: 85-106.

Kotsos, MP, Aligiannis, N and Mitakou, S (2007) 'A new flavonoid diglycoside and triterpenoids from *Stachys spinosa* L. (Lamiaceae)'. *Biochemical Systematics and Ecology*, 35: 381-385.

Kowalczyk, B and Olechnowicz-Stepień, W (1989) Published. 'Phytochemical investigation on *Fraxinus excelsior* leaves'. *Planta medica* 55, 1989 35th ann cong med plant res. Braunschweig. pp.623.

Koysomboon, S *et al.* (2006) 'Antimycobacterial flavonoids from *Derris indica*'. *Phytochemistry*, 67: 1034-1040.

Krauß, S, Michaelis, L and Vetter, W (2017) 'Phytol fatty acid esters in vegetables pose a risk for patients suffering from Refsum's disease'. *PLoS One*, 12: e0188035.

Krauß, S and Vetter, W (2018) 'Phytol and Phytol Fatty Acid Esters: Occurrence, Concentrations, and Relevance'. *European Journal of Lipid Science and Technology*, 120: 1700387.

Kukić, J, Dobrić, S and Petrović, S (2007) 'Influence of Some *Stachys* Taxa on Carrageenan-Induced Paw Edema in Rats'. *Pharmaceutical Biology*, 45: 560-563.

Kumar, A and Jha, A (2017) 'Drug Development Strategies'. *Anticandidal Agents*. Academic Press: 63-71.

Kumar, D *et al.* (2012) 'Anti-anxiety activity of *Stachys tibetica* Vatke'. *Chinese journal of natural medicines*, 11: 240-244.

Kumar, NP *et al.* (2019) 'Plasma Proinflammatory Cytokines Are Markers of Disease Severity and Bacterial Burden in Pulmonary Tuberculosis'. *Open Forum Infectious Diseases*, 6.

Kumar, P *et al.* (2013) 'Anti-mycobacterial activity of plumericin and isoplumericin against MDR *Mycobacterium tuberculosis*'. *Pulmonary Pharmacology and Therapeutics*, 26: 332-335.

Kumar, S and Kashyap, P (2015) 'In-vivo anti-inflammatory activity of a methanolic extract of *Fraxinus micrantha*'. *ARC J Pharma Sci*, 1: 1-4.

Lan, X *et al.* (2017) 'Pinocembrin protects hemorrhagic brain primarily by inhibiting toll-like receptor 4 and reducing M1 phenotype microglia'. *Brain, Behavior, and Immunity*, 61: 326-339.

Lan, X *et al.* (2016) 'The Natural Flavonoid Pinocembrin: Molecular Targets and Potential Therapeutic Applications'. *Molecular Neurobiology*, 53: 1794-1801.

Lange, C *et al.* (2014) 'Management of patients with multidrug-resistant/extensively drug-resistant tuberculosis in Europe: a TBNET consensus statement'. *European Respiratory Journal*, 44: 23.

Larsen, MM *et al.* (2010) 'Using a phylogenetic approach to selection of target plants in drug discovery of acetylcholinesterase inhibiting alkaloids in Amaryllidaceae tribe *Galantheae*'. *Biochemical Systematics and Ecology*, 38: 1026-1034.

Le, DAT *et al.* (2015) 'Anti-inflammatory triterpene and other components from *Kandelia candel* (L.) Druce'. *Natural Product Sciences*.

- Lechner, D, Gibbons, S and Bucar, F (2008) 'Modulation of isoniazid susceptibility by flavonoids in *Mycobacterium*'. *Phytochemistry Letters*, 1: 71-75.
- Lee, C-K and Chang, M-H (2000) 'The Chemical Constituents from the Heartwood of *Eucalyptus Citriodora*'. *Journal of the Chinese Chemical Society*, 47: 555-560.
- Lee, W *et al.* (2013) 'Anti-inflammatory Effects of Oleanolic Acid on LPS-Induced Inflammation *In Vitro* and *In Vivo*'. *Inflammation*, 36: 94-102.
- Leeson, PD *et al.* (2021) 'Target-Based Evaluation of "Drug-Like" Properties and Ligand Efficiencies'. *Journal of Medicinal Chemistry*.
- Lekphrom, R, Kanokmedhakul, S and Kanokmedhakul, K (2009) 'Bioactive styryllactones and alkaloid from flowers of *Goniothalamus laoticus*'. *Journal of Ethnopharmacology*, 125: 47-50.
- León-Díaz, R *et al.* (2010) 'Antimycobacterial neolignans isolated from *Aristolochia taliscana*'. *Memorias do Instituto Oswaldo Cruz*, 105: 45-51.
- Lewu, F, Grierson, D and Afolayan, A (2006) 'The leaves of *Pelargonium sidoides* may substitute for its roots in the treatment of bacterial infections'. *Biological Conservation*, 128: 582-584.
- Li, H *et al.* (2016) 'Correcting the impact of docking pose generation error on binding affinity prediction'. *BMC Bioinformatics*, 17: 308.
- Li, L *et al.* (2013) 'Rho kinase inhibition activity of pinocembrin in rat aortic rings contracted by angiotensin II'. *Chinese journal of natural medicines*, 11: 258-263.
- Li, M *et al.* (2015a) 'Oleanolic Acid Attenuates Insulin Resistance via NF- κ B to Regulate the IRS1-GLUT4 Pathway in HepG2 Cells'. *Evidence-Based Complementary and Alternative Medicine*, 2015: 643102.
- Li, S *et al.* (2015b) 'Parthenolide inhibits LPS-induced inflammatory cytokines through the toll-like receptor 4 signal pathway in THP-1 cells'. *Acta Biochimica et Biophysica Sinica*, 47: 368-375.
- Li, X *et al.* (2020) 'Oleanolic acid administration alleviates neuropathic pain after a peripheral nerve injury by regulating microglia polarization-mediated neuroinflammation'. *RSC Advances*, 10: 12920-12928.
- Liao, P-C *et al.* (2018) 'Identification of β -Sitosterol as in Vitro Anti-Inflammatory Constituent in *Moringa oleifera*'. *Journal of Agricultural and Food Chemistry*, 66: 10748-10759.
- Libby, P (2006) 'Inflammation and cardiovascular disease mechanisms'. *American Journal of Clinical Nutrition*, 83: 456s-460s.
- Lin, C-Y *et al.* (2014) 'Pheophytin a inhibits inflammation via suppression of LPS-induced nitric oxide synthase-2, prostaglandin E2, and interleukin-1 β of macrophages'. *International Journal of Molecular Sciences*, 15: 22819-22834.

- Lin, C-Y *et al.* (2017) 'Lipopolysaccharide-Induced Nitric Oxide, Prostaglandin E2, and Cytokine Production of Mouse and Human Macrophages Are Suppressed by Pheophytin-b'. *International Journal of Molecular Sciences*, 18: 2637.
- Lin, PL and Flynn, JL (2010) 'Understanding latent tuberculosis: a moving target'. *Journal of Immunology*, 185: 15-22.
- Lippold, F *et al.* (2012) 'Fatty Acid Phytyl Ester Synthesis in Chloroplasts of Arabidopsis'. *The Plant Cell*, 24: 2001.
- Liu, CH, Liu, H and Ge, B (2017a) 'Innate immunity in tuberculosis: host defense vs pathogen evasion'. *Cellular & Molecular Immunology*, 14: 963-975.
- Liu, R *et al.* (2014a) 'Pinocembrin protects human brain microvascular endothelial cells against fibrillar amyloid- β (1-40) injury by suppressing the MAPK/NF- κ B inflammatory pathways'. *BioMed Research International*, 2014: 470393.
- Liu, R *et al.* (2014b) 'Pinocembrin improves cognition and protects the neurovascular unit in Alzheimer related deficits'. *Neurobiology of Aging*, 35: 1275-1285.
- Liu, R *et al.* (2012a) 'Pinocembrin protects against β -amyloid-induced toxicity in neurons through inhibiting receptor for advanced glycation end products (RAGE)-independent signaling pathways and regulating mitochondrion-mediated apoptosis'. *BMC Medicine*, 10: 105-105.
- Liu, T *et al.* (2017b) 'NF- κ B signaling in inflammation'. *Signal Transduction and Targeted Therapy*, 2: 17023.
- Liu, X *et al.* (2012b) 'Exploring anti-TB leads from natural products library originated from marine microbes and medicinal plants'. *Antonie van Leeuwenhoek*, 102: 447-461.
- Liu, Y-L *et al.* (1992) 'Isolation of potential cancer chemopreventive agents from *Eriodictyon californicum*'. *Journal of Natural Products*, 55: 357-363.
- López-Carreras, N *et al.* (2013) 'Short-term effect of an aqueous *Fraxinus excelsior* L. seed extract in spontaneously hypertensive rats'. *Food Research International*, 53: 81-87.
- Lopez-Carreras, N *et al.* (2014) 'Long-Term Effect of an Aqueous *Fraxinus excelsior* L. Seed Extract in Spontaneously Hypertensive Rats'. *International Journal of Hypertension*, 2014: 565212.
- Lou-Bonafonte, JM *et al.* (2018) 'Current Insights into the Biological Action of Squalene'. *Molecular Nutrition & Food Research*: e1800136.
- Lozano-Grande, MA *et al.* (2018) 'Plant Sources, Extraction Methods, and Uses of Squalene'. *International Journal of Agronomy*, 2018: 1829160.
- Lu, M-Y *et al.* (2015) 'N6-(2-Hydroxyethyl)adenosine in the Medicinal Mushroom *Cordyceps cicadae* Attenuates Lipopolysaccharide-Stimulated Pro-inflammatory

Responses by Suppressing TLR4-Mediated NF- κ B Signaling Pathways'. *Journal of Natural Products*, 78: 2452-2460.

Lucas, EH *et al.* (1951) 'The Occurrence of Antibacterial Substances in Seed Plants with Special Reference to *Mycobacterium Tuberculosis*'. *Bulletin of the Torrey Botanical Club*, 78: 310-321.

Ludwiczuk, A, Skalicka-Woźniak, K and Georgiev, MI (2017) 'Terpenoids'. In: Badal, S. and Delgoda, R. (eds.) *Pharmacognosy*. Boston: Academic Press: 233-266.

Luo, X *et al.* (2013) 'Zanthoxylum capense constituents with antimycobacterial activity against *Mycobacterium tuberculosis* in vitro and ex vivo within human macrophages'. *Journal of Ethnopharmacology*, 146: 417-422.

Luo, Y *et al.* (2006) 'Steryl esters and phenylethanol esters from *Syringa komarowii*'. *Steroids*, 71: 700-705.

Mahato, SB and Kundu, AP (1994) '¹³C NMR Spectra of pentacyclic triterpenoids—a compilation and some salient features'. *Phytochemistry*, 37: 1517-1575.

Maitre, T *et al.* (2017) 'Multidrug and extensively drug-resistant tuberculosis'. *Médecine et Maladies Infectieuses*, 47: 3-10.

Maleki, N *et al.* (2001) 'Potent anti-inflammatory activities of hydroalcoholic extract from aerial parts of *Stachys inflata* on rats'. *Journal of Ethnopharmacology*, 75: 213-218.

Manca, C *et al.* (2013) 'Host Targeted Activity of Pyrazinamide in *Mycobacterium tuberculosis* Infection'. *PLoS One*, 8: e74082.

Mandal, SC, Mandal, V and Das, AK (2015) 'Botanicals as a Screening Source of New Drugs: Past Success Stories and Present-Day Concerns'. In: Mandal, S.C., Mandal, V. and Das, A.K. (eds.) *Essentials of Botanical Extraction*. Boston: Academic Press: 19-33.

Mangwani, N, Singh, PK and Kumar, V (2020) 'Medicinal plants: Adjunct treatment to tuberculosis chemotherapy to prevent hepatic damage'. *Journal of Ayurveda and Integrative Medicine*, 11: 522-528.

Mankhi, AA, Ali, E and Mohammed, HN (2018) 'Estimation level of IL-12 in Blood of patients with tuberculosis'. *Journal of Global Pharma Technology*, 10: 21-27.

Mann, A *et al.* (2012) 'Antimycobacterial Friedelane-terpenoid from the Root Bark of *Terminalia avicennioides*'. *American Journal of Chemistry*, 1: 52-55.

Marshall, JS *et al.* (2018) 'An introduction to immunology and immunopathology'. *Allergy, Asthma & Clinical Immunology*, 14: 49.

Maskell, L *et al.* (2013) 'Distribution of Ash trees (*Fraxinus excelsior*) in Countryside Survey data'. *Centre for Ecology and Hydrology*.

- Mateos, R *et al.* (2008) 'New lipophilic tyrosyl esters. Comparative antioxidant evaluation with hydroxytyrosyl esters'. *Journal of Agricultural and Food Chemistry*, 56: 10960-10966.
- Mativandlela, S *et al.* (2007) 'Antitubercular Activity of Compounds Isolated from *Pelargonium sidoides*'. *Pharmaceutical Biology*, 45: 645-650.
- Mativandlela, S *et al.* (2009) 'Antimycobacterial Flavonoids from the Leaf Extract of *Galenia africana*'. *Journal of Natural Products*, 72: 2169-2171.
- Matsuo, A *et al.* (1996) 'Phaeophytins from a cell suspension culture of the liverwort *Plagiochila ovalifolia*'. *Phytochemistry*, 42: 427-430.
- Matysik, E *et al.* (2016) 'The new TLC method for separation and determination of multicomponent mixtures of plant extracts'. *Journal of analytical methods in chemistry*, 2016.
- Mavar-Manga, H *et al.* (2008) 'Anti-inflammatory compounds from leaves and root bark of *Alchornea cordifolia* (Schumach. & Thonn.) Müll. Arg'. *Journal of Ethnopharmacology*, 115: 25-29.
- Mbosso, E *et al.* (2008) 'Spathoside, a cerebroside and other antibacterial constituents of the stem bark of *Spathodea campanulata*'. *Natural Product Research*, 22: 296-304.
- McCutcheon, AR *et al.* (1997) 'Anti-Mycobacterial Screening of British Columbian Medicinal Plants'. *International Journal of Pharmacognosy*, 35: 77-83.
- McInturff, JE, Modlin, RL and Kim, J (2005) 'The Role of Toll-like Receptors in the Pathogenesis and Treatment of Dermatological Disease'. *Journal of Investigative Dermatology*, 125: 1-8.
- Medzhitov, R (2008) 'Origin and physiological roles of inflammation'. *Nature*, 454: 428-435.
- Medzhitov, R (2010) 'Inflammation 2010: new adventures of an old flame'. *Cell*, 140: 771-776.
- Mehta, A *et al.* (2013) 'Antimycobacterial activity of *Citrullus colocynthis* (L.) Schrad. against drug sensitive and drug resistant *Mycobacterium tuberculosis* and MOTT clinical isolates'. *Journal of Ethnopharmacology*, 149: 195-200.
- Méndez, J *et al.* (1968) 'Growth substances isolated from woody cuttings of *Alnus glutinosa* medic. and *Fraxinus excelsior* L'. *Phytochemistry*, 7: 575-579.
- Menković, N *et al.* (2011) 'Ethnobotanical study on traditional uses of wild medicinal plants in Prokletije Mountains (Montenegro)'. *Journal of Ethnopharmacology*, 133: 97-107.
- Middleton, P *et al.* (2010) 'Antioxidant, antibacterial activities and general toxicity of *Alnus glutinosa*, *Fraxinus excelsior* and *Papaver rhoeas*'. *Iranian Journal of Pharmaceutical Research*: 101-103.

Miele, M *et al.* (2012) 'Hazel and other sources of paclitaxel and related compounds'. *Phytochemistry Reviews*, 11: 211-225.

Migas, P, Cisowski, W and Dembińska-Migas, W (2005) 'Isoprene derivatives from the leaves and callus cultures of *Vaccinium corymbosum* var. bluecrop'. *Acta Poloniae Pharmaceutica*, 62: 45-51.

Miyase, T, Yamamoto, R and Ueno, A (1996) 'Phenylethanoid glycosides from *Stachys officinalis*'. *Phytochemistry*, 43: 475-479.

Mohamed Ael, H and Mohamed, NS (2014) 'A new trans-neoclerodane diterpene from *Stachys aegyptiaca*'. *Natural Product Research*, 28: 30-34.

Molla, Y, Wubetu, M and Dessie, B (2021) 'Anti-Tuberculosis Drug Induced Hepatotoxicity and Associated Factors among Tuberculosis Patients at Selected Hospitals, Ethiopia'. *Hepatic Medicine: Evidence and Research*, 13: 1-8.

Monto, F *et al.* (2014) 'Action of an extract from the seeds of *Fraxinus excelsior* L. on metabolic disorders in hypertensive and obese animal models'. *Food & Function*, 5: 786-796.

Moreau, RA *et al.* (2018) 'Phytosterols and their derivatives: Structural diversity, distribution, metabolism, analysis, and health-promoting uses'. *Progress in Lipid Research*, 70: 35-61.

Moreau, RA, Whitaker, BD and Hicks, KB (2002) 'Phytosterols, phytosteranols, and their conjugates in foods: structural diversity, quantitative analysis, and health-promoting uses'. *Progress in Lipid Research*, 41: 457-500.

Morgan, J *et al.* (2021) 'Classical CD4 T cells as the cornerstone of antimycobacterial immunity'. *Immunological Reviews*, 301: 10-29.

Morris, GM *et al.* (2009) 'AutoDock4 and AutoDockTools4: Automated docking with selective receptor flexibility'. *Journal of Computational Chemistry*, 30: 2785-2791.

Munoz, O, Pena, RC and Montenegro, G (2001) 'Iridoids from *Stachys grandidentata* (Labiatae)'. *Journal of Biosciences*, 56: 902-903.

Murata, T *et al.* (2008) 'Iridoid glycoside constituents of *Stachys lanata*'. *Journal of Natural Products*, 71: 1768-1770.

Murray, CW *et al.* (2014) 'Validity of ligand efficiency metrics'. *ACS Medicinal Chemistry Letters*, 5: 616-618.

Naicker, N, Sigal, A and Naidoo, K (2020) 'Metformin as Host-Directed Therapy for TB Treatment: Scoping Review'. *Frontiers in Microbiology*, 11.

Nair, JJ *et al.* (2012) 'Isolation of di(2-ethylhexyl) phthalate from a commercial South African cognate herbal mixture'. *South African Journal of Botany*, 80: 21-24.

Nakatani, Y, Ourisson, G and Beck, J (1981) 'Chemistry and biochemistry of Chinese drugs. VII.: cytostatic pheophytins from silkworm excreta, and derived photocytotoxic pheophorbides'. *Chemical and Pharmaceutical Bulletin*, 29: 2261-2269.

Narasimhan, P *et al.* (2013) 'Risk Factors for Tuberculosis'. *Pulmonary Medicine*, 2013: 828939.

National Health Service (2018) *Tuberculosis (TB)* Available at: <https://www.nhs.uk/conditions/tuberculosis-tb/>.

Navarro, A, De Las Heras, B and Villar, A (2001) 'Anti-inflammatory and immunomodulating properties of a sterol fraction from *Sideritis foetens* Clem'. *Biological and Pharmaceutical Bulletin*, 24: 470-473.

Nazreen, S *et al.* (2019) 'Chemical constituents with antimicrobial and antioxidant activity from the aerial parts of *Callistemon lanceolatus* (Sm.) Sweet'. *Natural Product Research*: 1-5.

Neves, JM *et al.* (2009) 'Ethnopharmacological notes about ancient uses of medicinal plants in Trás-os-Montes (northern of Portugal)'. *Journal of Ethnopharmacology*, 124: 270-283.

Newman, D, . and Cragg, GM (2016) 'Natural Products as Sources of New Drugs from 1981 to 2014'. *Journal of Natural Products*, 79: 629-661.

Newsom, S (2002) 'Stevens' cure: a secret remedy'. *Journal of the Royal Society of Medicine*, 95: 463-467.

Newton, K and Dixit, VM (2012) 'Signaling in innate immunity and inflammation'. *Cold Spring Harbor Perspectives in Biology*, 4.

Newton, S *et al.* (2002) 'The evaluation of forty-three plant species for in vitro antimycobacterial activities; isolation of active constituents from *Psoralea corylifolia* and *Sanguinaria canadensis*'. *Journal of Ethnopharmacology*, 79: 57-67.

Newton, S, Lau, C and Wright, CW (2000) 'A review of antimycobacterial natural products'. *Phytotherapy Research*, 14: 303-322.

Ng, VAS *et al.* (2015) 'Secondary metabolites from *Cycas edentata*'. *Journal of Pharmaceutical Sciences and Research*, 7: 643.

Nguyen, NT *et al.* (2020) 'Autodock Vina Adopts More Accurate Binding Poses but Autodock4 Forms Better Binding Affinity'. *Journal of Chemical Information and Modeling*, 60: 204-211.

Nieva-Echevarría, B *et al.* (2014) 'A method based on ¹H NMR spectral data useful to evaluate the hydrolysis level in complex lipid mixtures'. *Food Research International*, 66: 379-387.

Nishimura, H *et al.* (1991) 'Nine phenethyl alcohol glycosides from *Stachys sieboldii*'. *Phytochemistry*, 30: 965-969.

- Nissink, JW (2009) 'Simple size-independent measure of ligand efficiency'. *Journal of Chemical Information and Modeling*, 49: 1617-1622.
- Nyokat, N *et al.* (2017) 'Isolation and synthesis of pinocebrin and pinostrobin from *Artocarpus odoratissimus*'. *Malaysian Journal of Analytical Sciences*, 21: 1156-1161.
- O'Garra, A *et al.* (2013) 'The immune response in tuberculosis'. *Annual Review of Immunology*, 31: 475-527.
- O'Neill, LA, Bryant, CE and Doyle, SL (2009) 'Therapeutic targeting of Toll-like receptors for infectious and inflammatory diseases and cancer'. *Pharmacological Reviews*, 61: 177-197.
- Ojha, SN *et al.* (2020) 'Ethnomedicinal knowledge of a marginal hill community of Central Himalaya: diversity, usage pattern, and conservation concerns'. *Journal of Ethnobiology and Ethnomedicine*, 16: 29.
- Okunade, AL, Elvin-Lewis, MPF and Lewis, WH (2004) 'Natural antimycobacterial metabolites: current status'. *Phytochemistry*, 65: 1017-1032.
- Olaru, ID *et al.* (2015) 'Novel drugs against tuberculosis: a clinician's perspective'. *European Respiratory Journal*, 45: 1119-1131.
- Ortiz, A and Sansinenea, E (2018) 'Di-2-ethylhexylphthalate May Be a Natural Product, Rather than a Pollutant'. *Journal of Chemistry*, 2018: 6040814.
- Orwa, C, Mutua, A., Kindt, R., Simons A. , Jamnadass R., (2009) *Agroforestry database: a tree reference and selection guide version 4.0.* (Accessed: 12/6/2021).
- Pace, CN *et al.* (2011) 'Contribution of hydrophobic interactions to protein stability'. *Journal of Molecular Biology*, 408: 514-528.
- Palomino, JC and Martin, A (2014) 'Drug Resistance Mechanisms in *Mycobacterium tuberculosis*'. *Antibiotics*, 3: 317-340.
- Pålsson-McDermott, EM and O'Neill, LAJ (2004) 'Signal transduction by the lipopolysaccharide receptor, Toll-like receptor-4'. *Immunology*, 113: 153-162.
- Palucci, I and Delogu, G (2018) 'Host Directed Therapies for Tuberculosis: Futures Strategies for an Ancient Disease'. *Chemotherapy*, 63: 172-180.
- Pantsar, T and Poso, A (2018) 'Binding Affinity via Docking: Fact and Fiction'. *Molecules*, 23: 1899.
- Park, M-S, Gao, C and Stern, HA (2011) 'Estimating binding affinities by docking/scoring methods using variable protonation states'. *Proteins: Structure, Function, and Bioinformatics*, 79: 304-314.
- Park, S *et al.* (2014) 'Pheophytin a and chlorophyll a suppress neuroinflammatory responses in lipopolysaccharide and interferon- γ -stimulated BV2 microglia'. *Life Sciences*, 103: 59-67.

- Pateh, UU *et al.* (2009) 'Isolation of stigmasterol, β -sitosterol and 2-Hydroxyhexadecanoic acid methyl ester from the rhizomes of *Stylochiton Lancifolius* Pyer and Kotchy (Aeaceae)'. *Nigerian Journal of Pharmaceutical Sciences*, Vol. 7, No. 1,; 19-25.
- Patil, R *et al.* (2010) 'Optimized hydrophobic interactions and hydrogen bonding at the target-ligand interface leads the pathways of drug-designing'. *PloS One*, 5: e12029.
- Pedersen, D and Rosenbohm, C (2001) 'Dry Column Vacuum Chromatography'. *Synthesis*, 16: 2431-2434.
- Pereira, AS *et al.* (2002) 'Three series of high molecular weight alkanoates found in Amazonian plants'. *Phytochemistry*, 61: 711-719.
- Phillips, L (2013) 'Infectious disease: TB's revenge'. *Nature*, 493: 14-16.
- Physician", AE (1931) *Tuberculosis, Its Treatment and Cure with the Help of Umckaloabo (Stevens)*. London:B Fraser & Co.
- PlantFile online database (2018) *Fraxinus excelsior*. Available at: <http://plantfileonline.net/plants>.
- Pogliani, L *et al.* (1994) 'An NMR and molecular mechanics study of squalene and squalene derivatives'. *Chemistry and Physics of Lipids*, 70: 21-34.
- Pollier, J and Goossens, A (2012) 'Oleanolic acid'. *Phytochemistry*, 77: 10-15.
- Poukens-Renwart, P *et al.* (1992) 'Reversed-phase HPTLC densitometric evaluation of fraxin in *Fraxinus excelsior* leaves'. *Journal of Pharmaceutical and Biomedical Analysis*, 10: 1089-1091.
- Pranskuniene, Z *et al.* (2018) 'Ethnopharmaceutical knowledge in Samogitia region of Lithuania: where old traditions overlap with modern medicine'. *Journal of ethnobiology and ethnomedicine*, 14: 70-70.
- Prasad, M *et al.* (2019) 'Nano-antimicrobials: A New Paradigm for Combating Mycobacterial Resistance'. *Current Pharmaceutical Design*, 25.
- Ragasa, CY and Lim, K (2005) 'Secondary metabolites from *Schefflera odorata* Blanco'. *Philippine Journal of Science*, 134: 63.
- Rai, SN *et al.* (2019) 'Anti-inflammatory Activity of Ursolic Acid in MPTP-Induced Parkinsonian Mouse Model'. *Neurotoxicity Research*, 36: 452-462.
- Raja, A (2004) 'Immunology of tuberculosis'. *Indian Journal of Medical Research*, 120: 213-232.
- Rajab, MS *et al.* (1998) 'Antimycobacterial activity of (E)-phytol and derivatives: a preliminary structure-activity study'. *Planta Medica*, 64: 2-4.
- Ramani, T *et al.* (2015) 'Cytokines: The Good, the Bad, and the Deadly'. *International Journal of Toxicology*, 34: 355-365.

- Ramappa, V and Aithal, GP (2013) 'Hepatotoxicity Related to Anti-tuberculosis Drugs: Mechanisms and Management'. *Journal of Clinical and Experimental Hepatology*, 3: 37-49.
- Ramazanov, NS *et al.* (2017) 'Phytoecdysteroids-containing extract from *Stachys hissarica* plant and its wound-healing activity'. *Natural Product Research*, 31: 593-597.
- Rao, GN *et al.* (2000) 'Constituents of *Cassia auriculata*'. *Fitoterapia*, 71: 82-83.
- Rasool, N, Ahmad, VU and Malik, A (1991) 'Terpenoids from *Pentatropis spiralis*'. *Phytochemistry*, 30: 1331-1332.
- Rasul, A *et al.* (2013) 'Pinocembrin: A Novel Natural Compound with Versatile Pharmacological and Biological Activities'. *BioMed Research International*, 2013: 379850.
- Rathee, P *et al.* (2012) 'In-vitro cytotoxic activity of β -Sitosterol triacontenate isolated from *Capparis decidua* (Forsk.) Edgew'. *Asian Pacific Journal of Tropical Medicine*, 5: 225-230.
- Rayasam, GV and Balganes, TS (2015) 'Exploring the potential of adjunct therapy in tuberculosis'. *Trends in Pharmacological Sciences*, 36: 506-513.
- Reynolds, CH, Tounge, BA and Bembenek, SD (2008) 'Ligand Binding Efficiency: Trends, Physical Basis, and Implications'. *Journal of Medicinal Chemistry*, 51: 2432-2438.
- Rezazadeh, S *et al.* (2009) 'Anti-inflammatory and antihyperalgesic activities of *Stachys athorecalyx* extracts on CFA-induced inflammation'. *Journal of Medicinal Plants Research*, 3: 368-376.
- Rosmarin, D and Strober, BE (2005) 'The potential of interleukin 12 inhibition in the treatment of psoriasis'. *J Drugs Dermatol*, 4: 318-325.
- Royal Botanic Gardens (2019) "*Plants of the World Online*. *Fraxinus excelsior* L. Available at: <http://www.plantsoftheworldonline.org>.
- Said, MS *et al.* (2015) 'A new butenolide cinnamate and other biological active chemical constituents from *Polygonum glabrum*'. *Natural Product Research*, 29: 2080-2086.
- Sakai, S, Mayer-Barber, KD and Barber, DL (2014) 'Defining features of protective CD4 T cell responses to *Mycobacterium tuberculosis*'. *Current Opinion in Immunology*, 29: 137-142.
- Sakdarat, S *et al.* (2009) 'Bioactive constituents from the leaves of *Clinacanthus nutans* Lindau'. *Bioorganic and Medicinal Chemistry*, 17: 1857-1860.
- Salinero, C *et al.* (2012) '¹H-nuclear magnetic resonance analysis of the triacylglyceride composition of cold-pressed oil from *Camellia japonica*'. *Molecules*, 17: 6716-6727.

Saludes, JP *et al.* (2002) 'Antitubercular constituents from the hexane fraction of *Morinda citrifolia* Linn. (Rubiaceae)'. *Phytotherapy Research*, 16: 683-685.

Sang, H *et al.* (2012) 'Inhibitory effect of the combination therapy of simvastatin and pinocembrin on atherosclerosis in ApoE-deficient mice'. *Lipids in Health and Disease*, 11: 166-166.

Santhi, N and Aishwarya, S (2011) 'Insights from the molecular docking of withanolide derivatives to the target protein PknG from *Mycobacterium tuberculosis*'. *Bioinformation*, 7: 1-4.

Sanz, M *et al.* (2012) 'LC-DAD/ESI-MS/MS study of phenolic compounds in ash (*Fraxinus excelsior* L. and *F. americana* L.) heartwood. Effect of toasting intensity at cooperage'. *Journal of Mass Spectrometry*, 47: 905-918.

Sarfraz, I *et al.* (2017) '*Fraxinus*: A Plant with Versatile Pharmacological and Biological Activities'. *Evidence-Based Complementary and Alternative Medicine*, 2017: 4269868.

Sasikumar, K, Ghosh, AR and Dusthacker, A (2018) 'Antimycobacterial potentials of quercetin and rutin against *Mycobacterium tuberculosis* H37Rv'. *3 Biotech*, 8: 427-427.

Sathishkumar, N *et al.* (2013) 'Computer-aided identification of EGFR tyrosine kinase inhibitors using ginsenosides from *Panax ginseng*'. *Computers in Biology and Medicine*, 43: 786-797.

Savva, A and Roger, T (2013) 'Targeting toll-like receptors: promising therapeutic strategies for the management of sepsis-associated pathology and infectious diseases'. *Frontiers in Immunology*, 4: 387-387.

Scherr, N *et al.* (2007) 'Structural basis for the specific inhibition of protein kinase G, a virulence factor of *Mycobacterium tuberculosis*'. *Proceedings of the National Academy of Sciences of the United States of America*, 104: 12151-12156.

Scherr, N *et al.* (2009) 'Survival of Pathogenic Mycobacteria in Macrophages Is Mediated through Autophosphorylation of Protein Kinase G'. *Journal of Bacteriology*, 191: 4546-4554.

Schwikkard, SL, Mulholland, DA and Hutchings, A (1998) 'Phaeophytins from *Tapura fischeri*'. *Phytochemistry*, 49: 2391-2394.

Sechehaye, A (1930) *The Treatment of Tuberculosis with Umckaloabo (Stevens' Cure)*. London: B Fraser & Co.,

Seebacher, W *et al.* (2003) 'Complete assignments of ¹H and ¹³C NMR resonances of oleanolic acid, 18 α -oleanolic acid, ursolic acid and their 11-oxo derivatives'. *Magnetic Resonance in Chemistry*, 41: 636-638.

Seidel, V and Taylor, PW (2004) 'In vitro activity of extracts and constituents of *Pelagonium* against rapidly growing *Mycobacteria*'. *International Journal of Antimicrobial Agents*, 23: 613-619.

Seo, DY *et al.* (2018) 'Ursolic acid in health and disease'. *The Korean journal of physiology & pharmacology : official journal of the Korean Physiological Society and the Korean Society of Pharmacology*, 22: 235-248.

Shailaja, VL *et al.* (2019) 'A natural anticancer pigment, Pheophytin a, from a seagrass acts as a high affinity human mitochondrial translocator protein (TSPO) ligand, in silico, to reduce mitochondrial membrane Potential ($\Delta\psi_{mit}$) in adenocarcinomic A549 cells'. *Phytomedicine*, 61: 152858.

Shakeri, A *et al.* (2019) 'LC-ESI/LTQ Orbitrap/MS/MS and GC-MS profiling of *Stachys parviflora* L. and evaluation of its biological activities'. *Journal of Pharmaceutical and Biomedical Analysis*, 168: 209-216.

Shakya, AK (2016) 'Medicinal plants: Future source of new drugs'. *International Journal of Herbal Medicine* 4: 6.

Sharifi-Rad, J *et al.* (2017) 'Medicinal plants used in the treatment of tuberculosis - Ethnobotanical and ethnopharmacological approaches'. *Biotechnology Advances*.

Shirley, M (2020) 'Pretomanid in drug-resistant tuberculosis: a profile of its use'. *Drugs & Therapy Perspectives*, 36: 273-279.

Sieniawska, E *et al.* (2020) 'Plant-based Food Products for Antimycobacterial Therapy'. *eFood*, 1.

Singh, M *et al.* (2012) 'Protective effect of curcumin, silymarin and N-acetylcysteine on antitubercular drug-induced hepatotoxicity assessed in an in vitro model'. *Human and Experimental Toxicology*, 31: 788-797.

Singh, N *et al.* (2015) 'Identification of Novel Inhibitors of *Mycobacterium tuberculosis* PknG Using Pharmacophore Based Virtual Screening, Docking, Molecular Dynamics Simulation, and Their Biological Evaluation'. *Journal of Chemical Information and Modeling*, 55: 1120-1129.

Singh, V and Mizrahi, V (2017) 'Identification and validation of novel drug targets in *Mycobacterium tuberculosis*'. *Drug Discovery Today*, 22: 503-509.

Singhal, A *et al.* (2014) 'Metformin as adjunct antituberculosis therapy'. *Science Translational Medicine*, 6: 263ra159-263ra159.

Skaltsa, H *et al.* (2000) 'Inhibition of prostaglandin E2 and leukotriene C4 in mouse peritoneal macrophages and thromboxane B2 production in human platelets by flavonoids from *Stachys chrysantha* and *Stachys candida*'. *Biological and Pharmaceutical Bulletin*, 23: 47-53.

Skerry, C *et al.* (2012) 'Adjunctive TNF Inhibition with Standard Treatment Enhances Bacterial Clearance in a Murine Model of Necrotic TB Granulomas'. *PloS One*, 7: e39680.

Slimani, W, Zerizer, S and Kabouche, Z (2020) 'Immunomodulatory and Anti-Arthritic Activities of *Stachys circinata*'. *Jordan Journal of Biological Sciences*, 13.

- Sliwoski, G *et al.* (2014) 'Computational Methods in Drug Discovery'. *Pharmacological Reviews*, 66: 334-395.
- Solovic, I *et al.* (2010) 'The risk of tuberculosis related to tumour necrosis factor antagonist therapies: a TBNET consensus statement'. *Eur Respiratory Soc.*
- Songsiang, U *et al.* (2009) 'Bioactive constituents from the stems of *Dalbergia parviflora*'. *Fitoterapia*, 80: 427-431.
- Soromou, LW *et al.* (2012) 'In vitro and in vivo protection provided by pinocembrin against lipopolysaccharide-induced inflammatory responses'. *International Immunopharmacology*, 14: 66-74.
- Spanova, M and Daum, G (2011) 'Squalene – biochemistry, molecular biology, process biotechnology, and applications'. *European Journal of Lipid Science and Technology*, 113: 1299-1320.
- Spjut, RW (1985) 'Limitations of a random screen: Search for new anticancer drugs in higher plants'. *Economic Botany*, 39: 266-288.
- Stallmach, A, Hagel, S and Bruns, T (2010) 'Adverse effects of biologics used for treating IBD'. *Best Practice & Research Clinical Gastroenterology*, 24: 167-182.
- Stefanova, Z *et al.* (1995) 'Effect of a total extract from *Fraxinus ornus* stem bark and esculin on zymosan- and carrageenan-induced paw oedema in mice'. *Journal of Ethnopharmacology*, 46: 101-106.
- Su, Q *et al.* (2018) 'Pinocembrin protects endothelial cells from oxidized LDL-induced injury'. *Cytokine*, 111: 475-480.
- Subramoniam, A *et al.* (2012) 'Chlorophyll revisited: anti-inflammatory activities of chlorophyll a and inhibition of expression of TNF- α gene by the same'. *Inflammation*, 35: 959-966.
- Sun, Y *et al.* (2019) 'The biosynthesis of camptothecin derivatives by *Camptotheca acuminata* seedlings'. *Natural Product Research*: 1-5.
- Sundaramurthy, V and Pieters, J (2007) 'Interactions of pathogenic *mycobacteria* with host macrophages'. *Microbes Infect*, 9: 1671-1679.
- Sung, H-Y *et al.* (2010) 'Oleanolic acid reduces markers of differentiation in 3T3-L1 adipocytes'. *Nutrition Research*, 30: 831-839.
- Suriyanarayanan, B, Shanmugam, K and Santhosh, RS (2013) 'Synthetic quercetin inhibits mycobacterial growth possibly by interacting with DNA gyrase'. *Rom Biotechnol Lett*, 18: 8587-8593.
- Suttiarporn, P *et al.* (2015) 'Structures of phytosterols and triterpenoids with potential anti-cancer activity in bran of black non-glutinous rice'. *Nutrients*, 7: 1672-1687.
- Szekely, R *et al.* (2008) 'A novel drug discovery concept for tuberculosis: inhibition of bacterial and host cell signalling'. *Immunology Letters*, 116: 225-231.

- Takeda, K and Akira, S (2005) 'Toll-like receptors in innate immunity'. *International Immunology*, 17: 1-14.
- Takeuchi, O and Akira, S (2010) 'Pattern recognition receptors and inflammation'. *Cell*, 140: 805-820.
- Tanachatchairatana, T *et al.* (2008) 'Antimycobacterial Activity of Cinnamate-Based Esters of the Triterpenes Betulinic, Oleanolic and Ursolic Acids'. *Chemical and Pharmaceutical Bulletin*, 56: 194-198.
- Tanjung, M, Tjahjandarie, TS and Sentosa, MH (2013) 'Antioxidant and cytotoxic agent from the rhizomes of *Kaempferia pandurata*'. *Asian Pacific Journal of Tropical Disease*, 3: 401-404.
- Targett, NM, Kilcoyne, JP and Green, B (1979) 'Vacuum liquid chromatography: an alternative to common chromatographic methods'. *The Journal of Organic Chemistry*, 44: 4962-4964.
- Tasioula-margari, M and Okogeri, O (2001) 'Isolation and Characterization of Virgin Olive Oil Phenolic Compounds by HPLC/UV and GC-MS'. *Journal of Food Science*, 66: 530-534.
- Tayarani-Najaran, Z *et al.* (2017) 'Cytotoxic and apoptotic effects of different extracts of *Artemisia biennis* Willd. on K562 and HL-60 cell lines'. *Iranian journal of basic medical sciences*, 20: 166-171.
- Thoss, V *et al.* (2012) 'Triacylglycerol composition of British bluebell (*Hyacinthoides non-scripta*) seed oil'. *RSC Advances*, 2: 5314-5322.
- Tiberi, S *et al.* (2018) 'New drugs and perspectives for new anti-tuberculosis regimens'. *Pulmonology*, 24: 86-98.
- Tissut, M and Egger, K (1972) 'Les glycosides flavoniques foliaires de quelques arbres, au cours du cycle vegetatif'. *Phytochemistry*, 11: 631-634.
- Tobin, DM (2015) 'Host-Directed Therapies for Tuberculosis'. *Cold Spring Harbor Perspectives in Medicine*, 5: a021196.
- Tobyn, G, Denham, A and Whitelegg, M (2011) 'CHAPTER 29 - *Stachys officinalis*, wood betony'. In: Tobyn, G., Denham, A. and Whitelegg, M. (eds.) *Medical Herbs*. Edinburgh: Churchill Livingstone: 307-316.
- Tomaz, ACdA *et al.* (2008) 'Chemical constituents from *Richardia grandiflora* (Cham. & Schltdl.) Steud. (Rubiaceae)'. *Revista Brasileira de Farmacognosia*, 18: 47-52.
- Tomou, EM, Barda, C and Skaltsa, H (2020) 'Genus *Stachys*: A Review of Traditional Uses, Phytochemistry and Bioactivity'. *Medicines*, 7.
- Torrado, E and Cooper, AM (2013) 'Cytokines in the Balance of Protection and Pathology During Mycobacterial Infections'. In: Divangahi, M. (ed.) *The New Paradigm of Immunity to Tuberculosis*. New York, NY: Springer New York: 121-140.

- Tostmann, A *et al.* (2008) 'Antituberculosis drug-induced hepatotoxicity: concise up-to-date review'. *Journal of Gastroenterology and Hepatology*, 23: 192-202.
- Tosun, F *et al.* (2004) 'Antimycobacterial screening of some Turkish plants'. *Journal of Ethnopharmacology*, 95: 273-275.
- Trinchieri, G (1995) 'Interleukin-12: A Proinflammatory Cytokine with Immunoregulatory Functions that Bridge Innate Resistance and Antigen-Specific Adaptive Immunity'. *Annual Review of Immunology*, 13: 251-276.
- Tringali, C (2012) *Bioactive compounds from natural sources : natural products as lead compounds in drug discovery*. 2nd ed.. edn. Boca Raton, FL: Boca Raton, FL : CRC Press.
- Trott, O and Olson, A (2010) 'AutoDock Vina: improving the speed and accuracy of docking with a new scoring function, efficient optimization, and multithreading'. *Journal of Computational Chemistry*, 31: 455-461.
- Tsalamandris, S *et al.* (2019) 'The Role of Inflammation in Diabetes: Current Concepts and Future Perspectives'. *European cardiology*, 14: 50-59.
- Tufekci, KU *et al.* (2012) 'Inflammation in Parkinson's disease'. *Advances in Protein Chemistry and Structural Biology*, 88: 69-132.
- Tundis, R, Peruzzi, L and Menichini, F (2014) 'Phytochemical and biological studies of *Stachys* species in relation to chemotaxonomy: a review'. *Phytochemistry*, 102: 7-39.
- Uc-Cachón, AH *et al.* (2014) 'Naphthoquinones isolated from *Diospyros anisandra* exhibit potent activity against pan-resistant first-line drugs *Mycobacterium tuberculosis* strains'. *Pulmonary Pharmacology and Therapeutics*, 27: 114-120.
- Ughetto, T (2014) 'Glucosevia *Fraxinus excelsior* Extract Effectively Controls Blood Glucose Levels in Randomized, Controlled Trial'. *Integrative Medicine*, 13: 30-32.
- Valenzuela, B *et al.* (2018) 'Alpinone exhibited immunomodulatory and antiviral activities in Atlantic salmon'. *Fish & Shellfish Immunology*, 74: 76-83.
- van Bergen, PF *et al.* (1997) 'Organic geochemical studies of soils from the Rothamsted Classical Experiments—I. Total lipid extracts, solvent insoluble residues and humic acids from Broadbalk Wilderness'. *Organic Geochemistry*, 26: 117-135.
- van der Kooy, F, Meyer, JJM and Lall, N (2006) 'Antimycobacterial activity and possible mode of action of newly isolated neodiospyrin and other naphthoquinones from *Euclea natalensis*'. *South African Journal of Botany*, 72: 349-352.
- Vaure, C and Liu, Y (2014) 'A Comparative Review of Toll-Like Receptor 4 Expression and Functionality in Different Animal Species'. *Frontiers in Immunology*, 5.
- Veluthoor, S *et al.* (2012) 'Chapter 15 - Phytochemicals: In Pursuit of Antitubercular Drugs'. In: Atta ur, R. (ed.) *Studies in Natural Products Chemistry*. Elsevier: 417-463.

- Venditti, A *et al.* (2014) 'Characterization of secondary metabolites, biological activity and glandular trichomes of *Stachys tymphaea* Hausskn. from the Monti Sibillini National Park (Central Apennines, Italy)'. *Chemistry & Biodiversity*, 11: 245-261.
- Venditti, A *et al.* (2017) 'Polar constituents, protection against reactive oxygen species, and nutritional value of Chinese artichoke (*Stachys affinis* Bunge)'. *Food Chemistry*, 221: 473-481.
- Victor, FC and Gottlieb, AB (2002) 'TNF-alpha and apoptosis: implications for the pathogenesis and treatment of psoriasis'. *Journal of drugs in dermatology*, 1: 264-275.
- Visen, P *et al.* (2009) 'Acute effects of *Fraxinus excelsior* L. seed extract on postprandial glycemia and insulin secretion on healthy volunteers'. *Journal of Ethnopharmacology*, 126: 226-232.
- Vitalini, S *et al.* (2015) 'Plants, people and traditions: ethnobotanical survey in the Lombard Stelvio National Park and neighbouring areas (Central Alps, Italy)'. *Journal of Ethnopharmacology*, 173: 435-458.
- Vyas, SP and Goswami, R (2017) 'Striking the right immunological balance prevents progression of tuberculosis'. *Inflammation Research*, 66: 1031-1056.
- Wajant, H, Pfizenmaier, K and Scheurich, P (2003) 'Tumor necrosis factor signaling'. *Cell Death and Differentiation*, 10: 45-65.
- Walburger, A *et al.* (2004a) 'Protein kinase G from pathogenic *mycobacteria* promotes survival within macrophages'. *Science*, 304: 1800-1804.
- Walburger, A *et al.* (2004b) 'Protein Kinase G from Pathogenic *Mycobacteria* Promotes Survival Within Macrophages'. *Science*, 304: 1800-1804.
- Wallis, RS *et al.* (2004) 'A study of the safety, immunology, virology, and microbiology of adjunctive etanercept in HIV-1-associated tuberculosis'. *AIDS*, 18: 257-264.
- Wallis, RS, van Vuuren, C and Potgieter, S (2009) 'Adalimumab treatment of life-threatening tuberculosis'. *Clinical Infectious Diseases*, 48: 1429-1432.
- Wang, S-Y *et al.* (2009) 'Bioactivity-guided screening identifies pheophytin a as a potent anti-hepatitis C virus compound from *Lonicera hypoglauca* Miq'. *Biochemical and Biophysical Research Communications*, 385: 230-235.
- Wang, S *et al.* (2018) 'Screening and identification of a six-cytokine biosignature for detecting TB infection and discriminating active from latent TB'. *Journal of Translational Medicine*, 16: 206-206.
- Wang, W *et al.* (2020) 'Pinocembrin mitigates depressive-like behaviors induced by chronic unpredictable mild stress through ameliorating neuroinflammation and apoptosis'. *Molecular Medicine*, 26: 53.

Wang, X *et al.* (2013) 'Oleanolic acid improves hepatic insulin resistance via antioxidant, hypolipidemic and anti-inflammatory effects'. *Molecular and Cellular Endocrinology*, 376: 70-80.

Waszkowycz, B, Clark, DE and Gancia, E (2011) 'Outstanding challenges in protein–ligand docking and structure-based virtual screening'. *Wiley Interdisciplinary Reviews: Computational Molecular Science*, 1: 229-259.

Wellen, KE and Hotamisligil, GS (2005) 'Inflammation, stress, and diabetes'. *The Journal of clinical investigation*, 115: 1111-1119.

Wong, EB, Cohen, KA and Bishai, WR (2013) 'Rising to the challenge: new therapies for tuberculosis'. *Trends in Microbiology*, 21: 493-501.

World Health Organization (2018a) *Tuberculosis*. Available at: <http://www.who.int/en/news-room/fact-sheets/detail/tuberculosis> (Accessed: 2018, February 16).

World Health Organization (2018b) *What is TB? How is it treated?* Available at: <http://www.who.int/features/qa/08/en/>.

World Health Organization (2020a) 'Tuberculosis TB, Global tuberculosis report 2020'. Available at: <https://apps.who.int/iris/bitstream/handle/10665/336069/9789240013131-eng.pdf>.

World Health Organization (2020b) *WHO operational handbook on tuberculosis. Module 4: treatment - drug-resistant tuberculosis treatment*. . Geneva: World Health Organization.

Wright, C *et al.* (2007) 'Herbal medicines as diuretics: a review of the scientific evidence'. *Journal of Ethnopharmacology*, 114: 1-31.

Wright, JLC *et al.* (1978) 'Identification of C-24 alkyl epimers of marine sterols by ¹³C nuclear magnetic resonance spectroscopy'. *Canadian Journal of Chemistry*, 56: 1898-1903.

Wu, M-J *et al.* (2004) '*Glossogyne tenuifolia* acts to inhibit inflammatory mediator production in a macrophage cell line by downregulating LPS-induced NF-κB'. *Journal of Biomedical Science*, 11: 186-199.

Yaacob, NS *et al.* (2015) 'Anti-Tumor Action, Clinical Biochemistry Profile and Phytochemical Constituents of a Pharmacologically Active Fraction of *S. crispus* in NMU-Induced Rat Mammary Tumour Model'. *PloS One*, 10: e0126426.

Yadav, AK *et al.* (2013) 'Screening of flavonoids for antitubercular activity and their structure–activity relationships'. *Medicinal Chemistry Research*, 22: 2706-2716.

Yamamoto, Y and Gaynor, RB (2001) 'Therapeutic potential of inhibition of the NF-κB pathway in the treatment of inflammation and cancer'. *The Journal of Clinical Investigation*, 107: 135-142.

- Yang, N *et al.* (2013) 'Pinocembrin, a major flavonoid in propolis, improves the biological functions of EPCs derived from rat bone marrow through the PI3K-eNOS-NO signaling pathway'. *Cytotechnology*, 65: 541-551.
- Yang, TW *et al.* (2017) 'Side effects associated with the treatment of multidrug-resistant tuberculosis at a tuberculosis referral hospital in South Korea: A retrospective study'. *Medicine*, 96: e7482-e7482.
- Yew, WW and Leung, CC (2006) 'Antituberculosis drugs and hepatotoxicity'. *Respirology*, 11: 699-707.
- Young, C, Walzl, G and Du Plessis, N (2020) 'Therapeutic host-directed strategies to improve outcome in tuberculosis'. *Mucosal Immunology*, 13: 190-204.
- Younis, T *et al.* (2016a) '*Fraxinus xanthoxyloides* leaves reduced the level of inflammatory mediators during in vitro and in vivo studies'. *BMC Complementary and Alternative Medicine*, 16: 230.
- Younis, T *et al.* (2016b) '*Fraxinus xanthoxyloides* leaves reduced the level of inflammatory mediators during in vitro and in vivo studies'. *BMC Complementary and Alternative Medicine*, 16: 230-230.
- Yuan, L *et al.* (2019) 'Phytosterols Suppress Phagocytosis and Inhibit Inflammatory Mediators via ERK Pathway on LPS-Triggered Inflammatory Responses in RAW264.7 Macrophages and the Correlation with Their Structure'. *Foods*, 8: 582.
- Zang, LL *et al.* (2014) 'Research progress of ursolic acid's anti-tumor actions'. *Chinese Journal of Integrative Medicine*, 20: 72-79.
- Zeid, IZ *et al.* (2012) 'Antimicrobial Antioxidant Daucane Sesquiterpenes from *Ferula hermonis* Boiss'. *Phytotherapy Research*, 26: 579-586.
- Zerin, T *et al.* (2016) 'Anti-inflammatory potential of ursolic acid in *Mycobacterium tuberculosis*-sensitized and concanavalin A-stimulated cells'. *Molecular Medicine Reports*, 13: 2736-2744.
- Zhang, D *et al.* (2015) 'Pinocembrin inhibits matrix metalloproteinase expression in chondrocytes'. *IUBMB Life*, 67: 36-41.
- Zhang, J-M and An, J (2007) 'Cytokines, inflammation, and pain'. *International Anesthesiology Clinics*, 45: 27-37.
- Zhang, Y-Z and Li, Y-Y (2014) 'Inflammatory bowel disease: pathogenesis'. *World Journal of Gastroenterology*, 20: 91-99.
- Zhang, Y *et al.* (2020) 'A dual effect of ursolic acid to the treatment of multiple sclerosis through both immunomodulation and direct remyelination'. *Proceedings of the National Academy of Sciences*, 117: 9082.
- Zhao, H *et al.* (2013) 'Efficient synthesis and anti-fungal activity of oleanolic acid oxime esters'. *Molecules*, 18: 3615-3629.

Zhao, J *et al.* (2019) 'Ursolic acid exhibits anti-inflammatory effects through blocking TLR4-MyD88 pathway mediated by autophagy'. *Cytokine*, 123: 154726.

Zheng, Y *et al.* (2014) 'Identification of plant-derived natural products as potential inhibitors of the *Mycobacterium tuberculosis* proteasome'. *BMC Complementary and Alternative Medicine*, 14: 400.

Zhou, L-t *et al.* (2015) 'Pinocembrin inhibits lipopolysaccharide-induced inflammatory mediators production in BV2 microglial cells through suppression of PI3K/Akt/NF- κ B pathway'. *European Journal of Pharmacology*, 761: 211-216.

Žiberna, L *et al.* (2017) 'Oleanolic Acid Alters Multiple Cell Signaling Pathways: Implication in Cancer Prevention and Therapy'. *International Journal of Molecular Sciences*, 18: 643.

Zulet, MA *et al.* (2014) 'A *Fraxinus excelsior* L. seeds/fruits extract benefits glucose homeostasis and adiposity related markers in elderly overweight/obese subjects: a longitudinal, randomized, crossover, double-blind, placebo-controlled nutritional intervention study'. *Phytomedicine*, 21: 1162-1169.

Zumla, A *et al.* (2015) 'Inflammation and tuberculosis: host-directed therapies'. *Journal of Internal Medicine*, 277: 373-387.

Zundler, S and Neurath, MF (2015) 'Interleukin-12: Functional activities and implications for disease'. *Cytokine & Growth Factor Reviews*, 26: 559-568.